2010
Office of Fossil Energy Fuel Cell Program Annual Report

Increase Energy Security
Eliminate Carbon Footprint
Enhance Water Conservation

SECA
Solid State Energy Conversion Alliance

U.S. DEPARTMENT OF ENERGY

NETL

DOE/NETL-2010/1439

2010
OFFICE OF FOSSIL ENERGY
FUEL CELL PROGRAM ANNUAL REPORT

October 2010

Table of Contents

III. SECA CORE RESEARCH & DEVELOPMENT (CONTINUED)

I. INTRODUCTION

I. Introduction

Competitive Innovation: Accelerating Technology Development

The U.S. Department of Energy (DOE) Office of Fossil Energy, through the National Energy Technology Laboratory (NETL) and in collaboration with private industry, universities and national laboratories, has forged Government-industry partnerships under the Solid State Energy Conversion Alliance (SECA) to reduce the cost of solid oxide fuel cells (SOFCs). This fuel cell technology shall form the basis for integrated gasification fuel cell (IGFC) systems utilizing coal for clean and efficient central power generation. IGFC systems incorporating SECA SOFC technology address environmental, climate change, and water concerns associated with fossil fuel use while simultaneously establishing a foundation for a secure energy future in the United States.

With the successful completion of the first phase of the SECA Cost Reduction program element in 2006, where initial cost and prototype test goals were achieved, SECA moved one step closer to realizing its vision of cost-effective, near-zero-emission fuel cell technology for commercial applications. SECA moved another step closer in 2009, when two of the Industry Teams successfully completed the first phase of Coal-Based Systems validation testing – metric tests for 10 kilowatt (kW) stacks in accordance with the SECA minimum requirements of greater than 5,000 hours of operation and degradation of less than 4.0 percent per 1,000 hours (<4%/1,000 hr). In the final quarter of Fiscal Year (FY) 2010, the Industry Teams will progress further with testing of ≥25 kW stacks to validate achievement of SECA's cost goals of $175/kW (stack) and $700/kW (power block). These cost goals are based upon high-volume production in 2007 dollars.

Successful validation testing in accordance with rigorous DOE guidance reflects the excellent progress being made toward the SECA goals. A coal-based SOFC power generation system that meets the goals will achieve environmental regulations compliance with effectively no carbon footprint, near-zero water requirements, essentially zero nitrogen oxides (NOx), and the lowest available cost of electricity. This technology makes substantial strides in realizing clean, economic energy production from coal in any state in the United States.

The SECA fuel cell program is a critical element of the DOE's Office of Fossil Energy technology portfolio. From an energy security perspective, coal is a primary resource for reducing dependence on imported oil and natural gas. More than half of the nation's electricity supply is generated from coal – developing technology to ensure its environmentally clean and climate friendly use is of crucial national importance. SECA technology offers greater than 99 percent carbon capture, less than 0.5 parts per million (ppm) NOx emission, reduced water requirements, and a coal-to-electricity efficiency exceeding 50 percent on a higher heating value (HHV) basis and as high as 60 percent HHV for advanced pressurized systems. The SECA cost goals of $175/kW stacks and $700/kW power blocks (2007 U.S. dollar basis) pursued under the SECA Cost Reduction program element will ensure that the cost of electricity to the user will not exceed what is typical today. Concurrently, the SECA Coal-Based Systems program element will scale and integrate SECA SOFC technology for use in large IGFC systems. Cross-cutting research and development (R&D) and testing support are provided by SECA's Core Technology Program element.

SECA is comprised of three groups: Industry Teams, Core Technology Program participants, and federal government management. The Industry Teams within the SECA Cost Reduction and Coal-Based Systems program elements design the fuel cells and handle most hardware and market penetration issues. The Core Technology Program element, made up of universities, national laboratories, small businesses, and other R&D organizations, addresses applied technological issues common to all Industry Teams. Findings and inventions under the Core Technology Program are made available to all Industry Teams under unique intellectual property provisions that serve to accelerate development. The federal government management facilitates interaction between Industry Teams and the Core Technology Program as well as establishes technical priorities and approaches.

Across the United States, SECA Core Technology Program participants are working on dozens of fuel cell projects, led by the brightest minds from leading universities, national laboratories and businesses. These competitively-selected projects provide vital R&D and testing in support of the Industry Teams.

In the same spirit of healthy competition, the Industry Teams leverage the collective ingenuity of the Core Technology Program to independently pursue innovations in fuel cell design that can be mass-produced at lower cost. Focusing on Cost Reduction and Coal-Based Systems, the Industry Teams are working to solve the challenges of fuel cell technology, each using different design and manufacturing approaches. As a result, the SECA program is rich in innovation, allowing it to reach its goals much faster.

Fuel Cell Research and Development

The Office of Fossil Energy and NETL are pleased to present this FY 2010 Fuel Cell Program Annual Report, a compilation of abstracts from the fuel cell projects managed through these offices. These abstracts are divided into subsections as detailed in the following.

SECA Industry Teams — Coal-Based Systems

Through its Coal-Based Systems program element, SECA seeks to leverage successes in the Cost Reduction program element; scale SOFC cells and stacks to sizes appropriate for central power generation applications; and integrate the SOFC, associated balance of plant, and coal gasification technology to create an IGFC system. Industry Teams will focus on developing large megawatt-scale systems while continuing SECA Cost Reduction activities. It is anticipated that the best technology from any Industry Team will be available for incorporation into one or more of the SECA Coal-Based Systems projects. Key R&D topics include materials (cathodes, interconnects, seals, etc.), manufacturing, failure analysis, system integration, coal contaminants, balance of plant, controls and instrumentation, and pressurization.

SECA Industry Teams — Cost Reduction

To achieve cost targets, Industry Teams are refining and validating advanced technology in ≥25 kW SOFC stacks that can be mass-produced, aggregated, and scaled to meet a broad range of applications. This development

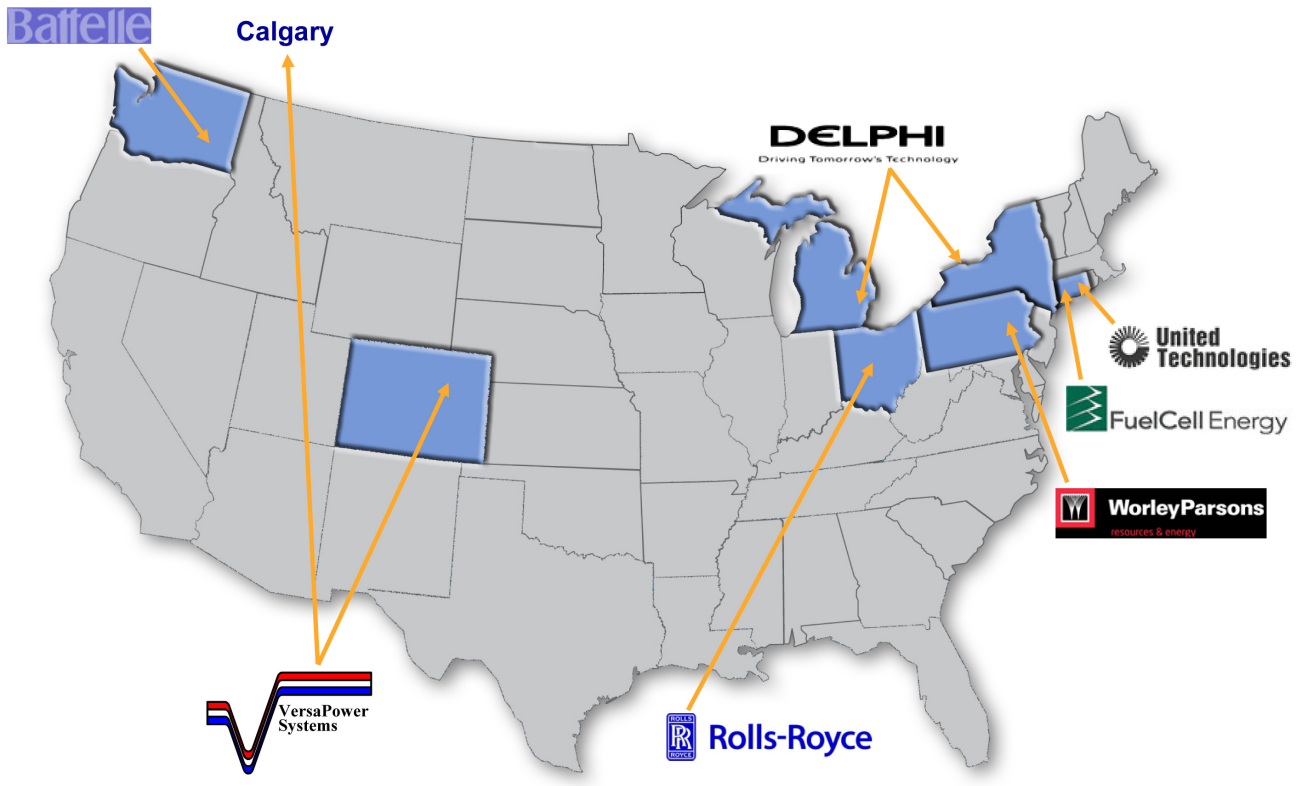

SECA Industry Teams and Major Subcontractors

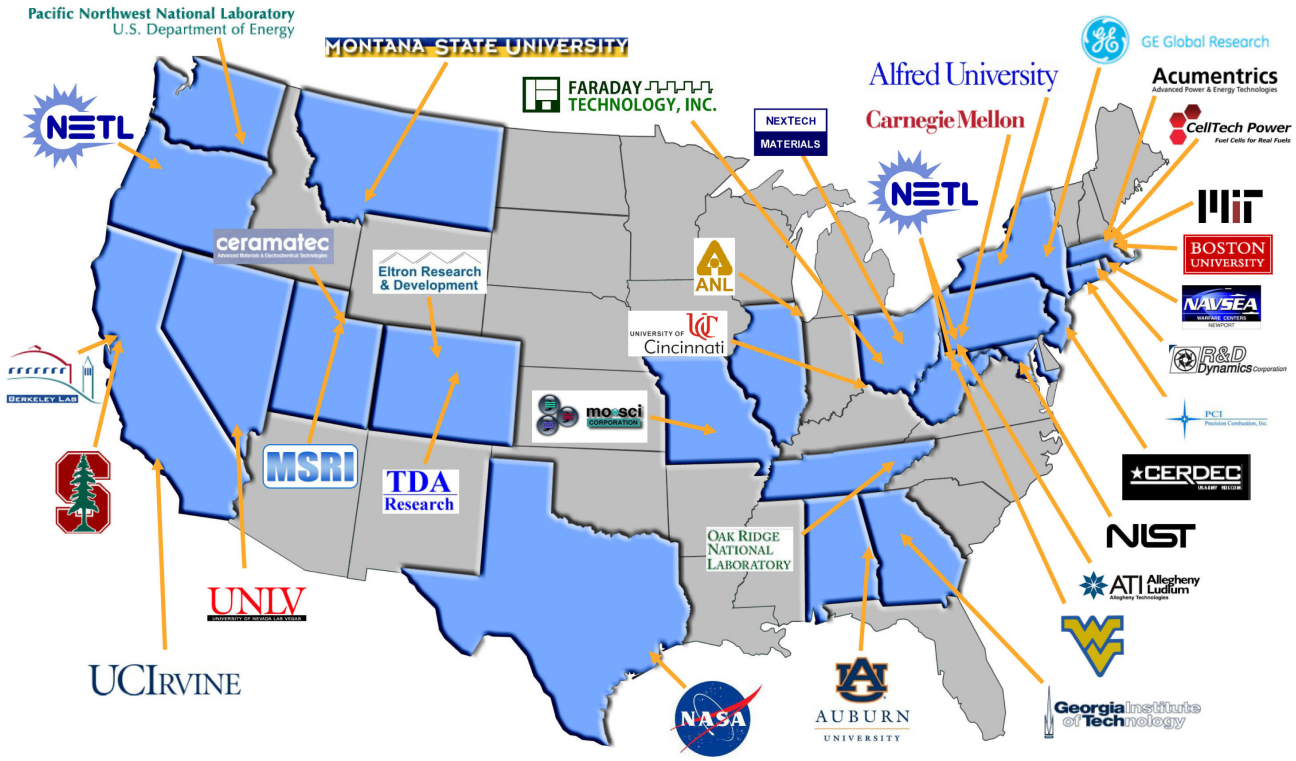

SECA Core Technology Program and Other R&D Participants

activity is blending established manufacturing processes with state-of-the-art fuel cell technology advancements in order to leverage the advantages of economies of production (high-volume mass production) and scale to reduce fuel cell costs. Achieving the cost targets requires reaching a full spectrum of large markets, such as auxiliary power units (APUs) for trucks and recreational vehicles, as well as other markets such as residential-commercial-industrial power, a wide range of distributed generation, and specialized applications for the military. Adoption of common stack technology for these vast markets will create the opportunity for the high-volume production required to reduce cost to commercially viable levels.

SECA Core R&D

The Core Technology Program provides comprehensive applied research support in nine focus areas. This program structure, along with special intellectual property provisions (exception to the Bayh-Dole Act), reduces R&D cost by leveraging resources so that the Industry Teams do not engage in separate, redundant applied research projects, paying multiple times for the same technical solutions. Diligent DOE management of the Core Technology Program with this approach also ensures that only major issues are addressed. SECA's goal is to raise the technology bar in large strides rather than small steps. Core Technology Program areas of research are also funded by special topics under DOE Small Business Innovation Research (SBIR), Small Business Technology Transfer, and Experimental Program to Stimulate Competitive Research solicitations. The Core Technology Program focus areas include the following:

- **Cathodes** – Improve the stability and performance of fuel cell cathodes using state-of-the-art concepts and methodologies.
- **Anodes and Coal Contaminants** – Determine potential coal syngas contaminants and their impact on anode performance.
- **Interconnects and Contact Materials** – Develop stable, low-cost metallic interconnects and interconnect contact materials operating in the temperature range of 650 to 850°C with acceptably low area-specific resistance (ASR) and stability over the service lifetime.
- **Seals** – Develop materials and designs exhibiting adequate sealing performance with the requisite chemical and phase stability in long-term service.
- **Cross-Cutting Materials and Manufacturing** – Develop materials and manufacturing technologies

that improve fuel cell reliability, performance, and ability to tolerate any fuel or air contaminants, and that achieve cost reductions.

- **Fuel Processing** – Develop fuel processing technologies that will meet application requirements such as zero water consumption, space and volume constraints, and transient capability.
- **Power Electronics** – Optimize efficiency and cost in conversion of fuel cell output to usable DC (direct current) and AC (alternating current) power.
- **Modeling and Simulation** – Create models to determine a reliable operating space and to guide manufacturing.
- **Balance of Plant** – Develop high-temperature heat exchangers and blowers to enable high system efficiency and low cost.

Innovative Concepts

SECA Innovative Concepts will assess the feasibility of a coal power plant based upon a direct coal SOFC and will validate the performance, robustness, cost and scalability of metallic supported cell designs for use in coal-based SOFC power systems.

Advanced Research

The SECA Advanced Research program provides cross-cutting, multidisciplinary research that leads to advanced electrochemical technologies minimizing the environmental consequences of using fossil fuels in energy generation. This program supports future advances in the SECA and Office of Fossil Energy Coal and Power programs by developing novel electrochemical energy-conversion and integrated technologies that advance the efficiency, reliability, and cost goals of fuel cell systems.

Key Program Accomplishments

SECA Industry Teams – Coal-Based Systems

SOFC Developers Achieve New Milestones in System Efficiency and Cost by Implementing the Next Generation of Thin Cell Technology. FuelCell Energy, Inc. and its technology partner, Versa Power Systems, Inc. initiated the manufacturing of new SOFC technologies based on improved materials and thinner anode structures. The new generation of cells has demonstrated significant performance gains, an expanded range of operating temperature, and long-term stability as compared to the previous baseline technology. The cell manufacturing process is based on tape-casting, screen-printing, and co-firing processes that have been optimized to take advantage of the new materials and thin cell technology. Over 46 stacks have been fabricated and tested, with cell sizes up to 1,000 cm^2 and cell counts up to 92 cells. A recent milestone in technology development was achieved by fabrication and testing of the first-of-a-kind >30 kW stack tower based on anode-supported planar cells. This significant achievement paves the road for future large-scale SOFC power stations and distributed generation systems. Utilizing the improved class of cell and stack technologies, a nominal 400 megawatt (MW) coal-based baseline system was developed. The system offers 58.7% electrical efficiency based on high heating value of coal while capturing more than 99% of carbon in the syngas as carbon dioxide. The baseline SOFC system consumes 75% less water compared to pulverized coal combustion plants using scrubbing technologies for carbon capture and has a footprint comparable to integrated gasification combined cycle plants. The recent factory equipment cost estimates have shown an SOFC power island cost of $414/kW in 2002 dollars, approaching the DOE cost target for a coal-based system.

Power Density Further Increased and Durability Improved for Solid Oxide Fuel Cells Targeted for Centralized Coal-Based Power Plants. Rolls-Royce Fuel Cell Systems (RRFCS) has demonstrated higher power densities for its integrated planar SOFC, reducing the cost of power block modules for an integrated coal-gasification fuel cell combined cycle plant that is projected to allow sequestration of 90% of carbon dioxide and achieve an overall efficiency of >50%. Further improvement by 36% of the power density at normal system operating conditions has been achieved through substitution and modification of the active layers of the cell. With this 2009-2010 advancement, the power density has now increased 73% cumulatively over the course of the SECA program. Operation of fuel cells at higher power densities allows smaller overall fuel cell systems at equivalent power ratings, which cascades into an overall lower cost for the power plant and lower cost of electricity. Coincident with the performance improvement has been improvement in the long-term durability achieved through mitigation of a key degradation mechanism present within the electrical interconnect formed between adjacent cells. System modeling studies have resulted in selection of a revised cycle for operation of the pressurized Rolls-Royce SOFC system as part of an advanced IGFC plan. The IGFC cycle is now common to that required for the 1-MW distributed power generation product under development by RRFCS, allowing a nearer-term validation to utilities of the commercial readiness of SOFC technology demonstration prior to adoption at the larger scale as required for the IGFC. Rolls-Royce has produced fuel cell modules on their pilot production line in Canton.

SOFCs Successfully Scaled for Large-Scale Stationary Applications. UTC Power is developing conceptual process designs of a wide range of power systems ranging from 250 kW up to 100+ MW with a focus on meeting the system efficiency and carbon separation targets specified in the SECA minimum requirements. Delphi, in partnership with Battelle Memorial Institute under the SECA Cost Reduction program, has continued advancement of SOFC technology. Cell and stack fabrication capabilities have been expanded and scaled up to high rates with improved process controls to maintain the highest quality standards. An improved 4th generation cell design with increased active area has been fabricated and tested. Power density has exceeded SECA 2011 goals with performance of 0.81 V/cell using 48.5% H_2, 48.5% N_2, 3% H_2O fuel. Utilizing the new cell design, a 25-cell stack has been built and demonstrated to produce power in excess of 5 kW. The Gen 4 stack is being used as the basis for a proof-of-concept power plant being developed by UTC Power. Phase I test results on simulated coal gas will be used to validate models that have been developed to aid in the design of the stationary SOFC power module.

SECA Industry Teams – Cost Reduction

SOFCs Successfully Tested for Coal-Based System Analysis. Delphi, in partnership with Battelle Memorial Institute under SECA, successfully fabricated and tested two 30-cell Generation 3.2 stacks. The stacks were instrumented with thermocouples on dummy repeating units to measure internal stack temperatures, as well as temperatures at the inlet and outlet of the stack. A stack test stand was also updated to run various load profiles and simulated coal syngas compositions as part of the project. Data were collected, analyzed, and reported to SECA. These data on the operation of state-of-the-art SOFC stacks shall be used for model validation and calibration in order to assess the impact of stack and system operating conditions on cell temperatures.

SECA Core R&D – Cathodes

Correlations Between Electrical Conductance and Lattice Parameter of SOFC Cathode Materials Discovered. Measurements of the out-of-plane lattice parameter of a $La_{0.6}Sr_{0.4}Co_{0.2}Fe_{0.8}O_{3-\delta}$ (LSCF) thin film and its electrical conductance at Argonne National Laboratory have revealed time-dependent changes in both of these quantities in response to an applied direct current electrical field. Experiments were performed that simultaneously measured X-ray diffraction along with conductance from an (001) oriented 20 nm LSCF film grown on a 100 nm gadolinium-doped ceria (GDC) (001) film deposited on a yttria-stabilized zirconia (YSZ) (001) substrate. The LSCF film was found to expand normal to the surface as oxygen partial pressure was decreased, or as a negative cathodic potential was applied to the LSCF/GDC/YSZ stack. A simultaneous measurement of the conductance during the application of this negative cathodic potential revealed a rapid decrease, then a plateau, followed by another rapid decrease in conductance. This two-step drop indicates that more than one process controls the conductance of these LSCF thin films. The length of the plateau generally becomes shorter as the applied bias becomes more negative and as the temperature is increased from 500°C to 700°C, but more studies are required to confirm this behavior. The kinetics of the lattice parameter change becomes much faster after the conductance has plateaued and then dropped. The size of the lattice parameter change, and hence the inferred oxygen vacancy concentration change, is only weakly dependent on temperature.

Role of Structure, Surface Chemistry, and Oxygen Reduction in SOFC Cathode Materials Investigated. Over the last year, using X-ray absorption spectroscopy (XAS), Boston University has clearly shown the charge state of the Mn ion in lanthanum strontium manganite (LSM) to be closely related to the cathode polarization resistance changes as measured by impedance spectroscopy. Further, using O-edge XAS, Boston University has shown segregation of Sr to the surface of the LSM thin films under cathodic conditions and confirmed these results using total X-ray fluorescence. Using electrical conductivity relaxation experiments and diffusion experiments, the surface exchange coefficient on epitaxial LSM thin films was measured and found to be 4 X 10^{-9} cm/s, and the diffusivity of oxygen was shown to be on the order of ~5 X 10^{-9} cm^2/s at 800°C. In the next phase of the project, Boston University expects to correlate oxygen transport kinetics to the thin film surface structure using in situ X-ray experiments.

Surface Engineered Films of Cathode Materials Produced and Characterized. Carnegie Mellon University (CMU) has demonstrated that surface engineered films of cathode materials can be produced and their structural and chemical properties characterized in detail. Crystallographic anisotropies were observed for epitaxial LSM single-crystal films in their oxygen uptake kinetics, where low index orientation varies by a factor of 4 in SOFC conditions. Furthermore, the surface exchange coefficient can vary greatly at low thicknesses and as a function of the support (substrate), both of which are relevant for SOFC electrocatalysis. Both electrical conductivity relaxation (ECR) and Kelvin probe spectroscopy (KPS) equipment can be used to simultaneously measure oxygen uptake, indicating that chemisorption and incorporation can be distinguished when their time constants are significantly

different, as observed for LSM. CMU will continue to produce a series of surface engineered films and will investigate (1) their structural properties, (2) their stabilities, and (3) their oxygen uptake kinetics using ECR and KPS measurements. By fabricating a matrix of related materials and carrying out these measurements, CMU will be able to provide a large amount of data to determine the key parameters that correlate surface structure to surface activity.

Method Developed for Predicting New Cathodes. Eltron Research & Development Inc. has demonstrated an approach for predicting potentially good cathode electrocatalyst formulations using existing experimental data. The use of artificial neural networks (ANNs) provides an input section, initial predictor of performance and properties of compositions selected, and a down-selection filter for a more complete structure and properties prediction system to be developed in Phase II. The model being developed relates physicochemical descriptors to cathode performance or to a metric proportional to it. Performance was fit to a function of the descriptors using an ANN, which can predict, classify, and cluster performance results. This approach allows for materials properties prediction and also enables prediction of material structure and structure-property relationships from the input of a proposed material composition. Using this approach, no fewer than four candidate materials were identified which should possess oxygen electroreduction activity comparable to or better than existing cathode materials.

Catalyst Infiltration of Cathodes Promises Improved Performance and Stability. Georgia Institute of Technology has demonstrated that the performance and stability of an LSCF cathode can be enhanced by infiltration of a catalyst such as LSM, scandia-doped ceria, or lanthanum calcium chromite. Microanalyses of the structure, composition, and morphology of the surfaces and interfaces in an LSM-infiltrated LSCF cathode reveal that a thin (~50 nm) LSM film is relatively stable on the surface of an LSCF substrate after annealing at 850°C for 900 hours, although the regularity of atom arrangement in the outer layer of the film was reduced from long to short range order. The inner layer of the LSM film and the underlying LSCF maintain their respective crystal structures and their structural coherence. For an LSM-infiltrated porous LSCF cathode, an amorphous layer (~2 to 20 nm) was formed on the surface of LSCF grains. Energy dispersive X-ray spectroscopy analysis of the amorphous layer suggests that it contains La, Sr, Co, Fe, and Mn; this surface lanthanum strontium cobalt iron manganite (LSCFM) layer may have enhanced oxygen ion conductivity due to the disorder of the high concentration of defects. Also, there was no evidence that Sr was enriched near LSCF surfaces. Thus, the resulting coating of LSCFM not only promotes facile transport of oxygen ions to the underlying LSCF but also inhibits formation of Sr-oxide on the LSCF surfaces. Considering the improvement in performance and stability achieved by infiltration, it is anticipated that the implementation of catalyst-infiltrated cathode may help to meet DOE cost goals.

Promising Cathode Contact Materials Identified. Lawrence Berkeley National Laboratory (LBNL) is undertaking a new project in FY 2010, addressing cathode contact material selection and development. The primary challenge addressed during FY 2010 concerns electrical connection and bonding between the interconnect and SOFC cathode layers. Historically, cathode materials such as LSM have been used as a cathode contact material (CCM) paste to bond the cell to the interconnect. High temperature is typically required to achieve good bonding, however, leading to rapid oxidation of the stainless steel interconnect. If a temperature low enough to avoid oxidation of the steel (<1,000°C) during the bonding step is employed, poor bonding and eventual delamination of the contact material occur. The goal of the work at LBNL is to identify candidate cathode materials displaying adequate properties after bonding at <1,000°C. A list of candidate cathode contact compositions was purchased from Praxair or fabricated by a glycine nitrate process. The properties of primary relevance, including conductivity, sintering behavior, coefficient of thermal expansion, and reactivity with manganese-cobalt spinel (MCO) and LSCF, were then determined. The summary of this screening effort suggested that the most promising candidates are LSCF and lanthanum strontium copper ferrite (LSCuF) (chosen for extensive sintering at low temperature) and strontium samarium cobaltite and lanthanum strontium cobaltite (LSC) (chosen for high conductivity). These four materials were then incorporated into ASR specimens in which electrical resistance of the LSCF/CCM/MCO junction was monitored over time. LSC and LSCuF are the most promising compositions tested to date. They provided low and stable ASR for 200 hours at 800°C. LSCuF survived 5 thermal cycles at 10°C/min.

Cathode Surface Electronic Structure and Chemical State Probed. Massachusetts Institute of Technology has probed the evolution of the surface topographic and electronic structure and chemical state of $La_{0.7}Sr_{0.3}MnO_3$ thin films using scanning tunneling microscopy and spectroscopy and X-ray photoelectron spectroscopy at elevated temperature and reactive gas environment, in particular to identify the structural nature of surface segregation on LSM. A layer-by-layer structure was found with a step height of 3.9 Å, close to the lattice parameter of LSM. Up to 500°C, the topography and the step heights remained the same, statistically within 2-4%, implying that no phase

separation took place on the top layers of the film. The low oxygen pressures, down to 10^{-10} mbar, at elevated temperatures promoted segregation of Sr by 12-20% on the A-site, accompanied by a smaller increase of (La+Sr)/Mn. The results suggest two possible structures for Sr segregation: the replacement of La by Sr on the AO-surface of the LSM, which retains a perovskite termination, or a separate AO-oxide phase nucleating on the defected lower layers. The electronic structure on LSM surface transitions from semiconducting to metallic at high temperatures, and the electron tunneling is affected by the partial pressure of oxygen.

Non-Destructive Characterization of Surfaces and Interfaces of SOFC-Related Materials Continued in Order to Identify Surface and Interface Properties during SOFC Operation. Using X-ray absorption spectroscopy and X-ray resonant scattering in the soft-X-ray energy region, Montana State University has compared the elemental distribution and chemical state of pristine and degraded LSCF/GDC interfaces, showing that prolonged operation of the cell results in La cation motion in these regions, strongly modifying the A-site and B-site occupancies of the La and Sr as well as the electronic structure of the Fe atom (due to a modification of the tetragonal distortion of the oxygen cage around the Fe atom). Furthermore, the degradation is dependent on operational conditions, especially the local cell potential occurring predominantly on the oxygen ion in-flow side. The potential at the surface of the LSCF is observed to modify the valency of surface transition metal atoms (here Cr is used as a tag element to clearly demonstrate the surface valency change from trivalent Cr to hexavalent Cr).

Infiltration Parameters for High-Activity SOFC Cathode Established. Researchers at the National Energy Technology Laboratory completed an initial study establishing experimental conditions of infiltration processes intended to tailor the microstructure of a Sr- and Co-doped $LaFeO_3$ cathode of an SOFC. The infiltration technique introduces nano-sized particulates of pyrochlore-structured $(LaSr)_2Zr_2O_7$ and perovskite-structured $(LaSr)CoO_3$ throughout the electrode pore surface to improve electrode reactivity. Experimental parameters, including concentration of infiltrate solution, infiltrate dosage, calcination temperature, and backbone structure, were scrutinized for the infiltrates to generalize the relationship between the evolved microstructures and cell performance. By applying the infiltration process to the cathode of a standard commercial button cell (MSRI Co.), researchers have decreased the ASR of cathode polarization from 0.68 ohm·cm^2 in the uninfiltrated cathode to 0.27 ohm·cm^2 in the infiltrated cathode. Based on the accumulated data and understanding, researchers expect to suggest required infiltration conditions for a specific electrode system, which is defined by its composition and microstructure.

New Cell Characterization Capability: In Situ High-Temperature X-Ray Diffraction (XRD) Analysis of Operating SOFC Cathodes. A test stand has been developed at Pacific Northwest National Laboratory that allows anode-supported SOFCs to be operated in the heating chamber of a high-temperature X-ray diffractometer. This allows for collection of XRD spectra of SOFC cathodes under actual operating conditions. The initial test configuration, which included a fine gold mesh current collector above the cathode, only allowed for very weak detection of LSCF-6428 diffraction peaks. Improved results were obtained by applying a gold paste current collector only to the perimeter of the cathode and by narrowing the width of the beam so that it impinges only on the cathode and not on the current collector around its edges. Due to the small diameter of the cathode, this configuration provides adequate current collection and also produces strong XRD patterns of the cathode material. It is anticipated that this capability will allow for detection of changes in cathode structure and/or secondary phase formation which may occur during long-term cell operation.

Study of the Electronic Structure of Cathode Materials Promotes Understanding of Oxygen Incorporation into Fuel Cell Cathodes. A theoretical study of oxygen on manganite surfaces conducted by Walter Harrison of Stanford University suggested a new understanding of the incorporation of oxygen into fuel cell cathodes. Oxygen is now understood to adhere to the surface as neutral atoms or molecules, then enter neutral oxygen vacancies, or F centers, without the successive ionization steps usually assumed. These neutral oxygen vacancies in the cathode are supplied by the neutralization of positively charged electrolyte vacancies at the electrolyte-cathode interface. Understanding of these mechanisms followed from the calculation of the electronic structure of the oxygen, of the cathode substrate, and of the interaction between the two. The limiting step in the process appeared to be the tendency of the adsorbed oxygen to avoid sites adjacent to oxygen surface vacancies. There is hope that further understanding may lead to a way to circumvent this limitation.

SECA Core R&D – Anodes and Coal Contaminants

Perovskite Adsorbents for Arsenic and Phosphorus Removal from Coal-Derived Synthesis Gas Streams Successfully Produced. During Phase I research in FY 2010, Eltron Research & Development, Inc. finished the design, synthesis, and initial testing of perovskite-based adsorbents for the removal of arsenic and phosphorus from coal-derived synthesis gas in order to protect Ni in

SOFC anodes from these poisons. The sorbents were designed to form both thermally and chemically stable arsenides and phosphides in order to prevent the re-release of these poisons at high temperatures or during interactions with high-pressure steam. Preferred sorbents produced at Eltron demonstrated As and P *adsorption efficiencies* as high as 73% versus 47% for a commercial Cu/ZnO material under ambient pressure and at 300°C under an argon stream containing 300-800 ppm As and 30–250 ppm P flowing at 2,000 hr^{-1}. Preferred sorbents also demonstrated As and P *adsorption capacities* as high as 4.5% versus 1.0% for a commercial Cu/ZnO material under ambient pressure and at 300°C under an argon stream containing 300-800 ppm As and 30–250 ppm P flowing at 2,000 hr^{-1}. Eltron sorbents contain no noble metals and are projected to cost <$5/lb on an industrial scale.

Thermodynamic and Experimental Analysis of SOFC Anode and Trace Coal Material Interactions Completed. A thermodynamic analysis of the interactions of trace materials present in coal syngas with the anode of a SOFC was performed in detail at the National Energy Technology Laboratory using a survey of 15 common gasifiers. The analysis shows that the bulk syngas composition affects the extent of anode secondary phase formation, with arsenic, phosphorus, and antimony combining with nickel to form the primary reaction products. These products are known to degrade fuel cell performance, and therefore need to be understood in order to predict fuel cell performance. The information gained from the analysis will be used to design effective clean-up strategies for integrated fuel cell/gasification systems. A paper describing this work was accepted for publication in the Journal of Power Sources.

A technique was developed that provides measurement of trace metal present in liquid- and/or gas-phase process streams at concentrations below 1 part per billion (ppb). The technique uses a modified gas chromatograph – inductively coupled plasma/mass spectrometer (GC-ICP/MS), which reduces the time required for sample collection and analysis by a factor of 50 compared to established methods. To perform the analysis, kinetic energy discrimination (KED) factors were developed to correlate a known spike of cesium (^{133}Cs) to all other analytes in liquid-phase samples. The KED factors were then used to simultaneously test an "unknown" sample of 44 liquid-phase analytes, each with a concentration of 10 ppb (mass), and 2 gas-phase analytes, each with a concentration of 1 ppm (vol), using ^{133}Cs as an internal standard. The technique's accuracy compares favorably to traditional ICP/MS methods, and concentration within 50% of the actual value for the liquid-phase analytes and 30% for the gas-phase analytes was measured. This new approach allows improved response when measuring trace components in coal syngas or flue gas, which is important for assessing clean-up requirements for advanced coal power production systems, including integrated gasification and fuel cell technology.

SECA Core R&D – Interconnects and Contact Materials

Coated Ferritic Stainless Steels Improve SOFC Performance and Cost Efficiency. In an interagency and industrial-partner collaboration, researchers at the National Energy Technology Laboratory (NETL), ATI Allegheny Ludlum Corp., and Pacific Northwest National Laboratory have successfully modified the metallic alloy AISI 441 to help achieve SOFC electrical interconnect requirements for lifetimes of 40,000 hours or more. AISI 441 is an inexpensive ferritic stainless steel. Experimental work at Pacific Northwest National Laboratory and ATI Allegheny Ludlum indicated that, with a special coating, AISI 441 exhibits very low and nearly constant area-specific resistance throughout 5,000 hours of testing. A rare earth treatment integral to the special coating and a manufacturing process that reduces silica formation have been developed by NETL and ATI, respectively. In addition to these breakthroughs, the cost of commercially available AISI 441 is predicted to be considerably lower (~$3.10/lb) than the cost of producing state-of-the-art high-temperature metal alloys suitable for SOFC electrical interconnect service.

Innovative Process for Application of $(Mn,Co)_3O_4$ Spinel Coatings onto SOFC Interconnects Demonstrated. Faraday Technology and West Virginia University are developing a cost-effective manufacturing process for application of $(Mn,Co)_3O_4$ spinel coatings onto SOFC interconnects to minimize chromia scale growth and chromium evaporation that can cause unacceptable degradation in the SOFC electrochemical performance. The manufacturing process involves using pulse reverse electrodeposition for application of a Mn-Co alloy coating onto the interconnect surface and subsequent conversion to the $(Mn,Co)_3O_4$ spinel. Faraday Technology and West Virginia University demonstrated that the electrodeposition process could produce uniform, dense, crack-free, well-adhered Mn-Co alloy coatings of various compositions on a 5 cm x 5 cm T441 stainless steel interconnect surface. A post-deposition thermal treatment converted the Mn-Co alloy coatings to $(Mn,Co)_3O_4$ spinels in which a coating thickness of ~3 µm was shown to be sufficient to mitigate chromia diffusion after 500 hours of thermal exposure at 800°C. A preliminary economic analysis based on using batch manufacturing for the pulse

reverse electrodeposition process demonstrated that the innovative coating technology can meet DOE's high-volume target of 1,600,000 plates per annum for 250 MW of fuel cell stacks at a cost of ~$1.87 per 25 cm x 25 cm coated interconnect.

Long-Term Evaluation of Protective Interconnect Coatings Exceeds 1 Year. In previous work at Pacific Northwest National Laboratory, $(Mn,Co)_3O_4$ (MC) spinels have been systematically investigated and applied as protection layers on a variety of candidate SOFC interconnect steels. Recently, the primary emphasis has been on the application of spinel coatings to AISI 441 ferritic stainless steel, which is being investigated as an interconnect alloy. A Ce-modified version of the coating has been developed to improve the interfacial adhesion between the steel substrate and the oxide scale that grows beneath the spinel coating. Long-term tests of Ce-modified MC spinel coatings on AISI 441 ferritic stainless steel indicate that these coatings exhibit low, stable ASR for over 10,000 hours at 800°C (tests are still in progress). Also, ongoing tests at 850°C indicate low, stable ASR for over 4,000 hours. In related work, an ultrasonic spray process has been developed for fabrication of MC spinel coatings onto steel interconnects and cell frames. Using a Design of Experiment approach, the preferred slurry and spray parameters for application and heat treatment of MC coatings onto 441 stainless steel were identified. Both wide and narrow mode spray processes have been optimized. ASR testing of the sprayed coatings indicated excellent performance comparable to previous coatings applied via screen-printing methods. Also, in an effort to reduce materials cost, coatings with reduced Co content are being evaluated. Co-free (Mn oxide only) coatings exhibited low initial ASR, but the ASR increased steadily over time at an unacceptably high rate. On the other hand, preliminary results for coatings with reduced Co content (i.e., Co:Mn ratio less than the standard 50:50 molar ratio) showed much improved stability over the Mn oxide coatings.

Multi-Site Doping of Yttrium Chromite Results in Optimized SOFC Interconnect Properties. The effect of cobalt, nickel, and copper doping on thermal, structural, and electrical characteristics of calcium-doped yttrium chromite was studied at Pacific Northwest National Laboratory. Yttrium chromite doped with 20% Ca on A-site and up to 30% cobalt, 15% nickel, and 10% copper on B-site showed a single-phase orthorhombic perovskite structure between 25 and 1,200°C over a wide range of oxygen partial pressures. A small amount of copper doping (~2%) remarkably enhanced sinterability, and the electrical conductivity was significantly improved by cobalt and nickel doping. Nickel doping stabilizes defect structure towards reduction, resulting in improved electrical conductivity and dimensional stability in reducing atmosphere. The thermal expansion coefficient can be adjusted and closely matched with that of 8 mol% YSZ through an optimum amount of doping, and oxygen ion leakage current due to exposure to dual atmospheres was shown to be acceptably low using oxygen permeation experiments. A chemical compatibility study between $Y_{0.8}Ca_{0.2}Cr_{0.85}Co_{0.1}Ni_{0.03}Cu_{0.02}O_{3\pm\delta}$ and other cell components indicated that the formation of detrimental secondary phase is not expected at processing temperature. Overall, yttrium chromite with ~20% calcium on the A-site and optimum amounts of cobalt, nickel, and/or copper on the B-site appears to be a promising candidate for interconnect applications in high-temperature SOFCs.

SECA Core R&D – Seals

New Viscous Glass Sealants May Improve SOFC Stack Lifetime. Alfred University has identified two new glass composition regimes that show promise for improved viscous glass SOFC sealants. Initial glass sealant candidates in the galliosilicate and germanosilicate compositions show promising behavior for sealing to YSZ and stainless steels in SOFC stacks. Optimized galliosilicate glasses exhibit desirable viscosity behavior, allowing seal formation at 850°C. Optimized germanosilicate compositions can form seals near 650°C with minimal alkali content, and retain a large amorphous content even after running at 850°C for 150 hours. The germanosilicate glasses are rather fluid at 850°C, yet some compositions still exhibit minimal interaction with YSZ after 1,500 hours, and thus show promise as the next-generation SOFC sealant.

Viscous Sealing Glass Successfully Identified for SOFCs. MO-SCI Corporation successfully identified and tested several glass compositions that could be used as viscous seals for SOFCs. The glasses possess desirable viscosity characteristics; that is, they have softening points in the temperature range expected for SOFC operations (650-850°C), and so cracks that might form in the glass upon thermal cycling should be closed upon reheating through a 'viscous healing' mechanism. The new glasses have relatively low liquidous temperatures (<800°C) and so do not exhibit significant crystallization when held at SOFC operating temperatures. Excessive crystallization will change the viscosity behavior and may jeopardize the viscous healing characteristics of the seal. The new glasses wet both aluminized SS441 and NiO/YSZ substrates, forming hermetic seals that have survived, in one case, >2,000-hour thermal cycles between room temperature and 750°C.

Innovative Self-Repairable Seals for SOFCs Developed. A functioning SOFC requires high-temperature seals that prevent the mixing of fuel and oxidant streams as well as prevent reactant escape to

the surrounding environment. A novel in situ self-healing sealing glass concept has been advanced by the University of Cincinnati. Glasses were fabricated and characterized, and seal testing was completed to demonstrate in situ self-repair capability of the glass seals. Seal tests displayed excellent seal performance, including in situ self-repair of cracked/leaking seals. The self-healing concept requires glasses with low viscosity at the SOFC operating temperature of 800°C, but this requirement may lead to excessive flow of the glass under load in areas forming the seal. To address this challenge, a modification to glass properties such as creep via addition of particulate fillers is being pursued in the current project. The underlying idea is that non-reactive ceramic particulate filler is expected to form glass-ceramic composite and increase the glass transition/glass softening temperatures and seal viscosity, thereby increasing the creep resistance of the glass-composite seals under load. In addition, the incorporation of an appropriate filler can affect the coefficient of thermal expansion of the glass-ceramic, providing additional flexibility for developing sealing glasses that reduce mismatch stresses and improve seal reliability. Filler materials have been successfully identified, and the glass-ceramic composites that have been fabricated are expected to help in meeting DOE cost and performance goals.

SECA Core R&D – Cross-Cutting Materials and Manufacturing

Manufacturing Analysis of SOFC Components Shows Low-Cost Paths Provide Excellent Performance. For SOFCs to become economically viable, low-cost and effective manufacturing processes are essential. NexTech Materials has demonstrated that protective coatings for the metallic components in an SOFC stack can be applied by low-cost, easily scaled processes. The project has found that aerosol spray deposition (ASD) of ceramic coatings on metal SOFC interconnects provides impressive corrosion resistance and compelling process economics. ASD coatings significantly exceed the performance requirements of the SOFCs, offering stable area-specific resistance values as low as 4-7 $m\Omega\text{-}cm^2$ after 1,000 hours of operation at 800°C in wet air, with repeated thermal cycling. The cost of ASD-coated large (625 cm^2) interconnects is projected to be within DOE targets, at a cost of less than $2/part. These promising results have already led to ongoing evaluations with SOFC integrators.

Effect of Long-Term Exposure on Phase Stability of Candidate Glass Seal Materials Determined. In FY 2010, the Oak Ridge National Laboratory (ORNL) SECA team successfully characterized the microstructural changes in candidate glass seal materials after 5,000 hours aging at 800°C in air and steam+H_2+N_2 environments. Devitrification kinetics, surface phase evolution, pore size distribution, and glass transition temperature were characterized as a function of long-term SOFC environment exposure. The effect of SOFC environment exposure on the physical and mechanical properties of 8 mol% YSZ electrolytes was characterized. In addition to the environmental exposure studies, the ORNL team completed a study that determined the uncertainty associated with the quantitative chemical compositional analysis of glass seal materials. ORNL supported the SECA industrial teams in the characterization of potential glass seal materials.

SECA Core R&D – Fuel Processing

Low-Temperature Plasma and Radio-Frequency Electromagnetic Fields Investigated for Enhanced Catalytic Activity in Fuel Reformers. Two novel fuel reforming technologies have been investigated at the National Energy Technology Laboratory (NETL) to improve the quality and yields of syngas for fuel cells: enhanced catalysis via radio-frequency (RF) electromagnetic fields and low-temperature plasma-assisted reforming. Two individual systems were successfully designed and incorporated into NETL's catalyst and fuel processing units. Proof-of-concept trials were performed, and both technologies showed promising results for improving syngas yields and reducing unwanted byproduct formation (coke, olefin compounds). Specifically, the low-temperature plasma system demonstrated energy conversion efficiencies (from fuel to products) as high as 83%, with 50% conversion of fuel directly to syngas (H_2 and CO only) and 33% preserved in the form of light hydrocarbons (mostly CH_4) with little or no evidence of coking. Further testing is in progress to repeat initial results, quantify by-product reduction levels with greater accuracy, and find optimal operating conditions, such as RF and plasma operating frequencies and power levels. A synergistic relationship between these advanced technologies and traditional metal-based catalysis has been identified, and future work will include efforts to understand the underlying physical mechanisms responsible for enhanced reforming.

Molten Catalytic Coal Reactor Constructed to Produce High-Methane Content Syngas. One goal of research at the National Energy Technology Laboratory (NETL) is to generate a high methane content syngas via the steam gasification of coal with molten alkali salts as catalysts. The high methane content syngas is an ideal fuel for generating electricity in an SOFC because it significantly reduces the parasitic cooling loads of the SOFC. The integration of a molten catalytic gasifier or a fluidized bed catalytic gasifier with a SOFC is one of

only a few ways to reach an overall electrical efficiency of 60% while allowing the co-production of hydrogen and/or methane during times of off-peak electricity demand. The goal of NETL's research is to expand the operating range of molten catalytic gasifiers by lowering the temperature with mixed alkali salts and lowering the pressure so as to improve integration with SOFCs that operate at or just above atmospheric pressures. NETL has successfully constructed a new molten catalytic reactor system and has begun baseline testing of the system. Construction and baseline testing of the reactor system will now allow for experiments to begin to determine the kinetics of molten salt steam-gasification and to determine the methane composition of the gas that would power a SOFC.

Diesel Reformer Operation Demonstrated for Water Neutrality. Precision Combustion, Inc. (PCI) has successfully demonstrated diesel autothermal reforming (ATR) operation under a water-neutral condition using both direct anode recycle approach and condensation approach for recovering exhaust water. The operating conditions of the proposed water recovery approaches have been optimized, and the reactor performance has been extensively characterized and evaluated. A durability test was performed to demonstrate stable catalyst performance under water-neutral conditions when operating the diesel reformer using simulated anode exhaust mixture. For the condensation approach, test results showed that a sufficient amount of water can be recovered to allow for Microlith®-based fuel reformer operation under a water-neutral condition at ambient temperatures as high as 50°C. PCI has also successfully developed a low-pressure-drop nozzle that operates with Tier II diesel. This result is significant because it reduces parasitic power requirements of the auxiliary power unit system while providing more uniform flow over a wide operating range. Finally, alternative catalysts were evaluated in order to develop a highly selective, sulfur-tolerant multifunctional reforming catalyst for fuel reformation at low cost. Results from preliminary catalyst testing demonstrated potential for a reduced-cost, highly efficient reformer system that can accomplish complete fuel conversion and ~85% reforming efficiency.

SECA Core R&D – Modeling and Simulation

Model Predicts Cathode Contact Materials Densification. Pacific Northwest National Laboratory has developed modeling tools to evaluate the effects of material volumetric changes during SOFC stack assembly on load distribution and component stresses. Volumetric changes (resulting from processes such as contact material sintering, glass-ceramic seal devitrification, and anode reduction) are important to determine residual stresses in the cells and their effect on reliability. The constitutive model was used with existing dilatometric measurements to simulate actual cathode contact materials currently under development and evaluate the sensitivity of final density to temperature, processing time, initial grain size, remote loading, layer thickness, and mechanical constraint. The model predicted that useful densification greater than 90% is possible based on the experimental data for low-temperature sintering, but sufficient strength is still required to accommodate high residual stresses up to 15 MPa.

Capability Stack Simulation Tools Enhanced. The existing SOFC-MP (Solid Oxide Fuel Cell – Multi-Physics) tools developed by Pacific Northwest National Laboratory were significantly updated to add new capabilities. For the three-dimensional stack modeling tool, memory usage was improved such that 50-cell stacks can be solved on a 64-bit Linux platform. For the two-dimensional stack modeling tool, numerous improvements were made to increase accuracy, usability, efficiency, and capability. Enhancements include simulation of mixed fuels, user-defined methane reforming rates, user-defined electrochemistry routines, simulation on targeted average current density or fuel utilization, simulation of stack current-voltage curve, and cell-to-cell variations on geometry and fuel/oxidant properties. This modeling tool was successfully validated against literature benchmarks for several single-cell cases and a 5-cell stack. Results for multi-cell stacks with more than 100 cells and cell-to-cell variations possible in tall stack experiments were also demonstrated.

SECA Core R&D – Balance of Plant

Hybrid Heat Exchanger Successfully Demonstrated for SOFC Generators. Acumentrics Corporation, in conjunction with Blasch Precision Ceramics, has successfully integrated a ceramic monolith into a combination cross-flow ceramic and counter-flow metallic cathode air recuperator. This arrangement takes advantage of a high-temperature, near-net-shape cast cross-flow ceramic core, while enabling the use of lower-grade metallic alloys in the medium-to-low temperature counter-flow metallic section. The hybrid recuperator is capable of meeting the >80% effectiveness required in residential- and commercial-scale solid oxide fuel generators. The robustness of the design was demonstrated through duration and thermal cycle testing.

Efficient Low-Cost Blower Being Developed for 3 to 10 kW SOFC Systems. R&D Dynamics Corporation is developing a low-cost cathode air blower which will cost less than $100 at a production volume of 50,000 units per year. The blower being developed

is efficient, reliable, oil-free, maintenance-free, and compact. Design for Manufacturing and Assembly techniques were used to reduce the cost of the blower. The blower was designed with only 17 parts. The blower was detail designed, and a prototype unit was manufactured. A low-cost controller was developed and tested for the blower. The prototype unit was tested, and performance data were collected. The blower is further optimized for performance improvements. The low-cost and efficient blower will help DOE meet its cost target goals for small SOFC systems.

Innovative Concepts

Low Degradation, High Performance of LSCF-Based SOFCs Successfully Demonstrated. GE Global Research has made significant progress in mitigating performance degradation of lanthanum strontium cobalt ferrite (LSCF)-based SOFCs. A high-performance LSCF-based cathode architecture and processing route was demonstrated to have no measurable performance degradation over 1,000 hours at 800°C measured at 0.7 V using a gold cathode current collector. Subsequent test results using 441HP ferritic stainless steel current collectors with protective spinel coatings, operating at ~1 W/cm^2, yielded a 1.9%/1,000 hr power density degradation rate that decreased with time and approached an asymptotic value over the 1,500-hour test. The observed resistance increase was purely ohmic, with no loss in catalytic activity. Further, the resistance change could be directly attributed to the resistance associated with the anticipated growth of chromium oxide on the stainless steel current collector.

NexTech Demonstrates Advanced Electrolyte-Supported Planar SOFCs. NexTech Materials is validating an advanced planar SOFC design for megawatt-scale power generation systems. This design, termed the *FlexCell*, offers intrinsic scalability to large areas, as well as other important attributes that translate to high performance and efficiency. The overall goal of the project is to demonstrate these promising attributes with electrolyte-supported *FlexCells* made with YSZ. In Phase I, NexTech demonstrated that high performance can be achieved with YSZ-based *FlexCells* and scaled the fabrication of YSZ-based *FlexCells* to 500-cm^2 areas. A manufacturing cost analysis confirmed that full-scale (250 MW) production costs of *FlexCells* will be less than $50/kW, and NexTech identified paths to reduce costs to less than $40/kW. In collaboration with The Ohio State University, a finite element analysis model of mechanical robustness was established, which has been applied to the design of large-area (500-cm^2 area) *FlexCells* for fabrication and testing in Phase II of the project.

Advanced Research

Direct Reduction of Tin Oxide with Coal Successfully Investigated. In support of the liquid tin anode fuel cell (LTAFC) research at the National Energy Technology Laboratory, a series of direct reduction tests with coal was conducted on samples of pure tin oxide. These tests successfully determined reduction efficiencies at the fuel cell operating temperature, and the fate of contaminants supplied by the coal ash component. Results have demonstrated that reduction efficiencies of approximately 90% or greater can be achieved for both eastern and western coals at 1,000°C, while virtually all critical contaminants report to the slag component at a mass distribution of 90% or higher. This trend is independent of the coal used and suggests that effective slag cleaning of these contaminants is possible. Future work will investigate direct reduction with coal of a dilute tin oxide component within a molten tin bath, to better simulate the LTAFC environment.

Oxygen Transport Measurements Improved in Molten Metal Anodes. National Energy Technology Laboratory researchers have completed spatial thermal probing and observed isothermal conditions within the liquid tin anode of an SOFC. Equipment was designed and constructed to facilitate independent positioning of sensors to allow direct measurement of spatial gradients in temperature and potential within the liquid tin. With these upgrades, the researchers have been able to confirm that thermally induced convection is not affecting oxygen diffusion measurements. The recent upgrades have also facilitated measurement of oxygen diffusion within the molten tin, showing values that approach those reported in the literature. Researchers have used the new equipment to probe the spatial variations in potential within the tin while investigating the recent observation of enhanced effective oxygen diffusion in the presence of hydrogen fuel. Researchers speculate that the improvement in the effective oxygen diffusion rate is attributable to modest hydrogen transport into the tin, which could extend the tin/fuel reaction layer into the tin bulk and consequently enhance the cell performance. Through better understanding of oxygen transport within the liquid tin anode, improvements to direct carbon conversion efficiencies of SOFCs may be possible.

Navy Evaluates SECA Fuel Cells for Undersea Vehicle Application. The Naval Undersea Warfare Center, Division Newport (NUWCDIVNPT) is collaborating with DOE to examine the effect of pure oxygen on SOFC stacks and to provide proof-of-concept system demonstrations. NUWCDIVNPT's role is to provide independent testing and evaluation of SOFC stacks being developed under the DOE's SECA program.

System demonstrations have consisted of an SOFC stack integrated with fuel processor, high-temperature anode recycle blower, and carbon dioxide sorbent. This system has attained an overall fuel utilization over 75%, oxygen utilization over 95%, and fuel efficiency over 50% lower heating value. These pure oxygen studies have shown up to 10% efficiency gains by using pure oxygen instead of air, and SOFCs show promise for use in undersea vehicles and other spin-off applications.

SECA Adds SBIR Projects

Several new Phase I projects were selected in 2010 under an SBIR solicitation. TDA Research will assess a post-SOFC residual fuel oxidizer for carbon capture, NexTech Materials will perform a comprehensive manufacturing cost analysis of volume manufacturing of SOFC stacks, and CellTech Power will assess the direct utilization of coal in a liquid tin anode SOFC.

2010 Annual SECA Workshop in Pittsburgh, Pennsylvania

The SECA program held its 11th annual workshop July 27–29, 2010, in Pittsburgh, Pennsylvania. Principal investigators of projects made up-to-date presentations. The findings and recommendations will be used by DOE to guide future work and by to make programmatic and funding decisions for the upcoming fiscal years. The workshop proceedings can be found on the program's website at http://www.netl.doe.gov/seca/.

Summary

SECA will meet its final cost goal of $175/kW stacks by the end of 2010. Ongoing cell performance and scaling improvements will undoubtedly result in additional cost reduction and the testing of larger SOFC stacks. Technological spinoffs of SOFCs into a variety of other applications, especially APUs for heavy-duty trucks, related military power applications for the Department of Defense, and potential manned space craft applications for the National Aeronautics and Space Administration will add to market penetration, increase manufacturing production volume, and lower SOFC cost.

By developing fuel cells to operate cost effectively on coal gas as well as natural gas, bio-fuels, diesel, and hydrogen, SECA is solving today's environmental, climate change, fuel availability, and energy security issues. SECA fuel cells are ideal for use in central generation applications, enabling high efficiency, diverse opportunities for carbon capture (e.g., post-power block), lower criteria pollutant emissions (e.g., less than 0.5 ppm NOx, regardless of fuel), and water conservation. IGFC system configurations utilizing near-term gasification and syngas cleaning technologies will generate power from coal with overall efficiencies of 50 percent (HHV, coal to AC power), including the coal gasification and carbon capture processes. Advanced systems are capable of efficiencies of 60 percent. In conjunction with SECA-driven fuel cell cost reduction, these IGFC systems will enable the clean, efficient and cost-effective use of the nation's most abundant fossil fuel. The once distant vision of using clean, low-cost fuel cell technology for everyday applications is now within reach.

II. SECA INDUSTRY TEAMS

A. Coal-Based Systems

II.A.1 SECA Coal-Based Systems – FuelCell Energy

Hossein Ghezel-Ayagh
FuelCell Energy, Inc.
3 Great Pasture Road
Danbury, CT 06813
Phone: (203) 825-6048; Fax: (203) 825-6273
E-mail: hghezel@fce.com

DOE Project Manager: Travis Shultz
Phone: (304) 285-1370
E-mail: Travis.Shultz @netl.doe.gov

Subcontractors:
- Versa Power Systems, Inc., Littleton, CO
- WorleyParsons Group, Inc., Reading, PA

Contract Number: 41837

Start Date: February 27, 2004
End Date: September 30, 2010

FY 2010 Objectives

- Improve anode supported solid oxide fuel cell (SOFC) cell components to enhance cell performance, lower performance degradation rate, and decrease cost.
- Incorporate the cell component improvements in fabrication of scaled-up cells and stacks.
- Design, build and test a >25 kW SOFC stack tower to validate the concept for incorporation in >250 kW scale modules.
- Demonstrate cell/stack size, design and material improvements to reduce cost of the SOFC stack to $100/kW (2002 U.S. dollars [USD]).
- Develop a >250 kW-class stack module design concept suitable for incorporation in Module Demonstration Unit (MDU) and central coal power plants.
- Develop the conceptual design of a MDU system for validation (in Phase III of the project) of the SOFC module performance and endurance.
- Develop a >100 MW baseline integrated gasification fuel cell (IGFC) system with electrical efficiency >50% (coal higher heating value [HHV]) and capability for >90% of carbon capture (as CO_2) from coal syngas.
- Finalize fuel cell test article design for validation test to determine fuel cell power block system factory cost, fuel cell stack cost, and fuel cell power density.
- Initiate 5,000 h metric test of a >25 kW scaled-up stack tower to demonstrate that a steady-state degradation of <2%/1,000 h is achievable.
- Verify the baseline system power block factory cost of <$400/kW (2000 USD) and a power density of >300 mW/cm^2 based on metric test of a >25 kW scaled-up stack tower.

Accomplishments

- Improvements in cell materials have reduced performance degradation rate at 750°C to <0.3%/1,000 h (at 500 mA/cm^2, over ~7,500 h period), in an 81 cm^2 active area cell. The cell performance degradation rate at 800°C has also been reduced to 0.46%/1,000 h (at 500 mA/cm^2), in a 5,000 h test of an 81 cm^2 cell.
- Thin anode substrate cells with increased mechanical strength have been developed for cost reduction. These cells scaled up to 550 cm^2 active area (25 cm x 25 cm cell size) and implemented in 16-cell stacks have shown a performance improvement of up to 8% at high fuel utilization conditions compared to baseline cells (Phase I). This accomplishment will result in more than 25% cell material cost reduction.
- Performance improvements have been recognized in the advanced cell technology based on improved cathodes and thin anodes. The improvements encompass a wide range of temperature from 650°C to 800°C, with an impressive 18% gain in voltage observed at the low temperature of 650°C (and 740 mA/cm^2) in an 81 cm^2 active area cell.
- Manufacturing of scaled up (25 cm x 25 cm) cells based on the new generation of high-performance thin cell technology was initiated. The cell manufacturing process is based on the third generation tape-casting, screen-printing and co-firing (TSC-3) process optimized to take advantage of the new cell materials and thin cell technology. Over 600 thin cells have been fabricated.
- Cell area scale up to 1,000 cm^2 active area (33 cm x 33 cm cell size) has been advanced with fabrication and testing of a 10-cell stack. The stack achieved an average cell voltage of 800 mV at 388 mA/cm^2 and 80% fuel utilization.
- The baseline stack building block has been scaled up from 64-cell (Phase I level) to 92-cell size utilizing the 550 cm^2 active area cells. Four 92-cell blocks have been built based on Phase II earlier cell technology to validate the stack design. In the tests at the controlled environment, the stack achieved peak power of 19.87 kW and a power density of 0.393 W/cm^2.
- More than 46 stacks (229 kW direct current [DC] total) with cell count ranging from 16 to 92 were fabricated and tested.

- Cost analysis of a recently fabricated 92-cell SOFC stack block, based on the Fiscal Year 2009 metric test performance, showed an estimated stack cost of $153/kW DC (2002 USD). Progress made in stack scale up as well as improvements in the stack design related to internal reforming were the key reasons for the significant reduction in cost from Phase I estimates. Further cost reduction is anticipated from the thin TSC-3 cell technology.
- Stack tower concept suitable for large-scale SOFC modules was successfully demonstrated. Recently, a stack tower using two 92-cell blocks was built, representing early Phase II stack technology. The stack tower test achieved a DC power output of 30.2 kW.
- A 250 kW module design has been developed based on an array of eight stack towers each containing two stack blocks.
- A Baseline Power Plant (>400 MW) system utilizing catalytic gasification was developed. After comprehensive optimization studies, a system electrical efficiency of 58.7% (high heating value of coal) was achieved surpassing the U.S. Department of Energy (DOE) target. This achievement is significant as the system also captures >99% of carbon (as CO_2) in the syngas. The system consumes 75% less water compared to pulverized coal combustion plants utilizing scrubbing technology for carbon capture.
- The Baseline Power Plant system developed is projected to have an interim factory cost of ~414 $/kWac (2002 USD) for the SOFC power island. The layout of the system was developed resulting in a footprint comparable to an integrated gasification combined cycle (IGCC) power plant.
- A system configuration for the 250 kW SOFC MDU was developed. The system offers an electrical efficiency of 61% (based on lower heating value [LHV] of natural gas).

Introduction

FuelCell Energy, Inc. (FCE) is in Phase II of a multi-phase project to develop SOFC modules and power blocks for application in coal-based IGFC power plants. The primary objective of the project is to develop affordable and highly efficient multi-MW SOFC systems that have near-zero emissions of SO_x and NO_x, low water consumption, and amenability to greenhouse gas (carbon dioxide) capture.

FCE utilizes the SOFC technology of its partner, Versa Power Systems (VPS), in the development of IGFC power plants. VPS has well-established processes, quality control procedures, and equipment for the manufacturing of fuel cells. Key research and development activities for the project include: cell and stack size scale up, SOFC performance optimization, increasing stack manufacturing capacity, and MW-class system conceptual design.

Approach

Fuel cell development work has been focused on key cell issues related to cost reduction, endurance improvement and performance enhancement. The main technical approach includes extension of the operating temperature window, reduction of average operating temperature, thermo-mechanical strength improvement, and scaled-up cell stack fabrication process development. The emphasis is placed on the development of a thin anode substrate with increased thermo-mechanical strength. Material solutions with enhanced electrochemical properties are being evaluated. Laboratory process and equipment retooling have been utilized to support the cell scale up process development to 33 cm x 33 cm size. Various cell component design considerations, such as anode substrate thickness and porosity, have been evaluated to identify the optimum cell configuration for operation at high power density on coal syngas. Parameters such as performance (power, thermal management, and efficiency), design simplicity, technical risk, manufacturability, and cost have been considered in the design selection process.

The Baseline Power Plant conceptual design focuses on evaluation of process alternatives that will increase power plant efficiency, meet carbon capture requirements, and minimize cost of the power plant's power island. Various process configuration analyses and parametric studies were conducted considering voltage, current density, fuel utilization, stream recycle levels, and process components. Concurrent with the Baseline Power Plant design work, conceptual design of a >250 kW MDU is continued with process configuration evaluations and operating parameter studies.

Results

The on-going endurance tests of the improved cathodes and modified anodes in single cells (81 cm^2 active area) continue to demonstrate very low performance degradation rates at 750°C. A cell test has accumulated over ~7,500 h with an average performance degradation rate of less than 0.3%/1,000 h (at 500 mA/cm^2), as shown in Figure 1. To expand the operating temperature window (for stack implementation of the cell technology), the performance degradation rate at temperatures other than 750°C is also being reduced. Significant progress has been made at 800°C, based on better understanding of the degradation mechanism and material improvements.

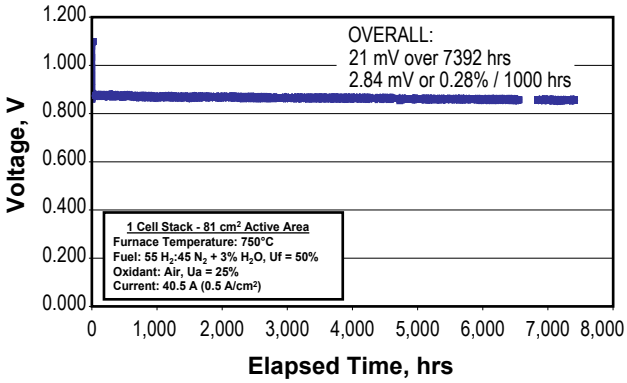

FIGURE 1. Endurance Test of a Modified Anode Cell (81 cm^2 active area) at 750°C and 500 mA/cm^2

The cell performance degradation rate has been reduced to 0.46%/1,000 h (at 500 mA/cm^2), as demonstrated in a 5,000 h test. Efforts to reduce the degradation rates at 650°C and 700°C continue.

A major advancement in the SOFC technology area was the development of thin anode substrate cells for cost reduction. Improving intrinsic anode substrate strength is a key strategy for implementing thin cells in a stack. Anode substrates showing more than 50% improvement in biaxial strength compared to the standard anode substrates were developed. Scaled-up thin cells with anode substrate thickness of 0.57 mm and 25 cm x 25 cm cell size (550 cm^2 active area) were produced using the tape-casting, screen-printing and co-firing (TSC) process. The cells were tested in a 16-cell stack. Additional cell material improvements related to cathodes and modified anodes, for enhanced cell performance and reduced performance degradation rate, were also implemented in a third generation of the SOFC technology (TSC-3). These TSC-3 cells are being evaluated, with standard 1 mm thick anode substrate and 0.57 mm thick anode substrate. Table 1 shows the performance observed (at 388 mA/cm^2) for a range of fuel utilizations in these stack tests. A performance improvement of ~8%, with ~2% points

TABLE 1. Performance Comparison of 16-Cell Stacks (550 cm^2 cell area) Containing Baseline 1 mm Anode Substrate TSC-2 Cells and Thin TSC-3 Cells

Fuel Utilization (%)	16 cell stack, 550 cm^2 TSC2 cells Stack 057235-0037	16 cell stack, 550 cm^2 thin TSC3 cells Stack 057235-0044	Performance Enhancement
50	0.823	0.886	7.7%
60	0.817	0.879	7.6%
70	0.804	0.866	7.7%
80	0.785	0.847	7.9%

FIGURE 2. 92-Cell SOFC Stack Block

from anode substrate thickness reduction, has been observed compared to the standard thickness TSC-2 cells (baseline). Endurance testing is in progress. A cell material cost reduction of 25% is anticipated from the anode substrate thickness reduction.

Effort in cell manufacturing process development has been focused on 25 cm x 25 cm thin cells. Over 600 thin cells have been fabricated. The overall process yield has been improved as the advanced thin cell technology is moved from the research and development stage to the pilot manufacturing stage.

The stack building block has been scaled up from a 64 to 92-cell count (550 cm^2 cell active area) as shown in Figure 2. Three 92-cell stacks were built (using cells representing earlier cell technology) and performance tested to validate the stack design and provide two 92-cell stack blocks needed to assemble a stack tower. Table 2 presents a summary of the 92-cell stack performance achieved. Performance of all three stacks was quite comparable. The DC output of the 92-cell block is ~18 kW. In the tests, the stack block achieved a peak power of 19.87 kW and a power density of 0.393 W/cm^2.

Development of 1,000 cm^2 active area cells was advanced to the short stack level. A 10-cell stack was

TABLE 2. 92-Cell Stack Block (550 cm^2 cell area) Performance

		GT57607-001 NOC (248-272h)	GT57607-001 Peak (555-579h)	GT57607-002 NOC(12-36h)	GT57607-003 NOC(4-28h)
Inputs	Fuel Utilization	68.3%	65.3%	68.4%	68.1%
	In-Stack Reforming	70.0%	60.0%	70.1%	70.0%
	Air Utilization		13.8%	14.1%	14.0%
	Stack Current (Current Density)	250.9 A (456 mA/cm²)	281.2 A (511 mA/cm²)	251.2 A (457 mA/cm²)	250.4 A (455 mA/cm²)
	Stack Furnace Temperature	704 C	700 C	705 C	715 C
Outputs	Stack Block Voltage (Average Cell Voltage)	71.823 V (0.781 V)	70.744 V (0.769 V)	72.044 V (0.783 V)	73.939 V (0.804 V)
	Stack Block Power (Power Density)	17,992 W (0.356 W/cm²)	19,868 W (0.393 W/cm²)	18,099 W (0.358 W/cm²)	18,517 W (0.366 W/cm²)
	Cathode Out Temperature	779 C	780 C	779 C	789 C

built and tested at Phase II normal operating conditions. The stack performed successfully during the fuel utilization (50 to 80% utilization) test, with an average cell voltage of 800 mV at 388 mA/cm^2 and 80% fuel utilization. The large area stacks significantly increase cell power output, as the cell voltage level is maintained during the scale up. As shown in Figure 3, a DC power output of 4 kW was observed at 500 mA/cm^2 for the 10-cell stack, during the peak power test.

A stack tower concept suitable for large-scale SOFC modules was successfully demonstrated. Stack towers were assembled consisting of multiple stack building blocks, utilizing the 550 cm^2 active area cells. A recent tower test was conducted on a stack tower built using two 92-cell blocks representing early Phase II stack technology. Figure 4 shows a picture of the completed stack tower. The stack tower test accumulated over 1,000 h, achieving a DC power output of 30.2 kW at 210 A (382 mA/cm^2).

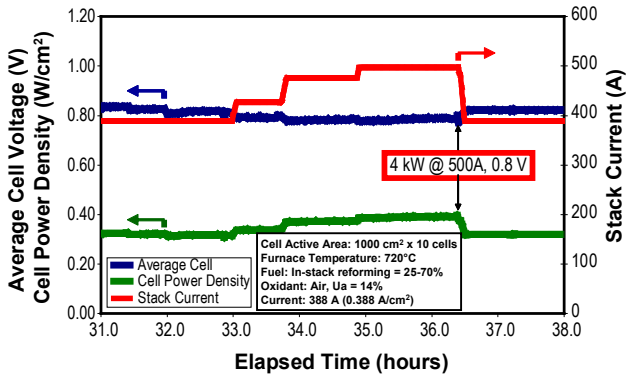

FIGURE 3. 1,000 cm^2 Cell Area 10-Cell Stack Peak Power Test Results

The SOFC module concept development was focused on the design of a >250 kW module based on a stack tower array of eight towers each containing two 96-cell stack blocks. The towers are arranged in two quads of 4 towers, with each quad assembled on a single fixed-end base. The quad base design, providing the support structure and facilitating the gas flow distribution to towers, is in progress. The SOFC module enclosure design, as shown in Figure 5, features removable panels to allow access. Instrumentation and electrical boxes on the two sides provide the penetrations to the enclosure, for routing instrumentation and attaching electrical bus components. The overall size is within standard

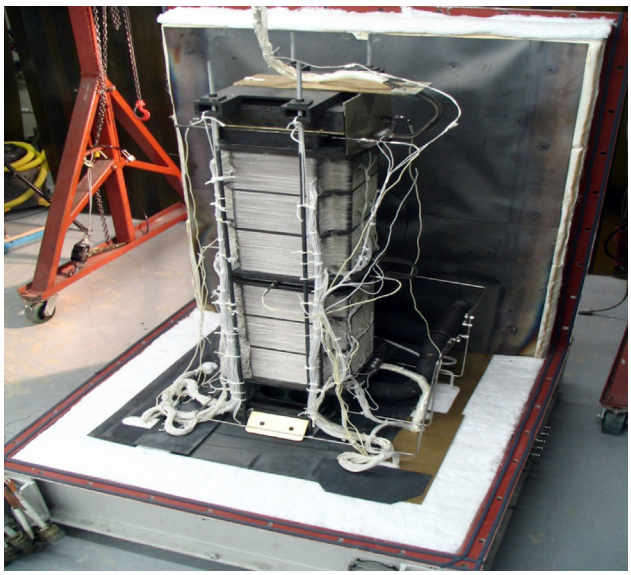

FIGURE 4. Stack Tower Assembled Using Phase II Stack Blocks (Two 92-cell Blocks, 550 cm^2 Active Area Cells)

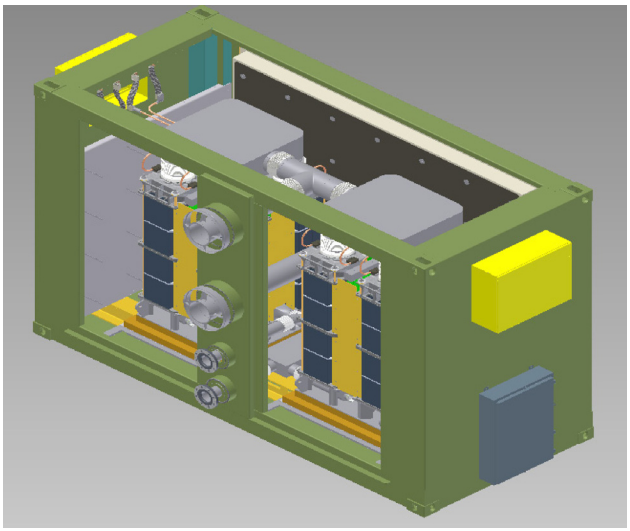

FIGURE 5. 250 kW SOFC Module with Front and Top Panels Removed

shipping limits to keep transportation and handling costs down.

Advanced Baseline System configuration development and analysis resulted in a highly efficient coal-based power plant. The system employs catalytic gasification and warm gas clean-up to provide coal syngas fuel for the SOFC. The system also employs oxy-combustion of the anode exhaust for CO_2 capture using a portion of the oxygen from the air separation unit at the gasification site. A comprehensive system optimization effort, including modification of subsystem operating conditions and updating of equipment performance parameters/assumptions, was carried out. The improvements resulted in a system electrical efficiency of 58.7% based on the HHV of coal, while capturing >99% of carbon (in the syngas) as CO_2. Water balances were generated to analyze the Baseline Power Plant system water usage. The SOFC system consumes 75% less water compared to pulverized coal combustion plants (using scrubbing technology for carbon capture). The IGFC systems have significantly less water consumption because of their higher system efficiency. A conceptual layout of the Baseline Power Plant (general arrangement of the power island) was developed. The footprint of the IGFC plant was found to be comparable to IGCC plant. Preliminary factory cost estimates have shown an SOFC power island cost of $414/kW in 2002 USD, approaching the DOE cost target for a coal-based system. The estimate includes the stack module, inverter, interconnect piping and other balance-of-plant (BOP) equipment.

A design basis document for 250 kW (nominal) SOFC MDU, was generated. This plant will have a ≥250kW SOFC module and the BOP supporting the fuel cell module. The MDU will serve as a system platform for the SOFC module test demonstration required in Phase III of the Solid State Energy Conversion Alliance (SECA) project. Several system configuration options were developed for the MDU and system simulations were carried out to guide the 250 kW MDU conceptual design. The configurations considered included anode recycle, cathode recycle, and fuel humidifier options. A configuration was down-selected based on the system performance comparison and a preliminary cost analysis. The system offers an electrical efficiency of >60% based on lower heating value of natural gas.

Conclusions and Future Directions

Advances in thin cell technology combined with progress in cell material have resulted in leap-frogging developments in both reduction of stack cost and increase in cell performance. A new generation of cells (TSC-3), combining the improved cathodes and modified anodes with thin cell technology, has been scaled up to 550 cm^2 active area. The scaled-up cells have shown outstanding voltaic efficiency and stability of operation. Stacks made from these cells have been operated successfully at fuel utilizations in excess of 80% and system representative gas compositions. The future cell development efforts are focused on expanding the operating temperature window to accommodate larger temperature gradients in a stack. Effort is directed to reducing the performance degradation rate at the low end of the temperature spectrum observed in the stack.

New grounds were also broken in stack scale-up technology. A stack building block based on the 550 cm^2 active area cells was scaled up successfully from a 64 to 92-cell count. Performance characterization tests at updated system representative conditions have demonstrated the 92-cell block DC power output of 18 kW with a power density of 0.356 W/cm^2. The large cell area in combination with increased stack cell count is aimed at the reduction of the overall stack cost. The stack tower concept for SOFC module application has been demonstrated successfully by assembling a tower using two 92-cell stack blocks and generating a DC power output of 30.2 kW. Implementation of thin TSC-3 cell technology in the stack block is in progress. A stack tower will be built from two 92-cell stack blocks containing thin TSC-3 technology cells to initiate the end-of-Phase II metric test. A >250 kW SOFC module concept has been developed based on an array of eight stack towers arranged in two quads. The quad base design, providing the support structure and facilitating the gas flow distribution to towers, is in progress.

An advanced Baseline Power Plant system (>400 MW) offering 58.7% electrical efficiency (coal HHV), while capturing >99% of carbon (in the syngas) as CO_2, has been developed. The system cost analysis has shown a path to the DOE cost target of 400 $/kW (2002 USD). System simulations and analyses to assess the suitability of biomass/coal blend gasifiers for

application to the SOFC-based systems are planned as a part of Phase III effort. A configuration for the >250 kW MDU system has been developed. The system offers an electrical efficiency of 61% (natural gas LHV), suitable for the distributed generation. The 250 kW power plant will be utilized as a platform for demonstration of the SECA developed technology. This system is suitable for large-scale coal-based power generation as well as the distributed generation applications using biomass and natural gas fuels.

FY 2010 Publications/Presentations

1. Hossein Ghezel-Ayagh, James Walzak, Stephen Jolly, Dilip Patel, and David Stauffer, "Design Optimization of Integrated Coal Gasification Solid Oxide Fuel Cell Systems," Proceedings of the ASME 2010 Eighth International Fuel Cell Science, Engineering and Technology Conference, FuelCell 2010-33191, June 14–16, 2010.

2. Hossein Ghezel-Ayagh, Rich Way, Peng Huang, Jim Walzak, Stephen Jolly, Dilip Patel, Mike Lukas, Carl Willman, Keith Davis, David Stauffer, Vladimir Vaysman, Brian Borglum, Eric Tang, Michael Pastula, and Randy Petri, "Integrated Coal Gasification and Solid Oxide Fuel Cell Systems for Centralized Power Generation," ECS Transactions - 2009 Fuel Cell Seminar & Exposition.

II.A.2 SECA Coal-Based Systems - Rolls-Royce

Richard Goettler (Primary Contact), Greg Rush, Ted Ohrn, Mark Scotto
Rolls-Royce Fuel Cell Systems (U.S.) Inc. (RRFCS)
6065 Strip Avenue NW
North Canton, OH 44720
Phone: (330) 491-4821; Fax: (330) 491-4808
E-mail: richard.goettler@rrfcs.com

DOE Project Manager: Patcharin Burke
Phone: (412) 386-7378
E-mail: Patcharin.Burke@netl.doe.gov

Subcontractors:
- Rolls-Royce Fuel Cell Systems Limited, Loughborough and Derby, United Kingdom
- Case Western Reserve University, Cleveland, OH
- University of Connecticut, Storrs, CT
- Matrix Innovations, Lynchburg, VA
- Oak Ridge National Laboratory, Oak Ridge, TN
- Pacific Northwest National Laboratory, Richland, WA

Contract Number: FE0000303

Start Date: September 1, 2009
End Date: June 30, 2011

FY 2010 Objectives

- Further reduce cell area specific resistance (ASR) to maximize system efficiency and lower average and peak stack operating temperatures.
- Demonstrate a next generation stack design which achieves high fuel utilization (~80%) to meet system efficiency targets.
- Mitigate degradation mechanisms to ensure meeting the Solid State Energy Conversion Alliance (SECA) program power degradation target of <2%/1,000 hours during stack metric tests.
- Perform electrochemical durability testing for the next generation cell technology over the range of system operating conditions to estimate the degradation rate expected for the stack metric test.
- Prepare an activity-based stack cost model.

Accomplishments

- A further increase of 36% in the power density has been demonstrated for the RRFCS integrated-planar (IP) solid oxide fuel cell (SOFC) through modification of the electrolyte and cathode material sets. The cumulative power density improvement has been 73% since the beginning of the project. Latest cell technology shifts peak stack operating temperature from 970°C to 920°C to minimize thermally activated degradation mechanisms.
- A key degradation mechanism associated with the electrical connection between individual cells has been mitigated through a design and materials change. Durability testing at average system operating conditions (860°C, 6.4 bar_a, 80% fuel utilization) exhibit degradation rate less than the SECA 2%/1,000-hour target.
- Investigated a moisture effect for lanthanum strontium manganite (LSM)-based cathodes causing power loss, accentuated at lower temperatures. Identified alternate cathodes showing less impact of moisture and steam exposure.
- Tested a next generation stack technology utilizing redesigned manifold components for improved fuel distribution and substrates with increased permeability characteristics. Combined these changes enable stacks operating at the 80% fuel utilization target. Stack average ASR at system operating conditions is 0.32 ohm-cm^2 achieving an average power density of 320 mW/cm^2.
- Submitted a preliminary stack cost model which will be updated upon obtaining actual peak power levels from the 15 kW metric stack test.

Introduction

The RRFCS SECA project is aimed at demonstrating the viability of the RRFCS IP-SOFC technology, which is being developed for the distributed energy market, for eventual scale up to a megawatt-scale system suitable for incorporation into centralized power generation facilities employing coal gasification and carbon sequestration. The integrated gasification fuel cell (IGFC) systems offer efficiencies of >50% (higher heating value), inclusive of CO_2 capture. The RRFCS stack concept is based on thin planar cells which are series-connected on a fuel-carrying porous ceramic support substrate [1]. These active substrates are the elemental building block of the fuel cell stack and are grouped together to form a megawatt-scale IP-SOFC system as shown in Figure 1. These cells are applied onto the substrates using well established thick film screen printing techniques. Contrary to other SOFC developers who seek ever larger single-cell active areas, RRFCS desires smaller cells to reduce current levels and achieve lower ohmic (I^2R) losses. RRFCS currently prints 60 cells of ~1.3 cm^2 on each side of the substrate. This represents a switch in design philosophy from a low voltage, high current fuel

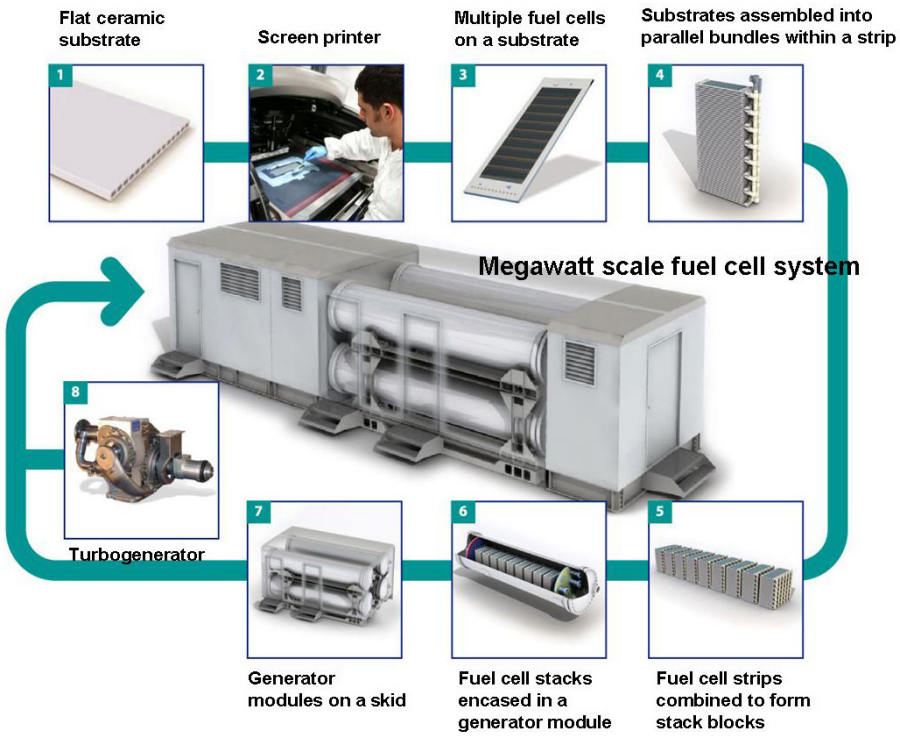

FIGURE 1. Schematic of the Planned RRFCS 1 MW Distributed Power Generation System

cell to a high voltage, low current approach. Substrates having the narrow 60-cell design (adopted pre-SECA) allow the use of lower conductivity and lower cost-basis materials to meet in-plane conductance requirements which has been an important materials substitution for achieving the DOE costs targets of <$700/kWe (in 2007$). Further progression in the performance (ASR) of the RRFCS technology has occurred over the past year and the focus of the project is now on validating the long-term durability under the system conditions selected for the RRFCS IP-SOFC power block module of the IGFC plant.

Approach

Achieving a successful 5,000-hour end-of-phase 15 kWe stack test requires thorough screening of the latest active cell layers at the full system operating conditions to verify the ability to meet the SECA program 2%/1,000-hour degradation target prior to commencement of the milestone stack test. Acquiring a system relevant electrochemical database for a pressurized SOFC system presents additional challenges over that faced by atmospheric system developers: mainly the higher cost associated with pressure containment. RRFCS has established an array of pressurized test stands ranging from subscale substrates for testing single and 5-cell articles, bundle rigs (~350 W) which tests the fundamental stack assembly unit, block rigs (~20 kW) and tier rigs (~125-250 kW).

RRFCS utilizes subscale atmospheric test stands for performance screening of alternate active cell layers and preliminary durability assessments prior to pressurized testing. Atmospheric test stands are employed to perform quality assurance testing of full-scale substrates exiting the printing line. Manufacturing of the fuel cell stacks are performed on the Process Verification Line (PVL), now located in Canton, Ohio, and includes a screen printing line representative of that required for a high volume factory. RRFCS has established supply chains for substrates, powders, inks and stack manifolding components. The PVL processes being utilized in Canton have been in practice within RRFCS since 2005, and are now being applied and optimized for the smaller pitch 60-cell substrate design and the new active layer material sets. The experience on the PVL along with the assembly operations have guided the inputs for the activity-based stack manufacturing cost model that has been developed for estimating high-volume manufacturing costs for the fuel cell module. Projected stack costs are in the $200/kW range for a cell technology providing an average system ASR of 0.32 ohm-cm^2. Final cost estimates will be based on the peak power output derived from the 15 kW metric stack test.

Not only must the fuel cell stack meet electrochemical performance and durability targets, it must demonstrate structural integrity to meet reliability/mean-time to failure necessary for commercial launch. Stack mechanical reliability is being investigated in collaboration with Oak Ridge National Laboratory

where detailed mechanical characterization of the substrate and fully processed and tested active substrates will be performed. A detailed understanding of the requirements for substrate diffusivity, based on modeling and validated with electrochemical testing, is being performed to achieve a substrate microstructure that provides sufficient transport of reactant and product gases, while maximizing structural properties. Studies of the interactions between the substrate material and the glass used to seal the inactive regions will be performed by Pacific Northwest National Laboratory, as reactivity and evolving thermal stress states could impact substrate strength. The University of Connecticut is performing assessments of the alloys selected by RRFCS for the balance of plant components, with particular emphasis on chromium release rates and alternate alloys and/or coatings for mitigating chromium volatility.

Results

RRFCS has achieved improvements in the performance of its cells, reported as a lower ASR. This is being driven by a desire to lower stack operating temperatures to minimize thermally activated degradation mechanisms. Progress on ASR reduction is summarized in Figure 2 for single cells operating at stack inlet fuel composition and stack representative flow rates. At the planned average system stack temperature of 860°C the ASR improvement upon transition from the pre-SECA 30-cell substrate technology to the 60-cell technology is 0.1 ohm-cm^2. Additional performance improvements totaling 0.1 ohm-cm^2 have been achieved through a switch of electrolyte composition and modification to the LSM-based cathode to reduce over-potential losses. These ASR improvements translate to an approximate 73% increase in power density over the course of the project.

Testing under the reduced stack operating temperatures has led to observations that ambient levels of air moisture cause performance degradation. This effect is shown in Figure 3 where a 3% moisture level that would be representative of that present in a high relative humidity region causes continual degradation over 1,000 hours operating at 800°C and 6.4 bar$_a$. The degradation trend is halted upon reduction of the steam level. A cathode moisture effect has recently been reported by other research groups [2,3]. The RRFCS studies have shown that the steam effect is most pronounced at lower temperatures, less than approximately 825°C. The cause of this steam effect is not fully understood, but impedance spectroscopy shows polarization changes and increases associated with diffusion processes. A modification to the LSM-based cathode shows a much reduced steam effect, as does testing of an alternate class of cathodes.

Aggressive testing at peak stack temperatures of 920°C and stack outlet fuel utilization conditions has been performed to identify the key degradation mechanisms which must be addressed to achieve the long-term degradation targets required for commercial

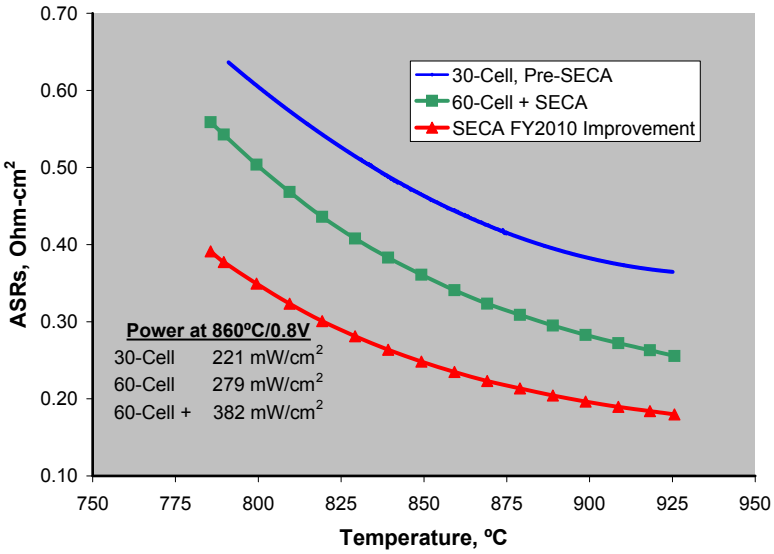

FIGURE 2. ASR Improvement and Power Density Improvement Compared at the Single Cell Level (1 bar$_a$ testing, system stack inlet fuel composition and flow rate)

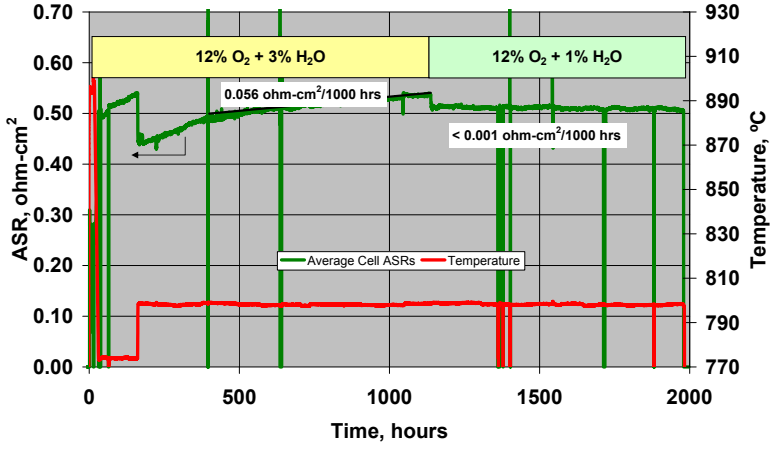

FIGURE 3. Moisture Effect Observed for LSM-Based Cathode (6.4 bar$_a$, 455 mA/cm^2, bundle mid-point fuel)

products. Post-test analysis results pointed to materials migration at the primary interconnect which connects adjacent cells on the substrate as the degradation mechanism showing an accelerating rate upon exceeding 1,000 hours of operation at these most severe stack conditions. Through modification of the interconnect design and materials changes, the degradation mechanism has been eliminated as confirmed by detailed post-test analysis. The active cell materials have been finalized for the Phase 1 metric stack test with pressurized durability testing exhibiting constant current power degradation rates less than 1%/1,000 hours. The durability challenge for the 40,000-hour life ultimately desired for commercial units is the microstructure stability of the anode-side material sets. Anode side durability has been observed to be significantly improved through use of the higher permeability substrates with testing over 1,600 hours at 925°C and 90% fuel utilization conditions showing stable performance and improved microstructure stability. Optimization of the anode is being pursued to further minimize coarsening and migration mechanisms.

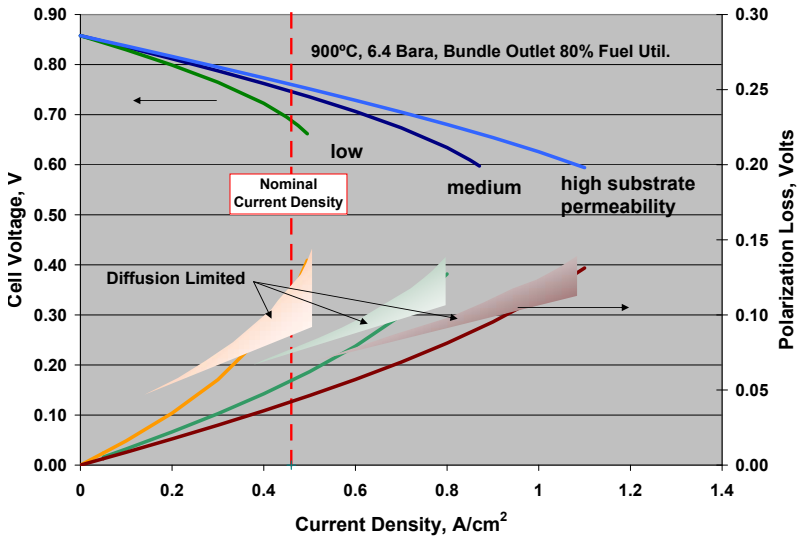

FIGURE 4. Modeling Results Showing Effect of Substrate Permeability on Cell Performance and Diffusion Resistance Contributions (900°C, 6.4 bar_a, bundle outlet 80% fuel utilization)

Additional systems analysis for the IGFC has been performed leading to a revised cycle for the SOFC module relying on cold gas clean-up (Selexol) rather than the initial cycle choice of warm gas cleanup (RTI International process). The main benefit is lower peak steam levels within the anode loop at target fuel utilizations which serves to minimize ASR increase associated with gas diffusive losses and anode degradation mechanisms.

Peak steam levels within the stack are also being managed through optimization of the substrate permeability and redesign of the manifold components to improve intra-bundle and bundle-to-bundle fuel flow distribution. A gaseous counter diffusion model has been utilized to extend the understanding of how key substrate characteristics such as porosity, tortuosity and mean pore radius, as determined through accurate permeability measurements, influence the electrochemical performance of the RRFCS active substrate [4]. Substrates exhibiting low to medium permeability characteristics show diffusional electrochemical resistance at the range of current densities (~380-500 mA/cm^2) present within the block (Figure 4) as determined through electrochemical models that have been validated with experimental data. Such analysis has guided refinement of the functional specification for the substrates being supplied to RRFCS. A new design of inlet and outlet manifolds of the parallel bundles comprising the strip and the stack component which connects substrate-to-substrate within a bundle has been completed. The redesigned manifolds provide improved balancing of flow between all the bundles within a strip. These stack component design changes along with optimized substrate permeability characteristics will allow achievement of 80% fuel utilization without undesirable levels of diffusive losses caused by fuel starved regions within bundles. Computational fluid dynamics analysis shows that these design changes can minimize fuel flow mal-distribution to <5% for the critical last substrate within the bundle where peak stack fuel utilization conditions exist.

Bundles incorporating the design changes to the substrate, manifolds, and the latest lower ASR cell technology have been manufactured and assembled in Canton. These bundles are under long-term testing at system relevant conditions and are exhibiting the predicted performance. At average stack conditions the bundle is exhibiting an ASR value of 0.32 ohm-cm^2 while operating at an 80% fuel utilization condition. This corresponds to a stack direct current electrical efficiency of ~64%.

Conclusions and Future Directions

In Fiscal Year 2010 RRFCS has made significant progress in the ASR reduction of its IP-SOFC technology. Concurrent with the cell advances has been a redesign of stack components including the substrate permeability characteristics and the fuel manifolds utilized in the all-ceramic stack design to achieve improved flow uniformity, thus allowing operation of the fuel cell stacks at high fuel utilization while avoiding

diffusional resistance losses. This latest cell and stack technology is now being produced on the manufacturing line in Canton, Ohio, and validated at full scale through single substrate qualification testing and bundle level pressurized testing providing the confidence to move forward into block level testing. A strip (~3.5 kW) incorporating the latest cell and stack technology will be tested during the initial commissioning run of the pressurized test stand that has been assembled in Canton, Ohio (funded by RRFCS capital and Ohio's Third Frontier) for performing the ~15 kW Phase 1 stack metric. Further analysis and modeling of the IGFC system will be performed using the latest stack performance levels, DOE's base concepts on IGFC system integration and reasonable assumptions for operating conditions of the fuel cell stack to refine estimates of the efficiencies possible for an IGFC plant incorporating the RRFCS pressurized SOFC module.

FY 2010 Publications/Presentations

1. Presentation at 2010 SECA Workshop, Pittsburgh, Pennsylvania, July 27–29, 2010.

References

1. U.S. Patent 7,422,820.

2. A. Hagen et al., "Effect of Humidity in Air on Performance and Long-Term Durability of SOFCS," ECS Transactions, 25(2) 439-446 (2009).

3. J. Nielsen et al., "Effect of Cathode Gas Humidification on Performance and Durability of Solid Oxide Fuel Cells," Solid State Ionics, 181 517-24 (2010).

4. J.B. Young and B. Todd, "Modeling of Multi-Component Gas Flows in Capillaries and Porous Solids," International Journal of Heat and Mass Transfer, 48 5338-5353 (2005).

II.A.3 SECA Coal-Based Systems - UTC Power

David D. Brengel (Primary Contact),
Gary Blake (Delphi), Larry Chick (Delphi),
John A. Ferro (Project Director),
Karl Haltiner (Delphi), Toby Junker (UTRC),
Subhasish Mukerjee (Delphi), Ellen Sun (UTRC)
UTC Power
195 Governors Highway
South Windsor, CT 06074
Phone: (860) 727-2478; Fax: (860) 353-4135
E-mail: david.brengel@utcpower.com

DOE Project Manager: Briggs White
Phone: (304) 285-5437
E-mail: Briggs.White@netl.doe.gov

Subcontractors:
- Delphi, West Henrietta, NY
- United Technologies Research Center (UTRC), East Hartford, CT
- Battelle/Pacific Northwest National Laboratory, Richland, WA

Contract Number: NT0003894

Start Date: October 1, 2008
End Date: September 30, 2010

FY 2010 Objectives

- Develop accelerated testing methodology for cell aging.
- Complete evaluation of combining high temperature firing operations (anode, electrolyte and interlayer).
- Complete evaluation of material sets for long-term stability.
- Complete cell cost reduction analysis.
- Demonstrate a 5 kW stack.
- Complete the design model for a 25 kW stack module.
- Deliver stacks for the 25 kW stack module to UTC Power.
- Complete the stack cost analysis.
- Complete installation of the stack build stand.
- Complete the detailed design of a test stand capable of testing a stack up to 50 kW.
- Procure, build and commission a test stand capable of testing a stack up to 50 kW.
- Develop a test plan for the 25 kW stack test consistent with the Solid State Energy Conversion Alliance (SECA) minimum requirements.
- Complete a detailed system analysis of a 250-1000 kW solid oxide fuel cell (SOFC) power module operating on either pre-reformed natural gas or coal syngas with respect to performance and operability.
- Complete the conceptual design of a 5 MW proof-of-concept system.
- Complete the system cost analysis for the baseline integrated gasification fuel cell (IGFC) system.

Accomplishments

- Expanded cell and stack fabrication, and test capability for Gen 4 stacks.
- Fabricated and tested multiple Gen 4 short stacks.
- Completed the design of a 25 kW test article for the SECA peak power and steady-state tests.
- Demonstrated a Gen 4 stack module producing 5.06 kW (503 mW/cm^2) at 0.81 V/cell using 48.5% H_2, 48.5% N_2, 3% H_2O fuel.
- Developed a low cost, high volume manufacturable process for Gen 4 stack components.
- Demonstrated greater than 7,500 hours durability using Gen 3.2 stacks.
- Demonstrated 200 thermal cycles using Gen 3.2 stacks.
- Completed interim stack cost analysis studies.
- Completed the detailed design, including a failure modes and effects analysis and hazard analysis, of a test stand capable of testing a stack up to 50 kW.
- Procured all major components, including the fully completed fluid skid, and initated the final assembly of a test stand capable of testing a stack up to 50 kW.
- Developed a test plan for the 25 kW stack test consistent with the SECA minimum requirements and the baseline IGFC system.
- Completed an initial down-select of the 250-1000 kW SOFC power module operating on pre-reformed natural gas based on performance, durability, operability and cost.
- Initiated the system cost analysis for the baseline IGFC system.
- Developed the conceptual design of an atmospheric IGFC system with an SOFC/gas tubine/steam turbine (GT/ST) cycle achieving an efficiency of 57 percent (higher heating value [HHV]).

Introduction

UTC Power is a world leader in developing and producing fuel cells that generate energy for buildings and for transportation, space and defense applications. UTC Power has recently developed and begun shipments of its newest generation fuel cell system for the commercial combined heat and power market. Delphi has been developing SOFC systems since 1999. After demonstrating its first generation SOFC power system in 2001, Delphi teamed with Battelle under the SECA program to improve the basic cell and stack technology, while Delphi developed the system integration, system packaging and assembly.

In addition to its high power density, another key advantage of the SOFC is its high system efficiency, particularly when its high temperature co-product heat can be used in combination with its electrical output. For example, the addition of a bottoming cycle with a steam turbine-generator can increase the overall efficiency to greater than 50 percent, significantly higher than the 35-40 percent efficiency for a typical coal-fired power plant.

UTC Power is developing conceptual process designs of a wide range of power systems ranging from 250 kW up to 100+ MW with a focus on meeting the system efficiency and carbon separation targets specified in the SECA minimum requirements. Designs for a sub-MW system for distributed power generation and a 5 MW proof-of-concept system will be developed, as well as a conceptual design and costing for a baseload power plant that separates greater than 90 percent of the carbon from the coal feedstock at an efficiency of 50 percent (HHV). In support of the design of a 250-1,000 kW SOFC power module, UTC Power will develop and build a test stand capable of testing a stack up to 50 kW, and will subsequently test a ≥25 kW Delphi stack for at least 1,500 hours in Phase I on a simulated coal syngas.

UTRC has developed stack materials and processes in support of the stack development effort led by Delphi. UTRC is focused on the key technical challenges for stack scale up and durability, including the evaluation of coated alloys, the development and evaluation of advanced seal concepts and materials, and the development of coating materials and processes for multiple stack components.

Approach

Delphi utilized a staged approach to develop a modular SOFC system for a range of fuels and applications. Major subsystems and individual components were developed and tested as building blocks for applications in targeted markets. These were then integrated into a "close-coupled" architecture for integrated bench testing, as well as a stationary power unit and an auxiliary power unit (APU) for the stationary and transportation markets, respectively.

UTC Power is using first principles-based models developed from performance data to prepare mass and energy balances and to predict the performance of the concept designs. Results from the mass and energy balances are used for trade studies, component sizing and costing. To design highly efficient SOFC/GT hybrid systems, UTC Power is working closely with Pratt & Whitney to establish turbine performance models. Using these models, both atmospheric and pressurized SOFC designs are being developed. Final designs are selected to meet the desired cost and performance targets.

UTC Power is using a well-defined work process with multiple, gated reviews to develop the 50 kW test stand from the conceptual design phase through the readiness phase, with an emphasis on reliability and simplicity. Key challenges include ensuring chromia is properly mitigated and unintended shutdowns are minimized during the duration of the stack test.

UTRC is conducting long-term oxidation, rapid thermal cycling, and area specific resistance measurements for coated alloy evaluation, utilizing advanced material characterization techniques including high resolution transmission electron microscopy and focused ion bean. Seal performance is evaluated via thermal cycling tests. Coating processes are being developed with an emphasis on both performance and cost, optimized at the coupon level and scaled up for stack components.

Results

The SECA Coal-Based Systems (CBS) project is a continuation of the core hardware development activities begun in the SECA Cost Reduction project. The efforts in the SECA CBS are more application-driven as Delphi and UTC Power move this technology closer to pilot and production releases. The SECA CBS project will support and address the development of fuel cells for central generation applications. This market has unique demands, and development tasks must address specific issues that are economic drivers of the design and application.

Stack design efforts have focused on optimizing the current design and adding features such as a cassette containing thermocouples in the center of the stack to get better temperature feedback. Development also focused on investigating different concepts for scaling up the active area footprint. Work on stack models has focused on developing algorithms that describe the current-voltage (I-V) response of an SOFC cell at a particular temperature and fuel composition. Such

algorithms are essential to detailed stack models, such as the MARC-SECA code, which are used to predict the temperature, current, gas composition and, indirectly, the mechanical stress distributions within a large-scale, multi-cell stack. The algorithm is used by the model to predict the I-V response of each localized node within the mesh based on the local temperature and local anode gas composition. The cathode gas composition could also have a significant effect on the I-V response if the cathode air is allowed to become appreciably depleted in oxygen.

Delphi continues to make progress with improved cell fabrication techniques by focusing on material and process improvements. Battelle Pacific Northwest Division and Delphi continue to partner in the area of cathode powder and paste development to develop cell material sets that lead to improved electrochemical performance while being robust to potential failures such as cathode layer delamination. Delphi continues to work closely with commercial suppliers of production materials to develop a consistent supply of production grade material and optimize the material properties to provide robust performance in the solid oxide fuel cell stack and ultimately the fuel cell system. Figure 1 compares the performance of a 25-cell Gen 4 stack to a 40-cell Gen 3.2 stack on 48.5% H_2, 3% H_2O, rest N_2 fuel. The Gen 4 stack produced 5.06 kW (503 mW/cm²) at 0.81 V/cell with I-V performance comparable to the Gen 3 stack.

The principles of the Delphi Manufacturing System Design are being applied to develop control and quality standards for each step of the manufacturing process. By focusing efforts in these areas early in the development process, Delphi has been able to scale up the fabrication process to mass quantities while maintaining the highest quality standards.

UTC Power has developed a library of models for simple-cycle SOFC power plants and used them to model a previously designed power plant concept (Figure 2). The power plant desulfurizes natural gas

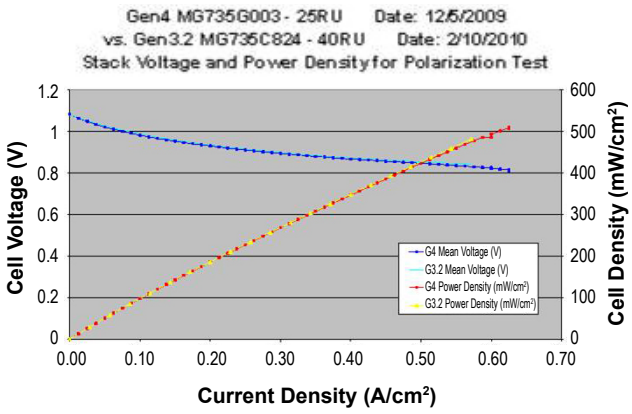

FIGURE 1. A Comparison of Gen 3.2 and Gen 4 Stack Performances (I-V Curves)

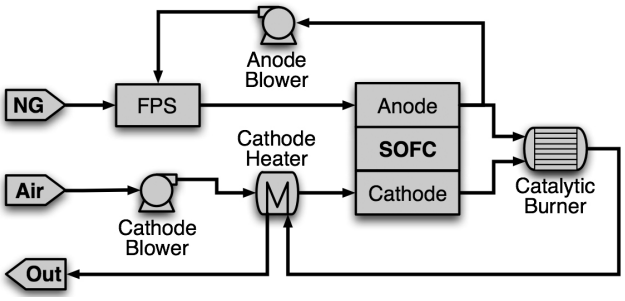

FIGURE 2. Process flow diagram of conceptual 400 kW natural gas (NG)-fueled SOFC power module. In the fuel processing system (FPS), NG is desulfurized and pre-reformed. Anode recycle provides water to the pre-reformer and ensures high plant efficiency.

and pre-reforms hydrocarbons higher than methane to eliminate the risk of carbon formation in the stack. Anode recycle provides water to the steam reformer and ensures a high system efficiency of greater than 55 percent (lower heating value). To date, conceptual designs of three IGFC systems meeting the desired efficiency and carbon separation targets have been completed. An atmospheric IGFC system with an SOFC/GT/ST cycle achieves an efficiency of 57 percent (HHV).

UTC Power also successfully completed the detailed design phase review for the 50 kW test stand, procured all major components, including the fully completed fluid skid, and initiated the final assembly of the test stand. Subsequent efforts will include the commissioning of the test stand and subsequent test of the ≥25 kW Delphi stack on simulated coal syngas. This test will demonstrate 5,000 hours of durability, 1,500 hours of which will occur in Phase I.

UTRC has characterized the effectiveness of manganese cobalt oxide (MCO) for both ferritic stainless steels and Ni-based superalloys. MCO is effective in improving oxidation resistance of ferritic stainless steels, but does not influence oxidation behavior of Ni-based superalloys such as Haynes 230. MCO adheres well to the alloy substrates during rapid thermal cycling tests using a “drop bottom” furnace and no coating spallation has been observed. Glass candidates consistently exhibit self-healing behavior at temperatures above 300°C. Thin uniform MCO and aluminide coatings have been obtained on coupons and processes are being scaled up for stack components.

Conclusions and Future Directions

SECA CBS is focused on the stationary markets, with Delphi leading the development of the stack for a coal syngas-based MW-scale power module. Product and process improvements were initiated for the current stack design, and for the development of the

next generation stack design. Development of the large active area footprint stack will continue for stationary applications.

The present sub-MW power module design meets all design specifications. Current and future work efforts are directed at developing a packaged system design with improved reliability and cost. Study of the IGFC systems shows that the GT-based hybrid systems have superior performance compared to systems employing only a steam bottoming cycle. In Fiscal Year 2010, a 5 MW proof-of-concept power plant will be designed based on the selected IGFC system (>100 MW) that meets the $400/kW (2002) power block cost target. The test of a >25 kW Delphi stack for at least 1,500 hours in Phase I on a simulated coal syngas will serve to validate the models used to design the 250-1,000 kW SOFC power module.

MCO is effective in both containing chromia and improving oxidation resistance for stainless steels. MCO coating applied at UTRC adheres well to alloy substrates during thermal cycling. Two material candidates have been identified as self-healing glass seals. Progress has been made in developing cost effective coating processes. Areas warranting continuation during FY 2010 include evaluation of coated stack components and validation of coating processes via stack testing.

FY 2010 Publications/Presentations

1. L. Chen, E. Sun, J. Yamanis, and N. Magdefrau, "Oxidation Kinetics of $Mn_{1.5}Co_{1.5}O_4$ Coated Haynes 230 and Crofer 22 APU for Solid Oxide Fuel Cell Interconnects," *J. of the Electrochem. Soc.* **157** (6) B931-B942 (2010).

2. David D. Brengel, "SOFC Program Review," 10th Annual SECA Workshop, Pittsburgh, Pennsylvania, July 14, 2009.

3. Rick Kerr, "Delphi SOFC Development Update," 10th Annual SECA Workshop, Pittsburgh, Pennsylvania, July 14, 2009.

4. Steven Shaffer, "Solid Oxide Fuel Cell Development for Transportation and Stationary Applications: Latest Update on Stack and System Performance," Fuel Cell Seminar, Palm Springs, California, November 17, 2009.

5. Neal Magdefrau, D. Frame, Lei Chen, E.Y. Sun, S. Tulyani, J. Holowczak, and J. Yamanis, "High Temperature Materials for SOFC Seal Applications," presented at the 34rd International Conference on Advanced Ceramics and Composites, Daytona Beach, Florida, January 27, 2010.

6. Lei Chen, D. Frame, N. Magdefrau, E.Y. Sun, and J. Yamanis, "$Mn_{1.5}Co_{1.5}O_4$ Based Spinel as Interconnect Coating for SOFC," presented at the 34rd International Conference on Advanced Ceramics and Composites, Daytona Beach, Florida, January 27, 2010.

7. Dan Hennessey, "Solid Oxide Fuel Cell Development for Auxiliary Power in Heavy Duty Vehicle Applications," DOE Hydrogen Program Peer Review; Washington, D.C., June 7–11, 2010.

8. Shivakumar Kameswaran, Handa Xi, S. Tobias Junker, Slaven Peles, Jean Yamanis and Ellen Sun, "Model-Based System Design of Highly-Efficient Integrated Gasification Fuel Cell Power Plants," paper # FuelCell2010-33219, Proceedings of the ASME 2010 Eighth International Fuel Cell Science, Engineering and Technology Conference FuelCell2010, Brooklyn, New York, June 14–16, 2010.

9. Sven Tobias Junker and Handa Xi, "Control of Stationary and Mobile Solid Oxide Fuel Cell Systems - A UTRC Perspective on Current Status and Future Directions," 2010 American Control Conference, Baltimore, Maryland, June 30 – July 2, 2010.

II. SECA INDUSTRY TEAMS
B. Cost Reduction

II.B.1 Solid State Energy Conversion Alliance Delphi SOFC

Steven Shaffer (Primary Contact), Gary Blake, Karl Haltiner, Subhasish Mukerjee, David Schumann, Gail Geiger, Larry Chick
Delphi Automotive Systems LLC
5725 Delphi Drive
Troy, MI 48098
Phone: (585) 359-6615; Fax: (585) 359-6061
E-mail: steven.shaffer@delphi.com

DOE Project Manager: Maria Reidpath
Phone: (304) 285-4140
E-mail: Maria.Reidpath@netl.doe.gov

Subcontractors:
- Battelle/Pacific Northwest National Laboratory, Richland, WA
- Electricore, Inc., Valencia, CA
- United Technologies Research Center, East Hartford, CT

Contract Number: 41246

Start Date: July 1, 2002
End Date: December 31, 2011

FY 2010 Objectives

The objective of this Fiscal Year 2010 work was to evaluate the performance of a solid oxide fuel cell (SOFC) stack for use in coal based system analyses. This was accomplished by:

- Building two 30-cell Gen 3.2 stacks.
- Updating the test stand for the tests.
- Testing the stacks.
- Collecting the data and reporting.

Accomplishments

- Two instrumented planar 30-cell SOFC stacks were fabricated with power densities of 469 mW per cm^2 and 480 mW per cm^2 for the coal-based system analysis.
- A test stand was upgraded to test the fabricated stack with various fuel compositions under varying loads.
- The tests were conducted, and the data was collected and analyzed.

Introduction

Delphi, in partnership with Battelle Memorial Institute under the Solid State Energy Conversion Alliance (SECA) program, is developing cost-effective 3-5 kW solid oxide fuel cell (SOFC) power systems for a range of fuels (natural gas, diesel, gasoline, and bio-fuels) and applications such as heavy-duty truck auxiliary power units (APUs), stationary distributed power generation, automotive, and niche applications in the military sector. During Phase I of the SECA project, the Delphi team was able to demonstrate test cells with power density more than required to meet the SECA 2011 goals. For SECA Phase II, Delphi aggressively pursued performance targets which drove SOFC stack, subsystem performance, and cost reduction. Delphi also utilized technical progress and market research to focus effort on development of the first diesel-powered SOFC APU for use by commercial vehicles. Emphasis in the first half of SECA Phase II was placed on achieving Phase II performance metrics on diesel fuel. Progress was made toward Phase II system targets: specifically, thermal cycling and power degradation rate. Results on natural gas stationary systems met target with reduced efficiency and power, and increased degradation rate were as anticipated when using diesel fuel. The project is currently on hold. As an addendum to the project, Delphi had an assignment to evaluate performance of an SOFC stack for use in coal-based system analyses.

Approach

For the additional work, Delphi did the following:

1. **Build.** Delphi fabricated two 30-cell Generation 3.2 (Gen 3.2) stacks for the test. Each stack had two thermal "dummy" cassettes with seven thermocouples each for mapping temperatures from the inlet to the outlet.
2. **Upgrade stand for the test.** The stand was upgraded for testing the different fuel compositions mentioned in the test plan. The stand needed to be upgraded for the different fuel compositions needed for these tests
3. **Testing of stack.** The stack was installed in the furnace and tested as per the test plan.
4. **Data collection and report.** All relevant data was collected and reported for use in the system analyses. This included polarization curves, temperature profiles and pressure data.

Results

Build

Two 30-cell Gen 3.2 stacks were fabricated successfully. Initial characterization was completed. Stack #833 produced 1,477 Watts at a power density of 469 mW per cm^2 at 570 mA per cm^2 (average voltage of 0.82 Volts, 750°C, 48.5% H_2, 3% N_2, rest H_2O fuel [see Figure 1]).

Stack #834 produced 1,512 Watts of power at a power density of 480 mW per cm^2 at 570 mA per cm^2 (average voltage of 0.84 Volts, 750°C, 48.5% H_2, 3% N_2, rest H_2O fuel). Both the stacks have good sealing and will be used for further evaluation with simulated coal gas reformate.

Upgrade Stand for the Test

The stands were successfully upgraded to allow for testing of all the different fuel compositions. The stand was optimized to be able to test the high steam content in the fuels as stated in the fuel compositions. A dummy stack was used to debug the stand. Table 1 shows the simulated reformate compositions that were tested. Figure 2 shows the stand that was developed to carry out this test.

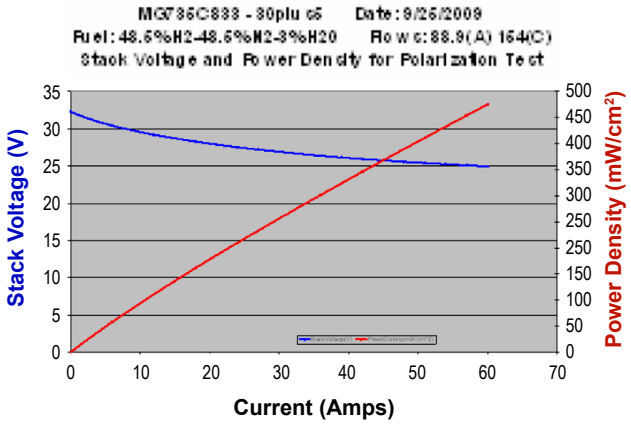

FIGURE 1. Stack #833: Current-Voltage Curve

TABLE 1. Simulated Reformate Compositions

	Fuel Composition					
Blend	**H_2**	**CH_4**	**CO**	**CO_2**	**N_2**	**H_2O**
Delphi Standard	48.5%				48.5%	3.0%
SECA CBS 1	63.5%				14.4%	22.1%
SECA CBS 2	12.5%	17.0%	5.0%	21.5%	4.9%	39.1%
SECA CBS 3	12.9%	9.0%	7.1%	39.8%	0.6%	30.6%
SECA CBS 4	17.0%	2.0%	24.0%	9.0%	1.0%	47.0%

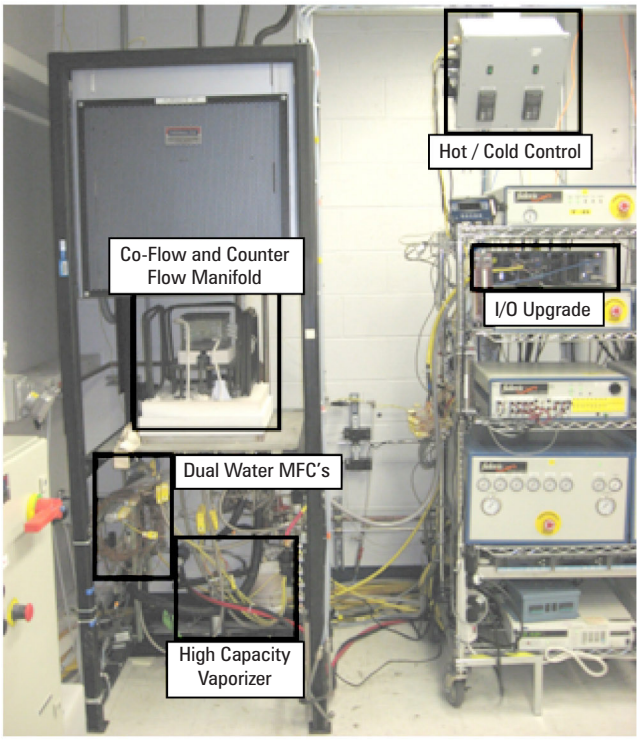

FIGURE 2. Test Stand Improvements

Hot / Cold Control (complete)

Added capability to vary cathode and anode inlet temperature, allowing for greater stack temperature control during max power sweeps.

I/O Upgrade (complete)

Increased Thermocouple Channels to handle additional TC Dummy readings

Co-Flow and Counter Flow Manifold (complete)

Modified test manifold pre-heating tubes to enable simultaneous testing with co-flow and counter flow conditions

Dual Water MFC's (complete)

Increased overall turndown by installing low flow and high flow water meters. Added capability to humidify 30 cell flows up to 50% water

High Capacity Vaporizer (complete)

Increased vaporization capacity to handle water flow rates for 50% humidification levels.

Test Stand Software (complete)

Various upgrades to match hardware changes

MFC = Multi-Function Controller

Testing of Stack

Stack testing is completed with data logged. With the stack at operating temperature (700-800°C inlet temperature), load was applied to get constant utilization polarization curves. For each reformate composition multiple constant fuel utilization polarization curves were measured. Each operating point was held for achieving steady-state operation. The tests were terminated when an individual voltage of a cell reaches a limiting condition (0.6 V) or reach a max temperature (840°C). Stacks were tested in co-flow configuration and counter-flow mode. Data collected includes polarization curves at given utilization (individual cell voltages versus current density), temperature profiles throughout the test and pressure (inlet, outlet).

Table 2 and Figure 3 show data from the series of co-flow tests with the referenced simulated reformate compositions. The trends observed demonstrates the impact of internal reforming in the reformate compositions with methane due to endothermic reforming. Having a higher inlet temperature with these reformates is beneficial for maintaining higher voltage. The high steam compositions impact open circuit voltage and therefore the voltages at 30 Amps (286 mA per cm^2) and 60 Amps (570 mA per cm^2) compared to the standard blends. Overall, the tests gave us a very useful understanding of performance and temperature distribution within the stack and more importantly within the plane of the repeating unit.

Data Collection and Report

Data processing was completed per schedule and report submitted to SECA.

Conclusions and Future Directions

The stacks have been built, tested and analyzed with the report delivered to SECA per the contract. Two Gen 3.2 stacks and a catalytic partial oxidation reformer will be built and delivered to the National Aeronautics and Space Administration as part of a new addendum to the original contract. This project is on hold.

FY 2010 Publications/Presentations

1. SECA Semi-Annual Report.

TABLE 2. Test Matrix

Fuel Iteration	Utilization Set Point	Inlet Anode Temp.
Delphi Standard A	30%	725°C
Delphi Standard B	50%	725°C
Delphi Standard C	70%	725°C
SECA CBS 1 A	30%	700°C
SECA CBS 1 B	30%	725°C
SECA CBS 1 C	30%	750°C
SECA CBS 1 D	50%	700°C
SECA CBS 1 E	50%	725°C
SECA CBS 1 F	50%	750°C
SECA CBS 1 G	70%	700°C
SECA CBS 1 H	70%	725°C
SECA CBS 1 I	70%	750°C
Delphi Standard B	50%	725°C
SECA CBS 2 A	30%	750°C
SECA CBS 2 B	30%	800°C
SECA CBS 2 C	50%	750°C
SECA CBS 2 D	50%	800°C
SECA CBS 2 E	70%	750°C
SECA CBS 2 F	70%	800°C
SECA CBS 2 G	70%	820°C
Delphi Standard B	50%	725°C
SECA CBS 3 A	30%	750°C
SECA CBS 3 B	30%	800°C
SECA CBS 3 C	50%	750°C
SECA CBS 3 D	50%	800°C
SECA CBS 3 E	70%	750°C
SECA CBS 3 F	70%	800°C
SECA CBS 3 G	70%	820°C
Delphi Standard B	50%	725°C
SECA CBS 4 A	30%	750°C
SECA CBS 4 B	30%	800°C
SECA CBS 4 C	50%	750°C
SECA CBS 4 D	50%	800°C
SECA CBS 4 E	70%	750°C
SECA CBS 4 F	70%	800°C
SECA CBS 4 G	70%	820°C
Delphi Standard B	50%	725°C

	Fuel Composition					
Blend	**H_2**	**CH_4**	**CO**	**CO_2**	**N_2**	**H_2O**
Delphi Standard	48.5%				48.5%	3.0%
SECA CBS 1	63.5%				14.4%	22.1%
SECA CBS 2	12.5%	17.0%	5.0%	21.5%	4.9%	39.1%
SECA CBS 3	12.9%	9.0%	7.1%	39.8%	0.6%	30.6%
SECA CBS 4	17.0%	2.0%	24.0%	9.0%	1.0%	47.0%

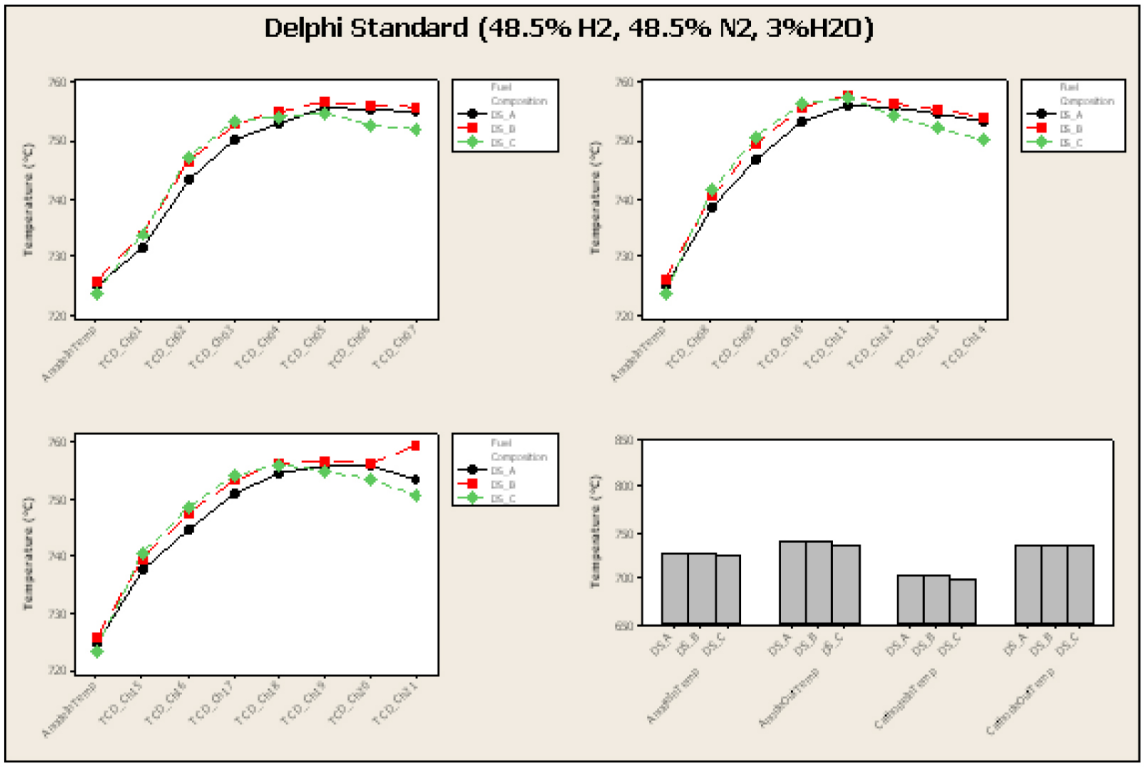

FIGURE 3. SECA Delphi Standard – Temperature Data at 30 Amps (286 mA per cm^2)

III. SECA CORE RESEARCH & DEVELOPMENT

A. Cathodes

III.A.1 Synchrotron X-Ray Studies of SOFC Cathodes

P.H. Fuoss (Primary Contact), K.-C. Chang, J.A. Eastman, T.T. Fister, D.D. Fong, B.J. Ingram, H. You
Argonne National Laboratory (ANL)
9700 S. Cass Ave.
Argonne, IL 60439
Phone: (630) 252-3289; Fax: (630) 252-7777
E-mail: fuoss@anl.gov

DOE Project Manager: Briggs White
Phone: (304) 285-5437
E-mail: Briggs.White@netl.doe.gov

Contract Number: FWP49071

Start Date: June 2007
End Date: May 2011

FY 2010 Objectives

- In situ X-ray scattering measurements of the structure and atomic scale chemistry in $La_{0.6}Sr_{0.4}Co_{0.2}Fe_{0.8}O_{3-\delta}$ (LSCF) will be measured as a function of temperature and oxygen partial pressure (pO_2).
- Crystallographic and phase-diagram (temperature versus pO_2) studies of recently discovered surface reconstructions will be used to help understand the chemistry of LSCF (001) surfaces.
- Grazing-incidence powder diffraction will be used to identify possible phase transformations and segregation on the surface of the cathodes during the electrode polarization and heating.
- Grazing-incidence, depth-sensitive spectroscopic X-ray techniques will be used to identify the chemical composition and oxidation states of $La_{1-x}Sr_xMnO_3$ (LSM), $La_{1-x}Sr_xCoO_3$ (LSC), and LSCF as a function of pO_2 and electrochemical condition.
- Correlate the structure and chemical states determined from in situ measurements with ex situ measurements from the literature and supplemental measurements performed at ANL, Carnegie Mellon University, (CMU) and Massachusetts Institute of Technology (MIT).

Accomplishments

- Determined the lattice parameter and electrical conductance of thin LSCF as functions of temperature and pO_2.
- Discovered that the LSCF (001) surface is reconstructed, and determined the sensitivity of the reconstruction's X-ray diffraction peaks to temperature and pO_2.
- Measured and modeled the lateral potential drops from an LSCF on yttria-stabilized zirconia (YSZ) thin film when using a series of wires as current collector.
- Prepared $La_{1-x}Sr_xMn_{1-y}Ta_yO_3$ cathodes and measured the area specific resistance as a function of temperature for y=0.01, 0.05 and 0.10.
- Found that, upon high temperature annealing, Sr segregates to the surface, new phases form, and there are elemental chemical shifts on the surfaces of LSCF films grown on YSZ(111) or gadolinium-doped ceria (GDC)/YSZ(001) with a strong dependence on the distance from the working electrodes.
- Demonstrated that a thin LSM overlayer increases stability of LSCF films compared to bare LSCF films without the overlayer under similar annealing conditions.

Introduction

The performance of solid oxide fuel cells (SOFCs) is strongly influenced by the nanoscale structure and chemistry of electrode materials under operating conditions. However, because SOFCs are operated at elevated temperatures and at near-atmospheric pressure, the utilization of traditional surface science techniques, which typically involve vacuum conditions near room temperature, requires validation. The studies being performed in this project provide the needed understanding of in situ/ex situ correlations. The results also enable the development of molecular-level models for stimulating the rational design and development of high performance cathode materials.

Approach

We employ in situ X-ray scattering and spectroscopy technologies developed at ANL to both measure equilibrium structures of SOFC cathode materials at elevated temperatures and under controlled oxygen partial pressures. We examine the dynamic structural and chemical changes that occur at the cathode side of a fuel cell under conditions that simulate actual operating conditions. This work, particularly sample preparation, microscopy measurements, ultra-high vacuum-based surface characterizations, and theoretical studies, is

performed in collaboration with investigators at several universities including CMU, Stanford, and MIT.

Results

During Fiscal Year 2010, experiments were performed that simultaneously measured X-ray diffraction along with direct current conductance from an (001) oriented 20 nm LSCF film grown on a 100 nm GDC (001) film deposited on a YSZ (001) substrate. Figure 1 shows the expansion of the LSCF film derived from the location of the LSCF (004) diffraction peak as a function of oxygen partial pressure (pO_2) and electrical bias applied across the LSCF/GDC/YSZ stack. The LSCF expansion is directly related to the oxygen vacancy concentration. Figure 2 shows the associated conductance of the film as a function of time for each of four oxygen partial pressures. Note the rapid decrease, then a plateau, followed by another rapid decrease in conductance for the 0.15 Torr conductance. This two-step drop indicates that more than one process controls the conductance of these LSCF thin films. The length of the plateau generally becomes shorter as the applied bias becomes more negative and as the temperature is increased from 500°C to 700°C but more studies are required to confirm this behavior. The kinetics of the lattice parameter change becomes much faster after the conductance has plateaued and then dropped. The size of the lattice parameter change, and hence the inferred oxygen vacancy concentration change, is only weakly dependent on temperature.

Due to their polar nature, it is expected that the surfaces of LSM, LSC and LSCF would have significantly different structures than the bulk. Since the primary role of these materials is to catalyze the oxygen reduction reaction, and since catalysis is primarily a surface phenomenon, determining the

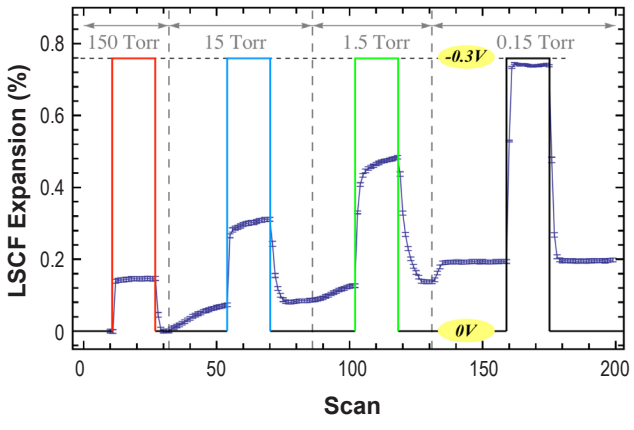

FIGURE 1. The expansion of the out-of-plane lattice parameter of an LSCF film at 500°C as a function of time and oxygen partial pressure for zero applied potential and a -0.3 V cathodic potential. Each scan takes 48 seconds, so the total elapsed time is approximately 3 hours.

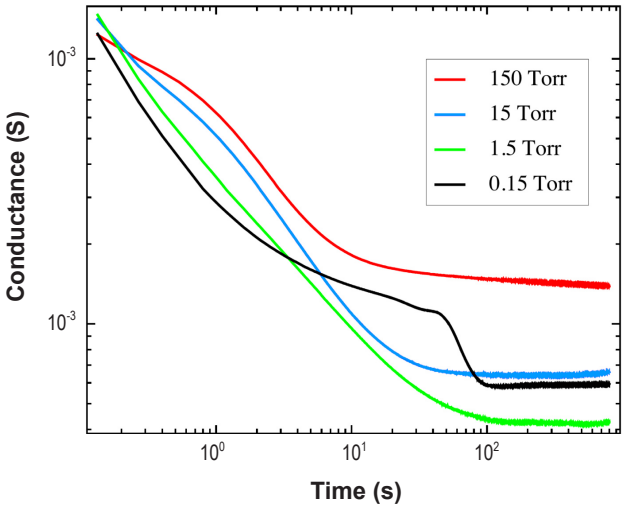

FIGURE 2. Conductance as a function of time while exposed to an applied potential of -0.3 V (cathodic) at different pO_2. The time periods for the conductance curves correspond to the four dramatic shifts in the LSCF lattice parameter exhibited in Figure 1.

atomic structure of the surfaces of LSM, LSC, and LSCF under environmental conditions relevant to SOFC operation is important. In earlier work, we found that a dominant reordering in these three materials is pO_2- and temperature-dependent segregation of strontium to the surface. However, we recently discovered that the LSCF (001) surface reconstructs into a surface with a much larger unit cell than the underlying bulk material. Figure 3 shows X-ray diffraction peaks from a 5 nm thick film of (001)-oriented LSCF grown on a niobium-doped (0.5 wt%) $SrTiO_3$ substrate. The azimuthal scan parallel to the surface shows three times as many diffraction peaks as would be expected from the bulk (i.e., the unit cell is three times larger) while the X-ray diffraction normal to the surface indicates that this reconstructed surface layer is two monolayers thick. From the complete data set, the atomic rearrangements that occur under conditions consistent with an operating fuel cell will be identified.

The effect of applied electrochemical polarization on surface properties of thin film cathode materials has been investigated. The electronic sheet resistance of very thin films limits current flow resulting in potential drops laterally from the working electrode (i.e., platinum wire current collectors). This potential drop is expected to be dependent on the ratio of ionic to electronic resistance, and will reduce the surface potential driving oxygen reduction. The lateral potential was investigated using a thin film specimen with a series of parallel Pt-wire current collectors pressure contacted to its surface. The lateral potential along the surface was measured while a constant potential was applied between the working electrode (one of the Pt wires) and the counter electrode (Pt mesh on the bottom

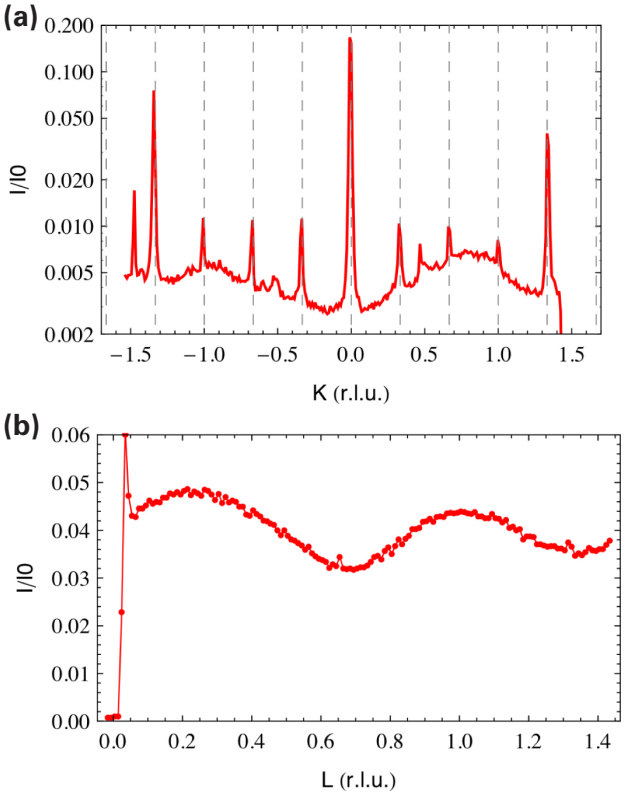

FIGURE 3. (a) The azimuthal scan through H = 4/3, L=0 shows peaks at ⅓-order positions, as highlighted by the dashed gridlines. The additional peaks locations such as K=-1.5 are from surface particles. (b) The periodicity of the crystal truncation rod from the (5/3,0) reflection indicates a four-monolayer-thick reconstruction. Both scans were taken at 750°C, 150 Torr pO_2.

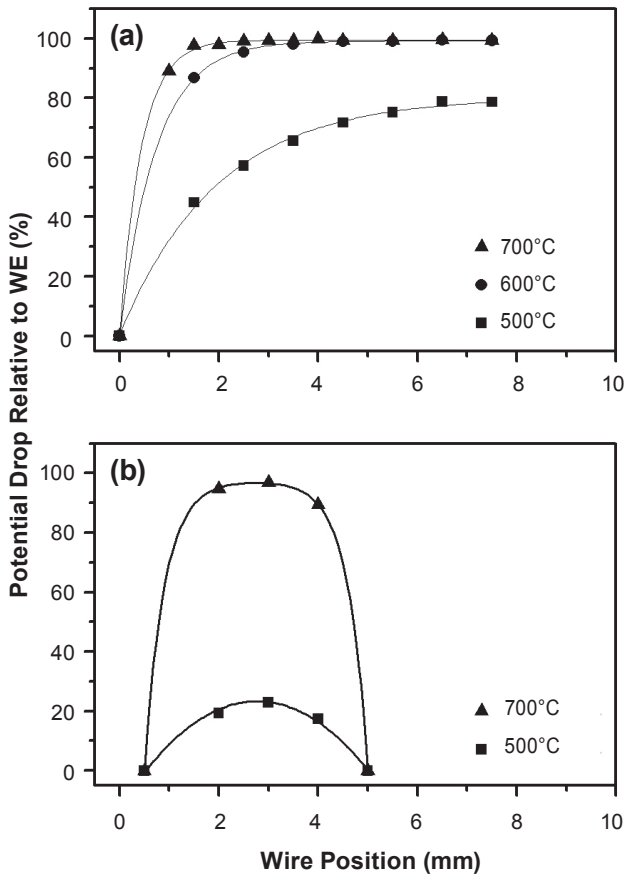

FIGURE 4. (a) The surface potential relative to the working electrode (a single Pt wire located at x = 0 mm) on LSCF/(111) YSZ. (b) The surface potential relative to the working electrode (two electrically shorted Pt wires at x = 0.5 and 5 mm) on LSCF/GDC/(001)YSZ.

of the substrate). The results for a 20 nm LSCF thin films on (001) YSZ/GDC single crystal substrates for cathodic polarization of 200 mV exhibit a significant dependence on temperature, whereas, the applied potential has no obvious effect on the lateral potential drop (Figure 4a). At 700°C, the surface potential drops ~90% relative to the working electrode within 1 mm. The observed surface polarization is similar for LSCF films on (111) YSZ, suggesting that the crystallographic surface termination does not modify the expected isotropic current flow in the bulk of the thin film. The spacing and orientation of the platinum wires needed to optimize the surface exposure and electrochemical polarization was investigated by measuring the surface potential between two parallel wires that are electrically shorted (Figure 4b). There is a large potential drop at 700°C even in the case of a parallel wire working electrode; therefore, wire placement must be optimized for each experiment to insure reliable results.

The effect of applied potential on 20 nm thick LSCF films thermally equilibrated by pre-annealing at 800°C for 55 hours was measured. At 800°C, the surface oxidation state of Co and Fe gradually changed from those of the bulk and, as shown in Figure 5, those changes persisted after cooling to room temperature. X-ray spectra that highlight the surface or the bulk (by varying the X-ray incidence angle) show a marked shift in the Co K-edges. Similar Fe K edge spectra show a less pronounced but still discernible shift in the peak position. The spectral changes are fairly uniform across the sample demonstrating that they are primarily due to annealing at high temperature. Electrochemical measurements indicate that the applied potential drops off rapidly from the wires at 800°C and the X-ray spectra would have shown a strong change with distance from the contact wires if there was a significant dependence on the applied potential (up to -5 V during annealing in these measurements). However, examination after cooling the sample to room temperature revealed that the area under the wire has a higher B cation concentration (data not shown) than areas away from the wire. The surface B cation concentration enhancement disappears ~0.8 mm away from the active wire, a result that is consistent with the electrochemical measurements.

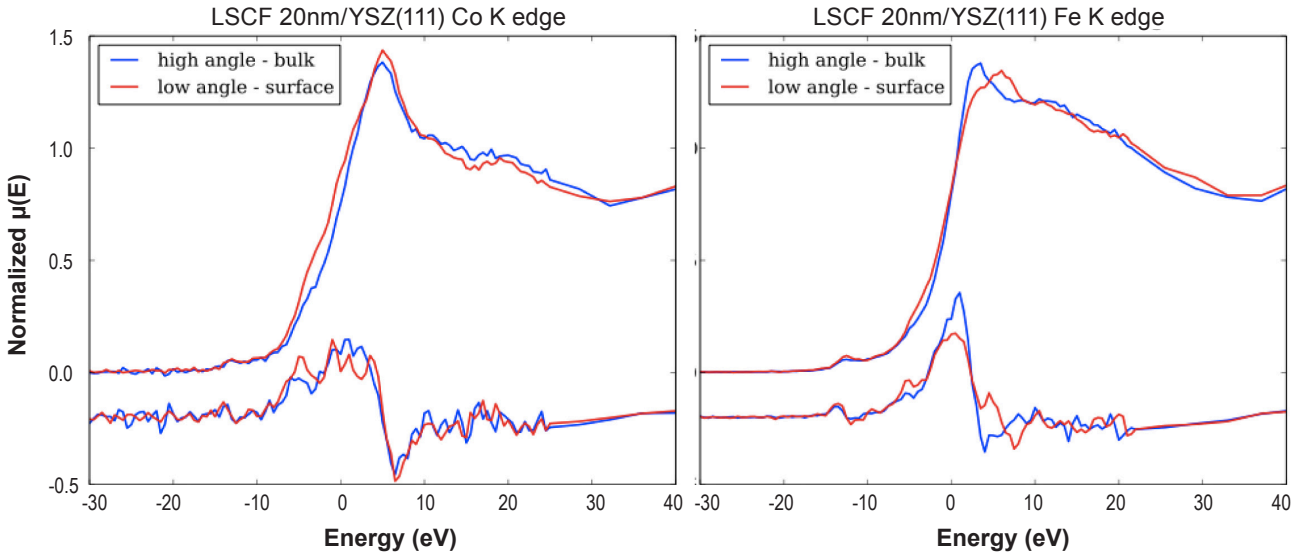

FIGURE 5. Co and Fe K-edge X-ray absorption near-edge structure from a 20 nm LSCF(011) film on YSZ(111) at the active working electrode position. The Co K-edge differs significantly between the surface and bulk while the Fe K edge differences are less pronounced.

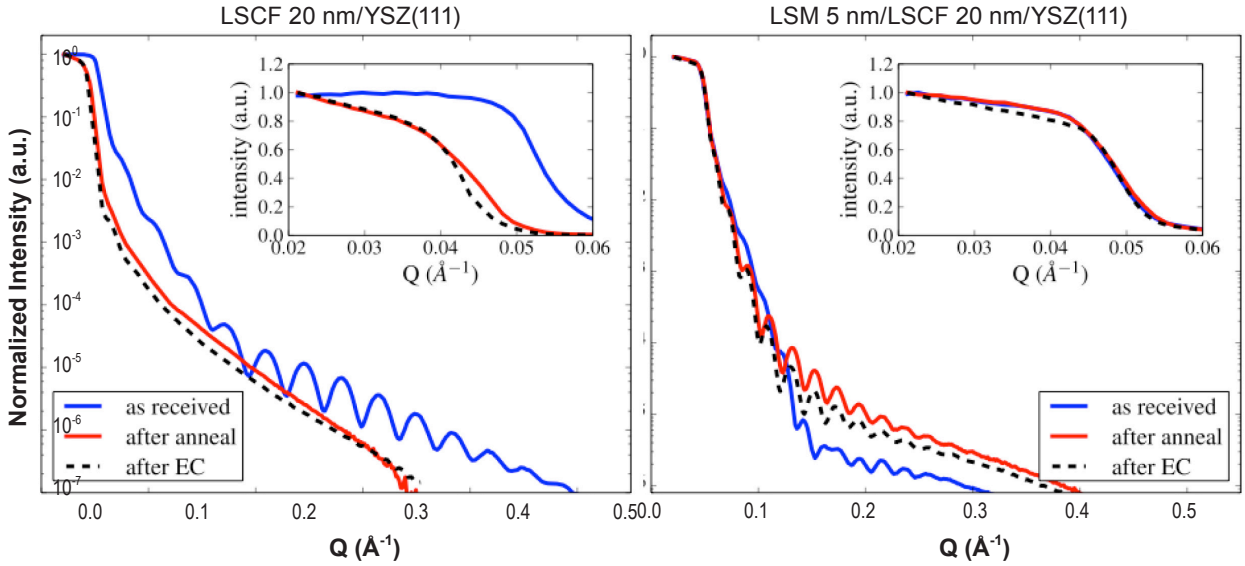

FIGURE 6. Reflectivity scans of (a) LSCF and (b) LSM-capped LSCF. Insets show blow-ups of the low angle data that can be used to determine the critical angle for total reflectivity. Note that the uncapped LSCF becomes rough after annealing, as evidenced by the disappearance of the fringes. Also, annealing results in a significant decrease of the critical angle in LSCF indicating that the electron density at the surface has decreased. In contrast, changes in roughness and critical angle after annealing are insignificant for the LSM-capped sample.

To model an LSCF system with LSM infiltrations, the effect of an LSM overlayer on the stability of LSCF grown on a YSZ (111) oriented substrate was studied. In contrast to LSCF on YSZ (111) where the X-ray reflectivity fringes and critical angles change significantly upon annealing (Figure 6a), little change in the reflectivity data (Figure 6b) is found after annealing when there is an LSM overlayer. This result suggests that LSM stabilizes the interfaces of the thin films under annealing conditions. No evidence of Mn intermixing with the other B site cations was found in total reflection X-ray fluorescence measurements (not shown), which is further evidence for the stable LSCF film and the protective nature of LSM overlayer.

LSM was doped with various levels of tantalum in an effort to develop enhanced cathode materials through surface modifications. Tantalum has been shown to be an active oxygen reduction catalyst. Preliminary results were promising and indicated a 5 and 10% improvement in performance for Ta-substituted LSM relative to

standard LSM electrodes. Based on these results and the guiding principle of surface modification via infiltration, LSM electrodes were prepared with excess Ta/Ta_2O_5 that was expected to decorate the surface and grain boundaries of the LSM. The Ta-enhanced LSM was screen printed on a YSZ substrate as a composite YSZ/LSM+Ta electrode. The area specific resistance of $LSMTa_{0.05}$, $LSMTa_{0.10}$, LSM+10%Ta, LSM and LSF composite electrodes were compared, and the addition of Ta_2O_5 to LSM was found to improve the performance of LSM to values comparable to LSF. The physical morphology (e.g., 8YSZ/perovskite ratio and particle size) of the different electrode materials was ostensibly identical. The atomic distribution of tantalum is unknown at this time, but EDS has confirmed the nominal composition and X-ray diffraction has confirmed a single phase perovskite structure. The long-term stability of Ta-enhanced LSM is good; however, performance degradation was observed to be higher than standard LSM electrodes.

Conclusions and Future Directions

- Simultaneous measurements of the LSCF lattice parameter and electrical conductance have revealed a multi-step conduction process that is sensitive to both oxygen partial pressure and the magnitude of an applied, cathodic bias.
- The LSCF (001) surface has been found to reconstruct into a larger unit cell (in contrast to both LSM and LSC).
- Chemical shifts of Co and Fe have been determined for LSCF using X-ray spectroscopy techniques and those measurements confirm that Co is more strongly interacting with oxygen than Fe.
- An LSM overlayer is found to stabilize the LSCF surface, a property that may enhance the usefulness of LSM as a cathode intercalant.

Extended measurements of the simultaneous lattice parameter change and electrical conductance of LSCF thin films will be used to identify the mechanisms of conduction in this important SOFC material. Structural studies of the atomic arrangements on the low index LSCF surfaces will be performed with the goal of providing insight into the catalytic mechanisms on those surfaces. Further investigations of LSM/LSCF thin films will be performed to identify how the LSM layer chemically and structurally enhances the stability of the underlying LSCF film. The possible enhancement of the oxygen reduction activities due to the LSM overlayer, reported in literature, will be examined by measuring the chemical states of the interfacial elements. Finally, improved cell configurations will improve the sensitivity of X-ray signals to the electrochemical conditions of LSCF films with or without an LSM overlayer and allow for a clearer understanding of the functioning of these important materials in the operating environment of an SOFC.

FY 2010 Publications/Presentations

1. Tim Fister, Dillon Fong, Jeff Eastman, Hakim Iddir, Peter Zapol, Hui Du, Paul Salvador, and Paul Fuoss, "Total reflection inelastic x-ray scattering: a direct probe of defect chemistry in thin films," 2010 Spring MRS Meeting, San Francisco, April 5–9, 2010.

2. Tim Fister, Stephan Hruszkewycz, Dillon Fong, Jeff Eastman, Paul Fuoss, Hui Du, and Paul Salvador, "In situ synchrotron measurements of surface compensation mechanisms in $La_{0.6}Sr_{0.4}Co_{0.2}Fe_{0.8}O_{3-\delta}$ thin films," APS March Meeting, Portland, March 15–19, 2010.

3. Tim Fister, Dillon Fong, Jeff Eastman, Hui Du, Paul Salvador, and Paul Fuoss, "In situ characterization of oxygen reduction and exchange in $La_{0.6}Sr_{0.4}Co_{0.2}Fe_{0.8}O_{3-\delta}$ at elevated temperature and pO_2," 2009 Fall MRS Meeting, Boston, November 30-December 4, 2009.

4. Tim Fister, Dillon Fong, Paul Fuoss, Hakim Iddir, Peter Zapol, Robert Gordon, Mali Balasubramanian, Balasubramaniam Kavaipatti, and Paul Salvador, "Total reflection inelastic x-ray scattering from a 10 nm $La_{0.6}Sr_{0.4}Co_{0.2}Fe_{0.8}O_{3-\delta}$ thin film," 2009 X-Ray Science Gordon Conference, Waterville, Maine, August 2–7, 2009.

5. Kee-Chul Chang, Brian Ingram, Daniel Hennessy, Balasubramaniam Kavaipatti, Paul Salvador, and Hoydoo You, "In situ x-ray techniques for model oxide fuel cell cathodes," 2009 X-Ray Science Gordon Conference, Waterville, Maine, August 2–7, 2009.

6. M. Krumpelt, T.A. Cruse, B.J. Ingram, J.L. Routbort, S. Wang, P.A. Salvador, et al., "The Effect of Chromium Oxyhydroxide on Solid Oxide Fuel Cells," J. Electrochem. Soc., **157**, B228-B233 (2010).

III.A.2 Solid Oxide Fuel Cell Cathodes: Unraveling the Relationship Among Structure, Surface Chemistry and Oxygen Reduction

Srikanth Gopalan
15 St. Mary's Street
Department of Mechanical Engineering
Boston University
Boston, MA 02215
Phone: (617) 358-2297
E-mail: sgopalan@bu.edu

DOE Project Manager: Patcharin Burke
Phone: (412) 386-7378
E-mail: Patcharin.Burke@netl.doe.gov

Contract Number: NT0004104

Start Date: September 1, 2008
End Date: September 30, 2011

FY 2010 Objectives

- Continue deposition of high quality epitaxial and polycrystalline cathodic thin films.
- Obtain in situ/ex situ correlations between electrochemical impedance spectroscopy (EIS) and X-ray absorption and emission spectroscopy (XAS and XES).
- Use in situ X-ray chamber to obtain high temperature surface structure and composition analysis.
- Obtain kinetics data on oxygen exchange on cathode thin films using electrical conductivity relaxation and one-dimensional diffusion experiment.

Accomplishments

- We have continued to deposit high-quality lanthanum strontium manganite (LSM) thin films as evidenced by high-resolution transmission electron microscopy (TEM) and roughness measurements using atomic force microscopy.
- Ex situ measurements using XES and XAS have clearly shown the charge state of the Mn ion in LSM to be closely related to the cathode polarization resistance changes as measured by impedance spectroscopy.
- Total reflection X-ray fluorescence data clearly show segregation of Sr to the surface of the LSM thin films.
- The surface exchange coefficient on epitaxial LSM thin films have been found to be $4x10^{-9}$ cm/s and the diffusivity of oxygen in LSM thin films has been measured to be on the order of ~$5x10^{-9}$ cm^2/s.

Introduction

Many of the specific details of the oxygen reduction reaction in a solid oxide fuel cell (SOFC) remain poorly understood. Surface chemistry directly influences the nature of oxygen reduction reaction pathways on the SOFC cathodes and the rates at which the individual processes proceed. From semi-empirical correlations between the chemistry and structure of oxide surfaces and their electrocatalytic performance, the true cause-and-effect relationships in the oxygen reduction processes at the cathode could be elucidated. This would provide valuable guidance in improving cathode performance.

Approach

In this work, we aim to acquire such surface-specific chemical and structural data on heteroepitaxial thin films of LSM and lanthanum strontium cobalt ferrite (LSCF) cathodes on single-crystals of yttria-stabilized zirconia (YSZ) and YSZ coated with a barrier layer of rare-earth doped ceria (e.g. Y_2O_3-doped CeO_2 or YDC) electrolytes. This is being accomplished using a combination of analytical spectroscopic techniques and TEM. Further, we also aim to employ soft X-ray spectroscopies, namely XES/XAS, to correlate changes in the thin film polarization resistance to the surface chemical composition and the charge state of the Mn ion. The overall goal is to understand the role of surface atomic and electronic structure on the oxygen exchange reaction.

Results

We have performed EIS of our dense films to confirm the suitability of studying dense films for studying the "burn-in" effect. Figure 1 presents the results of an EIS using 70 nm thick LSM/YSZ(111) samples which were heated to 800°C in air and a potentiostat/galvanostat. These measurements were taken with a frequency response analyzer which was used to both apply a -1 V cathodic bias across the sample for 5 days and perform impedance measurements with an applied 10 mV frequency ranged from 65 KHz to 10 mHz second arc emerges at a higher frequency with a peak frequency of 65 Hz.

In order to retain the final condition of our films we used a rapid quenching method to study samples exposed to SOFC atmospheric conditions and operation i.e. (800°C to room temperature within 5 seconds) for lanthanum strontium manganese oxide (LSMO) films exposed at 800°C in air without a bias and with a -1 V bias. Our study also included LSMO films cooled in thermal equilibrium in order to determine the ability of the quenching to preserve their final state (which will be discussed further in section B). The samples were sealed in evacuated glass vials until released and mounted within a dry N_2 glove box environment and immediately inserted into the ultra-high vacuum (UHV) analysis chambers. Exposure to atmospheric conditions was limited to at most 4 minutes.

Mn L-edge XAS results shown in Figure 1 show clearly that in addition to the charge state, it is also possible to track changes to the surface chemical composition of thin film electrodes. Using O-K edge XAS in the TEY mode (not shown here) we have also been able to identify segregation of Sr to the surface of the LSM thin films upon exposure to the operational conditions of the SOFC cathode. The segregation of Sr to the surface of the cathode has also been confirmed using X-ray fluorescence (XRF) shown in Figure 2.

It is satisfying to confirm Sr segregation to the surface of LSM films using two different synchrotron based techniques.

We have also measured the oxygen surface exchange coefficient ($4x10^{-9}$ cm/s) on these epitaxial thin films and their diffusivity ($5x10^{-9}$ cm^2/s) under cathodic conditions. The surface exchange coefficients in particular are somewhat smaller than what has been reported in the literature. However, literature measurements are typically on bulk polycrystalline samples, which have a high surface roughness, porosity and other types of

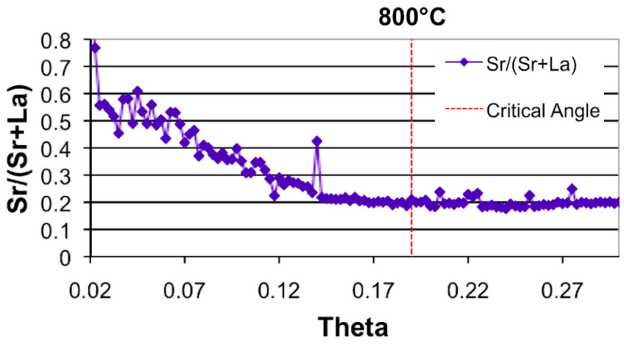

FIGURE 2. In situ XRF Results Showing Segregation of Strontium to the Surface of Annealed LSM Thin Films at 800°C in Air

defects. In future we will attempt to correlate the oxygen surface exchange kinetics with the surface structural and compositional measurements, which we expect to track through synchrotron X-ray measurements.

Conclusions and Future Directions

Thus far we have shown that XES/XAS spectroscopies are valuable tools to correlate the change in cathodic polarization resistance with the Mn charge state. Using XAS in TEY mode, we have also confirmed the segregation of Sr to the LSM surface. This has also been independently confirmed using total reflection X-ray fluorescence.

In the future, we expect to accomplish the following.

1. Ex situ/in situ correlations using XAS/XES on LSCF thin films.
2. In situ X-ray experiments correlated with electrical conductivity relaxation on LSCF thin films.
3. Correlation of oxygen transport kinetics with X-ray structure of LSCF thin films.

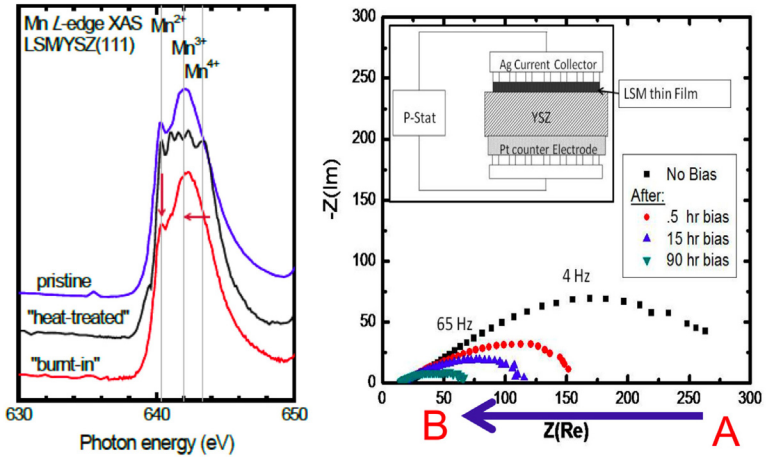

FIGURE 1. (left) XAS Results and (right) Impedance Spectroscopy Results on Three Different LSM Thin Films

III.A.3 SOFC Cathode Surface Chemistry and Optimization Studies

Paul A. Salvador (Primary Contact), Lu Yan, Shanling Wang, K. R. Balasubramaniam, and Hui Du
Carnegie Mellon University
Department of Materials Science and Engineering
5000 Forbes Avenue
Pittsburgh, PA 15206
Phone: (412) 268-2703; Fax: (412) 268-3113
E-mail: paul7@andrew.cmu.edu

Collaborators: Drs. Paul Fuoss,[a] Jeff Eastman,[a] Tim Fister,[a] Brian Ingram,[a] Hoydoo You,[a] Kee-Chul Chang,[a] Bilge Yildez,[b] Helia Jalili,[b] C. Heske,[c] S. Krause[c]
[a] Argonne National Laboratory
9700 South Cass Avenue
Argonne, IL 60439-4837
[b] Massachusetts Institute of Technology
Department of Nuclear Science and Engineering
77 Massachusetts Avenue, Rm: 24-210
Cambridge, MA 02139
[c] University of Nevada, Las Vegas
Department of Chemistry
4505 Maryland Parkway, Box 454003
Las Vegas, NV 89154

DOE Project Manager: Patcharin Burke
Phone: (412) 386-7378
E-mail: Patcharin.Burke@netl.doe.gov

Contract Number: NT0004105

Start Date: September 1, 2008
End Date: February 28, 2010

FY 2010 Objectives

- Develop samples of cathode materials having specific surface structures and chemistries using thin film preparation methods, as requested by collaborators.
- Provide lanthanum strontium manganese oxide (LSM), lanthanum strontium cobalt oxide (LSC), and lanthanum strontium cobalt iron oxide (LSCF) samples for surface characterization to collaborators at the Argonne National Laboratory Advanced Photon Source (ANL-APS), Massachusetts Institute of Technology (MIT), and the University of Nevada Las Vegas (UNLV).
- Refine investigations into the oxygen uptake kinetics in thin film samples: specifically LSM (100), (110), and (111) at different thicknesses and on different substrates, and to relate these to potential infiltrated cathodes.
- Use Kelvin probe spectroscopy (KPS) on LSM samples to demonstrate sensitivity to different steps in the oxygen uptake reaction.

Accomplishments

- Further developed single-crystal, epitaxial, textured, and polycrystalline thin films of LSM, LSC, and LSCF with low roughness values on both insulating and electrolytic substrates of various geometries that were used in both in-house and collaborators' experimental facilities to understand the nature of the surface chemistry/reactivity of cathode materials.
- Thin film samples were characterized at: the ANL-APS as a function of temperature (T), pressure (P), and electrochemistry for their surface compositions, structures, and charge states; at MIT for their local electronic properties using scanning tunneling spectroscopy and electrochemical properties with electrochemical impedance spectroscopy; at UNLV with Auger electron spectroscopy and X-ray photoelectron spectroscopy, and at Carnegie Mellon University (CMU) with X-ray diffraction, atomic force microscopy, electrical conductivity relaxation (ECR), KPS, and piezoelectric crystal microbalance.
- Demonstrated that the surface chemical exchange coefficient of LSM was independent of thickness on $SrTiO_3$ (STO) and refined the interpretations of the anisotropies observed. A 4-fold difference was observed between low index orientations for films of 600 nm for the three low index orientations at 800°C in conditions similar to cathode electrochemical conditions.
- Demonstrated that epitaxial thin film samples of LSM exhibit substrate dependent properties, indicating that infiltrated cathodes may have complex behavior not predicted by bulk investigations. Over a factor of two orders of magnitude was observed for nominally identical films on different substrates, indicating infiltrated nanoparticles may exhibit degraded properties.
- Implemented a simultaneous ECR/KPS testing method for thin film characterization in atmospheric pressure using mixed gases to control the pO_2, and demonstrated a two-step process occurs during oxygen uptake on LSM: fast adsorption and slow incorporation. This provides an experimental path for investigating whether surface engineering can be used to optimize cathode properties separately.

Introduction and Approach

The cathode in solid oxide fuel cells (SOFCs) is responsible for the reduction of O_2 gas and its incorporation into the electrolyte. When SOFCs are operated at specific current densities/voltages, the oxygen incorporation (or uptake) process can contribute significantly to the losses of the cell, thereby limiting the performance of the SOFC system. Two major options exist for improving the cathode performance by specifically targeting the oxygen incorporation process: changing the component solid materials or adding yet another material (a catalyst) to the existing frameworks [1,2]. We aim to address both approaches in this work by (1) developing an experimental project that allows us to probe the nature of atomic scale surface chemistry and its role in oxygen incorporation in LSM, LSC, lanthanum strontium iron oxide, and LSCF (and related cathode materials) and (2) determining the optimal catalyst chemistry from both an activity and stability perspective [3-7]. Realizing these goals will lead to improved cathode performance in SOFCs and an acceleration of introduction of new materials into SOFCs to allow for the DOE Solid State Energy Conversion Alliance (SECA) program to meet performance metrics.

Generally speaking, the limitations in designing highly active cathodes for oxygen incorporation arise from the general lack of direct correlations between surface/interface chemistry/structure and performance of SOFC cathode materials over the appropriate ranges SOFC operational conditions [8]. In this work, we aim to fill this need by (1) developing experimental protocols that will provide a sensitive measure of activity/stability in operational conditions and by (2) determining key correlations between structure (solid state atomic, electronic, crystallographic, and chemical) and electrochemical performance (mass and charge transfer) parameters in surface engineered samples. At CMU, we are generating surface engineered samples and providing them to a range of collaborators who characterize the samples. Several groups at ANL have investigated samples using high-energy synchrotron X-ray techniques at the ANL-APS [4,9]. A group at MIT uses scanning-tunneling spectroscopy and electrochemical impedance spectroscopy are carried out to determine electrical characteristics of the films [7]. A group at UNLV carries out experimental electronic structure determination of thin film surfaces. Separate reports will be provided by these collaborators. In this report, we describe the progress at CMU on sample preparation, especially on measurement of the oxygen uptake kinetics using simultaneous ECR and KPS.

Results

As indicated in past publications and reports [4,10-13] and in forthcoming publications [14,15] we have been providing high-quality surface-engineered thin films to collaborators, who are working on identifying surface chemistries and properties that lead to improved electrocatalytic performance [4,11-13]. It is essential to characterize the details of the thin film structure to interpret properly experimental observations. At CMU, we carry out the necessary processing and characterization to ensure samples have the characteristics requested from collaborators. Reports from collaborators are given elsewhere.

As described in our last two annual reports [10,16], we have developed ECR capabilities to investigate the behavior of epitaxial films and characterized the orientation dependence of the oxidation and reduction reactions at oxygen pressures of 50 to 500 mTorr (6-60 x 10^{-5} atm), similar to the effective oxygen activity in the active cathode. This year we improved the analysis of the data from the chamber [14] and measured the properties over a range of thicknesses and temperatures to confirm the interpretation of our observations arising from k_{chem} [14]. How this was done for (100)-oriented films of LSM on STO is shown in Figure 1, which plots the ECR relaxation time, τ, versus film thickness L (from which $k_{chem} = L/\tau$) [14]. The inset

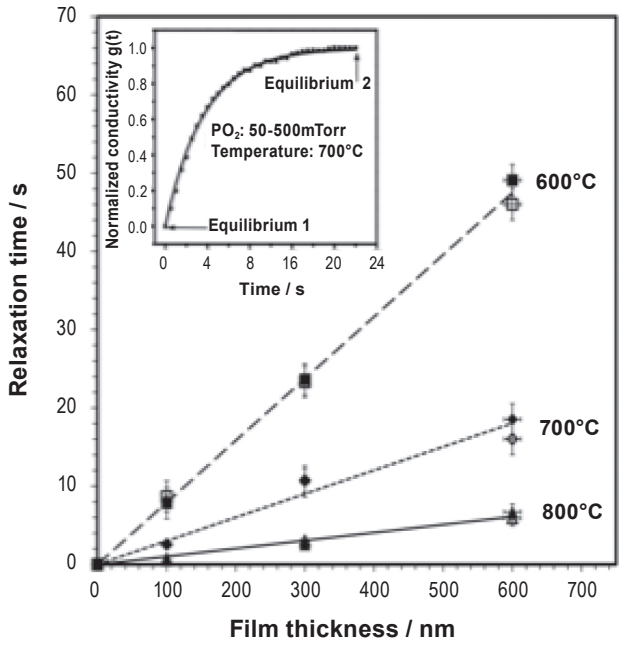

FIGURE 1. Dependence of the ECR relaxation time, based on an exponential fit to ECR data (shown in the inset for a 100 nm thick film at T = 700°C), on film thickness (100–600 nm) and temperature (600–800°C).

shows the actual ECR data. The linear dependence of τ with L indicates that k_{chem} the material response is accurately interpreted in the surface controlled regime, which is rarely done in the literature on the topic. The details of the orientation dependence of films having L = 600 nm have been submitted for publication, including a detailed comparison with available literature reports [15]. Overall, a factor of 4 difference was observed for the different low-index orientations for oxidation and reduction, with (100) being the least active surface and (111) the most active surface from 600 to 800°C. It should be pointed out that we have measured, in another project, that the surfaces of LSM in real cathodes are very close to being randomly distributed, meaning that the local exchange rates vary at least by a factor of 4 (high index surfaces were not investigated here, but will be in Fiscal Year 2011).

This year we posed three questions relative to the ECR response of LSM relative to their use as infiltrates in SOFCs. (1) Does the response of LSM vary with the thickness (size) of the film (infiltrate)? (2) Does the response of LSM vary with the material on which the film (infiltrate) is supported? And, (3) can KPS and ECR be used simultaneously to identify distinct steps in the oxygen reduction reaction? As described in the following, the answers to all three are yes; but, these need to be further explored to understand how infiltrates behave in SOFC cathodes.

The ECR relaxation times (measured at 600°C) of (100)-oriented films deposited on STO and $NdGaO_3$ (NGO) are shown in Figure 2. The film thickness ranges from 40 to 150 nm and the lines are meant as guides to the eye. As discussed above in regard to Figure 1, the relaxation time should decrease in a linear fashion with a decrease in thickness, ultimately passing through the origin of the plot. As seen for all films below 100 nm in thickness, the relaxation time actually increases with decreasing thickness. These films are expected to be surface controlled, relative to the bulk film properties. The origin of the decrease in the effective k_{chem} at small thicknesses remains to be explored, though likely candidates include a number of strain-related effects, defect population variations, defect ordering, substrate influence, a change in the rate limiting process, and finite size effects (some of which are interrelated). In any case, thicknesses of infiltrated materials vary from a few nm to a few hundred nanometers, which are precisely in the range reported here.

A two order of magnitude variation is observed in the k_{chem} values determined from the data presented in Figure 2, which depends both on thickness and support (substrate). For LSM on STO, oxidation and reduction are approximately equal in rate. However, for LSM on NGO, the oxidation and reduction rates vary greatly and both are significantly lower than their counterpart for the LSM on STO. For example at 40 nm, $k_{chem, red} \approx 2.4 \times 10^{-8}$ cm/s for LSM on NGO. At 50 nm,

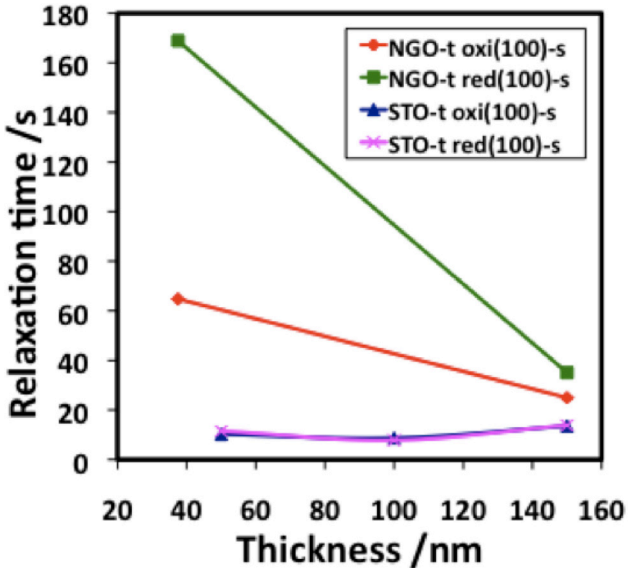

FIGURE 2. Dependence of the relaxation time as a function of substrate (STO and NGO) and chemical process (oxidation or reduction) for films below 150 nm.

$k_{chem, red} \approx 5 \times 10^{-7}$ cm/s for LSM on STO. Meanwhile, the values for thick films in the linear regime on STO are $k_{chem, red} \approx 1.2 \times 10^{-6}$ cm/s. For the strained epitaxial films presented here, the surface exchange rates decreased, indicating that the catalytic activity of LSM decreases in such cases. We will determine the importance of such variations in FY 2011.

To cover the range of oxygen pressures expected in the cathode ($1x10^{-5}$ to $1x10^{0}$) and to simultaneously interrogate the surface with ECR and KPS, we installed and began operating a new high-temperature test chamber that operates at 1 atm using mixed gases to control the partial pressure of oxygen. Overall the materials properties of our films behave as expected in the higher pressure range and ECR produced values similar to our earlier investigations using the low-pressure chamber. As such we focus here on the use of the KPS/ECR simultaneously.

Kelvin probe spectroscopy measures the contact potential difference between a reference material and the sample under test [17], which is given by the work function (WF) difference in general. The contact potential difference is firstly related to the difference in the electrochemical potential of the bulk electrons in the sample and reference, generally given by the difference in the WFs. The WF of the sample can be related to the bulk Fermi level, ϕ_S^B, and any surface dipole, ϕ_S^D, an electron must traverse to escape the sample. This surface dipole is sensitive to surface states including adsorbed species [17-22]. Figure 3 shows three schematics of the work function difference that could be measured in a system that that goes from a

reduced state (left) to a transient chemisorbed state with the bulk out of equilibrium in the new oxidized condition (center) to the equilibrium oxidized state (right). Both ϕ_S^B and ϕ_S^D can vary between the reduced and oxidized state, which require knowledge of the material's defect chemistry to de-convolute the two values from the overall the response. What is more relevant to exploring materials responses is the transient state. In the case shown in Figure 3, the initial transient leads to a large change in ϕ_S^D with no change in ϕ_S^B. In this case, we expect a large change in the contact potential difference (CPD) and almost no change in the conductivity, since the bulk has not changed. Such observations have been made previously on ceramics [17-22], but not on thin films of controlled orientations and thicknesses of SOFC compositions.

Figure 4 illustrates the data collected from a combination of ECR and KPS in transient modes at 600°C, both on oxidation and reduction (other conditions are given in the Figure). What is immediately evident is that the ECR data behaves as presented earlier, while the KPS data behave in a very different fashion. In the KPS, an instantaneous (faster than our experimental set-up can measure) change occurs in the CPD, while the ECR shows almost no change in the conductivity, indicative of a very fast development of a large surface dipole. This agrees with reports that LSM has a fast chemisorption step and a slow incorporation step of oxygen [23]. The decay from the initial state to the final state can be modeled using known values for the Fermi level shift under these conditions [20,21] to determine the change in the surface dipole. Oxidation

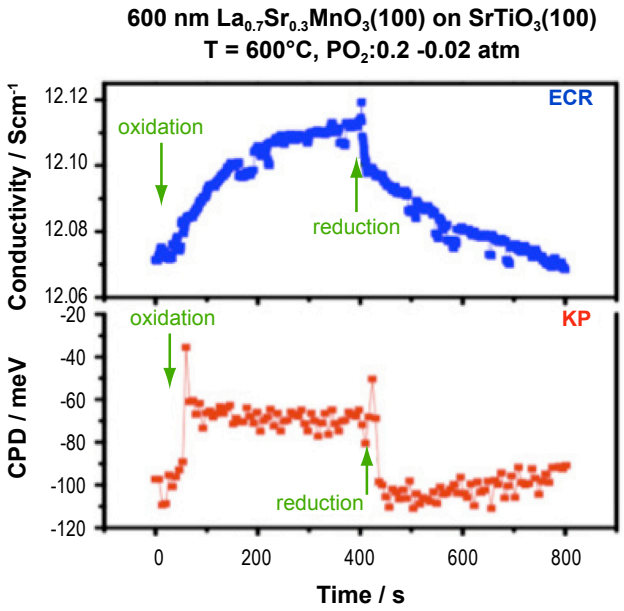

FIGURE 4. Transient conductivity and contact potential difference measured on the same film in identical conditions, listed above the figures. Both the oxidation and reduction processes are shown, whose starting points are shown.

and reduction occur in similar fashions: the surface dipole changes quickly and then the system decays to it final state, as described in Figure 3 for oxidation. In FY 2011 we will use this to characterize LSM, LSCF, and LSC, as well as surface engineered materials to determine if adsorption and incorporation can be independently optimized to allow for optimal infiltrates to be designed.

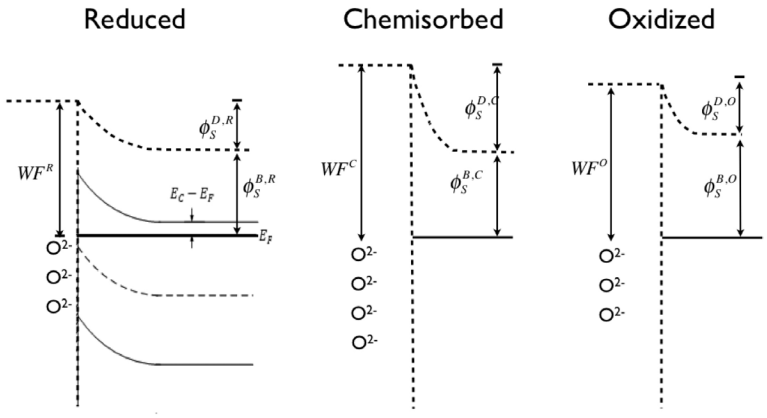

FIGURE 3. Schematic of the work function, including the Fermi level and surface dipole (from surface states/adsorbates, for a reduced (R), a chemisorbed (C), and an oxidized state (O), respectively from left to right, during an oxidation process. WF^i denotes the measured work function in the *i*th state, where *i* indicates the state. E_F indicates the Fermi level, $\phi_S^{B,i}$ and $\phi_S^{D,i}$ represent the potential contribution to the work function from the bulk (B) and dipole (D) in the *i*th state. The dashed upper line running in the horizontal direction represents the reference level, O^{2-} represents adsorbed oxide ions, the dashed vertical line represents the surface of the cathode, the dark horizontal line represents E_F.

Conclusions and Future Directions

We have demonstrated that surface engineered films of cathode materials can be produced and characterized in detail for the structural and chemical properties. Crystallographic anisotropies were observed for epitaxial LSM single crystal films in their oxygen uptake kinetics, where low index orientation vary by a factor of 4 in SOFC conditions of temperature and effective pressure. Furthermore, the surface exchange coefficient can vary greatly at low thicknesses and as a function of the support (substrate), both of which are relevant for SOFC electrocatalysis. Both ECR and KPS equipment can be used to simultaneously measure oxygen uptake, indicating that chemisorption and incorporation can be distinguished when their time constants are significantly

different, as observed for LSM. We will continue to produce a series of surface engineered films and will investigate (1) their structural properties, (2) their stabilities, and (3) their oxygen uptake kinetics using ECR and KPS measurements. By fabricating a matrix of related materials and carrying out these measurements, we will be able to provide a large amount of data to determine the key parameters that correlate surface structure to surface activity, with the aim of providing information to the DOE-SECA program to improve cathode activity by design.

FY 2010 Publications/Presentations

1. L. Yan, B. Kavaipatti, S. Wang, H. Du, and P. Salvador, "Electrical Conductivity Relaxation Study of Solid Oxide Fuel Cell Cathodes Using Epitaxial (001)-Oriented Strontium-Doped Lanthanum Manganite Thin Films," *Mat. Res. Soc. Symp. Proc.*, submitted (2010).

2. K. Katsiev, B. Yildiz, K.R. Balasubramaniam, and P.A. Salvador, "Electron Tunneling Characteristics on $La_{0.7}Sr_{0.3}MnO_3$ Thin-Film Surfaces at High Temperature," *Applied Physics Letters*, **95**(9), 092106 (2009). DOI: 10.1063/1.3204022.

3. Khabibulakh Katsiev, Bilge Yildiz, Balasubramaniam Kavaipatti, and Paul Salvador, "Electronic and Chemical State of $La_{0.7}Sr_{0.3}MnO_3$ and Dense Thin-Film Cathode Surfaces," *Meet. Abstr. - Electrochem. Soc.* **902** 1336 (2009).

4. "Thin-film Cathode Fabrication and Characterization," presented at the 10th Annual SECA Workshop, Pittsburgh, Pennsylvania, July 14–16, 2009.

5. "Experimental Investigations to Support Computational Modeling of SOFCs," presented at Pacific Northwest National Laboratory, Energy & Environment/Fluid and Computational Engineering Group, Richland, Washington, October 22, 2009.

6. "Correlations of Electronic and Chemical State on $La_{0.7}Sr_{0.3}MnO_3$ Dense Thin-Film Cathode Surfaces," presented by collaborators at 216th ECS Meeting, Vienna, Austria, October 6, 2009.

7. "Effects of Crystallographic Orientation on the Oxygen Exchange Rate of SOFC Cathode Thin Films," presented by student at MS&T 2009 Conference, Pittsburgh, Pennsylvania, October 27, 2009.

8. "In situ X-ray Characterization of Oxygen Reduction in $La_{0.6}Sr_{0.4}Co_{0.2}Fe_{0.8}O_{3-\delta}$ at Elevated Temperature and Variable Oxygen Partial Pressure," presented by collaborator at MRS Fall Meeting 2009, Boston, Massachusetts, November 30, 2009.

9. "Total Reflection Inelastic X-ray Scattering, a Direct Probe of Defect Chemistry in Thin Films," presented by collaborator at MRS Spring Meeting 2010, San Francisco, California, April, 2010.

10. "Investigation of High Temperature Catalytic Activity of Solid Oxide Fuel Cell Cathode Using Surface Engineered Thin Films," presented by student at MRS Spring Meeting 2010, San Francisco, California, April, 2010.

11. "Correlations of Structural, Chemical and Electronic State on $La_{0.8}Sr_{0.2}MnO_3$ Dense Thin-film Surfaces," presented by collaborator at MRS Spring Meeting 2010, San Francisco, California, April, 2010.

References

1. E. Maguire, B. Gharbage, and F.M.B. Marques, "Cathode Materials for Intermediate Temperature SOFCs," *Solid State Ionics* (2000).

2. N.Q. Minh (1995). Science and Technology of Ceramic Fuel Cells, Elsevier Science.

3. K.-C. Chang, B. Ingram, K.R. Balasubramaniam, B. Yildiz, D. Hennessy, P.A. Salvador, N. Leyarovska, and H. You, "In situ Synchrotron X-ray Studies of Dense Thin-film Strontium-doped Lanthanum Manganite Solid Oxide Fuel Cell Cathodes," *Mat. Res. Soc. Symp. Proc* **1126** 1126-S08-10.1-6 (2009).

4. T.T. Fister, D.D. Fong, J.A. Eastman, P.M. Baldo, M.J. Highland, P.H. Fuoss, K.R. Balasubramaniam, J.C. Meador, and P.A. Salvador, "In situ Characterization of Strontium Surface Segregation in Epitaxial $La_{0.7}Sr_{0.3}MnO_3$ Thin Films as a Function of Oxygen Partial Pressure," *Applied Physics Letters* **93** [15]151904 (2008).

5. P.A. Salvador, J. Meador, K.R. Balasubramaniam, P. Fuoss, J. Eastman, D. Fong, and P. Baldo, "SOFC Cathode Surface Chemistry and Optimization Studies," *FY 2007 Office of Fossil Energy Fuel Cell Program Annual Report,* U.S. Department of Energy Paper IV.A.4, 1-5 (2007).

6. P.A. Salvador, L. Yan, S. Wang, K.R. Balasubramaniam, P. Fuoss, J. Eastman, D. Fong, T. Fister, P. Baldo, H. You, K.-C. Chang, B. Yildiz, and I.B. Misirlioglu, "SOFC Cathode Chemistry and Optimization Studies," *FY 2008 Office of Fossil Energy Fuel Cell Program Annual Report,* U.S. Department of Energy Paper III.A.2, 1-5 (2008).

7. K. Katsiev, B. Yildiz, P.A. Salvador, and K.R. Balasubramaniam, "Electron Tunneling Characteristics on $La_{0.7}Sr_{0.3}MnO_3$ Thin-Film Surfaces at High Temperature," *Applied Physics Letters* (2009 in press).

8. J. Fleig, H. Kim, J. Jamnik, and J. Maier (2008). Oxygen Reduction Kinetics of Lanthanum Manganite (LSM) Model Cathodes: Partial Pressure Dependence and Rate-Limiting Steps. Fuel Cells. **8:** 330-337.

9. K.-C. Chang, B. Ingram, K.R. Balasubramaniam, B. Yildiz, D. Hennessy, P.A. Salvador, N. Leyarovska, and H. You, "In situ Synchrotron X-ray Studies of Dense Thin-film Strontium-doped Lanthanum Manganite Solid Oxide Fuel Cell Cathodes," *Mat. Res. Soc. Symp. Proc* (in press 2009).

10. P.A. Salvador, L. Yan, S. Wang, K.R. Balasubramaniam, P. Fuoss, J. Eastman, D. Fong, T. Fister, P. Baldo, H. You, K.-C. Chang, B. Yildiz, K. Katsiev, C. Heske, and S. Krause, "SOFC Cathode Surface Chemistry and Optimization Studies," *FY 2009 Office of Fossil Energy Fuel Cell Program*

Annual Report, U.S. Department of Energy Paper III.A.3, 1-6 (2009).

11. K. Katsiev, B. Yildiz, K.R. Balasubramaniam, and P.A. Salvador, "Electron Tunneling Characteristics on $La_{0.7}Sr_{0.3}MnO_3$ Thin-Film Surfaces at High Temperature," *Applied Physics Letters* **95** [9]092106 (2009).

12. K.-C. Chang, B. Ingram, K.R. Balasubramaniam, B. Yildiz, D. Hennessy, P.A. Salvador, N. Leyarovska, and H. You, "In situ Synchrotron X-ray Studies of Dense Thin-film Strontium-doped Lanthanum Manganite Solid Oxide Fuel Cell Cathodes," *Mat. Res. Soc. Symp. Proc.* **1126** 1126-S08-10 (2009).

13. P.A. Salvador, J. Meador, K.R. Balasubramaniam, P. Fuoss, J. Eastman, D. Fong, and P. Baldo, "SOFC Cathode Surface Chemistry and Optimization Studies," *FY 2007 Office of Fossil Energy Fuel Cell Program Annual Report*, U.S. Department of Energy Paper IV.A.4, 1-5 (2007).

14. L. Yan, B. Kavaipatti, S. Wang, H. Du, and P. Salvador, "Electrical Conductivity Relaxation Study of Solid Oxide Fuel Cell Cathodes Using Epitaxial (001)-Oriented Strontium-Doped Lanthanum Manganite Thin Films," *Mat. Res. Soc. Symp. Proc.* submitted (2010).

15. L. Yan, K.R. Balasubramaniam, S. Wang, H. Du, and P.A. Salvador, "Effects of Crystallographic Orientation on the Oxygen Exchange Rate of $La_{0.7}Sr_{0.3}MnO_3$ Thin Films," *Solid State Ionics* **submitted** (2010).

16. P.A. Salvador, L. Yan, S. Wang, K.R. Balasubramaniam, P. Fuoss, J. Eastman, D. Fong, T. Fister, P. Baldo, H. You, K.-C. Chang, B. Yildiz, and I.B. Misirlioglu, "SOFC Cathode Chemistry and Optimization Studies," *FY 2008 Office of Fossil Energy Fuel Cell Program Annual Report*, U.S. Department of Energy Paper III.A.2, 1-5 (2008).

17. J. Nowotny and I. Sikora, "Work Function Measurement of Nonstoichiometric Oxides at High-Temperatures," *Zeitschrift Fur Physikalische Chemie-Frankfurt* **107** [1]87-98 (1977).

18. T. Bak, J. Nowotny, M. Rekas, and C.C. Sorrell, "Diffusion-Controlled Work Function Changes of (La,Sr) MnO_3," *Solid State Ionics* **117** [1-2]157-160 (1999).

19. S.P.S. Badwal, T. Bak, S.P. Jiang, J. Love, J. Nowotny, M. Rekas, C.C. Sorrell, and E.R. Vanced, "Application of Work Function Measurements for Surface Monitoring of Oxide Electrode Materials (La,Sr)(Co,Mn,Fe)O_3," *Journal of Physics and Chemistry of Solids* **62** 723-729 (2001).

20. T. Bak, J. Nowotny, M. Rekas, and C.C. Sorrell, "Non-Stoichiometry, Fermi Energy and Work Function of (La,Sr) MnO_3. II. Verification of theoretical model," *Journal of Physics and Chemistry of Solids* **62** [4]737-742 (2001).

21. T. Bak, J. Nowotny, M. Rekas, and C.C. Sorrell, "Non-Stoichiometry, Fermi Energy and Work Function of (La,Sr) MnO_3. I. Theoretical model," *Journal of Physics and Chemistry of Solids* **62** [4]731-735 (2001).

22. T. Bak, J. Nowotny, M. Rekas, C.C. Sorrell, and E.R. Vance, "Surface Electrical Properties of (La,Sr) (Co,Fe,Mn)O_3," *Solid State Ionics* **135** 563-565 (2000).

23. C.C. Kan, H.H. Kan, F.M. Van Assche, E.N. Armstrong, and E.D. Wachsman, "Investigating Oxygen Surface Exchange Kinetics of $La_{0.8}Sr_{0.2}MnO_{3-delta}$ and $La_{0.6}Sr_{0.4}Co_{0.2}Fe_{0.8}O_{3-delta}$ Using an Isotopic Tracer," *J Electrochem Soc.* **155:** B985-B993 (2008).

III.A.4 First Principles Identification of New Cathode Electrocatalysts for Fuel Cells

James H. White
Eltron Research & Development, Inc.
4600 Nautilus Court South
Boulder, CO 80301-3241
Phone: (303) 530-0263, ext. 114
Fax: (303) 530-0264
E-mail: jwhite@eltronresearch.com

DOE Project Manager: Briggs White
Phone: (304) 285-5437
E-mail: Briggs.White@netl.doe.gov

Contract Number: SC0000872

Start Date: July 20, 2009
End Date: April 19, 2010

FY 2010 Objectives

- Build a model for oxygen electro-reduction at solid oxide fuel cell (SOFC) temperatures based on the previous literature. Identify level(s) of description to be employed or investigated. Identify mechanistic steps associated with that level.
- Identify data in Eltron's data and knowledge base for SOFC cathodes, ceramic mixed conducting membranes and reducing (air) side catalysts, and other high temperature applications. Perform a thorough literature search. Tabulate all data. Identify oxygen electro-reduction performance metric or metrics for metal oxide materials.
- Find literature values of descriptors or calculate descriptors using methods ranging from simple empirical relationships to quantum mechanical methods.
- Using Eltron and literature data, correlate descriptors and performance data.
- Predict descriptors and properties giving rise to high performance.
- Propose new materials possessing the above properties.
- Synthesize, characterize, and test new materials using temperature programmed desorption (TPD) of O_2.

Accomplishments

- Identified overall Phase I approach and conducted a literature search pertaining to the performance of SOFC cathodes. The level of description to be used was identified, simplifying assumptions made, and an initial model and model equations proposed.
- Identified model equations relating performance metric(s) to physicochemical descriptors for unary metal oxides. Identified expressions relating surface and bulk descriptors and unary metal oxide descriptors and multi-component metal oxide performance.
- Identified a pool of physicochemical descriptors and their sources. Down-selected descriptors on the basis of availability and/or calculability and relevance to reaction mechanism. Chose oxygen exchange rate as a performance metric. Correlations between descriptors and performance metric(s) developed.
- Comprised a training set using descriptors and associated performance metric (oxygen exchange rate). This set was used to train a generalized regression neural network (GRNN), which related the performance metric to the descriptors.
- Performance (surface oxygen exchange rate) of 14 unary metal oxides in addition to those in the training set were predicted using the artificial neural network (ANN) encoded mode.
- A training set for multicomponent metal oxides was comprised using data for unary metal oxides by expansion in multiplets of the unary metal oxide data. The ANN trained with this set was then used to predict new multicomponent metal oxide cathode materials. Compared with existing literature fuel cell performance to determine suitability.
- Tested TPD as an *ersatz* for oxygen exchange rate measurements using unary metal oxides.
- Synthesized predicted preferred multicomponent metal oxides. TPD spectra of these materials were obtained and correlation between predicted exchange rate and peak desorption temperature developed.
- Identified correlations between peak desorption temperature and the descriptors comprising the training set and between descriptors in the training set.
- Identified potentially valuable surface techniques for obtaining surface descriptors of value in predicting SOFC cathode performance.

Introduction

Eltron Research & Development is in Phase I of a three-phase project to develop new cathode electrocatalyst materials and methodologies for their selection. SOFC performance is limited by poor oxygen reduction kinetics. Thus, new cathode materials are needed. However, their identification is limited by the combinatorial nature of the problem, the narrow range of existing SOFC cathode compositions, and lack of a suitable approach for predicting the efficacy of cathode electrocatalyst candidates. The approach being followed is to identify a correlational model relating a cathode performance metric to various descriptors. The rate of oxygen exchange is related to surface (and atomistic) descriptors and the model applied using ANNs. This approach allows new areas of composition space to be searched using existing data.

Phase I consisted of identification of cathode performance metrics and material descriptors, development and demonstration of a correlational model for materials prediction, and experimental confirmation of predictions. Additionally, surface data relating to adsorption/desorption of oxygen on candidate materials was obtained.

Approach

The approach under development involves identification of a model which can predict potentially good cathode electrocatalyst formulations using existing experimental data for component unary metal oxides and the best set of such descriptors. The use of ANNs provides an input section, initial predictor of performance and properties of compositions selected, and a down-selection filter for more complete structure and properties prediction system to be developed in Phase II.

The model being developed relates physicochemical descriptors to cathode performance or to a metric proportional to it. Performance was fit to a function of the descriptors using an ANN, which can predict, classify, and cluster performance results. This approach allows for materials properties prediction and also enables prediction of material structure and structure-property relationships from the input of a proposed material composition. In order to implement this approach, the following general steps were taken: 1) Select or identify material descriptors. 2) Identify cathode performance descriptor(s). 3) Identify governing mathematical relationships between performance and descriptors. 4) Determine, obtain, or calculate material descriptors. 5) Survey existing data, including Eltron's and literature data. For the sake of accuracy, descriptor data was obtained from the literature. In some instances, simple formulas were used in calculating specific descriptors (e.g., cation polarizing power).

Reaction Mechanism. The mechanism employed was as described in Kinoshita [1]. This consists of the steps: 1) gas diffusion in electrode pores; 2) adsorption of O_2 on electrode surface; 3) surface diffusion of adsorbed O_2 to three phase boundary; 4) dissociation of adsorbed O_2; 5) diffusion of adsorbed oxygen atom to electrochemical reaction site; 6) electrochemical reaction of adsorbed oxygen; and 7) neutralization of electron holes.

Level of Description. The level of description invoked depended both on what was being sought in the model and on the assumptions made about the electrochemical system. Initially, the electrocatalyst attributes of the materials were sought. This was focused primarily on intrinsic activity and, thus, on microscopic aspects of the material. It was then necessary to have the ability to predict transport properties of the materials which required a hydrodynamic level.

Results

Model Equations. Mathematically the appropriate relationships were of the following form:

General cathode performance:

$$P = f(\chi_1, \chi_2, \chi_3, \cdots \chi_i) \quad (1)$$

where P = a cathode performance metric and $\chi_i = i$-th descriptor. The performance measure here would ideally be a direct measure of overall cathode activity. In the intrinsically kinetic limited regime, the cathode performance may be represented in the following form:

Cathode performance:

$$P_{kinetic} = f(\chi_{surf,1}, \chi_{surf,2}, \chi_{surf,3}, \cdots \chi_{surf,i}) \quad (2)$$

It must be true that:

$$\chi_{surf,i} = g(x_{bulk,i}) \quad (3)$$

i.e., that the surface descriptors possess some (albeit not necessarily known) functional relationship to bulk properties.

In addition to the cathode performance obtained under kinetic conditions, mass transport limited performance may also be expressed in the form:

$$P_{transport} = f(\chi_{bulk,1}, \chi_{bulk,2}, \chi_{bulk,3}, \cdots \chi_{bulk,i}) \quad (4)$$

Finally, the role of macroscopic features (e.g., porosity, electrode/electrolyte interface, current collector/cathode interface, grain size, etc.) and non-

idealities may be incorporated into a "form factor" expression:

$$FF = f(\text{macroscopic features, non-idealities, etc.}) \quad (5)$$

Material Descriptors. Descriptors were drawn from a number of properties categories but invariably bore a fundamental relationship to the intrinsic activities of electrocatalyst candidates. After searching the literature for measures of performance, the oxygen exchange rate, $r_{ox,exch}$, was chosen. Use of other, electrochemical figures of merit in an ANN-based model were quickly ruled out because of the absence of cathode-only data (i.e., data not convolved with non-cathode effects or phenomena) and because of the lack of an adequate database of material compositions.

The choice of material descriptors was based on a down-selection process utilizing a number of criteria (appropriateness, availability of experimental values, measurability, calculability, and availability of performance figures of merit for the material). The descriptor set actually chosen was selected from the mixture of surface and bulk descriptors. A key inclusion here was acid-base related variables (e.g., surface probe molecule vibrational frequencies and cation polarizing power) because of the acid-base characteristics of oxygen adsorption on metal oxides. The oxygen acts as a Lewis base in that unshared pairs of electrons interact with oxygen ion vacancies or with metal cations.

The Model. The model utilized the following assumptions: 1) oxygen electro-reduction is kinetically limited; 2) transferability of phenomena and descriptors from unary to multi-component metal oxides; 3) superposability: properties of multi-component metal oxides are functions of those of unary metal oxides; 4) active sites are coordinatively unsaturated; 5) electrode performance is a function of its structure and composition; 6) electrode performance descriptors relate to electrocatalyst structure and composition; 7) electrode performance can be expanded as a function of descriptors; 8) microscopic reversibility applies, i.e., the global O_2 reduction reaction is invariant under time reversal; and 9) there is a fundamental relationship between the rate of oxygen exchange at a cathode surface and the electro-reduction activity of the cathode material. The model was expressed as:

$$P = f(r_{ox\ exch,\ multiple}) \quad (6)$$

$$r_{ox\ exch,\ unary} = f(\chi_{bulk,1}, \chi_{bulk,2}, \chi_{bulk,3}, \cdots \chi_{bulk,i}) \quad (7)$$

$$r_{ox\ exch,\ multiple} = f(r_{ox\ exch,\ unary,1}, r_{ox\ exch,\ unary,2}, r_{ox\ exch,\ unary,3}, \ldots, r_{ox\ exch,\ unary,i}) \quad (8)$$

i.e., cathode performance is a function or functional of the oxygen exchange rate, which in turn can be expressed as a function of materials descriptors (even bulk descriptors), and finally, the exchange rate for the multiple component material is a function of that for unary oxides. The above model was encoded into an ANN in order to obtain its solution.

A total of 16 descriptors and their correlations with values of the oxygen exchange rate, $r_{O2,exch}$ were initially investigated. These consisted of ionization potential; work function; cation radius; cation-anion bond length; surface metal-oxygen bond energy; O1s binding energy; optical basicity; sanderson electronegativity; cation polarizability; polarizing power; C-O stretch in adsorbed CO; N-H stretch in adsorbed pyridine; N-H stretch in adsorbed NH_3; specific refractivity; molecular electronic polarizability; molecular electronic polarizability/molecular volume; and dielectric constant. Further down-selection of descriptors was obtained by considering the R^2 values for oxygen exchange rate versus each descriptor. Based on these correlations, descriptors were down-selected to eight. Additional values were obtained or added to the table after a number of iterations of the modeling process. This was further reduced to only three descriptors because of the limited number performance data points. The three descriptors chosen were the ionization potential of cations plus one electron (IP), the sum of cationic and oxygen anion radii ($r_M^+ + r_O^{2-}$), and the polarizing power of cations (PP = q/r). The descriptor/performance metric data constituted the basis of the training set for the ANN (package from Ward Systems, Inc.: Neuro Shell Predictor – a GRNN-based routine) model.

This data set were shown sufficient for training the ANN for predicting unary metal oxides. Multi-component metal oxides were more difficult to treat: transferability and superposability of descriptors as described above were invoked to model the complex metal oxide systems. Practically, this meant expanding the above data set to multiply the number of entries as well as number of descriptors. Data for component unary oxides were then entered into each field. The stoichiometric coefficients were given values of either 0 or 1 with the first indicating the absence of a component and 1 its presence. In this manner, the amount of data in the training set could be expanded and the training set applied to enable prediction of performance of multi-component metal oxides. ANNs were trained and tested using the data sets above. Physical descriptor data for unknowns was then presented to the ANN, resulting in a production set containing the sought predicted values.

Having built the model to be used and established correlations between descriptors and the performance metric (rate of oxygen exchange), the predictive power of the method was tested, first using unary metal oxides and then mixed metal oxides. Although the reliability of these predictions cannot be ascertained without experimental data, some of the predictions are quite reasonable. For example, silver oxide is anticipated to be the best of the unary materials predicted because of

the well known mobility of oxygen on silver and silver oxide and the thermal instability of the latter.

Use of an ANN trained on a multicomponent data set gave an R^2 of 0.95 with 16 neurons in the input layer and 82 in the hidden layers. Applying this to a rather lengthy list (82) of candidate multi-component oxide compositions resulted in a set of predictions for these compositions. The potential usefulness of the approach is indicated by consideration of the data presented in Table 1 which shows the best and worst compositions predicted.

TABLE 1. Summary of Predicted Materials Showing Best and Worst Variants

Existing Material	Log($r_{02,exch}$)	New Material	Log($r_{02,exch}$)
$Ba_{0.5}Sr_{0.5}Co_{0.2}Fe_{0.8}O_3$	1.75	$Ba_{0.5}Sr_{0.5}Co_{0.2}Cu_{0.8}O_3$	2.49
$LaMnO_3$	0.26	$Ce_{0.45}La_{0.05}Mn_{0.25}Cu_{0.25}O_2$	1.33
$(La_{0.8}Sr_{0.2})_{0.9}MnO_3$	1.14	$Fe_{0.6}Mn_{0.3}Cu_{0.1}O_{1.3}$	1.20
$La_{0.6}Sr_{0.4}Co_{0.2}Fe_{0.8}O_3$	1.11	$Sr_{1.4}La_{0.6}AlCuO_5$	1.07
$LaSrCo_2O_6$	1.00	–	–
$PrBaCo_2O_5$	0.99	–	–
$MgAl_2O_4$	-0.35	–	–
Y_2Zr_207	-1.30	–	–

These data show expected or intuitive trends. For example, the spinel $MgAl_2O_4$ and the pyrochlore $Y_2Zr_2O_7$ are anticipated to be very poor oxygen electrocatalysts, while the perovskites $Ba_{0.5}Sr_{0.5}Co_{0.2}Fe_{0.8}O_3$, $(La_{0.8}Sr_{0.2})_{0.9}MnO_3$, and $La_{0.6}Sr_{0.4}Co_{0.2}Fe_{0.8}O_3$ are known from the literature to be good cathode electrocatalysts. More importantly, the exchange rates for a number of new materials were also predicted. On the right hand (third and fourth columns) of Table 1, four materials displaying exchange rates comparable or better than existing materials are presented. All of these were ultimately synthesized and tested using TPD.

Measurement of oxygen thermal desorption spectra (TPD) of unary metal oxides as well as candidate cathode materials was performed because of the difficulty of performing electrochemical experiments or radioisotope exchange measurements during Phase I. TPD spectra were obtained. This consisted of heating a sample of material from 100 to 450°C or 100 to 550°C at a rate of 2°C/min. Data obtained for unary metal oxides is presented in Figure 1. These data show a significant correlation ($R^2 = 0.71$) between predicted oxygen exchange rate and the TPD surface oxygen peak. Similarly, plotting the same data for multi-component oxides versus TPD peak temperature gave the data shown in Figure 2.

This data is distinguished from that for the unary metal oxides in that the logarithmic shape of the curve is absent. Rather, more of a peaked dependence is in

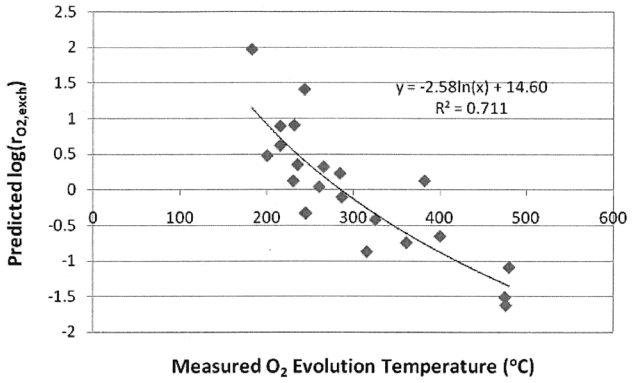

FIGURE 1. Predicted Normalized log($r_{02,exch.}$) for Unary Metal Oxides Versus Temperature of Peak Oxygen Desorption

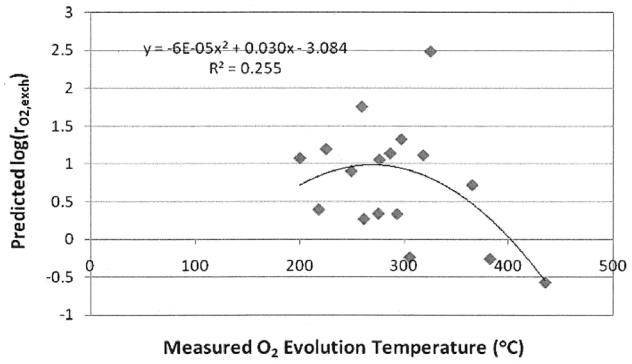

FIGURE 2. Predicted log($r_{02,exch}$) versus Measured Peak Desorption Temperature for MultiComponent Metal Oxides

evidence. Fitting to a parabolic function gave a non-zero and even significant correlation.

The oxygen exchange rate thus correlates well with surface oxygen evolution temperature for unary oxides, as shown in Figure 1, above. Correlations between TPD and other variables were considered in finally selecting descriptors. For example, peak temperature of surface oxygen desorption was correlated versus five descriptors as was O1s binding energy and the surface CO stretch frequency. In addition, correlation with a surface pyridine stretch was poor and while that with a bulk bandgap relied upon a complex fitting function. Identifying new descriptors for use in the ANN training required considerations of correlations between variables. Other data showed that, while there is weak correlation between bond length and ionization energy, cation polarizing power is strongly correlated with ionization energy and with bond length. Thus, when deciding on which descriptor for TPD peak to displace, polarizing power (PP) was selected because of its strong correlation with the other descriptors.

Replacing PP by the TPD peak temperature resulted in the ANN training giving predicted versus

actual $\log(r_{O_2,exch})$ with an R^2 value of 0.95 using a multicomponent training set analogous to that employed as above. However, use of this in predicting new materials was not attempted in Phase I.

Insofar as the prospects for the "new" materials on the right side of Table 1 are concerned, three of the four candidates ($Ce_{0.45}La_{0.05}Mn_{0.25}Cu_{0.25}O_2$, $Fe_{0.6}Mn_{0.3}Cu_{0.1}O_{1.3}$, and $Sr_{1.4}La_{0.6}AlCuO_5$) have been utilized by Eltron for other applications (de-volatile organic compound catalysis, chemical looping combustion carrier, and direct decomposition de-NOx catalysis) and have shown requisite stabilities for those applications. That all have performed very well in their respective capacities is a strong indication that they will be useful in cathode electrocatalysis as well since those applications all rely on fast and facile oxygen exchange chemistry. The remaining candidate ($Ba_{0.5}Sr_{0.5}Co_{0.2}Cu_{0.8}O_3$) [2] is anticipated to have exceptional electroreduction activity, as it is the copper analog of $Ba_{0.5}Sr_{0.5}Co_{0.2}Cu_{0.8}O_3$ which has been demonstrated to be an extremely active cathode material. However, neither of these materials should tolerate atmospheric CO_2 well and their stability properties are not fully defined.

Techniques for obtaining surface descriptors are summarized in Table 2. Descriptions of the techniques in relation to metal oxide surfaces can be found in a number of sources, especially Henrich and Cox [3], Fierro [4], and Woodruff [5].

TABLE 2. Summary of Surface Descriptors Identified in Phase I

Descriptor	Symbol	Surface Technique(s)
Work Function	φ	PES, Kelvin probe
Cation radius + O^{2-} radius	$r_M^{n+} + r_O^{2-}$	SEXAFS (also gives cation coordination number)
Surface metal-oxygen bond energy	$E_{MO,surf}$	TPD
O1s binding energy	$BE\ O1s$	XPS
C-O stretch in CO	υ_{CO}	Surface IR
N-H stretch in pyridine	υ_{Pyr}	Surface IR
N-H stretch in ammonia	υ_{NH}	Surface IR
Band gap	ΔU_g	UPS
Electron Density of States	$g(E)$	UPS
Surface vacancy concentration	$C_{vac,surf}$	Surface conductivity

PES = Photoemission spectroscopy
SEXAFS = Surface extended X-ray absorption fine structure
TPD = Temperature programmed desorption
XPS = X-ray photoelectron spectroscopy
IR = Infrared
UPS = Ultraviolet photoelectron spectroscopy

Conclusions and Future Directions

The key objectives of the Phase I were met. Specifically, a model correlating performance figures of merit with material physicochemical variables was built, the model was encoded in an ANN, and new cathode materials predicted using the model. Experimental verification of the approach was obtained using TPD.

Future work will consist of expanding the descriptor and cathode performance database by synthesizing and characterizing cathode candidates, further refinement of the model developed, and by incorporating preferred candidates into SOFCs.

References

1. K. Kinoshita, "Electrochemical Oxygen Technology," Wiley, New York, p. 73 (1992).

2. X. Sun, S. Li, J. Sun, X. Liu, and B. Zhu, Int. J. Electrochem. Sci., 2, 462 (2007).

3. V.E. Henrich and P.A. Cox, "The Surface Science of Metal Oxides," Cambridge, Cambridge, 1994.

4. (a) B.M. Reddy, in "Metal Oxides: Chemistry and Applications," J.L.G. Fierro, Taylor and Francis, Boca Raton, p. 215 (2006). (b) G.J. Hutchings and M.S. Scurrell, CATTECH, 7, 90 (2003).

5. D.P. Woodruff, "Oxide Surfaces (The Chemical Physics of Solid Surfaces)," Elsevier Science, 2001.

III.A.5 Theory, Investigation and Stability of Cathode Electro-Catalytic Activity

Meilin Liu (Primary Contact), Wentao Qin, Mingfei Liu, Matt Lynch, Jongjin Choi, Lifang Nie
Georgia Institute of Technology
School of Materials Science and Engineering
771 Ferst Drive
Atlanta, GA 30332-0245
Phone: (404) 894-6114; Fax: (404) 894-9140
E-mail: meilin.liu@mse.gatech.edu

DOE Project Manager: Briggs White
Phone: (304) 285-5437
E-mail: Briggs.White@netl.doe.gov

Contract Number: NT0006557

Start Date: September 1, 2008
End Date: August 31, 2011

FY 2010 Objectives

- Characterize the surface composition, morphology, and electro-catalytic properties of a catalyst infiltrated $La_{0.6}Sr_{0.4}Co_{0.2}Fe_{0.8}O_{3-\delta}$ (LSCF) cathode.
- Establish the scientific basis for rational design of high-performance cathodes by combining a porous backbone (such as LSCF) with a thin catalyst coating.

Accomplishments

- Developed a general and empirical method for designing thin-film test cells based on continuum modeling.
- Optimized a sol-gel process for fabrication of $La_xSr_{1-x}MnO_{3-\delta}$ (LSM) coating on LSCF pellets and porous LSCF cathodes.
- Demonstrated that the performance and stability of LSCF cathodes can be improved with a thin film coating of a suitable catalyst (e.g., LSM, $Sm_{0.2}Ce_{0.8}O_{1.95-\delta}$ [SDC], and $La_{1.95}Ca_{0.05}Ce_2O_{7-\delta}$ [LCC]) and evaluated possible sources of improvement using micro-kinetic modeling.
- Characterized the detailed structure, composition, and morphology of LSM and LSCF surfaces and the LSM/LSCF interfaces prepared under different conditions: (i) as prepared, (ii) after annealing at 850°C for more than 900 hrs, and (iii) under conditions similar to fuel cell operation (active direct current polarization).
- Demonstrated that a thin-film LSM coating on an LSCF substrate is stable at 850°C for more than 900 hrs.
- Demonstrated that the interfacial polarization resistance and activation energy of an LSCF cathode can be significantly reduced with infiltration of SDC.

Introduction

One of the reasons that LSCF-based cathodes show much better performance than those based on LSM is that LSCF has much higher ionic and electronic conductivity than LSM, significantly extending the active sites beyond the triple-phase boundaries [1]. One obvious downfall for LSCF is that it reacts adversely with yttria-stabilized zirconia (YSZ), which can be mitigated by the use of a buffer layer of doped-CeO_2 between LSCF and YSZ [2]. However, the catalytic activity of the stand-alone LSCF cathodes is likely to be limited by the surface catalytic properties. Further, the long-term stability of LSCF cathodes is a concern. Thus, it is hypothesized that the *performance* and *stability* of a porous LSCF cathode may be improved by the application of a catalytically active coating through infiltration. The selection of the catalytic materials as well as the detailed microstructures of the porous LSCF and the catalyst layer may critically impact the performance of the proposed cathodes. The objective of this project is to optimize the composition and morphology of the catalyst layer and microstructure of the LSCF backbone for better performance.

Approach

LSM films were prepared using several fabrication techniques. Sputtering was used to fabricate test cells for fundamental study of the LSM electrode; a sol-gel process was used for deposition of LSM films on LSCF pellets to examine the microstructure evolution during annealing at high temperatures with and without cathodic polarization. Further, the sol-gel process is also used to produce a thin-film LSM coating on porous LSCF electrodes through infiltration [3]. A general and empirical method based on continuum modeling was developed for designing thin film test cells and for interpretation of electrochemical testing results. The effect of LSM, SDC, and LCC coatings on LSCF cathodes performance were determined using symmetric and anode-supported button cells. The detailed structure, composition, and morphology of the LSM

surface, the LSCF surface, and the LSM/LSCF interfaces in LSM-infiltrated LSCF cathodes were characterized using scanning and transmission electron microscopy (SEM and TEM) and spectroscopy. The microscopic details of the cathodes are also to be correlated directly with their electrochemical performance.

Results

A General and Empirical Method for Designing Test Cells

We have developed a model for evaluation of the sheet resistance in thin film working electrodes for the exploration of fundamental properties of the mixed ionic electronic conductor of interest. Figure 1(a) shows the alternating current solution of a distribution of resistor-capacitor parallel circuits over the surface of the film, solved for with different film conductance (the product of the film thickness t_m and the conductivity σ). At low film conductance, an extraneous high-frequency feature appears in the impedance concomitant with an increase in the overall zero-frequency total resistance. This effect is detrimental and it must be avoided, and the only way to do that is to design test cells properly to limit sheet resistance. The empirical model was used to do that. Figure 1(b) shows a selection chart plotting the contour of the logarithm of the critical current collector spacing (in microns) for a particular current collector configuration leading to no more than a 0.5% increase in the total resistance as a function of the polarization resistance and film conductance. Such plots allow the determination of constraints upon a current collector in order to limit sheet resistance in a film. The ability to design and fabricate test cells with good thin-film working electrode of acceptable sheet resistance is vital to evaluating the fundamental properties of LSCF and LSM films.

LSM Coating on Porous LSCF Cathode

In order to better control the infiltration process, a water-free sol-gel infiltration process was developed. This new approach uses 2-methoxyethanol and acetic acid to replace water as solvents, and strontium acetate and manganese acetate as metal organic precursors to replace nitrate precursors. The water-free LSM sol showed improved wettability on the LSCF surface. We have successfully fabricated dense LSM films with desired structure, composition, morphology, and thickness on the LSCF surface.

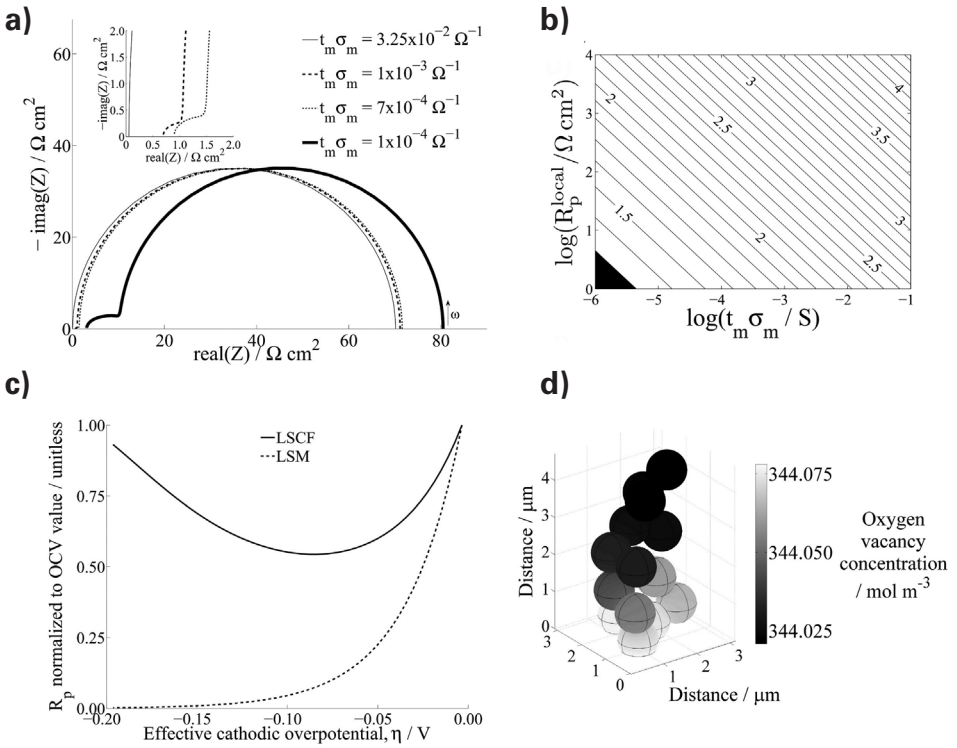

FIGURE 1. Key continuum modeling results: (a) Impedance response for different film conductance simulated using the empirical sheet resistance model for a simple resistor-capacitor circuit distributed over the film. (b) Generated charts for selecting the maximum current collector spacing for a discrete-contact current collector arrangement. (c) Polarization resistance of LSM and LSCF normalized to the open circuit voltage (OCV) value simulated using the micro-kinetic model. (d) Oxygen vacancy distribution in the porous representation of LSCF.

Interface Study of LSM/LSCF

Water-free sol-gel LSM was spin-coated on an LSCF pellet, producing an LSM film with thickness ranging from 42 nm to 50 nm. Compositions of the derived LSM films were determined to be $La_{16.0}Sr_{4.1}Mn_{20}$, which yields an A/B ratio of ~1.0. The sol-gel LSM on LSCF pellet was subsequently annealed at 850°C for 900 hours. Figures 2 (a) and (b) present a TEM and Z-contrast images of the film, respectively. The film thickness is 48 nm and comparable to that before annealing. The observation is critical as it pertains to mass-stability of the LSM. Nonetheless, the LSM film has lost long range order of atomic arrangement, as indicated by the electron diffraction pattern shown in Figure 2 (c), except at its bottom portion up to about 10 nm thick. Surface of the crystalline phase of LSM is outlined by the yellow dashed curve in Figure 2 (d), and the interface by the orange dashed line. Structure coherence of perovskite lattices of both phases are maintained, which is demonstrated in Figures 2 (e) and (f). Profiles of elemental concentration and atomic percent, presented in Figure 2(g) and (h), show the concentration of Co is nearly constant within the bottom portion of the LSM film and tapers off near the film surface. The fastest Co diffusion observed is consistent with the high Co diffusion rate in LSM. In neither the as-deposited nor the annealed LSM is the surface Sr-enrichment seen. The Sr-enrichment has been widely accepted as the major cause of LSCF cathodes' instability and performance degradation [4]. The Sr profiles presented in Figures 2 (g) and (h) suggest the LSM coating has prevented the Sr-enrichment which may be associated with the stability improvement of the LSCF cathode.

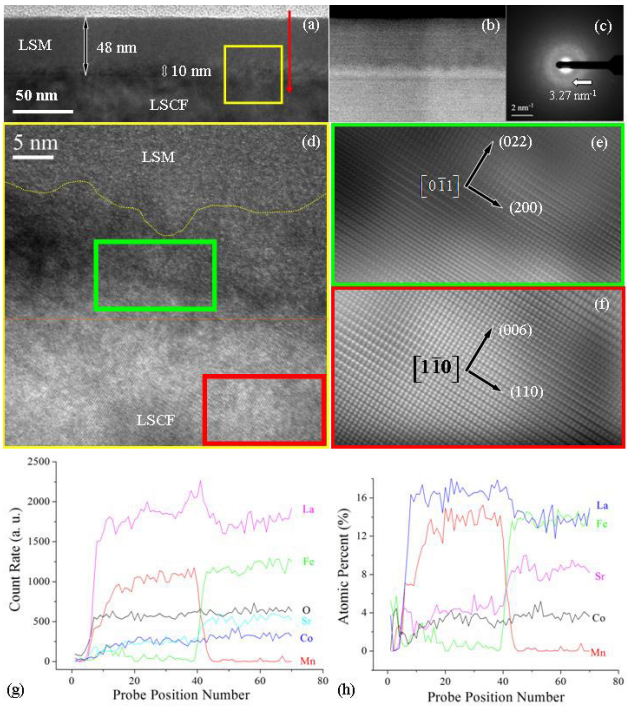

FIGURE 2. Microanalysis of LSM films derived from a sol-gel process on LSCF pellets after annealing at 850ºC at 900 hours. (a) TEM image. The yellow square marks an area along the LSM/LSCF interface and whose magnified view is presented in (d). The red and single-headed arrow illustrates the profile line associated with profiles presented in (g) and (h). (b) Z-contrast image. (c) Electron diffraction from the top amorphous portion of the LSM layer. The green and red rectangles in (d) illustrate areas whose Fourier-filtered images are presented in (e) and (f), respectively. The yellow dashed curve and the orange dashed line in (d) mark the termination of LSM zone-axis fringes, and the approximate LSM/LSCF interface, respectively. (g) profile of energy dispersive X-ray spectroscopy (EDS) count rate and (h) profile of atomic percent.

Figure 3 (a) is a TEM image of an LSCF grain in the LSM-infiltrated cathode subjected to 900 hours of operation. Presented in Figure 4 (a) are some typical performances of the cells with LSCF cathodes (with and without LSM modification). The LSCF grain maintains the perovskite structure, as revealed by its lattice fringes deep in the bulk and at the edge of the LSCF grain in Figures 3 (a)-(e). The surface layer contains all the cations of LSCF and LSM, and lacks long range order of atomic arrangement as shown in the electron diffraction pattern presented in Figure 3 (f). Thickness of the surface layer ranges from 2 to 23 nm as shown in Figure 3 (a). Profiles of elemental concentration and atomic percent are presented in Figure 3 (g) to (j), which shows peaks of Mn at the grain boundary and the grain surface. The profiles similarly do not show any surface-enrichment of Sr.

TEM observations suggest that the thickness of the LSM films derived from a sol-gel process on an LSCF pellet was largely preserved during annealing at 850ºC for 900 hours. However, it appears that Mn migration along the LSCF grain surface, combined with evolution of LSM on the LSCF grain, led to the formation of a thin layer of LSM that contained some Co. The degree of regularity of atom arrangement is also reduced (from long to short range order), which favors oxygen ion conductivity. On the other hand, the thickness of the LSM layer is very small, ranging from 2 to 23 nm. The small thickness is expected to ease transport of the oxygen ions to the LSCF.

Cathode Performance and Stability Improvements by LSM Coating on LSCF Surface

To demonstrate the performance and stability improvements induced by LSM infiltration, long-term tests have been performed with anode-supported cells. Shown in Figure 4 (a) are the current densities of a cell with a blank LSCF cathode and two cells with LSM-coated LSCF cathode tested at 750°C for about 900 hours at a constant voltage of 0.7 V. The LSM coatings were fabricated with two techniques: solution infiltration and gas phase deposition. The performance improvement was immediate for the

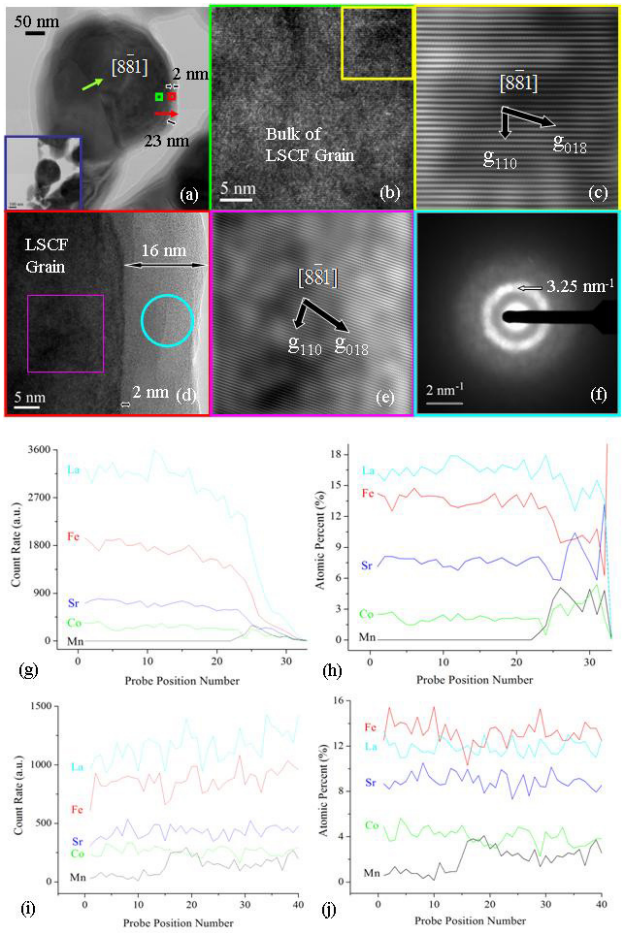

FIGURE 3. Microanalysis of porous LSCF cathode infiltrated with LSM after operation (under a constant cell voltage of 0.7 V) at 750°C for 900 hours. (a) TEM images of LSCF grain in the porous cathode infiltrated with water-based LSM solution and after 900 hours of operation at 750ºC. The color squares mark areas that were zoomed in and are displayed in (b) to (f). The color arrows denote profile lines. The inset provides a lower magnification image of the LSCF grain. (b) High resolution TEM image of the LSCF grain within the green square in (a). (c) Fourier-filtered image of the yellow square in (b). (d) High resolution TEM image of surface of the LSCF grain within the red square in (a). (e) Fourier-filtered image of the magenta square in (d). (f) Convergent beam electron diffraction from surface layer within the blue circle in (d). EDS profiles of count rates and atomic percents for the red (g) and (h), and yellow (i) and (j), profile lines marked in (a). The atomic percents were acquired based on standard-less quantification, and normalization of total percentage of metallic elements to 40%.

LSCF cathode modified by gas phase deposition, but delayed for about 100 hours for the one modified with infiltration. This delay and the subsequent increase in performance are attributed to the activation of LSM under cathodic polarization. However, performance and stability improvements have been observed for both modifications, indicating that the LSM coatings on LSCF cathode surfaces have improved the performance and stability of the LSCF cathodes.

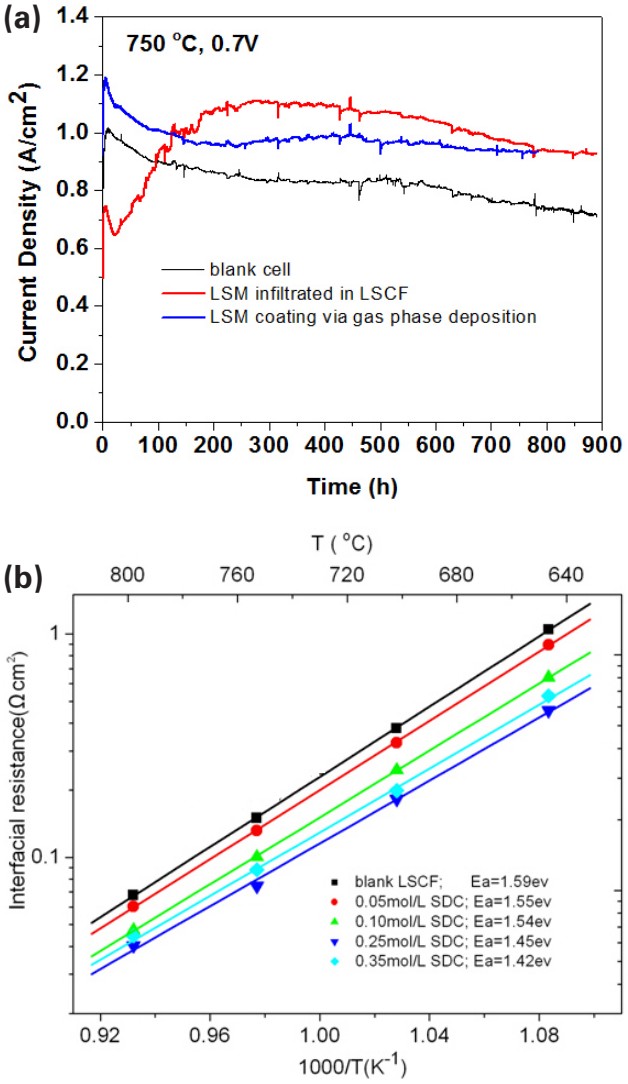

FIGURE 4. (a) Current densities of cells with blank and LSM-coated LSCF cathodes as measured at 750°C under a constant cell voltage of 0.7 V. Humidified hydrogen was used as fuel and stationary air as oxidant. (b) Interfacial polarization resistances and activation energies of blank and SDC-infiltrated LSCF cathodes.

A possible explanation for the kinetic response of uncoated and LSM-coated LSCF under cathodic polarization lies in the solid-state defect chemistry of the two materials. Figure 1 (c) shows the simulated response of the polarization resistance of LSCF and LSM under bias, normalized to the OCV value, and generated using a micro-kinetic modeling technique that links steady-state defect concentrations to oxygen reduction rate on the surface assuming no bulk transport losses. In this particular simulation, the oxygen reduction rate is set to be directly proportional to the steady-state surface oxygen vacancy concentration to the value at equilibrium. The trend of LSCF polarization resistance has reasonable qualitative agreement with experimental data for uncoated (blank) LSCF films.

The trend for LSM is suggestive of the experimental observation of the LSM-coated LSCF thin-film working electrode: the polarization resistance drops very quickly with increasingly negative cathodic overpotential compared to LSCF and does not increase once large cathodic overpotentials are reached. A surface with an LSM coating therefore may have a larger polarization resistance under OCV but be more highly activated under bias resulting in a lower net polarization resistance at operating voltage. This micro-kinetic technique along with consideration of transport can also be applied onto porous microstructures. Figure 1 (d) shows the solution for the distribution of oxygen vacancies under a small cathodic bias in a porous LSCF structure. Such simulations can be used to better understand the response of porous electrodes, connect experimental results of LSM-infiltrated cathodes to theory, and to help design novel porous structures.

Exploration of $Sm_{0.2}Ce_{0.8}O_{1.95-\delta}$(SDC) as a Catalyst Material

The main objective of the project is to develop a catalytically active coating onto the LSCF backbone to improve the performance and stability of a porous LSCF cathode. A new catalyst material of SDC has been developed. Presented in Figure 4 (b) are the polarization resistances for a blank LSCF cathode and for SDC infiltrated LSCF cathodes as measured using impedance spectroscopy at 650-800°C under open circuit conditions. Clearly, the electrode polarization resistances were significantly reduced with increasing the loading of SDC coating on LSCF surface, reaching the lowest polarization resistances of 0.074 and 0.44 Ω cm^2 at 750°C and 650°C, respectively, when 0.25 mol L^{-1} SDC solution was used for infiltration. These numbers are about half of those for a blank LSCF cathode without SDC infiltration measured under the same conditions. However, further increase of the concentration to 0.35 mol L^{-1} resulted in higher polarization resistance. It is believed that excess SDC may degrade the charge transfer processes along the surface and across the interfaces; it may reduce the cathode porosity and block the gas transports. It is also noted that the blank LSCF cathode had the highest activation energies among all the electrodes, similar to those reported in the literature [5]. However, the activation energies for the SDC-infiltrated LSCF were reduced slightly, suggesting that the O_2 reduction on the cathode surface was enhanced by the SDC coating on LSCF surface.

Conclusions

An electrochemical model for design of test cells has been developed for the exploration of fundamental properties of electrode materials. We have also developed a sol-gel infiltration process for successful fabrication of dense LSM films with desired structure, composition, morphology, and thickness on LSCF surface. The ability to design and fabricate test cells with good thin-film working electrode of acceptable sheet resistance is vital to evaluating the fundamental properties of LSCF and LSM films. It is also demonstrated that the stability and performance of an LSCF cathode can be improved by the introduction of a thin-film catalyst (e.g., LSM and SDC) though an infiltration process. Electron microscopy revealed that Mn is distributed along LSCF grain boundaries and on the exposed LSCF grain surface. However, a thin film of LSM coating on LSCF seems to be stable after annealing at 850°C for 900 hours of operation. Further, there was no evidence to suggest that Sr has enriched near LSCF surface covered by LSM. The observed improvements in performance and stability of LSM infiltrated LSCF may be attributed to the microscopic features: a stable and uniform LSM film on LSCF.

Patents Issued

1. Meilin Liu, Ze Liu, Mingfei Liu, Lifang Nie, David Spencer Mebane, Lane Wilson, and Wayne Surdoval, "Solid oxide fuel cells having porous cathodes infiltrated with oxygen-reducing catalysts." United States Application No. 12/837,757, July 2010.

FY 2010 Publications/Presentations

1. L.F. Nie, M.F. Liu, Y.J. Zhang, and M. Liu, "$La_{0.6}Sr_{0.4}Co_{0.2}Fe_{0.8}O_{3-\delta}$ Cathodes Infiltrated with Samarium-Doped Cerium Oxide for Solid Oxide Fuel Cells," *Journal of Power Sources*, 195(15), 4704-4708, 2010.

2. M. Lynch and M. Liu, "Investigation of Sheet Resistance in Thin-Film Mixed-Conducting Solid Oxide Fuel Cell Cathode Test Cells," *Journal of Power Sources*, 195(16), 5155-5166, 2010.

3. M. Lynch, D. Mebane, and M. Liu, "Numerical Continuum Modeling and Simulation of Mixed-Conducting Thin-Film and Patterned Electrodes," *Ceramic Engineering and Science Proceedings* (Advances in Solid Oxide Fuel Cells V), 2009, 129-136.

4. M.E. Lynch, X. Li, L. Yang, D. Mebane, and M. Liu, "Investigation of SOFC Cathode Kinetics by Means of Continuum Modeling and Well-Defined Electrodes," 217th Meeting of The Electrochemical Society, Vancouver, British Columbia, Canada, April 2010.

5. X.X. Li, M.E. Lynch, M.F. Liu, X.Y. Lou, and M. Liu, "Investigating Catalytic Properties of Cathode Materials Using Patterned Electrodes," 217th Meeting of The Electrochemical Society, Vancouver, British Columbia, Canada, April 2010.

6. M.E. Lynch, D.S. Mebane, Y.M. Choi, and M. Liu, "Numerical Continuum Modeling of Thin Film Solid Oxide Fuel Cell Cathode Materials," (invited) International Center for Materials Research Workshop on Modeling of Fuel Cell Electrocatalysts, Santa Barbara, California, USA, July 2009.

References

1. S.P. Jiang, "A Comparison of O-2 Reduction Reactions on Porous (La,Sr)MnO_3 and (La,Sr)(Co,Fe)O-3 Electrodes," *Solid State Ionics*, 146(1-2): p. 1-22, 2002.

2. D. Stover, H.P. Buchkremer, and S. Uhlenbruck, "Processing and Properties of the Ceramic Conductive Multilayer Device Solid Oxide Fuel Cell (SOFC)," *Ceramics International* 30, 1107-1113, 2004.

3. T.Z. Sholklapper, C. Lu, C.P. Jacobson, S.J. Visco, and L.C. De Jonghe, "LSM-Infiltrated Solid Oxide Fuel Cell Cathodes," *Electrochemical and Solid-State Letters*, 9(8):A376–A378, 2006.

4. S.P. Simner, M.D. Anderson, M.H. Engelhard, and J.W. Stevenson, "Degradation Mechanisms of La-Sr-Co-Fe-O_3 SOFC Cathodes," *Electrochemical and Solid State Letters*, 9(10): p. A478-A481, 2006.

5. S. Bebelis, et al., "Electrochemical Characterization of Perovskite-Based SOFC Cathodes," *Journal of Applied Electrochemistry*, 37(1): p. 15-20, 2007.

III.A.6 Catalyst Infiltration in Support of Anode Support Cell Development

Lutgard DeJonghe (Primary Contact),
Michael C. Tucker, Lei Cheng
Lawrence Berkeley National Laboratory (LBNL)
MS 62-203
1 Cyclotron Rd.
Berkeley, CA 94720
Phone: (510) 486-6138; Fax: (510) 486-4881
E-mail: lcdejonghe@lbl.gov

DOE Project Manager: Joseph Stoffa
Phone: (304) 285-0285
E-mail: Joseph.Stoffa@netl.doe.gov

Contract Number: MSD-NETL-01

Start Date: October 1, 2009
End Date: September 30, 2010

FY 2010 Objectives

- Quantify performance of commercially-available lab-scale fuel cells.
- Identify and develop candidate materials, architectures and concepts to solve issues related to delamination and degradation of cathode contact material.
- Target high-risk/high-benefit strategies and novel technical approaches.

Accomplishments

- Assessed baseline performance of lab-scale cells from Ningbo Institute of Material Technology and Engineering (NIMTE), using hydrogen fuel and coal gas with 0-55 ppm H_2S. Fabricated test rig enabling suitable steam-to-carbon ratio to prevent coking in gas inlet manifold.
- Screened a long list of candidate cathode materials for suitability as cathode contact pastes. Determined conductivity, sintering behavior, coefficient of thermal expansion (CTE), reactivity with lanthanum strontium cobaltite ferrite (LSCF) and $MnCo_2O_4$ (MCO) neighbor materials and bonding.
- Determined area specific resistance (ASR) of most promising candidates at 800°C for 200 h.
- Identified novel cathode contact schemes and materials. Determined feasibility of novel approaches, and selected most promising candidates for further development.

Introduction

The main focus of the LBNL project is to support industrial Solid State Energy Conversion Alliance (SECA) teams in their effort to commercialize solid oxide fuel cell (SOFC) technology that meets the SECA performance and cost targets. In order to achieve this goal, it is necessary to improve the performance of SOFC components through selection of appropriate materials and development of novel yet inexpensive alternative materials, architectures and concepts. The primary challenge addressed by LBNL during Fiscal Year 2010 concerns electrical connection and bonding between the interconnect and cathode layers, shown in Figure 1. Historically, cathode materials such as lanthanum strontium manganite are used as a cathode contact material (CCM) paste to bond the cell to the interconnect. High temperature is typically required to achieve good bonding, however, leading to rapid oxidation of the stainless steel interconnect. If a temperature low enough to avoid oxidation of the steel (<1,000°C) during the bonding step is employed, poor bonding and eventual delamination of the contact material occur. The goals of the work at LBNL are to: (a) screen known candidate cathode materials to ascertain whether they can be used as CCMs displaying adequate properties after bonding at <1,000°C; and (b) identify and develop novel materials, architectures, and approaches to solving this issue.

Approach

Accordingly, in FY 2010 the LBNL core effort has been focused on the following issues:

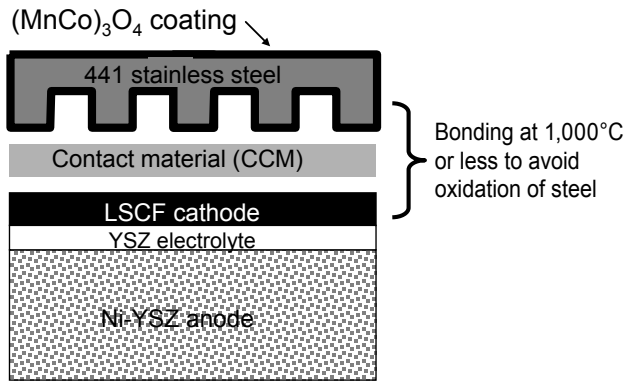

FIGURE 1. Schematic of CCM Placement in Cell Stack

- Identification of cathode materials from the existing literature that offer promise as candidate cathode-interconnect contact materials.
- Synthesis and characterization of candidate materials, including determination of sintering behavior, conductivity, bonding, CTE, and reaction with neighbor materials.
- Down-selection of the most promising candidates, and determination of the long-term stability of their ASR in relevant test geometries using model cathode and interconnect layers.
- Demonstration of the best materials in lab-scale cells operating under realistic conditions.
- Novel materials and architectures have also been pursued, wherein the bonding and electronic connection functions of the CCM material are separated, and composite materials are used to provide the dual functionality.

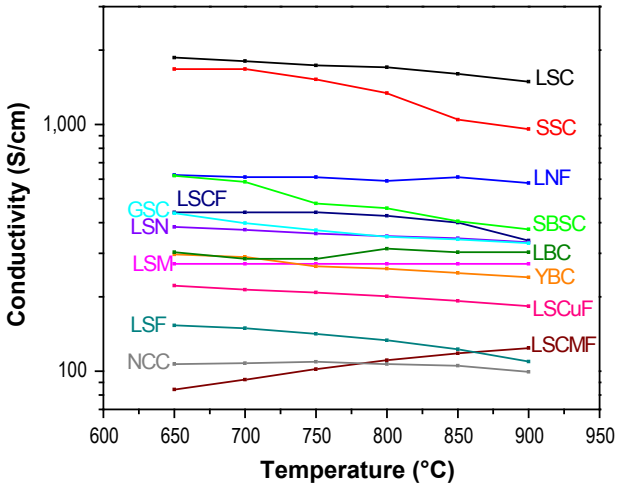

FIGURE 2. Conductivity of Various CCM Compositions

Results

Testing of Commercially-Available Cells

To expedite development of CCM materials, a low-cost commercially-available lab-scale cell with reproducible performance and stability would be very helpful. Quotes for 1-1.5" diameter button cells were obtained from various manufacturers. By far, the most reasonably priced were obtained from NIMTE in China. Several cells were tested with hydrogen and coal gas as fuel. The cells provided about 450 mW/cm^2 at 800ºC. Although the degradation rate was high (up to 40%/1,000 h), degradation was linear. The performance of the cells was not close to state-of-the-art, but they are suitable for use in seal, CCM, interconnect, and other short-term studies that don't require high power density.

Screening of Candidate CCM Materials

Table 1 lists the cathode compositions that were identified as candidates for application as CCM materials. The compositions were purchased from Praxair or fabricated by glycine-nitrate process (GNP). The properties of primary relevance, including conductivity, sintering behavior, CTE, and reactivity with MCO and LSCF were then determined.

The primary functions of the CCM are bonding and electrical connection. Therefore, sintering and conductivity were the first properties to be assessed. Conductivity was determined for fully-sintered bars of the CCM materials over the range 650-900ºC. The results are shown in Figure 2. Strontium samarium cobaltite (SSC) and lanthanum strontium chromite (LSC) displayed the highest conductivities. Sintering behavior was determined using dilatometry. It is expected that the cell-to-interconnect bonding step will occur at 900-1,000ºC to avoid excessive oxidation of the stainless steel. Therefore, the shrinkage observed at these temperature points is reported in Table 1. LSCF and lanthanum strontium copper ferrite (LSCuF) provided the highest extent of sintering.

CTE for the compositions was determined using a dilatometer, and is reported in Table 1. Although there was a very wide range of values, it is expected that the effect of high CTE can be mitigated by geometrically optimized cell and stack design or by addition of low-CTE filler materials to the CCM layer. Therefore, otherwise promising compositions were not ruled out solely on the basis of high CTE.

In the fuel cell stack, the CCM layer is in contact with the LSCF cathode and MCO coating on the stainless steel interconnect. Therefore, it is important to characterize the extent of reaction expected between these materials. Pellets of mixed CCM/LSCF or CCM/MCO were prepared and reacted in air for 120 h at 800ºC (to mimic operation conditions) and 10 h at 1,000ºC (to mimic bonding step conditions). X-ray diffraction was used to determine the extent of reaction, which is summarized in Table 1.

The summary of this screening effort suggested that the most promising CCM candidates are LSCF and LSCuF (chosen for extensive sintering at low temperature) and SSC and LSC (chosen for high conductivity).

These four materials were then incorporated into ASR specimens in which electrical resistance of the LSCF/CCM/MCO junction was monitored over time. Figure 3 shows a schematic of the sample geometry. Figure 4 shows the ASR as a function of time. LSC and LSCuF provided low and stable ASR for 200 h at 800°C. LSCuF survived five thermal cycles at 10°C/min.

TABLE 1. Candidate CCM Compositions and Summarized Results of Screening Tests

						Reacts with MnCo?		Reacts with LSCF?		
		Incipient Sintering Point (°C)	Shrinkage at 900°C	Shrinkage at 1000°C	CTE at 800°C	800°C 150h	1000°C 10h	800°C 150h	1000°C 10h	Conductivity of bulk dense pellet 800°C (S/cm)
La0.6Sr0.4Co0.8Fe0.2	LSCF	637	2.7	**7.6**	17.3	NO	NO	N/A	N/A	426
La0.8Sr0.2Cu0.9Fe0.1O2.5	LSCuF	820	1.1	**10.1**	15.5	NO	NO	NO	NO	201
La0.7Sr0.3CoO3	LSC	677	1.1	3.3	18.7	NO	NO	Minor	Minor	**1702**
Sm0.5Sr0.5CoO3	SSC	740	0.5	2.3	22	NO	Trace	NO	NO	**1338**
SmBa0.5Sr0.5Co2O5	SBSC	708	1.6	3.4	22	NO	Trace	YES	YES	458
GdSrCo2O5	GSC	760	1.3	3.2	19.5	NO	Trace	YES	YES	350
La0.65Sr0.30MnO3	LSM	784	0.7	3.3	12.8	NO	NO	YES	YES	272
LaBaCo2O5	LBC	770	0.7	2.3	25	NO	NO	Minor	Minor	314
YBaCo2O5	YBC	689	1.7	3.8	16.8	NO	YES	YES	YES	260
Nd1.8Ce0.2CuO4	NCC	657	1.5	**5.5**	14.5	YES	YES	YES	YES	107
La0.8Sr0.2Co0.3Mn0.1Fe0.6O3	LSCMF	786	0.4	2.1	17.6	NO	NO	N/A	N/A	110
La0.98Ni0.6Fe0.4O3	LNF	932	0	1.1	13.8	NO	NO	YES	YES	589
La1.2Sr0.8NiO4	LSN	975	0	0.1	13.5	Minor	YES	NO	NO	352
La0.7Sr0.3FeO3	LSF	690	0.3	0.9	13.3	NO	NO	NO	NO	133

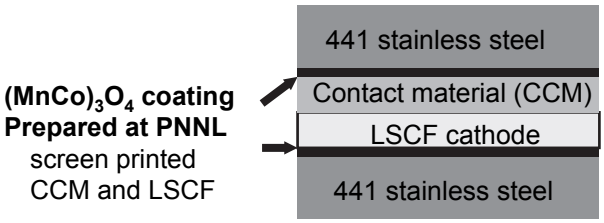

FIGURE 3. Sample Geometry for ASR Experiments

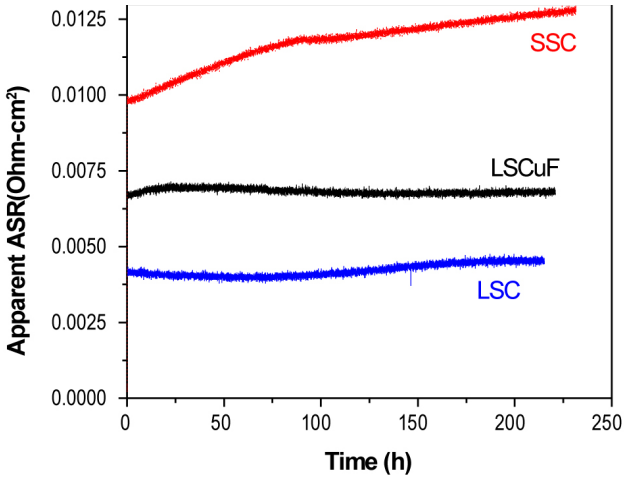

FIGURE 4. ASR for Various CCM Compositions at 800°C

Conclusions and Future Directions

- Many candidate CCM compositions were synthesized and screened for relevant physical properties.
- LSCF, LSCuF, SSC, and LSC were chosen as the most promising candidates, and ASR testing was conducted with these compositions. Initial results indicate that LSCuF and LSC provide low, stable ASR.
- Assessment of mechanical properties, tolerance to thermal cycling, and post-mortem analysis are under way.
- Novel solutions to the CCM issue will be developed in the future.

Special Recognitions & Awards/Patents Issued

1. Patent disclosure: Thermal management material for high-temperature electrochemical device.

FY 2010 Publications/Presentations

1. M. Tucker, G. Lau, L. DeJonghe, and S. Visco, "Progress in Metal-Supported SOFCs," presentation at SOFC-XI, Vienna, Austria, October 2009.

2. M. Tucker, G. Lau, L. DeJonghe, and S. Visco, "Progress in Metal-Supported SOFCs," presentation at Fuel Cell Seminar, Palm Springs, California, November 2009.

3. M. Tucker, G. Lau, and L. DeJonghe, "Longevity of Metal-Supported SOFCs," presentation at Daytona Beach Ceramics Conference, Daytona Beach, Florida, January 2010.

4. M. Tucker, L. Cheng, and L. DeJonghe, "Cathode Contact Materials for SOFCs," poster presentation at European Fuel Cell Forum, Lucerne, Switzerland, July 2010.

5. M. Tucker, L. Cheng, and L. DeJonghe, "Cathode Contact Materials for SOFCs," presentation at 11th Annual SECA Workshop, Pittsburgh, Pennsylvania, July 2010.

III.A.7 Correlations of Electronic and Chemical State on $La_{0.7}Sr_{0.3}MnO_3$ Dense Thin-Film Cathode Surfaces

Bilge Yildiz (Primary Contact), Helia Jalili
Massachusetts Institute of Technology
Nuclear Science & Engineering Department
77 Massachusetts Avenue, 24-210
Cambridge, MA 02139
Phone: (617) 324-4009; Fax: (617) 258-8863
E-mail: byildiz@mit.edu

DOE Project Manager: Briggs White
Phone: (304) 285-5437
E-mail: Briggs.White@netl.doe.gov

Subcontractors:
Clemens Heske and Stefan Krause
University of Nevada, Las Vegas (UNLV)
Las Vegas, NV

Contract Number: NT0004117

Phase I Start Date: October 1, 2008
Phase I End Date: March 31, 2010
Phase II Start Date: April 1, 2010
Phase II End Date: September 30, 2011

FY 2010 Objectives

- Observation of local electronic structure, electron tunneling properties, and chemical characteristics on $La_{0.7}Sr_{0.3}MnO_3$ (LSM) dense thin-film model cathodes at elevated temperatures and reactive gas environment with oxygen.
- Identify correlations between surface chemical state and electron exchange characteristics on LSM as a function of temperature.
- Identify the structural nature of A-site surface segregation on perovskite LSM at high temperature and high oxygen pressure. Quantify the changes in A-site/B-site cation ratio, by in situ treatment in the measurement chamber.

Accomplishments

- Observation of a layer-by-layer structure on LSM films with step size of 3.9 Å close to the lattice parameter of LSM by using scanning tunneling microscopy (STM). Top layers were atomically flat, with roughness less than 0.1 nm whereas the bottom layer was more defected. At high temperature of 580°C and high oxygen pressure of 10^{-3} mbar, no evident change of morphology was observed and step heights remained the same, suggesting that the surface perovskite layered structure remained stable.
- X-ray photoelectron spectroscopy (XPS) results showed that the low PO_2 (ultra-high vacuum, UHV) environment promotes segregation of A-site with a pronounced change on the Sr content. This result implies two possible structures which is associated with increased Sr-content: 1) Sr-segregation is occurring mainly on a perovskite AO-terminated surface, on which Sr replaces La atoms, and 2) Sr segregation, in the form of a separate oxide, as SrO, takes place only on the defected lower layers which we didn't have enough resolution/ control to probe yet.

Introduction

Amongst the various types of fuel cells, the solid oxide fuel cell (SOFC) is particularly attractive given its fuel flexibility (hydrocarbons, hydrogen or even CO) and high conversion efficiencies enabled by its relatively high operating temperature (800-1,000°C). In addition, the SOFCs can work in a reversible mode, for example, coupled to a nuclear plant or concentrated solar power, to produce electricity, and hydrogen or syngas for liquid fuels synthesis, alternating the product streams between days and nights. Fundamental understanding of the surface electronic and chemical state of the cathode is needed to enable rational design of materials for intermediate temperature and more durable SOFCs. For this purpose, probing the cathode surfaces at high temperature and O_2 environment is an asset to relate the surface structure and chemistry to the oxygen reduction kinetics at the atomistic level [1,2].

The relation of equilibrium surface segregation, that is the enhancement or depletion of a certain cation in the cathode structure at a given temperature and pressure, to oxygen reduction kinetics is an outstanding question. In the perovskite structured cathode material $La_{(1-x)}Sr_xMnO_3$ the ratio of A-site to B-site cations (A/B) can deviate from stoichiometric ratios significantly [3], driven for example by an enrichment of Sr or La cations on the surface. However, the origin of the A-site segregation, the structure of the segregated surface, and the temperature and pressure conditions that promote this segregation remain open.

The change of A/B could originate from different mechanisms including Sr enrichment at the A-site, i.e., Sr replacing La on the perovskite terminated surface [4],

formation of a separate oxide layer (Sr,La)-O [5], and formation of Ruddlesden Popper phases ($(La,Sr)_2MnO_4$) [6]. Fister et al. [4] reported Sr surface segregation using in situ synchrotron measurements of total reflection fluorescence over a wide range of temperature, T, and oxygen pressure, P_{O2} for $La_{0.7}Sr_{0.3}MnO_3$. He observed the surface segregated Sr increases as oxygen pressure decreases, and interpreted that Sr replaces La on the AO-terminated surface of the perovskite. Fister proposed the surface oxygen vacancy concentration controls the degree of segregation. Another hypothesis about the origin of A-site segregation is the formation of the A-site containing oxides (SrO or La_2O_3) separated on the surface, shown by Liu et al [5]. High resolution transmission electron microscopy images from the LSM and other perovskite surfaces clearly showed the formation of an A-oxide on the surface. The last hypothesis that we note here proposes that the A-site rich structure originates from the formation of the layered Ruddlesden Popper phases ($(La,Sr)_2MnO_4$), which was shown using angle resolved X-ray photoelectron spectroscopy on thin LSM films [6].

Experimental Approach

STM was used to investigate the surface morphology and electronic structure at elevated temperatures and oxygen environment. This information was combined with the chemical composition on LSM using XPS.

The experiments were performed in a modified UHV system design by Omicron Nanotechnology, Inc., with the base pressure lower than 5×10^{-10} Torr. The microscope chamber is equipped with a variable temperature STM and non-contact atomic force microscope. The analysis chamber was equipped with a five-channel hemispherical electron analyzer and X-ray source for the XPS. A heater was installed on the manipulator arm that allows us to heat the sample while performing XPS analysis.

The samples in this investigation were epitaxially grown $La_{0.7}Sr_{0.3}MnO_3$ on $SrTiO_3$ substrate using the pulsed laser deposition technique. The as-grown films were cleaned in ultrasonic bath with 99.99% purity ethyl-alcohol, followed by Ar blow drying. In order to remove the carbon contamination, sample cleaning for the STM experiments was performed by heating the samples in oxygen for 30 min at $5x10^{-6}$ mbar in the UHV chamber. This resulted in a significant reduction of the carbon content.

During the cleaning of the samples in oxygen, the high-temperature STM/scanning tunneling spectroscopy, and the XPS experiments, the sample was radiatively heated by using a pyrolytic boron nitride (PBN) heater. 10^{-3} mbar oxygen pressure localized in the vicinity of the sample's surface was created during the STM measurements via direct oxygen dosing by a retractable dozer equipped with high precision leak valve. STM at room temperature (RT) and high temperatures (HT) up to 580°C was performed in the constant-current mode using Pt/Ir tips. The bias voltage of 1-2 V applied to the sample during STM measurement and the tunneling current, *I*, ranged from 50-500 pA.

Results

Surface Phase on LSM Film

Effect of the annealing in the non-UHV partial pressure of oxygen and in UHV at temperatures up to 580°C was studied in consecutive steps of temperature. Figure 1(a,b) shows the room temperature STM image of the as-grown film of LSM/$SrTiO_3$ (STO) after a 30 min heating in oxygen pressure of 10^{-6} mbar at 500°C to clean its surface. Figure 1(a) shows the morphology of the surface over large area of 500×500 nm^2. Surface is smooth with well resolved step edges. Figure 1(b) shows the zoomed-in image and the white line corresponds to the position of the height profile taken. Figure 1(c)

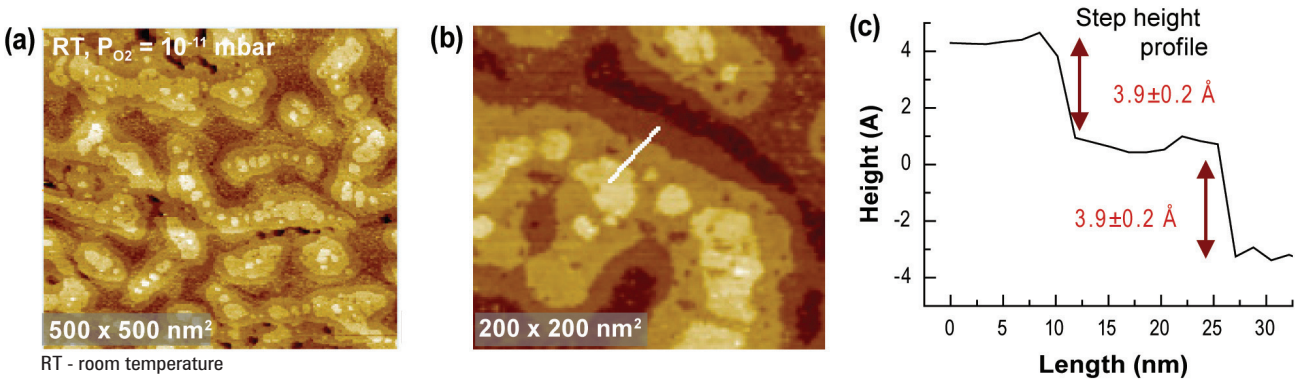

FIGURE 1. LSM surface morphology, and step height analysis of the 10 nm thick LSM thin film grown on STO substrate. (a) Large area 500×500 nm^2 image, (b) the zoomed-in image for clarity on the step height analysis, (c) the cross sectional height-profile measured from (b), with a height difference between each step as 3.9±0.2 Å.

shows that the step height between each layer is 3.9±0.2 Å. The potential phases that can form on the surface of the LSM film with their respective lattice constants are summarized in Table 1. Comparing the lattice parameters of the compounds listed in Table 1 and the step height between each layer obtained from the STM measurements, we found that the LSM lattice parameter has the closest match (3.88 Å) to the measured step height differences. This implies that the LSM surface consists of several monolayers of LSM before being subject to oxidizing or reducing under controlled conditions. However, the bottom most layer exposed on the surface is not as smooth as the top layers and it has a defected structure. The smooth and well-defined top layers will be used in the next sections as a reference from which the surface may deviate upon cation segregation on the surface.

TABLE 1. Possible Phases That Can Stabilize on the LSM Surface and Their Respective Lattice Parameters

Compound	Lattice Parameters
[7] $La_{0.7}Sr_{0.3}MnO_3$	a=b=c=3.88 Å
[8] SrO	a=b=c=5.16 Å
[9] $SrCO_3$	a=5.1, b=8.4, c=6.0 Å
[10] La_2O_3	A=b=3.4, c=6.1 Å
[11] $(La,Sr)_2MnO_4$	a=b=3.84, c=12.5 Å

Measure of Phase Separation with Temperature and P_{O2}

Figure 2 shows the surface morphology of the LSM at three different conditions, (a) RT and UHV pressure, (b) T = 500°C and $P_{O2\text{-surface}} \sim 10^{-3}$ mbar, and (c) 500°C, $P_{O2} = 10^{-11}$ mbar. No distinct change in surface morphology was observed upon annealing up to 500°C. Even at a high temperature of 580°C, the step size between each layer remained the same (3.9±0.2 Å) when in oxygen pressure. Results shown in Figure 2 indicated no evidence of secondary phase formation that was detectable in morphology and/or change of the step size between each layer. In order to quantitatively and more accurately analyze the size distribution from Figure 2, we took a statistical approach. For this purpose, we applied the Histogram analysis using the scanning probe image processor[1] image and data analysis software (12). Figure 3(a) shows the histogram obtained for Figure 2(c). Each peak in the histogram (Figure 3(a)) corresponds to the height of each layer, and the integral of each peak determines the area fraction contributed by each layer. For the specific case that was shown in Figure 3(a), from right to left, the first peak located at 8 Å, arise from the contribution of the top-most layer, the second peak corresponds to the second top layer and so on. To get good statistics, the analysis was performed for about 20 different images each at RT (black curve) and at HT (red curve). These results are summarized in Figure 3(c). As shown in Figure 3(c), there is only a small difference (2-4%) between the size distribution at HT and RT.

Chemical Composition on LSM Film

To capture the changes in chemical state arising during and posterior to the annealing process, and correlate these to the structural changes summarized in Figure 3, we performed XPS measurements on the as-received and the annealed samples. Figure 4(a) on the left side (black curve) shows the ratio of the content of A-site cations to B-site cations, (La+Sr)/Mn, and on the right side (red curve) shows the ratio of Sr to A-site Sr/(Sr+La) for four different treatments; at RT and HT for the UHV annealed sample as well as the oxygen annealed sample. Figure 4(a) indicates several interesting points: 1) The starting condition of the surface is A-site rich. Given the step-height corresponding to the LSM lattrice parameter, we deduce

[1] http://www.nanoscience.com/products/SPIP/SPIP.html

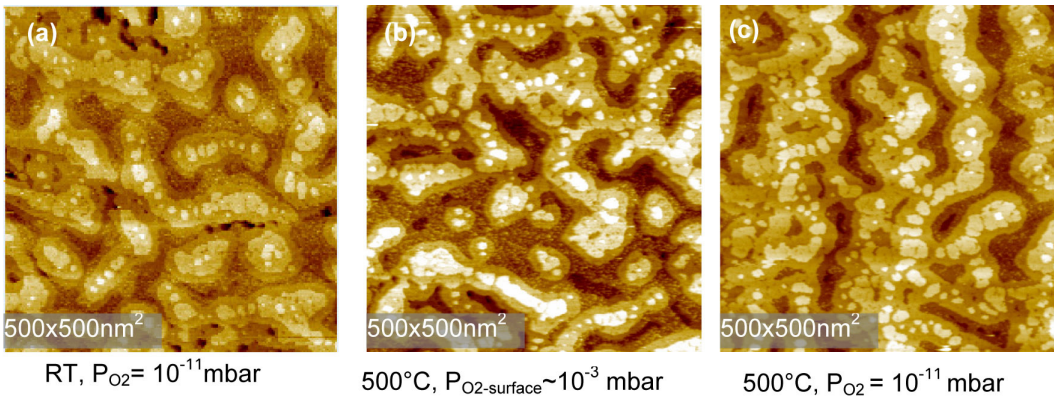

FIGURE 2. Surface morphology of the 10 nm LSM on STO (a) at room temperature after cleaning the surface, (b) at 500°C in oxygen ($P_{02}=10^{-3}$ mbar), (c) at 500°C in oxygen ($P_{02}=10^{-11}$ mbar).

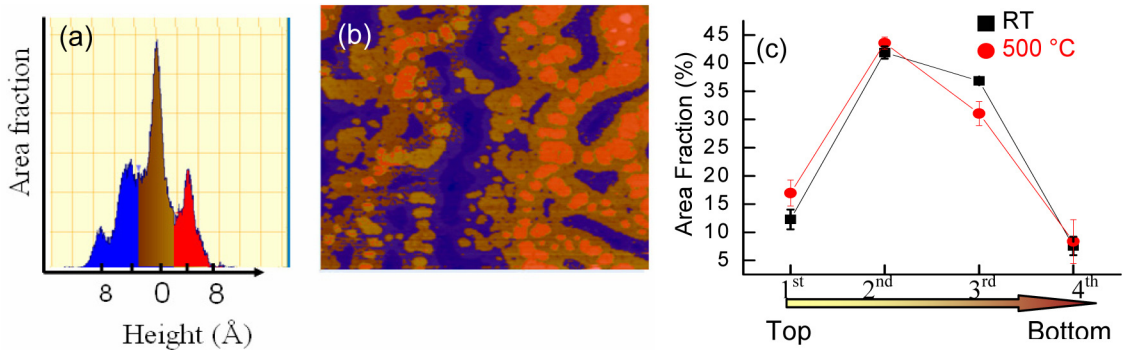

FIGURE 3. (a) and (b) show the STM image and the corresponding histogram diagram representing the area fraction of each layer, (c) summarizes the quantified size distribution of each layer at RT (black curve) and HT (red curve). For each temperature, these data were obtained from histograms as shown in (a).

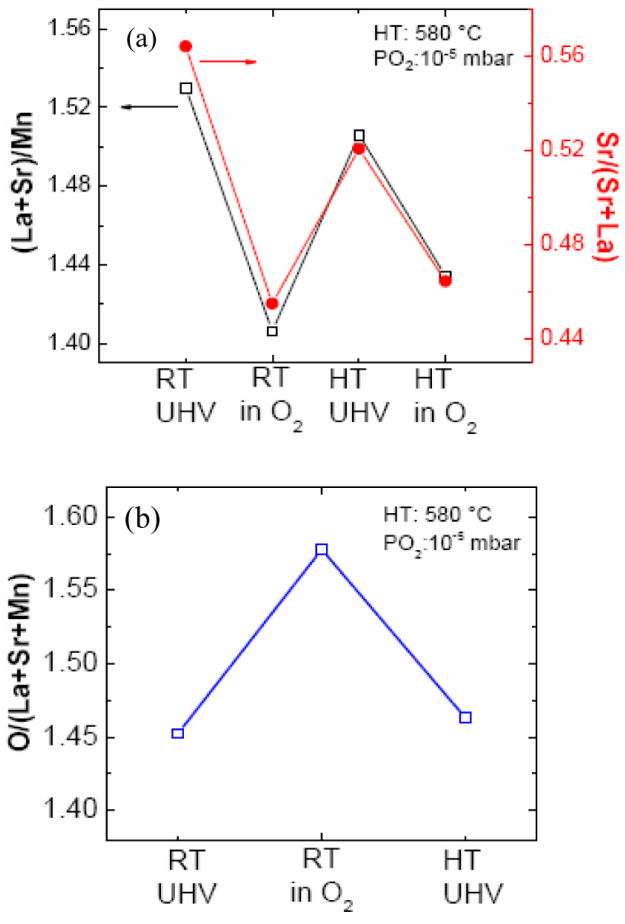

FIGURE 4. The XPS data obtained for LSM/STO at different conditions of RT and HT in UHV and oxygen partial pressure. (a) Black curve: ratio of A- to B-site, Red curve: ratio of Sr to A-site. (b) Ratio of oxygen to the rest of the cations.

that the surface is made of AO-terminated perovskite layers. 2) Annealing the sample in UHV and/or oxygen promotes an increase of A-site. 3) Increase of Sr is more evident on the UHV-annealed sample compared to the oxygen-annealed sample. Figure 4(b) shows the oxygen content relative to the cations. As one would expect, the surface oxygen content decreases as the pressure reduces, nevertheless, surface oxygen was present even at HT and UHV conditions, implying that the surface was not reduced to a state including only the metal cations.

In order to deduce the nature of the segregation and the surface structure upon segregation, data from histogram analysis were compared with the XPS data. XPS data revealed a 12-20% relative change in the Sr content on the A-site during the treatments of the surface at various temperatures and oxygen pressures. The STM statistical analysis showed only a small difference (2-4%) between the size distribution at HT and RT, and no other changes in the morphology on the flat top layers were observed. Comparing the 12-20% chemical change with the max 2-4% change in the area of the surface layers suggests that the A-site and Sr-site rich surface can not arise due to a secondary phase formation as a separate oxide phase on the top layers of the LSM film in the conditions we tested. Also considering the fact that the step sizes between each layer stayed the same (3.9 Å) regardless of T and PO_2, we also rule out the possibility of Ruddlesden Popper phase, $(La,Sr)_2MnO_4$ with a Z-axis lattice constant of c=12.5 Å. The only mechanism that we can not rule out based on our current results is the replacement of La by Sr on the A-O terminated surface that retains its perovskite layered structure up to 500°C. However, due to defected nature of the bottom layer of the surface morphology that makes limits resolution limit of the present measurements, we have not excluded the possibility of Sr surface segregation as a separate phase on the bottom defected layer.

Conclusions and Future Directions

Evolution of surface morphology, electronic structure and chemical state was studied as a function of

temperature and oxygen pressure using STM and XPS. The STM showed that the surface had a layer-by-layer structure with a step height of 3.9 Å, close to lattice parameter of LSM. Two different morphologies were depicted. Top layers were flat with roughness less than 0.1 nm whereas the bottom layer was defected, making it difficult to resolve possible secondary phase formation on the bottom layer. At a high temperature of 500°C and oxygen pressures of 10^{-10}-10^{-5} mbar, no evident change of morphology was observed, and the layered nature of the surface and step height remained the same.

The XPS data and analysis indicated that the low P_{O2} (UHV) environment promotes segregation of A-site with a pronounced change on the Sr content. The significant changes on the Sr content, accompanied by only a small change on the surface morphology suggests two possible structures for Sr segregation on LSM in the T and P_{O2} conditions reported here; the replacement of La by Sr on the AO-terminated surface of the LSM which retains a perovskite termination; or a separate AO-oxide phase nucleating on the defected lower layers. High resolution STM with refined XPS analysis will be performed to resolve these two possible structures at the atomistic scale. Systematic studies to investigate the surface phases and their relation to surface electron transfer properties are under progress.

Special Recognitions & Awards/Patents Issued

1. High temperature STM capability noted in the MIT and departmental news:
http://web.mit.edu/nse/research/spotlight/yildiz_july-2010.html
http://web.mit.edu/newsoffice/2010/nse-electro-interfaces.html

FY 2010 Publications/Presentations

1. Presentations at the ECS Fall Meeting, 2009, Vienna; MRS Spring Meeting, 2010, San Francisco; ECS Spring Meeting, 2010, Vancouver; and E-MRS Spring Meeting, 2010, Strasbourg.

2. Conference publication: "Structural, Chemical and Electronic State on $La_{0.7}Sr_{0.3}MnO_3$ Dense Thin-film Surfaces at High Temperature – *Surface Segregation*," Helia Jalili, Yan Chen, and Bilge Yildiz, ECS Transactions, 2010.

References

1. S.B. Adler, *Chem Rev*, **104**, 4791 (2004).

2. F.S. Baumann, J. Fleig, M. Konuma, U. Starke, H.U. Habermeier, and J. Maier, *J. Electrochem. Soc.*, **152**, A2074 (2005).

3. K. Katsiev, B. Yildiz, K. Balasubramaniam, and P.A. Salvador, *Appl. Phys. Lett.*, **95**, - (2009).

4. T.T. Fister, D.D. Fong, J.A. Eastman, P.M. Baldo, M.J. Highland, P.H. Fuoss, K.R. Balasubramaniam, J.C. Meador, and P.A. Salvador, *Appl. Phys. Lett.*, **93**, 151904 (2008).

5. Private communication with Prof. Meilin Liu, Georgia Tech University.

6. H. Dulli, P.A. Dowben, S.H. Liou, and E.W. Plummer, *Phys Rev B*, **62**, 14629 (2000).

7. M.C. Martin, G. Shirane, Y. Endoh, K. Hirota, Y. Moritomo, and Y. Tokura, *Phys Rev B*, **53**, 14285 (1996).

8. R. Bertacco, J.P. Contour, A. Barthelemy, and J. Olivier, *Surf Sci*, **511**, 366 (2002).

9. T. Thongtem, N. Tipcompor, A. Phuruangrat, and S. Thongtem, *Mater. Lett.*, **64**, 510-512 (2010).

10. C.G. Hu, H. Liu, W.T. Dong, Y.Y. Zhang, G. Bao, C.S. Lao, and Z.L. Wang, *Adv. Mater.*, **19**, 470 (2007).

11. F. Zheng and L.R. Pederson, *J. Electrochem. Soc.*, **146**, 2810 (1999).

III.A.8 Synchrotron Studies of SOFC Cathode Materials

Y.U. Idzerda
Department of Physics
Montana State University
Phone: (406) 994-7838; Fax: (406) 994-7838
E-mail: Idzerda@physics.montana.edu

DOE Project Manager: Patcharin Burke
Phone: (412) 386-7378
E-mail: Patcharin.Burke@netl.doe.gov

Contract Number: NT0004115

Start Date: September 3, 2008
End Date: September 2, 2011

FY 2010 Objectives

- Characterize atomic variations and modifications occurring in the nanometer range, in the cathode/electrolyte interface region of solid oxide fuel cell (SOFC)-related materials.
- Correlate these modifications to electric potential, ion current, gaseous environment, and possible synergistic effects between them.
- Identify A-site and B-site occupancy and in Y-doping of $SrTiO_3$.

Accomplishments

- Observations of the power curves for lanthanum strontium cobalt ferrite/gadolinia-doped ceria (LSCF/GDC) sandwich structures driven with potentials ranging from 350 mV to 500 mV at 800°C for 100 hours of operation, suggest that an initial onset occurs after a fixed oxygen ion flow has occurred and demonstrates that the form of degradation can be monitored and an identification of films that display a long-term reduction in performance can be made. The X-ray absorption spectroscopy (XAS) spectra for the Fe and Co in these materials shows a distinct and repeatable variation in the electronic structure, suggesting a strong chemical modification in the interfacial region due to cation diffusion (La) in the opposite direction of the oxygen vacancy flow. Reversing the ion flow does not reverse the degradation, but does degrade the second LSCF/GDC interface.
- Observed that the La cation diffusion strongly modifies the A-site:B-site occupations in the interfacial region and may be present elsewhere in the SOFC material.
- Observed cation diffusion in response to oxygen vacancy motion by direct comparison with spectra acquired for interface degradation due to interfacial stress.
- Demonstrated that the Cr that has migrated to the cathode has a different chemical state after oxygen ion flow on the side of the electrolyte where the oxygen molecules dissociate and oxygen ion flow is initiated.
- Obtained baseline XAS spectra for LSCF/GDC interfaces, and have initiated thin cathode film growth on $DyScO_3$ substrates.
- Expanded the research directions (as suggested) and completed the testing and are using a second test station that uses an electrical potential rather than a chemical potential to drive ion currents for direct comparison with our in situ studies.

Introduction

One poorly understood area of SOFC systems is the interfacial region between the electrolyte and the cathode and/or anode. As the electrodes become thinner to enhance performance, this interfacial behavior becomes a dominant contributor to the overall SOFC performance. If the material properties of the electrolyte/cathode/anode at the interface significantly differ from the bulk properties, these buried regions, which are difficult to probe, may become the dominant inhibitor of electron or oxygen vacancy transport. Fortunately, X-rays have a significant penetration depth and have been shown to be sensitive to the electronic and crystalline structure of these interfacial regions.

In addition, identifying the mechanisms for intrinsic degradation of SOFC structures remains an important and fundamentally interesting problem. Connecting this mechanism to operational parameters including ion flow, overpotentials, and gaseous environments will lead to improved performance and durability.

Approach

Element specific XAS will be used to determine the A-site and B-site occupations (and vacancies) for the perovskite ABO_3 systems. The electronic structure of Y-doped $SrTiO_3$ (0-10% atomic doping) will be examined to determine if the A-site and B-site occupation and oxygen vancy concentration can be better quantified. Diffuse X-ray resonant scattering will be used to quantify the evolution of the interface width of relevant materials to determine Sr enrichment

at surface/interface regions and to further identify the distribution of A-site:B-site occupancies. In addition, increasing interest in the magnetic properties in relation to the catalytic and transport properties of the surface/interface of these materials has led to the examination the high-temperature magnetic properties by high-temperature vibrating sample magnetometry (bulk behavior) and by using X-ray absorption and X-ray magnetic circular dichroism (the differential absorption of circular polarized X-rays) to determine the elemental behavior of the magnetism. This will require use of a high-temperature cell, and, since oxygen vacancies may play a role in the high-temperature magnetism, control of the oxygen stoichiometry within the material during the high vacuum measurements.

Results

Clear indicators of interfacial degradation have been established and the underlying mechanism continues to be identified. The total oxygen ion flux and potentials required for the onset of a reduction in the oxygen vacancy flow (power reduction) has been established. The cation diffusion in response to oxygen vacancy motion has been quantified and baseline XAS spectra for LSCF/$DyScO_3$ interfaces have been obtained. Observations of the power curves for LSCF/GDC sandwich structures driven with potentials ranging from 350 mV to 500 mV at 800°C for 100 hours of operation, suggest that an initial onset occurs after a fixed oxygen ion flow has occurred and demonstrates that the form of degradation can be monitored and films that display a long-term reduction in performance can be identified. The XAS spectra for the Fe and Co in these materials shows a distinct and repeatable variation in the electronic structure, suggesting a strong chemical modification in the interfacial region due to cation diffusion (La) in the opposite direction of the oxygen vacancy flow. Reversing the ion flow does not reverse the degradation, but does degrade the second LSCF/GDC interface.

In addition, the research directions have been expanded to identify signatures for the A-site and B-site occupations in a first step to determining their relative occupation. La cation diffusion strongly modifies the A-site:B-site occupations in the interfacial region and may be present elsewhere in the SOFC material. As a demonstration of the ability to identify A-site and B-site occupation, we have examined the Y-doped $SrTiO_3$ (STO) SOFC material (0% to 10% atomic doping of Y). At issue is whether the Y substitutes for the A-site Sr or the B-site Ti and with what valence. Other researchers have identified the Y as substituting into the structure as Y^{3+} and predominantly in the Sr A-site. Of less certainty are the responses of the Ti, Sr, and O occupancies to maintain charge neutrality.

To address this, we have measured the L_{23} edge XAS for Ti, Sr, and Y for 2%-10% Y concentrations in STO and compared them to pure $SrTiO_3$, TiO_2, and Y_2O_3. Figure 1 shows that the Sr and Y electronic structure remain essentially unchanged. The direct comparison with the Y_2O_3 powder standard confirms that the Y substitutes as Y^{3+}, as was previously observed, and the Sr electronic structure remains essentially unchanged from pure $SrTiO_3$. These observations are consistent with the viewpoint that the Y is substitutional into the Sr site. The Ti XAS spectra (not shown) identifies that the Ti remains in the Ti^{4+} valence and the changes in the spectra (increase in the L_2-edge features) is consistent with a small increase in oxygen vacancies. Charge neutrality is maintained through the introduction of oxygen vacancies and the alloy is more correctly reported as $Y_xSr_{1-x}TiO_{3-\delta}$. More importantly, the A-site and B-site occupancy can be quantified using XAS of the relevant materials and can be applied to lanthanum strontium transition metal (LSTM) overlayers on GCD, YSZ, and $DyScO_3$ substrates.

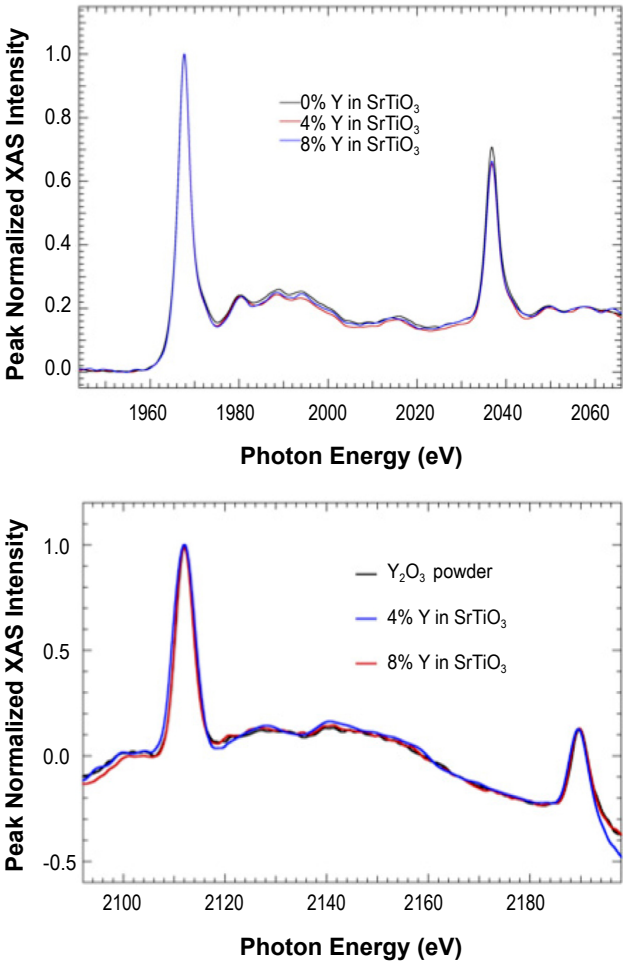

FIGURE 1. Peak area normalized XAS spectra of the (top) Sr L_{23}-edge and (bottom) Y L_{23}-edge for Y-doped $SrTiO_3$ for different Y concentrations (atomic percent). Also shown is the Y L_{23}-edge for Y_2O_3 reference powder.

To identify the mechanism of oxygen ion flow reduction due to possible interface mechanisms, the Fe and Co L_{23} XAS spectra has been measured for cells with demonstrated degradation for both the oxygen in-flow and oxygen out-flow interfaces. The spectra were measured before and after use for 100 hours at 800°C at the 500 mV driving potentials. In Figure 2, the changes in the electronic structure of the Fe and Co L_{23}-edge XAS spectra are shown before and after use on the oxygen ion in-flow side of the LSCF/GDC sandwich structure (oxygen vacancies flow into this region and are filled with oxygen ions, eliminating the vacancy). The data was acquired at beamline U4B of the National Synchrotron Light Source in the sample current (total electron yield) mode. This type of acquisition is sensitive to the first 20 nm of the material of interest. The measured variation in the Fe and Co edge suggests that changes have occurred in the interfacial region for both the Fe and Co but only on one side (oxygen ion in-flow) of the structure. The measured XAS spectra of the materials prior to use are identical to baseline spectra. The spectra on the out-flow side (oxygen vacancy creation) show no variation for the LSCF electronic structure, indicating that the direction of oxygen vacancy flow is critical.

To further identify the mechanism of degradation, diffuse X-ray resonant scattering (diffuse XRS) has been performed on these materials at the La M_5-edge. Diffuse XRS has been shown to yield the elemental distribution within the interfacial area between these two layers. The width of the diffuse peak corresponds to the in-plane correlation length (similar to grain size) and the ratio of the specular to diffuse intensity can be used to quantify the perpendicular root mean square-roughness (interface width). Figure 3, shows that after operation which has led to operational degradation, the La has further diffused at the LSCF/GDC interface so that the interface width is increased by 80%. This La redistribution must result in an enhanced Sr concentration within this region and a stronger variation of the Sr A-site:B-site ratio.

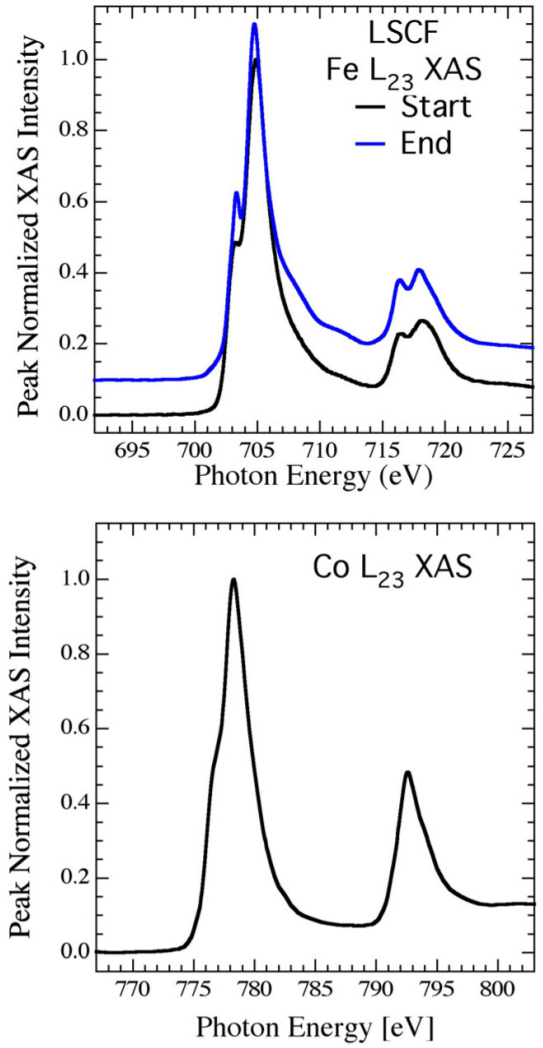

FIGURE 2. The Fe and Co L_{23}-Edge XAS of LSCF before and after Oxygen Vacancy Flow at 800°C and 0.5 V for 100 Hours

Conclusions and Future Directions

The utility of XAS and diffuse XRS has been used to demonstrate that oxygen ion flow and applied electrical potentials can modify the surface and interfacial regions of SOFC materials. The addition of Y to $SrTiO_3$ at the few percent level (well beyond the electronic doping of STO) results in Y substituting as Y^{+3} in the Sr A-site

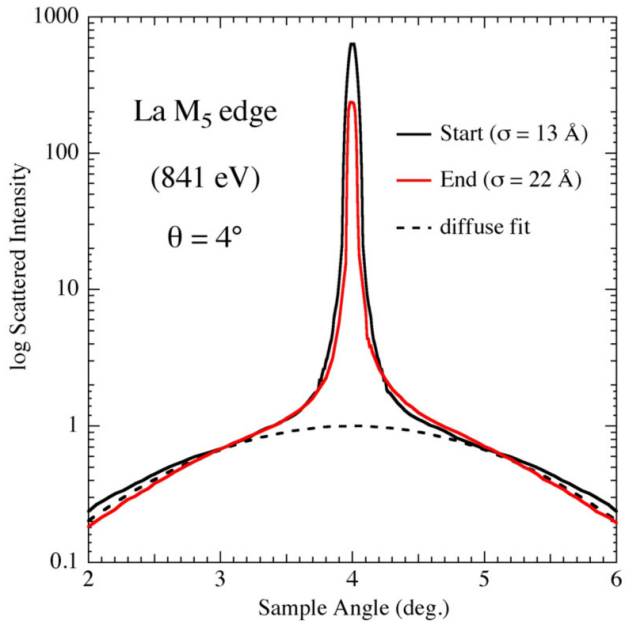

FIGURE 3. Diffuse XRS Spectra of La M_5 Edge Acquired at the LSCF/GDC Interface after 100 Hours Oxygen Ion Flow

with the emergence of oxygen vacancies which can be quantified from the Ti XAS spectra.

The major focus in the future will be to examine the high-temperature magnetic properties of lanthanum strontium transition metal oxide (LSTMO) materials. The Y-doped $SrTiO_3$ SOFC material (0% to 10% atomic doping of Y) will continue to be examined as well as Mo-doped and V-doped $SrTiO_3$ SOFC materials where a stronger quantification of the A-site to B-site occupation of the Sr, Ti, and dopant atom are expected with doping concentration.

FY 2010 Publications

1. M. Finsterbusch, A. Lussier, Z. Zuh, R.J. Smith, J.A. Schaefer, and Y.U. Idzerda, "Effect of Cr_2O_3 on the ^{18}O Tracer Incorporation in SOFC Materials," Solid State Ionics **181**, 640-645 (2010).

FY 2010 Presentations

1. A. Lussier, M. Finsterbusch, and Y.U. Idzerda, "Cathode/Electrolyte Interface Material Studies," 10th Annual SECA Workshop, Pittsburgh, Pennsylvania, July 14–16, 2009.

2. A. Lussier, M. Finsterbusch, and Y.U. Idzerda, "Degradation Mechanisms in Oxygen Ion Conducting Materials," March Mtg. Amer. Phys. Soc., Portland, Oregon, March 15–19, 2010.

3. M. Finsterbusch, A. Lussier, E. Negusse, and Y.U. Idzerda, "Modified Cr Valence in Symmetric Oxygen Ion Conducting Half Cells with Ion Flow," March Mtg. Amer. Phys. Soc., Portland, Oregon, March 15–19, 2010.

4. B. Anderson, P. Rugheimer, and Y.U. Idzerda, "Manganese Doped Scandium Oxide as a Cathode for Fuel Cells," March Mtg. Amer. Phys. Soc., Portland, Oregon, March 15–19, 2010.

III.A.9 DOE/NETL In-House Cathode R&D

Kirk Gerdes
U.S. Department of Energy
National Energy Technology Laboratory
3610 Collins Ferry Rd.
Morgantown, WV 26507
Phone: (304) 285-4342; Fax: (304) 285-4469
E-mail: Kirk.Gerdes@netl.doe.gov

Contract Number: 10-220621 6923
(In-house cathode R&D)

Start Date: October 1, 2009
End Date: September 30, 2010

FY 2010 Objectives

- Identify and develop at least one material to infiltrate standard solid oxide fuel cell (SOFC) cathode.
- Generate at least one infiltration vehicle suitable for dispersion of infiltrate throughout cathode pore structure.
- Test 10 cases of infiltrated cells parametrically on process parameters identified to provide proper control of nano-particle synthesis on cathode materials (calcination temperature, solution composition, etc.).
- Generate public report on the key conclusions from the work.

Accomplishments

- Developed cathode infiltrate materials including $(LaSr)_2Zr_2O_7$.
- Prepared two vehicles for applying infiltrate to cathode pores. One method is based on a glycine-nitrate process, one is based on a citric acid process.
- Confirmed formation of desired infiltrate through X-ray diffraction (XRD) analysis. Minimized secondary phase formation by adoption of glycine-based methods.
- Characterized microstructure of infiltrated cathode and evaluated distribution of infiltrate material within cathode pore structure as a function of precursor solution concentration and number of infiltrations performed.
- Investigated electrochemical performance of infiltrated cells using standard tests including current/voltage/power monitoring and impedance spectroscopy. More than 30 cell tests were completed.

Introduction

An SOFC is a device which generates electrical energy by exchanging oxygen ions between an oxygen containing process stream such as air and a process stream containing an oxidizeable material such as hydrogen. The SOFC cathode facilitates the reduction of oxygen to an ionic form in preparation for transport across the impermeable electrolyte membrane. This electrochemical oxygen reduction process is sensitive to the material composition and physical structure of the cathode, and the oxygen reduction reaction (ORR) efficiency can be impacted by chemical or structural alterations.

One method proposed to improve the efficiency of the ORR at the cathode is to supply catalytic material at the active sites within the pores of the cathode. Although an SOFC cathode is typically composed of a 60 μm thick porous ceramic, the cathode is particularly active at the locations within 1-10 μm of the interface between cathode and electrolyte, and material deposition is therefore preferred at the deeper location. The primary challenges of cathode infiltration are: 1) ensuring that the desired infiltrate material phase is deposited; 2) distribution of infiltrate into the active regions of the cathode is achieved; 3) the material is stable as evaluated by electrochemical, thermochemical, and thermomechanical performance metrics. Achievement of targeted cathode infiltration resulting in improved cathode activity and long-term stability is the target of the present research effort.

Approach

In this project, a porous ceramic SOFC cathode of standard composition ($La_{1-x}Sr_xMnO_3$ or $La_{1-x}Sr_xFe_{1-y}Co_yO_3$) is infiltrated with materials intended to alter the chemical activity of the cathode and enhance the ORR. Materials suitable for infiltration into the cathode are identified, the materials are generated and infiltrated, and the impact on cathode performance is electrochemically evaluated. Materials demonstrating improved cathode performance are also screened through extended testing to ensure that long-term stability will be adequate to meet lifetime performance metrics.

Initially the material $(La,Sr)_2Zr_2O_7$ (LSZ) is used to develop the infiltrate generation protocols and the infiltrate vehicle formulations. After choosing the desired material, the desired phase is infiltrated into the porous cathode at concentrations from 1-30 wt%.

The quality of infiltration is evaluated visually on the basis of infiltrate particle size and uniformity of infiltrate coverage. Infiltrated cells are then operated electrochemically for up to 200 hours at 750-800°C using hydrogen as the fuel source. Cells under test are also periodically probed with electrochemical impedance spectroscopy, and results are used to examine changes in the electrode polarization and cell ohmic resistance. The results are used to evaluate the performance of all candidate materials in order to identify the infiltrate demonstrating the greatest performance improvement and/or greatest stability.

Results

In the short duration of this project, substantial success has been achieved. The LSZ phase selected was created using a glycine-nitrate process. As indicated in Figure 1, the desired phase begins forming at temperatures as low as 950°C, with clear indications that the pure LSZ phase is generated as the temperature approaches 1,150°C. The sintering temperature for the infiltration process is then selected to exceed 950°C, so that the pure phase will be formed in the test pieces.

The infiltrate solution is composed of precursor nitrate salts dissolved in a liquid mixture intended to solubilize the salts and control solution viscosity and pH. The solution is applied to the cathode using a syringe in a series of infiltration steps interspersed with drying steps. The solution concentration and total applied volume are controlled to sufficiently wet the cathode pores while preventing deposition of infiltrate on the surface of the cathode structure. Infiltration steps are repeated until the desired mass of infiltrate is applied to the cathode and then a final sintering step is completed. An example of a cathode infiltrated using this procedure is shown in Figure 2. In this image, the lanthanum strontium cobaltite ferrite (LSCF) cathode backbone having particle sizes of approximately 200-500 nm at the active layer near the electrode/electrolyte interface is infiltrated with LSZ material having particle and feature sizes <100 nm. The scanning electron microscopy (SEM) images are supported by calculations indicating that the surface is essentially covered by a complete layer of LSZ at 31 wt% infiltration. Addition of less material will result in a sparse surface coverage, while addition of further infiltrate will begin to constrict the pores.

A series of cells prepared using the above material and described infiltration methods were tested to determine the impact of cathode infiltrate content on electrochemical performance. Electrochemical performance is evaluated using electrochemical impedance spectroscopy (EIS) in which the cell was held at an operating current of ~0.25 A/cm^2 and a small amplitude alternating current is applied to the cell at frequencies from approximately 0.1 Hz to 1 kHz. Figure 3 depicts EIS data indicating that total cell

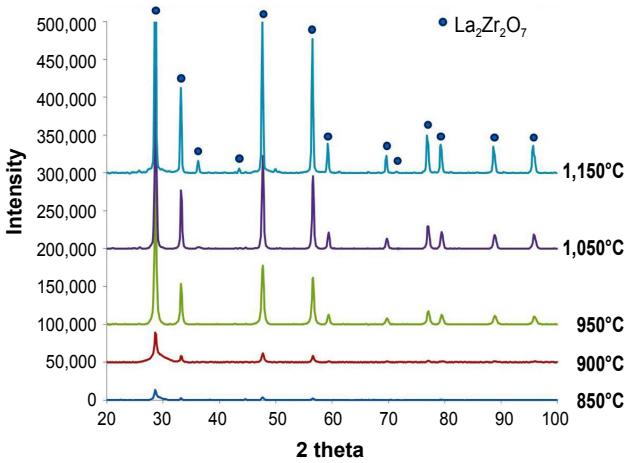

FIGURE 1. XRD pattern of powders derived from LSZ nitrate solution. Reacting agent and citric acid were added to the solutions.

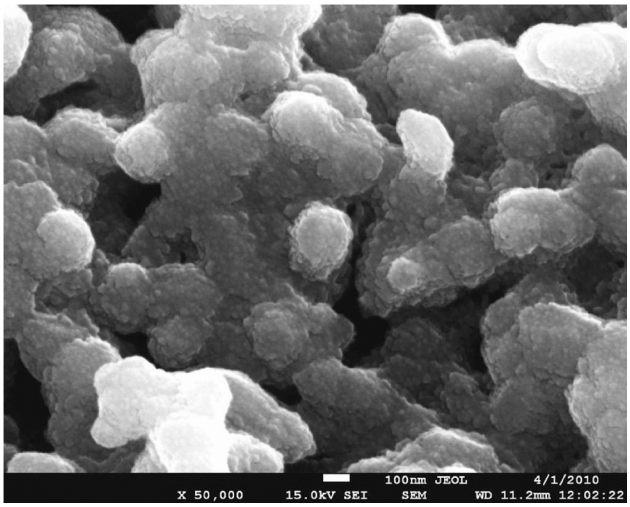

FIGURE 2. SEM microstructure of LSCF cathode infiltrated with 31 wt% LSZ.

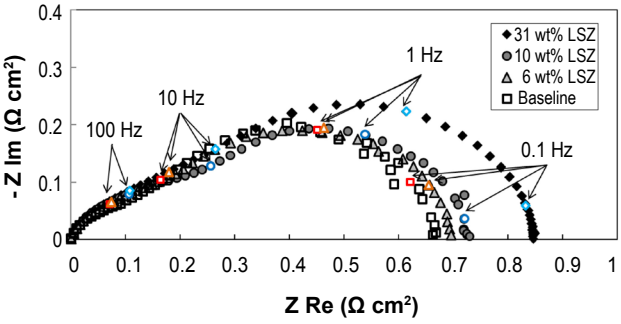

FIGURE 3. Impedance measured at open circuit voltage after 24-hour operation under 0.5 A at 750°C. Ohmic resistance was subtracted for clear comparison of polarization resistance.

polarization actually increases for loadings exceeding 6 wt% with no clear effect for cathode loadings less than 6 wt%. Increased cell polarization indicates that the cell becomes less active and therefore less efficient. As cathode loading increases the peak frequencies also shift slightly to lower values and the impedance curves at lower frequencies appear to grow in magnitude. Growth of lower frequency curves indicates that lower frequency processes are contributing in greater proportion to the total polarization resistance as the infiltrate content increases in the cathode.

The infiltrated cells are also tested after 24 hours of operation to determine the total cell overpotential, that is, the total cell voltage losses. Overpotential is tested as a function of current density for each infiltrate loading and the data are depicted in Figure 4. The initial data indicate that addition of any infiltrate to the cathode has a neutral or negative impact on the cell overpotential. These preliminary data produce a direct correlation between infiltrate content and total overpotential, and the data consistently show neutral or increased overpotential (decreased efficiency) as infiltrate content increases. Although the 6 wt% loading appears to indicate a decrease in cell polarization, the preliminary effort has not yet produced enough cell test data to statistically verify the significance of the observation in this test.

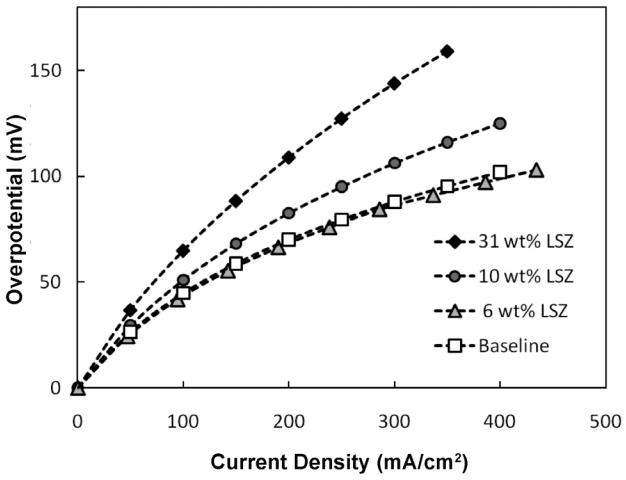

FIGURE 4. Electrode (anode+cathode) overpotential calculated from voltage-current polarization data measured after 24-hour operation under 0.5 A at 750°C.

Although the EIS data indicate that infiltration of the LSZ material into an LSCF cathode is probably deactivating the cathode (and suppressing the ORR rate), infiltrate materials may also serve a valuable purpose by suppressing migration of cathode material and providing enhanced cathode stability. The subject of the present effort remains identification of infiltrate materials which will enhance the cathode activity, although it may be valuable to re-investigate the low range loading (<6 wt%) of LSZ to evaluate the material's impact on cathode stability.

Conclusions and Future Directions

The Fiscal Year 2010 effort has provided valuable core data upon which further infiltration efforts can be initiated. In particular, the present effort has generated an infiltrate material and generated an infiltrate solution capable of penetrating to the cathode active layer and distributing infiltrate uniformly throughout. The infiltrated cathode was tested using typical electrochemical methods, and the data obtained clearly indicated the impact of adding infiltrate to the cathode. For the particular system under test (LSZ in LSCF), the infiltrate material did not have a significantly positive impact for any loading, and indeed has a negative impact on cathode activity as infiltrate loading increases.

Future efforts should include evaluation of infiltrate materials other than LSZ. The results and experience gained from the present techniques can be used to rapidly screen other materials related to the LSZ system or common mixed ionic-electronic conductors. The battery of chemical and electrochemical characterization methods already developed is considered sufficient for future efforts to rapidly screen the activity of other potentially active materials.

FY 2010 Publications/Presentations

1. Poster presentation, "Cathode Infiltration Using LSZ and Mixed Ionic Electronic Conductor," SECA 2010, Pittsburgh, Pennsylvania.

III.A.10 Development of SOFC Cathodes

J.S. Hardy (Primary Contact), J.W. Templeton, Z. Lu, J.W. Stevenson
Pacific Northwest National Laboratory
P.O. Box 999, MS K2-44
Richland, WA 99352
Phone: (509) 375-2627; Fax: (509) 375-2186
E-mail: john.hardy@pnl.gov

DOE Project Manager: Briggs White
Phone: (304) 285-5437
E-mail: Briggs.White@netl.doe.gov

Contract Number: FWP40552

Start Date: October 1, 2009
End Date: September 30, 2010

FY 2010 Objectives

- Develop solid oxide fuel cell (SOFC) electrodes offering high performance and long-term stability at intermediate SOFC operating temperatures (650-850ºC).
- Determine the effects of potential volatile constituents of a candidate sealing glass on SOFC cathode performance.
- Investigate the effects of composition and processing parameters on performance and stability of Sr-doped lanthanum cobalt ferrite (LSCF)-based cells.
- Develop an economical, scalable process for fabricating a dense samarium-doped ceria (SDC) interlayer.

Accomplishments

- Determined that the stability and performance of lanthanum strontium manganite/yttria-stabilized zirconia(LSM/YSZ) cathodes are affected by SCN-1[1] glass but LSCF cathodes are not significantly affected.
- Demonstrated the importance of cathode sintering temperature optimization.
- Operated an SOFC in a high temperature X-ray diffractometer (HTXRD).
- Began long-term tests of LSCF cathodes with varying A-site stoichiometry.

[1] SCN-1 is a glass belonging to the system SiO_2-CaO-Na_2O

Introduction

Minimization of electrode polarization processes at intermediate temperatures represents one of the greatest challenges in obtaining high, stable power densities from SOFCs. While it is generally agreed that cathode polarization processes are a major contributor to power degradation during long-term operation of SOFCs, the specific mechanism(s) are still not well understood. One school of thought is that it is at least in part due to evolution of Sr from the LSCF lattice during cell operation [1-3] which affects cell performance in at least two ways. First, the Sr diffuses to the YSZ interface where it reacts to form electrically resistive $SrZrO_3$. As it diffuses, the Sr is likely to migrate by surface diffusion and is unlikely to escape oxidation to SrO which is also a highly resistive oxide. Sr-enrichment and/or SrO at the surfaces and interfaces on the cathode side of the cell would be expected to interfere with the oxygen reduction and charge transfer reactions and thereby also affect nonohmic polarization. Secondly, depletion of Sr from the LSCF lattice and enrichment at its surface is also likely to affect the cathodic performance of LSCF. The observed precipitation of Sr from the LSCF lattice suggests that under SOFC operating conditions, the stable chemical composition of LSCF is one with a higher degree of Sr-deficiency. Thus, in Fiscal Year 2010, long-term tests of anode-supported cells with LSCF cathodes that have varying levels of A-site- and Sr-deficiency have been initiated. The impact of cathode sintering temperature on cell performance and stability has also been examined and development of higher density SDC interlayers is underway. Additionally, capabilities are being developed to run in situ HTXRD measurements on SOFC cathodes during cell operation to determine whether additional insight into the mechanisms of power degradation can be gained through such measurements.

Another potential cathode-related challenge facing stack developers is degradation of cathode performance over time due to interaction between the cathode material and gas species volatilized from other stack components, such as alloy interconnects (e.g., Cr) and/or glass seals (e.g., B, Na, K). The potentially deleterious effects of volatile Cr species on cathode performance have been the subject of numerous studies, while effects of volatile seal constituents have received very limited attention to date. During FY 2010, a study of the possible impact of constituent evaporation from candidate sealing glass SCN-1 on the performance and stability of SOFC cathodes has been performed.

Approach

Typical Cell Preparation and Testing. The following procedure was adopted for preparing and testing all anode-supported button cells except for those used in experiments for which deviation from this procedure was required. These experiments and the associated procedural modifications will be described below. Anode-supported electrolyte bilayers were fabricated through a non-aqueous tape-casting and lamination process. Green tapes of the electrolyte (YSZ), functional anode layer and bulk anode layer were laminated together and then co-sintered in air. After sintering, the thickness and diameter of the bilayers were approximately 1 mm and 25 mm, respectively, with a dense electrolyte membrane (~8 µm thick). SDC interlayers were applied to the anode-supported YSZ membranes via screen printing an ink that was made from 40 wt% submicron (~0.2 µm) SDC powder (Praxair Specialty Ceramics, Woodinville, Washington) in V-006 binder (Heraeus, West Conshohocken, Pennsylvania). The screen-printed SDC layer was then co-sintered with the anode current collector (Ni mesh embedded in NiO paste) at 1,200°C for 2 hours. LSCF powder with the nominal composition $La_{0.6}Sr_{0.4}Co_{0.2}Fe_{0.8}O_{3-\delta}$ (Praxair Specialty Ceramics) that had been attrition milled for 5-10 hours was applied by screen-printing and then sintered at 1,100°C. The cathode area after sintering was 2 cm^2 and was the active cell area used to calculate power density. The cathode contact material was Sr-doped lanthanum cobaltite (LSC). The cells were sealed to alumina test fixtures using a glass sealing material. Current-voltage and electrochemical impedance spectroscopy (EIS) data were recorded at various temperatures from 600 to 850°C using a Solartron 1480 Multistat and 1255 Frequency Response Analyzer. During EIS measurements, cells were subjected to direct current operating voltages in the range of open circuit voltage to 0.5 V. The typical alternating current amplitude was 20 mA. The fuel side gas (H_2-3% H_2O) was supplied to the anode at 200 sccm. Air was supplied to the cathode at 400 sccm.

Cathode Sintering Temperature. In order to determine the impact of sintering temperature on cell performance and stability, a number of cells were fabricated and tested according to the above procedure except that the cathodes were sintered at various temperatures between 900 and 1,150°C.

A-site Stoichiometry. Cells were fabricated and tested according to the above procedure using LSCF cathodes with varying degrees of A-site deficiency and Sr-deficiency. The A-site deficient compositions have the chemical formula $(La_{0.6}Sr_{0.4})_{1-x}Co_{0.2}Fe_{0.8}O_{3-\delta}$ and the Sr-deficient compositions have the chemical formula $La_{0.6}Sr_{0.4-x}Co_{0.2}Fe_{0.8}O_{3-\delta}$ where x = 0.02, 0.05, and 0.10 in both cases. The cathode powders for this study were supplied by Fuel Cell Materials.

SDC Interlayer Densification. Many alternatives were pursued in an effort to increase the density of screen-printed SDC interlayers. Screenprint inks were made using 20-100% nanoscale SDC powder (Fuel Cell Materials, Lewis Center, Ohio) that had a specific surface area of 199 m^2/g with the balance of the powder being the standard submicron SDC described above. Other inks were made using submicron SDC that had been doped with 1-10 mol% of Li, Fe, Zn, Mn, Al, Bi, Co, or Cu. Additionally, inks were made using 2 mol% Cu-doped SDC at 20-80% solids loading in various binder systems, including B-75717 (Ferro Electronic Materials, Cleveland, Ohio), ESL 450 (ESL Electroscience, King of Prussia, Pennsylania), and the standard V-006. For these tests, after the SDC layer was sintered, the specimens were sectioned and polished for scanning electron microscopy (SEM).

In Situ HTXRD. Cells to be tested in the HTXRD were reduced to ~13 mm in diameter and the cathode area was reduced to 0.5 cm^2. Additionally, in order to avoid shielding the cathode from the impinging X-rays, the LSC contact layer was not used. Instead, a gold paste current collector was applied to the cathode and contacted by gold mesh. Otherwise, cells were operated in the heating chamber of the HTXRD according to the above procedure with gas flow rates of 100 sccm fuel and 300 sccm air.

Concentration Polarization. Investigations of the impact of concentration polarization on SOFC performance were carried out under varying cathode gas (oxidizer) conditions, including stagnant air, 500 sccm of flowing air, and 500 sccm of flowing oxygen.

SCN-1 Glass Compatibility. Commercial button cells (H.C. Starck Ceramics, Selb, Germany) using LSCF and LSM/YSZ cathodes were exposed to SCN-1 glass that had been sintered at 850°C in a Pt crucible that was subsequently inserted into the gas line that feeds air to the cathode. The SCN-1 glass was then pushed into the hot zone of the furnace until it was less than 1 cm upstream from the cathode side of the cell. This was done without interrupting cell operation. Control samples were treated exactly the same as the test specimens except that there is no glass in the Pt crucible that is inserted into the air stream.

Results

Due to space constraints, the results of the various studies carried out in FY 2010 will be briefly summarized here with an attempt being made to convey the highlights of each.

Cathode Sintering Temperature. The objective of the study was to demonstrate the impact of sintering

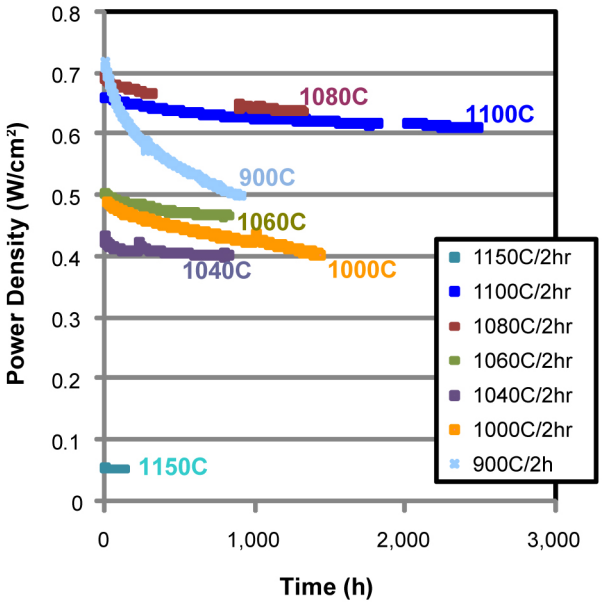

FIGURE 1. The Power Density as a Function of Time for Cells with LSCF Cathodes Fired for 2 hours at Various Temperatures

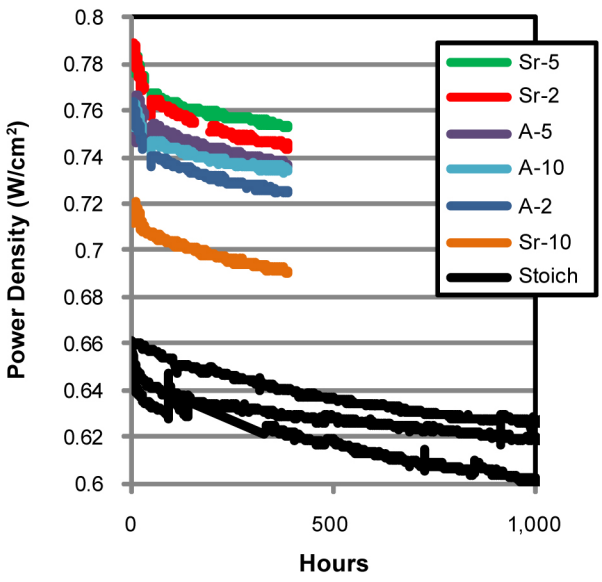

FIGURE 2. The Power Density as a Function of Time for Cells with Cathodes Made from A-Site- and Sr-Deficient LSCF as Compared to Stoichiometric LSCF Cells

temperature on LSCF cathode performance and stability and the importance of optimizing the sintering temperature for a given cathode powder. Figure 1 shows the power density as a function of time for cells with cathodes fabricated from the same LSCF cathode ink in which the only variable was the temperature at which the cathode was sintered for 2 hours. It is readily obvious that the best combination of performance and stability was exhibited when the sintering temperature was between 1,080 and 1,100°C. It should be noted that the sintering conditions found to be optimal for this specific LSCF powder are not generally applicable to all LSCF cathodes for a number of reasons including differences in composition, synthesis method, particle size and morphology, deposition method, and processing history. However, for a given LSCF powder, cathode performance and stability can be greatly affected based on the sintering conditions.

A-site Stoichiometry. Figure 2 is a plot of the performance as a function of time for cells with cathodes made from A-site- and Sr-deficient LSCF together with the performance of three previously tested cells using stoichiometric LSCF. The chemical formulae for A-site- and Sr-deficient compositions have been given above and are designated in the legend of Figure 2 as "A -*x*" or "Sr -*x*" where *x* is a number representing the percent A-site deficiency arising from the depletion of proportional amounts of La and Sr or depletion of only Sr, respectively. Meanwhile, the stoichiometric LSCF compositions are designated "Stoich" in the legend. Additionally, the legend keys for the cells have been arranged in the same order from top to bottom as the cells appear in the performance chart (i.e., from highest to lowest power density). For the first ~30 hours, the cells were operating at constant voltage (0.8 V) before a software glitch caused the data acquisition to stop. When the problem was recognized, the cells were switched to constant current mode which was the condition that had been used in the previous measurements of cells with stoichiometric cathodes. While in constant voltage mode, the degradation rates were quite high relative to those of the cells with stoichiometric cathodes. However, after switching to constant current mode, the degradation rates appear to be very similar to those of the stoichiometric cathodes that had also been operated at constant current. All of the cells with non-stoichiometric LSCF cathodes exhibit significantly higher power densities than those with stoichiometric LSCF. These tests are scheduled to run for 1,000 hours and to be repeated two additional times for a total of three sets of 1,000-hour tests. Until additional iterations of the test have been completed, the significance of the difference between the non-stoichiometric cells cannot be verified, but it appears that the Sr -10 specimen is the only one that is significantly underperforming relative to the others, while yet significantly outperforming the stoichimetric LSCF cells.

SDC Interlayer Densification. While dilatometry results indicated that an increasing ratio of nanoscale SDC powder mixed into the standard submicron SDC led to lower sintering temperatures, attempts to sinter screen-printed SDC layers containing nanoscale powder proved unsuccessful due to delamination. However, SEM of SDC that had been doped with various elements and sintered onto an anode-electrolyte bilayer at 1,200°C

for 2 hours revealed that Cu- and Co-doped SDC provided the greatest improvement in interlayer density when compared to the undoped SDC. Attempts were then made to further increase the interlayer density by repeatedly infiltrating dried, but unfired, Cu-doped SDC layers with nitrate solutions containing the constituents of Cu-doped SDC before firing. However, this attempt to improve the green density did not significantly improve the density of the sintered interlayer. SDC interlayers fabricated from ink formulations that were made using three different commercially-available binder systems, each loaded with at least three different concentrations of Cu-doped SDC powder, were examined with SEM. It was found that the ESL 450 and B-75717 binders could be loaded with 80 wt% and 70 wt% Cu-doped SDC, respectively, and still be thin enough for screen printing, whereas the V-006 binder could only be loaded with 40 wt% before becoming too viscous for reliable screen printing. Under SEM, it was found that higher solids loadings resulted in significantly improved density in the fired layers. However, at 70 or 80 wt% solids loading, the layers made using ESL 450 were cracked and delaminated, while those made using B-75717 and 70 wt% solids remained continuous and adhered to the electrolyte. By attrition milling the SDC powder for only 1 hour instead of 7-8 hours, the average particle size was increased from ~0.2 µm to ~0.4 µm. This increase in particle size made it possible to increase the maximum solids loading in the B-75717 binder to 80 wt%, however, SEM of the resulting interlayers after sintering revealed that the density was still higher when the ~0.2 µm powder was loaded at 70 wt%. Figure 3 includes SEM micrographs of sinter interlayer made using (a) 40 wt% undoped SDC in V-006, (b) 40 wt% Cu-doped SDC in V-006, (c) 70 wt% Cu-doped SDC in B-75717, and (d) 80 wt% ~0.4 µm Cu-doped SDC in B-75717.

In Situ HTXRD. A test stand has been developed that allows 13 mm diameter anode-supported SOFCs to be operated in the heating chamber of a HTXRD. The performance results of a cell that was operated in the HTXRD are plotted in Figure 4. The cell degraded rapidly, losing about 50% power in less than 200 hours. This cell had utilized a fine gold mesh current collector that had been cold rolled to a thickness of less than 40 µm and connected to the cathode using small dots of gold paste. Unfortunately, XRD results indicated that the gold mesh only allowed very weak detection of LSCF diffraction peaks. Efforts to determine a current collector configuration that would allow detection of a strong signal from the LSCF cathode found that having a current collector in the path of the X-rays had to be avoided or the LSCF peaks were greatly diminished in resulting scans. Therefore, a gold paste current collector applied only to the perimeter of the cathode has been adopted and a shim has been designed that narrows the width of the beam so that it impinges only

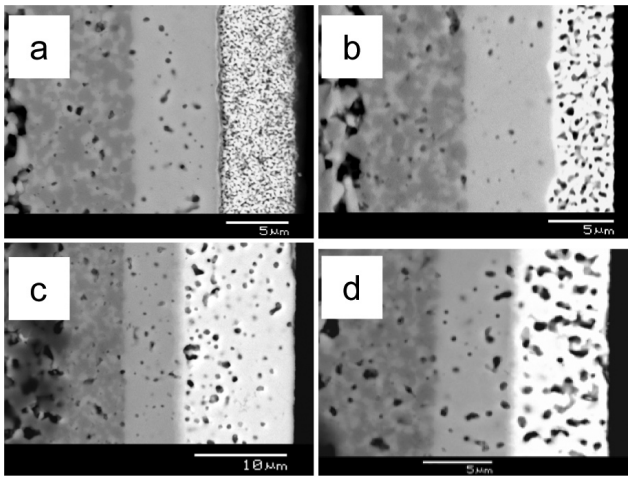

FIGURE 3. SEM Micrographs of (a) 40 wt% Undoped SDC in V-006, (b) 40 wt% Cu-Doped SDC in V-006, (c) 70 wt% Cu-Doped SDC in B-75717, and (d) 80 wt% ~0.4 μm Cu-Doped SDC in B-75717

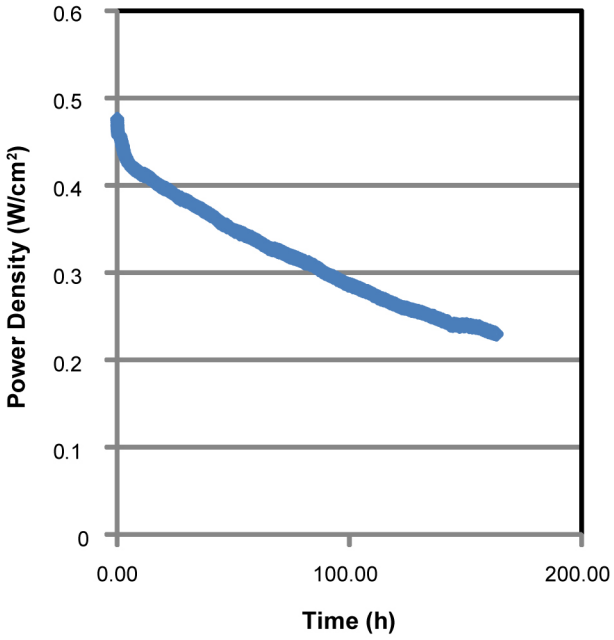

FIGURE 4. The Power Density as a Function of Time for a Cell That Was Operated in the HTXRD

on the cathode and not on the current collector around its edges. Due to the small diameter of the cathode, this configuration should provide adequate current collection, and XRD analysis of fully fixtured cells in this configuration has produced strong LSCF peaks.

Concentration Polarization. Figure 5 shows EIS results of a cell with an LSCF cathode and flowing oxygen as the oxidizer gas. It was found that the non-ohmic polarization resistance continuously decreases with increasing current density when other constituents

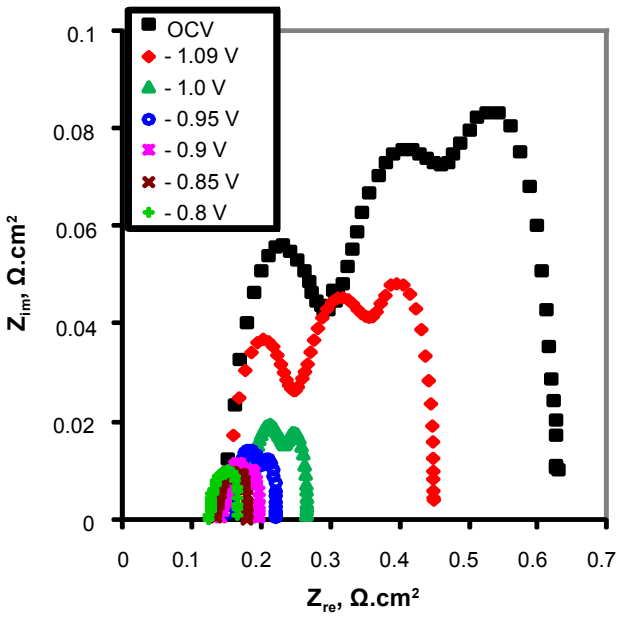

FIGURE 5. EIS Results of a Cell at 750°C with an LSCF Cathode and Flowing Oxygen as the Oxidizer Gas

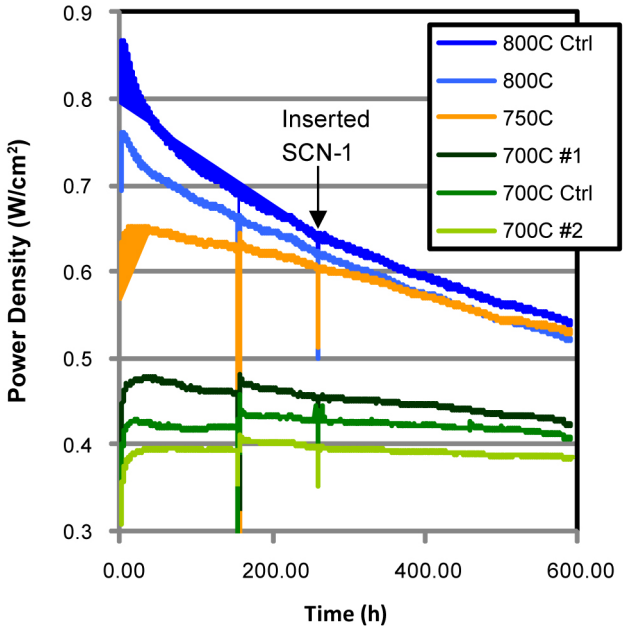

FIGURE 6. The Power Density of LSCF Cells as a Function of Time before and after SCN-1 Glass Exposure

besides oxygen are not present in the oxidizer gas. EIS measurements on this cell under flowing and stagnant air also showed a decrease with current density initially, but a minimum was reached because a low frequency arc associated with concentration polarization arose and increased in size with increasing current density. This suggests that perhaps LSCF cathodes possess sufficient cathodic activity to operate at high current densities if oxygen starvation due to diffusion limitations can be avoided.

SCN-1 Glass Compatibility. Figure 6 is a chart of the power density of LSCF cells as a function of time before and after SCN-1 glass introduction. The glass was inserted ~260 hours into the experiment and had no distinguishable effect on the performance of the LSCF cells at any of the operating temperatures investigated. Analysis of impedance spectroscopy also found no effect attributable to glass insertion. This was not the case for cells with LSM/YSZ cathodes. For LSM/YSZ cells at 800 and 850°C, insertion of the SCN-1 glass caused the power to briefly decline by ~1-2% while the control sample at 850°C did not exhibit a similar decline in power. All of the affected samples reached a minimum in power density and began to recover within 6 hours, achieving their previous power levels generally within 24 hours. EIS analysis of the LSM/YSZ cells concurred with the transient effect of SCN-1 glass on 800 and 850°C cells, as there was no remnant effect of the glass seen in the impedance spectra measured 125 hours after the glass was inserted. However, the EIS data also suggested that the SCN-1 glass had a sustained effect on the LSM/YSZ cells at 750°C that was not obvious from an initial look at the long-term performance results. The ohmic and polarization resistances of the 750°C control sample with no glass followed a similar trend to those of the samples at 800 and 850°C (i.e., no abrupt change in slope when the glass was inserted), but the two 750°C test samples exposed to the SCN-1 glass both exhibited a sudden increase in the slope of both the ohmic and polarization resistances as a function of time at this point. Once the effect of the glass on the 750°C LSM/YSZ cells was made evident by the impedance data, a closer look at the long-term performance data indeed showed that performance of the two test samples did degrade at a faster rate after glass insertion than that of the control sample.

Conclusions and Future Directions

Cathode sintering temperature optimization should be carried out for LSCF cathodes as sintering temperature has a significant impact on performance and stability. Although testing is still underway, all the levels of A-site deficiency in LSCF that are currently being tested seem to have brought about a significant improvement in power density as compared to stoichiometric LSCF cathodes and do not appear to have significantly affected degradation rates. These tests will be carried out to the planned 1,000-hour duration and the tests will be repeated twice more. Great progress has been made in improving the density of screen-printed SDC interlayers through Cu-doping and improving the ink formulation with B-75717 binder and an increase in the solids loading to 70 wt%. Interlayers will be made

with Co-doped SDC in the improved ink formulation and examined with SEM and button cell tests will be performed on cells made using ink formulations that are found to produce the best SDC interlayers. It has been demonstrated that SOFC testing can be performed in the HTXRD and that strong diffraction patterns from the cathode can be detected if the current collectors are attached to the perimeter of the cathode. Next, we will acquire HTXRD patterns from an LSCF cathode during SOFC operation. Concentration polarization studies indicated that perhaps more emphasis should be placed on microstructure optimization to avoid diffusion limitations and concentration polarization. It was found that SCN-1 glass seal material had no significant effect on LSCF cathodes but did affect LSM/YSZ cathodes.

FY 2010 Publications/Presentations

1. Z. Lu, X.D. Zhou, D. Fisher, J.W. Templeton, J.W. Stevenson, N. Wu, and A. Ignatiev, "Enhanced Performance of an Anode-Supported YSZ Thin Electrolyte Fuel Cell with a Laser-Deposited $Sm_{0.2}Ce_{0.8}O_{1.9}$ Interlayer," *Electrochem. Comm.* **12**(2), 179-182 (2010).

2. X.D. Zhou, L.R. Pederson, J.W. Templeton, and J.W. Stevenson, "Electrochemical Performance and Stability of the Cathode for Solid Oxide Fuel Cells. I. Cross Validation of Polarization Measurements by Impedance Spectroscopy and Current-Potential Sweep," *J. Electrochem. Soc.* **157**(2):B220-B227 (2009).

3. Z. Lu, L.R. Pederson, J.S. Hardy, J.W. Templeton, and J.W. Stevenson, "On the Ohmic Resistance of the Anode-Supported Solid Oxide Fuel Cells (SOFC)," Presented at 34th International Conference and Exposition on Advanced Ceramics and Composites (ICACC), Daytona Beach, Florida (2010).

4. X.D. Zhou, S.P. Simner, J.W. Templeton, Z. Nie, J.W. Stevenson, and B.P. Gorman, "Electrochemical Performance and Stability of the Cathode for Solid Oxide Fuel Cells II. Role of Ni Diffusion on LSM Performance," *J. Electrochem. Soc.* **157**(5):B643-B649 (2010).

References

1. S.P Simner, M.D. Anderson, M.H. Engelhard, and J.W. Stevenson, *Electrochemical and Solid State Letters*, **9**, A478 (2006).

2. A. Mai, M. Becker, W. Assenmacher, F. Tietz, D. Hathiramani, E. Ivers-Tiffée, D. Stover, and W. Mader, *Solid State Ionics*, **177**, 1965 (2006).

3. C. Endler, A. Leonide, A. Weber, F. Tietz, and E. Ivers-Tiffée, *ECS Transactions*, **25**, 2381 (2009).

III.A.11 Electronic Structure of Cathode Materials

Walter A. Harrison
GLAM/McCullough Bldg.
Stanford University
Stanford, CA 94305-4045
Phone: (650) 723-4224
E-mail: walt@stanford.edu

DOE Project Manager: Briggs White
Phone: (304) 285-5437
E-mail: Briggs.White@netl.doe.gov

Subcontractors:
- Research and Development Solutions, LLC
- Leonardo Technology Incorporated (after March 2010)

Contract Number: PPM 300.02.08

Start Date: January 7, 2008
End Date: October 31, 2009

FY 2010 Objectives

- Calculate the energy of oxygen atoms versus distance from $SrMnO_3$ (SMO) and $LaMnO_3$ (LMO) surfaces.
- Calculate the corresponding energy for molecules at both surfaces.
- Explore energy-loss mechanisms for incoming atoms and molecules.

Accomplishments

- Successfully obtained the energy of approaching oxygen atoms, showing a deep minimum on both SMO and LMO.
- Obtained a much shallower minimum energy for oxygen molecules for both parallel and perpendicular orientation, except stronger for O_2 on SMO.
- Found mechanisms for energy loss from vibrational excitation and for electronic excitation through level crossing.

Introduction

During Fiscal Year 2009 we undertook the calculation of Madelung electrostatic energies associated with the surfaces of SMO and LMO, which needed to be added to our calculation of cluster-orbital energies in order to obtain meaningful surface energies. We planned to move on to the study of oxygen atoms and molecules near these surfaces. That is just what we did, but it appeared that the direct electrostatic energies obtained with Madelung calculations were much less central than they were for surface energies. More important was the presence of occupied electronic states in the oxygen atom, higher in energy than empty states in the manganite substrate. Such an occurrence leads to unphysical results in any full density functional theory (DFT) calculation, and would also give incorrect results in our approximate method unless corrected. We exactly solved a two-electron problem which contained this difficulty, and extended the correction to oxygen near a surface. This same two-electron problem also provided a new, clear formulation of the van der Waals interaction between oxygen and a surface, which we also incorporated. This enabled us to carry out a rather complete analysis of oxygen atoms and molecules approaching the SMO and LMO surfaces.

Approach

The electronic structure of these conducting manganites which are used as fuel cell cathodes is fundamentally different from that of the more familiar semiconductors [1-3]. Here the important electrons are localized near individual manganese ions, forming local cluster states associated with the manganese ion and its six nearest-neighbor oxygen ions. The magnetic moments of the localized electrons on each cluster are aligned with each other to form local moments, coupled to those on neighboring clusters by Heisenberg exchange, forming antiferromagnetic arrays. There are no energy bands as there are in semiconductors and electrical conduction occurs through small-polaron hopping, or tunneling [2,3]. This distinction is not present in DFT, the current state-of-the-art computational method for electronic structure, which then proceeds as if there *were* energy bands. In fact it turns out that the total energy for some aspects would be very similar for the two types of systems so that the DFT calculations can give meaningful results sometimes, but not always, even though the corresponding electronic structure is incorrect. In contrast, we make simplified calculations for the correct cluster states in order to obtain total energies. At the same time we incorporate two many-body effects, also absent from DFT calculations. One distinguishes ionization energies from electron affinities on localized states, and the second gives the van der Waal's coupling which dominates the interaction with a substrate at large distances.

Results

We began with a simple description of the oxygen molecule, following Reference 1 but adjusting the parameters which enter to give the observed internuclear distance and binding energy. We then represented the electronic structure of the substrate in terms of the cluster orbitals described above, and used in References 2 and 3, to calculate a wide range of properties. For clusters at a (100) surface, the manganese ions had only five neighbors, so the calculation of cluster orbitals was modified to correspond to these surface clusters. This gave energy diagrams presented in Figure 1.

One sees here the difficulty mentioned earlier in the up-spin electron in the oxygen atom, shown to the far right, which is higher in energy than empty substrate orbitals to the left. This was rectified in our approach by adding a Coulomb repulsion U between d-state electrons, but reduced by $-e^2/r$ for transfer from the atom a distance r from the substrate cluster. (This correction was not shown in Figure 1.) This kept the electron appropriately occupying the atomic state when the atom was far from the surface. The corresponding correction was added also for approaching molecules, still appropriate though there were no occupied orbitals actually higher than those empty, as seen in the figure. We also added the van der Waals interaction (not shown in the figure) which varies as $1/z^6$, and is negligible at large spacing.

As the molecule approaches the surface, the van der Waals interaction begins to enter and then direct coupling V_{pdm} between the cluster orbitals and the atom or molecule at a distance z. This then shifts the levels for an approaching oxygen atom as shown in Figure 2 for SMO. The most interesting aspect is the total energy, shown in black, which is obtained as the sum of the energies of the occupied electronic states. It shows a deep minimum of –2.9 eV near $z = 1.8$ Å. This indicates that such an atom can indeed be strongly bound to the manganese substrate, in fact more strongly bound than if it were bound to another oxygen atom as a molecule at large distance. Thus a dissociative adsorption of the oxygen molecule is energetically allowed.

Another interesting feature of these curves is seen by noting that an atom approaching, with energy near zero at very large z, will retain the same total energy, increasing its kinetic energy down to $z = 1.8$, and then striking the surface, like a hammer, and reflecting back from $z = 1.5$ Å and leaving the surface. There can be no capture without a mechanism for energy loss. In fact, closer examination of Figure 2 shows a possible electronic mechanism for such energy loss. We note that near 1.4 Å the occupied up-spin σ state crosses the empty up-spin x^2–y^2 state. For this calculation, with the oxygen atom exactly above the substrate manganese ion, symmetry prevents any transfer of the electron, which would remain in the σ state through the crossing on the way in and as moving outward. If its trajectory is slightly displaced from this vertical line, the two states become coupled and the electron might, or might not, make a transition to the x^2–y^2 state. There is a "sweet spot" over the manganese ion through which the electron will most likely continue in the σ state through the crossing, and outside of which it will most likely make a transition. Thus, an electron can be captured by the substrate for an atom arriving at an angle with the surface through the sweet spot, and leaving outside of it,

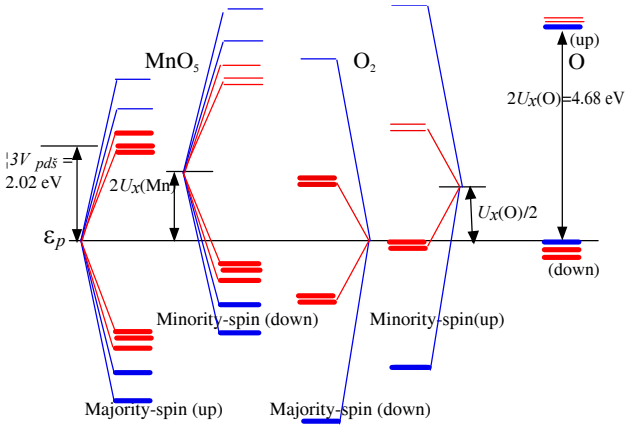

FIGURE 1. Energy levels, all measured from the oxygen majority-spin p-state energy, for the MnO_5 surface cluster in $SrMnO_3$ on the left, for an oxygen molecule in the middle, and for the oxygen atom on the right, showing the majority-spin and minority-spin levels for each. Each line represents one level; closely-spaced lines are degenerate levels. e_g levels for MnO_5 and σ-levels for O are shown in blue, t_g levels for MnO_5 and ϖ levels for O are shown in red. Those occupied in the ground state for the neutral oxygen atom, molecule, and for the Mn^{4+} clusters in $SrMnO_3$ are drawn heavy. In $LaMnO_3$ the lower of the two upper majority-spin e_g states is also occupied.

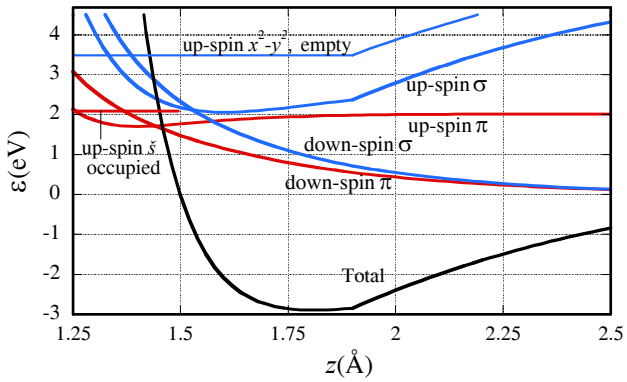

FIGURE 2. Highest occupied states of each category for an O atom, as a function of the distance z to an Mn ion under it in a SMO substrate. The total, in black, includes additional repulsions, is a minimum near 1.8 Å, and is measured from the energy at large distances. The cusps at 1.90 Å arise from taking $U-e^2/d$ equal to zero for distances less than that, and are not physical. The lowest empty state is also shown.

or arriving outside the sweet spot and leaving through it. The electron would remain in this high-energy state and the atom would not have sufficient energy to leave the surface, bound near the bottom of the total-energy curve in Figure 2. This would actually not occur for an oxygen atom with thermal incoming energy, since the atom would be reflected back before reaching this level crossing. It is nevertheless an interesting mechanism for capture of oxygen by a substrate which should be kept in mind in studying capture by a cathode.

The same calculation was carried out for an atom coming down on an LMO surface. In that case, the energy was lower if we reversed the spin of the incoming atom from that given in Figure 1, but it led to curves analogous to that in Figure 2. The total energy reached a minimum energy of –1.51 eV at $z = 1.86$ Å, not quite as strongly bound as for SMO. In both cases the resulting bond could be considered a polar covalent bond [1]. We carried out the corresponding calculation for an oxygen *molecule* on as SMO substrate, both for molecular axes oriented perpendicular to, and parallel to the surface. For perpendicular orientation the bond was very weak, –0.015 eV at 3.8 Å. It certainly would be considered a van der Waals bond. For a molecular axis parallel to the surface we again obtained a strong bond of the molecule to the Mn site, –0.90 eV at 1.49 Å. The van der Waals interaction was again dominant, but the covalent contribution brought it to smaller spacing and greater bonding. Keeping the axis parallel to the surface, the energy was actually minimum with the molecular axis rotated 45° from the cube axes of the substrate. This binding energy was sufficient that an energy of 0.32 eV would be required to spit the molecule into individual atoms bound to the surface. As for the *atom* approaching, there was no accessible level crossing, but for the molecule coming on LMO with parallel orientation, a level crossing did occur for an incident kinetic energy of 0.63 eV, so a small fraction of molecules might be captured through such a crossing. However, the bonding of the molecule on LMO is extremely weak, below thermal energies, so bonding of the molecule might not be anticipated.

It was interesting to learn that similar questions had been studied by Kotomin, et al. [4], using full density-functional calculations. They looked only at close molecules on LMO so the difficulty of unphysical properties at large spacing did not arise. Many of their results were similar to ours, and they looked at barriers to diffusion of vacancies in the surface plane, which we had not done. However, at least one conclusion was in strong disagreement with ours: they found a binding of an oxygen molecule by –1.13 eV on LMO, where we found very tiny binding. This is an important case, into which we looked, and about which we have corresponded with the author. If we proceed with a band calculation, using parameters from Reference 1, this becomes a calculation similar to theirs, though with additional approximations. However, for this band calculation, with rather broad overlapping bands, we find a large binding similar to theirs. Our view is that the energy-band description is *not* appropriate, that the electrons are localized on individual clusters with well-separated levels, and thus that the weak bonding we find is the correct physical solution. We may however regard the question as not fully resolved.

We also considered the possibility of vibrational excitations in the substrate providing a mechanism for capture, modeling the SMO lattice as shown to the right in Figure 3. It was then straight-forward to use the total energy as a function of z from Figure 2 to calculate the classical trajectory of an incoming oxygen atom, leading to the displacements as a function of time shown to the left in Figure 3. The acceleration of the atom to high energy as it approaches the surface indeed causes it to strike to the surface with sufficient force to lose most of its energy to the lattice and be captured. Thus in the case of oxygen atoms, the capture is easy, and there is no need for electronic energy loss through a sweet spot. For the much more gentle approach of molecules to the surfaces, the molecule generally recoiled with negligible loss of energy. Only in the case of O_2 on SMO was the loss sufficient to provide capture. This of course also

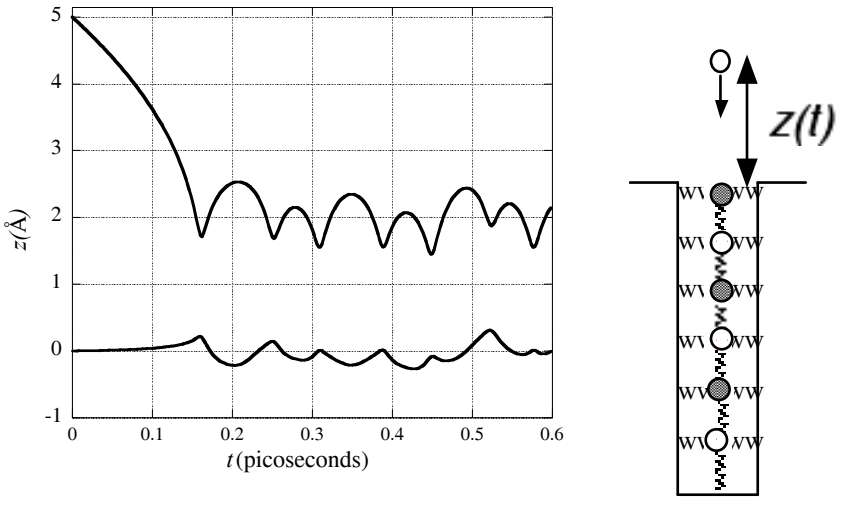

FIGURE 3. The upper curve is the position of an O atom, initially approaching an Mn ion in a surface plane of SMO from directly above with 100 meV kinetic energy. The substrate was modeled as illustrated to the right, but with a chain of ten atoms, alternately Mn and O. Below is shown the position of the top (Mn) ion of the chain.

allows capture on $La_{1-x}Sr_xMnO_3$ but there is a factor of x reduction in the capture rate since it occurs only over the Mn^{4+} sites arising from having Sr ions present.

It seemed that thermal desorption spectroscopy might be a promising experimental approach for studying these adsorptions, though this is not part of our current project. We used the absorption energies for molecules on Mn^{4+} sites to predict thermal desorption curves for lanthanum strontium manganite, which were included in the oxygen-on-manganite publication.

Finally, we considered a substrate with oxygen vacancies. They are expected to have comparable populations on the surface as in the bulk, and we found that if an oxygen atom or molecule were bound to one of the two Mn sites adjacent to the vacancy, it could role without activation energy into the vacancy, incorporating that oxygen in the substrate. This however brought up another very important consequence of the localized electronic structure of the manganites. In an ionic crystal such as rock salt, an anion vacancy will be positively charged, but will attract the extra electron present to form an *F center* in the crystal, a neutral color center the properties of which have been widely studied (e.g., Reference 1). In ZrO_2 doped with Y, the material of choice for the electrolyte in oxide fuel cells, the oxygen vacancy is *caused* by the negatively charged yttrium dopant, substituting for zirconium, with a concentration of oxygen vacancies equal to half that of the yttrium concentration, required by charge neutrality. It is energetically more favorable to have oxygen vacancies than to remove electrons from the deep valence-band states of the zirconia. In $La_{1-x}Sr_xMnO_3$ the fraction of Mn clusters which are Mn^{4+} rather than Mn^{3+} is x, to maintain charge neutrality. Similarly, if we introduce vacancies of charge 2+ into SMO we may expect charge neutrality to be maintained by producing two more Mn^{3+} clusters, and it will be energetically favorable for those two Mn^{3+} ions to be the two neighbors to the vacant oxygen site, producing a neutral F center as in NaCl. The very important conclusion is that vacancies in $La_{1-x}Sr_xMnO_3$ (LSM) are expected to diffuse as a neutral species. In the operation of the fuel cell, the current is carried by positively charged vacancies in the zirconia electrolyte, which are neutralized at the interface with the cathode, leaving neutral vacancies to diffuse to the surface. Thus, when oxygen atoms or molecules are captured or absorbed in the cathode, there is no necessity for an ionization step. Contrary to the general view, we expect no ionization of the oxygen at the cathode surface.

This however causes an important problem. We expect that surface oxygen vacancies will have both neighboring Mn ions as Mn^{3+}, and we found the strongest binding of the oxygen is for SMO, or on Mn^{4+} ions in LSM. We conclude that the adsorbed oxygen tends to avoid the sites neighboring on vacancies, an effect which may be responsible for the tiny fractional uptake of oxygen on a cathode surface. This difficulty may not be intrinsic in the sense that occupation of the neighboring sites might be catalyzed by some appropriate agent, though we have not yet come up with such an agent. All of these findings concerning oxygen on $La_{1-x}Sr_xMnO_3$ have been described more completely in our 2010 publication [5].

Conclusions and Future Directions

During the year we completed a theoretical study of oxygen on manganite surfaces, which resulted in a modified view of cathode behavior. Oxygen is understood to adhere to the surface as neutral atoms or molecules, and then enter neutral oxygen vacancies, or F centers, without the successive ionization steps usually assumed. These neutral oxygen vacancies in the cathode are supplied by the neutralization of positively charged electrolyte vacancies at the electrolyte-cathode interface. Where our calculated results differed importantly from full-scale DFT calculations, we have argued that our approach should be the more reliable. The limiting step in the process of incorporating oxygen in the cathode may be the tendency of the adsorbed oxygen to avoid sites adjacent to oxygen surface vacancies. There is hope that further understanding may lead to a way to circumvent this limitation.

The contract ended in November, 2009, and the effort was terminated except for processing the publication of a Physical Review paper on the work. The project was restarted March 15, 2010, under the auspices of Leonardo Technology Incorporated. In the new project we are focusing on problems more closely related to two experimental parts of the fuel cell project, the near-edge X-ray absorption fine structure study at the University of Nevada, Las Vegas, and faraday probe studies at Carnegie Mellon University. Both of these depend heavily on the charges acquired by ions in the bulk and at the surface, and the resulting potentials which are obtainable through the Madelung calculations such as were used for total energy calculations, and described in the annual report for 2009. The insights obtainable through this study should not only help clarify the meaning of the experimental results, but also provide insight into the surface behavior. We hope in particular to consider edges where the cathode, the electrolyte, and the air environment intersect.

FY 2010 Publications/Presentations

1. Walter A. Harrison, "Oxygen Atoms and Molecules at $La_{1-x}Sr_xMnO_3$ Surfaces," Phys. Rev. B **81**, 045433 (2010) (arXiv:0911.2268).

References

1. Walter A. Harrison, "Elementary Electronic Structure," World Scientific (Singapore, 1999), revised edition (2004).

2. Walter A. Harrison, "Tight-Binding Theory of Manganese and Iron Oxides," arXiv:0803.0994, Phys. Rev. B **77**.130001 (2008).

3. Walter A. Harrison, "Tight-Binding Theory of Lanthanum Strontium Manganate," arXiv:0807.2248, submitted to Phys. Rev. but not accepted.

4. Eugene A. Kotomin, Yuri A. Mastrikov, Eugene Heifets, and Jaochim Maier, Phys. Chem. Chem. Phys. **10**, 4644 (2008).

5. Walter A. Harrison, "Oxygen atoms and molecules at $La_{1-x}Sr_xMnO_3$ surfaces," Phys. Rev. B **81**, 045433 (2010) (arXiv:0911.2268).

III. SECA CORE RESEARCH & DEVELOPMENT

B. Anodes and Coal Contaminants

III.B.1 Perovskite Adsorbents for Warm-Gas Arsenic and Phosphorus Removal

Erick J. Schutte
Eltron Research & Development, Inc.
4600 Nautilus Court South
Boulder, CO 80301-3241
Phone: (303) 530-0263; Fax: (303) 530-0264
E-mail: eschutte@eltronresearch.com

DOE Project Manager: Joseph Stoffa
Phone: (304) 285-0285
E-mail: Joseph.Stoffa@netl.doe.gov

Contract Number: SC0000871

Start Date: July 20, 2010
End Date: April 19, 2010

FY 2010 Objectives

- Formulate and synthesize perovskite-based adsorbents containing elements that very strongly bind arsenic and phosphorus as well as sulfur and other impurities which will likely poison nickel catalysts in solid oxide fuel cells (SOFCs).
- Demonstrate rapid uptake of arsenic and phosphorus by the adsorbents.
- Demonstrate retention of arsenic and phosphorus by the adsorbents under high pressure steam at temperatures ranging from 250-400°C.

Accomplishments

- Preferred sorbents demonstrated As and P adsorption efficiencies as high as 73% versus 47% for a commercial Cu/ZnO material under ambient pressure and at 300°C under an argon stream containing 300-800 ppm As and 30-250 ppm P flowing at 2,000 hr^{-1}.
- Preferred sorbents demonstrated As and P adsorption capacities as high as 4.5% versus 1.0% for a commercial Cu/ZnO material under ambient pressure and at 300°C under an argon stream containing 300-800 ppm As and 30-250 ppm P flowing at 2,000 hr^{-1}.
- Preferred sorbents contain no noble metals and are projected to cost <$5/lb.

Introduction

Synthesis gas produced by gasification of coal is contaminated with arsenic, phosphorus, and other toxic metals that poison nickel catalysts in SOFCs at concentrations >20 parts *per billion*. Current, zinc-based sorbents are limited by reactions with steam that release arsenic and phosphorus to parts per million levels and require that a polishing filter be developed which reduces arsenic and phosphorus to low parts per billion concentrations, while operating in steam above 250°C and at pressures between one and five atmospheres. During the Phase I project Eltron focused on designing solid sorbents to very strongly bind arsenic, phosphorus and other potential poisons originating from coal forming compounds which have high melting points (>1,200°C) to prevent poison release at high temperatures or by interactions with high pressure steam.

Approach

During the Phase I project Eltron focused on designing solid sorbents to very strongly bind arsenic, phosphorus and other potential poisons originating from coal forming compounds which would possess thermal and chemical stability within the environments expected downstream from a coal gasifier/water-gas shift (WGS) system and upstream of a SOFC. Various perovskite and other ceramic-based materials were examined which contained elements known to form those types of bonds with both arsenic and phosphorus.

Testing was accomplished using a fixed bed system in which elemental arsenic and elemental phosphorus were placed in effusion cells and heated to produce vapors of the given elements prior to a sweep gas being directed through the cells and into the main reactor. Nickel-coated coupons placed both prior to and directly after the sorbent bed were used to identify the entry and exit of the arsenic and/or phosphorus. An additional reactor was designed which was similar to the initial test reactor but was capable of handling high pressures and employing steam and a simulated WGS gas mixture in addition to the arsenic and phosphorus, in order to more closely mimic environments expected in a industrial gasifier-SOFC system.

Results

Sixteen different proprietary perovskite powders to be used as adsorbents for removal of phosphorus and arsenic were prepared by standard solid-state processing procedures. Powders of the starting materials were rotated on a ball mill for several hours to produce a homogenous mixture of the powdered starting materials. Solid-state reactions were then initiated by placing mixtures of starting materials in alumina crucibles, followed by calcining at 1,200°C for 12 hours. The

perovskite powders were subjected to attrition milling for 4 hours at an agitator speed of 400 rpm to further reduce particle size to the sub-micron range. Nine of the 16 perovskite sorbents were extruded into cylindrical pellets, similar in size and shape to optimized commercial pellets of $CuO/ZnO/Al_2O_3$ for sulfur removal. For this project, all materials were extruded with a diameter of ¼". The extrudates were then sliced into cylinders of desired height (¼") after passing through the die. The cylinders were sintered by heating them at a rate of 1°C min^{-1} to the desired temperature of 1,300°C, dwelling at temperature for 4 hours, and then cooling at a rate of 1°C min^{-1} to room temperature. The sintered cylinders were crushed into smaller pieces which were sieved to between 6 and 12 mesh. These granules were initially used in the fixed beds exposed to vapors of phosphorous and arsenic during testing.

All perovskite materials were characterized after synthesis and after use as adsorbents by routine, standard analytical methods. Surface area analysis of the adsorbents was performed by Brunauer-Emmett-Teller gas adsorption. Surface areas of selected extruded sorbents and a commercial Cu/ZnO sorbent material can be seen in Table 1.

TABLE 1. Surface Area of Select Extruded Sorbents

Batch	Surface Area, m^2/g
K53-01	14.1
K53-HSA	48.3
K56-01	7.5
K57-01	12.1
K59-01	5.3
Commercial	77.4

Other characterization tasks such as X-ray diffraction (XRD) (before and after use), scanning electron microscopy and X-ray spectroscopy (before and after use), and thermogravimetric analysis to determine loss of near-surface oxygen under reducing conditions as a function of temperature were performed on selected adsorbents.

Two reactors, one for general breakthrough testing and one for testing under simulated industrial conditions, were employed during the Phase I. The first, seen on the left of Figure 1, was used solely to test arsenic, phosphorus and arsenic/phosphorus containing gas streams. The design features two effusion cells one for phosphorus and one for arsenic placed on either side of the main reactor chamber. The vapor pressure of the elements within the effusion cells was controlled through uniform heating of the cells in small, custom-made ovens. A small orifice in the effusion cells was connected to a sweep line, allowing for a controlled release of phosphorus and/or arsenic into

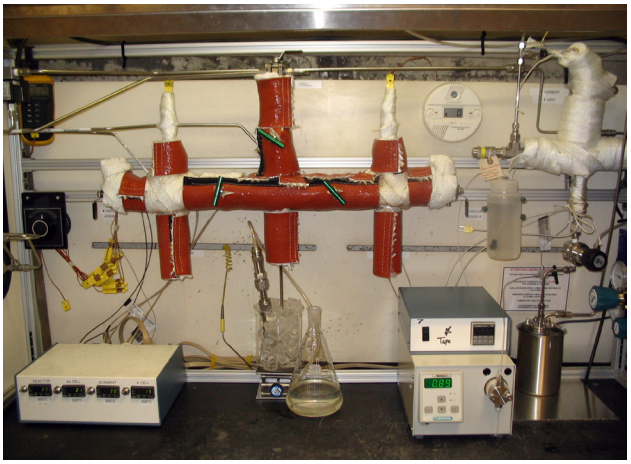

FIGURE 1. General Breakthrough (left) and Simulated Syn-Gas/Pressure (right) Reactors Designed and Built at Eltron for Sorbent Testing in Phase I

an inert gas stream of argon which carried the elements along a heated and insulated stainless steel pathway to the sorbent bed. The system also equipped with lines for introduction of hydrogen for pre-reduction of the sorbent bed prior to testing. Adsorbent beds were housed in tubes of 316 stainless steel and heated externally. The entire reactor was wrapped extensively in insulation in order to reduce the possibility "cold spot" formation that could result in condensation of arsenic and phosphorus on the reactor walls. Temperatures were monitored via 11 thermocouples placed strategically along the length of the entire reactor system.

The second reactor was constructed to handle pressures up to 5 bar and the addition of a steam-laden synthesis gas mixture to the arsenic and phosphorus streams; it can be seen on the right of Figure 1. The reactor system was equipped with lines for simulated syngas and the hydrogen used to pre-reduce sorbents. A piston pump was installed on the reactor that was capable of delivering enough water to the system to yield a steam concentration of up to 20%. Heat exchanger coils were used to raise steam from the water delivered by the pump prior to mixing with the dry synthesis gas/arsine/phosphine mixture.

Perovskite-based adsorbents were exposed to phosphorus and arsenic vapors in argon carrier gas at concentrations between 20 and 400 ppm by volume. Early shakedown tests with an inert sorbent bed in place found that heating the phosphorus bed at 450°C and the arsenic bed at 525°C yielded the appropriate amount of elemental vapor when using an argon sweep flow of 60 ml/min. This was determined by first weighing the element filled alumina boats prior to heating for 3 hours under 60 ml/min argon flow, then re-weighing the boats and calculating the mass of Ar and/or P released over time, assuming the forms of both elements were As_4 and

P_4. The assumption of As_4 and P_4 gaseous species was made based on thermodynamic equilibrium modeling.

The design of the sorbent test bed itself involved the placement of two sintered steal filter elements coated with 100 nm thin films of Ni both immediately prior to, and after, the 4-5 g sorbent bed. At parts per million concentrations, both arsenic and phosphorus form bulk compounds with nickel under warm-gas conditions. Bulk compounds in the films were detected by XRD and X-ray elemental spectroscopy, helping us confirm the presence of As and P prior to the sorbent (upstream coupon) and whether the sorbent was effective in removing those contaminants (downstream coupon).

In all, there were six different sorbents tested for 3-hour periods, under ambient pressure, and at 300°C in the As/P up-take reactor during Phase I. Control experiments with phosphorus and arsenic in argon carrier gas were deemed successful if thin films of nickel placed downstream of the adsorbents *did not* transform into bulk phosphides or arsenides. Calculated adsorption efficiencies for the six sorbents tested can be seen in Table 2.

TABLE 2. Arsenic and Phosphorus Adsorption Efficiencies

Adsorbent	As/P Sorption Efficiency (%)	Sorbent Mass Change (%)
K57-01	72.33	4.52
K59-01	23.60	0.82
Commercial	47.01	1.01
K53-01	27.87	0.56
K53-HSA	72.96	4.45
K56-01	41.56	1.09

All tests were run for 3 hours with a 1 hour H_2 reduction phase prior to arsenic and phosphorus exposure. The adsorption efficiencies were calculated by determining the amount of arsenic and phosphorus which was vaporized during the test and then comparing that total to the weight gain experienced by the sorbent. It should be noted that the nickel coupons placed downstream of the preferred sorbents did not contain any substantial arsenic or phosphorus after testing. This suggests that our sorbents may in fact possess much higher efficiencies and capacities but deposition of elemental arsenic and phosphorus occurred within the reactor body prior the sorbent bed, despite our best efforts at prevention, and thus never reached the bed to be adsorbed.

Conclusions and Future Directions

Preferred sorbents demonstrated As and P adsorption efficiencies as high as 73% and adsorption capacities as high as 4.5% versus 47% and 1.0%, respectively for a commercial Cu/ZnO material tested under ambient pressure and at 300°C under an argon stream containing 300-800 ppm As and 30-250 ppm P flowing at 2,000 hr^{-1}. The preferred sorbents from the Phase I also contain no noble metals which aids in keeping their projected costs on an industrial scale to ~$5/lb.

Specific technical objectives of the Phase II are as follows:

- Design, synthesize and optimize down-selected and new mixed metal oxide sorbents that most tightly bind arsenic, phosphorus and sulfur and will minimize release of the resulting arsenides, phosphides and sulfides into gas streams containing especially steam, hydrogen, carbon monoxide and carbon dioxide.
- Design, test and optimize sorbent catalysts that accelerate adsorption and dissociation of molecular hydrogen and H_2S, allowing partial reduction of the sorbent oxide lattice for incorporation of catalyst poisons such as arsenic, phosphorus and sulfur.
- Design and construct a reactor capable of testing As, P and S capturing sorbents that incorporates high temperatures (>250°C), high pressures (1-5 atmospheres), can be safely operated using highly toxic gases such as H_2S, AsH_3 and PH_3 and has a downstream gas analysis system capable of accurate and consistent determination of As, P and S concentrations down to and below 20 ppb.
- Perform a scale-up of the optimum sorbent discovered in the Phase II in order to provide enough material for slipstream testing on the commercial and pilot-scale gasification streams of potential Phase III partners.
- Prove that bed(s) of sorbent adequately protect current commercial SOFCs from arsenic and phosphorus poisoning.
- Perform a detailed technical and economic engineering analysis to determine the technical and economic viability of the sulfur sorbents and the system engineered to employ them.

Specific questions to be answered during Phase II are as follows:

- Do adsorbents containing various 1st row transition metals uptake and strongly bind arsenic and phosphorus as predicted by theory?
- Will adsorbents containing various rare earth elements, known for excellent binding of sulfur, also aid binding of phosphates?
- Do higher surface areas obtained through co-precipitation synthesis methods lead to improvements in sorbent performance?
- Does presence of sulfur affect performance of preferred sorbents?

- Does presence of steam affect performance of preferred sorbents?
- What affect does high pressure have on sorbent performance?
- Are accurate and repeatable As and P detection levels <20 ppb possible using the the novel testing method described within Eltron's Phase II proposal?
- Does scale-up of preferred sorbent lead to a decline in sorbent performance?
- Are the economics associated with both large-scale catalyst manufacturing and fixed bed sorbent installation downstream of a water-gas shift generator on a coal gasification unit positive? Do they indicate real commercial potential?

FY 2010 Publications/Presentations

1. Erick Schutte, "Perovskite Adsorbents for Warm-Gas Arsenic and Phosphorus Removal," Presented at the 11th Annual SECA Workshop, Pittsburgh, Pennsylvania, July 27–29, 2010.

III.B.2 Novel SOFC Anodes with Enhanced Tolerance to Coal Contaminants

Joon-Ho Koh
Materials & Systems Research, Inc. (MSRI)
5395 West 700 South
Salt Lake City, UT 84104
Phone: (801) 530-4987 Ext. 18; Fax: (801) 530-4820
E-mail: jkoh@msrihome.com

DOE Project Manager: Maria Reidpath
Phone: (304) 285-4140
E-mail: Maria.Reidpath@netl.doe.gov

Contract Number: SC0001659

Start Date: July 1, 2009
End Date: March 31, 2010

FY 2010 Objectives

- Design of solid oxide fuel cell (SOFC) anodes based on the current nickel and zirconia cermet but with some modifications on anode support and/or interlayer.
- Fabrication of planar SOFCs (from a small button size to 100 cm² active area) with the standard and various other formulations for anode support and/or interlayer.
- Electrochemical testing on the fabricated cells with H_2S, PH_3, and AsH_3.
- Post-mortem analysis on the tested cells as well as analysis on pristine cells.
- A short-stack demonstration test, using cells of the most promising anode formulation, with simulated coal syngas and key contaminants.

Accomplishments

The key observation and achievement in Phase I are summarized as follows:

- Demonstrated that MSRI's current state-of-the-art cells have tolerance to H_2S in the concentration range of 1~50 ppm.
- Designed modified anode SOFC formulations, taking into account the feasibility of cell fabrication and the cost for cell materials, that will facilitate further development of SOFC anodes with tolerance to coal gas contaminants while maintaining or improving cell performance.
- Successfully fabricated and tested planar cells, from a button size to a larger size (100 cm²), with several modified anode designs.

Introduction

SOFCs will play a key role in a highly efficient near-zero emission coal-based power generation system. To achieve the target system efficiency, SOFC anodes must be able to tolerate or mitigate the effect of certain coal contaminant compounds such as hydrogen sulfide, arsine, and phosphine.

Improved power generation technologies will help the nation make more efficient and environmentally responsible use of its abundant domestic coal reserves. The proposed effort will contribute to the development of a near-zero emission coal-based power generation system. SOFCs are one of the key technologies for integrated gasification fuel cell systems. Naturally occurring coal has many impurities, some of which end up in the syngas that is used as fuel for SOFCs [1,2]. To achieve the U.S. DOE goals such as efficiency greater than 50% (coal higher heating value to electrical power), it is essential the SOFC anode can tolerate or mitigate the effect of those impurities. The output of the proposed effort can contribute to the DOE-sponsored Solid State Energy Conversion Alliance (SECA) project that will develop commercially-viable SOFC power generation systems.

Approach

While a complete replacement of the current nickel and zirconia cermet anode is neither practically beneficial nor technically feasible for many reasons, some modification on the current anode may enhance resistance to the key coal contaminants. MSRI is working toward the development of SOFC anodes that would have enhanced tolerance to coal contaminants while maintaining electrochemical cell performance.

Results

Experiments during this Small Business Innovation Research Phase I project focused on investigating the effect of H_2S. Although the effect of H_2S on SOFCs has been studied and reported by many groups during the last decade, the results vary and they have not been able to lead to a conclusive understanding. MSRI has been continuously modifying the SOFC planar cell design and fabrication process for reliable performance and high yield. Our most recent cells have been tested for the effect of H_2S during Phase I of this project. Initial tests were carried out on button cells (~1 inch diameter) and later tests were conducted with 100 cm²

cells. The main focus in these tests is on electrochemical cell performance under the practical SOFC operating condition. The change of cell voltage was observed with and without H_2S. The initial cell voltage was typically in the range of 0.7~0.8 V. Tests were repeated on different cells to observe consistency and reliability of test results. Figure 1 shows one of the button cell test results at 750°C with a discharge current of 0.6 A. The cell voltage is stable and there is also no significant degradation caused by the presence of 1.2 ppm H_2S.

The next test was done with a larger cell (100 cm² cathode area). A single cell was tested with all the standard stack components (interconnect and sealing gasket). This cell was subject to a thermal cycle before the test with H_2S. In this test, a much higher concentration of H_2S was used. The concentration of H_2S was 100 ppm in the cylinder. Because the fuel gas to the anode was 50% H_2 (balance N_2), the concentration of H_2S introduced to the anode was 50 ppm. This is far beyond the target range of H_2S and other contaminants considered in this project. Tests with such a higher concentration of H_2S were carried out, mainly because the effect of H_2S on the tested cells was not observed otherwise. The tests with 50 ppm H_2S were conducted at various temperatures. The degradation was more noticeable at lower temperatures in general. In any case, when the fuel gas was switched back to 50% H_2 without H_2S, the cell voltage recovered. The degradation of cell voltage at 810°C is 3~4 mV and stable after the drop of voltage (Figure 2). In all the tests carried out during Phase I, the fuel gas did not include water vapor.

The 100 cm² cell size is directly applicable for small to medium size SOFC application systems (or up to a 10 kW-scale power generation unit). This cell size is also considered useful for testing of generally large cells for investigation of many stack development issues including long-term contaminant effects, sealing gaskets, interconnect, etc., because a 100 cm² cell testing involves all stack components and their effects on cell performance while it does not require any big or specially-designed testing facility. The 100 cm² cell test results are considered more reliable and informative than button cell test results. It is very encouraging that the 100 cm² cell test results in this Phase I effort have shown tolerance to H_2S consistently up to 50 ppm. Most of the SOFC applications are based on various forms of fossil-fuel resources such as coal syngas (SECA) and logistic fuels (military) which contain a significant amount of sulfur.

The Phase I effort also resulted in a modified anode cell formulation which can maximize the cell/stack performance in the presence of sulfur and other contaminants in coal syngas. The modified anode formulation is still based on the nickel and zirconia cermet, but several aspects were further addressed to realize the project goal. A brief summary of the modified anode design approach is described in what follows.

The use of precious metals (Pt, Rh, Pd, Ru, Ir, Os) was excluded due to their high cost. The electrocatalytic materials of interest are a group of relatively low-cost transition metals (Ti, V, Cr, Mn, Fe, Co, Ni, Cu, Mo, and W). These transition metal electrocatalysts are initially in the form of oxides and therefore they are sintered in their primary oxide forms together with nickel oxide and zirconia during the cell fabrication process. In order to go through a sintering process properly, a metal electrocatalyst should have a melting point higher than the sintering temperature in its stable oxide forms. The melting temperature of a metallic phase should also be significantly higher than the SOFC operating temperature (which would be 700~850°C, taking into account a significant temperature rise due to heat generated during fuel cell reactions). Another important aspect is the reduction behavior of the metal

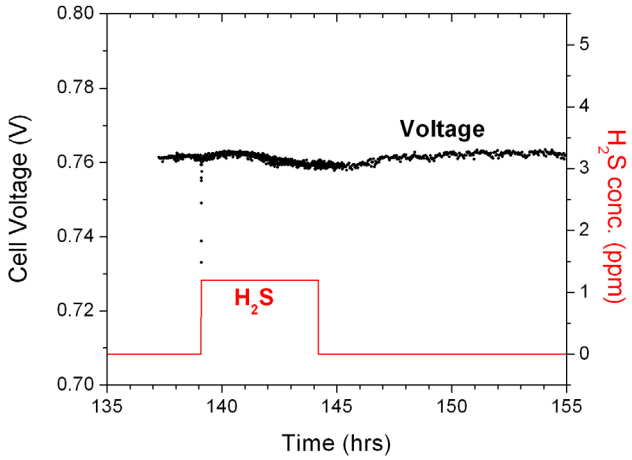

FIGURE 1. Performance of a Standard Anode Button Cell with H_2S (1.2 ppm) at 750°C

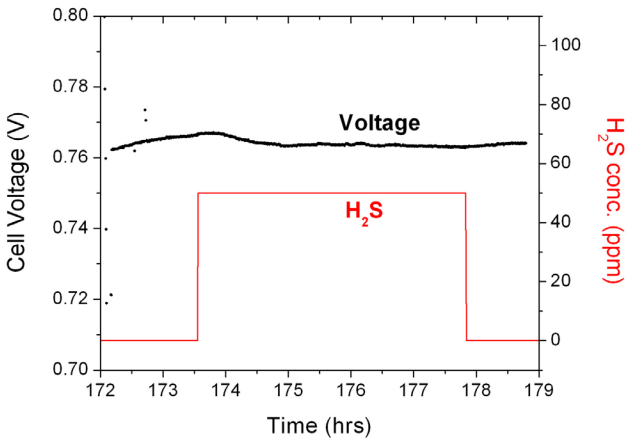

FIGURE 2. Performance of a Standard Anode 100 cm² Cell with H_2S (50 ppm) at 810°C

oxides into their metallic phases. This is important because SOFC cells are usually sintered in oxides and then in situ reduced under a flow of diluted hydrogen during a pre-conditioning (or initial heating) process after stack assembly. All these requirements for metal electrocatalysts have been reviewed with their physical properties and thermodynamic data. The Ellingham diagram, which is based on the standard free energies for formation of oxides, was used for evaluation the reduction behavior of metal oxides.

For a modified anode interlayer, Co and Fe are probably the easiest to implement, from the cell fabrication point of view. The properties of these two metals (and their oxides) and their reducibility are close to those of Ni. Some transition metals (Ti, Cr, and Mn) may be co-sintered (in their oxide forms) with Ni and zirconia, but their reduction to metallic phases will not be as easy as that of the NiO+ ytrria-stabilized zirconia (YSZ) anode. Other transition metals (Cu, Mo, W, or V) would need a different method (e.g. infiltration or impregnation of metal precursors followed by low-temperature firing) if they are to be used in the SOFC anode.

For a modified anode support, iron (Fe) appears to be the only material that can be considered either as an alternative to nickel or a bimetallic phase with nickel. This is because, in the current standard anode-supported planar SOFC design, the anode metal electrocatalyst takes approximately 70% of all the cell component materials being used. Except iron, all the transition metals cheaper than nickel have some problems with their properties or in cell fabrication. For example, zinc (Zn) melts at ~400°C and copper (Cu) cannot make an anode support because its oxide does not have a sufficiently high melting point with regard to the typical sintering temperature.

Electrical conductivity of the transition metals is generally large enough once they are completely reduced from initial oxides. The contribution to cell performance from the anode will be more likely influenced by ionic conduction in the anode interlayer and also by microstructural stability. A mixed ionic and electronic conductor based on zirconia is recommended as an alternative to YSZ in the modified anode interlayer.

Thermodynamic data for nickel sulfides, nickel phosphides, and nickel arsenides are available from the literature [3]. These are compared in Figure 3. It shows that nickel phosphides are more favorable thermodynamically than nickel sulfides and nickel arsenides. Based on this thermodynamics, the presence of phosphine is expected to have more significant effect on SOFC performance than the presence of sulfur and arsine, when the anode is Ni+YSZ. In general, however, there appears to be lack of thermodynamic information available to predict the effects of these contaminants on non-nickel-based SOFC anodes.

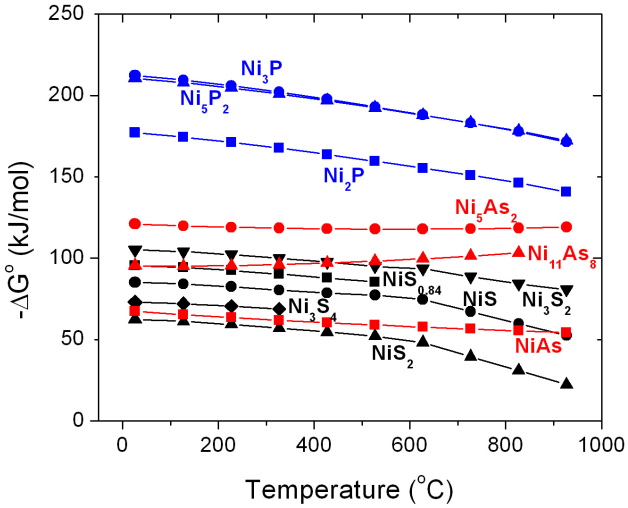

FIGURE 3. Comparison of the Standard Free Energy Change for Formation of Nickel Sulfides, Phosphides, and Arsenides

Several cells, based on the modified anode formulation, were fabricated during Phase I of this project. Two different anode formulations were implemented into the current 100 cm² cell fabrication process. These 100 cm² cells were successfully fabricated and tested. Their initial performance (power curve or current-voltage characteristics) is compared to the standard anode cell (Ni+YSZ) in Figure 4. To maximize the performance and stability of newly formulated cells, the process conditions (e.g., sintering temperature and duration) need to be fine-tuned for each modification. For this reason, the power curves of two modified anode cells in Figure 4 are certainly not the best performance for each modified design. Nevertheless, the performance of these cells is quite close to that of the standard cell.

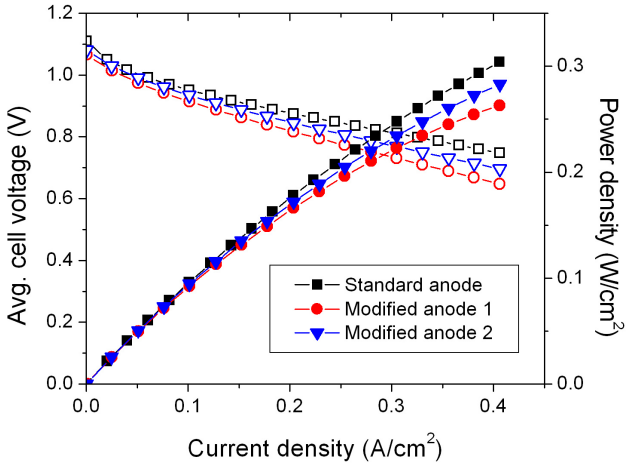

FIGURE 4. Comparison of the Current-Voltage-Power Curves of 100 cm² Cells

The successfully fabricated 100 cm² cells with modified anode designs and their satisfactory performance are very encouraging milestone achieved during Phase I. This indicates that cells with the proposed anode modification approach can be fabricated from a button size to a large size. With further optimization of the process conditions for each modification, the performance of those modified cells will be maximized. This will allow investigation of the effect of coal gas contaminants on variously formulated cells. Such an effort is planned in Phase II of this project.

Conclusions and Future Directions

The key observation and achievement in Phase I are summarized as follows:

- MSRI's current standard cells have shown consistent tolerance to H_2S in the concentration range of 1~50 ppm.
- A new cell formulation was designed further to develop SOFC anodes having tolerance to coal gas contaminants. The new cell design is based on the current standard nickel and zirconia cermet anode, with some modifications taking into account cell manufacturability and cost.
- Several cells with modified anodes, from a button size to a larger size (100 cm²), were successfully fabricated and tested. Their initial performance is satisfactory.

Future studies in Phase II are planned to achieve the following objectives:

- To fabricate planar SOFCs (from a small button size to a 100 cm² active area cell size) with the standard and various other formulations for anode support and/or interlayer based on the Phase I design approach.
- To conduct electrochemical testing on those fabricated cells with 1~10 ppm PH_3 and AsH_3.
- To conduct further validation testing on the MSRI's standard cells, which showed promising performance with 1~50 ppm H_2S in the Phase I tests.
- To conduct post-mortem analysis on the tested cells as well as analysis on pristine cells.
- To conduct a short-stack demonstration test, using cells of the most promising anode formulation, with simulated coal syngas and key contaminants.

References

1. C. Xu, J.W. Zondlo, H.O. Finklea, O. Demircan, M. Gong, and X. Liu, "The Effect of Phosphine in Syngas on Ni-YSZ Anode-Supported Solid Oxide Fuel Cells," *Journal of Power Sources* **193** (2009) 739-746.

2. J.P. Trembly, R.S. Gemmen, and D.J. Bayless, "The Effect of Coal Syngas Containing AsH_3 on the Performance of SOFCs: Investigations into the Effect of Operational Temperature, Current Density and AsH_3 Concentration," *Journal of Power Sources* **171** (2007) 818-825.

3. I. Barin, "Thermochemical Data of Pure Substances: Parts I and II," 3rd Edition, VCH Publication, Weinheim (1995).

III.B.3 DOE/NETL In-House Contaminant R&D

Kirk Gerdes
U.S. Department of Energy
National Energy Technology Laboratory (NETL)
3610 Collins Ferry Rd.
Morgantown, WV 26507
Phone: (304) 285-4342; Fax: (304) 285-4469
E-mail: Kirk.Gerdes@netl.doe.gov

Contract Number: 10-220621 6923
(In-house contaminant R&D)

Start Date: October 1, 2009
End Date: September 30, 2010

FY 2010 Objectives

- Quantify the effect of solid oxide fuel cell (SOFC) exposure to process contaminants including Selexol, arsenic, selenium, and aromatic hydrocarbons. At least two 500-hour tests will be done on these species to generate data for lifetime prediction.
- Demonstrate the Fiscal Year 2009 devised protocol for gas phase analysis using the gas chromatograph-inductively coupled plasma/mass spectrometer (GC-ICP/MS) system with individual contaminant test skid and operate system on AsH_3, PH_3, H_2Se, Hg, ethylene, benzene, naphthalene, Selexol, and/or other elements.
- Compare one standard ICP/MS sample digestion method to the direct gas-phase injection methods developed under this project.

Accomplishments

- Standard anode-supported SOFC button cells composed of Ni-yttria-stabilized zirconia (YSZ)/YSZ/lanthanum strontium manganite exposed to simulated syngas containing ~1 ppm Selexol for 500 hours.
- A calibration procedure applicable to gas phase analysis of trace metal content in an industrially relevant process stream was developed. Results were compiled and the detailed procedure was submitted to a peer reviewed journal. This study represents the first known publication of calibration pertinent to direct gas phase analysis of a high temperature process stream containing trace metals.
- An operating method for gas phase analysis of trace metal content by GC-ICP/MS was drafted. Operating results for gas phase operation and analysis were compared to samples generated from standard liquid digestion methods. A formal report will be compiled and submitted to a peer reviewed journal for publication in FY 2011.
- The GC-ICP/MS analytical system was remotely deployed to a gasification facility (National Carbon Capture Center/Power Systems Development Facility, Wilsonville, AL) to generate gas phase trace metal analysis in support of on-going contaminant sorbent testing for a commercial sorbent developer.
- Results of a thermodynamic analysis of nickel-based SOFC anode interactions with trace materials in coal-derived synthesis gas were compiled in a report published by the peer reviewed Journal of Power Sources.
- The individual contaminant test skid was modified to allow exposure of SOFC to simultaneous gas phase contaminant materials including cyclic hydrocarbons (benzene, naphthalene), arsenic, phosphorus, and selenium. The test facility is one of two known facilities capable of precisely exposing SOFC to arsenic and selenium.

Introduction

High efficiency electricity producing systems containing SOFCs are the subject of substantial federally supported research. Many of the system designs considered include a coal gasification unit coupled to a gas processing system that provides synthesis gas to the SOFC. The coal gasification process may volatilize some of the naturally occurring trace materials found in the coal. Nickel-based SOFC anodes have been theoretically and experimentally shown to negatively interact with trace metal species contained in synthesis gas derived from coal gasification.

In order to operate SOFCs on coal fuel sources, the trace materials that are reactive with the fuel cell anode must first be identified. Trace material exposure limits acceptable for maintaining SOFC performance must also be determined as a function of operating conditions. Results of this research effort are used to design cleanup systems that will reduce the trace material content of the fuel stream to operationally acceptable levels.

Approach

The research is comprised of two primary research activities. In activity 1, representative SOFC test specimens are exposed to trace contaminant materials in a controlled laboratory environment during 500-hour tests under physically relevant operating conditions. During the test, the SOFC performance is continuously

monitored through a series of electrochemical tests including current/power/voltage monitoring and electrical impedance spectroscopy. After the tests, the SOFC specimens are observed with microscopic and spectroscopic techniques to investigate the impact of contaminant exposure on material composition and structure. Electrochemical testing results are compared to micro/spectroscopic details and modes of contaminant attack and processes of anode degradation are postulated.

In activity 2, a technique is developed to quantify the trace metal content of the synthesis gas exposed to the SOFC using a GC-ICP/MS device. Existing techniques of ICP/MS and GC-ICP/MS have been widely demonstrated using liquid phase samples, but effective techniques have not been reported for direct gas phase analysis. The technique developed in this activity captures and analyzes gas phase samples for trace metal in less than 5 minutes and compares favorably to traditional techniques which require sample capture periods of 4-12 hours.

Results

In FY 2010, the individual contaminant exposure testing activity completed the analysis of the SOFC performance impact of exposure to higher hydrocarbons and began investigating the impact of Selexol exposure. Exposure analysis for higher hydrocarbons indicated that by assuming a baseline cell degradation rate (continuous, linear thermochemical or thermomechanical degradation) of 0.25%/1,000 hours and a minimum acceptable cell operating voltage of 0.7 V, a maximum exposure limit could be determined. The maximum exposure limit for benzene was determined to be 150 ppm, although this result was limited by the maximum concentration of benzene exposure applied in the tests (150 ppm). The maximum acceptable exposure concentration of naphthalene was determined to be 110 ppm.

Collected electrochemical impedance data were normalized to remove cell ohmic resistance contributions (Figure 1). The data indicate that the cell polarization increased in magnitude and the peak frequency of the contributing processes became smaller as exposure time increased. Such behavior indicates that resistances associated with lower frequency processes (such as mass transfer) are becoming more dominant.

Post-operational microscopy and spectroscopy were performed on the cells exposed to benzene and naphthalene to search for the physical source of the performance degradation. No bulk surface carbon was observed and no bulk carbon was observed in the pores. Surface sensitive measurements collected by X-ray photoelectron spectroscopy revealed no surface carbon deposits. Some transmission electron microscopy (TEM) analysis was performed which detected small secondary

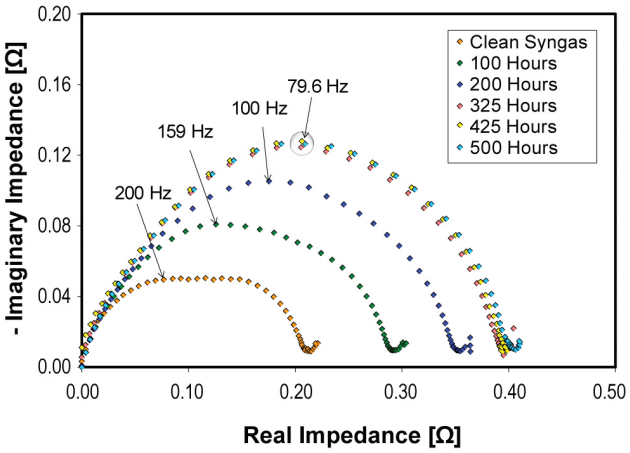

FIGURE 1. Electochemical impedance spectroscopy data collected for 500-hour operation of SOFC on synthesis gas doped with 500 ppm naphthalene.

phase inclusion (<10 nm in diameter), but due to the small size the exact identification of the phase is not yet complete. The preliminary result indicates that the small secondary phases may be a Ni_yC_x phase, but analysis of these specimens by TEM and other spectroscopic techniques will continue in FY 2011.

The FY 2010 gas phase trace metal analysis activity using GC-ICP/MS generated the first known method intended to calibrate an ICP/MS instrument for direct gas phase analysis. The procedure demonstrated a method of calibration whereby a detector response to a known element concentration is compared to the relative detector response of an unknown analyte in order to provide a correlated quantification of the unknown analyte. This process is referred to as a "semi-quantitative" calibration and analysis technique, and leverages empirically determined instrument responses that depend primarily on the analyte mass and instrument tuning parameters. An empirical parameter set is also obtained that describes the conditions of the ionization media, an argon plasma typically generated at a power of greater than 1,000 W. These two empirical factors were demonstrated to predict the concentration of nearly all elements in an "unknown" matrix containing more than 45 species at a concentration of 10 ppb, as shown in Figure 2. For this complex system, the semi-quantitative accuracy was better than 50% for most elements. This accuracy compares favorably with the accuracy of traditional ICP/MS, and is expected to be improved through continuing research in FY 2011.

A second major accomplishment of the trace metal analysis activity was the demonstration of the devised calibration method to accurately predict the concentrations of a mixed phase sample. In this analysis, the 45 element liquid phase sample was injected simultaneously with a gas phase sample

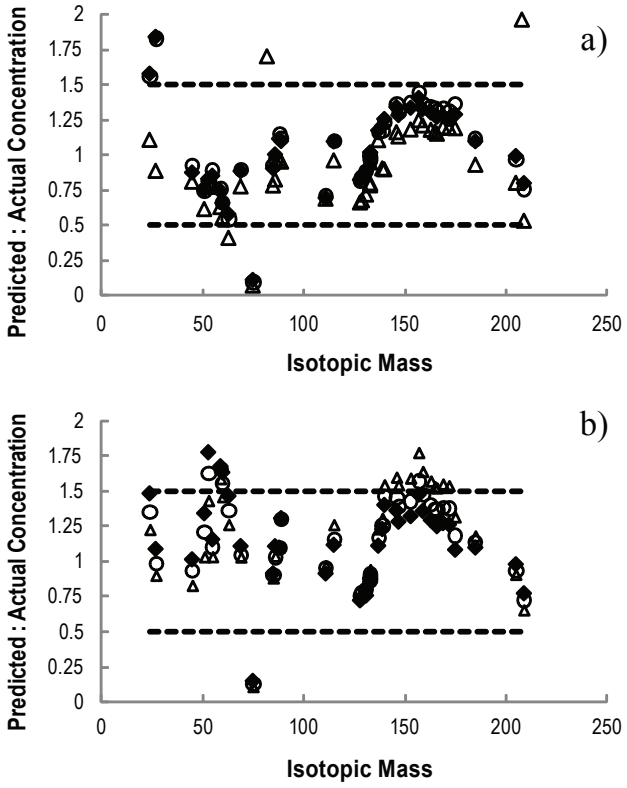

FIGURE 2. Ratio of predicted to actual concentration for a 45-element standard analyzed using semi-quantitative analysis at 1,000 W (△), 1,200 W (○), and 1,500 W (◆) for No Gas (a) and He-3 (b) modes. The dashed lines (– –) depict +/- 50% accuracy.

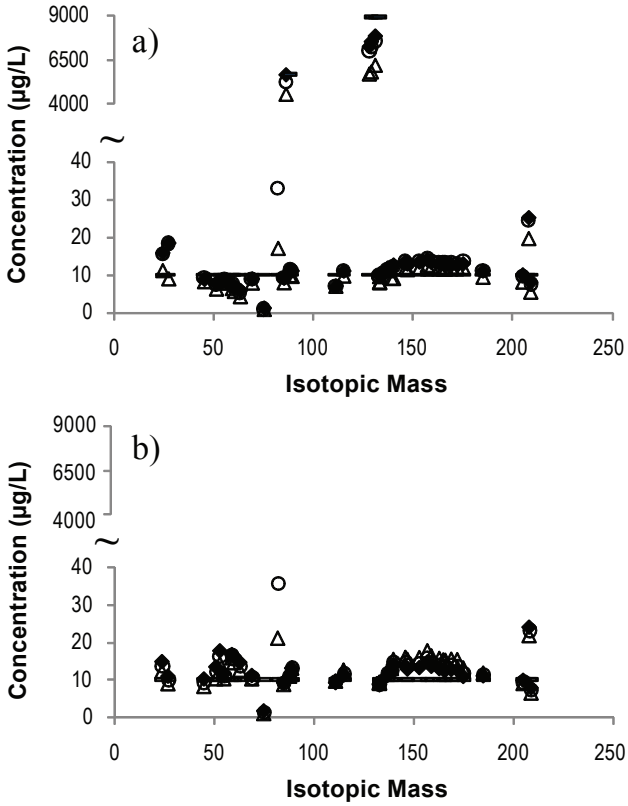

FIGURE 3. Predicted concentration for a 45 element liquid standard with simultaneous detection of a 2-element gas phase standard 1,000 W (△), 1,200 W (○), and 1,500 W (◆) for No Gas (a) and He-3 (b) modes. Mixed phase injection over three orders of magnitude dynamic range is demonstrated. Actual elemental concentrations are represented by dashes (—) for each element.

containing krypton and xenon at relative concentrations that were more than three orders of magnitude greater than those in the liquid sample. As shown in Figure 3, the concentrations were semi-quantitatively predicted at better than 50% for most elements with a dynamic linear detector response over three orders of magnitude. This important result validates the application of the developed method to direct gas phase analysis and indicates the technique's suitability for collection and analysis of industrially relevant process streams containing trace metals.

Conclusions and Future Directions

The in-house contaminants research and development effort in FY 2011 will extend the research completed during the two primary FY 2010 activities. Investigation of trace material exposure will be extended to include additional trace metal species such as arsenic and selenium. The experimental efforts will continue to focus on determination of acceptable trace material exposure, and for beginning more detailed investigation of processes by which anode degradation due to contaminant exposure occurs. The activity pertaining to development of analytical methods for direct gas phase analysis for trace metals will continue by further refining the accuracy of the empirical predictions. Improvement of the empirical factors should tighten the uncertainty in reported results and improve semi-quantitative evaluations of concentration in an unknown sample. The analytical system will further be deployed to support materials and performance testing of other technologies (catalysts, sorbents, membranes, etc.) in industrially relevant processes, as possible.

FY 2010 Publications/Presentations

1. A. Martinez, K. Gerdes, R. Gemmen, and J. Poston, "Thermodynamic analysis of interactions between Ni-based solid oxide fuel cells (SOFC) anodes and trace species in a survey of coal syngas," *Journal of Power Sources*, **195**, 16 (August 2010) **5206-12**.

2. K. Gerdes and K. Carter, "Calibration method for direct GC-ICP/MS analysis of gas phase samples," submitted to *Spectrochemica Acta B*.

3. K. Gerdes, "U.S. DOE SOFC testing at NCCC-PSDF," NCCC/PSDF – DOE review (November 9, 2009) Wilsonville, Alabama.

III.B.4 Sorbents for Warm Temperature Removal of Arsenic and Phosphorous from Coal-Derived Synthesis Gas

Dr. Gokhan Alptekin
TDA Research, Inc.
12345 W. 52nd Avenue
Wheat Ridge, CO 80033
Phone: (303) 422-7819
E-mail: galptekin@tda.com

DOE Project Manager: Joseph Stoffa
Phone: (304) 285-0285
E-mail: Joseph.Stoffa@netl.doe.gov

Contract Number: SC0001492

Start Date: July 20, 2009

End Date: April 19, 2010

Introduction

Gasification converts coal and other heavy hydrocarbon feedstocks into synthesis gas feed streams that can be used as a fuel for highly efficient power generation cycles. Integrated gasification fuel cell (IGFC) systems are attractive alternatives to current power generation technologies in large-scale stationary applications. Electrochemical oxidation of the synthesis gas fuel in a solid oxide fuel cell (SOFC) and takes place at lower temperatures (650°C to 850°C) than combustion-based power generation technologies, thereby greatly reduces the emissions of nitrogen oxides. In a carbon-constrained world, SOFCs also promise to lower CO_2 emissions due to their highly efficient operation. Further, because the fuel and oxidant streams are separate and CO_2 can be recovered in a concentrated form, any CO_2 emissions can also be captured and sequestered much more efficiently.

However, coal-derived synthesis gas contains a myriad of trace contaminants that may poison the fuel cell electrocatalyst. Recent investigations sponsored by the U.S. DOE have shown that in addition to sulfur, the SOFCs are particularly susceptible to poisoning by the trace amounts of phosphorus and arsenic present in the coal-derived synthesis gas. Due to the complex nature of the synthesis gas and the molecular permutations by which these impurities are present, it is difficult to formulate a fuel cell electrocatalyst that is resistant to all contaminants. Therefore, the synthesis gas feed must be treated before it enters the fuel cell system to ensure that the concentrations of these contaminants are reduced to levels that allow long-term stable operation of the fuel cell. Several researchers have shown that the contaminant concentrations must be reduced to less than 20 ppbv in the fuel gas to prevent degradation of the cell performance.

Approach

Although several adsorption technologies are available to remove arsenic and phosphorous impurities (mainly to prevent emissions from semi-conductor manufacturing plants), none of these technologies are applicable to warm gas clean-up, which could significantly improve the efficiency of the IGFC power cycle.

TDA Research (TDA) is developing a low-cost, high-capacity expendable chemical sorbent that can remove the arsenic, phosphorous, sulfur and other trace metal (e.g., mercury) from coal-derived synthesis gas at warm-gas temperatures (260°C, above the dew point of the synthesis gas). The sorbent will reduce the concentration of all of these contaminants to ppbv levels, protecting the fuel cell (see Table 1). Unlike the commercially available physical adsorbents used for trace metal removal or for sulfur polishing, this sorbent operates above the dew point of the synthesis gases (220-260°C) enabling the power cycle to operate with a very high efficiency.

TABLE 1. Sorbent Capacity for Target Contaminants (lb of contaminant removed per lb of sorbent)

Contaminant	Sorbent Capacity
H_2S	7.75%
PH_3	7.00%
AsH_3	2.79%

Results

In the Phase I work, TDA identified a sorbent composition that can effectively remove the target synthesis gas contaminants at the desired temperature range. The sorbent achieved a high capacity while reducing the contaminant concentrations to less than 10 ppbv under representative conditions. The best sorbent formulation developed for this application achieved a high capacity for all target contaminants (e.g., 2.79 wt% capacity for arsenic, 3.6 wt% for PH_3, and up to 7.75 wt% capacity for sulfur) while removing greater than 99% of the contaminants under representative conditions. Pre-breakthrough concentrations of less than 10 ppbv each for AsH_3 and PH_3, which was the detection limit of the measurement device,

were measured. (The thermodynamic equilibrium calculations suggest that parts per trillion levels are readily achievable). In addition, it was shown that the sorbent could achieve 0.08 wt% Hg capacity at 220°C under representative conditions, enabling an all high temperature warm gas clean-up technology for the IGFC plant (assuming that existing warm gas bulk desulfurization and CO_2 systems are in place). A semi-moving bed reactor was designed to house the sorbents, which allows achievement of a high sorbent utilization, reducing the sorbent replacement and capital costs.

Based on the experimental data, a preliminary engineering analysis was carried out to estimate the cost of cleaning of the synthesis gas for a 100 MWe IGFC plant. Using the gas composition from an oxygen-blown slagging gasifier and contaminant concentrations reported based on Eastman Chemicals' operating experience in the Kingsport, TN plant, it was estimated that the guard bed reactor will consume ~303 lb sorbent per day (equivalent of ~50.6 tons of sorbent per year). At $4/lb estimated sorbent cost, the sorbent replacement will be estimated to be $443,199 at 100% capacity factor for the clean-up system. The cost of all major process equipment used in the clean-up system was estimated to be $3.77 million ($37.7/kWe). Based on annualized capital cost and operating and maintenance expenses, it was estimated that the total cost of cleaning the synthesis gas will be $3.19 per 1,000 kg gas. The overall impact of the clean-up process on the cost of electricity is estimated as $0.0025/kWh, representing less than ~3.3% of the cost of electricity (assuming $0.0753/kWh as the selling price of electricity).

Future Directions

In Phase II, TDA Research will continue to improve the sorbent. The production rate and batch size will be scaled up using high throughput equipment. A slipstream will be demonstrated using actual coal-derived synthesis gas to fully assess the technical viability of the new gas clean-up concept.

III.B.5 Investigation of Modified Ni-YSZ-Based Anode for High Impurities Containing Syngas Fuels

Dr. Conghua Wang
TreadStone Technologies, Inc.
201 Washington Road
Princeton, NJ 08540
Phone: (609) 734-3071; Fax: (609) 734-2967
E-mail: cwang@TreadStone-Technologies.com

DOE Project Manager: Joseph Stoffa
Phone: (304) 285-0285
E-mail: Joseph.Stoffa@netl.doe.gov

Contract Number: NT0006343

Start Date: June 2009
End Date: May 2010

FY 2010 Objectives

- Investigate migration rate and approaches to mitigate the risk by preparing yttria-stabilized zirconia (YSZ) disks and characterize the diffusion rate. Investigate barrier layers that reduce diffusion.
- Identify anode reaction catalyst using syngas fuels.

Accomplishments

Proof-of-concept experimental results indicate that the modified YSZ anode material is capable of with standing increase tolerance to impurities under simulated gas feeds.

Introduction

TreadStone Technologies, Inc. initiated work to investigate modified Ni-YSZ-based anodes that improves its resistance to impurities contained in syngas fuels from coal-based power plants. Improved power generation technologies will help the nation make more efficient and environmentally responsible use of its abundant domestic coal reserves. Accordingly, advances in solid oxide fuel cells (SOFC) technology are sought for integrated gasification fuel cell (IGFC) systems. IGFC systems are attractive alternatives to current technologies in large-scale stationary applications. SOFCs offer considerable opportunities with respect to CO_2 capture (by keeping the fuel and oxidant streams separate) and lower CO_2 generation (as a result of higher efficiency). With these advantages, systems containing improved fuel cell technology in combination with heat recovery subsystems and commercial CO_2 capture technology can meet Department of Energy (DOE) goals: efficiency greater than 50% from coal (higher heat value) to electrical power, NOx emissions less than 15 ppm with 0.5 ppm readily achievable, carbon capture greater than 90% with 99% achievable, and a significantly reduced water footprint. Consistent with these goals, the DOE-sponsored Solid State Energy Conversion Alliance will develop commercially-viable ($400/kW) SOFC power generation systems by the year 2010. This SOFC technology has potential application in military fuel cell projects.

Approach

The primary objective of this project is to provide proof-of-concept demonstration, using existing proprietary concepts and technology, of utilizing high-impurity tolerant SOFC anodes to mitigate the costs of coal gas cleanup. Ni-YSZ anodes are used because of their wide use, high power density, and long-term stability. Ni-YSZ anodes were modified by providing a barrier layer for improved sulfur tolerance and carbon deposition resistance. To establish the feasibility of this approach, the effects of the barrier layer on the long-term stability of the anode and power density of the cell were evaluated. TreadStone used a diffusion barrier that minimizes or eliminates migration into YSZ, and identified a high performance catalyst to improve the anode activity.

Results

Proof-of-concept experimental results indicate that the modified YSZ anode material is capable of withstanding increase tolerance to impurities under simulated gas feeds.

Conclusions and Future Directions

Further experiments of the modified Ni-YSZ anode are needed to demonstrate its performance at longer processing times (>100 hours) including impurity tolerance and long-term stability of the modified anode. The modified Ni-YSZ-based cell would need to be scaled-up to the full-size cell and stack demonstration. The necessary modification of the current low cost Ni-YSZ anode fabrication process needs to be explored and its impact on the fabrication cost needs to be evaluated.

III.B.6 Utilization of Coal Syngas in High Temperature Fuel Cells: Degradation Mechanisms and Lifetime Prediction

Prof. Ismail Celik
West Virginia University (WVU)
P.O. Box 6106
Morgantown, WV 26506
Phone: (304) 293-3209; Fax: (304) 293-6689
E-mail: ismail.celik@mail.wvu.edu

DOE Project Manager: Briggs White
Phone: (304) 285-5437
E-mail: Briggs.White@netl.doe.gov

Contract Number: 46299

Start Date: August 1, 2009
End Date: July 31, 2012

FY 2010 Objectives

- Identify the tolerance limits of solid oxide fuel cell (SOFC) anode for specific impurities.
- Predict the lifetime of the anode for a given impurity level.
- Develop remedies for impurity effects.
- Implement new characterization methods.

Accomplishments

- Observed that PH_3 forms nickel phosphide (Ni_xP_y) secondary phases inside the SOFC anode.
- Showed that HCl impurity does not affect the performance of the SOFC anode but it poses problems to tubing, metal interconnects and other corrodible materials.
- Showed that H_2S in biogas causes catastrophic failure even at moderate concentrations.
- Measured the conductivity of a SOFC anode using in situ techniques and found that it does not change appreciably upon exposure to PH_3.
- Observed that cell degradation due to PH_3 exposure is not a definite function of the over-potential.
- A layer of NiO ribbon is observed at the interface between NI and yttria-stabilized zirconia (YSZ) in recent transmission electron microscopy (TEM) experiments.
- Optical measurements of temperature changes were performed on the anode as a function of current density and fuel composition.
- Extended the SOFC modeling code to simulate planar cells running with coal syngas.
- Conducted parametric investigation to study the electrochemical and structural performance of both button and planar SOFCs.
- Fabricated high performance button cells using cost effective techniques.
- Lanthanum-doped ceria (LDC) impregnation technique for sulfur tolerance was optimized.

Introduction

This project is a continuation of an earlier three-year project supported under the U.S. Department of Energy Experimental Program to Stimulate Competitive Research (EPSCoR), a program designed to enhance the capabilities of EPSCoR states in energy research and economic development through the support of advanced research at academic institutions. The long-term goal is to establish an internationally recognized, sustainable fuel cell research center for coal-based clean power generation which serves as a technology resource for the emerging fuel cell industry in West Virginia. Towards this goal, we formed a multidisciplinary team of research professionals who have worked together for several years and have strong credentials in their respective areas of expertise. Our strengths are in applying nano-technology to develop and fabricate materials for advanced coal-based fuel cells; state-of-the-art material characterization and fuel cell testing facilities involving both ex situ and in situ measurement techniques; and multi-dimensional modeling of fuel cells at various scales using high-performance computing. During the first phase of the project, we developed a laboratory infrastructure, solidified interactive working relationships, and attained national recognition for the work conducted by the center in the area of coal-based clean power generation via fuel cells. The research cluster has proven itself to be sustainable with team members working together on other related projects. Based on the progress made, we obtained a three-year continuation of funding from DOE EPSCoR with cost share from the National Energy Technology Laboratory, West Virginia State, and WVU. Under the second phase of the project, two new WVU faculty, Dr. Edward Sabolsky and Dr. Xueyan Song, joined our group which made the research cluster even more versatile. The goal under this project is to further expand the infrastructure for fuel cell research at WVU, to increase our reputation as a centre of excellence and thus ensure continued funding. The proposed technical objectives of the project are to establish the tolerance

limits of contaminant levels in the coal syngas for SOFCs and to predict the lifetime of the cells for a given contaminant levels.

Approach

The research cluster is based on a multi-scale, multi-disciplinary approach conducted by eight faculty members in four departments at WVU. The work is organized under three integrated projects: 1) characterization of contaminant effects; 2) multi-scale continuum modeling; and 3) anode material development. The knowledge base gained from experiments (Projects 1 and 3) will be used in multi-scale computational models (Projects 2) to establish the tolerance limits for the impurities and to predict the life time of SOFCs operating on syngas with contaminants.

Results

Characterization of Contaminant Effects

The objectives of this project are to identify the degradation mechanisms and to characterize the micro-structure details using state-of-the-art testing. Effects of PH_3 and HCl on a Ni-YSZ anode-supported SOFC were tested. The results show that the degradation rate is larger at higher cell working temperatures using syngas with PH_3 though PH_3 is more reactive with Ni in the anode at lower working temperature and produces nickel phosphide (Ni_xP_y) secondary phases (see Figure 1). The dominant compositions of Ni_xP_y on the cell anode are Ni_5P_2 with H_2O present, and $Ni_{12}P_5$ without H_2O present. The production of Ni_xP_y can be generated on the cell anode using syngas or dry H_2 fuel with 10 ppm PH_3 contaminant (see Figure 1). Further, the appearance of Ni_xP_y phases is independent of the electrochemical reactions in the cell [1]. The Ni-YSZ anode-supported cell has higher tolerance of HCl impurity. The cell series and polarization resistances remained almost constant during exposure to 100 ppm HCl for 400-hour testing [2]. HCl in syngas poses a challenge not only to the tubing but also to any interconnects based on stainless steel or other corrodible materials. This issue cannot be ignored in SOFC systems using coal syngas. Tolerance tests of H_2S-laden biogas fuel on Ni-YSZ anode-supported SOFC were performed. The application of 20 ppm H_2S to the cell caused complete cell failure in very short time [3] (see Figure 2). Half cell testing along with equilibrium calculations showed that the PH_3 forms phosphates and deactivates the catalyst which is exacerbated by both temperature and PH_3 concentration [4]. Conductivity of the anode was monitored during the operation an SOFC button cell using van der Pauw technique. No significant change was observed in the conductivity of the anode when exposed to PH_3. Performance degradation during the 170 hours exposure is not due to loss of anode conductivity [5]. The effect of overpotential on degradation rate was explored in an experiment where the cell was operated at a constant voltage for at least 24 hours during exposure to syngas with PH_3. The results indicate that the rate of power loss is not a definite function of the overvoltage [6] (see Figure 3). In situ infared temperature measurement was carried out at the anode surface as a function of loading current densities to investigate the polarization effects on electrode reactions. Recent results from TEM experiments show that in the anode triple phase boundary area, a layer of ribbon NiO grain covers the entire interface between Ni and YSZ. One plausible explanation is that oxygen in the NiO ribbon (~10 nm wide) comes from the YSZ. The results show that NiO

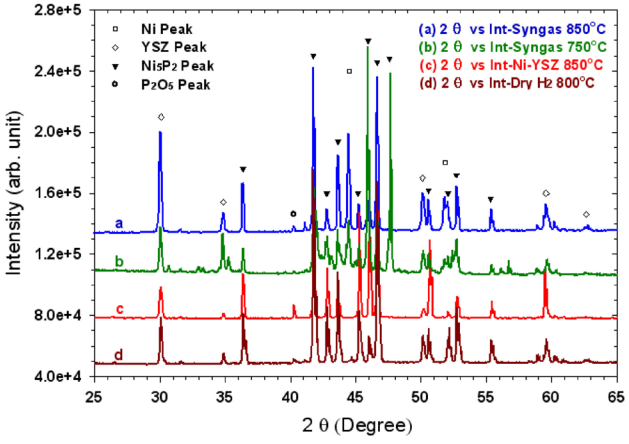

FIGURE 1. The XRD Spectra of the Top Cell Anode Surface after 200-hour Exposure to 10 ppm PH_3 in (a) Syngas Fuel at 850°C, (b) Syngas Fuel at 750°C, (c) Syngas Fuel at 850°C by Using Ni-YSZ Disc and (d) Dry H_2 at 800°C with 0.5 A/cm^2 Load

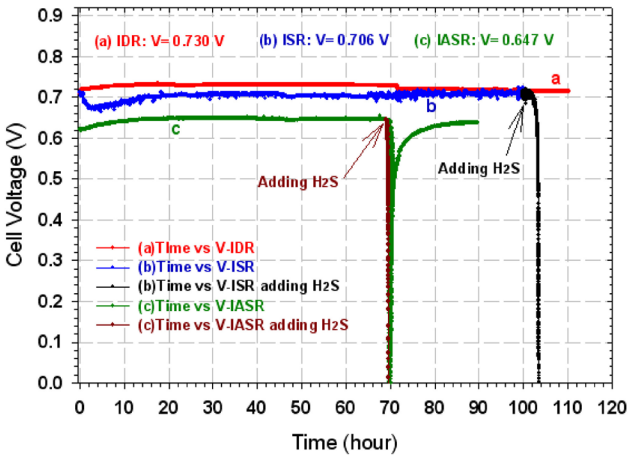

FIGURE 2. Cell Voltage vs. Time for (a) Internal Dry Reforming (IDR), (b) Internal Steam Reforming (ISR), (c) Internal Air-Steam Reforming (IASR)

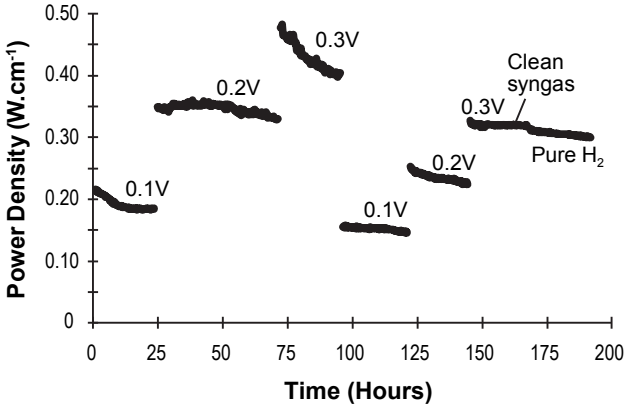

FIGURE 3. Power Degradation at Different Over-Potentials during and after Exposure to PH_3

was formed even when operated in pure hydrogen atmosphere.

Continuum Level Modeling

The objective of this project is to utilize the knowledge base obtained from short-term experiments at relatively higher concentrations of contaminants to develop theoretical models that could accurately predict the degradation behavior of cells operating on syngas with very low levels of impurities for long durations. A new phenomenological one-dimensional model was formulated to simulate the typical degradation patterns observed for coal syngas contaminants. The model parameters were calibrated to match the experimental degradation rates reported in literature for arsine (AsH_3) and phosphine (PH_3). The results at various temperatures and contaminant concentrations closely emulate the characteristic behavior of SOFC anodes exposed to these most detrimental syngas contaminants (see Figure 4). Multi-phase equilibrium calculations were performed to aid experiments in identifying the possible stable forms of the impurities under SOFC operating conditions [4]. Large planar cells operating on coal syngas were simulated using in-house modeling code DREAM SOFC and the results were used in structural durability predictions. On the structural modeling front, an alternative anode durability model was developed to incorporate thermo-mechanical as well as fuel gas contaminant effects on the anode microstructure. This model is implemented in finite element analysis and simulations were performed under different conditions [7]. The model is enhanced to predict the long-term structural behavior for a co-flow planar SOFC anode exposed to phosphine (PH_3).

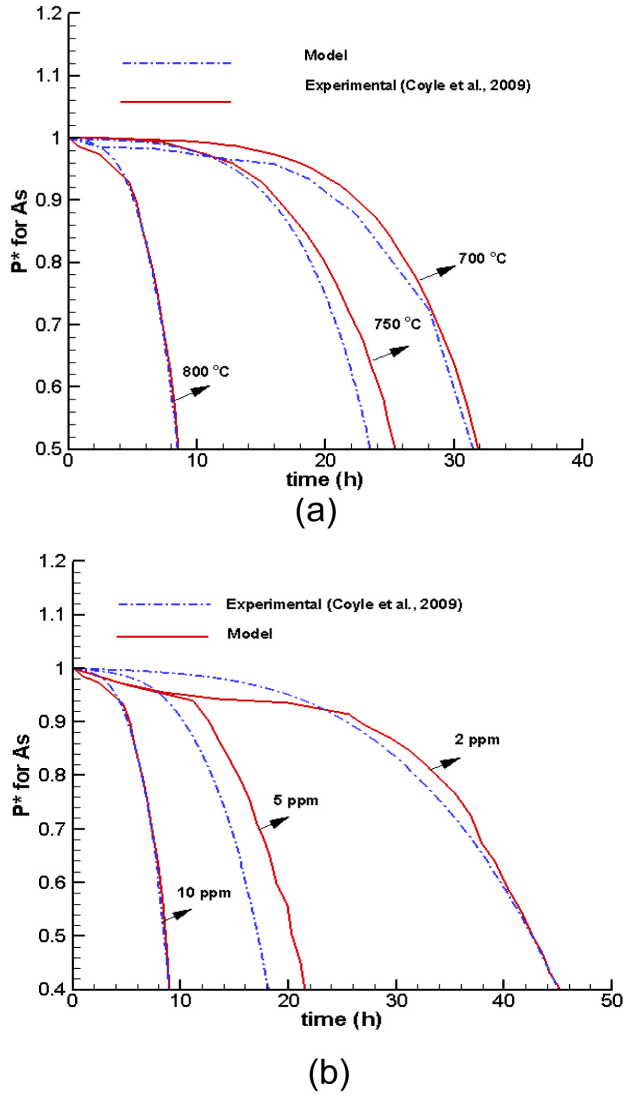

FIGURE 4. Modified Power Density vs. Time at 0.05 A/cm^2 for AsH_3: (a) Effect of Temperature, (b) Effect of Concentration

Anode Materials Development

The aim of this project is to fabricate SOFCs with high performance for syngas operation and to improve stability of the SOFC anode in sulfur and phosphorus-containing syngas. Anode-supported SOFC cells with performance over 0.8W/cm^2 and stable open circuit voltage have been successfully fabricated in WVU by a cost-effective process of die-pressing, drop-coating and co-sintering of Ni-YSZ anode and YSZ electrolyte. Impregnation of $La_xCe_{1-x}O_2$ (LDC) oxide coating into electrolyte-supported SOFC anode was optimized to further enhance anode tolerance against up to 20 ppm H_2S in coal syngas. The tolerance effects introduced by LDC coating through suppressing the on-set and degree of sulfur poisoning was proved on both anode and electrolyte supported cells. An in-depth study on

fundamental reaction mechanisms of S and P with the SOFC anode were performed by theoretical analysis together with detailed surface and bulk material characterization techniques of scanning electron microscope, cross-section X-ray photon spectroscopy (XPS) and X-ray diffraction (XRD). Results identified different mechanisms dominating at the anode surface and anode/electrolyte interface for P poisoning. MIEC (Mixed Ionic-Electronic Conductivity) ceramic oxides are being investigated as alternative anode materials to replace the Ni-cermet anode in PH_3-containing syngas [8].

In order to address the differences in button cell testing compared to conventional planar stack designs, work on the fabrication and testing of commercial-size planar cells for practical kilowatt-size systems has been initiated. Planar SOFCs are currently being fabricated by WVU with active areas in the range of 30-100-cm^2.

Conclusions and Future Directions

Substantial progress has been made on all fronts of the project. Experiments were conducted to study degradation of the SOFC anode due to three different impurities: P, S and Cl. Phosphorus impurity was extensively studied and the modes and mechanisms for the degradation were identified. Tests were conducted on both commercial and in-house built cells. The in-house button cells are shown to be on par with the commercial ones and work is in progress to manufacture large planar cells. A unique in situ test bench was designed and used in some of the tests. Parametric studies were conducted using in-house simulation tools to predict the electrochemical and structural performance of SOFCs. A new phenomenological model is developed which is shown to accurately predict SOFC anode degradation due syngas trace impurities.

In the future, tolerance tests will continue for impurities such as S, P, Cd, Cl, etc., and the changes occurring at the anode with respect to both microstructure and composition will be investigated. XPS combined with sputtering will be used in post-mortem analysis to resolve some of the questions about the nature of the products formed by the impurities. Out-of-plane surface deformations will be measured at specified time intervals each with a series of increasing applied pressure. The test results will facilitate the understanding of the mechanisms as well as provide quantitative evaluation of the long-term SOFC structural degradation under coal syngas. The infrared temperature measurement technique will be further refined in order to get a precise measurement on the small spot location of the button cell surface during SOFC operation. Analyses similar to that done for the phosphorus impurity will be extended for Cd and Cl. The results will be used to determine the governing factors that lead to degradation of SOFC anodes that are exposed to the impurity-containing syngas. On the cell manufacturing front, future research will focus on optimization of the fabrication process for a doped ceria coating on the MSRI cell to enhance sulfur tolerance. The phenomenological degradation model will be extended for the case of simultaneous exposure to multiple impurities. Material parameters for the durability model will be estimated using an in situ experimental setup. The durability model will be applied on a planar SOFC anode to estimate thermo-mechanical and syngas contaminants degradation effects and hence predict its structural service life.

Special Recognitions & Awards/Patents Issued

1. Dr. Ismail Celik received the prestigious Robert C. Byrd Professorship at West Virginia University.

2. Dr. Edward Sabolsky received the Prestigious 2010 Ralph E. Powe Junior Faculty Award from Oak Ridge Associated Universities (ORAU).

3. Dr. Xingbo Liu received 2010 Early Career Faculty Fellow Award from The Minerals, Metals, & Materials Society.

4. Dr. Xueyan Song received U.S. Air Force Summer Faculty Fellowship award for 2010.

5. Dr. Nick Wu and Dr. Xingbo Liu received the Outstanding Researcher Awards from College of Engineering & Mineral Resources, West Virginia University for year 2008-2009.

FY 2010 Publications/Presentations

1. C. Xu, J.W. Zondlo, H.O. Finklea, O. Demircan, M. Gong, and X. Liu, "The effect of phosphine in syngas on Ni–YSZ anode-supported solid oxide fuel cells," *Journal of Power Sources* 193 (2009) 739–746.

2. C. Xu, M. Gong, X. Liu, H.O. Finklea, and J.W. Zondlo, "The effect of HCl in syngas on Ni-YSZ anode-supported solid oxide fuel cells," *Journal of Power Sources* 195 (2010) 2149-2158.

3. C. Xu, J.W. Zondlo, M. Gong, F. Elizalde-Blancas, X. Liu, and I.B. Celik, "Tolerance tests of H_2S-laden biogas fuel on solid oxide fuel cells," *Journal of Power Sources* 195 (2010) 4583-4592.

4. M. Zhi, F.N. Cayan, I. Celik, S.R. Pakalpati, R. Gemmen, and N.Q. Wu, "Temperature and impurity concentration effects on degradation of nickel/yttria stabilized zirconia anode in PH_3 containing coal syngas," *Fuel Cells* 10, Issue 1, 174-180.

5. O. Demircan, C. Xu, John Zondlo, and H.O. Finklea, "In situ Van der Pauw measurements of the Ni/YSZ anode during exposure to syngas with phosphine contaminant," *Journal of Power Sources* 194 (2009) 214–219.

6. O. Demircan, W. Zhang, C. Xu, J. Zondlo, and H.O. Finklea, "The effect of overpotential on performance degradation of the SOFC Ni/YSZ anode during exposure

to syngas with phosphine contaminant," *Journal of Power Sources* 195 (2010) 3091-3096.

7. G. Iqbal, H. Guo, B. Kang, and O. Marina, "Durability prediction of solid oxide fuel cell anode material under thermomechanical and fuel gas contaminant effects," *Journal of Applied Ceramic Technology*, doi: 10.1111/j.1744-7402.2009.02415.

8. M. Gong, D. Bierschenk, J. Haag, K.R. Poeppelmeier, S.A. Barnett, C. Xu, J.W. Zondlo, and X. Liu, "Degradation of $LaSr_2Fe_2CrO_{9-\delta}$ solid oxide fuel cell anodes in phosphine-containing fuels," *Journal of Power Sources* 195 (2010) 4013-4021.

III. SECA CORE RESEARCH & DEVELOPMENT

C. Interconnects and Contact Materials

III.C.1 Evaluation of a Functional Interconnect System for SOFCs

Matthew D. Bender
ATI Allegheny Ludlum
Technical and Commercial Center
1300 Pacific Avenue
Natrona Heights, PA 15065
Phone: (724) 226-6575
E-mail: Matt.Bender@ATImetals.com

DOE Project Manager: Robin Ames
Phone: (304) 285-2078
E-mail: Robin.Ames@netl.doe.gov

Contract Number: 42513

Start Date: January 1, 2006
End Date: September 30, 2010

FY 2010 Objectives

- Optimize alloy compositions of ferritic stainless steels with coatings applied for oxidation resistance and enhancement of electrical properties.
- Evaluate surface treatments to maximize performance in solid oxide fuel cell (SOFC) environments.
- Demonstrate significant improvement in critical SOFC-related properties for interconnect systems incorporating new or modified alloy compositions and surface modifications.

Accomplishments

- A third generation of both low-chromium and high-chromium SOFC interconnect alloy compositions were designed and processed (melted, hot-rolled, cold-rolled, and annealed). Seven new experimental alloys were evaluated.
- Area specific resistance (ASR) testing of coated alloy samples was completed for exposure times as long as 3,200 hours at temperature. The rate of increase in ASR once the test systems reached steady-state conditions was observed to be as low as 0.8 $m\Omega \cdot cm^2$/1,000 hours for a coated Fe-17Cr alloy and 1.4 $m\Omega \cdot cm^2$/1,000 hours for a coated Fe-26Cr alloy.
- Long-term oxidation testing was completed in simulated cathode environments (humidified air) at 800-900°C for exposure times up to 1,000 hours at temperature. Systematic trends in breakaway oxidation behavior were related to deliberate variations in composition.
- Post-processing techniques were performed on flat-rolled ATI 441HP™ stainless steel as a means to incrementally reduce the rate of oxidation, which should yield beneficial effects to the electrical properties of the surface. Testing of this surface-modified material continues.
- Four additional lower-chromium (13-18 wt% Cr) alloys were designed and processed to explore the sufficiency of coated, very low-chromium stainless steels as SOFC interconnect alloys.

Introduction

This project is focused on evaluating the performance of affordable materials integrated into systems for use as SOFC interconnects. Interconnects can be a source of degradation of fuel cell stack performance by the formation and growth of electrically resistive surface oxide layers. It is critical to control which types of oxides form and to minimize layer growth for an extended period of time.

The reference point for this project is a monolithic ferritic stainless steel; examples include ATI 441HP™ stainless steel (UNS S44100) and E-BRITE® alloy (UNS S44627). These were chosen for their combination of low cost, general availability, and performance characteristics. Functionality can be added to these basic interconnect materials at the cost of increased complexity. Modifications are aimed at tailoring the relevant properties of a surface to its local environment in the fuel cell and include special processing, surface treatments, and applied coatings.

Approach

Two methods for increasing metallic interconnect performance are being explored. The first is to incorporate minor but impactful modifications to alloy compositions in what are essentially commercially available materials. A set of six alloy compositions was reduced to practice, based on current state-of-the-art information and the results from Phase I of this project. An additional set of seven alloy compositions was then further evaluated, exploring the compositional space around the top two performing alloys of the initial six.

The second approach is to alter the surface of the stainless steel by post-fabrication processing to yield long-lasting benefits by removing or sequestering elements (e.g., silicon and/or aluminum) which form resistive interfacial phases. This may be possible by annealing in specific atmospheres followed by chemical

cleaning in some cases. Other post-fabrication methods modify the sub-surface grain structure to improve formation of the oxide. Alternatively, an external oxidation-resistant and electrically conductive coating can be applied to remove the stainless steel surface from direct contact with the SOFC environment.

Results

Seven experimental compositions were melted to explore relatively minor modifications to commercially available alloys, notable E-BRITE and ATI 441HP alloys, which are iron-chromium ferritic stainless steels alloyed with a small amount of niobium. The significant difference between the two primary groups of alloys tested is the chromium content. The modified E-BRITE alloys contain a high level of chromium (23-26 wt%) while the modified ATI 441HP alloys have lower chromium content (nominally 17 wt%). Table 1 contains a review of the alloys used for testing in the current study. It is mixed between commercially available alloys and experimentally melted and processed material (designated EXP followed by a heat number). The experimental compositions tested in this matrix are further modifications of EXP. 580-6 and EXP. 580-5, which were alloys that performed well in earlier experimentation.

Evaluation of this set of test materials was completed with ASR testing carried out on coated alloy substrates. The coatings were of the cerium-modified manganese cobaltite spinel type developed by researchers at the Pacific Northwest National Laboratory (PNNL) [1]. The coatings were applied at PNNL on small specimens provided by ATI Allegheny Ludlum with an unaltered, non-directional dull finish produced by cold rolling, annealing, and acid pickling.

ASR test parameters were typical of those used in the industry – 800°C test temperature, lanthanum strontium manganate ceramic contact layer, and a constant current density of 0.5 A/cm^2 of contact area. The test results are summarized in Table 2, with the critical metric being the rate of ASR increase as a function of time, made specific to an interval of 1,000 hours for ease of interpretation. This value was obtained by taking the linear slope as a function of time of each individual ASR curve. After extended exposure times, the curves generally reach a constant or steady-state region where the value remains constant. A good target for fuel cell performance is an ASR of less than 0.1 Ω·cm^2 after 40,000 hours.

The important findings from this testing are now summarized. The cerium-modified manganese cobaltite spinel coatings continue to be effective in reducing the rate of ASR increase for nearly all of the alloys tested. The combined effect of the base alloy and coating may obscure the differences between

TABLE 1. Overview of Test Material (weight percent)

Alloy	Cr	Nb	Si	Others
ATI 441HP™ alloy	17.5	0.3	0.4	0.3 Mn, 0.2 Ti
EXP. 580-6	17	0.3	0.15	0.3 Mn, 0.2 Ti
EXP. 580-6 MOD1	17.3	0.5	0.15	0.3 Mn, 0.2 Ti
EXP. 580-6 MOD2	17.3	0.7	0.15	0.3 Mn, 0.2 Ti
EXP. 580-6 MOD3	17.3	0.7	0.35	0.3 Mn, 0.2 Ti
EXP. 580-6 MOD4	17.3	0.3	0.35	0.3 Mn, 0.0 Ti
EXP. 580-6 MOD5	17.3	0.3	0.35	0.8 Mn, 0.2 Ti
E-BRITE® alloy	26	0.2	0.3	1 Mo
EXP. 580-5	26	0.2	0.3	1 Mo, 0.3 Mn, 0.1Ti
EXP. 580-5 MOD1	26	0.5	0.35	1 Mo, 0.3 Mn, 0.2 Ti
EXP. 580-5 MOD2	24	0.3	0.35	1 Mo, 0.3 Mn, 0.2 Ti

TABLE 2. Overview of ASR Test Results

Sample ID	ASR Evolution Rate (mΩ·cm^2/1,000h)	
	Uncoated	Coated
ATI 441HP™ alloy	35.4	0.8
EXP. 580-6	25.1	6.9
EXP. 580-6 MOD1	no test	4.6
EXP. 580-6 MOD2	no test	1.6
EXP. 580-6 MOD3	no test	0.8
EXP. 580-6 MOD4	no test	77.1
EXP. 580-6 MOD5	no test	118.6
E-BRITE® alloy	936.5	21.1
EXP. 580-5	38.1	1.4
EXP. 580-5 MOD1	no test	4.4
EXP. 580-5 MOD2	no test	2.4

performances of the base experimental alloys to some extent. The coated commercial ATI 441HP alloy yielded the best long-term performance in the test matrix. Test results for this alloy are shown in Figure 1. Previously, in testing the uncoated condition, it was found that EXP. 580-6 exhibited a moderate but significant improvement in performance over standard Type 441. Three additional observations were made for the coated ATI 441HP samples: 1) the addition of Nb (EXP. 580-6 MOD3) did not show an improvement beyond the commercial alloy composition; 2) the elimination of Ti (EXP. 580-6 MOD4) was detrimental to alloy performance; and 3) the addition of a higher amount of Mn (EXP. 580-6 MOD5) was detrimental to alloy performance after 1,500 hours of testing.

The minor modification of a 0.3 wt% Mn addition to a base E-BRITE alloy composition continued to yield the best long-term performance of higher-chromium alloys. EXP. 580-5 alloy exhibited a very low steady state of ASR increase. For coated higher-chromium alloys, an increase in Nb content (EXP. 580-5 MOD1) does not appear to be beneficial. Additionally, a drop in material performance is associated with a reduction in Cr content (EXP. 580-5 MOD2).

While alloys based on the ATI 441HP stainless steel have shown encouraging test results, previous testing has

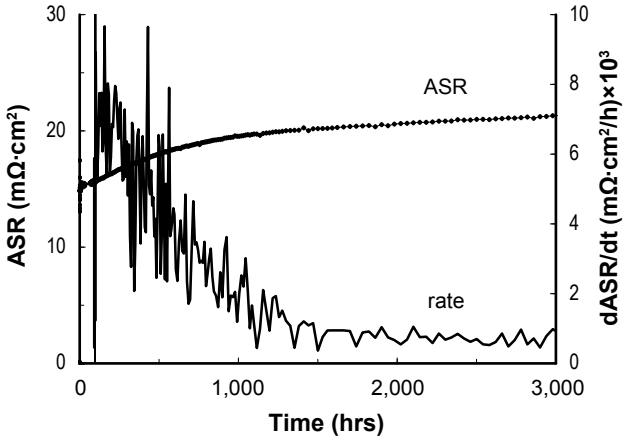

FIGURE 1. ASR as a Function of Time and Instantaneous Slope for ATI 441HP™ Alloy Coated with the PNNL Cerium-Modified Manganese Cobaltite Spinel Coating

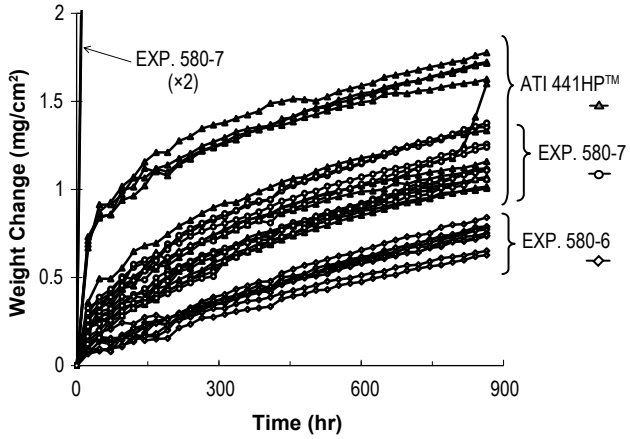

FIGURE 2. Oxidation Weight Change Data as a Function of Time for Samples Exposed to Air Containing 10% Water Vapor at 850°C

shown there to be somewhat unpredictable behavior in terms of oxidation resistance and ASR evolution at the upper end of the SOFC operating temperature range. Prior analysis indicated that the silicon level may have a role in retarding accelerated oxidation. An experiment to test large numbers of samples from several alloy compositions was completed in order to generate data for an analysis of the potential for breakaway oxidation. The alloy compositions for this study are summarized in Table 3. The major difference between the alloys is the silicon content. Evaluation of these alloys took the form of relatively simple gravimetric oxidation testing (weight change measurements) uncoated coupons at 800, 850, and 900°C in air containing 10% water vapor. Test results from the 850 and 800°C experiments are shown in Figures 2 and 3, respectively. At 850°C, there are two clear bands of data for EXP. 580-7 and EXP. 580-6 samples. Additionally, breakaway oxidation occurred in two EXP. 580-7 samples early in the testing. The ATI 441HP samples group in two separate bands. At 800°C, there are two clear bands of data for EXP. 580-6 and ATI 441HP samples. The EXP. 580-7 data extends across this entire region. Five EXP. 580-7 samples had breakaway oxidation early in the testing. The inflection point in the 800°C data was caused by a slight increase in temperature of the furnace midway through the test.

TABLE 3. Overview of Test Material (weight percent)

Alloy	Cr	Nb	Si	Others
ATI 441HP™ alloy	17.5	0.3	0.4	0.3 Mn, 0.2 Ti
EXP. 580-6	17	0.3	0.15	0.3 Mn, 0.2 Ti
EXP. 580-7	17	0.3	0.05	0.3 Mn, 0.2 Ti

The important findings from this testing are now summarized. At both 800 and 850°C, the alloy with 0.15 wt% (EXP. 580-6) performed better than the alloy

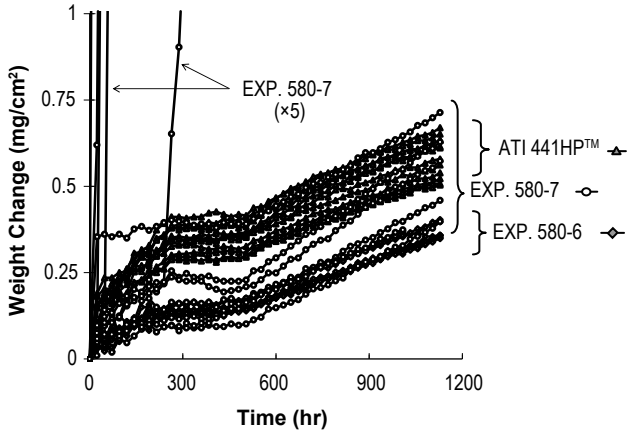

FIGURE 3. Oxidation Weight Change Data as a Function of Time for Samples Exposed to Air Containing 10% Water Vapor at 800°C

with higher silicon content (0.40 wt%), but also better than the alloy with lower silicon content (EXP. 580-7). The EXP. 580-7 alloy showed some instability at the early test times, while the other two alloys did not. At 900°C, EXP. 580-6 alloy continues to perform better than the other two alloys. In summary, the modified ATI 441HP alloys with too low of a silicon content do not appear to be beneficial at any temperature tested (800-900°C), and there appears to be an optimum silicon content level between 0.05 and 0.40 wt% for reducing susceptibility to breakaway oxidation.

The alternative approach to modifying performance is to alter the surface of the stainless steel by post-fabrication processing. Samples from a production coil of ATI 441HP stainless steel underwent various post-processing treatments including desiliconization, surface blasting, surface grinding, and temper rolling. Cold work has been shown to reduce the rate of oxidation.

The blasting and grinding methods should alter the near-surface grain structure, while temper rolling should alter the through-thickness grain structure, whereby improving the diffusion of chromium to the surface. The desiliconization process should selectively remove silicon from the surface, which should prevent electrically resistive phases from forming at the scale-metal interface during exposure to SOFC operating conditions. Coated test coupons from each treatment are currently undergoing long-term oxidation testing in air at 800°C and will be characterized at the conclusion of the test. ASR testing of coated test coupons was recently initiated.

Conclusions and Future Directions

- Coated experimental alloys with compositions based on modifications to the basic ATI 441HP alloy melted for this study have exhibited low observed rates of ASR increase. The value determined for a manganese cobaltite spinel-coated ATI 441HP alloy was the lowest at 0.8 $m\Omega \cdot cm^2$/1,000 hours after 3,200 hours at 800°C in air.
- Compositions based on modifications to the basic E-BRITE alloy tailored for SOFC interconnect applications have exhibited low observed rates of ASR increase. Specifically, the value determined for a manganese cobaltite spinel-coated Fe-26Cr alloy with manganese addition was 1.4 $m\Omega \cdot cm^2$/1,000 hours after 3,200 hours at 800°C in air. This is an order of magnitude better than the coated base composition. The commercial E-BRITE composition with manganese addition may be a robust alloy alternative to ATI 441HP alloy should the oxidation resistance and ASR properties of lower-chromium alloys be found to be insufficient during scale up of SOFC technology.
- Oxidation testing of a large number of samples showed that while the silicon content of an alloy may have a role in retarding accelerated oxidation, there seems to be an intermediate optimal silicon content providing the best long-term resistance to breakaway oxidation of a modified ATI 441HP stainless steel. An experimental alloy with moderate silicon content outperformed both the commercial alloy with higher silicon content and a second experimental alloy with lower silicon content. This research suggests that removal of all silicon from the ATI 441HP alloy is not beneficial for SOFC interconnect performance.
- Sample preparation of flat-rolled ATI 441HP stainless steel with post-processing techniques was completed as a means to incrementally reduce the rate of oxidation, which should yield beneficial effects on the electrical properties of the surface. Surface-modified material will be characterized following a long-term oxidation test and will be investigated using ASR testing.
- Sample sheets from four low-chromium (13-18 wt% Cr) experimental alloys were produced and provided to Jeffrey Fergus of Auburn University. An investigation into alloy performance and the characterization of the interaction between the formed oxide and applied manganese cobaltite spinel type coating on these low-chromium alloys will continue into Fiscal Year 2011.

Special Recognitions & Awards/Patents Issued

1. U.S. and associated foreign patents have been filed on higher-Cr content alloy compositions (application numbers 20060286433, 20060286432, and 20060285993) and on the silicon removal process (application number 20080236710).

FY 2010 Publications/Presentations

1. Quarterly status report for Project 42513, October 2009.

2. Quarterly status report for Project 42513, January 2010.

3. Status review presentation at NETL, Morgantown for Project 42513, March 2010.

4. Quarterly status report for Project 42513, April 2010.

References

1. Zhenguo Yang, Guanguang Xia, Zimin Nie, Joshua Templeton, and Jeffry W. Stevenson, "Ce-Modified $(Mn, Co)_3O_4$ Spinel Coatings on Ferritic Stainless Steels for SOFC Interconnect Applications," *Electrochem. Solid-State Lett.*, Volume 11, Issue 8, 2008: B140-B143.

III.C.2 Effect of SOFC Interconnect-Coating Interactions on Coating Properties and Performance

Jeffrey W. Fergus
Auburn University
Materials Research and Education Center
275 Wilmore Laboratories
Auburn, AL 36849
Phone: (334) 844-3405; Fax: (334) 844-3400
E-mail: jwfergus@eng.auburn.edu

DOE BES Project Manager:
Timothy Fitzsimmons
Phone: (301) 903-9830
E-mail: Tim.Fitzsimmons@science.doe.gov

DOE NETL Project Manager: Briggs White
Phone: (304) 285-5437
E-mail: Briggs.White@netl.doe.gov

Contract Number: 46497

Start Date: June 15, 2008
End Date: June 14, 2011

FY 2010 Objectives

- Determine the mechanism of the reaction between chromium and the spinel manganese-cobalt oxide coating material.
- Identify coating compositions with improved performance.

Accomplishments

- The two-layer growth mechanism for the reaction between the spinel $(Mn,Co)_3O_4$ and Cr_2O_3 was established.
- The addition of iron or titanium to $(Mn,Co)_3O_4$ was shown to reduce the amount of reaction with Cr_2O_3 without significantly decreasing the electrical conductivity or changing the coefficient of thermal expansion (CTE).

Introduction

The high operating temperature of solid oxide fuel cells (SOFCs), which provides their excellent fuel flexibility, can lead to degradation of individual fuel cell components. One form of degradation is chromium poisoning of the cathode, which results from volatilization of chromium from the chromia scale formed on alloys used for the interconnect. The amount of chromium volatilization, and thus the associated cell poisoning, can be minimized by applying a ceramic coating to the alloy surface. One promising coating material systems is the spinel $(Mn,Co)_3O_4$ [1-4], which has been shown to reduce chromium volatilization [5,6].

Although chromium can form a spinel phase with other transition metals, chromium has not been observed in the coating during use in a SOFC [7,8]. However, with time, interaction of the coating with the chromia scale or with other SOFC components can lead to changes in the coating composition, which can affect properties and thus performance. The purpose of this work is to study the interaction between chromia and potential interconnect coating materials to provide information needed to design effective coatings for long-time SOFC operation.

Approach

The project addresses three aspects of coating properties and performance: i) thermodynamics, ii) transport properties and iii) physical properties. The thermodynamic aspects include phase equilibria, crystal structure stability and chemical activity. The transport properties to be evaluated include conductivity and diffusion rates. The physical properties are those that are important for coating performance, such as the CTE. These aspects will be evaluated for the original coating composition and for compositions resulting from interaction of the coating with other fuel cell components by preparing bulk analogues of the compositions expected after the interaction occurs. Characterization of these bulk analogues will provide valuable information for evaluating any changes in the performance after interaction with other components. Finally, the results will be used to identify compositions with potentially improved performance and these promising compositions will be similarly evaluated. This knowledge and understanding will allow coatings to be designed so that the expected compositional changes during operation increase the conductivity in an amount that offsets the increase in resistance due to growth the chromia scale. In this case, the coating electrical resistance, and thus the associated overpotential, would be constant with time, so fuel cell performance would not degrade during operation.

Results

The previously reported results were for reaction of coating materials at 1,000-1,200°C, which is higher

than the typical operating temperature for intermediate temperature SOFCs, so lower temperature exposures have been evaluated. Scanning electron microscopy (SEM) images of the surfaces of $Mn_{1.5}Co_{1.5}O_4$ after reaction with Cr_2O_3 for 72 hours in air at 1,000°C, 900°C and 800°C are shown in Figure 1. The morphologies of the surfaces that had been in contact with chromia are faceted and appear similar to the previously reported observations at 1,200°C indicating that may they may form by the same mechanism. One notable difference is that at lower temperatures, i.e., 800°C (Figure 1c) and 900°C (Figure 1b), the surface compositions are lower than those observed at higher temperatures, i.e., 1,000°C (Figure 1a). This is in contrast to the previously reported results at 1,200°C, where a faceted microstructure formed only when the maximum chromium content, i.e., $(Mn,Co)Cr_2O_4$, was formed. The faceted morphology is indicative of a reaction layer formed by the diffusion of cobalt and manganese from $(Mn,Co)_3O_4$ through the reaction layer. At 1,200°C, this mechanism only occurs when the chromium content reaches the maximum in the spinel phase, i.e., $(Mn,Co)Cr_2O_4$, in which case Cr^{3+} ions occupy the octahedral sites, so manganese and cobalt are predominantly in the tetrahedral sites with a valence of 2+. At lower temperatures, growth controlled by cobalt and manganese diffusion, which is desirable for minimizing chromium volatility, occurs for lower chromium content. This mechanism is consistent with observations of negligible chromium in $(Mn,Co)_3O_4$ interconnect coatings during SOFC operation.

The conductivities of coating materials were determined using 4-point direct current conductivity measurements. Figure 2 shows that the measured conductivities of $(Mn,Co)_3O_4$ are in agreement with previous reports and confirms the high conductivity of the 1:1 Mn:Co composition (i.e., $Mn_{1.5}Co_{1.5}O_4$). Figure 3 shows that the addition of chromium significantly decreases the conductivity, which indicates that the reaction layer could lead to an increase in the electrical resistance across the interface.

As discussed above, the transport properties of spinel phases depend on ion site occupancy. Through collaboration with the Indonesian National Nuclear Energy Agency (BATAN), neutron diffraction was performed on $Mn_{1.5}Co_{1.5}O_4$, $MnCo_2O_4$ and $Mn_{0.4}Co_{0.6}Cr_2O_4$. The results indicate that chromium has the strongest preference for octahedral sites and that manganese has a stronger preference for octahedral sites as compared to cobalt.

Since chromium has a strong preference for the octahedral site in the spinel structure, the solubility and/or diffusivity of chromium could be decreased

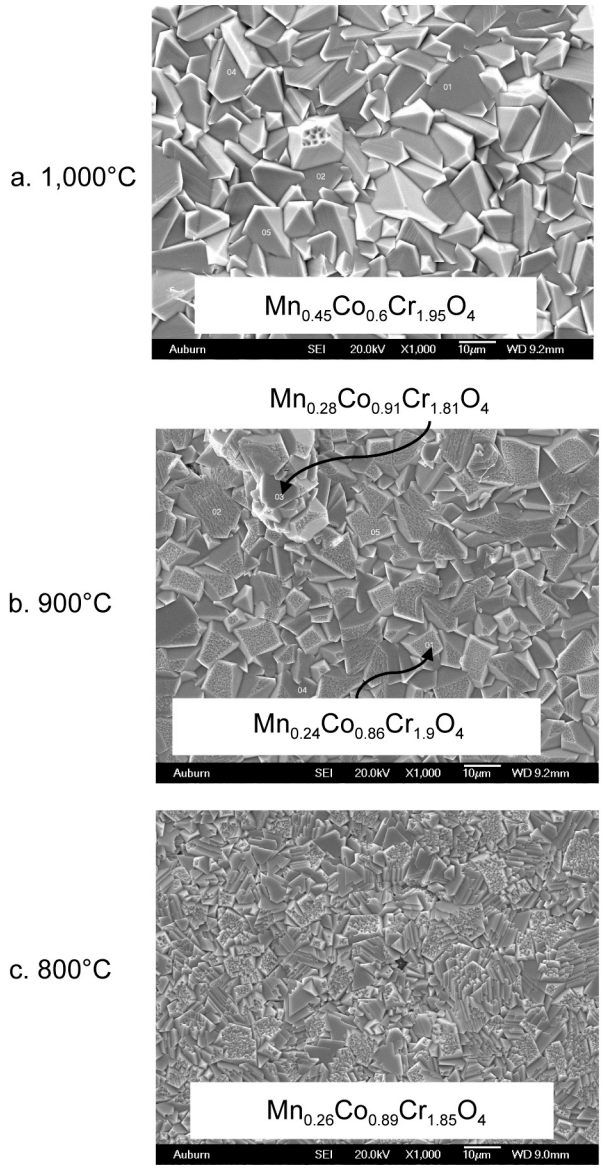

FIGURE 1. SEM Micrographs of Surfaces of $Mn_{1.5}Co_{1.5}O_4$ and after Reaction in Air for 72 hours at 1,000°C (a), 900°C (b) and 800°C (c)

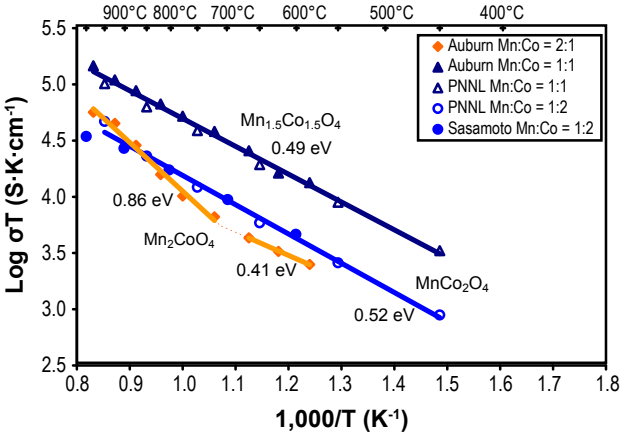

FIGURE 2. Conductivity of $(Mn,Co)_3O_4$ Compared with Results from Pacific Northwest National Laboratory (PNNL) [9] and Sasamoto *et al.* [10]

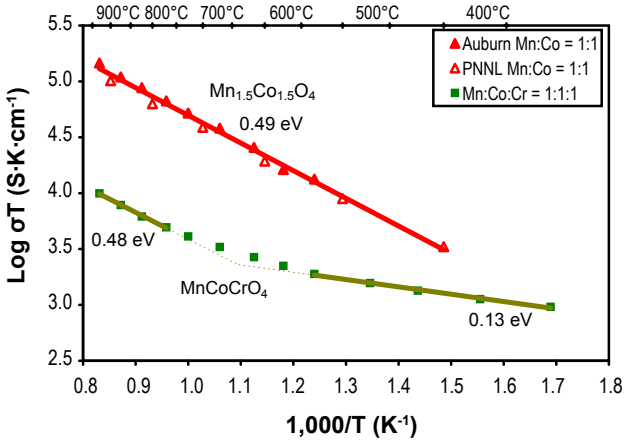

FIGURE 3. Effect of Cr on Conductivity of $(Mn,Co)_3O_4$ (PNNL [9])

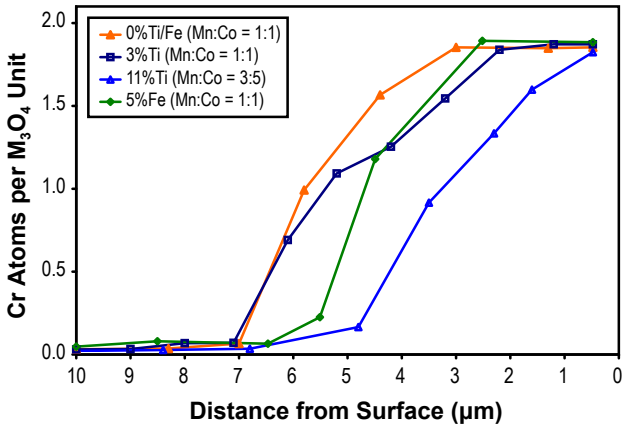

FIGURE 4. Chromium Composition through Cross-Section between Cr_2O_3 and Doped (Ti/Fe) or Undoped $(Mn,Co)_3O_4$ after 336 hours at 800°C

by doping with other ions with preference for the octahedral sites. To evaluate this possibility, $(Mn,Co)_3O_4$ was doped with titanium, iron or yttrium. The chromium composition gradients as determined by energy dispersive X-ray spectroscopy at the cross-section between Cr_2O_3 and doped/undoped $(Mn,Co)_3O_4$ after 336 hours at 800°C are shown in Figure 4. The thickness of the reaction layer (i.e., $(Mn,Co)Cr_2O_4$) is decreased for all dopants, particularly for the sample with 11% Ti and the higher Co content (i.e., $MnCo_{1.66}Ti_{0.34}O_4$). The chromium concentration gradient in the reaction layer for this composition and an analogous iron-doped composition (i.e., $MnCo_{1.66}Fe_{0.34}O_4$) after reaction at 900°C for 144 hours are shown in Figure 5. The reaction layer thickness for the iron-doped composition is slightly thinner, but its CTE is higher than that of the titanium-doped composition. Figure 6 shows that the conductivity of the iron-doped composition is higher than that of the titanium-doped composition, although the conductivity of the titanium-doped composition is still relatively good (i.e., slightly higher than $MnCo_2O_4$). Both dopants are beneficial, but which of the two provides the best performance will depend on the relative importance of electrical resistance and the thermal stresses from the CTE mismatch.

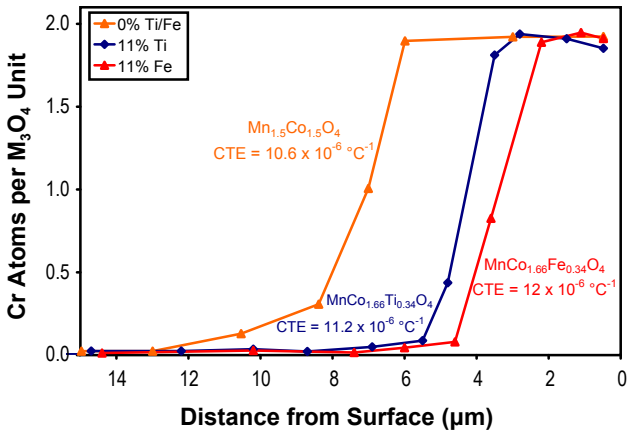

FIGURE 5. Chromium Composition through Cross-Section between Cr_2O_3 and Doped (Ti/Fe) or Undoped $(Mn,Co)_3O_4$ after 144 hours at 900°C

Conclusions and Future Directions

The effect of dopant additions will be evaluated by measuring the properties of the compositions formed in the reaction layer between the coating and the chromia scale. Information on the coating properties, combined with predications of the compositions and thicknesses of the reaction layer from the kinetic studies, will be used to evaluate the expected coating performance during long-term use.

Through support from the Solid State Energy Conversion Alliance Program, Allegheny Technologies

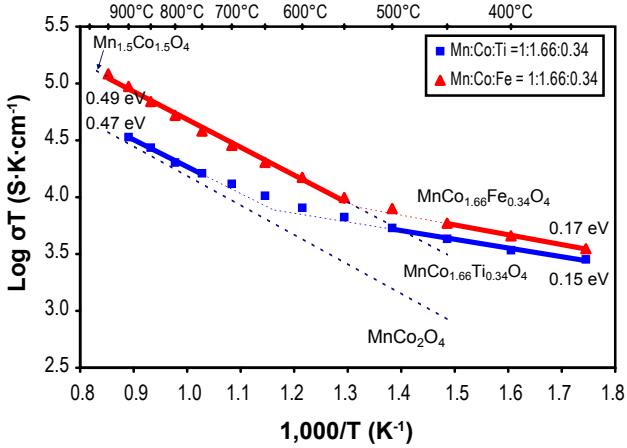

FIGURE 6. Effect of Iron and Titanium on the Conductivity of $(Mn,Co)_3O_4$ in Air

Inc. has produced alloys containing the alloying additions in the commercial alloy 441, but with various chromium contents. The stability of these alloys with and without coatings produced by PNNL will be evaluated to determine if the application of a protective coating will allow for the use of an alloy with a lower chromium content.

FY 2010 Publications/Presentations

1. A. Purwanto, A. Fajar, H. Mugirahardjo, J.W. Fergus, and K. Wang, "Cation Distribution in Spinel $(Mn,Co,Cr)_3O_4$ at Room Temperature," *Journal of Applied Crystallography* **43** (2010) 394-400.

2. J. Fergus, K. Wang, and Y. Liu, "Equilibria in Spinel Coatings for Solid Oxide Fuel Cell Interconnects," *Materials Science & Technology (MS&T)* 2009 (2009) 312-321.

3. J. Fergus, K. Wang and Y. Liu, "Interactions between $(Mn,Co)_3O_4$ SOFC Interconnect Coating Materials and Chromia," in *Supplemental Proceedings: Volume 2: Materials Characterization, Computation, Modeling and Energy* (The Minerals, Metals & Materials Society, 2010) 473-480.

4. J.W. Fergus, "Interconnect-Coating Interactions: Mn-Co Spinel Oxides," 10th Annual SECA Workshop, Pittsburgh, Pennsylvania, 15 July 2009.

5. J.W. Fergus, "Materials Degradation in Solid Oxide Fuel Cells," National Research Council, National Research Council Institute for Fuel Cell Innovation, Vancouver, British Columbia, 28 April 2010.

6. J.W. Fergus, "Materials Degradation in Solid Oxide Fuel Cells," Invited presentation for Symposium on Assessing Environmental Degradation, 2010 ASM Annual Symposium, GE Global Research, Niskayuna, New York, 19 May 2010.

References

1. Y. Larring and T. Norby, "Spinel and perovskite functional layers between Plansee metallic interconnect (Cr-5 wt% Fe-1 wt% Y_2O_3) and ceramic $(La_{0.85}Sr_{0.15})_{0.91}MnO_3$ cathode materials for solid oxide fuel cells," *J. Electrochem. Soc.* **Vol. 147**, 2000, pp. 3251-3256.

2. Z. Yang, G.-G. Xia, G.D. Maupin, and J.W. Stevenson, "Conductive protection layers on oxidation resistance alloys for SOFC interconnect applications," *Surf. Coating Tech.* **Vol. 201**, 2006, pp. 4476-4483.

3. M.R. Bateni, P. Wei, X. Deng, and A. Petric, "Spinel coatings for UNS 430 stainless steel interconnects," *Surf. Coating Tech.* **Vol. 201**, 2007, pp. 4677-4684.

4. M.J. Garcia-Vargas, M. Zahid, F. Tietz, and A. Aslanides, "Use of SOFC metallic interconnect coated with spinel protective layers using the APS technology," *ECS Trans.* **Vol. 7**, 2007, pp. 2399-2405.

5. H. Kurokawa, C.P. Jacobson, L.C. DeJonghe, and S.J. Visco, "Chromium vaporization of bare and of coated iron-chromium alloys at 1073 K," *Solid State Ionics* **Vol. 178**, 2007, pp. 287-296.

6. C. Collins, J. Lucas, T.L. Buchanan, M. Kopczyk, A. Kayani, P.E. Gannon, M.C. Deibert, R.J. Smith, D.-S. Choi, and V.I. Gorokhovsky, "Chromium volatility of coated and uncoated steel interconnects for SOFCs," *Surf. Coating Tech.* **Vol. 201,** 2006, pp. 4467-4470.

7. Z. Yang, G.-G. Xia, H.-H. Li, and J.W. Stevenson, "$(Mn,Co)_3O_4$ spinel coatings on ferritic stainless steels for SOFC interconnect applications," *Int. J. Hydrogen Energy* **Vol. 32**, 2007, pp. 3648-3654.

8. Z. Yang, G. Xia, and J.W. Stevenson, "$Mn_{1.5}Co_{1.5}O_4$ spinel protection layers on ferritic stainless steels for SOFC interconnect applications," *Electrochem. Solid-State Lett.* **Vol. 8**, 2005, pp. A168-A170.

9. Z. Yang, G.-G. Xia, H.-H. Li, and J.W. Stevenson, "$(Mn,Co)_3O_4$ spinel coatings on ferritic stainless steels for SOFC interconnect applications," *Int. J. Hydrogen Energy* **Vol. 32** [16] (2007) 3648-3654.

10. T. Sasamoto, N. Sumi, A. Shimaji, O. Yamamoto, and Y. Abe, "High temperature electrical properties of the spinel-type oxide $MnCo_2O_4$-$NiMn_2O_4$," *J. Mater. Sci. Soc. Jpn.* **Vol. 33** [1] (1996) 32-37.

III.C.3 Electrodeposited Mn-Co Alloy Coatings for SOFC Interconnects

Heather McCrabb (Primary Contact),
Dr. Timothy Hall
Faraday Technology, Inc.
315 Huls Drive
Clayton, OH 45315
Phone: (937) 836-7749; Fax: (937) 836-9498
E-mail: heathermccrabb@faradaytechnology.com

DOE Project Manager: Robin Ames
Phone: (304) 285-0978
E-mail: Robin.Ames@netl.doe.gov

Subcontractor:
West Virginia University, Morgantown, WV

Contract Number: 86387

Start Date: July 20, 2009
End Date: April 19, 2010

FY 2010 Objectives

- Determine the range of coating percent compositions that the electrodeposition process can deposit.
- Demonstrate that the electrodeposition process can deposit Mn-Co alloy coatings with a thickness range of 3-10 μm.
- Determine the alloy coating quality when varying alloy compositions and thickness.
- Determine the spinel coating quality by demonstrating a low and stable area specific resistance (ASR), minimal porosity, minimal thickness variation, and good adhesion to the interconnect surface.
- Conduct a preliminary economic analysis to determine if the process is suitable for high volume manufacturing.

Accomplishments

- Deposited a range of Mn-Co alloy coating compositions ranging from 5% to 95% Co using the FARADAYIC Electrodeposition Process.
- Deposited the Mn-Co alloy with a coating thickness range of 3-10 microns.
- Determined the coating thickness uniformity, porosity, adhesion and deposition rate.
- Demonstrated a low, stable ASR after 500 hours at 800°C for various coating composition and thickness values.
- Demonstrated that the FARADAYIC Electrodeposition Process is economically viable for production of $(Mn,Co)_3O_4$ spinel coatings for SOFC interconnects.

Introduction

Commercialization of solid oxide fuel cells (SOFCs) requires low-cost components, materials and manufacturing processes. Specifically, the interconnect material and coating used in SOFCs represent 45% of the total material cost for the typical stack [1]; therefore it is desirable that new materials and manufacturing technologies be developed that effectively increase system durability while decreasing production costs. The decrease in the SOFC operating temperatures from 1,000ºC to between 650 and 850ºC has enabled the use of less expensive chromia-forming ferritic stainless steels as interconnects instead of $LaCrO_3$ ceramic. However, even newly developed ferritic alloys such as SS441 and Crofer 22 APU, cannot completely eliminate the chromia scale growth and chromium evaporation into cells that can cause unacceptable degradation in the SOFC electrochemical performance. One attractive method to resolve the chromia scale growth and diffusion issues is to electrodeposit a Mn-Co alloy coating onto the interconnect surface and subsequently convert it to a $(Mn,Co)_3O_4$ spinel.

Faraday and West Virginia University are working to develop, optimize, and validate the FARADAYIC Electrodeposition Process as an effective and economical manufacturing method for coating interconnect materials used in SOFC stacks with Mn-Co alloys. The FARADAYIC Process utilizes pulse and pulse reverse waveforms and simple electrolyte solutions for manufacturing the interconnect coatings. A preliminary economic analysis based on using batch manufacturing suggests that the innovative coating technology can meet DOE's high volume target of 1,600,000 plates per annum for 250 MW of fuel cell stacks at a cost of ~$1.87 per 25 cm x 25 cm coated interconnect.

Approach

The FARADAYIC Electrodeposition Process is a pulse/pulse reverse plating process that controls the electric field and the boundary layer to reduce gradients (composition, thickness, or morphological) in the formed coating. The novel aspect of this technology is the manner in which the electric field and double layer are controlled and how these parameters can

inherently control the properties of the coating. For instance, when using a direct current overpotential for deposition, the composition, thickness, and morphology of the deposit is controlled by the surface texture of the substrate/electrode. With the use of the FARADAYIC Electrodeposition Process the electric field can be tuned to reduce effects of the substrate and obtain better overall control of the deposit's properties. In addition, the cell geometry, plating bath flow, and shape of the applied electric field influence the current distribution that develops on the surface of the substrate. The main advantages of the proposed technology, as compared to conventional, direct current electrodeposition, are:

- Enhanced process control: Since the process proceeds only under the influence of an electric field, the processing time is exact and uniform across the plate.
- Enhanced surface structure and thickness control: The FARADYAIC Process parameters can be selected to minimize the diffusion boundary layer, decreasing the effect of substrate surface morphology on the deposit properties across an area.

Results

Mn-Co alloy coatings were electrodeposited onto 5 cm x 5 cm T441 stainless steel substrates from a sulfate-based electrolyte containing ammonium sulfate and boric acid at 50°C using a pulse reverse waveform [2]. The coatings were electrodeposited in a cell designed to facilitate uniform flow across the surface of a flat substrate [3]. Formation of the $(Mn,Co)_3O_4$ spinel was achieved by subsequently baking the samples at 800°C in air for 72 hr. The coating uniformity, surface morphology and alloy composition of the coatings as deposited and after the 72 hr bake were investigated using optical and scanning electron microscopy (SEM) and energy dispersive X-ray spectroscopy (EDX). Figure 1 exemplifies the data collected to evaluate the uniformity of the as-deposited coatings. It shows that the coating composition and thickness remain constant within the experimental error of the evaluation apparatus, an optical microscope (±1.5 µm at 40x) or the EDX (±5%).

Furthermore, the spinel coating adhesion was evaluated using a Rockwell hardness tester to apply a load onto a 1/16" diameter ball indenter in order to penetrate the oxide scale on the substrates surface [4]. The loads were stair-stepped between 60 and 150 kgf to determine the critical level that spallation occurred on each specimen after the Mn-Co alloy coating was thermally oxidized in air at 800°C for 72 hrs. Figure 2 shows that the post-bake spinel coatings did not spall regardless of the applied load, indicating good adhesion between the spinel coating and the T441 interconnect substrate.

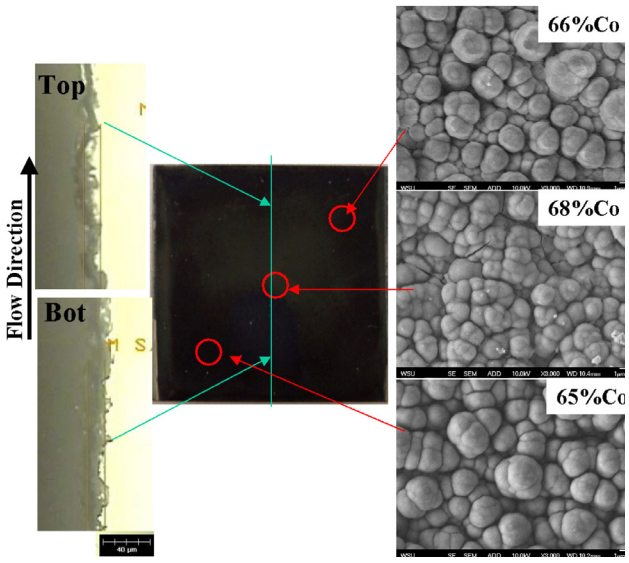

FIGURE 1. Exemplifies the data set collected to validate the uniformity of the as-deposited substrate. Left) Optical microscope images of cross-section of the centerline on the top and bottom of the sample. Center) Digital photograph of as-deposited surface. Right) SEM-EDX images and % compositions of surface structure of three separate areas.

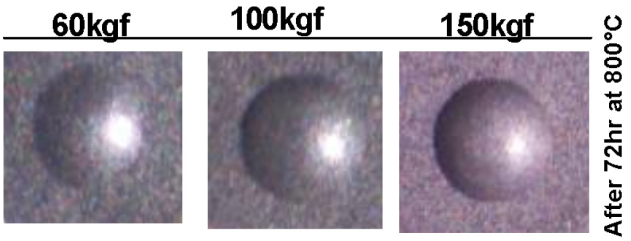

FIGURE 2. Typical adhesiveness for Mn-Co spinel coatings prepared using the FARADAYIC Process. No coating spallation was observed, regardless of applied load.

Figure 3 provides SEM images and EDX lines scans for coating cross sections of three samples with the same alloy composition at three different alloy thicknesses (3, 7 and 10 µm) after thermal exposure for 500 hr at 800°C. Each sample's coating can be divided into two parts: 1) Mn-Co-based oxide layer and 2) chromium-based oxide layer. The SEM/EDX analyses shows the presence of an inner chromium-based oxide layer at the interface of the oxide layer and the substrate, which suggests oxygen transport through Mn-Co-based oxides and chromium diffusion from the substrate during oxidation. The top sample in Figure 3 (metal coating of 3 µm) shows a Mn-Co-based oxide scale of about 3.0 µm and then a chromium-based oxide scale of about 1.3 µm on the metal substrate. The middle sample in Figure 3 (7 µm metal deposit) shows a Mn-Co-based oxide layer of about 13.2 µm and

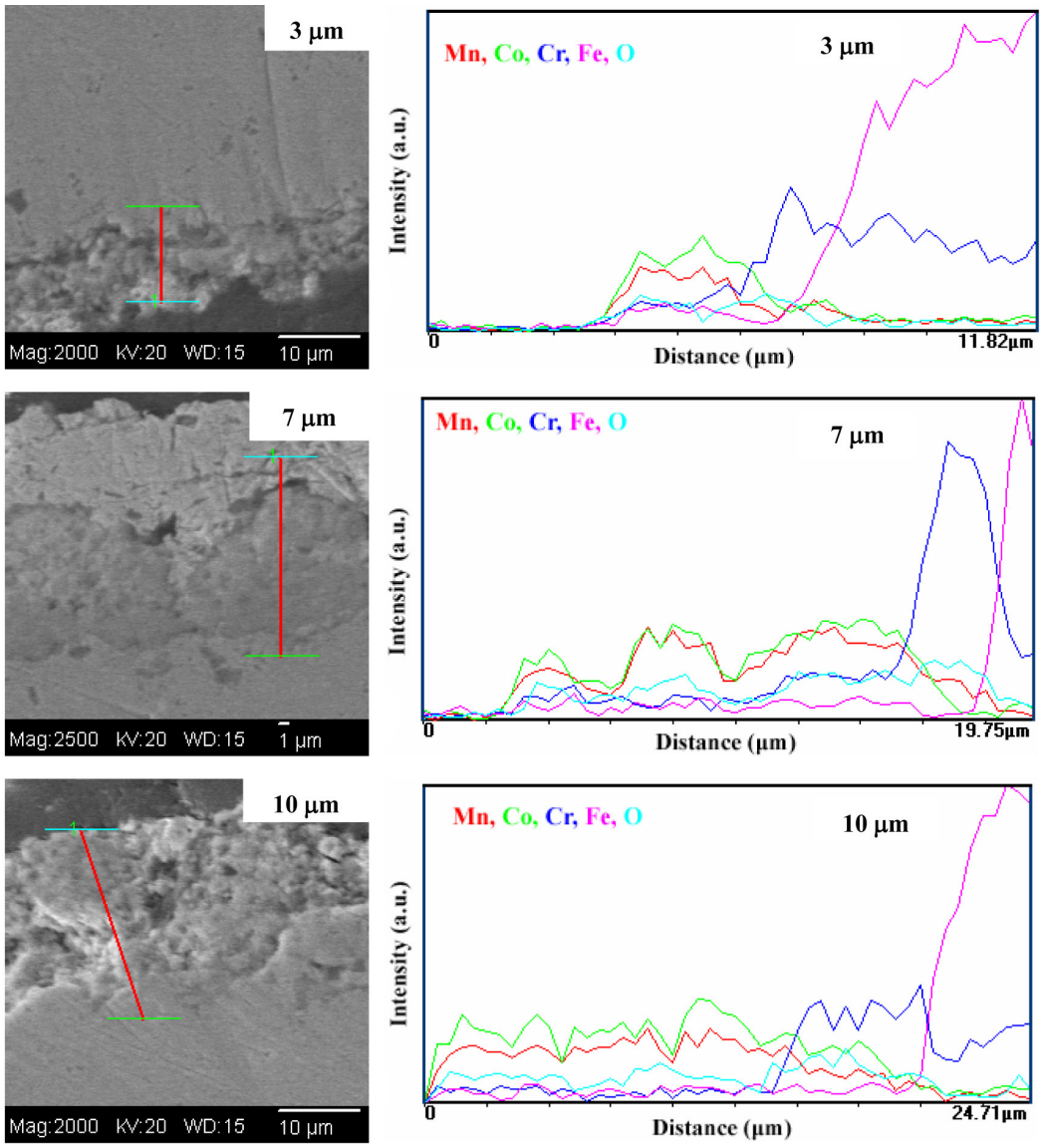

FIGURE 3. SEM/EDX analyses of a 3 mm (top), 7 mm (middle), and 10 mm (bottom) thick $(Mn,Co)_3O_4$ spinel coating after 500 hrs of thermal exposure at 800°C.

chromium-based oxide layer of about 2.6 µm. While the sample at the bottom of Figure 3 (with a 10 µm metal coating) shows a Mn-Co-based oxide layer of about 15.5 µm and a chromium-based oxide layer of about 5.4 µm. Therefore, both the thickness of Mn-Co-based oxide layer and chromium-based oxide layer increases as the original Mn-Co alloy coating thickness increases. The data at the top of Figure 3 demonstrates that the thinnest coating (3 µm) exhibits minimal porosity and as such, has the potential to effectively suppress the chromium penetration to the surface after 500 hr at 800°C. Additionally, coatings have demonstrated a low and stable ASR below the DOE performance target of 100 $m\Omega cm^2$ after 500 hr at 800°C.

A preliminary manufacturing throughput and cost analysis of the FARADAYIC Electrodeposition Process for high-volume manufacturing of Mn-Co spinel interconnect coatings has been conducted. Electrodeposition is widely considered an inexpensive, scalable, non-line-of-sight industrial manufacturing process and the addition of pulse/pulse-reverse processing, i.e. the FARADAYIC Process, offers a further enhancement to the electrodeposition process through the control of grain size, morphology, stress, and composition of the deposits. The preliminary cost analysis is based upon an annual production volume of 250 MW of fuel cell stacks for which approximately 1,600,000 interconnect plates would need to be coated per year. The throughput assessment considers the

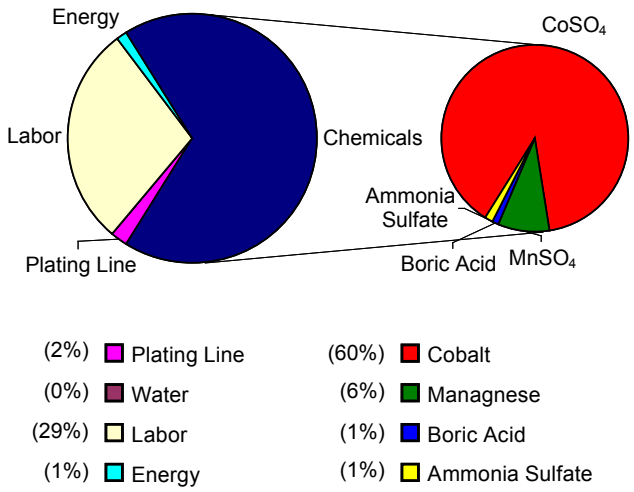

FIGURE 4. Cost analysis of coating process based upon batch manufacturing of 1,600,000 plates per annum at a cost of ~$1.87 per 25 cm x 25 cm coated interconnect.

FARADAYIC Electrodeposition Process as a batch manufacturing process. Figure 4 provides the cost analysis of the FARADAYIC Electrodeposition Process based upon batch manufacturing of 1,600,000 plates per annum at a cost of ~$1.87 per 25 cm x 2 cm coated interconnect.

Conclusions and Future Directions

A cost-effective process to apply high-quality coatings to SOFC interconnects in a mass production scenario is being developed. The FARADAYIC Electrodeposition Process can be used to deposit a Mn-Co alloy with a controlled composition and thickness that can subsequently be converted to a spinel by thermal exposure at high temperatures in an oxidizing environment. Preliminary results indicate that the FARADAYIC Electrodeposition Process:

- Can deposit a range of Mn-Co alloy coating compositions ranging from 5% to 95% Co.
- Can deposit the Mn-Co alloy with a coating thickness range of 3-10 microns.
- Exhibits minimal porosity according to ASM 2460, SEM images and EDX line scans.
- Exhibits minimal thickness variation and is well adherent to the T441 substrate.
- Demonstrates a low, stable area specific resistance below the DOE performance target of 100 $m\Omega cm^2$.
- Is economically viable for production of $(Mn,Co)_3O_4$ spinel coatings for SOFC interconnects and can meet DOE's high volume target of 1,600,000 plates per annum at a cost of ~$1.87 per 25 cm x 25 cm coated interconnect for a batch manufacturing process.

Development of the FARADAYIC Electrodeposition Process is on-going with the following activities planned:

- Development, optimization and validation of the FARADAYIC Electrodeposition Process for 10 cm x 10 cm single and dual-sided grooved interconnect materials.
- Mitigation of chromium diffusion by determining the controlling mechanism through in situ high temperature X-ray diffraction measurements and X-ray photoelectron spectroscopy depth profiling.
- Development of a more comprehensive economic assessment of the electrodeposition coating process as it relates to interconnect manufacturing.

FY 2010 Publications/Presentations

1. T.D. Hall, H.A. McCrabb, J. Wu, H. Zhang, X. Liu, and E.J. Taylor, "Electrodeposition of CoMn onto Stainless Steels Interconnects for Increased Lifetimes in SOFCs," 217th Meeting of the Electrochemical Society, Vancouver, British Columbia (April 2010).

References

1. Eric J. Carlson, Suresh Sriramulu, Peter Teagan, and Yong Yang, "Cost Modeling of SOFC Technology," First International Conference on Fuel Cell Development and Deployment, University of Connecticut, Storrs, Connecticut, March 10, 2004.

2. J. Wu, Y. Jiang, C. Johnson, and X. Liu, Journal of Power Sources 177 (2008) 376-385.

3. L. Gebhart, J. Sun, P. Miller, and E.J. Taylor, "Electroplating Cell with Hydrodynamics Facilitating More Uniform Deposition across a Workpiece during Plating," U.S. Patent No. 7,553,401 issued June 30, 2010.

4. X. Sun et. al., Journal of Power Sources 176 (2008) 167.

III.C.4 Thickness Effects on SOFC Interconnects

Paul D. Jablonski
National Energy Technology Laboratory (NETL)
1450 Queen Avenue, SW
Albany, OR 97321
Phone: (541) 967-5982; Fax: (541) 967-5958
E-mail: Paul.Jablonski@netl.doe.gov

Contract Number: FY10.MSE.1610248.691.01

Start Date: December 15, 2009
End Date: September 30, 2010

FY 2010 Objectives

- Employ computational modeling to evaluate the thickness, chemistry and temperature effects on the interdiffusion of Ni and a ferritic stainless steel.
- Construct diffusion couples of Ni/Fe16Cr and Ni/441SS and expose them to solid oxide fuel cell (SOFC) relevant conditions in order to evaluate the computational predictions.

Accomplishments

- Previous efforts by NETL have resulted in a U.S. patent (7,553,517) which infuses reactive elements (RE) into the interconnect surface in a low cost and reliable method resulting in a 3x (or more) reduction in oxidation rate.
- The Ni/stainless steel interdiffusion under SOFC operating conditions has been calculated for times up to nearly 32 years.
- Preliminary interdiffusion experiments are in good agreement with the predictions.

Introduction

SOFCs are energy conversion devices which transform fuel to electrical energy in the absence of combustion. They have the potential for high efficiencies especially when part of an integrated fuel utilization system [1-5]. A great leap forward was made upon the development of cell components that could operate in the reduced temperature range of 700-800°C as compared to previous systems which operated typically at 1,000°C or so [6-11]. With this temperature reduction it became possible to consider metallic components for interconnects which have the advantage of being low cost and more easily manufactured in comparison to their ceramic counterparts. An interconnect within a planar SOFC joins repeat units of the anode/electrolyte/cathode assembly in order to build up useful levels of current and voltage. In doing this it separates the fuel and air, and it also becomes part of the electrical circuit. Even at elevated operating temperatures, candidate metallic interconnect alloys have low resistivity compared to their ceramic cell counterparts. However, alloys being considered for SOFC interconnects such as the Ni-based alloy Haynes 230 or ferritic stainless steels such as 430ss or 441ss oxidize on both the anode and cathode side of the fuel cell. This is because these materials are chromia formers. Chrome oxidizes at very low partial pressure of oxygen (P_{O2}~10^{-23} Pa, 800°C) which is easily reached in the moist fuel environment (the oxidant reacts with the fuel on the anode side of the cell to form water and/or carbon dioxide). Fortunately, the chrome-rich oxides that form on the alloys are intrinsic semi conductors under typical SOFC operation conditions. Nevertheless, oxide scale growth on the interconnect leads to reduced SOFC performance over time. Thus, much work has been done to slow the oxide scale growth rate and minimize or prevent Cr evaporation (and thus poisoning) on the air side of the interconnect [12-23]. One measure of the effectiveness of these improvements is the area specific resistance (ASR) test [11,16,24]. In its most complete form, an ASR test is basically a four point probe resistivity measurement over a specified area under SOFC relevant conditions including temperature and gas exposure. When testing the ASR on interconnect materials, a pair of samples are typically pre-oxidized under the conditions of interest then sandwiched together for measurement at temperature. Interestingly, the ASR on the fuel side can be significantly higher than that on the air side (~50x or more) [25-28]. The present understanding of this phenomena is that the oxide that forms on the anode side is porous, cracked and poorly adherent under the anodic conditions of the interconnect.

Pure Ni does not oxidize under SOFC anodic conditions (the equilibrium partial pressure of oxygen to oxidize Ni: P_{O2}~10^{-9} Pa, 800°C). There have been several attempts to evaluate a bi-metal of Ni/chromia forming metal. Nielsen et al. [29] performed experiments on a 200 µm thick Fe22Cr alloy with a 7 µm thick Ni plate at 850°C for up to 1,150 h. What they observed was very low in-stack ASR on the anode side (<1 mΩcm^2). However, they also observed significant interdiffusion after the 1,150 h exposure (not surprising since Cr tracer diffusion predicts an interdiffusion of about 12 µm) leaving little hope for long term stability of such an interconnect. It is interesting to note that in the work of Nielsen they also Ni plated the cathode

side and they reported a reduced ASR on that side as well (~10 mΩcm^2), presumably as a result of increased scale conductivity when doped with Ni. Likewise, Shaigan et al. [30] electroplated ~7 µm thick layer of Ni or Ni/$LaCrO_3$ onto 1 mm thick 430ss and exposed them to air oxidizing conditions at 800°C for up to 2,040 h. While they reported significantly lower ASR on the coated coupons (~5 mΩcm^2) they also reported significant interdiffusion between the coating and the substrate. Under these conditions, the Cr tracer diffusion predicts an interdiffusion of about 8 µm. Fu et al. [31] applied a ~75 µm thick Ni layer on 430ss by atmospheric plasma spray (APS) technology and exposed these coupons to moist hydrogen conditions at 800°C for up to 250 h. While they did report low ASR on the Ni coated coupons (~12 mΩcm^2), they also reported the formation of Cr-Fe rich oxides at the Ni-430ss interface, presumably due to the porous nature of the APS coating. In each of these cases the ASR was reduced by the application of a Ni coating (compare the above results to ~1 Ωcm^2 which was reported after 200 h/800°C [26]). From these results we may conclude that it is advantageous to apply a Ni layer to at least the fuel side of the interconnect. Thus, the stability and lifetime prediction of a Ni coating on a ferritic steel substrate would be of interest for SOFC application.

As has been demonstrated in the literature [29-31], when Ni is applied to a ferritic stainless steel the two will interdiffuse over time at the normal SOFC operating conditions. The critical question is this: Under what conditions (Ni thickness and operating temperature) would the Ni layer be expected to survive?

The goal of this research is to explore the interdiffusion of Ni with ferritic stainless steel with numerical predictions and experimental verification in order to get a life estimate and to better predict the required Ni and stainless thicknesses for a given set of conditions.

Approach

A computational approach was selected in order to estimate the amount of interdiffusion out beyond the 40,000 h desired life. The commercial software DICTRA (DIffusion Controlled TRAnsformations) was utilized employing the diffusivity database MOB2 along with the thermodynamic database TCFe6. Both mobility and thermodynamic databases are needed because in a DICTRA diffusion simulation multicomponent diffusion equations of the type:

$$J_k = -\sum_{j=1}^{n-1} \tilde{D}_{kj}^{n} \frac{\partial C_j}{\partial z} \quad \text{(Equation 1)}$$

are solved using a complete (n-1) x (n-1) temperature and concentration dependent diffusivity matrix. The diffusivity matrix $\tilde{D}_{kj}^{n}$ is calculated from parameters stored in the mobility and thermodynamic databases. Thus, it is possible to calculate diffusion within a multicomponent system. In the present simulation, the system consists of 100 µm thick Ni (left side) next to 400 µm thick model ferritic stainless steel (Fe-16Cr). In order to better capture the details at the interface, a geometric grid point array was utilized which had closer grid point spacing at either side of the interface between the two phases. Simulation temperatures of 750, 800, and 850°C were examined out to 1(10)^9 s (nearly 278,000 h).

Results

The computational results showed that Cr from the ferrite phase reaches 1 weight percent at about 37 µm into the Ni but does not reach the outer (left side) of the Ni as a result of the simulation of 1.44(10)^8 s (40,000 h) at 750°C (Figure 1). The FCC/BCC interface moves from its original 100 µm location to about 113 µm from the left side as a result of this diffusion. A small two-phase region was observed at the FCC/BCC interface and is exhibited as a vertical segment in the Cr composition versus position plot. The Cr was slightly reduced in the adjacent ferritic material (down from 16 to about 15.3 weight percent). This Cr depletion on the ferritic side of the diffusion couple extended to the far right side of the ferritic phase (not shown in the figure) and is 15.98 weight percent. Under the same conditions the 1 weight percent Fe level reaches about 24 µm into the Ni but did not reach the outer (left side) of the

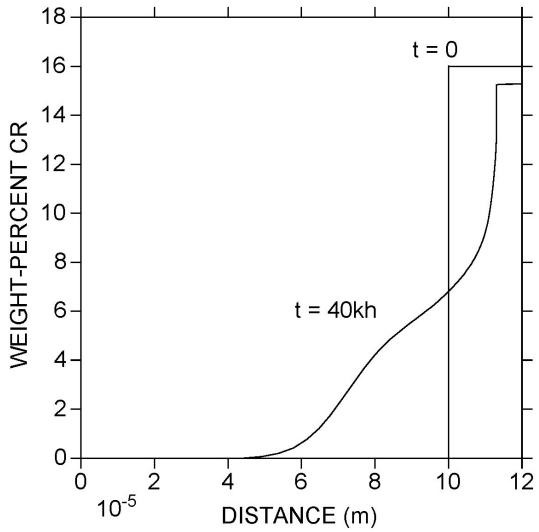

FIGURE 1. The weight percent Cr is shown as a function of distance (m) in the plot for t = 0 and 1.44(10)^{8}s (0 and 40,000 h) at 750°C. The pure Ni ranged from 0 to 10(10)$^{-5}$m at t = 0. The Cr diffused about 80 µm into the Ni but did not reach the outer (left side) of the Ni. Note that the Cr depletion shown on the ferritic side did not extend all the way to the right side (outer ferritic).

Ni. Thus, at the 1 weight percent level, Cr is the faster diffusing species in this system.

At 800°C, the Cr from the ferrite phase diffuses fully through the 100 µm Ni as a result of the simulation of $1.44(10)^8$ s (40,000 h) reaching about 0.3 weight percent Cr on the far left (outer Ni) side. The Cr level reaches 1 weight percent at about 77 µm into the Ni. The face centered cubic/body centered cubic (FCC/BCC) interface moves from its original 100 µm location to about 131 µm from the left side as a result of this diffusion. The Cr was slightly reduced in the adjacent ferritic material, down from 16 to about 15.5 weight percent. This Cr depletion on the ferritic side of the diffusion couple extended to the right side of the ferritic phase and is 15.8 weight percent on this outer surface. Under the same conditions the Fe does not diffuse fully through the 100 µm Ni and reaches 1 weight percent about 72 µm into the Ni.

At 850°C, the Cr from the ferrite phase diffuses fully through the 100 µm Ni as a result of the simulation of $1.44(10)^8$ s (40,000 h) reaching about 5.6 weight percent Cr on the far left side. The FCC/BCC interface moves from its original 100 µm location to about 175 µm from the left side as a result of this diffusion. The Cr was slightly reduced in the adjacent ferritic material, down from 16 to about 15.7 weight percent. This Cr depletion on the ferritic side of the diffusion couple extended to the right side of the ferritic phase and is 15.8 weight percent on this outer surface. Under the same conditions the Fe diffuses fully through the 100 µm Ni and reaches about 12 weight percent on the outer (left side) of the Ni. Likewise, the Ni diffuses all the way through the ferritic phase reaching about 0.9 weight percent on the outside of the ferritic phase.

It has been found that Cr diffuses further into the Ni layer than does the Fe at the 1 weight percent level. In order to estimate the time to breach the Ni, the position of 1 weight percent Cr within the Ni layer was recorded for a series of time steps at 750°C with 100 µm Ni up to $1.44(10)^8$ s. A similar series was recorded for the 800 and 850°C simulations, but these employed 500 µm Ni in order to avoid breaching the Ni. Figure 2 shows a plot of square root of time vs. diffusion distance into the Ni layer for the three different temperatures. All were found to fit the following equation:

$$X_{Ni}^{Cr=1} = a + bt^{0.5} \quad \text{(Equation 2)}$$

where $X_{Ni}^{Cr=1}$ is the distance into the Ni from the original FCC/BCC interface where the Cr level reaches 1 weight percent, a and b are constants and t is time in s. Table 1 contains a compilation of these coefficients as well as predictions of times to breach the 100 µm Ni as well as diffusion distances after $1.44(10)^8$ s at the three temperatures. At 750°C it is predicted that it will take more than double the $1.44(10)^8$ s life cycle to reach 1 weight percent Cr outside a 100 µm Ni layer while at 800 and 850°C the time to reach this level of Cr drops by an order of magnitude or so for each 50°C increase in temperature. Another way to consider these results is the Ni thickness for a $1.44(10)^8$ s life cycle (presuming that 1 weight percent Cr is the critical level). At 750°C a 37 µm Ni layer is required while a 77 µm layer is required at 800°C and a 150 µm layer is required at 850°C. Thus, for every 50°C increase in temperature the Ni required is approximately doubled.

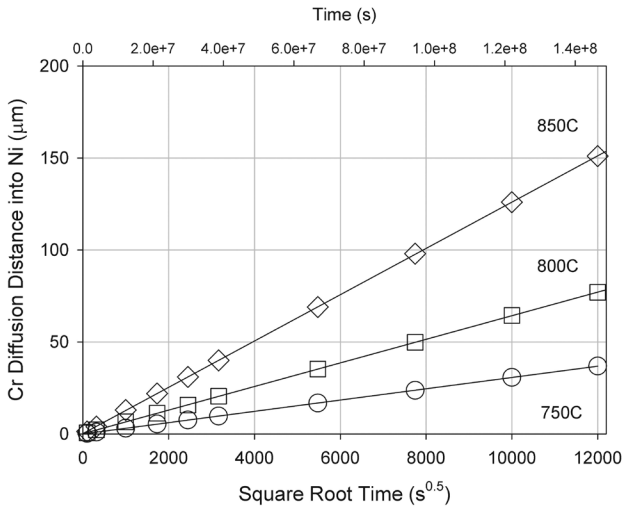

FIGURE 2. The distance that Cr from the ferritic stainless steel diffuses into Ni is plotted as a function of the square root of time in the figure. For the 750°C test, 100 µm Ni was used while 500 µm Ni was used for the higher temperatures. Each of the curves is linear with the square root of time. The curve fit coefficients are found in Table 1.

TABLE 1. The coefficients to Equation 2 are found in the table below as are the times to breach 100 µm Ni as well as the distance to reach 1 weight percent Cr after $1.44(10)^8$ s at the respective temperatures.

T(°C)	a (µm)	b (µm $s^{-0.5}$)	$t_i(X_{Ni}^{Cr=1}$ =100 µm)	$X_{Ni}^{Cr=1}$, (t = $1.44(10)^8$ s)
750	2.77 $(10)^{-2}$	$3.07(10)^{-3}$	$1.1(10)^9$ s	37 µm
800	0.119	$6.42(10)^{-2}$	$2.4(10)^8$	77
850	0.185	$1.26(10)^{-2}$	$6.3(10)^7$	150

Whenever results to a complex or long-term problem are desired, it is sometimes useful to consider simulations to predict the solution. In the present case, the desired 40,000 h life cycle for an SOFC is slightly over 4.5 years. Thus, it could conceivably take over 20 years to complete five experimental trials if run in series while such a series of simulations could be completed in a matter of days or weeks. However, in order to be useful, the validity of the predictions must be somehow

tested. Of the 35 or so references that Jönsson used in his development of the Mobility database for DICTRA, 19 of these are over a temperature and composition range relevant to the present work [32]. In his assessment report, Jönsson showed that the simulated diffusivities give a satisfactory description of the experimental data [32]. Thus, the foundation of this present work is sound. A further check of the results is a comparison of the predictions to the tracer diffusivity [33] based diffusion distance. Table 2 contains the distance that the Cr has diffused into the Ni to reach the 1 weight percent level. Note that these values come directly from the simulations rather than the curve fit to Equation 2 which are given in Table 1. First a quick comparison to the values based on Equation 2 is warranted. In general, the predictions based on Equation 1 agree within about 5% with the values of the simulation. Comparing the value of $X_{Ni}^{Cr=1}$ with the tracer diffusion distance shows that they agree within a factor of ~2 which is fairly good for diffusion distances and the fact that one is describing tracer diffusion and the other chemical diffusion. Thus, the diffusion distance and life estimates presented in this work appear reasonable.

TABLE 2. The distance into Ni to reach 1 weight percent Cr after $1.44(10)^8$ s is compared to the tracer diffusion distance for Cr in Ni [33] at the respective temperatures.

T (°C)	$X_{Ni}^{Cr=1}$ (μm)	Tracer
750	37 μm	17 μm
800	77	35
850	150	68

The best check on the validity of the predictions would be experimental verification. We constructed a Ni/Fe16Cr diffusion couple and exposed it to 850°C for 1,000 h. The experimental results compare favorably to the predictions (Figure 3). Another reasonable approach would be if experimental results were available in the literature. Yen et al. [34] report on a diffusion couple of Ni/Fe-16Cr at 750°C/200 h. Unfortunately, the work presented by Yen is clearly in error. Within the Ni/Fe-16Cr diffusion couple, there are a couple of points measuring over 60 weight percent Cr and another measuring over 40 weight percent Cr. Nickel does not stabilize Cr rich phases in ferritic stainless steels. Even if it did, they report little or no Ni in the vicinity of the 60 weight percent Cr; however, Fe-16Cr is single phase at 750°C (it is at 850°C as well). The only reasonable conclusion is that this region of high Cr pre-existed in the ferritic material. Indeed, the ferritic material was made by arc melting a button of elemental constituents followed by equilibrating at 750°C/720 h. Such a high level of Cr could not segregate due to non-equilibrium solidification [35, 36]. If it had been, it is unlikely that such a low temperature anneal would have homogenized

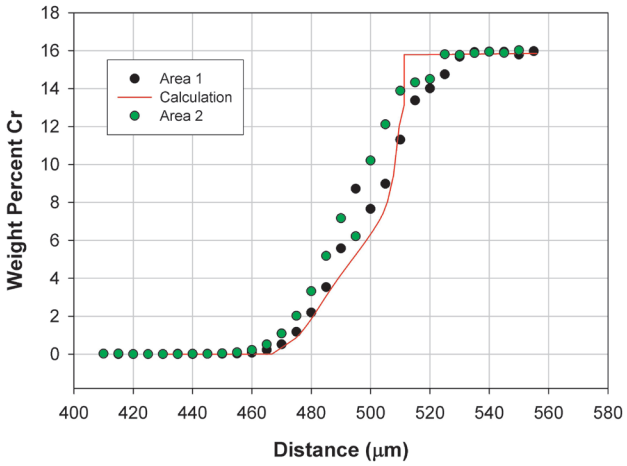

FIGURE 3. The weight percent Cr is shown as a function of distance (μm) in the plot. The symbols are measured results from diffusion couple experiments while the line is the computational predictions which compare favorably to the measurements. Conditions: 850°C/1,000 h.

the material [37]. Thus, the only conclusion that can be reached is that their melting technique failed to fully alloy in all of the melt stock. Our own experience is that making alloys in a button furnace can be tricky at best [38] especially when melting metals of dissimilar melting points or densities. The densities of Fe and Cr are not that different however the melting temperatures differ by over 300°C. Thus, a button melt operator can create a molten pool of liquid Fe and still have solid Cr within the pool. It is also noteworthy that only a limited amount of superheat is achievable in such a furnace. This is why large differences in the melting temperature of constituents can be problematic. The critical factors in being able to fully alloy in all the constituents also include the size of the materials, how long the material is held molten and the size of the hearth and electrode (both relate to the size of the molten pool at any one time). None of these criteria were discussed by Yen et al. [34] and may not have been considered. Thus, the ferritic component of their diffusion couple has a dubious pedigree. Regarding their reported interdiffusion with Ni, even the most conservative reading of their results suggests diffusion distances on the order of 40 μm while tracer diffusion data suggest a distance of about 1 μm and this work suggests a distance of about 2.5 μm (Equation 2, Table 1). The discrepancy between the experimental results and the two predictions suggests a source beyond experimental error. At this temperature, grain boundary diffusion could be a significant contributor; however, no grain size was specified for either component of the diffusion couple. At any rate, because of the errors cited, these results cannot be used to test the predictions of the present work.

Conclusions and Future Directions

There is a significant opportunity to impact the goals of reduced SOFC performance degradation and improved lifetime prediction. Ni is a proven performer on the SOFC anode side. Previous researchers have failed to address the required Ni thickness for long term performance. A combined approach of computational modeling and experimental verification has been used to address this challenge. Next fiscal year we propose to insert an engineered interconnect (Ni cladding on the anode side and surface treatment on the cathode side) into an SOFC test stack to evaluate the long term performance and stability.

Special Recognitions & Awards/Patents Issued

1. U.S. Patent 7,553,517, Method of Applying a Cerium Diffusion Coating to a Metallic Alloy, June 30, 2009.

FY 2010 Publications/Presentations

1. Jablonski, Cowen and Sears, *J Power Sources* (2010).

2. Invited Talk: 2010 ASM Annual Symposium.

References

1. Fuel Cell Handbook, 7th ed., EG&G Technical Services, under contract number DE-AM26-99FT40575 with U.S. Department of Energy, Office of Fossil Energy, National Energy Technology Laboratory, Ch. 1, (2004).

2. Fuel Cell Handbook, 7th ed., EG&G Technical Services, under contract number DE-AM26-99FT40575 with U.S. Department of Energy, Office of Fossil Energy, National Energy Technology Laboratory, Ch. 7, (2004).

3. Mark C. Williams, Joseph P. Strakey, and Wayne A. Surdoval, J. of Power Sources 143 (2005) 101-196.

4. Mark C. Williams, Joseph P. Strakey, Wayne A. Surdoval, and Lane C. Wilson, Solid State Ionics, 177 (2006) 2039-2044.

5. Mark C. Williams, Joseph P. Strakey, and Wayne A. Surdoval, J. of Power Sources 159 (2006) 1241-1247.

6. S. de Souza, S.J. Visco, and L.C. De Jonghe, Solid State Ionics 98 (1997) 57.

7. H. Ishihara, H. Matsuda, and Y. Takita, J. Am. Chem. Soc. 116 (1994) 3801.

8. M. Feng and J.B. Goodenough, Eur. J. Solid State Inorg. Chem. T31 (1994) 663.

9. P. Huang and A. Petric, J. Electrochem. Soc. 143 (5) (1996) 1644.

10. K.Q. Huang, R. Tichy, and J.B. Goodenough, J. Am. Ceram. Soc. 81 (1998) 2565.

11. W.Z. Zhu and S.C. Deevi, Mat. Res. Bull., 38 (2003) 957-972.

12. S.P. Simner, M.D. Anderson, G.-G. Xia, Z. Yang, L.R. Pederson, and J.W. Stevenson, J. Electrochem. Soc. 152 (4) (2005) A740.

13. M.C. Tucker, H. Kurokawa, C.P. Jacobson, L.C. De Jonghe, and S.J. Visco, J. Power Sources 160 (2006) 130.

14. M. Kumpelt, T. Kaun, T.A. Cruse, and M. Hash, SECA Annual Workshop, May 11–13, 2004, available at http://www.seca.doe.gov.

15. S.P.S. Badwal, R. Deller, K. Foger, Y. Ramprakash, and J.P. Zhang, Solid State Ionics 99 (1997) 297.

16. J.W. Fergus, Mater. Sci. Eng. A397 (2005) 271.

17. Y. Matsuzaki and I. Yasuda, Solid State Ionics 132 (2000) 271.

18. S.P. Jiang, J.P. Zhand, and X.G. Zheng, J. Eur. Ceram. Soc. 22 (2002) 361.

19. Z. Yang, G. Xia, P. Singh, and J.W. Stevenson, J. Power Sources 155 (2006) 246.

20. X. Chen, P.Y. Hou, C.P. Jacobson, S.J. Visco, and L.C. De Jonghe, Solid State Ionics 176 (2005) 425-433.

21. Z. Yang, G. Xia, G. Maupin and J. Stevenson, Surface and Coatings Technology, 201 (2006) 4476-4483.

22. Junwei Wu, Christopher D. Johnson, Randall S. Gemmen, and Xingbo Liu, Journal of Power Sources 189 (2009) 1106.

23. D.E. Alman and P.D. Jablonski, Int. J. Hydrogen Energy 32 (2007) 793.

24. P. Piccardo, P. Gannon, S. Chevalier, M. Viviani, A. Barbucci, G. Caboche, R. Amendola, and S. Fontana, Surf. Coat. Tech 202 (2007) 1221-1225.

25. D.M. England and A.V. Virkar, J. Electrochem. Soc. 146 (9) (1999) 3196-3202.

26. D.M. England and A.V. Virkar, J. Electrochem. Soc. 148 (4) (2001) A330-A338.

27. Y. Liu, J. Power Sources, 179 (2008) 286-291.

28. T.J. Armstrong, M.A. Homel, and A.V. Virkar, in: Solid Oxide Fuel Cells VIII–Electrochemical Society, S.C. Singhal, M. Dokiya (Eds.), Penington, New Jersey (2003) 841-850.

29. K.A. Nielsen, A.R. Dinesen, L. Korcakova, L. Mikkelsen, P.V. Hendriksen, and F.W. Poulsen, Fuel Cells 06 (2006) No. 2, 100-106.

30. N. Shaigan, D.G. Ivey, and W. Chen, J. Power Sources 183 (2008) 651-659.

31. C. Fu, K. Sun, X. Chen, N. Zhang, and D. Zhou, Corrosion Sci. 50 (2008) 1926-1931.

32. B. Jönsson and Z. Metallkd. 86 (1995) 686-692.

33. Smithells Metals Reference Book, 7th ed., E.A. Brandes and G.B. Brook ed., Butterworth-Heinemann Ltd, (1992).

34. Y. Yen, J. Su, and D. Huang, J. Alloys and Compounds 457 (2008) 270-278.

35. E. Scheil and Z. Metallkd., 1942, vol. 34, pp. 70-72.

36. G.H. Gulliver, J. Inst. Met. 1913, vol. 9, pp. 120-57.

37. P.D. Jablonski and C.J. Cowen, Met Trans B., 40B 182 (2009).

38. P.D. Jablonski and E. Argetsinger, unpublished research, NETL (2005).

III.C.5 Development of SOFC Interconnects and Coatings

Guan-guang "Gordon" Xia (Primary Contact), Jung-Pyung Choi, Joshua Templeton, Xiaohong Li, Zimin Nie, Tak Keun Oh, and Jeff Stevenson
Pacific Northwest National Laboratory (PNNL)
P.O. Box 999, MS K2-44
Richland, WA 99352
Phone: (509) 371-6261; Fax: (509) 375-2186
E-mail: Guan-Guang.Xia@pnl.gov

DOE Project Monitor: Briggs White
Phone: (304) 285-5437
E-mail: Briggs.White@netl.doe.gov

Contract Number: FWP40552

Start Date: October 1, 2009
End Date: September 30, 2010

FY 2010 Objectives

- Develop cost-effective, optimized materials for intermediate temperature solid oxide fuel cell (SOFC) interconnect applications.
- Identify, understand, and mitigate degradation processes in interconnects and at interconnect interfaces.

Accomplishments

- Evaluated performance of spinel-coated ferritic stainless steel interconnect materials under single- and dual-atmosphere exposure conditions.
- Optimized composition and processing parameters of Ce-modified MnCo spinel coatings.

Introduction

In previous work, $(Mn,Co)_3O_4$ (MC) spinels have been systematically investigated and applied as protection layers on a variety of candidate SOFC interconnect steels. In recent years, the primary emphasis has been on the application of spinel coatings to AISI 441 ferritic stainless steel, which is being investigated as an interconnect alloy by PNNL in collaboration with Allegheny Ludlum and the National Energy Technology Laboratory. 441 is prepared via conventional melt metallurgy and is therefore less expensive that other candidate steels, such as Crofer22APU, which utilize vacuum processing to reduce the Si content to very low levels. Additions of Nb and Ti to the 441 tie up residual Si in Laves phase at grain boundaries, eliminating the need for expensive processing. To mitigate scale adhesion issues, Ce-modified MC (Ce-MC) coatings (e.g., $Ce_{0.02}Mn_{1.49}Co_{1.49}O_4$) were developed, which combines the advantages of rare earth (RE) surface treatment or additions, and the MC spinel coating. The stability and electrical performance of 441 coated with Ce-MC protection layers were validated in short-term and long-term (1 year) testing. These tests indicated that the spinel protection layers helped minimize the interfacial electrical resistance and mitigate the scale growth beneath the spinel coatings on 441. In addition, the Ce-modified coatings improved the scale adherence and overall interconnect surface stability.

Approach

To supplement and confirm previous test results, additional long-term area specific resistance (ASR) tests are being carried out to evaluate the long-term performance and structural stability of Ce-MC coatings on AISI441. The AISI441 was provided by the manufacturer, Allegheny Technologies Inc. MC and Ce-MC spinel powders were applied to selected alloy coupons using a slurry-based approach, and sintered to form protective coatings. The electrical resistance of bare and coated 441 is measured by applying a four-probe direct current measurement technique to simulated interconnect/coating/contact material/cathode structures. In addition to baseline testing of spinel-coated 441 at 800°C, the effects of a) physical surface modifications to the 441, and b) higher temperature (850°C) are being studied.

Alternative protective coating compositions are also being developed and evaluated, with an emphasis on reduction of coating cost (e.g., reduction of Co content and/or elimination of reducing atmosphere heat treatments).

Results

Figure 1 shows long-term ASR test results of bare 441, MC coated 441, and Ce-MC coated 441. Some of the tests are still in progress; all tests were performed at 800ºC, except where noted in the legend. In contrast to the bare (uncoated) 441, the ASRs of both the MC and Ce-MC coated 441 were low and remained essentially unchanged at 800 and 850°C, indicating good stability (and high reproducibility) of the coated steel coupons. Oxidation studies have also been performed on coated 441 coupons at 800 and 850°C; results are shown in Figure 2. As expected, the oxidation kinetics were faster

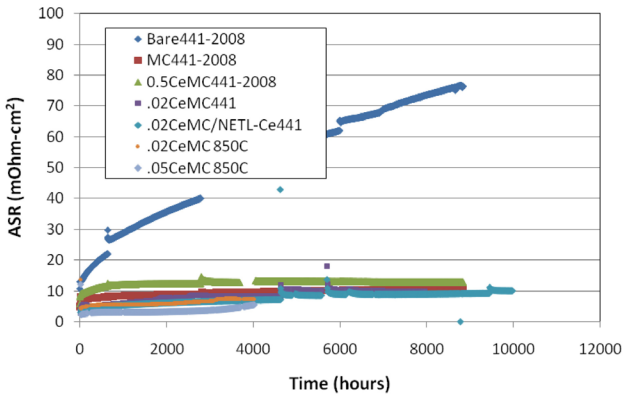

FIGURE 1. Area specific resistance of $Mn_{1.5}Co_{1.5}O_4$ (MC) coated and Ce-modified MC coated AISI 441, in comparison with that of bare 441. The measurements were carried out at 800°C in air except where noted in the legend.

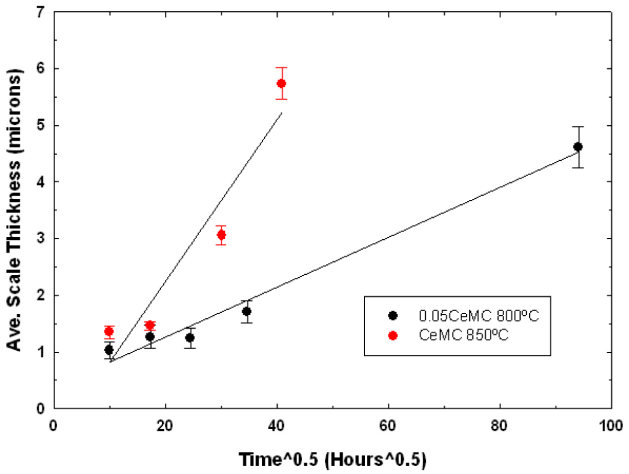

FIGURE 2. Average oxide scale thickness as a function of time for spinel-coated AISI 441 at 800 and 850°C in air.

at the higher temperature (see Table 1). While the 850°C ASR tests showed excellent stability, oxidation tests on coated 441 coupons at 850°C indicated spallation at the scale/alloy interface after ~1,500 hours. No obvious differences in coating/scale/alloy chemistry were observed during post-test scanning electron microscopy/energy dispersive spectroscopy (SEM/EDS) analysis, suggesting that the spallation may have been primarily related to increased thermal stresses (due to coefficient of thermal expansion mismatch) resulting from increased oxide scale thickness at the higher temperature. To mitigate possible spallation issues at this higher temperature, a variety of physical surface modifications to the 441 are being considered; oxidation testing of the modified steel is in progress.

TABLE 1. Parabolic Rate Constants for Bare and Coated AISI 441 Stainless Steel

k_p (g^2/cm^4-s)	800°C	850°C
Ce-MC coated 441	2×10^{-14}	1×10^{-13}
Bare 441	5×10^{-14}	3×10^{-13}

In related work, intended to allow for scale-up of PNNL's protective coating processes, ultrasonic spray techniques previously developed for aluminized coatings were optimized for the application of MC spinel coatings. Unlike previously developed screen-printing fabrication techniques, spray-based processes allow for application of protective coatings to selected regions of "shaped" SOFC interconnects and other components. A "Design of Experiment" approach was used to optimize the spray process, with the specific experiments being determined through an L16 Orthogonal Array developed for each spray mode (wide and narrow). The Gray-Taguchi methodology was applied to three results: coating thickness, pore area per unit of total area, and the amount of material used for the sample coating process. In addition, analysis of variance (ANOVA) was performed to determine which factor was most influential in the spray process. After the optimization process was completed, ASR tests demonstrated that the optimized spray processes (using either a wide spray or narrow spray mode) produced coatings that resulted in low stable ASR that were similar to the results obtained for coatings applied by screen-printing (Figure 3).

As mentioned above, alternative protective coating compositions are also being developed and evaluated, with an emphasis on reduction of coating cost. One cost reduction approach involves reduction, or even elimination, of the Co content of the coating. For the Co-free case, Mn oxide coatings, prepared from Mn powder precursors, were evaluated. The Mn powders

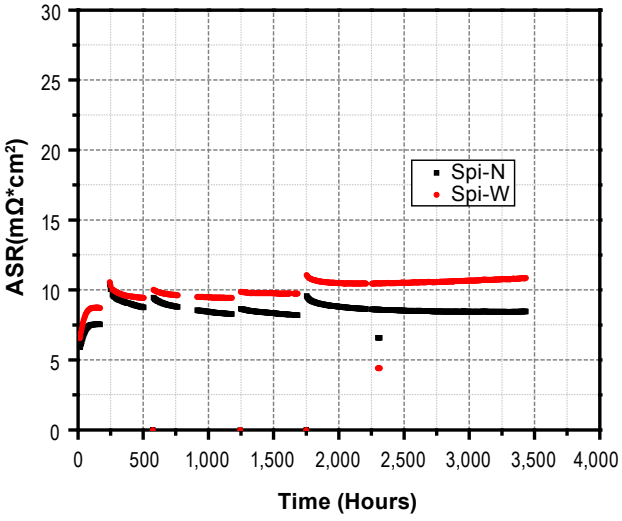

FIGURE 3. ASR of spinel-coated AISI 441; the spinel coatings were applied using wide or narrow mode ultrasonic spray process. The measurements were carried out at 800°C in air.

were milled to different sizes (in cyclohexane to prevent oxidation) and then evaluated separately and in mixtures to determine the optimized precursor condition for maximum coating density. The binder to solids ratio of the screen-printing inks was also optimized for maximum coating density. Once the optimized coating fabrication conditions were determined, coated AISI 441 coupons were subjected to ASR testing. While low initial ASRs were obtained on the optimized coatings, the ASR was found to increase significantly over time (Figure 4). The increase in ASR correlated well with an observed increase in scale thickness under the Mn oxide coating, indicating that the coatings were unable to substantially reduce oxidation of the steel. This could be attributable to unobserved gas transport paths through the coating, or to high oxygen ion conductivity in the coating. More encouraging preliminary results have been obtained for MC compositions with reduced Co content (i.e., Co content less than the standard Mn:Co = 50:50 mole ratio). While initial ASR values were somewhat higher than for the standard MC composition, a coating with Mn:Co = 85:15 weight ratio showed nearly stable ASR over more than 1,500 hours of testing at 800ºC (Figure 5). Post-test SEM/EDS analysis on a similar sample after 500 hours of testing indicated that, similar to standard MC coatings, the reduced Co coating was effective in blocking Cr transport from the oxide scale.

Conclusions and Future Directions

Long-term ASR tests validated the long-term structural and electrical performance stability (and reproducibility) of spinel-coated 441 under intermediate temperature SOFC operating conditions. The long-term tests also confirmed the effectiveness of the spinel coating as a Cr barrier that sealed off Cr and prevented Cr-migration into cathode contact materials. Gray-Taguchi/ANOVA methodologies were used to optimize ultrasonic spray processes intended for application of spinel coatings to complex interconnects. Attempts to completely eliminate Co from the protective coatings yielded low initial ASRs, but the ASRs increased steadily over time, indicating the need for some Co in the coating. Samples of AISI 441 with coatings having reduced Co content (compared to the standard spinel coating) have demonstrated encouraging stability over 1,500-hour test times.

Future research directions include long-term testing in realistic stack environments (using PNNL's Solid State Energy Conversion Alliance Core Technology Program stack test fixture), testing at temperatures higher than 800ºC to determine upper service limits for the coated 441, continued efforts to reduce coating cost, and further implementation of spray-based fabrication processes.

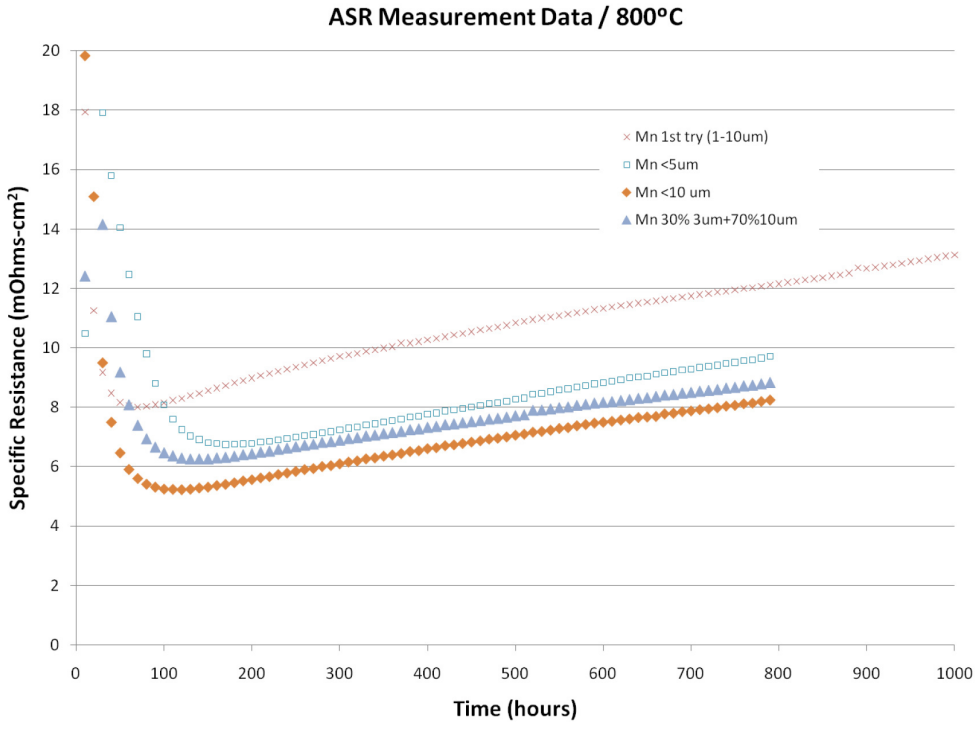

FIGURE 4. ASR of AISI 441 with Mn oxide coating prepared from Mn powder precursors. The measurements were carried out at 800°C in air.

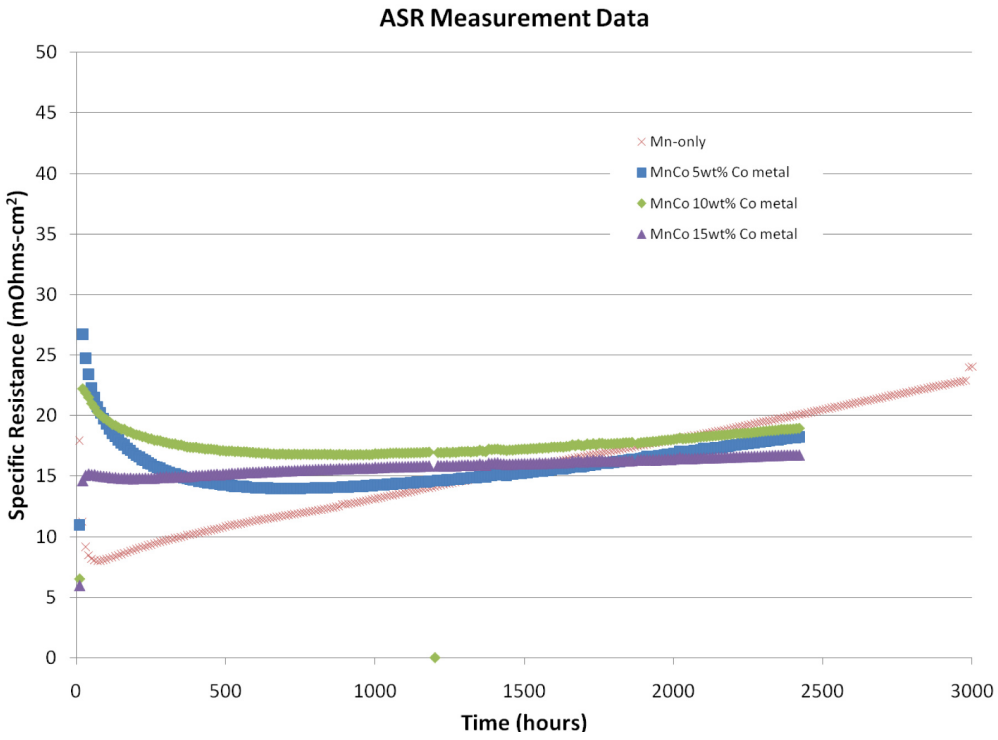

FIGURE 5. ASR of AISI 441 with MnCo oxide coatings with varying Co content. The measurements were carried out at 800°C in air.

FY 2010 Publications/Presentations

1. J.P. Choi, K.S. Weil, Y.S. Chou, J.W. Stevenson, Z. Yang, and G.G. Xia, "Advanced Novel Interconnect Coatings for Hermetic Sealing and Mitigation of Cr Volatility in Planar SOFC Stacks," 139th Annual TMS Meeting, Seattle, Washington, February 15–18, 2010.

2. J.W. Stevenson, G. Yang, G. Xia, J. Templeton, and J. Choi, "Development of Alloy-based SOFC Interconnects," 34th International Conference on Advanced Ceramics and Composites, Daytona Beach, Florida, January 24–29, 2010.

3. J.P. Choi, K.S. Weil, Y.S. Chou, and J.W. Stevenson, "Novel Dual MnCo Spinel Coating with Alumina for Planar SOFC Stacks," Materials Science & Technology 2009, Pittsburgh, Pennsylvania, October 29, 2009.

4. X. Li, J. Templeton, G. Xia, Z. Yang, Z. Nie, and J.W. Stevenson, "Recent Progress in Development of Protective Coatings for SOFC Interconnect," 37th International Conference on Metallurgical Coatings and Thin Films, San Diego, California, April 26, 2010.

5. J.W. Stevenson, G. Xia, J. Choi, J. Templeton, T. Oh, and Z. Nie, "Development of SOFC Interconnects and Coatings," 11th Annual SECA Workshop, Pittsburgh, Pennsylvania, July 28, 2010.

III.C.6 Development of Cathode Contact Materials for SOFC

Guan-guang "Gordon" Xia (Primary Contact), Zigui Lu, Joshua Templeton, Xiaohong Li, Zimin Nie, Tak Keun Oh, and Jeff Stevenson
Pacific Northwest National Laboratory (PNNL)
P.O. Box 999, MS K2-44
Richland, WA 99352
Phone: (509) 371-6261; Fax: (509) 375-2186
E-mail: Guan-Guang.Xia@pnl.gov

DOE Project Monitor: Briggs White
Phone: (304) 285-5437
E-mail: Briggs.White@netl.doe.gov

Contract Number: FWP40552

Start Date: October 1, 2009
End Date: September 30, 2010

FY 2010 Objectives

- Develop and investigate cost-effective contact materials and fabrication processes for cathode/interconnect interfaces that demonstrate long-term chemical, electrical, and structural stability.
- Identify, understand, and mitigate degradation processes at cathode/interconnect interfaces.

Accomplishments

- Determined solid oxide fuel cell (SOFC)-relevant properties of candidate cathode contact materials.
- Evaluated performance of candidate cathode contact materials using simulated cathode/contact material/interconnect test configurations.

Introduction

Optimization of interconnect materials and coatings is a necessary, but not sufficient, condition for obtaining stable stack performance. The complete solution to interconnect-related challenges must also take into account the electrode/interconnect interfaces. Thus, it is necessary to develop a complete materials system, which includes not only the interconnect itself, but also stable, high performance contact materials for electrode/interconnect interfaces.

Requirements for successful development of cathode contact materials include:

- High electrical conductivity to minimize the resistance of the contact layer and the contact interfaces.
- Chemical compatibility with the interconnect and the perovskite cathode. If reaction occurs, the resulting reaction products should be stable and conductive.
- Appropriate thermal expansion behavior and high thermo-chemical and structural stability in the SOFC operating environment.
- Appropriate bond-forming ability and sintering activity for increased contact area, decreased contact resistance, and adequate interfacial structural stability and strength.
- Low cost.

Finding suitable materials for electrical contact layers at the cathode interface can be especially challenging, particularly in intermediate temperature (IT) (650-850°C) SOFCs where high-temperature oxidation-resistant alloys are used as interconnects. The contact layer must provide a low resistance contact between a conductive oxide cathode (e.g., lanthanum strontium manganese oxide [LSM], lanthanum nickel iron oxide [LSF], or lanthanum strontium cobalt iron oxide [LSCF]) and the interconnect (possibly coated). Therefore, there always exists a ceramic/metal interface, and possible additional ceramic/ceramic interfaces as well, all of which potentially contribute to high contact resistance and power loss. Many conductive oxides, such as those commonly used as cathodes, demonstrate high electrical conductivity and chemical compatibility, but these oxides usually exhibit low sintering activity at typical IT-SOFC stack sealing temperatures (825-950°C). On the other hand, many conductive oxides with a low sintering temperature are highly reactive and demonstrate poor compatibility and stability. Consequently, there is a pressing need for optimized, cost-effective contact materials for cathode-side applications.

Approach

During Fiscal Year 2010, primary emphasis was on the use of sintering aids and novel processing techniques to enhance sintering/bonding of candidate contact materials. Composition-microstructure-property relationships were determined for SOFC-relevant properties including sintering activity, coefficient of thermal expansion (CTE), electrical conductivity, and bond strength. Evaluation of the electrical resistance and chemical stability of simulated cathode/contact material/interconnect structures was performed using

interfacial electrical resistance tests followed by post-test analysis (scanning electron microscopy [SEM], energy dispersive spectroscopy, transmission electron microscopy, X-ray diffraction, etc). Bond strength was evaluated through tensile testing of simulated cathode/contact material/interconnect structures.

Results

$LaNi_{0.6}Fe_{0.4}O_3$ (LNF-6040) was evaluated as a potential cathode contact material, based on its high electrical conductivity and good CTE match to other SOFC components. To enhance its sintering activity, several potential sintering aids were added to the LNF. The sintering aids were introduced by milling the sintering aid powder with LNF powder. Densification results (linear sintering shrinkage as a function of temperature, as measured via constant heating rate [3°C/min] dilatometry) are shown in Figure 1. Bi_2O_3 clearly had the most influence in terms of lowering the onset of sintering. As shown in Figure 2, several levels of Bi_2O_3 addition were found to be result in similar, low values of area specific resistance (ASR) when tested in a cathode/contact material/coated interconnect configuration.

The effect of sintering aids on $La_{0.8}Sr_{0.2}MnO_3$ (LSM-20) was also investigated. Dilatometric shrinkage results for a variety of sintering aids are shown in Figure 3. As shown in Figure 4, low values of ASR were obtained in cathode/contact material/coated interconnect configuration testing. However, while both of these contact material systems (LNF and LSM) resulted in low ASR, post-test SEM analysis did not indicate significantly higher density within the sintering aid-containing contact material compared to the base material without the sintering aid. Also, similar to the base material, adhesion to at least one of the adjacent

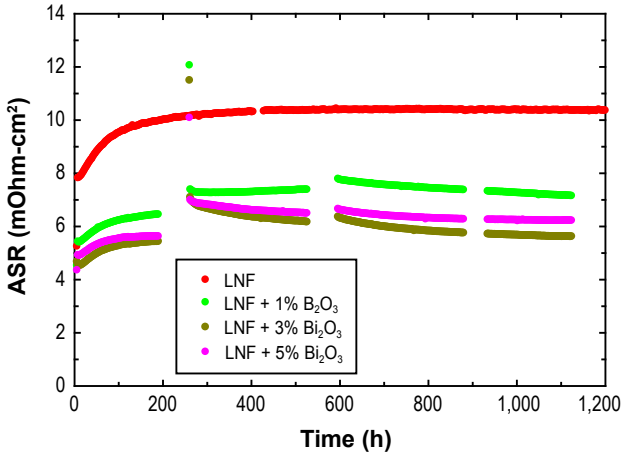

FIGURE 2. ASR Test Results for LNF with Bi_2O_3 Sintering Aid

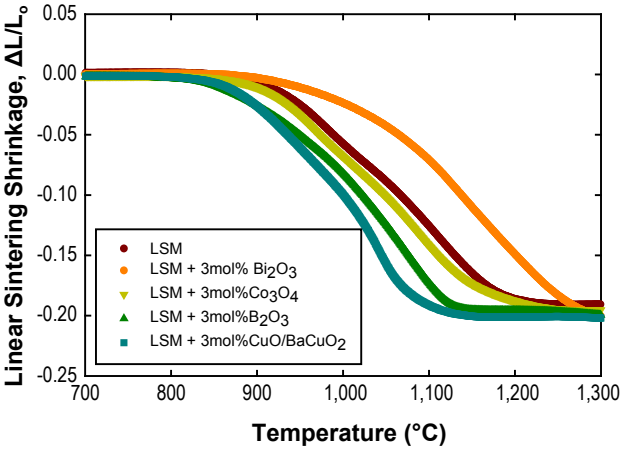

FIGURE 3. Dilatometric Sintering Shrinkage Plots for LSM with the Indicated Sintering Aids

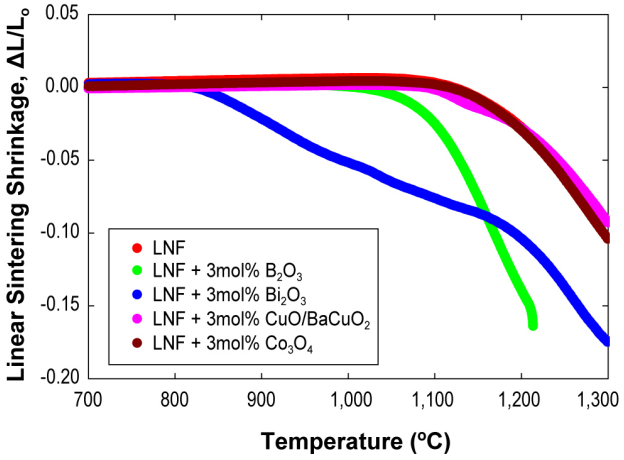

FIGURE 1. Dilatometric Sintering Shrinkage Plots for LNF with the Indicated Sintering Aids

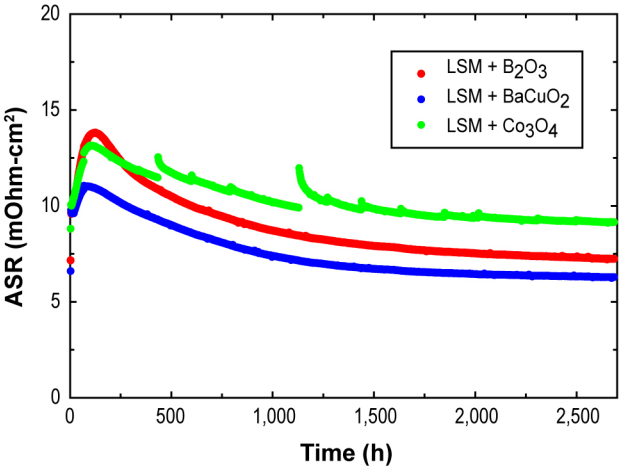

FIGURE 4. ASR Test Results for LSM with the Indicated Sintering Aids

materials (cathode or interconnect coating) was minimal, as evidenced by interfacial separation in the SEM micrographs.

A third candidate oxide, $La_{0.68}Sr_{0.4}Co_{0.2}Fe_{0.8}O_3$ (LSCF-6428) is under investigation. Dilatometric results for a variety of sintering aids (added in oxide form) are shown in Figure 5. For the temperature range of interest (850-1,000°C), CuO produced the most pronounced increase in sintering activity. It was also observed that the sintering activity showed little dependence on the amount of CuO added (within the range of 3-10 mol%). As shown in Figure 6, very low values of ASR were obtained with CuO-LSCF in cathode/contact material/coated interconnect configuration testing. Post-test SEM analysis will be performed to determine whether the LSCF contact material exhibits better strength/bonding than the LNF and LSM based materials.

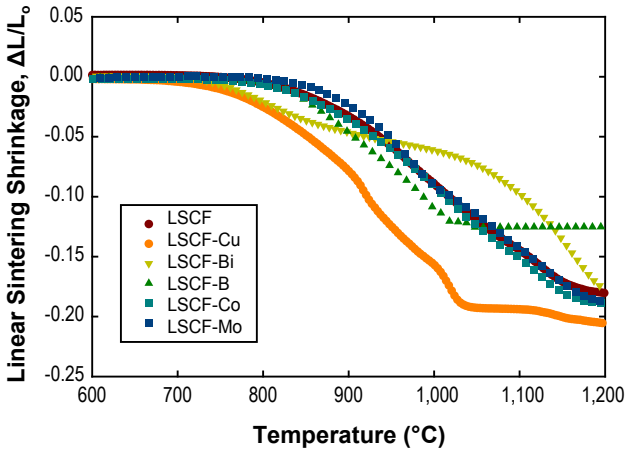

FIGURE 5. Dilatometric Sintering Shrinkage Plots for LSCF with the Indicated Sintering Aids

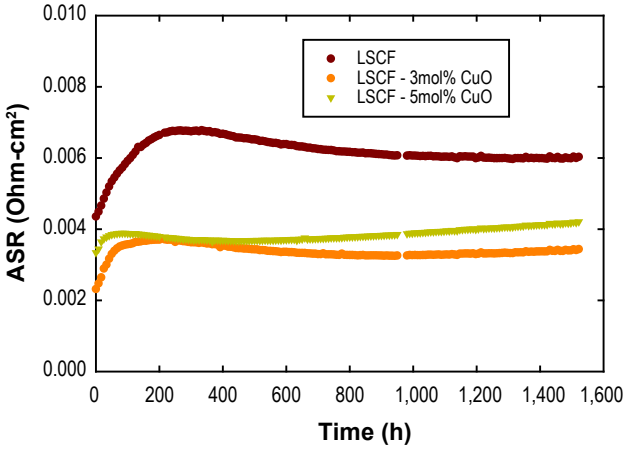

FIGURE 6. ASR Test Results for LSCF with CuO Sintering Aid

Tensile test methods have been developed and are being implemented in order to quantify the bulk and interfacial mechanical properties of cathode/contact material/interconnect structures. These tests will allow for determination of the effects of contact material composition, cathode and interconnect surface morphology, and processing variables on the mechanical properties of the cathode contact zone.

Conclusions and Future Directions

Sintering activity of LSM, LNF, and LSCF perovskite oxides was adjusted through minor additions of secondary oxide phases. Electrical tests on the modified materials indicated low, stable ASR for simulated cathode/contact material/interconnect structures, but it was not clear that intrinsic strength or bonding strength at the contact interfaces was improved.

Future research directions include evaluation of reaction sintering approaches as a means of increasing intrinsic and interfacial bond strengths, and long-term testing in realistic stack environments (using PNNL's Solid State Energy Conversion Alliance Core Technology Program stack test fixture). Reaction sintering fabrication techniques, in which multiple phase precursors are reacted to form a final single phase material, have been successfully developed for protective $(Mn,Co)_3O_4$ spinel coatings on IT-SOFC interconnects. The energy released during the formation of the final phase (enthalpy of formation) provides additional energy (besides the reduction of surface energy) for the densification process.

FY 2010 Publications/Presentations

1. G. Xia, Z. Lu, J.D. Templeton, Z.G. Yang, and J.W. Stevenson, "Recent Progress in Cathode/Interconnect Contact Materials R&D for SOFC at PNNL," 139th Annual TMS Meeting, Seattle, Washington, February 15–18, 2010.

2. G. Xia, G. Yang, Z. Lu, J. Templeton, and J.W. Stevenson, "Recent Progress in Cathode/Interconnect Contact Materials R&D for SOFCs at PNNL," 34th International Conference on Advanced Ceramics and Composites, Daytona Beach, Florida, January 24–29, 2010.

3. Y. Chou, C.A. Ellefson, R.T. Williams, J. Choi, and J.W. Stevenson, "A Study of the LSM Cathode Contact Strength with $(Mn,Co)_3O_4$ Spinel Coated Surface," 34th International Conference on Advanced Ceramics and Composites, Daytona Beach, Florida, January 24–29, 2010.

4. J.W. Stevenson, G. Xia, Z. Lu, X. Li, Z. Nie, T. Oh, and J. Templeton, "Development of Cathode Contact Materials for SOFC," 11th Annual SECA Workshop, Pittsburgh, Pennsylvania, July 28, 2010.

III.C.7 Development of Ceramic Interconnect Materials for SOFC

Kyung Joong Yoon (Primary Contact),
Jeff W. Stevenson, Olga A. Marina
Pacific Northwest National Laboratory (PNNL)
K2-44, P.O. Box 999
Richland, WA 99354
Phone: (509) 372-4255; Fax: (509) 375-2186
E-mail: kyungjoong.yoon@pnl.gov

DOE Project Manager: Briggs White
Phone: (304) 285-5437
E-mail: Briggs.White@netl.doe.gov

Contract Number: FWP40552

Start Date: October 1, 2009
End Date: September 30, 2010

FY 2010 Objective

Develop ceramic interconnect materials with improved thermal and electrical properties.

Accomplishments

- Improved electrical conductivity, sintering behavior, and dimensional stability through doping with cobalt, nickel, and copper on B-site of Ca-doped yttrium chromite.
- Matched thermal expansion coefficient of Ca-doped yttrium chromite with that of 8 mol% yttria-stabilized zirconia (YSZ) by adjusting the amount of B-site doping.
- Measured sufficiently low oxygen ion "leakage" current.
- Confirmed chemical compatibility of doped yttrium chromite with other cell components at cell processing temperature.

Introduction

Currently, acceptor-doped lanthanum chromite is the state-of-the-art ceramic interconnect material for high temperature solid oxide fuel cells (SOFCs) due to its fairly good electronic conductivity and chemical stability in both oxidizing and reducing atmospheres, and thermal compatibility with other cell components. The major challenge for acceptor-doped lanthanum chromite for SOFC interconnect applications is its inferior sintering behavior in air, which has been attributed to the development of a thin layer of Cr_2O_3 at the interparticle necks during the initial stages of sintering. In addition, lanthanum chromite is reactive with YSZ electrolyte at high temperatures, forming a highly resistive lanthanum zirconate phase ($La_2Zr_2O_7$), which further complicates the co-firing processes. Acceptor-doped yttrium chromite is considered to be one of the promising alternatives to acceptor-doped lanthanum chromite because it is more stable with respect to the formation of hydroxides in SOFC operating conditions, and the formation of impurity phases can be effectively avoided at co-firing temperatures. In addition, calcium-doped yttrium chromite exhibits higher mechanical strength than lanthanum chromite-based materials. The major drawback of yttrium chromite is considered to be its lower electrical conductivity than lanthanum chromite. The properties of yttrium chromites could possibly be improved and optimized by partial substitution of chromium with various transition metals. During Fiscal Year 2010, PNNL investigated the effect of various transition metal doping on chemical stability, sintering and thermal expansion behavior, microstructure, electronic and ionic conductivity, and chemical compatibility with other cell components to develop the optimized ceramic interconnect material.

Approach

Various compositions of Ca- and transition metal-doped yttrium chromites were synthesized using the glycine nitrate process. The precursors of metal nitrates were standardized by gravimetric analysis, and mixed according to the desired stoichiometry with glycine. The glycine nitrate mixtures were combusted, and the raw powders were calcined at 1,200°C for 2 hours in air. After calcination, phase purity was verified using X-ray diffraction (XRD) analysis (Philips 3100 XRG, Philips Analytical Inc.). The powders were annealed at 900°C in buffered hydrogen (pO_2=~10^{-17} atm) for 8 hours and examined with XRD to confirm the chemical stability in reducing atmosphere. The phase stability between 25 and 1,200°C was studied using a Philips X'Pert-MPD X-ray diffractometer with secondary beam graphite monochromated Cu Kα radiation, equipped with an Anton Paar HTK1200 high-temperature chamber. Rectangular specimens were prepared by uniaxial pressing at 35 MPa followed by isostatic pressing at 200 MPa. Sintering shrinkage was measured at temperatures up to 1,400°C in a dilatometer using 3×3×14 mm bars, and the sintered samples were used to measure thermal expansion coefficients (TECs) in the temperature range of 100-900°C in air. Electrical conductivity measurements were performed by a four-probe direct current method using 3×3×30 mm rectangular bars sintered at 1,400-1,700°C for 12 hours

to achieve the maximum density. The electrical contacts were made using Pt wires and Pt paste, and conductivity was measured in the temperature range 700-900°C while varying the oxygen partial pressure by mixing oxygen and nitrogen for oxidizing atmospheres (pO_2=0.001-0.21 atm), and carbon dioxide and forming gas (3% H_2 in N_2) for reducing atmospheres (pO_2=10^{-17}-10^{-11} atm). Oxygen permeation measurements were performed on a ~98% dense discs in the temperature range 400-900°C. The ~2.5 mm thick discs were uniaxially pressed at 35 MPa and isostatically pressed at 200 MPa followed by sintering at 1,450°C, and then mounted between two alumina tubes and sealed with gold O-rings at 900°C by pressure loading. Forming gas (3% H_2 in N_2) was fed to the permeate side, and air was supplied to the feed side, each at a constant flow rate of 30 cm^3 min^{-1}. The oxygen partial pressure of the H_2/N_2 output gas on the permeate side was measured using a zirconia-based oxygen sensor, and the oxygen flux through the disc was calculated based on the assumption that the increase in the total amount of oxygen in the permeate gas (resulting in increases in the oxygen partial pressure, ΔpO_2, and water vapor partial pressure, ΔpH_2O) is entirely due to oxygen ion permeation through the disc. The gas composition of the output gas was obtained from the H_2-H_2O equilibrium condition using the measured oxygen partial pressure. In chemical compatibility studies, doped yttrium chromite powder was mixed with NiO, 8 mol% YSZ, and Sr-doped lanthanum manganite (LSM) powders to obtain a 50:50 weight ratio, ball-milled for 24 hours and fired in air at 1,200~1,400°C for 12 hours. The resulting specimen was crushed and the powder was analyzed by XRD.

Results

In this study, calcium content on the A-site was fixed at 20% and the B-site was doped with various amounts of cobalt, nickel, or copper. The XRD analysis in Figure 1 shows the single phase formation of an orthorhombic perovskite structure up to 30% cobalt, 15% nickel, or 10% copper. The phase stability after annealing at 800°C for 12 hours in a reducing environment ($pO_2 = 4\times10^{-22}$ atm) was confirmed using XRD. XRD patterns indicated no phase change due to the exposure to reducing atmosphere. Chromite-based perovskite oxides can undergo an orthorhombic-rhombohedral phase transformation, which can cause problems during thermal cycling due to non-linear thermal expansion behavior and loss of mechanical strength. Especially, calcium-doped lanthanum chromite was reported to show a significant degradation in mechanical properties between 300 and 500°C because of the orthorhombic-rhombohedral phase transition. The phase stability of doped yttrium chromite between 25 and 1,200°C was examined using high-temperature XRD, and a single orthorhombic phase was found in

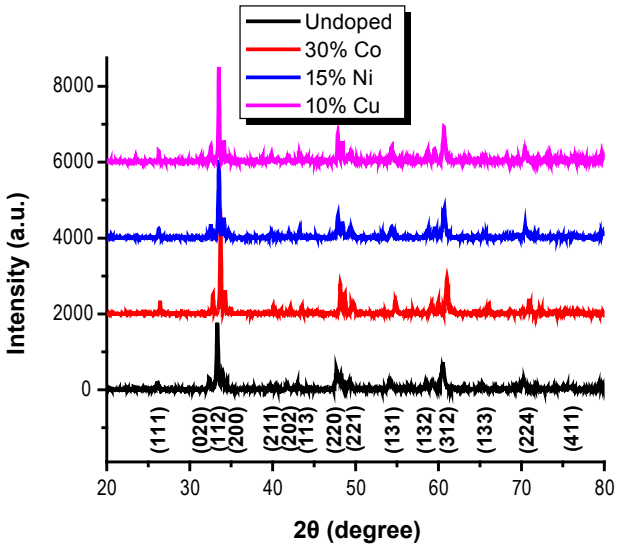

FIGURE 1. XRD Patterns of Ca- and Transition Metal-Doped Yttrium Chromite Powders after Calcinations at 1,200°C in Air for 2 Hours

the entire temperature range. Therefore, calcium- and transition metal-doped yttrium chromite is expected to show better mechanical strength during thermal cycling than calcium-doped lanthanum chromite.

Figure 2 shows the sintering behaviors of doped yttrium chromites between 600 and 1,400°C. Sinterability was enhanced with nickel and cobalt doping and further improved with the addition of a small amount of copper (2%). Without B-site doping, approximately 3% of sintering shrinkage was observed during heating up to 1,400°C, while sintering was remarkably enhanced with 10% cobalt, 3% nickel, or 2% copper on B-site showing ~20% of sintering shrinkage at 1,250°C. In Figure 2, inflection points are observed in the sintering curves between 1,200~1,300°C for some compositions. Inflections in sintering curves generally suggest a change in the sintering mechanism at that point. Pronounced curvature change in the sintering curve is usually an indication of the generation of a liquid phase, and further study is required to clarify the sintering mechanism of this system.

In TEC measurements, there was no indication of non-linear thermal expansion behavior between room temperature and 900°C, which further confirms the phase stability. TEC increased with increasing nickel and cobalt content. Measured values were 9.8×10^{-6} K^{-1} for $Y_{0.8}Ca_{0.2}CrO_{3\pm\delta}$, 10.7×10^{-6} K^{-1} for $Y_{0.8}Ca_{0.2}Cr_{0.9}Co_{0.1}O_{3\pm\delta}$, 10.2×10^{-6} K^{-1} for $Y_{0.8}Ca_{0.2}Cr_{0.9}Ni_{0.1}O_{3\pm\delta}$, and $11.7\times10^{-6}K^{-1}$ for $Y_{0.8}Ca_{0.2}Cr_{0.85}Co_{0.1}Ni_{0.03}Cu_{0.02}O_{3\pm\delta}$. It is important to match the thermal expansions of the cell components in order to minimize the thermal stress in the SOFC stack caused by thermal cycles, and it can closely match that of 8 mol% YSZ (~10.8×10^{-6} K^{-1}) with optimum amounts

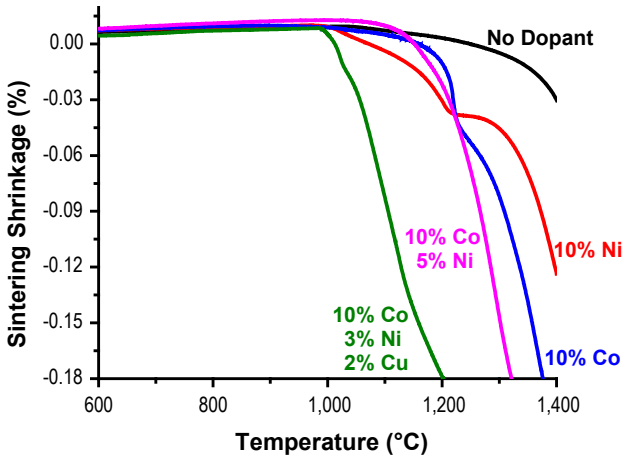

FIGURE 2. Sintering Behavior of Ca- and Transition Metal-Doped Yttrium Chromite between 600-1,400°C in Air

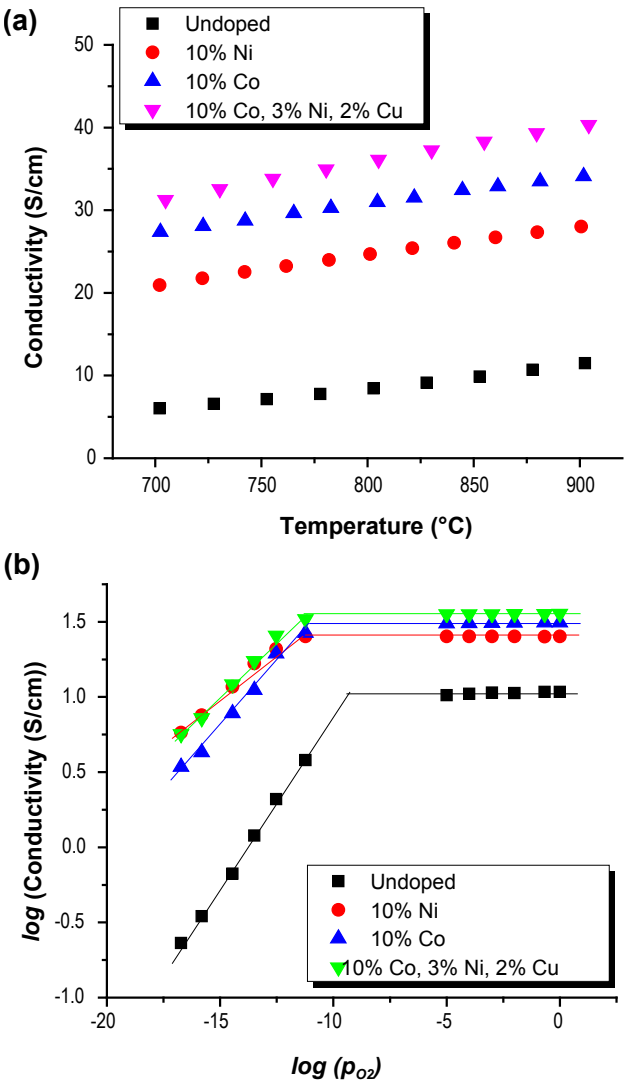

FIGURE 3. Electrical Conductivity of Ca- and Transition Metal-Doped Yttrium Chromite (a) Measured in the Temperature Range 700 to 900°C in Air, and (b) as a Function of Oxygen Partial Pressure between 10^{-17} and 1 atm at 800°C

of B-site dopants. Without B-site doping, the TEC of calcium-doped yttrium chromites linearly increases with calcium content, and requires more than 30% calcium for the TEC to match that of YSZ. However, chromite-based materials with more than 25% of calcium doping are considered to be less stable due to the secondary phase formation of calcium chromate ($CaCrO_4$). Therefore, it would be advantageous to control the TEC of yttrium chromite by adjusting the amount of B-site dopants and keep the calcium content below 25% to maintain stability.

The electrical conductivity of doped yttrium chromite was measured in the temperature range 700 to 900°C in air, as shown in Figure 3(a). The electrical conductivity increases with temperature, which indicates a thermally activated conduction mechanism. Cobalt and nickel doping on the B-site leads to a substantial increase in conductivity, and measured values were 8 S/cm for $Y_{0.8}Ca_{0.2}CrO_{3\pm\delta}$, 24 S/cm for $Y_{0.8}Ca_{0.2}Cr_{0.9}Ni_{0.1}O_{3\pm\delta}$, 30 S/cm for $Y_{0.8}Ca_{0.2}Cr_{0.9}Co_{0.1}O_{3\pm\delta}$, and 36 S/cm for $Y_{0.8}Ca_{0.2}Cr_{0.85}Co_{0.1}Ni_{0.03}Cu_{0.02}O_{3\pm\delta}$ at 800°C. Figure 3(b) shows the electrical conductivity as a function of oxygen partial pressure between 10^{-17} and 1 atm at 800°C. The conductivity remains constant throughout the high oxygen partial pressure region, and decreases with decreasing oxygen partial pressure below a critical oxygen partial pressure, which confirms the *p*-type conduction mechanism. At high oxygen partial pressure, the charge imbalance caused by the introduction of aliovalent dopants is compensated by the formation of holes. Therefore, the number of charge carriers is determined by the amount of doping, and the conductivity is independent of oxygen partial pressure. In a reducing atmosphere, loss of lattice oxygen to the atmosphere creates a doubly charged oxygen vacancy and consumes two holes, and the conductivity develops a strong dependence on oxygen partial pressure as the ionic charge compensation becomes predominant. In the low oxygen partial pressure region, the plots of $log(\sigma)$ versus $log(pO_2)$ for $Y_{0.8}Ca_{0.2}CrO_{3\pm\delta}$ and $Y_{0.8}Ca_{0.2}Cr_{0.9}Co_{0.1}O_{3\pm\delta}$ show $pO_2^{1/4}$ dependence. With Ni doping on the B-site, the electrical conductivity starts decreasing at a lower oxygen partial pressure (~10^{-12} atm) than $Y_{0.8}Ca_{0.2}CrO_{3\pm\delta}$ (~10^{-10} atm), and the slopes of the plot of $log(\sigma)$ versus $log(pO_2)$ for $Y_{0.8}Ca_{0.2}Cr_{0.9}Ni_{0.1}O_{3\pm\delta}$ and $Y_{0.8}Ca_{0.2}Cr_{0.85}Co_{0.1}Ni_{0.03}Cu_{0.02}O_{3\pm\delta}$ are smaller than 0.25, which indicates that the system does not reach the extreme reducing condition, and both ionic and electronic compensation mechanisms are operative with Ni doping. The electrical conductivity of $Y_{0.8}Ca_{0.2}Cr_{0.85}Co_{0.1}Ni_{0.03}Cu_{0.02}O_{3\pm\delta}$ at 800°C in reducing atmosphere ($pO_2 \approx 10^{-17}$ atm) was 5.6 S cm^{-1}, which is more than an order of magnitude higher than that of $Y_{0.8}Ca_{0.2}CrO_{3\pm\delta}$ (0.2 S cm^{-1}).

In a reducing environment, the lattice of chromite-based perovskite materials expands due to an increase in the ionic radius from 55.0 pm for Cr^{4+} to 61.5 pm for Cr^{3+} and/or increased coulombic repulsion between cations as the bridging oxygen ions are removed. It is important to minimize such chemical expansion because non-uniform expansion of any SOFC component, including the interconnect material, would cause internal stresses and deformation followed by a loss of electrical contact, gas seal failure, and crack formation. Doped yttrium chromite has been reported to demonstrate significantly lower chemical expansion (~40% less) in a reducing atmosphere than doped lanthanum chromite for the same acceptor dopant because the smaller size of the yttrium chromite unit cell has a "clamping" effect which hinders the reduction of Cr^{4+} to Cr^{3+} and oxygen evolution in a reducing atmosphere. The chemical expansions of doped yttrium chromite in the oxygen partial pressure range of 10^{-17}-0.21 atm at 800°C in Figure 4 shows that the expansion can be further reduced by nickel substitution while the effect of cobalt doping on the chemical expansion is insignificant. The expansions were referenced to the initial sample length at 800°C in air, and the isothermal expansion in a reducing atmosphere (pO_2=10^{-17} atm) decreased from 0.09% to 0.05% with 10% nickel substitution. The chemical expansion of $Y_{0.8}Ca_{0.2}Cr_{0.85}Co_{0.1}Ni_{0.03}Cu_{0.02}O_{3\pm\delta}$ was 0.07% under the same condition. The onset of the expansion occurred at low oxygen partial pressures and the magnitude of the expansion decreased with nickel doping. It was reported that the mechanical properties of yttrium chromite closely correlate with the chemical expansion behavior because lattice expansion caused by the oxygen vacancy formation degraded toughness and inherent grain strength, potentially leading to intragranular fracture. Therefore, nickel doping is suggested to improve the mechanical properties of yttrium chromites by improving the dimensional stability toward reduction. The isothermal expansion as well as the electrical conductivity can be directly related to the oxygen non-stoichiometry, and the comparison between Figures 3(b) and 4 indicates that there is a consistency between the trend in the electrical conductivity and that in chemical expansion behavior. The results suggest that nickel substitution on calcium-doped yttrium chromite stabilizes the defect structure and suppresses the oxygen vacancy formation in reducing environments, resulting in improved electrical performance and dimensional stability in SOFC operating conditions.

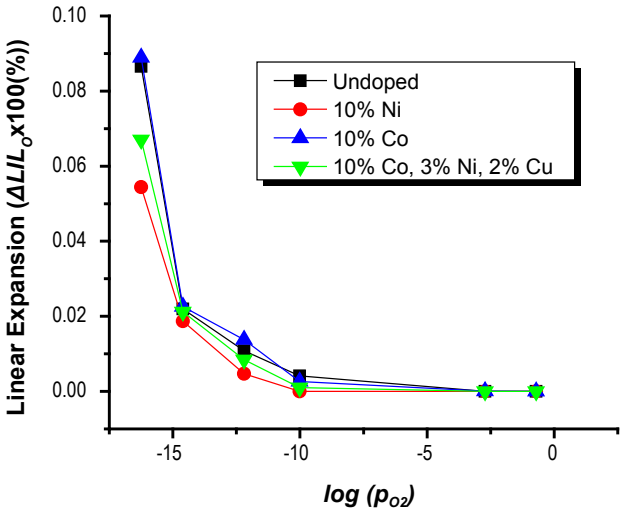

FIGURE 4. Chemical Expansions of Doped Yttrium Chromite in the Oxygen Partial Pressure Range of 10^{-17}-0.21 atm at 800°C

Electrochemical oxygen permeation through the interconnects can cause significant efficiency loss, especially for SOFC stack designs employing thin interconnects with high surface area because the SOFC interconnects are exposed to a large oxygen chemical potential gradient. Oxygen ionic leak current leads to an electrochemical consumption of fuel and reduction in the energy conversion efficiency. In this study, the SOFC operating condition was simulated by exposing one side of a dense disc to an oxidizing atmosphere (pO_2=0.21 atm) and the other side to a reducing atmosphere (pO_2=~10^{-20} atm). The oxygen permeation flux through the sample was determined by direct measurement of the oxygen partial pressure change in the reducing sweep gas. Figure 5(a) shows the oxygen fluxes through the samples containing 10% Co and 10% Ni normalized by the sample thickness (2.5 mm) as a function of temperature. Oxygen flux through the sample was negligible below 600°C, which verified the gas tightness of the system. It was assumed that the oxygen transport through the sample was diffusion-controlled because the sample was sufficiently thick to ignore the contribution of the surface exchange reaction. Therefore, the oxygen flux through the sample is determined by the ambipolar conductivity of the sample, and Figure 5(b) shows the temperature dependence of the ionic conductivity calculated by the Wagner equation. The relationship between $ln(\sigma_{ion}T)$ and $1/T$ shows a linear dependence, and the activation energies obtained from the slope were 104 kJmol^{-1} for 10% Ni and 93 kJmol^{-1} for 10% Co. The leakage current density through the interconnect due to oxygen permeation was calculated using the measured oxygen flux. The leakage current densities between the oxygen partial pressures of ~10^{-20} and 0.21 atm at 800°C for both compositions were calculated to be less than 5 mA cm^{-2} for a 20 μm thick interconnect. This value is comparable to the estimated leakage current of $La_{0.87}Sr_{0.13}Cr_{1.03}O_3$ under the similar condition (4 mA cm^{-2}), and is considered to be sufficiently low for practical use, because it has been reported that a permeation current density above 0.1 A cm^{-2} can greatly affect the cell efficiency.

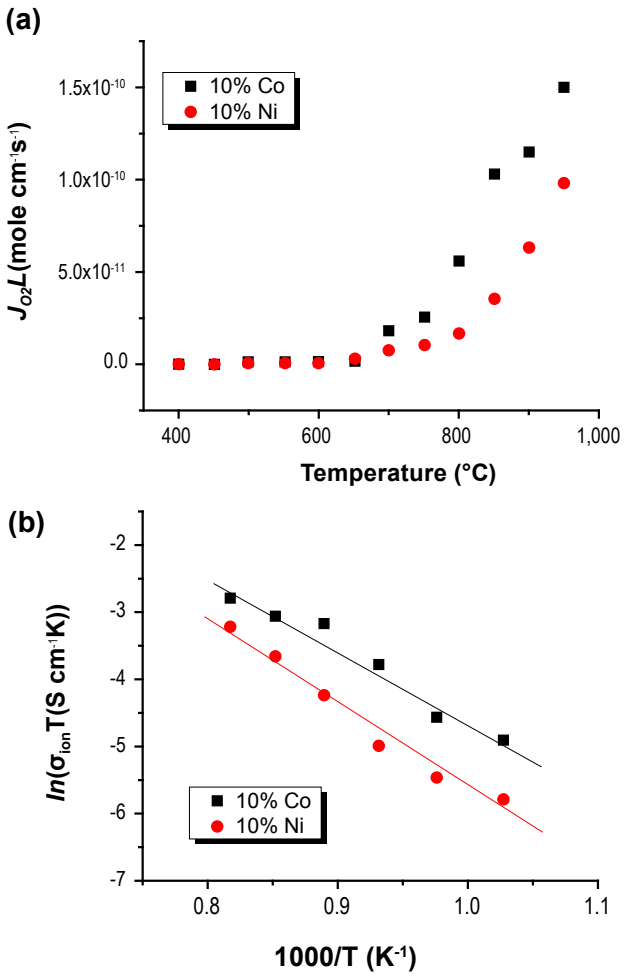

FIGURE 5. (a) Oxygen Flux Through Doped Yttrium Chromite Normalized by the Sample Thickness at Different Temperatures, and (b) Arrhenius Plot for the Ionic Conductivity Calculated from the Oxygen Flux

Chemical compatibility of the interconnect material with other cell components is a very important issue because chemical reactions between them can lead to an increase of the cell resistance and/or thermal stresses which cause subsequent cell failure. The chemical compatibility of $Y_{0.8}Ca_{0.2}Cr_{0.85}Co_{0.1}Ni_{0.03}Cu_{0.02}O_{3\pm\delta}$ with NiO, 8 mol% YSZ, and LSM was studied using XRD analysis. Figure 6 shows the XRD patterns of mixtures of 50 wt% of $Y_{0.8}Ca_{0.2}Cr_{0.85}Co_{0.1}Ni_{0.03}Cu_{0.02}O_{3\pm\delta}$ and 50 wt% of NiO fired at 1,400°C, 50 wt% of $Y_{0.8}Ca_{0.2}Cr_{0.85}Co_{0.1}Ni_{0.03}Cu_{0.02}O_{3\pm\delta}$ and 50 wt% of 8 mol% YSZ fired at 1,400°C, and 50 wt% of $Y_{0.8}Ca_{0.2}Cr_{0.85}Co_{0.1}Ni_{0.03}Cu_{0.02}O_{3\pm\delta}$ and 50 wt% of LSM fired at 1,200°C in air for 12 hours. The peaks of the composites correspond to those of the individual constituents, and no reaction products were observed. Since the conventional Ca-doped $LaCrO_3$ interconnect material can possibly react with other cell components under similar firing conditions and form a highly resistive secondary phases such as $La_2Zr_2O_7$, lanthanum

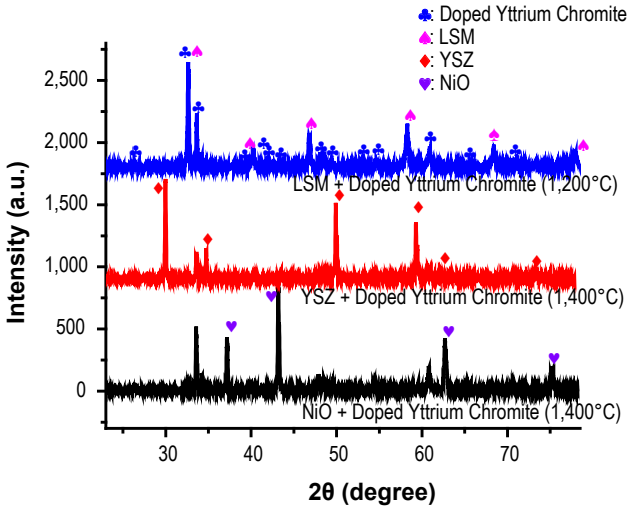

FIGURE 6. The XRD Patterns of Mixtures of 50 wt% of $Y_{0.8}Ca_{0.2}Cr_{0.85}Co_{0.1}Ni_{0.03}Cu_{0.02}O_{3\pm\delta}$ and 50 wt% of NiO Fired at 1,400°C, 50 wt% of $Y_{0.8}Ca_{0.2}Cr_{0.85}Co_{0.1}Ni_{0.03}Cu_{0.02}O_{3\pm\delta}$ and 50 wt% of 8 mol% YSZ Fired at 1,400°C, and 50 wt% of $Y_{0.8}Ca_{0.2}Cr_{0.85}Co_{0.1}Ni_{0.03}Cu_{0.02}O_{3\pm\delta}$ and 50 wt% of LSM Fired at 1,200°C in Air for 12 Hours

replacement with yttrium in the A-site is considered to be beneficial in suppressing the undesired reactions.

Conclusions and Future Directions

In this work, the effect of cobalt, nickel, and copper doping on thermal, structural, and electrical characteristics of calcium-doped yttrium chromite was studied. Yttrium chromite doped with 20% Ca on A-site and up to 30% cobalt, 15% nickel, and 10% copper on B-site showed a single phase orthorhombic perovskite structure between 25 and 1,200°C over a wide range of oxygen partial pressures. A small amount of copper doping (~2%) remarkably enhanced sinterability, and the electrical conductivity was significantly improved by cobalt and nickel doping. Nickel doping stabilizes defect structure towards reduction, resulting in improved electrical conductivity and dimensional stability in a reducing atmosphere. TEC can be adjusted and closely matched with that of 8 mol% YSZ through an optimum amount of doping, and oxygen ion leakage current due to exposure to dual atmospheres was shown to be acceptably low using oxygen permeation experiments. A chemical compatibility study between $Y_{0.8}Ca_{0.2}Cr_{0.85}Co_{0.1}Ni_{0.03}Cu_{0.02}O_{3\pm\delta}$ and other cell components indicated that the formation of detrimental secondary phase is not expected at processing temperature. Based on the results presented in this report, yttrium chromite with ~20% calcium on A-site and optimum amounts of cobalt, nickel, and/or copper on B-site is considered to be a promising candidate for interconnect applications in high temperature SOFCs. Future work will involve determination of composition-

processing-property relationships for a range of compositions for further optimization.

FY 2010 Publications/Presentations

1. K.J. Yoon, C.N. Cramer, E.C. Thomsen, C.A. Coyle, G.W. Coffey, and O.A. Marina, "Calcium- and Cobalt-Doped Yttrium Chromites as an Interconnect Material for Solid Oxide Fuel Cells," *Journal of the Electrochemical Society*, 157 (6) B856 - B861 (2010).

2. K.J. Yoon, C.N. Cramer, J.W. Stevenson, and O.A. Marina, "Improvement of Sintering, Thermal Behavior, and Electrical Properties of Calcium- and Transition Metal-Doped Yttrium Chromite," Electrochemical and Solid-State Letters, 13 (9) B101 – B105 (2010).

3. K.J. Yoon, C.N. Cramer, J.W. Stevenson, and O.A. Marina, "Advanced Ceramic Interconnect Material for Solid Oxide Fuel Cells: Electrical and Thermal Properties of Calcium- and Nickel-Doped Yttrium Chromites," *Journal of Power Sources*, 195 (2010) 7587-7593.

4. K.J. Yoon, J.W. Stevenson, and O.A. Marina, "Effect of Nickel Substitution on Defect Chemistry, Electrical Properties, and Dimensional Stability of Calcium-Doped Yttrium Chromite," Submitted (2010).

III. SECA CORE RESEARCH & DEVELOPMENT

D. Seals

III.D.1 Viscous Glass/Composite SOFC Sealants

Scott Misture (Primary Contact), James Shelby
NYS College of Ceramics at Alfred University
2 Pine St., Binns-Merrill Hall
Alfred, NY 14802
Phone: (607) 871-2438; Fax: (607) 871-2354
E-mail: misture@alfred.edu

DOE Project Manager: Joseph Stoffa
Phone: (304) 285-0285
E-mail: Joseph.Stoffa@netl.doe.gov

Contract Number: NT0005177

Start Date: October 1, 2008
End Date: September 30, 2011

FY 2010 Objectives

- Develop the new viscous glasses and glass/composite sealing materials needed to advance solid oxide fuel cell (SOFC) technologies.
- Improve our fundamental understanding of viscous sealants and their potential for meeting the desired sealing requirements and the nature and magnitude of the limitations of such materials.
- Optimize thermochemical and thermomechanical properties iteratively.

Accomplishments

- Down-selected sealants within the compositional regions of interest and tested the down-selected sealants for up to 1,500 h in contact with 8 mol% yttria-stabilized zirconia (8YSZ) and alumina.
- Expanded the compositional ranges with an additional 26 compositions to improve properties while decreasing alkali content, and tested the new sealants to 500 h thus far.
- Measured initial response of the sealants to exposure to dry H_2.
- Designed a new statistical compositional matrix that yielded 25 new compositions for testing.

Introduction

Large-scale production of SOFC laminate stacks is complicated by difficulties of sealing the stack components using a reliable method that is robust over the lifetime of the device. Candidate sealants should exhibit high coefficients of thermal expansion (CTE) values near 12 ppm/K, gas impermeability, minimal interaction with SOFC stack components for 40,000 hours between 600 and 850°C, and a maximum processing temperature of ~950°C [1]. Glass, glass-ceramic, and glass-ceramic composite seals are the best candidates for forming seals due to ease of manufacture and ability to control CTE, viscosity, and sealing temperatures with composition.

Many sealants currently being developed contain large amounts of alkaline earths such as barium or strontium which aids in seal formation below 1,000°C, yet form undesirable crystals when held at temperatures within the SOFC target operating temperature range [2-3]. Some contain undesirable amounts of boron which readily exhibits volatilization in a hydrogen atmosphere at SOFC operating temperatures [4]. The current project centers on developing new viscous oxide glass sealants that will flow at the operating temperature to reduce mechanical stresses between components but maintain the required hermeticity. By using glasses with lower alkaline earth content and reduced alkali content as well, we hope to avoid known reactivity issues. Compositions with gallium and germanium additions to silicate-based compositions appear to be promising candidates.

Approach

Initial candidate glass sealants were researched in the literature and using the SciGlass® Database to identify initial SOFC sealant compositions. These glasses were melted and screened by measuring thermophysical properties such as CTE, glass transition temperature, as well as flow and crystallization behavior at 850°C. Compositional modifications to reduce the alkali content were used to optimize properties that were undesirable in relation to the target properties.

An iterative approach of screening, down-selection and optimization is currently in a fourth iteration. Compositional regions of interest are moving towards non-alkali glass compositions with each successive iteration. Many of the new glass compositions exhibit improved properties and stability against interactions with aluminized stainless steel and 8YSZ. Heat treatments for ~1,500 h at the low (650°C) and high (850°C) operating temperatures are currently underway for new optimized compositions.

Results

Initial gallio-silicate glass compositions with 10 mol% alkali exhibited extensive crystallization and poor flow behavior for sealing at 850°C. Additions of B_2O_3 resulted in some non-alkali glasses capable of sealing at 850°C with the lowest glass transition temperature of ~650°C. Many of these compositions crystallized to a large extent after 100 h at 850°C. The fourth iteration of compositional modification of gallium based glasses is focused on low alkali silicates. These glasses exhibit Tg near 620°C and retain a high concentration of amorphous content after heat treatment. All the gallio-silicate glasses that passed the initial screenings are currently being tested at 650°C to assess the performance at lower operating temperature.

The germano-silicate glasses were studied extensively due to the highly desirable viscosity that allows sealing at ~700°C with Tg below 600°C. These glasses retain an amorphous content of ~70% even after 1,500 h at 850°C, for example as shown in Figure 1. It was discovered that ZnO containing glasses are undesirable for SOFC applications because of extensive vaporization of Zn under dry H_2 at 850°C. One of the Zn-free compositions in this series exhibited a stable interface with 8YSZ substrates after 1,500 h at 850°C. Microprobe measurements indicate limited diffusion of Zr and Y into the glass, even while the glass is very fluid. In contrast, a glass with 10% ZnO continued dissolving the 8YSZ through the long heat treatments which is undesirable when considering the target of 40,000 h lifetimes. The germano-silicate glasses without ZnO and with 10 mol% ZnO both performed well when sandwiched between 8YSZ and aluminized stainless steel. The glasses did not fracture on cooling and crystallization behavior did not notably change. The formation of a Cr-containing interfacial crystalline phase was apparent for seals in contact with aluminized stainless steel.

Some of the germano-silicate glasses were stable upon exposure to 700 torr of dry H_2 at 850°C, while others formed Ge metal colloids. Composite seals were formed by mixing powders of the sealing glass with alumina and 8YSZ. Some compositions remain highly amorphous with 8YSZ powders, while other compositions remain highly amorphous with alumina powders. Additional compositional modification of the germano-silicate glasses is underway concurrently with additional testing of the existing sealants.

A statistical compositional matrix has been created to incorporate the gallio-silicate and germano-silicate glasses to explore new compositional space. The design involves 25 new glasses and should allow optimization of desirable glass properties to formulate successful glass compositions consisting of nine components.

Conclusions and Future Directions

Within the first year of the project, we identified and modified two glass systems with promising properties. Galliosilicate glasses are candidates for glass sealants for use in SOFC operation conditions. Modified gallio-silicates exhibit more desirable viscosity behavior and are currently being optimized to reduce crystallization at 850°C. Germano-silicate glasses exhibit softening temperatures near 700°C and low glass transition temperatures. The compositions tested thus far have allowed us to build a statistical model to further improve properties in a new range of compositions.

The statistical compositional matrix should aid the formation of successful viscous sealants with glasses that contain as many as nine components. Future work will center on long-term testing of the optimized glasses.

FY 2010 Publications/Presentations

1. M.O. Naylor, J.E. Shelby, and S.T. Misture, "Viscous Sealants for Solid Oxide Fuel Cell Application," Presented at the American Ceramic Society Glass and Optical Materials Division Meeting. Corning, New York, 2010.

References

1. S.C. Singhal and K. Kendall, *High Temperature Solid Oxide Fuel Cells: Fundamentals, Design, and Applications;* pp. xvi, 405 p. Elsevier, Oxford; New York, 2003.

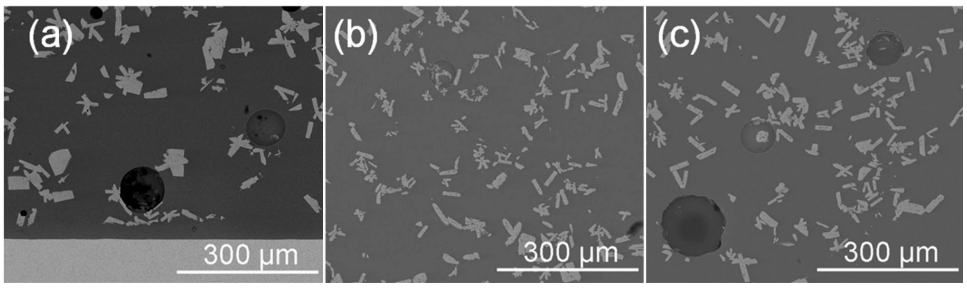

FIGURE 1. Scanning Electron Microscope Images of the Bulk Crystallization of One of the Germano-Silicate Sealants on 8YSZ Substrates Heat Treated at 850°C for 504 h (a), 1,026 h (b), and 1,530 h (c)

2. Z. Yang, J.W. Stevenson, and K.D. Meinhardt, "Chemical Interactions of Barium-Calcium-Aluminosilicate-Based Sealing Glasses with Oxidation Resistant Alloys," *Solid State Ionics,* **160** [3-4] 213-25 (2003).

3. M. Brochu, B.D. Gauntt, R. Shah, G. Miyake, and R.E. Loehman, "Comparison between Barium and Strontium-Glass Composites for Sealing Sofcs," *Journal of the European Ceramic Society,* **26** [15] 3307-13 (2006).

4. A. Flugel, M.D. Dolan, A.K. Varshneya, Y. Zheng, N. Coleman, M. Hall, D. Earl, and S.T. Misture, "Development of an Improved Devitrifiable Fuel Cell Sealing Glass," *Journal of the Electrochemical Society,* **154** [6] B601-B8 (2007).

III.D.2 Glass Composite to Coated Interconnect Seals for Long-Term Chemical Stability

Niladri Dasgupta (Primary Contact),
Bruce Butler, Erinn Sorge
Materials & Systems Research, Inc.
5395 West 700 South
Salt Lake City, UT 84104
Phone: (801) 530-4987 Ext. 17
Fax: (801) 530-4820
E-mail: ndasgupta@msrihome.com

DOE Project Manager: Joseph Stoffa
Phone: (304) 285-0285
E-mail: Joseph.Stoffa@netl.doe.gov

Contract Number: 85202

Start Date: June 30, 2008
End Date: August 13, 2010

FY 2010 Objectives

- Modify the Ba-Ca-Al-B silicate (BCAS) base-glass composition to accommodate required amounts of nano-MgO.
- Formulate glass-MgO compositions having the desired phases on crystallization.
- Optimize coating processes for doped lanthanum chromite and alumina on metallic interconnects.
- Investigate the thermal, chemical and mechanical stability of glass-MgO sealing compositions over 3,000 hours at 800°C.

Accomplishments

- Six base-glass compositions were prepared by systematically varying the BCAS glass composition.
- Two potential glass-MgO compositions (compositions 3 and 5) were selected from a list of custom formulations for long-term testing. The selection was made based on phase determination, thermal expansion behavior and wetting/flow characteristics.
- Flexible tapes of the above two compositions were successfully fabricated by tape-casting.
- The stability of crystalline phases and the coefficient of thermal expansion (CTE) was conclusively demonstrated for the above compositions after holding at 800°C for 1,000 hours. The percentage change in CTE was 1.7% for composition 3 and 4.2% for composition 5.
- A doped 8-10 µm thick lanthanum chromite coating was successfully applied to the sealing area of the metallic inteconnect by a combination of spraying and infiltration. It was established that the coating acts as an effective barrier layer against chromium migration and prevents undesirable reaction between the metallic interconnect and glass-based seal after 1,000 hours at 800°C.
- A 5-7 µm thick coating of aluminum oxide was successfully applied on metallic interconnect substrate by electrophoretic deposition.
- Excellent bonding was demonstrated at the sealing glass-8% mol yttria-stabilized zirconia (8YSZ) and sealing glass-coated Crofer interface after holding at 800°C for 500 hours.
- Preliminary short-term helium leak testing was used to confirm that compositions 3 and 5 have marginally better sealing ability than BCAS glass at 800°C.

Introduction

Solid oxide fuel cells (SOFCs) operate in the temperature range 650 to 850°C and typically function under an oxygen chemical potential gradient that develops across the electrolyte. A hermetic seal which prevents the intermingling of the cathode and anode side gases is a critical requirement for planar SOFCs as any leakage leads to reduced system performance, lower power-generation efficiency, poor fuel utilization [1,2] and accelerated degradation of the stack [2]. One popular approach for such seals is to use rigid bonded, specially tailored glass or glass ceramic compositions. The primary challenges in developing such seals are: i) maintaining proper viscosity in the glass, ii) matching the thermal expansion of the material with that of the primary cell components and stabilizing it as a function of time and temperature and iii) controlling their reactivity with metal components. An example of state-of-the-art sealing glass is a BCAS glass developed by the Pacific Northwest National Laboratory [3,4] which has a very good CTE match with other SOFC components after short-term crystallization. However, the CTE decreases significantly after ageing at 750°C for 1,000 hrs. The glass also reacts in contact with common metallic interconnects which results in the weakening of the seal joint. Recent attempts to remove these impediments by design of the glass composition [5,6] has met with limited success. Loehman [7] demonstrated that the flow, adhesion, thermal expansion and reactivity

of borate glasses can be controlled by the selective addition of oxide nanoparticles. Similar results were reported by Nielsen et al. [8] for sodium aluminosilicate glasses using nano-MgO filler.

The Phase I effort generally showed the beneficial effects of incorporating MgO in the base BCAS glass composition. While the maximum benefits in terms of long-term stability were derived in compositions with a threshold amount of MgO, most of the experiments were performed with lower levels of MgO in the glass because of its better fluidity. The first task of the current effort was therefore to make suitable modifications to the base glass composition in order to accommodate larger amounts of MgO in the glass. Therefore, the overall objective was to optimize a glass composition to which the addition of the required amount of MgO will result in a crystallized glass of the desired phase composition and with satisfactory flow and wetting characteristics. The developed compositions were to be tested up to 3,000 hours for phase development, reactivity and thermal expansion. In order to prevent reaction at the glass/metal-interconnect interface, techniques were developed for coating protective oxides like doped lanthanum chromite and aluminum oxide on metal substrates.

Approach

The overall approach for this project was to select a base-glass which is widely known to be compatible with standard SOFC materials and conditions and to eliminate some of its glaring deficiencies by i) adding suitable amounts of nano-MgO and ii) applying an appropriate protective coating to the area of the metallic interconnect in contact with the glass seal to reduce chemical reaction. It was concluded after the Phase I effort that the addition of a threshold quantity of nano-MgO ensures that a unique phase mix is formed in the crystalline glass that imparts durational stability to the thermal expansion coefficient. The approach in this phase of the investigation was to suitably modify the base-glass composition so as to ensure that the addition of the required amount of nano-MgO does not adversely affect the wettability and flowabilty of the glass. The other approach was to improve the doped lanthanum chromite protective interconnect coating developed in Phase I by modifying the spray parameters, introducing an infiltration step to reduce porosity and firing the coating in a reducing atmosphere to prevent oxide formation. A third approach was to develop an electrophoretic deposition technique for forming an aluminum oxide coating on metallic interconnects as an alternative to doped lanthanum chromite. The effectiveness of the steps taken was to be verified by phase analysis by X-ray diffraction (XRD), thermal expansion determination by dilatometry and interface integrity analysis by scanning electron microscopy (SEM) equipped with compositional analysis facility on samples heat treated at 800°C at various durations extending to 3,000 hours.

Results

Glass-MgO compositions were formulated with the following criteria in mind 1) to ensure that one or both of two phases A and B are the predominant crystalline phases in the crystallized glass; 2) the compositions flow well and wet the electrolyte and coated interconnect at the operating temperature of the SOFC stack. The first criterion was arrived at based on Phase I results which confirmed that phases A and B are stable over long durations of thermal treatment and have appropriately high thermal expansion values. Two glass-MgO compositions, 3 and 5 were found to form these crystalline phases and had suitable wetting and flow properties, and were selected for long duration evaluation. They were subjected to heating at 800°C for prolonged periods and then characterized for their thermal expansion and phase development along with the BCAS glass for comparison. Specimens were removed from the furnace every 500 hours. Figure 1 shows the XRD pattern for composition 5 after heat treatment at 800°C for 500 hours and 1,000 hours. The presence of crystalline phases A and B is clearly seen. Comparing the XRD traces for the two temperatures, it is apparent that the two phases are stable and they dominate the phase spectrum. Table 1 is a comparison of the CTE values for BCAS glass, composition 3 and composition 5 heated at 800°C for 0.5, 500 and 1,000 hours, respectively. The CTE of the BCAS glass is seen to reduce by 7.2 % when it is held for 1,000 hours at 800°C. This is one of the primary drawbacks for this glass and is known to happen because of the progressive

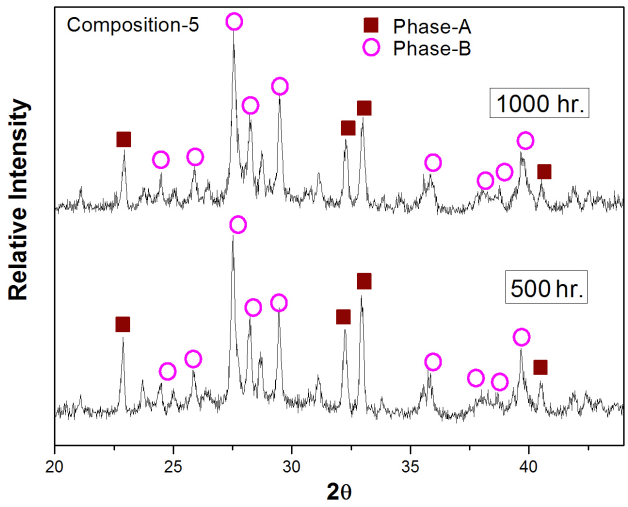

FIGURE 1. X-ray Diffraction Patterns for Glass-MgO Composition 5 Held at 800°C for 500 and 1,000 Hours

TABLE 1. A Comparison of the CTE Values of BCAS Glass, Composition 3 and Composition 5 Heated at 800°C for Different Durations

Duration	OG (BCAS Glass)	Composition 3	Composition 5
0.5 hours	11.1 x 10^{-6}/°C	11.8 x 10^{-6}/°C	11.8 x 10^{-6}/°C
500 hours	10.5 x 10^{-6}/°C	11.4 x 10^{-6}/°C	12.2 x 10^{-6}/°C
1,000 hours	10.3 x 10^{-6}/°C	11.6 x 10^{-6}/°C	12.3 x 10^{-6}/°C

crystallization of monoclinic celsian which has a CTE of 2.3 x 10^{-6}/°C. The CTE is expected to reduce further at longer durations of heat treatment. The CTE for composition 3 actually reduces marginally after 500 hours of heat treatment and then increases a little after 1,000 hours of heat treatment. The overall decrease after 1,000 hours is only 1.7% which may be essentially considered to be constant within experimental errors. For composition 5 there is actually an increase of 4.2% in the CTE after heating for 1,000 hours. Since the final value is within the desired range of (12-12.5) x 10^{-6}/°C, this may actually result in better sealing properties over longer durations of operation.

Electrophoretic deposition (EPD) of an aluminum oxide sol was used to apply a barrier coating of the oxide on a Crofer-22 foil substrate. Figure 2 shows an SEM micrograph of the inert oxide layer deposited on Crofer-22 foil by the gel electrophoretic method. The thickness of the coating is about 5 µm. The superimposed energy dispersive analysis by X-rays clearly shows the aluminum (red) and oxygen (yellow) concentration peaks corresponding to the aluminum oxide coating. XRD of the surface indicated broad peaks, suggesting that the coating is not fully crystallized to alpha-Al_2O_3 under moderate heat treatment (2 hrs at 500°C).

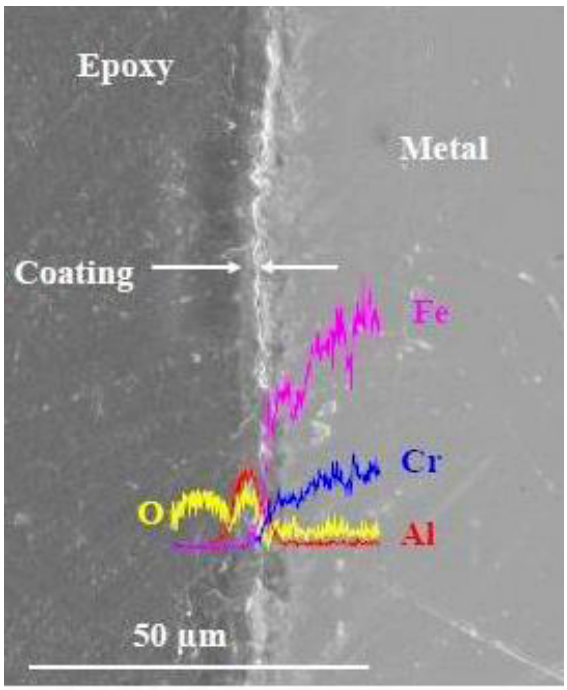

FIGURE 2. SEM Micrograph of Aluminum Oxide Layer Deposited on Crofer-22 Foil by Electrophoretic Deposition

The condition of the uncoated and coated metal/glass interface and the bonding of the glass to this interface and the 8YSZ interface is of particular interest. Figure 3 shows an SEM micrograph of a test specimen where glass-MgO composition 5 is sandwiched between an anode supported SOFC (with the 8YSZ electrolyte in contact with the glass) and a perovskite coated Crofer-22 foil heat treated at 800°C for 500 hours. At low magnification, the 8YSZ/glass as well as the glass/perovskite interface look well bonded. The magnified view of the glass/perovskite interface further indicates that the bonding is good and also that the

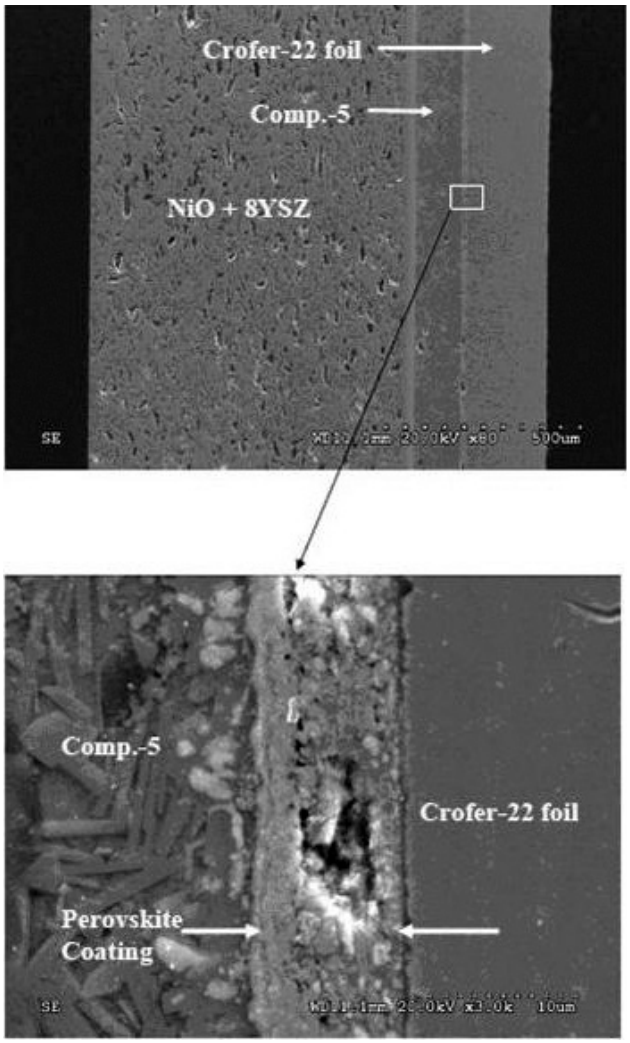

FIGURE 3. SEM Micrograph of Sectional View of a SOFC Cell _Glass-MgO_Crofer-22 (Doped $LaCrO_3$ Coated) Sandwich Heated at 800°C for 500 Hours

perovskite coating adheres well to the Crofer-22 surface, without any significant oxidation of the metal surface. Obviously, direct contact between the glass and the metal was very effectively prevented by the perovskite coating.

Conclusions and Future Directions

The results indicate that glass-MgO compositions 3 and 5 have stable crystalline phases and thermal expansion coefficients over prolonged durations at 800°C. They form clean and stable seal interfaces with the SOFC electrolyte (8 YSZ) and Crofer-22 metal foil coated with doped lanthanum chromite. Preliminary short-term leak tests on seal interfaces suggest that compositions 3 and 5 display better sealing characteristics than BCAS glass at 800°C. One may reasonably assume that the better stability of the CTE for the above glass-MgO compositions will impart superior leak resistance over longer durations when compared with BCAS glass.

The long-term tests will be completed for 3,000 hours duration. Mechanical properties will be evaluated for the two glass-MgO compositions. Elaborate leak testing will be carried out accompanied by thermal cycling. The compositions will be fabricated into gaskets and will be used in short and long stack tests having coated interconnects in order to evaluate their effectiveness under actual service conditions.

FY 2010 Publications/Presentations

1. Glass Composite to Coated Interconnect Seals for Long-Term Chemical Stability-Continuation Progress Report, Submitted to DOE, May 13, 2010.

References

1. T. Iwata and Y. Enami, "Analysis of Fuel Utilization Performance of Round Substrates, Planar Solid Oxide Fuel Cells," J. Electrochem. Soc., 145 (1998) 931.

2. J. Hartvigsen et al., Ceram. Trans., 65 (1996) 279.

3. Z. Yang, J.W. Stevenson, and K.D. Meinhardt, "Chemical Interactions of Barium-Calcium-Aluminosilicate-Based Sealing Glasses with Oxidation Resistant Alloys," Solid State Ionics, 160 (2003) 213-225.

4. K.D. Meinhardt, J.D. Vienna, T.R. Armstrong, and L.R. Pederson, "Glass-Ceramic Material and Method of Making," U.S. Patent No. 6,430,966 (2002).

5. R.K. Brow and D.S. Reis, "Designing Sealing Glasses for Solid Oxide Fuel Cells," ASM Materials Solutions Conference and Exposition, Columbus, Ohio, October 18–20, 2004.

6. R.N. Singh, "Sealing Technology for Solid Oxide Fuel Cells," Int. J. Appl. Ceram. Technol., 4 (2007) 134-144.

7. R. Loehman, "Development of High Performance Seals for Solid Oxide Fuel Cells," SECA Core Technology Program Review, Albany, New York, October 1, 2003.

8. K.A. Nielsen, M. Solvang, S.B.L. Nielsen, A.R. Dinesan, D. Beeaff and P.H. Larsen, "Glass Composite Seals for SOFC Application," J. Eur. Cer. Soc., 27 (2007) 1817-1822.

III.D.3 High-Temperature Viscous Sealing Glasses for Solid Oxide Fuel Cells

Cheol-Woon Kim
MO-SCI Corporation
4040 Hy Point North
Rolla, MO 65401
Phone: (573) 364-2338; Fax: (573) 364-9589
E-mail: ckim@mo-sci.com

DOE Project Manager: Joseph Stoffa
Phone: (304)-285-0285
E-mail: Joseph.Stoffa@netl.doe.gov

Subcontractor:
Missouri University of Science & Technology, Rolla, MO

Contract Number: SC0002491

Start Date: August 12, 2009
End Date: May 11, 2010

FY 2010 Objectives

- Develop glass compositions that exhibit stable thermomechanical properties, including viscosity, for use as seals for solid oxide fuel cells (SOFCs).
- Characterize the thermochemical reactions that occur at the seal/SOFC material interface and that involve volatilization of glass components under the operating conditions.
- Conduct leak tests and analyze the self-healing performance of candidate 'viscous glass' seals at high temperatures.

Accomplishments

- Phase I research identified new viscous glass compositions that exhibit promising sealing behavior for SOFCs. These alkali-free glasses have compositions from the BaO-B_2O_3-SiO_2 or BaO-B_2O_3-Al_2O_3-RO systems where RO represents alkaline earth oxides.
- The dilatometric softening points (T_s) and the glass transition temperatures (T_g) of the new glasses are below the lower bound of the SOFC operating temperature (650°C).
- The glasses do not crystallize in a differential scanning calorimeter (DSC) when heated at a rate of 10°C/min up to 1,000°C.
- These glasses have relatively low liquidus temperatures (T_L <800°C) and so can form viscous seals that do not substantially devitrify under SOFC operational conditions.
- Insignificant weight losses (volatility) occur from the glasses when held at 650 or 850°C in ambient air for 500 hours.
- These glasses show stability against crystallization in heat treatment tests for 500 hours in ambient air at 650 or 850°C.
- The viscosities of the new viscous sealing glasses were measured and 'self-healing' behavior, which is expected around a viscosity of 10^5 Pa-s, occurs in the temperature range of 725-750°C.
- Isokom temperatures for Glass 4 and 28 do not change after heat treatments for 500 hours at 650-850°C, indicating that these glasses are thermo-rheologically stable at SOFC operational temperatures.
- The new glasses wet both aluminized SS441 and NiO/YSZ substrates.
- The new glass seal survived 75 thermal cycles (room temperature to 750°C) over the course of >2,000 hours without failure of the hermetic seal at constant pressure of 0.5 psid.

Introduction

SOFCs require hermetic seals to prevent mixing of the fuel and oxidant streams within the cell stack and to seal the stack to the system manifold. Reliable sealing materials must (a) possess viscosity-temperature characteristics that are compatible with sealing requirements and that allow for stress relaxation and 'self-healing' without excessive flow, under pressure, that would compromise seal integrity; (b) be chemically compatible with SOFC components and so not alter the long-term thermo-mechanical stability of the seal by forming deleterious interfacial reaction products; (c) avoid the significant volatilization of glass constituents under the SOFC operational conditions that has been associated with other sealing materials, and so alter the viscous properties of the seal or the performance of the SOFC; and (d) possess dilatometric properties that are compatible with other SOFC components, and these properties must be stable over the course of the SOFC lifetime.

Approach

The use of 'viscous glass' seals provides one means of reducing the risk that thermal stresses will result in catastrophic failures, and may provide a means for the seal to 'recover' if cracks do form. Some

of the early work at Argonne National Laboratory identified compositions in the alkaline earth lanthanum aluminoborate system that remained viscous ($\eta > 10^3$ Pa-s) under operational conditions [1]. More recently, Singh [2] has proposed that SOFC seals be made from stable (non-crystallizing) glass compositions with glass transition temperatures (T_g) well below the SOFC operational temperature. On heating the seal above T_g, the rigid glass becomes viscous and any flaws within the seal (or at a seal interface) will 'heal' because of viscous flow. In addition to providing a means to 'repair' cracks in a seal caused by thermal stresses, the use of a viscous seal could also reduce the magnitude of those stresses compared with a rigid glass seal with the same thermal expansion characteristics since the stresses will be relieved at temperatures above T_g in the 'viscous glass' seal, reducing the effective ΔT over which thermal stresses develop.

The Phase I research successfully identified and tested several glass compositions that could be used as viscous seals for SOFCs. The glasses possess desirable viscosity characteristics and relatively low liquidus temperatures, exhibit no significant weight losses from the molten state when held in air, and survive thermal cycles over 2,000 hours.

Results

Phase I research performed at MO-SCI Corporation and the Missouri University of Science & Technology identified new viscous glass compositions that exhibit promising sealing behavior for SOFCs. These alkali-free glasses have compositions from the BaO-B_2O_3-SiO_2 or BaO-B_2O_3-Al_2O_3-RO systems, where RO represents alkaline earth oxides, and were melted in aluminosilicate crucibles in ambient air for 2-3 hours, typically at 1,100-1,150°C. The dilatometric softening points (T_s) and the glass transition temperatures (T_g) of the new glasses are below the lower bound of the SOFC operating temperature (650°C), see Table 1. The glasses do not crystallize in a DSC when heated at a rate of 10°C/min up to 1,000ºC (Figure 1). The glasses have coefficients of thermal expansion that are lower ($7\text{-}9\times10^{-6}$/°C) than those ($10\text{-}12.5\times10^{-6}$/°C) for typical SOFC components. These glasses have relatively low liquidus temperatures ($T_L < 800$°C) and so can form viscous seals that do not substantially devitrify under SOFC operational conditions. Table 2 shows that insignificant weight losses (volatility) occur from the glasses when held at 650 or 850°C in ambient air for 500 hours. These glasses also show stability against crystallization in heat treatment tests for 500 hours in ambient air at 650 or 850°C (Figure 2).

The viscosities of the new viscous sealing glasses (Glass 2, 4, and 28) were measured using a high temperature rotational viscometer for the viscosity range $1\text{-}10^4$ Pa-s and using the parallel plate technique

TABLE 1. Viscous Sealing Glasses Developed in Phase I and Their Thermal Properties

	Glass 2	Glass 4	Glass 28
Melting Temperature (°C)	1,150	1,150	1,100
T_g(°C) Measured from CTE Curve	619	599	581
Dilatometric T_s(°C)	650	632	615
CTE (40-500°C)	8.19×10^{-6}	7.32×10^{-6}	7.48×10^{-6}

CTE = Coefficient of thermal expansion

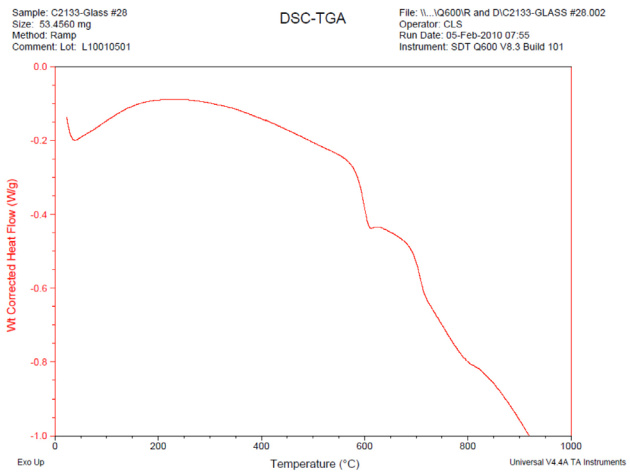

FIGURE 1. DSC analysis of the viscous sealing glasses (e.g., Glass #28); there are no obvious crystallization exotherms up to 1000°C.

TABLE 2. Five Hundred Hour Weight Loss (Volatility) Results for the Viscous Sealing Glasses Held in Air at the SOFC Operational Temperature Displaying Insignificant Weight Loss

	650°C / 500 hrs	850°C / 500 hrs
	% Weight Loss	
Glass #2	0.04	0.07
Glass #4	0.03	0.08
Glass #28	0.04	0.09

[3] for the viscosity range $10^5\text{-}10^{11}$ Pa-s. The viscosity-temperature data were analyzed by the new relationship recently proposed by Corning [4]. This new model (equation (1)) is based on fitting parameters that have physical meaning and is reported to provide more accurate predictions for extrapolated η-T curves than do other models:

$$\log \eta\,(T) = \log \eta_\infty - (12 - \log \eta_\infty)\frac{T_g}{T}\exp\left[\left(\frac{m}{12-\log \eta_\infty} - 1\right)\left(\frac{T_g}{T} - 1\right)\right] \quad (1)$$

where T is temperature in K, η is the viscosity in Pa·s, η_∞ is the high-temperature limit of viscosity, T_g is the glass transition temperature defined as the temperature at which the glass viscosity is 10^{12} Pa·s, and m is fragility

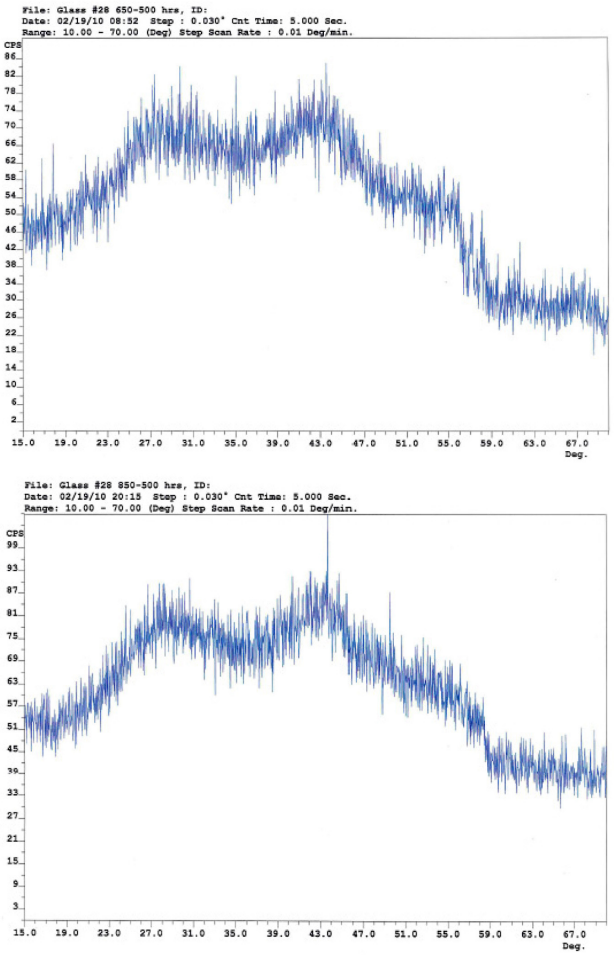

FIGURE 2. X-ray diffraction (XRD) patterns for the viscous sealing glass #28 held at the SOFC operational temperature exhibiting insignificant crystallization. Top: Held at 650°C for 500 hours. Bottom: Held at 850°C for 500 hours.

parameter. Table 3 lists the Corning viscosity model fitting parameters for each glass and the respective glass transition temperatures from dilatometry experiments. The very good agreement between the T_g predicted by the viscosity model and that measured by dilatometry is worth noting. Table 3 gives the isokom temperatures at log η (Pa-s) = 6.6. This is the Littleton softening point for soda lime silicate glasses and is sometimes described as the temperature at which a glass flows under its own weight. Singh [5] reports 'self-healing' behavior for an SOFC sealing glass with a viscosity of 10^5 Pa-s at 800ºC. From Table 3, similar behavior would be expected for the MO-SCI glasses (Glass 2, 4, and 28) at temperatures in the range of 725-750°C. This temperature range is below the liquidus temperatures for the glasses, and so experiments were conducted to determine if heat treatments in this temperature range affect the glass viscosities. Glass #2, #4, and #28 were heat treated at 650°C, 750°C, and 850°C for 500 hours to determine if the viscosities of the glasses change with time at SOFC operational temperatures. The parallel plate viscosity test was used to characterize viscosities of the heat-treated cylindrical glasses. Tables 4 and 5 list the isokom temperature at a viscosity of $10^{6.6}$ and 10^8 Pa-s, respectively for Glass 2, 4, and 28. The isokom temperatures of Glass #2 have increased by 15 to 20°C after the heat treatment at 850°C for 500 hours, compared to the 'as cast' glass and the samples heat-treated at 650 and 750°C for 500 hours. This increase may be due to the limited crystallization of the glass after the heat treatment. Isokom temperatures for Glass 4 and 28 do not differ after heat-treatments from those as-cast samples, indicating that these glasses are thermo-rheologically stable at SOFC operational temperatures.

Multi-layer sandwich seal samples were made using Glass #2, #4, or #28 and heat treated in ambient air at 800°C for 500 hours. The SOFC materials, aluminized SS441 interconnect alloys and NiO-YSZ bilayers, were supplied by Pacific Northwest National Laboratory. Figure 3 shows a scanning electron microscopy (SEM) image of the Glass #28/SS441 interface. The glassy layer in the micrograph is 40-50 µm thick. The glass clearly wets the metal - there are no voids at the glass/metal interface. Embedded in the glass are small particles and dendritic crystals. EDS (energy dispersive spectroscopy) analyses indicate that the dendritic crystals (spot a) could be a Ba-aluminosilicate phase (boron could not be detected with this EDS system). No silica was added to the base composition of Glass #28. It is possible that the silica detected in these crystals originated from the aluminosilicate crucible used to prepare the glass. The glassy region (spot b) near the interface with the SS441 substrate appears to be alumina-rich, relative to other components. The alumina-layer that forms on the SS441 alloy surface

TABLE 3. Corning Viscosity Model Fitting and Isokom Temperatures for Glass 2, 4, and 28

Glass	Fitting Parameters				Isokom T(°C), Log(η/Pa•s)=				
	Log η_∞	*m*	T_g(°C) fit	T_g(°C) CTE	11	9	6.6	4	2
Glass 2	-3.5	68.7	620	619	643	668	708	779	887
Glass 4	-3.5	65.2	594	585	615	643	685	762	868
Glass 28	-3.5	66.1	589	575	610	637	680	753	859

TABLE 4. Isokom Temperatures (°C) at Viscosity of $10^{6.6}$ Pa-s for Glass 2, 4, and 28 after Heat Treatment for 500 Hours

Glass	As-cast	650°C 500 hrs	750°C 500 hrs	850°C 500 hrs
Glass 2	713 ± 18	714 ± 4	715	733
Glass 4	689 ± 13	692 ± 2	not measured	689 ± 1
Glass 28	682 ± 11	684 ± 3	681	683

TABLE 5. Isokom Temperatures (°C) at Viscosity of 10^{8} Pa-s for Glass 2, 4, and 28 after Heat Treatment for 500 Hours

Glass	As-cast	650°C 500 hrs	750°C 500 hrs	850°C 500 hrs
Glass 2	679 ± 23	685 ± 1	679	700
Glass 4	660 ± 13	661 ± 1	not measured	656 ± 3
Glass 28	653 ± 13	653 ± 5	647	649

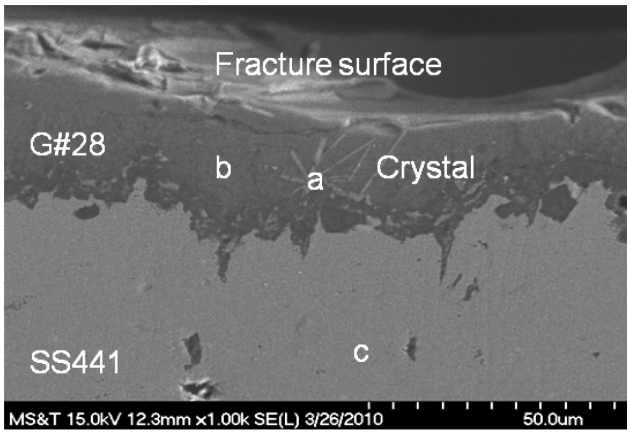

FIGURE 3. SEM image of the glass/metal interface in a sandwich seal sample of Glass #28 held in ambient air at 800°C for 500 hours.

when exposed to oxidizing conditions appears to dissolve into the glass, altering the glass composition across the sealing region.

Coupon sealing was conducted by sandwiching Glass #2, #4, or #28 paste between an aluminized SS441 disc (3.2 cm diameter and 1 mm thick) with a central hole (1 cm diameter) and an anode-supported (NiO-YSZ) thin electrolyte (YSZ) bilayer disc (2.1 cm diameter). The seal sandwich assembly was heated at 10°C/min to 850°C and held for 8 hours to remove binder and bubbles and to form the desired seal. The assembly was then transferred to a pressurized tube furnace and exposed to thermal cycles between room temperature and 750°C in ambient air at a differential pressure of 0.5 psi (26 torr). Glass #28 seal survived 75 thermal cycles over the course of >2,000 hours without failure of the hermetic seal, as summarized in Figure 4.

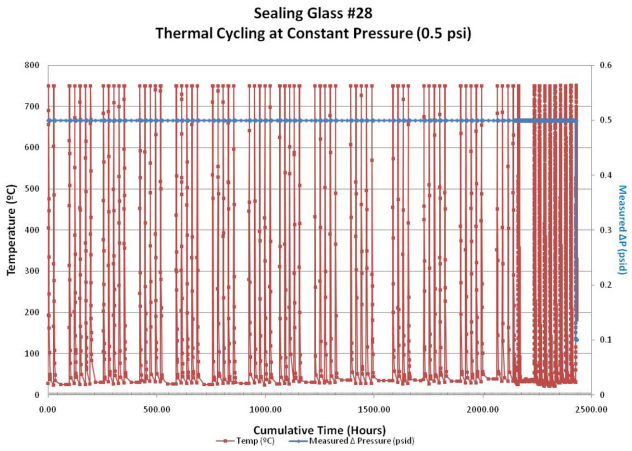

FIGURE 4. Demonstration of a hermetic seal made from SS441/Glass #28/NiO-YSZ bilayer. This seal survived 75 thermal cycles (room temperature to 750°C) in ambient air at a differential pressure of 0.5 psi (26 torr) for more than 2,000 hours.

Conclusions and Future Directions

Phase I research (DE-SC0002491) successfully identified and tested several glass compositions that could be used as viscous seals for SOFCs within the project budget and specified time period. The glasses possess desirable viscosity characteristics - that is, they have softening points in the temperature range expected for SOFC operations (650-850°C), and so cracks that might form in the glass on thermal cycling should be closed upon reheating through a 'viscous healing' mechanism. The new glasses have relatively low liquidus temperatures (< 800°C) and so do not exhibit significant crystallization when held at SOFC operational temperatures. Excessive crystallization will change the viscosity behavior and may jeopardize the viscous healing characteristics of the seal. In addition, the new glasses wet both aluminized SS441 and NiO/YSZ substrates, forming hermetic seals that have survived, in one case, 75 thermal cycles between room temperature and 750°C.

The glasses developed in Phase I exhibit no significant weight losses from the molten state when held in ambient air, but nothing is known about the thermochemical stability of the melts in wet environments. Simple seals have been prepared for the Phase I hermeticity tests and for the initial materials compatibility tests, but no attempts have been made to develop practical sealing materials from these new glasses. The glasses have thermal expansion coefficients ($7\text{-}9\times10^{-6}$/°C) that are lower than those for typical SOFC components and this could lead to the development of deleterious tensile stresses in the glass (or ceramic layer) when the seal is cooled to room temperature.

A molten seal is potentially more reactive with SOFC components than is a rigid, glass-ceramic seal. Reaction products are more rapidly transported from an interface with a molten material, promoting further reactions that could modify the properties of the seal or the SOFC component. Dissolution of oxides from SOFC components could modify the liquidus temperature or the viscosity of the molten glass, affecting the long-term thermo-mechanical stability of the seal.

FY 2010 Publications/Presentations

1. Cheol-Woon Kim, Cindy L. Schwartz, Joe Szabo, Kevin Barr, Ted E. Day, Richard K. Brow, and Zhongzhi Tang, "High-Temperature Viscous Sealing Glasses for Solid Oxide Fuel Cells," 11th Annual SECA Workshop, Pittsburgh, Pennsylvania, July 27–29, 2010.

References

1. I. Bloom and K.L. Ley (1995), "Compliant Sealants for Solid Oxide Fuel Cells and Other Ceramics," U.S. Patent 5,453,331, issued September 26, 1995; K.L. Ley, M. Krumpelt, R. Kumar, J.H. Meiser, and I. Bloom, "Glass-Ceramic Sealants for Solid Oxide Fuel Cells: Part I. Physical Properties," *J. Mat. Res.,* 11, 1489-1493.

2. R. Singh (2004), "High Temperature Seals for Solid Oxide Fuel Cells," Proceedings of SSM International Conference, Columbus, Ohio, October 18–20.

3. ASTM–American Society for Testing and Materials (2007), "Standard Test Method for Measurement of Viscosity of Glass Between 10^4 Pa·s and 10^8 Pa·s by Viscous Compression of a Solid Right Cylinder [Metric]," ASTM C 1351M – 96 (Reapproved 2007), ASTM International, West Conshohocken, Pennsylvania.

4. J.C. Mauro, et al. (2009), *PNAS,* 106 (47), 19780-4.

5. R. Singh (2008), "Innovative Seals for Solid Oxide Fuel Cells (SOFC)," Final Progress Report, DOE Award DE-FC26–04NT42227.

III.D.4 Innovative Self-Healing Seals for Solid Oxide Fuel Cells (SOFCs)

Professor Raj N. Singh
University of Cincinnati
Department of Chemical and Materials Engineering
Cincinnati, OH 45221-0012
Phone: (513) 556-5172; Fax: (513) 556-3773
E-mail: Raj.Singh@uc.edu

DOE Project Manager: Joseph Stoffa
Phone: (304) 285-0285
E-mail: Joseph.Stoffa@netl.doe.gov

Contract Number: FE0001390

Start Date: October 1, 2009
End Date: March 31, 2011

FY 2010 Objectives

- Develop self-healing glass composites containing fillers as seals for SOFCs.
- Select appropriate filler materials suitable for making glass-composites.
- Characterize stability of the self-healing composites glasses.

Accomplishments

- Self-healing glass composites were fabricated using alumina, magnesia, and zirconia fillers. Thermomechanical behaviors of the glass-composites were measured between 25-800°C.
- Preliminary results suggested that alumina and magnesia fillers might not be suitable for making useful glass-composites. However, the zirconia filler appeared promising.
- These results provide great promise towards meeting Solid State Energy Conversion Alliance (SECA) seals goals for SOFCs.

Introduction

A functioning SOFC requires seals that prevent electrode leakage and internal gas manifold leakage if internal gas manifolds are utilized. The seals must prevent the mixing of fuel and oxidant streams as well as prevent reactant escape to the surrounding environment. The seal material must be electrically isolating and be mechanically and chemically stable in contact with interfacing cell components in humid dual reducing and oxidizing conditions. Of particular importance is the ability to seal between metallic and ceramic components with differing coefficients of thermal expansion (CTE), and do so while exposed to temperature transients over a range from room temperature up to SOFC operating temperature (≈800°C). This project is developing innovative sealing concepts for both short- and long-term functionality of SOFCs, addressing the aforementioned issues.

Approach

A novel in situ self-healing sealing glass concept was advanced in the previous funding cycle of the SECA program. Glasses were fabricated and characterized to advance this concept and seal testing was done to demonstrate in situ self-repair capability of the glass seals. Seal tests displayed excellent seal performance including in situ self-repair of cracked/leaking seals. The self-healing concept requires glasses with low viscosity at the SOFC operating temperature of 800°C but this requirement may lead to excessive flow of the glass under load in areas forming the seal. To address this challenge, a modification to glass properties such as creep via addition of particulate fillers is proposed and being pursued in the current project. The underlying idea is that non-reactive ceramic particulate filler is expected to form glass-ceramic composite and increase the glass transition/glass softening temperatures and seal viscosity thereby increasing the creep resistance of the glass-composite seals under load. In addition, the incorporation of an appropriate filler can affect the coefficient of thermal expansion of the glass-ceramic thereby providing additional flexibility for developing sealing glasses with the optimum expansion mismatch among materials forming the seal thereby reducing mismatch stresses and improving seal reliability. This report summarizes progress made towards advancing this concept.

Results

A filler phase is required for sealing glasses as a part of this activity. The filler phase should be oxidation resistant at 800°C, strong, and have expansion behavior close to the sealing glass. Three types of fillers, i.e., Al_2O_3, yttria-stabilized zirconia (YSZ), and MgO, were selected for the initial screening effort for the project because these ceramics have expansion close to or higher than the glass and are electrical insulators. Al_2O_3 and YSZ have expansion slightly smaller than the glass and MgO has higher value than the glass. Samples of glass composites containing 30% by weight of Al_2O_3, YSZ, or MgO powders were fabricated

using tape casting, lamination, and sintering to make dense glass-ceramic composites. The composites were then characterized for CTE between 25-800°C and crystallization by X-ray diffraction.

Density of the composite and CTE of glass-30% Al_2O_3 composite were measured after processing. Density of the composite was measured after processing. Glass-30% Al_2O_3 composite was 98% dense, glass-30% MgO composite was 99.5% dense, and glass-30% YSZ composite was 99% dense.

Thermophysical (expansion) behavior of each of these composites is being measured to determine the role of particulate addition on select properties. The data for the glass and glass-30% Al_2O_3 composite are shown in Figure 1. It shows that the CTE decreased because of the addition of 30% alumina. In addition, the glass transition and softening temperatures increased for the composite. Both of these responses are as expected because the CTE of alumina is lower than the glass and addition of particulate to the glass is expected to increase viscosity and consequently the glass transition and softening temperatures. Thermophysical behaviors of the glass and glass-30% MgO composite are measured and shown in Figure 2. It shows that the CTE increased as a result of the MgO addition, which is expected behavior because the CTE of MgO is higher than the glass. However, the glass transition and softening behaviors show a significant change. In fact the data in Figure 2 show two humps in the CTE behavior; one around 600°C and another around 850°C. This behavior is a result of the reaction of MgO with glass and the X-ray diffraction data indicated formation of the enstatite ($MgSiO_3$) and fosterite (Mg_2SiO_4) phases. A significant amount of these crystalline phases are not desirable for self-healing behavior. As a result we do not plan further studies on glass-MgO composite in this project. The results for glass-30% YSZ composite are shown in Figure 3. The CTE of the glass-YSZ composite is lower than the glass, as expected, and the glass transition and softening temperatures increased with YSZ addition. The glass softening temperature for the glass-30% YSZ composite is ~700°C, which is significantly higher than the value of 570°C for the glass alone. In addition there was no crystallization of glass, which is desirable for self-healing behavior.

These results suggest that the best filler phase for further studies is YSZ because MgO reacts with the glass and Al_2O_3 produces a low CTE. Preliminary data from the glass-alumina composite also suggest reaction of alumina with the glass leading to formation of aluminum silicate. From these results YSZ is down-selected for further studies. Composites of glass-YSZ containing 10, 20, and 30% YSZ are being prepared for further characterization and CTE measurements. These composites will be placed on a YSZ plate and annealed in air and in moist fuel environments for up to 1,000 hours at 800°C to demonstrate stability. In addition, crystallization behavior upon annealing will be evaluated by X-ray diffraction along with the CTE data. These results will be reported in future for developing seals to meet the SECA goals for SOFCs.

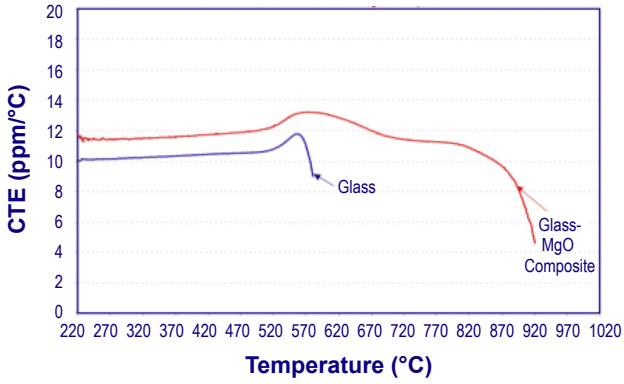

FIGURE 2. Coefficient of Thermal Expansion of a Glass and Glass-30% MgO Composite in the as Fabricated State

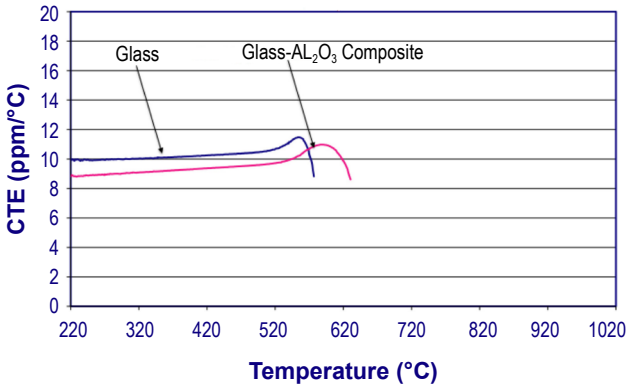

FIGURE 1. Coefficient of Thermal Expansion of a Glass and Glass-30% Al_2O_3 Composite in the as Fabricated State

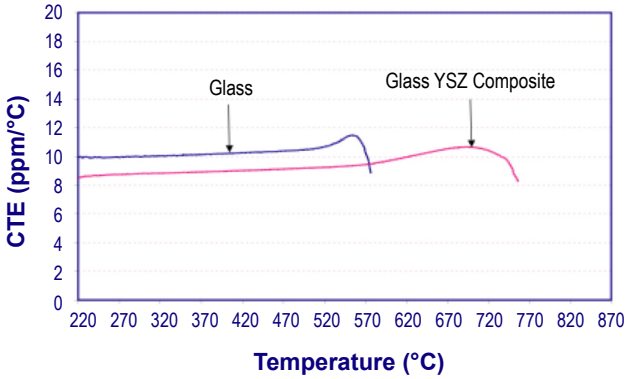

FIGURE 3. Coefficient of Thermal Expansion of a Glass and Glass-30% YSZ Composite in the as Fabricated State

Conclusions and Future Directions

- The self-healing glasses with and without fillers were fabricated and studied. Composites with alumina and magnesia fillers showed reactivity with the glass and inappropriate CTE for making seals for SOFCs.
- Glass-composites with zirconia filler showed good expansion matching and stability against reaction during processing. This system is down-selected for further testing.
- Plans are to further pursue long-term stability of the self-healing glass composites at 800°C in SOFC testing environment.

FY 2010 Publications/Presentations

1. Program Quarterly Reports (October 2009-March 2010).
2. Phase-I Annual Report (July 2010).

III. SECA CORE RESEARCH & DEVELOPMENT

E. Cross-Cutting Materials and Manufacturing

III.E.1 Manufacturing Analysis of SOFC Interconnect Coating Processes

Matthew M. Seabaugh (Primary Contact), Michael J. Day, Michael G. Beachy, Sergio Ibanez, Robin Kimbrell, and Scott L. Swartz
NexTech Materials, Ltd.
404 Enterprise Drive
Lewis Center, OH 43035
Phone: (614) 842-6606; Fax: (614) 842-6607
E-mail: m.seabaugh@nextechmaterials.com

DOE Project Manager: Briggs White
Phone: (304) 285-5437
E-mail: Briggs.White@netl.doe.gov

Contract Number: SC0001208

Start Date: August 12, 2009
End Date: May 11, 2010

FY 2010 Objectives

- Determine cost of manufacturing 625 cm^2 active area interconnect (IC) coatings that are dense, low resistance and durable for 40,000-hour operation.
- Determine whether electroplating or reduced atmosphere processing of spinel precursors represents the most cost effective and technically feasible route to interconnect coatings.
- Determine whether $(Mn,Co)_3O_4$-rare earth element composite coatings can be densified through modifications to materials precursors, process and annealing conditions.
- Identify a path to achieve a total interconnect cost <$7 each at 400 MW volume.
- Cost model powder deposition and electroplating processes at 400 MW/year scale.
- Assess the cost of powder deposition by aerosol spray deposition (ASD) and electrophoretic deposition (EPD) and down-select process.
- Achieve area specific resistance (ASR) <25 mΩ-cm^2 after 1,000 hours at 800°C in air.
- Achieve >90% dense composite coating via ASD or electrophoretic deposition.

Accomplishments

For solid oxide fuel cells (SOFCs) to become economically viable, low-cost and effective protective coatings must be developed for the metallic system and stack components. In Phase I of this effort, NexTech Materials demonstrated that:

- ASD of ceramic coatings on metal SOFC ICs provides impressive corrosion resistance and compelling process economics.
- ASD coatings offer stable ASR as low as 4-7 mΩ-cm^2 after 1,000 hours of operation at 800°C in wet air, with repeated thermal cycling.
- The cost of ASD coating large (625 cm^2) ICs is projected to be less than $2/part, within Solid State Energy Conversion Alliance (SECA) targets.

These concrete examples of the promise of ASD bode well for its commercialization. Phase I results have already led to ongoing evaluations with SOFC integrators.

Introduction

For DOE SECA teams, metallic ICs provide a path to meet the aggressive cost targets for SOFC stacks. Metal ICs can be produced by high volume production processes, as publicized by Delphi, Versa Power and General Electric. These developers have stated that their stack development hinges on the development of metal ICs with stability for >40,000 hours. To date, ferritic alloy corrosion has been too fast to meet SECA lifetime performance targets. However, formulations such as Crofer 22APU and ALSS441-HP have longer lifetimes and more stable corrosion products. Further, a number of oxide coating techniques have been proposed, with varying degrees of technical validation.

From our analysis, spinel, perovskite and composite oxide coatings can adequately protect metallic ICs. The main obstacle to implementation is the high cost of depositing thin, high density, defect-free coatings over large parts. The IC cost has been recently targeted at ~20% of stack cost, (~$5-7 for a 625 cm^2 active area IC), inclusive of manufacturing and materials costs. Current coating technologies cost tens to hundreds of dollars per part, making clear the need for a manufacturing assessment and optimization of IC coating.

Approach

Phase I was designed to assess economic viability of five competing coating technologies. The costs of capital equipment, materials, operating and associated activities were estimated based on prior experience, vendor quotes and estimates of throughput. Using these analyses, a down-selection was performed. The most cost effective coating processes were performance-evaluated, proving ASD to be a high value method to apply low resistance

TABLE 1. Comparison of Prevalent IC Coating Technologies *(Estimated at 400 MW/year production)*

Metric/Technique	Plasma	IBED	Electroplating	EPD	ASD
Coating Density	Intermed.	Excellent	High	Intermed.	*Intermed.*
Coating Thickness (μm)	>20	<5	1-10	5-20	*5-20*
Composition Flexibility	Good	Low	Limited	Excellent	*Excellent*
Capital Cost ($)	3.1M	3.7M	2.5M	2.2M	*1.5M*
Operating Cost ($)	1.1M	1.2M	1.6M	1.5M	*1.5M*
Coating Cost per Interconnect ($/part)	2.61	2.03	1.95	1.93	1.65
Coating Cost per Kilowatt ($/kW)	10.44	8.12	7.80	7.72	6.60

protective coatings to steel. Experiments informed by these analyses also identified opportunities for cost reduction.

Results

The Phase I cost modeling compared plasma spray deposition, electroplating, EPD, ASD and ion beam enhanced deposition (IBED). After a review of the relevant literature the process variables (Table 1) were tabulated and the process costs estimated using standard engineering methods (Figure 1).

$Mn_{1.5}Co_{1.5}O_{1.5}$ (MCO) powder was produced in 25 kg lots using mixed oxide routes at 1,000°C, resulting in a two-phase spinel mixture and surface area of >15 m^2/g. To demonstrate ASD effectiveness in protecting AL441HP substrates, MCO and MCO/CeO_2 composite (5% CeO_2 on metals basis) coatings were deposited and tested. Powder suspensions were deposited as 10 µm thick coatings on 240 µm thick coupons by aerosol spray. Coatings were applied symmetrically and sintered in forming gas (5% H_2 in N_2, 3% H_2O) 1,000°C for 4 hours, followed by oxidation (1,000°C for 2 hours). Top down and cross section of MCO coated samples were prepared and analyzed by scanning electron microscopy (Figure 2).

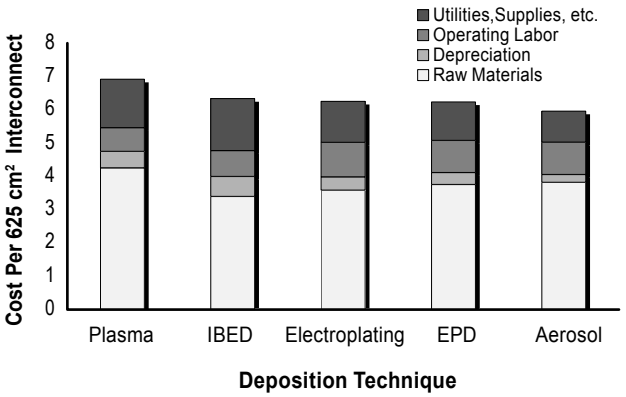

FIGURE 1. Cost Comparison of IC Coating Technologies (400 MW/year production)

MCO coated substrates were provided with lanthanum strontium manganite (LSM) conductive pads for electrical contact and dried. Platinum leads and mesh were bonded to the pads with LSM ink and cured at 1,000°C for one hour in air. The samples were electrically tested under an atmosphere of humidified air, at 800°C and 0.5 A/cm^2 for 500 hours (Figure 3). Based on these initial stability tests and subsequent thermal cycling and long-term endurance tests of over 1,000 hours, these coatings have been demonstrated to be robust, low resistance and stable over harsh operating conditions.

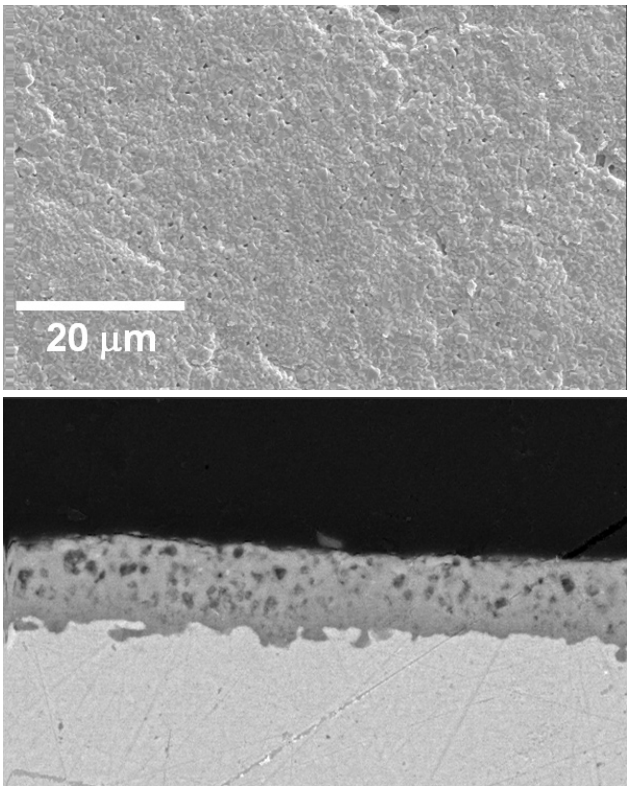

FIGURE 2. Top-Down and Cross-Sectional Image of ASD Coating of MCO on AL441-HP

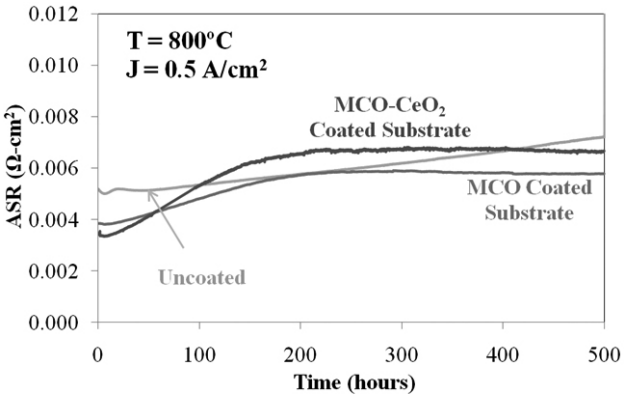

FIGURE 3. ASR of ASD Coatings of Different Materials on AL441-HP Alloy (tested at J = 0.5 A/cm^2, 800°C in humidified air)

Conclusions and Future Directions

The Phase I cost analysis showed that while the metal cost dominates the IC price, coating technologies can meet SECA cost targets. Evaluation of five coating processes showed that ASD was the most cost effective and test of ASD coatings demonstrated good uniformity, high density, and electrochemical stability over time and through thermal cycles. Further cost reduction opportunities were identified: reducing the coating thickness, using lower cost materials, using faster firing cycles, and by removing the oxidation step.

In the proposed Phase II effort, NexTech will develop and production validate cost models for ASD coating at various production volumes. Experimental work will continue to reinforce the value proposition of the coating approach for SECA teams. Specific areas of interest will be demonstrating process flexibility for a range of IC manufacturing routes, stack assembly protocols. Large scale (component size >160 cm^2) manufacturing trials and performance testing as single components and in short stacks will complement the manufacturing cost assessment.

Special Recognitions & Awards/Patents Issued

1. Pending Patent on Interconnect Coating Compositions.

FY 2010 Publications/Presentations

1. M. Seabaugh, et al., "Oxide Coatings for Metallic SOFC Interconnects," 7th International Symposium on Solid Oxide Fuel Cells (SOFC): Materials, Science, and Technology, Daytona, Florida, January 25, 2010.

2. M. Seabaugh, et al., "Next-Generation Ceramic Coatings for Stainless Steel SOFC Interconnects," Proceedings of the 9th European Solid Oxide Fuel Cell Forum, Lucerne, Switzerland, June 29 – July 2, 2010.

III.E.2 Reliability and Durability of Materials and Components for Solid Oxide Fuel Cells

Edgar Lara-Curzio (Primary Contact), Amit Shyam, Rosa Trejo, Dana McClurg, Joseph Muth and Melanie Kirkham

Other Contributors: Larry Walker, Beth Armstrong, Joe Giaquinto, David Glasgow, Michael Miller, and Jane Howe

Oak Ridge National Laboratory
1 Bethel Valley Rd.
Oak Ridge, TN 37831-6062
Phone: (865) 574-1749; Fax: (865) 574-4913
E-mail: laracurzioe@ornl.gov

DOE Project Manager: Patcharin Burke
Phone: (412) 386-7378
E-mail: Patcharin.Burke@netl.doe.gov

Contract Number: FEAA066

Start Date: October 1, 2009
End Date: September 30, 2010

FY 2010 Objectives

- Support the Solid State Energy Conversional Alliance (SECA) industrial teams in the development of reliable and durable solid oxide fuel cells (SOFCs).
- Identify and utilize test techniques to determine the physical and mechanical properties of SOFC component materials and the interfaces between them.
- Characterize candidate glasses developed for SOFC seal applications.
- Develop economically-viable sealing materials and concepts.

Accomplishments

- Successfully characterized the microstructural changes in candidate glass seals after 5,000 hours aging at 800°C in air and steam+H_2+N_2 environments.
- Determined the uncertainty associated with the quantitative chemical compositional analysis of glass seal materials.
- Supported the SECA industrial teams in the characterization of potential glass seal materials.

Introduction

A critical aspect of SOFC design is sealing. Intermediate temperature operation (650°C to 850°C) planar SOFC stacks consist of alternating fuel and air chambers, which are sealed from each other and connected to fuel and air delivery manifolds, respectively. These seals are subject to a demanding set of performance criteria in an extreme operating environment. In a majority of cases, the seals must have a low electrical conductivity, be chemically and mechanically stable in a high temperature reactive environment (moist reducing and/or oxidizing conditions), and demonstrate chemical compatibility with the cell and interconnect materials. Volatile constituents (e.g., alkalis, etc.) in the seal should be minimized to less than 1% weight loss over 40,000 hours. Fuel leakage should be less than one percent averaged over the seal area. The seal material must be capable of a service life of more than 40,000 hours and dozens of thermal cycles for stationary systems. In addition to the above factors, manufacturability and cost of the sealing material are critical factors in meeting the SECA program goals.

During the Fiscal Year 2010 reporting period, Oak Ridge National Laboratory (ORNL) continued investigating the effects of long-term environmental exposure to SOFC-relevant environments on the microstructure and properties of a barium alkali silicate glass[1]. Changes in the microstructure and thermophysical properties of glass test specimens that were exposed to air and steam+N_2+H_2 for 5,000 hours at 800°C were characterized. To assess the effect of environmental exposure on microstructure, including the precipitation of crystalline phases, the formation of pores and their evolution, X-ray diffraction, scanning electron microscopy (SEM) and transmission electron microscopy (TEM) were performed on the exposed test specimens.

During the reporting period, a methodology was established to determine the uncertainty associated with various quantitative techniques for chemical compositional analysis of glass seal materials. Various advanced engineering sealing concepts were also developed during the reporting period.

Finally, in the reporting period, another task involving the effect of SOFC relevant environment on the physical and mechanical properties of 8 mol% yttria-

[1] SCN-1, SEM-COM Company, Toledo, OH 43623

stabilized zirconia (8YSZ) was initiated. Results from this investigation will be reported in the final quarter of FY 2010.

Approach

The exposure tests for glass in air and a gas mixture of steam+H_2+N_2 were performed in a box furnace and a tubular furnace with environmental control capability, respectively. The glass exposure tests were performed at a temperature of 800°C and interrupted periodically for removal and characterization of test specimens. Two different substrates, namely alumina and 8YSZ, were used for the glass exposure tests. A suite of microstructural characterization techniques including SEM, high resolution TEM (HRTEM) and X-ray diffraction were applied to determine the phase stability, chemical reactions between the substrate and the glass and evolution of the crystalline phase(s) with exposure time. The viscosity of the bulk glass was determined by thermomechanical analysis (TMA). The wetting behavior of the glass on the two different substrates exposed to two different environments for different periods of exposure time was determined by contact angle measurements on ceramographically prepared cross-section of glass specimens. Image analysis[2] was performed to measure the contact angles and advanced image analysis techniques were developed to quantify the pore size distributions.

A design of experiments approach was implemented to determine the uncertainty in quantitative chemical compositional analysis of SCN glass using the following techniques: inductively coupled plasma-mass spectroscopy, inductively coupled plasma-atomic emission spectroscopy, neutron activation analysis and atom probe analysis. Advanced statistical techniques were applied to determine the precision and uncertainty associated with the above techniques for SCN glass (see footnote 1) and an additional National Institute of Standards and Technology standard reference material with a chemical composition similar to that of the glass seal material.

Results

The viscosity of glasses is an important parameter to predict their behavior if they were to be used in sealing applications. The viscosity of the sintered glass was determined by TMA. Two different viscosity measurement methodologies were employed: 1) the first methodology consisted of determining the viscosity under isothermal conditions at three different constant compressive loads[3]; and 2) the second methodology consisted of determining the glass viscosity at a constant heating rate (5 or 10°C/minute) under a constant compressive load. A summary of the viscosity values obtained at temperatures between 650 and 800°C is presented in Figure 1. The two methodologies give comparable values of viscosity with the values at the faster heating rate (10°C/minute – constant load of 0.25 N) diverging at higher temperatures. It is likely that these discrepancies arise due to differences between the test temperature and the actual temperature of the test specimen at the faster heating rate. The viscosity value decreases from ~10^7 Pa.s to ~10^5 Pa.s between 650 and 800°C, respectively. An Arrhenius-type activation energy of viscosity of ~280 kJ/mol was calculated in the temperature range of 650-800°C.

The wetting behavior of the glass seal material in the temperature range of interest is another important property that determines seal performance. The change in the contact angle of sintered SCN glass beads with 8YSZ and alumina substrates up to a 5,000-hr exposure at 800°C in air and steam+H_2+N_2 is presented in Figure 2. The contact angle measurements were performed at room temperature from the analysis of the cross-section of *different* test specimens that had been exposed for various periods of time. These results indicate that the value of the contact angle decreases with increasing time of exposure. It can be observed in Figure 2 that the steam+H_2+N_2 environment provides marginally better wetting conditions, which is likely due to changes in surface tension of the glass in steam-rich environments. Also these results suggest that under similar exposure conditions, the glass wets the 8YSZ substrate better than when compared to the alumina substrate. The above results are consistent with high temperature in situ observation of contact angles reported in the annual report of FY 2009.

Phase stability in air and wet-reducing environments is an important parameter that determines the long-term

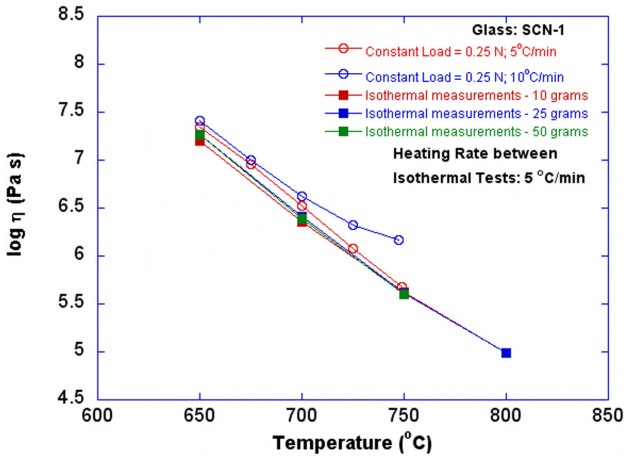

FIGURE 1. Viscosity of SCN Glass as a Function of Temperature Determined with the Isothermal and Constant Heating Rate Methodologies

[2] ImageJ®, National Institute of Health
[3] ASTM standard test method C1351

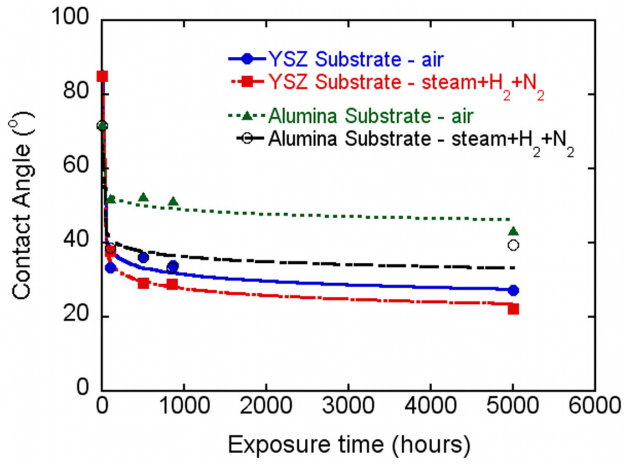

FIGURE 2. Effect of time of exposure on the contact angle of SCN glass in two different environments. Results for 8YSZ and alumina substrates are presented.

functional performance of viscous seals for SOFCs. During the reporting period, the kinetics of precipitation of crystalline phases and the microstructural stability of SCN glass on alumina and 8YSZ substrates were characterized. Figure 3 incorporates scanning electron micrographs of the cross-sections of SCN glass test specimens on 8YSZ substrates at the end of 5,000 hrs of exposure to air and steam+H_2+N_2 at 800°C. Cracks that appear to initiate in the glass are seen to propagate into the zirconia substrate, suggesting that the glass beads remain well bonded to the 8YSZ substrate. The precipitation of crystalline phases is evident in these micrographs. Complementary studies using X-ray diffraction revealed the nature of these phases, which consist of $KAlSi_3O_8$ and BaO. Qualitatively these results are similar to those obtained from the analysis of test specimens that had been exposed for 850 hrs and reported in FY 2009. Figure 4 shows scanning electron micrographs of the cross-sections of SCN glass test specimens on alumina substrates at the end of 5,000 hrs of exposure to air and steam+H_2+N_2 at 800°C. The presence of BaO precipitates close to the surface of the glass bead under the steam-rich exposure conditions is evident. In addition to the uniformly distributed $KAlSi_3O_8$ phase similar to the observations for the zirconia substrate, there was an additional layer of these precipitates close to the glass-substrate interface. The presence of this layer is likely due to the diffusion of aluminum ions from the substrate. HRTEM results confirmed the presence of this reaction layer at the interface of the alumina substrate and the glass bead under this exposure condition. These results indicate that the evaluated glass seal material is stable under SOFC operating conditions.

A qualitative analysis of the micrographs of test specimens in Figures 3 and 4 reveals the presence of a distribution of pores including large pores. Pore size distribution of specimens with various exposure conditions was quantified using image analysis techniques that were developed for the same purpose.

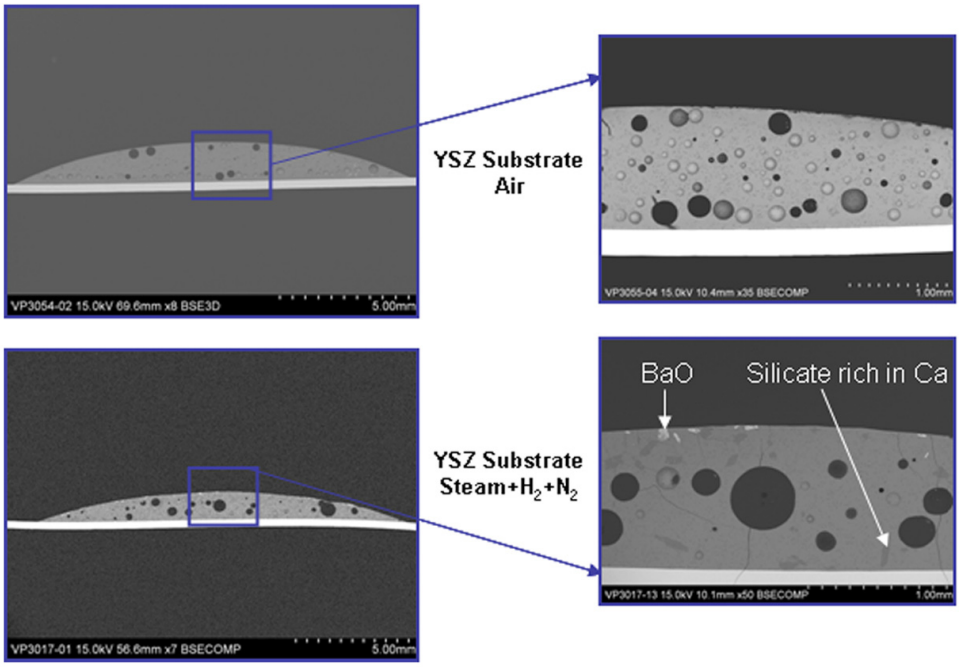

FIGURE 3. Cross-section SEM images of SCN glass specimens exposed for 5,000 hours on an 8YSZ substrate. The top and bottom images are for specimens exposed in air and steam+H_2+N_2 environments, respectively.

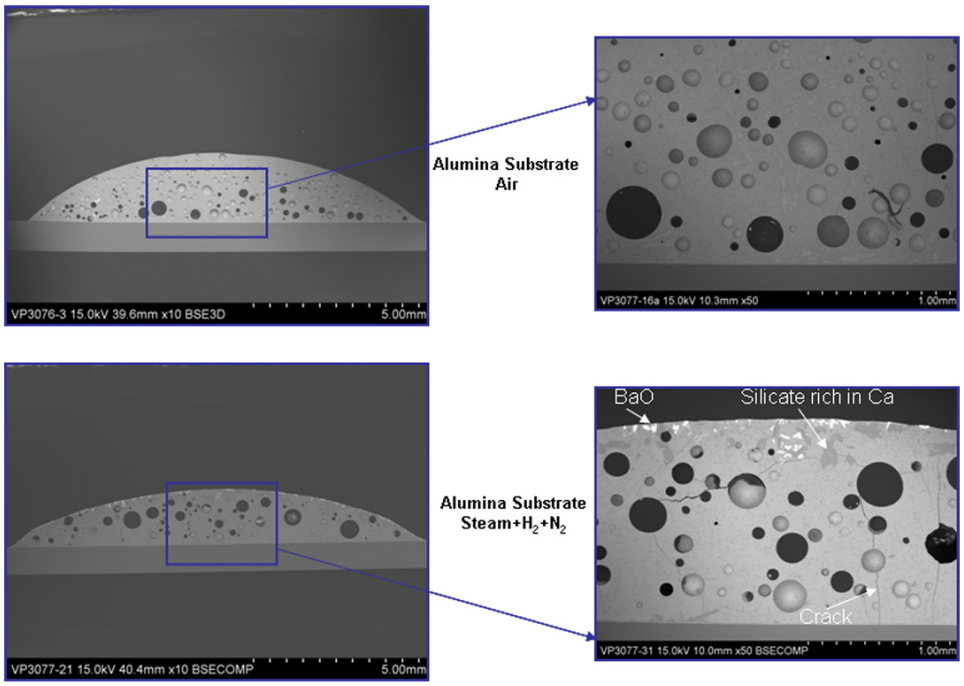

FIGURE 4. Cross-section SEM images of SCN glass specimens exposed for 5,000 hours on an alumina substrate. The top and bottom images are for specimens exposed in air and steam+H_2+N_2 environments, respectively.

As an example, the change in the pore size distribution with time of exposure in steam+H_2+N_2 environment for the glass bead on 8YSZ substrate is shown in Figure 5. The images and the graph in Figure 5 indicate that the pores coarsen with time.

Conclusions and Future Directions

Characterization of the cross-section of glass specimens that have been exposed to air and water vapor+H_2+N_2 environments at elevated temperature for up to 5,000 hrs have been completed. The results

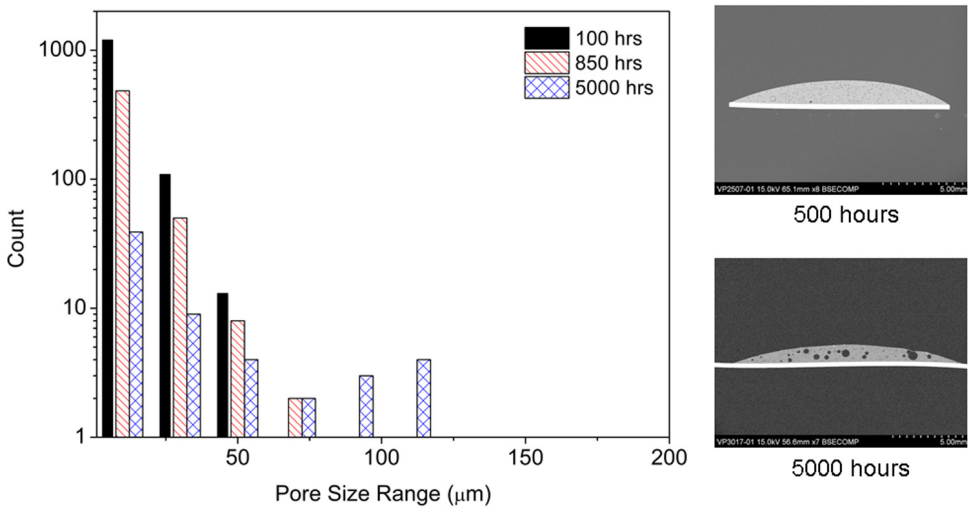

FIGURE 5. Pore-Size Distribution Changes for a Glass Bead on an 8YSZ Substrate under Steam+H_2+N_2 Exposure

of microstructural characterization and phase stability of the viscous glass seal material indicate that SCN glass is stable under SOFC operating conditions for long exposure times. Sets of test specimens continue being exposed to both air and water vapor+H_2+N_2 with the objective of achieving exposure times in excess of 20,000 hrs. The wetting and viscous flow behavior of SCNP glass under SOFC conditions was also determined in the reporting period.

The results from the characterization of these test specimens with 20,000+ hrs of exposure will be reported in the future. An interim report on the comparison of techniques to determine the chemical composition of glasses has been submitted to the National Energy Technology Laboratory. Future work includes the study and reporting of the effect of long-term SOFC environment exposure on the thermophysical and mechanical properties of 8YSZ substrates. Additional environmental exposures that create a pO_2 gradient in the 8YSZ specimen, e.g. air on one side and steam+H_2+N_2 on the other side of the test specimen are being planned. Development of viscous glass sealing system concepts remain a priority along with support to the SECA industrial teams. Test methodologies that quantify the adhesion strength of oxides that form on interconnects under SOFC operation conditions are also being investigated.

FY 2010 Publications/Presentations

1. Quarterly Report for 1st quarter Fiscal Year 2010, January 2010.

2. Quarterly Report for 2nd quarter Fiscal Year 2010, April 2010.

III.E.3 Development and Implementation of Stack Fixture Tests

Yeong-Shyung "Matt" Chou (Primary Contact), Edwin C. Thomsen, Jung-Pyung Choi, William E. Voldrich, Jeff Bonnett, and Jeff Stevenson
Pacific Northwest National Laboratory (PNNL)
K2-44, P.O. Box 999
Richland, WA 99354
Phone: (509) 375-2527; Fax: (509) 375-2186
E-mail: yeong-shyung.chou@pnl.gov

DOE Project Manager: Briggs White
Phone: (304) 285-5437
E-mail: Briggs.White@netl.doe.gov

Contract Number: FWP40552

Start Date: October 1, 2009
End Date: September 30, 2010

FY 2010 Objectives

- Develop a solid oxide fuel cell (SOFC) stack test fixture for use by PNNL and other Solid State Energy Conversion Alliance (SECA) Core Technology Program (CTP) participants.
- Implement the test fixture in evaluation/validation of new materials, processes, and design concepts developed by PNNL and other SECA CTP participants.

Accomplishments

- Developed second generation stack test fixture on behalf of SECA CTP.
- Successfully demonstrated second generation stack test fixture for single cell and three-cell short stack testing with candidate SOFC materials.

Introduction

PNNL and other SECA CTP participants use a wide range of materials characterization techniques (X-ray diffraction [XRD], scanning electron microscopy, energy dispersive spectroscopy [EDS], transmission electron microscopy, X-ray photoelectron spectroscopy [XPS], thermal gravimetric analysis, differential scanning calorimetry, particle size analysis, electrical conductivity, single and dual atmosphere oxidation, etc.) and sub-stack multiple component tests (e.g., "button" cell testing, area specific resistance testing of interconnect/cathode/cathode structures, and leak testing of cell/seal/interconnect structures) to evaluate the performance of newly developed materials, fabrication processes, and design concepts. In recent years, PNNL has developed and implemented a "stack" test fixture intended to evaluate/validate cell and stack component performance under realistic stack conditions. It is anticipated that results from these stack fixture tests will help to bridge the gap between typical CTP tests and the full-scale cells and stacks under development by the SECA industrial teams, and thus facilitate technology transfer from the CTP to those teams.

Approach

In Fiscal Year 2010, a second generation stack test fixture was designed and implemented. Similar to the first generation fixture, the single-cell second generation design is also based on a 50 mm x 50 mm cell, and includes a cell frame component as well as anode and cathode plates simulating the anode and cathode faces of an SOFC interconnect. The most significant difference between the first and second generation designs lies in the fact that the second generation design can be extended to multiple cell stack tests. As a result, the test fixture allows for the simultaneous testing of multiple cells, cell-to-frame and stack perimeter seals, anode and cathode contact materials, and interconnects (including coatings). Unlike the single-cell test setup, in the multiple cell tests the interconnects are exposed to a realistic dual atmosphere environment. Most components of the stack test fixture (cell frames, anode and cathode plates, contact pastes, and seals) are fabricated at PNNL. Stack fixtures are assembled and then sealed and tested in test stands consisting of a furnace, heat exchangers, gas handling system with mass flow controllers, and electrical characterization units. Electrochemical performance of the cells is measured under isothermal and/or thermal cyclic conditions. Once the tests complete, the fixtures are dis-assembled and their components are analyzed by appropriate characterization techniques such as optical and electron microscopy, EDS, XRD, XPS, etc. Results from the tests are compared to results obtained from testing of individual components and sub-stack structures to assess intrinsic stability and inter-component reactions, and their effects on performance under stack operating conditions.

Results

The development of the test fixture design has been iterative in nature, with results from the previous fixture tests helping to identify further design changes required

to optimize fixture performance. The second generation fixture (Gen2), which incorporates modifications to the previous first generation, version 3 design (Gen1. V3), is based on AISI 441 sheet stock of 0.133" and 0.040" thickness. Computer-aided design drawings of a three-cell short stack of the Gen2 fixture are shown in Figure 1. For a typical three-cell stack test, three cell frames and four interconnect plates are used along with eight mica-based seals separating each cell frame and interconnect plate. The stack is then compressed between two heat exchangers (air and fuel). Figure 2 shows photographs of the parts used in a three-cell stack test with voltage leads and current rods attached. The 50 mm x 50 mm cells were NiO/yttria-stabilized zirconia (YSZ) supported YSZ cells with Sr-doped lanthanum manganite (LSM)/YSZ cathode (H.C. Starck, Germany). The cells was first sealed onto aluminized 441 cell frame plates of 0.040" thickness at 950°C/2h in air using refractory sealing glass. Three cells on cell frame plates were then assembled with interconnect plates (machined from 0.133" thick 441 stock), and sealed with hybrid mica and glass perimeter seals. Pt or Ni wires for voltage sensing were spot welded onto cell frames and interconnects. Inconel 600 rods were also attached onto the interconnect plates as current leads. Contact pastes of NiO and LSM were applied to anodes and cathodes prior to assembly, and the components were then pressed between the two heat exchanger blocks for incoming air and fuel. Figure 3 shows an assembled three-cell stack test in the furnace. The assembly was slowly heated to the final sealing temperature of 930°C in flowing air. After sealing at 930°C for 2 hours, the stack was cooled to 800°C and a fuel of 5% H_2 in N_2 with 3% H_2O was supplied to the fuel channel. Both the fuel and air flow rates were then gradually increased until cell open circuit voltages (OCVs) of about 0.7-0.8 V were obtained, and then the fuel was switched to pure moist H_2 and flow rates were increased again. Once the cell OCVs stabilized, electrochemical performance measurements were conducted.

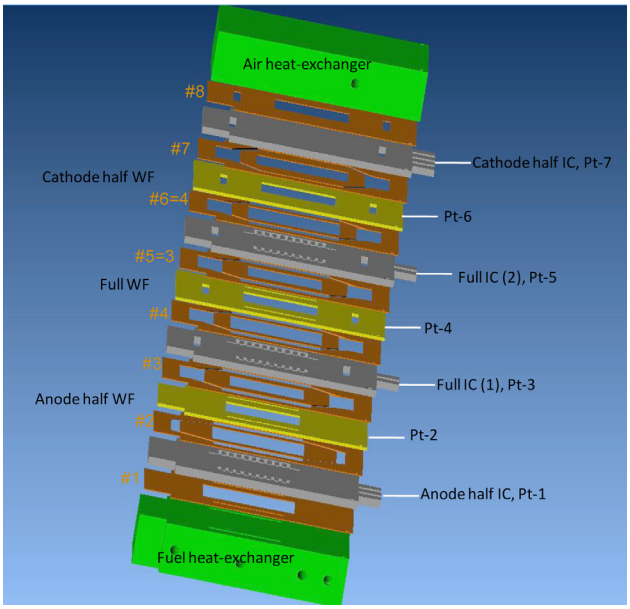

FIGURE 1. Second-Generation Three-Cell Stack Test Fixture

Three three-cell stack tests (Test #01, #02, and #03) were performed through June 2010. Test #01 showed satisfactory OCVs for cell 1 (1.077 V, bottom cell) and cell 2 (1.064 V, central cell). However, cell 3 exhibited a low OCV of only ~0.15 V. (The Nernst OCV should be 1.10 V for 97% H_2 + 3% H_2O versus air at 800°C). The test was then shut down to examine the components. At room temperature, no evidence of leakage was found around the perimeters of cell 3, so the fuel heat exchanger seals were replaced and the assembly was re-heated to 800°C. The OCV for both cells 1 and 2 increased to 1.084 V (cell 1) and 1.082 V (cell 2), but cell 3 OCV only increased to ~0.8 V. Cells 1 and 2 performed well with maximum power density reaching 400 and 450 mW/cm^2. The full cell and "half cell" (subtracting the resistance of the MnCo spinel coated interconnect plate) impedances showed little difference, indicating good performance of the spinel coating (applied by ultrasonic spraying). Overall, the short stack with two functional cells performed well in a constant current mode at 6 A (375 mA/cm^2) for ~500 hours at 800°C.

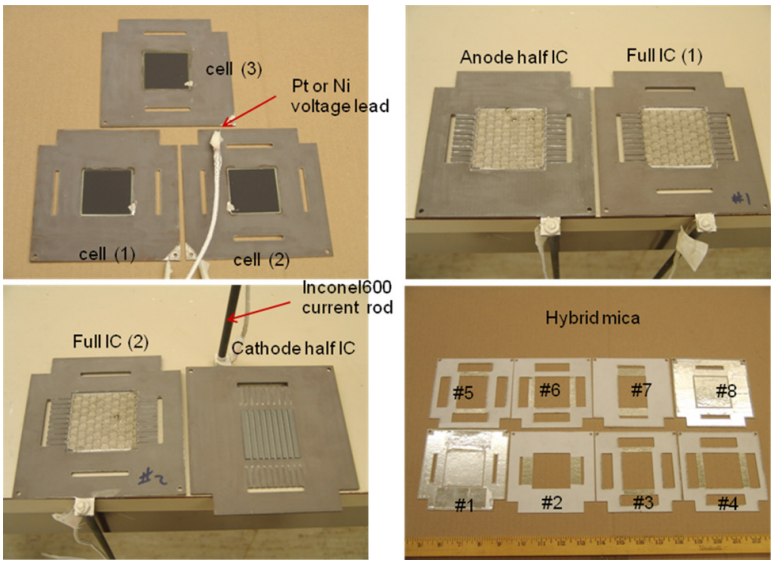

FIGURE 2. SOFC Parts Used for Second-Generation Three-Cell Stack Test

The second stack test (Test #02) also showed good OCVs for the bottom and middle cells (cells 1 and 2) and low OCV

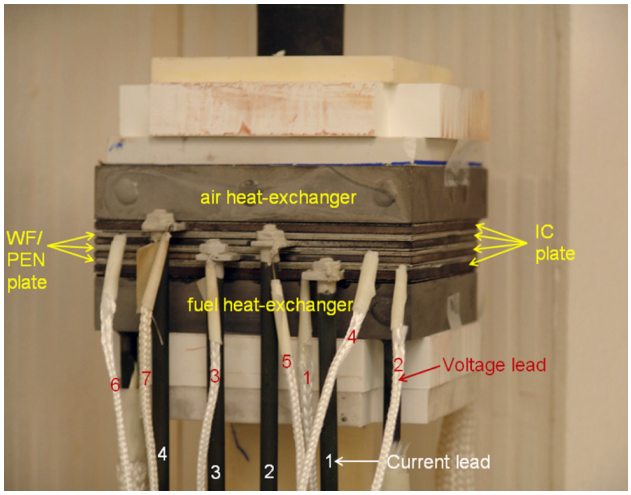

FIGURE 3. Assembled Three-Cell Stack Test in a Furnace

for the top cell (cell 3). The OCVs of the three cells were 1.070 V, 1.063 V, and 0.15 V for cell 1, cell 2, and cell 3, respectively, at 800°C. Again, cell 1 and cell 2 exhibited good performance; both cells had maximum power density ≥350 mW/cm^2. It was observed that cell 3 took a longer time to recover its original OCV when electrochemical measurements were performed, suggesting partial blockage of gas flow. Post-test examination of the mica seal for cell 3 revealed that the cause for poor OCV and performance of that cell in test runs #01 and #02 was the blockage of air flow caused by mica seal impingement into the air channel. After removal of the excess mica, the stack was re-assembled and reheated to 800°C. The OCVs were 1.059 V (cell 1), 1.074 V (cell 2), and ~1.0 V (cell 3). OCV of cell 3 was still lower than the other cells, but was substantially improved, and all 3 cells were exhibited reasonable current-voltage (I-V) curves and power density. During post-test analysis, some cell damage (cracks) along with brownish discoloration was observed on the cell. The cause for this damage is not clear at present, but may be related to the warping of window frame and interconnect plates and/or the fact that the current design used compliant corrugated Ni-mesh and Ni contact paste on the anode side and LSM contact paste with no compliant metallic mesh on the cathode side. This geometry and elasticity difference between Ni and LSM can put the positive electrode-electrolyte-negative electrode (PEN) to cell frame glass seal in tension (mode I) or shear (mode II) modes, since the compliant Ni mesh may not carry the load. In addition to warping issues, non-uniform thickness of the metallic plates (especially the full interconnect plates with four slots) could also contribute to an uneven stress distribution. Further improvement may be achieved by minimizing machining by using brazed thin plates instead of machined grooved parts.

Upon completion of post-test analysis of Test #02, a new stack (Test #03) was assembled and tested at 800°C at the same fuel and air conditions. This stack test was successful, as shown by the I-V sweeps and power density curves shown in Figures 4A and 4B, respectively. The measured OCVs were 1.08 V (cell 1), 1.07 V (cell 2), and 1.05 V (cell 3); these were attained using fuel and air flow rates of 1,300 sccm and 1,500 sccm, respectively. The maximum power densities were all ≥300 mW/cm^2. Impedance spectra of the full cell and "half cell" were also measured for all three cells, as shown in Figures 5A and 5B, respectively. The similarity of full and half cell spectra indicated that the conductance through the (Mn,Co)-spinel coating was very high, and that the electrical contact between the cathode and coating was good. The similarity of the ohmic resistance (high

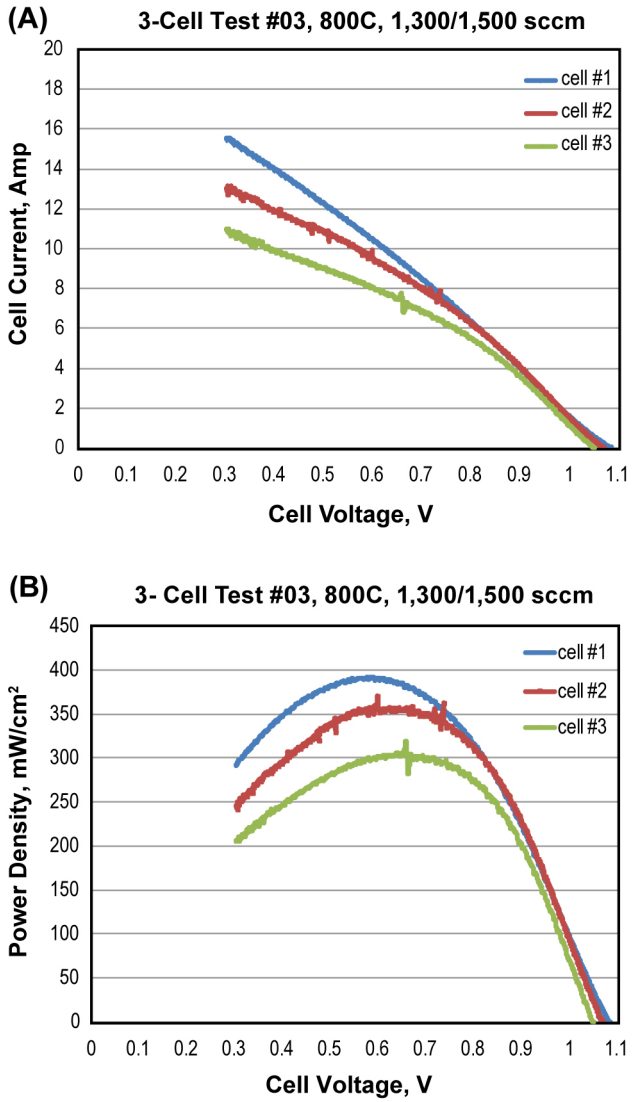

FIGURE 4. Electrochemical Performance of Three-Cell Stack Test #03 at 800°C, (A) I-V Sweep of Each Cell, and (B) Power Density Curve of Each Cell

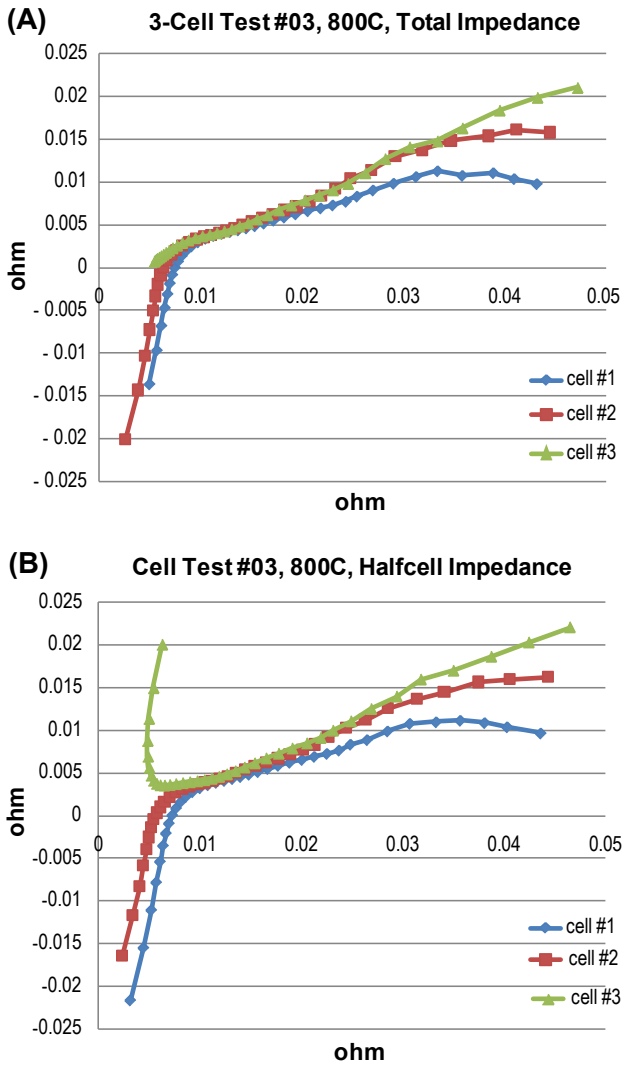

FIGURE 5. Impedance of Each Cell in Three-Cell Stack Test #03, (A) Full Cell Impedance, and (B) "Half Cell" Impedance

frequency intercept) of the three cells indicated good consistency in contact paste application and other stack fabrication details. Most of the observed cell impedance was non-ohmic, presumably due to electrode polarization, and was likely attributable to differences in fuel and/or air distribution.

Conclusions and Future Directions

The second generation stack test fixture was successfully demonstrated in three-cell stack tests at 800°C. The test fixture will bridge the gap between research level "button" cells and full-sized industrial stacks, and will be used to evaluate/validate new materials, processes, and design concepts developed by PNNL and other participants in the SECA CTP. Future improvements for the test fixture may include mass reduction through use of thinner AISI 441 stock, cathode contact reinforcement/modification for thermal cycle stability, and better flow channel design to achieve high fuel utilization.

FY 2010 Publications/Presentations

1. Y-S. Chou, J.W. Stevenson, and J-P Choi, "Effect of water content on SOFC single cell testing," MS&T 2009 Conference & Exhibition, Pittsburgh, Pennsylvania, October 26–30, 2009.

2. Y-S. Chou, J-P Choi, J.W. Stevenson, C-M Wang, G-G. Xia, and Z-G Yang, "SOFC materials evaluation in a standard test fixture," 2009 Fuel Cell Seminar, Palm Springs, California, November 16–19, 2009.

3. Y-S. Chou, J.W. Stevenson, and J-P Choi, "Evaluation of a single cell and candidate materials with high water content hydrogen in a generic solid oxide fuel cell stack test fixture, Part I: test fixture and electrochemical performance," Int'l J. Appl. Ceram. Tech. (in press).

III. SECA CORE RESEARCH & DEVELOPMENT

F. Fuel Processing

III.F.1 Reformer for Conversion of Diesel Fuel into CO and Hydrogen

Michael V. Mundschau (Primary Contact), David A. Gribble, Jr., Paul N. Plassmeyer and Lee M. Henton
Eltron Research & Development, Inc.
4600 Nautilus Court South
Boulder, CO 80301-3241
Phone: (303) 530-0263; Fax: (303) 530-0264
E-mail: mmundschau@eltronresearch.com

DOE Project Manager: Joseph Stoffa
Phone: (304) 285-0285
E-mail: Joseph.Stoffa@netl.doe.gov

Contract Number: 84394

Start Date: August 8, 2008
End Date: August 7, 2009

FY 2009-10 Objectives

- Design a reformer for converting commercial diesel fuel with a maximum of 15 parts per million by mass sulfur into a mixture of H_2 and CO.
- Demonstrate self-cleaning reactor walls that prevent deposition of carbonaceous residues and plugging of reformers by effusing air through the walls.
- Develop perovskite catalysts for dry partial oxidation of diesel fuel that are sulfur tolerant, stable near 950°C, resist deactivation by sintering and contain vacancies for enhancing mobility of oxygen anions allowing rapid oxidation of hydrocarbons and inhibition of deposition of carbon.

Accomplishments

- Distilled commercial diesel fuel; collecting 20% by mass of the most volatile components. Showed that the volatile fraction could be relatively easily re-vaporized and reformed by dry catalytic partial oxidation - eliminating steam and more complex fuel injectors and mixers. Nearly 90% of the carbon in the volatile fraction was converted into the desired CO, and about 75% of the hydrogen into H_2, with minimum deposition of carbon or naphthelene and no soot in the exhaust.
- Produced CO and H_2 by dry catalytic partial oxidation from volatile components of commercial diesel fuel that may have application in the regeneration of NOx traps used in pollution control of diesel engines.

Introduction

Dry catalytic partial oxidation of diesel fuel into H_2 and CO has potential applications for operation of solid oxide fuel cells and for regeneration of NOx traps used in pollution control of diesel exhaust. Reforming of diesel fuel into synthesis gas is also a first step in the production of pure hydrogen for proton exchange membrane fuel cells after water-gas shift and impurity removal using hydrogen transport membranes [1,2].

Dry partial oxidation of diesel fuel has a number of unique issues not encountered in the reforming of volatile fuels, fuels with higher H/C or O/C atomic ratios, or in steam reforming. Much effort in this research has been expended in understanding the fundamental science required for diesel fuel reforming. The major findings are summarized as follows.

The H/C atomic ratio in the fuel, along with the quantity of oxygen in the system, dictates the thermodynamic equilibrium temperature required to favor production of H_2 and CO over H_2O and CO_2 and to completely suppress formation of elemental carbon that can deactivate catalysts and plug reformers. Combustion analysis of commercial diesel fuel containing <15 ppmw sulfur, indicates H/C atomic ratios ranging from 1.87:1 to 1.78:1. To eliminate deposition of even single monolayers of carbon that might deactivate catalysts, calculations predict that catalysts must operate above about 950°C, assuming a stoichiometry of one mole of atomic oxygen for each mole of carbon in the fuel to form CO [3]. Temperatures required for partial oxidation of diesel fuel are considerably higher than that required for partial oxidation of methane with an atomic ratio of H/C of 4:1, or for steam and autothermal reforming of hydrocarbons where H_2O increases both H/C and O/C atomic ratios in the system.

The extreme temperatures required for dry partial oxidation of diesel fuel rule out most conventional high surface area, supported metallic catalysts that sinter and lose surface area and activity or that might be pyrophoric upon cycling between reducing conditions and exposure to air. For this high temperature application, refractory oxides with the perovskite crystal structure were selected [3]. The perovskites are designed to be electron conducting for the difficult reduction step: $O_2 + 4e^- = 2O^{2-}$ and are designed with oxygen-anion vacancies to enhance oxygen mobility and attack of adsorbed carbon from beneath. The perovskites have proven to be quite effective in suppressing deposition of carbon in catalyst beds [3]. Surface area is limited to about 1 $m^2 \cdot g^{-1}$, but at these extreme temperatures gas-

phase diffusion of large molecules is expected to be rate limiting rather than surface kinetics, and no great effort has been expended or deemed necessary to improve catalyst surface area.

Iron-based perovskites of general formula, $La_{1-x}(Ca,Sr)_xFeO_{3-\delta}$, have shown the best activity and stability of the base metal perovskites tested. Under appropriate thermodynamic conditions, Fe, Co and Ru, the three catalysts used in Fischer-Tropsch synthesis, catalyze the reverse reactions, converting *n*-alkanes into synthesis gas. Of the base metals, iron and cobalt best resist poisoning by sulfur at levels of 15 ppmw in diesel fuel [3]. Iridium, platinum and rhodium are the most sulfur-tolerant catalysts, based upon instability of their bulk sulfides at elevated temperatures [3], and Pt-Rh wire gauze operated near 1,000°C is sulfur-tolerant and thermally stable. The elements, Pt, Rh, Ru, Co and Fe are predicted to have catalytic activity for opening aromatic rings. However, the ability of iron in the perovskites tested to date to reform naphthalene is less than desired.

Thermodynamic and kinetic analysis indicates that elemental carbon is the preferred product in the fuel heating zone between 200-600°C [3]. Long-chain *n*-alkanes, such as *n*-hexadecane (cetane), are the least stable hydrocarbons in diesel fuel, cracking to form free radicals at autoignition temperatures near 205°C, well below the boiling point of 286.5°C. Carbon will deposit from long-chain ($>C_{12}$) *n*-alkanes well below their boiling points if heated above fuel cracking temperatures under oxygen lean conditions unless appropriate precautions are taken. Aromatic compounds such as naphthalene and benzene are the most stable molecules in the fuel, vaporizing well below their autoignition temperatures at 526°C and 562°C, respectively. Under oxygen-lean conditions, hydrocarbon free radicals react with high probability with other hydrocarbons, initiating radical polymerization and formation of tar and other carbonaceous residues. Because temperatures below about 950°C favor formation of graphite and soot, radical chain propagation in the heating zone leading to deep oxidation but also release of heat accelerating nucleation and growth of soot, must be suppressed.

Approach

Figure 1 shows schematically the laboratory porous membrane reactor. The fuel line and air brought in at the top are kept just below 200°C to minimize cracking of fuel and formation of tar. About 10% of the air required for partial oxidation is brought in with the fuel at the top through a porous baffle of yttria-stabilized zirconia fiber, stated by the manufacturer (Zircar Zirconia) to be 76% porous, which also acts as an infrared shield for the fuel line. It is desired that the oxygen in the cooler air react with hydrocarbon free radicals as they form in the gas phase of the heating zone between 205-562°C to produce easier-to-reform, small, oxygenated molecules that are very rapidly swept to the reformer hot zone operated above 950°C. Heat released by formation of the oxygenated compounds is partially absorbed by cooler air effusing through the walls of porous zirconia-toughed-alumina, stated by the manufacturer, Refractron, to be 40% porous. Inner walls in the heating zone are kept carbon-free by high local partial pressures of oxygen near the inner walls. Radical chains leading to polymerization and tar or to deep oxidation in the heating zone are terminated, in part, by the proximity of the walls of the relatively narrow porous tube (22-mm) and surfaces within the pores. It is also desired that air be effused throughout the length of the porous walls enclosing the bed of perovskite to produce a more uniform temperature distribution throughout the catalyst bed and to avoid hot spots at the entrance of the bed, which would be the case if all of the air and fuel were mixed before the entrance of the bed. Mobile lattice oxygen in the perovskite catalyst acts as a reservoir for oxygen in oxygen-lean regions, and the vacancy-rich perovskites act as sinks for excess oxygen in oxygen-rich regions.

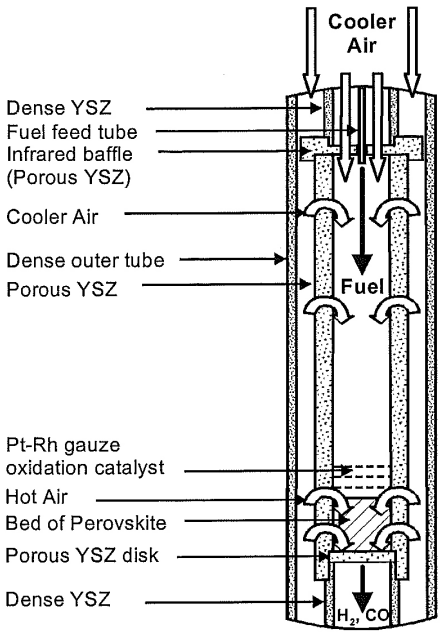

FIGURE 1. Schematic of a porous membrane reactor for reforming diesel fuel into synthesis gas. Cooler air (<200°C) is fed through walls of a narrow porous ceramic tube to suppress deposition of carbon on inner walls and to react with free radicals formed in the gas phase of the reformer heating zone. Pre-heated hot air (~900°C) is fed through porous walls to partial oxidation catalysts in the lower reformer hot zone.

Results

To circumvent need for complex and expensive liquid-fuel injectors and air mixers, diesel fuel was distilled below 200°C, and 20% by mass of the most

volatile components were collected into a reservoir. The distillate from the reservoir was relatively easily re-vaporized just below 200°C and entered the reformer in the gas phase. Figure 2 shows percent yields of carbon and hydrogen from dry partial oxidation of the distillate. Catalysts were very stable over the 72 h period tested. Nearly 90% of the carbon in the distillate was converted into the desired CO and about 75% of the hydrogen into molecular hydrogen. Very slight deposition of carbon occurred on the inner walls in the 2 cm above the catalyst, but exhaust and traps had no soot and negligible naphthalene. The catalyst was free of carbon. To suppress carbon, quantity of air was about 20% above that required for partial oxidation, and this produced the CO_2 and H_2O seen. Methane slip was evident, implying that the system was not brought to equilibrium or that methane formed in the cooler exhaust. Figure 3 plots the data as mole % (= volume %) of products in the reformate, that also contains 58 mol% N_2. Levels of CO and H_2 would be more than sufficient to regenerate NOx traps used in pollution control for diesel engines.

Figure 4 shows results for dry partial oxidation of full commercial diesel fuel (<15 ppmw S). Yields of desired CO and H_2 were less than that of the volatile distillate, and slight decay in yield was seen over 72 h. Tar appeared on the outer surface of the fuel nozzle and more carbon appeared deposited on

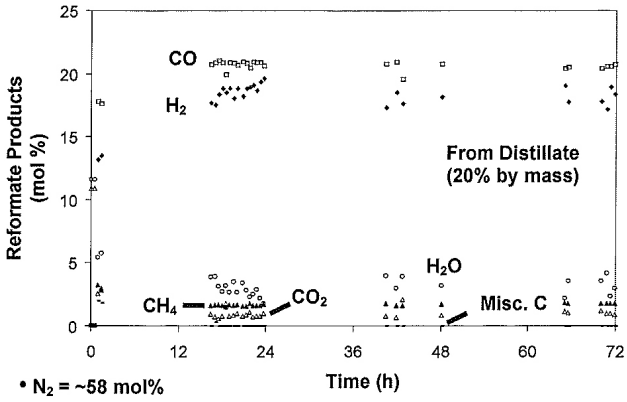

FIGURE 3. Reformate products as mole % (= volume %) from dry partial oxidation of the most volatile components distilled from diesel fuel. On-board reforming of components vaporized from diesel fuel may have application in regeneration of NOx traps used in pollution control of diesel exhaust.

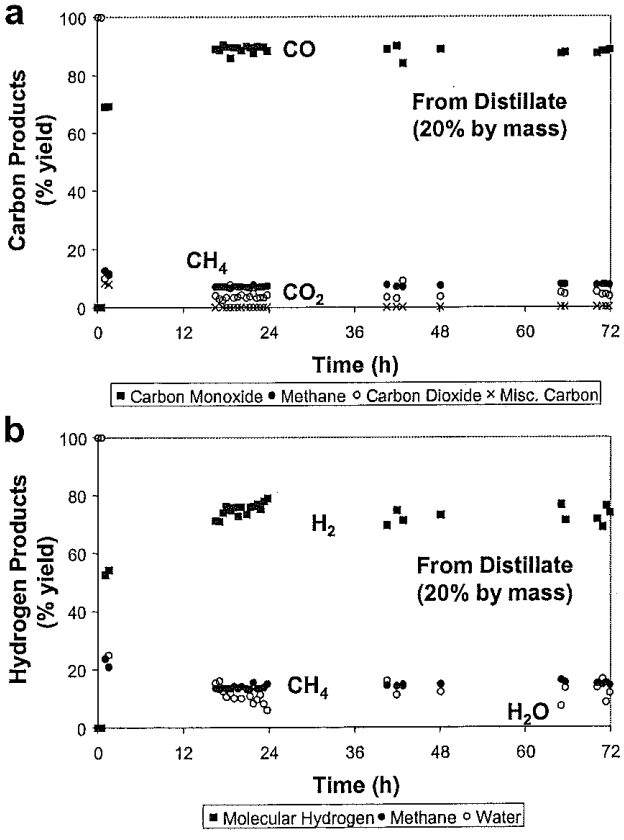

FIGURE 2. Percent yields of products containing (a) carbon and (b) hydrogen by dry partial oxidation of volatile compounds distilled from diesel fuel. Nearly 90% of the carbon in a distillate containing 20% by mass of the diesel fuel is converted into CO and 75% into molecular hydrogen.

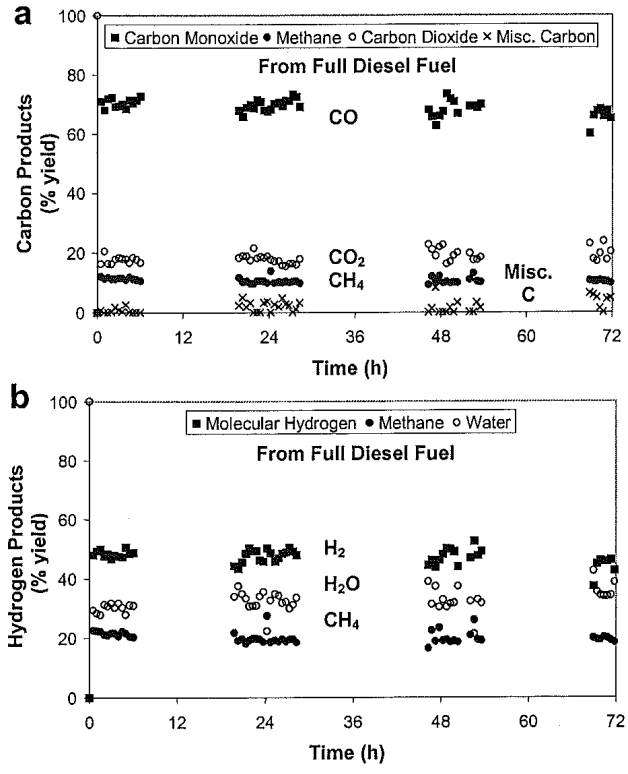

FIGURE 4. Percent yields of products containing (a) carbon and (b) hydrogen by dry partial oxidation of full commercial diesel fuel containing <15 ppmw sulfur. Although exhaust is soot-free, considerable naphthalene escapes through the catalyst bed, and yields of desired products are lower relative to reforming of the most volatile compounds distilled from diesel fuel.

inner walls, although there was no immediate danger of plugging the system. No soot was seen in the exhaust traps. However, considerable naphthalene was seen crystallized onto cooler exhaust lines and in the exhaust trap, implying inadequate catalyst activity for decomposition of naphthalene or formation of naphthalene in the system.

Conclusions and Future Directions

- Considerable work remains to produce a practical reformer for fuel cells. Sulfur even at levels of 15 ppmw in "ultra-low sulfur diesel" in the reformate is likely to poison nickel-based catalysts in solid oxide fuel cells. Parasitic power consumption for fuel injection, air flow and external heating of air fed to catalysts will need to be greatly reduced if efficient fuel cell systems are to be fabricated. Cost of all components will need to be greatly reduced.
- Narrow, self-cleaning walls of porous ceramic show promise for suppressing deposition of carbon in the critical diesel fuel heating zones but will require considerable effort to produce practical, cost-effective, devices.
- Perovskite catalysts, especially those containing iron, show promise as sulfur-tolerant, dry partial-oxidation catalysts for diesel fuel but will require further development.
- Dry partial oxidation of volatile components distilled from diesel fuel at temperatures below a modest 200°C might find immediate application for regeneration of NOx traps.

References

1. M.V. Mundschau, Hydrogen Separation Using Dense Composite Membranes: Part 1 Fundamentals, in: Inorganic Membranes for Energy and Environmental Applications, A. C. Bose, Editor (Springer, New York, 2009) pp. 125-153, DOI: 10.1007/978-0387-34526-0_8.

2. M.V. Mundschau, X. Xie, and C.R. Evenson IV, Superpermeable Hydrogen Transport Membranes, in: Nonporous Inorganic Membranes, A.F. Sammells and M.V. Mundschau, Editors (Wiley-VCH, Weinheim, 2006) pp. 107-138.

3. M.V. Mundschau, Christopher G. Burk and David A. Gribble, Jr., "Diesel Fuel Reforming Using Catalytic Membrane Reactors," *Catal. Today* 136 (2008), 190-205, DOI: 10.1016/j.cattod.2008.02.003, and references therein.

III.F.2 Oxide-Based Reforming Catalyst Evaluation and Development

Dushyant Shekhawat (Primary Contact), David A. Berry, Daniel J. Haynes[a], Mark W. Smith[b]
U. S. Department of Energy
National Energy Technology Laboratory
3610 Collins Ferry Road
Morgantown, WV 26507-0880
Phone: (304) 285-4634; Fax: (304) 285-0943
E-mail: Dushyant.Shekhawat@netl.doe.gov
[a]URS Corporation, 3610 Collins Ferry Rd.
Morgantown, WV 26507-0880
[b]REM Engineering Services, 3537 Collins Ferry Rd.
Morgantown, WV 26505-2374

Contract Number: 07-220611

Start Date: October 1, 2009
End Date: September 30, 2010

FY 2010 Objectives

- Conduct research towards development of a viable hydrocarbon reformer that is suitable for commercially representative fuel cell applications (e.g., diesel auxiliary power units).
- Perform temperature profile measurements during catalytic partial oxidation (CPOX) of diesel on pyrochlore coated monolith.
- Perform experimental studies (CPOX of diesel) on catalyst powders using the graded bed approach.
- Identify a scalable catalyst synthesis method that produces a pyrochlore-based catalyst with a comparable performance to the catalyst produced using the modified-Pechini method.
- Apply the optimized pyrochlore-based catalyst onto a structured catalyst such as monolith.

Accomplishments

- Prepared numerous oxide catalyst powders on oxygen-conducting supports; performed catalyst characterization by X-ray diffraction (XRD), inductively-coupled plasma (ICP), Brunauer-Emmett-Teller (BET), temperature-programmed reduction (TPR), temperature-programmed oxidation (TPO), X-ray photoelectron spectroscopy (XPS); evaluated activity and selectivity under several modes of reforming.
- Completed temperature profile measurements during CPOX of diesel on pyrochlore-coated monolith.
- Conducted several bed configurations to evaluate the optimal graded-bed approach.
- Evaluated several monoliths coated with different pyrochlore materials.
- Provisional patent application filed for method for designing reforming catalyst systems.

Introduction

The U.S. Department of Energy is sponsoring the development of high temperature fuel cell power systems based on solid oxide technology through its Solid State Energy Conversion Alliance (SECA) program. Diesel-fueled auxiliary power units are an important market segment for solid oxide fuel cell systems. The most promising route to hydrogen production from middle distillate fuels is catalytic reforming. The catalyst used in the fuel processor is a critical component of this system and must be able to provide a clean, tailored synthesis gas to the fuel cell stack for long-term operation.

However, carbon formation and deactivation by sulfur are still key challenges for CPOX catalysts. It has been shown that catalyst poisoning by sulfur and/or carbon is a structure sensitive reaction. Specifically, the deactivation mechanism by carbon and sulfur is influenced by the cluster size of the active metal. For example, larger metal clusters have a much stronger interaction with carbon and sulfur, than smaller, well-dispersed metal particles [1–3]. This problem becomes worse at the high reforming temperatures of CPOX, because conventional supported metals tend to sinter and agglomerate into even larger particles. Thus, the need for improved catalyst design/performance still exists.

For the past several years, the National Energy Technology Laboratory (NETL) has been developing new classes of structural oxide catalysts based on hexaluminate and pyrochlore architectures. These oxide catalysts are of interest primarily due to its refractory nature and its stability in high temperature reducing and oxidative environments. They also have the ability to "atomically-disperse" the active metal catalyst within an oxide framework that separates it from deposited metal catalysts that are more prone to sintering at high temperature with less control of particle size or "next nearest neighbor interactions." A series of hexaaluminates and pyrochlores with different formulations were prepared and evaluated for diesel reforming. Recently, one of the pyrochlore-based formulations demonstrated 1,000 hrs of successful diesel reforming. Now, the goal is to apply the optimized pyrochlore catalyst used in the 1,000 hr test

onto a structured material to produce a commercially representative form such as monolith, foams, pellets, etc.

Approach

Dispersing the metal throughout the structure may avoid the formation of larger metal clusters at the surface that are favorable sites for sulfur poisoning and carbon deposition, and thus may make the catalyst less susceptible to deactivation. Mixed metal oxides have become increasingly popular because of the ability to substitute different metals into their structure and maintain catalytic activity [3-5]. For example, prior research at NETL has demonstrated the ability to effectively incorporate Ni into the hexaaluminate structure $ANi_{0.4}Al_{11.6}O_{19-d}$ (A = La, Sr, and Ba) and successfully partially oxidize n-tetradecane with reduced carbon formation [5]. Liu and Krumpelt [6] have shown that the incorporation of Ru into a perovskite type structure ($LaCr_{0.95}$-$Ru_{0.05}O_3$) is catalytically active for the autothermal reforming of n-dodecane while exhibiting sulfur tolerance.

The general approach undertaken in this study has been to substitute catalytically active metals and dopants into the framework oxide lattice of specific pyrochlore materials to reduce the formation of large ensembles of active sites that are responsible for forming carbon and also for strongly adsorbing sulfur compounds also leading to deactivation. Select formulations of pyrochlore compounds were synthesized and evaluated for catalytic partial oxidation activity and selectivity of during reforming of n-tetradecane and dimethyl sulfide.

Temperature Profiling Tests: Temperature profiling experiments were performed during the CPOX of n-tetradecane. Conditions for the experiment are shown in Table 1. A quartz tube (19 mm inside diameter) fixed-bed reactor was used as reaction vessel for testing. The catalyst consisted of a square channel monolith (diameter = 18 mm; length = 50.4 mm; 15.7 channel/mm) provided by NexTech materials. It was comprised of an Al_2O_3 base structure coated with zirconia-doped ceria and LCZRh2Y pyrochlore catalyst. A 9.5 mm hole was bored through the center of the monolith to allow for axial bed temperature readings. Bed temperatures were measured at three locations, top, middle and bottom of the monolith using a 3-point temperature probe (BASF).

TABLE 1. CPOX Reaction Conditions for Temperature Profiling Study

Pre-heat (°C)	375
Reactor (°C)	800
N_2 Flow (sccm)	150
Air Flow (sccm)	631
Fuel Flow (ml/min)	0.18
O/C	1.2

Grade-Bed Tests: Successful reforming of diesel surrogate fuels has been previously demonstrated using noble metal-substituted catalysts [4,7,8]. However, these catalysts can be prohibitively expensive. Therefore, it has been decided to substitute a portion of the catalyst bed with less expensive catalysts that may provide acceptable levels of performance and significantly reduce cost. This approach has been referred to as the graded catalyst bed and very few similar studies have been reported with varying degrees of success [9-12].

Two mechanisms for the CPOX of methane have been proposed in literature: direct and indirect [13]. In the direct mechanism, methane is pyrolyzed to elemental carbon and H_2. Next the elemental carbon on the surface of the catalyst reacts with oxygen on the surface to form CO. Finally, H_2 and CO gas desorb from the surface to yield synthesis gas. In the indirect mechanism, sometimes called oxidation-reforming mechanism, the formation of the products takes place in two separate regions, or zones, of the reactor. First, a portion of the methane reacts with oxygen to form combustion products (H_2O and CO_2). This is followed by steam reforming (SR) and CO_2 (dry) reforming reactions with the remaining methane in the second region of the bed. The indirect mechanism is most likely the mechanism that dominates under typical operating conditions using a working catalyst.

The CPOX of higher hydrocarbons under typical operating conditions has been demonstrated to operate under a similar indirect mechanism [14], although cracking reactions are also present prior to contact with the catalyst. This has been supported in the literature by the presence of a high temperature spike in the front of the catalyst bed [15]. Figure 1 shows the major regions of a CPOX reactor for typical liquid hydrocarbons. It is this representation that was used to develop the graded catalyst bed approach.

It was desirable to select two compositions with significantly different levels of performance to examine the benefit of different combinations and configurations of the catalyst bed. The two compositions examined were a previously studied Ni-substituted barium hexaaluminate, BNHA, and a Rh-substituted pyrochlore, LCRh1ZY. The BNHA catalyst was known to deactivate within a short period of time under the selected reaction conditions given in Table 2. The LCRh1ZY catalyst was the same composition as the 1,000-hr formulation previously reported [16,17], but with 1 wt% Rh instead of 2 wt%, and without an oxygen-conducting support.

The two catalysts were configured in several different ways. The simplest tests consisted of dividing the bed in half and putting one composition on top and the other on the bottom, and then testing the reverse.

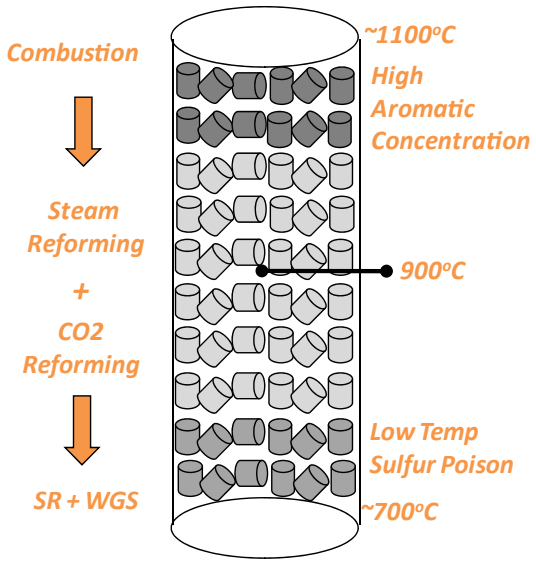

FIGURE 1. Diagram of CPOX Reaction Zones for Indirect Mechanism

TABLE 2. Operating Conditions for Graded Catalyst Bed Tests

O/C ratio	1.2
Temperature (°C)	900
Flow Rate (sccm)	400
GHSV (sccm/g_{cat}•hr)	25,000
Step 1	1 hr pure TD
Step 2	2 hr TD + 10 wt% MN + 50 ppm DBT
Step 3	2 hr pure TD

GHSV – gas hourly space velocity
TD – n-Tetradecane
MN – 1-Methylnaphthalene
DBT – Dibenzothiophene

The next configuration considered the reactor to consist of three regions, still using two different compositions. As shown in Figure 1, the top of the catalyst bed can get well above 1,000°C where combustion reactions occur. The middle of the catalyst bed where secondary reforming reactions begin is held at 900°C. The bottom of the catalyst bed has significantly lower temperatures as the endothermic reforming reactions dominate. With this in mind, it was hypothesized that the top and bottom regions of the catalyst bed is where the less expensive Ni-based catalysts more rapidly deactivate. In particular, the colder bottom of the bed is most susceptible to sulfur poisoning since the formation of metal sulfide species becomes thermodynamically favorable. Therefore, the configuration consisted of placing the Ni-based catalyst in the middle region of the bed, with the noble metal-based catalyst split between the top and bottom of the bed. One final catalyst bed configuration consisted of a 50/50 split of the two catalysts by weight evenly mixed throughout the bed.

Results

Temperature Profiling Tests: In parallel to the graded bed studies, temperature profiling measurements were performed to determine the length of the catalytic reaction zones. Under the presumption that the CPOX and oxygen-SR reactions proceed according to the reported two step oxidation-reforming mechanism (i.e., indirect mechanism) [18-22], temperature measurements down the length of the bed may distinguish not only the length of each reaction zone, but also the intensity of the reactions occurring at each point. The results will assist the graded bed studies to determine the proper location for a catalyst formulation which is optimized for the reactions occurring in that portion of the bed.

Temperature measurements taken down the length of the square channel monolith are shown in Figure 2. Consistent with the literature [18-22], higher temperatures are observed at the top of the bed likely due to the rapid consumption of a portion of the fuel with all available oxygen near the bed inlet. The temperature decreases as the heat generated by the initial oxidation is utilized to promote the endothermic reforming reactions, which convert the remaining fuel into synthesis gas. Although not endothermic, the equilibrium of the water-gas shift (WGS) reaction also occurs after the oxidation zone, and contributes to the synthesis gas selectivity.

From these results, a graded catalyst bed designed for each reaction zone would consist of at least two different formulations. Near the bed inlet, the ideal catalyst would maintain a reduced state (active form) in the presence of oxygen, and also have a high melting point to avoid sintering. Such properties are characteristic of noble metals like Rh, or Pt [23]. The short distance of the oxidation zone is advantageous and

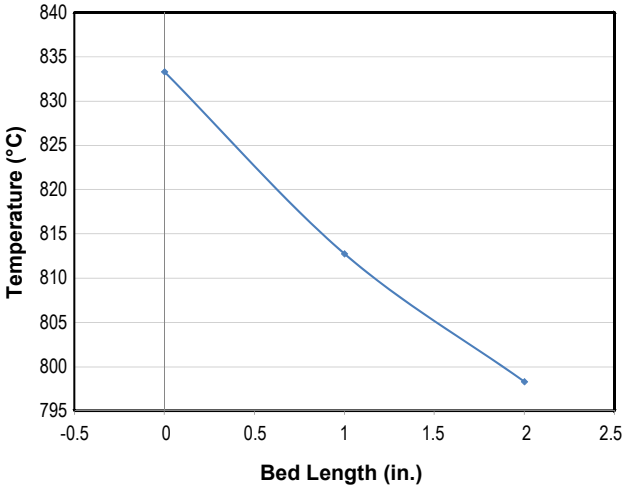

FIGURE 2. Temperature Profile of Monolith Catalyst Coated with Pyrochlore Catalyst; $T_{reactor}$ = 800°C; O/C=1.2

would require a small amount of these metals, which would make their use, especially the more expensive Rh, more economical. Ni may also be acceptable, but must be modified either through the partial substitution into an oxide-based structure, like a pyrochlore [8], or by the addition of a small amount of noble metals [24,25]. For the endothermic portion, catalysts active and selective for SR and WGS are desirable. Studies have found SR activity of metals to rank in the order of Rh, Ru>Pd, Ni>Pt>Co [26]. In the interest of cost, a catalyst comprised of mainly Ru, Pd, or Ni may be acceptable for this region.

Grade-Bed Tests: The results of the CPOx experiments for the graded catalyst beds are provided in Figure 3. The graded catalyst beds were compared to beds containing each of the two catalysts separately. Clearly the LCRh1ZY catalyst exhibited the best performance while the BNHA catalyst deactivated significantly during the 2 hr exposure to aromatic and sulfur species (Step 2). The graded bed configuration with the worst performance was the one with the LCRh1ZY catalyst in the top half of the bed and BNHA in the bottom half. This suggests that the Ni-based catalyst deactivates more rapidly in the bottom region. The three remaining configurations performed similarly, but the one consisting of the BNHA in the top half and LCRh1ZY in the bottom half of the bed exhibited a consistent decrease during Step 2 of the experiment, and did not recover to the same level in Step 3. The two best performing configurations were the evenly mixed bed and the bed consisting of the LCRh1ZY split between the top and bottom and BNHA in the middle. It should be noted that there was a 40/60 split by mass between the LCRh1ZY and BNHA in the latter configuration instead of 50/50, which may account for the slightly lower, though still stable performance during Step 2. Nevertheless, it is not clear why the mixed bed performed as well as it did. It has been suggested that the BNHA is functioning as sulfur scavenger which enhances the performance of the LCRh1ZY. It was determined that longer testing and the examination of additional catalyst compositions is necessary.

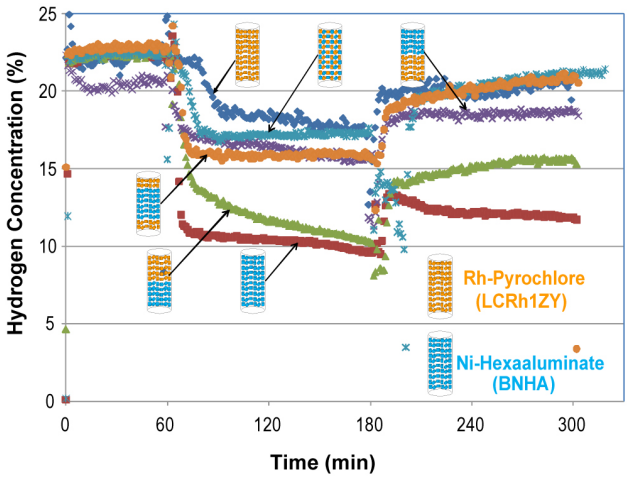

FIGURE 3. Performance of Graded Catalyst Bed Configurations in the CPOX of *n*-Tetradecane with Addition of Aromatic and Sulfur Species: GHSV = 25,000 scc/g_{cat} • hr, T = 900°C, P = 0.23 MPa, O/C = 1.2

After each CPOx experiment a temperature programmed oxidation (TPO) was conducted on the catalyst bed to calculate the amount of carbon formed. Table 3 provides the results of the TPOs for each configuration. The theoretical amount of carbon formed was calculated based on the rate of carbon formation per gram of catalyst from the runs conducted on the individual catalysts separately as single-composition beds. It is not surprising, based on the results in Figure 2, that the evenly mixed bed formed the least amount of carbon. However, the highest level of carbon formation unexpectedly occurred in the configuration consisting of the three catalyst zones. Of all the graded configurations, only the evenly mixed bed and the bed with the BNHA in the top and LCRh1ZY in the bottom regions of the bed produced less carbon than the theoretical amount. These results suggest that carbon formation in the bed is not strongly correlated to performance for this combination of catalytic materials. It may also be related to the fact that carbon is not deposited only on the catalysts' surfaces, but the reactor walls and bed material as well. Further, it should be noted that an inert catalyst bed produces ~0.63 g of carbon under these same operating conditions.

TABLE 3. Total Carbon Formed in Graded Catalyst Beds during CPOX Testing (Determined by TPO)

Top:Bottom	Total Carbon (g)	Theoretical (g)
1.0 g LCRh1ZY	0.49	—
1.0 g BNHA	1.88	—
0.5 g LCRh1ZY: 0.5 g BNHA	1.31	1.19
0.5 g BNHA: 0.5 g LCRh1ZY	1.13	1.19
0.2 g LCRh1ZY: 0.6 g BNHA: 0.2 g LCRh1ZY	1.41	1.32
0.5 g BNHA + 0.5 g LCRh1ZY	0.71	1.19

Conclusions and Future Directions

The graded catalyst bed studies conducted thus far have produced some very interesting results. It has been determined that the amount of expensive noble metal-based catalyst can be reduced by substituting less expensive Ni or Ru-based catalysts in sections of the bed that are less likely to deactivate them. Further,

the results strongly suggest that the bottom region of the catalyst bed is the most likely place that these less expensive catalysts will deactivate. Therefore, substituting these catalysts in the top and/or center of the bed may produce acceptable levels of performance and a significant reduction in overall catalyst cost. Remaining tests will consist of long-term studies to determine the optimum catalyst compositions and configurations. Finally, future work will focus on developing a finished commercial product comprised of a deposited catalyst/support system with multiple compositions that are active for the different reforming reactions taking place in hydrocarbon reforming.

Special Recognitions & Awards/Patents Issued

1. D.A. Berry, D. Shekhawat, M.W. Smith, and D. Haynes, "Methods for designing a reforming and/or combustion system," Provisional patent application filed (2010).

2. NETL-Organized American Institute of Chemical Engineers Conference Symposium, *2010 Spring National Meeting – Topical 2: Advanced Fossil Energy Utilization.*

FY 2010 Publications/Presentations

1. M.W. Smith, D.A. Berry, D. Shekhawat, D.J. Haynes, and J.J Spivey, "Partial Oxidation of Liquid Hydrocarbons in the Presence of Oxygen-Conducting Supports: Effect of Catalyst Layer Deposition," *Fuel* 89(6) (2010) 1193-1201.

2. D.J. Haynes, A. Campos, M.W. Smith, D.A. Berry, D. Shekhawat, and J.J. Spivey, "Reducing Deactivation of Ni-Metal during the Catalytic Partial Oxidation of a Surrogate Diesel Fuel Mixture," *Catal. Today* 154 (2010) 210-216.

3. M.W. Smith, D.A. Berry, D. Shekhawat, D.J. Haynes, and J.J. Spivey, "Catalytic Material Development for a SOFC Reforming System: Application of an Oxidative Steam Reforming Catalyst to a Monolithic Reactor (FuelCell2010-33198)," *8th International Fuel Cell Science, Engineering and Technology Conference*, American Society of Mechanical Engineers, Brooklyn, New York, June 14–16, 2010.

4. D.J. Haynes, D.A. Berry, D. Shekhawat, M.W. Smith, and J.J. Spivey, "Long Term Reforming of Commercial Diesel Fuel Using a Layered Pyrochlore Catalyst," *239th ACS National Meeting*, San Francisco, California, March 2010.

5. M.W. Smith, D.A. Berry, D. Shekhawat, D.J. Haynes, and J.J. Spivey, "Ni-substituted Oxide Catalysts with Oxygen Ion Conductivity for Hydrocarbon Reforming," *2010 Spring National Meeting*, American Institute of Chemical Engineers, San Antonio, Texas, March 21–25, 2010.

References

1. B.J. Wuensch, K.W. Eberman, C. Heremans, E.M. Ku, P. Onnerud, E.M.E. Yeo, S.M. Haile, J.K. Stalick, and J.D. Jorgensen, Solid State Ionics 129 (2000) 111.

2. K.V.G. Kutty, C.K. Mathews, T.N. Rao, and U.V. Varadaraju, Solid State Ionics 80 (1995) 99.

3. P. Erri, P. Dinka, and A. Varma, Chem. Eng. Sci. 61 (2006) 5328-5333.

4. D.J. Haynes, D.A. Berry, D. Shekhawat, and J.J Spivey, Catal. Today, 136 (2008) 206-213.

5. T.H. Gardner, D. Shekhawat, D.A. Berry, M.W. Smith, M. Salazar, E.L. Kugler, Appl. Catal. A: Gen. 323 (2007) 1-8.

6. D.J. Liu and M. Krumpelt, Int. J. Appl. Ceramics Tech. 2 (2005) 301-307.

7. D.J. Haynes, D.A. Berry, D. Shekhawat, and J.J Spivey, Catal. Today, 145 (2009) 121-126.

8. D.J. Haynes, A. Campos, M.W. Smith, D.A. Berry, D. Shekhawat, A. Roy, and J.J. Spivey, Catal. Today, 155 (2010) 84-91.

9. S. Shen, et al., "A Novel Two-Stage Reactor Process for Catalytic Oxidation of Methane to Synthesis Gas," in Stud. Surf. Sci.Catal., 2001, Elsevier. p. 99-104.

10. G.C.M. Tong, J. Flynn, and C.A. Leclerc, Catal. Lett., 102 (2005) 131-137.

11. J. Xu, W.S. Wei, A.Z. Tian, Y. Fan, X.J. Bao, and C.C. Yu, Catal. Today, 149 (2010) 191-195.

12. J. Zhu, M.S.M.M. Rahuman, J.G. van Ommen, and L. Lefferts, Appl. Catal. A: Gen., 259 (2004) 95-100.

13. A.P.E. York, T. Xiao, M.L.H. Green, and J.B. Claridge, Catal. Rev., 49 (2007) 511-560.

14. R. Subramanian, G.J. Panuccio, J.J. Krummenacher, I.C. Lee, and L.D. Schmidt, Chem. Eng. Sci., 59 (2004) 5501-5507.

15. G.J. Panuccio, K.A. Williams, and L.D. Schmidt, Chem. Eng. Sci., 61 (2006) 4207-4219.

16. M.W. Smith, D.A. Berry, D. Shekhawat, D.J. Haynes, and J.J. Spivey, "Catalytic Material Development for a SOFC Reforming System: Application of an Oxidative Steam Reforming Catalyst to a Monolithic Reactor," in 8th Intl Fuel Cell Sci., Eng. and Tech. Conf., 2010, American Society of Mechanical Engineers: Brooklyn, New York.

17. D.J. Haynes, D.A. Berry, D. Shekhawat, M.W. Smith, and J.J. Spivey, "Long Term Reforming of Commercial Diesel Fuel Using a Layered Pyrochlore Catalyst," in Spring National Meeting, 2010, American Chemical Society: San Francisco, California.

18. I. Aartun, H.J. Venvik, A. Holmen, P. Pfeifer, O. Görke, and K. Schubert, Catal. Today. 110 (2005) 98-107.

19. F. Basile, G. Fornasari, F. Trifirò, and A. Vaccari, Catal. Today, 64 (2001) 21-30.

20. R. Horn, K.A. Williams, N.J. Degenstein, and L.D. Schmidt, Chem. Eng. Sci., 62 (2007) 1298-1307.

21. B.C. Michael, D.N. Nare, and L.D. Schmidt, Chem. Eng. Sci., 65 (2010) 3893-3902.

22. G.J. Panuccio and L.D. Schmidt, Appl. Catal. A: Gen., 332 (2007) 171-182.

23. B.C. Enger, R. Lødeng, and A. Holmen, J. Catal., 262 (2009) 188-198.

24. M. Shiraga, D. Li, I. Atake, T. Shishido, Y. Oumi, T. Sano, and K. Takehira, App. Catal. A: Gen., 318 (2007) 143-154.

25. K. Yoshida, N. Begum, S.-i. Ito, and K. Tomishige, Appl. Catal. A: Gen., 358 (2009) 186-192.

26. G. Kolb, R. Zapf, V. Hessel, and H. Löwe, Appl. Catal. A: Gen., 277 (2004) 155-166.

III.F.3 Alternative Reforming Concepts: RF-Enhanced Catalysis and Low-Temperature Plasma

Dushyant Shekhawat (Primary Contact), David A. Berry, Michael J. Gallagher[a], and Richard M. Bergen[a]
U.S. Department of Energy
National Energy Technology Laboratory (NETL)
3610 Collins Ferry Road
Morgantown, WV 26507-0880
Phone: (304) 285-4634; Fax: (304) 285-0943
E-mail: Dushyant.Shekhawat@netl.doe.gov
[a]URS Corporation, Morgantown, WV

Contract Number: 07-220611

Start Date: October 1, 2009
End Date: September 30, 2010

FY 2010 Objectives

RF-Enhanced Catalysis:

- Modify current instrumentation of catalyst screening unit at NETL to incorporate radio frequency (RF)-enhanced catalytic system.
- Evaluate RF-field application to heavy hydrocarbon reforming catalysts.
- Examine fundamental parameters affect RF energy influence.

Low-Temperature Plasma:

- Modify current instrumentation of fuel processing unit at NETL to incorporate existing reverse vortex plasma reformer (previously constructed at Drexel University).
- Demonstrate stable operating performance of plasma reformer with various fuels including diesel.
- Conduct plasma characterization studies.
- Complete process optimization study.

Accomplishments

RF-Enhanced Catalysis:

- Completed modification of a catalyst screening unit (CSU) to incorporate the RF system.
- Demonstrated stable operation within a frequency range of 0.1-62 MHz at various power levels (0-100 W).
- Preliminary experiments showed a 20% increase in hydrogen and carbon monoxide yields with assistance from applied RF electromagnetic fields.

Low-Temperature Plasma:

- Completed modification of fuel processing unit to incorporate the plasma reformer.
- Demonstrated stable performance for the partial oxidation of n-tetradecane at various O/C ratios (0.8-1.1).
- The energy conversion efficiency (fuel-to-products) was shown to be as high as 83%, with 50% conversion of fuel directly to syngas (H_2 and CO only) and 33% preserved in the form of light hydrocarbons (mostly CH_4 and some C_2H_4).
- The presence of coke/carbon in the exhaust stream was visually monitored and not observed. Carbon and energy balances corroborate that very little, if any, solid carbonaceous material was formed as a product, even at O/C ratios ≤1 where it is thermodynamically favorable to be produced.
- A second generation plasma reformer was designed and being constructed to complete the process optimization studies and to resolve the fuel injection issues.

Introduction

The successful deployment of fuel cell technology for many market applications requires the use of hydrocarbon-based fuels. The U.S. Department of Energy is sponsoring development of high-temperature fuel cell power systems based on solid oxide technology through its Solid State Energy Conversion Alliance (SECA) program. The fuel processor is a critical component of these systems and must be able to provide a clean, tailored hydrogen-rich synthesis gas to the fuel cell stack for long-term operation. There are a number of barrier issues that must be overcome in using hydrocarbon fuels. Carbon formation, both during startup and long-term operation, must be minimized to avoid coking of the catalysts in the reformer and downstream fuel cell. Also, most fuels contain some level of sulfur that can poison both the reforming catalysts and the fuel cell anode. Much of the technology development thus far has focused on catalytic systems. Although widely used in high-steam commercial processes, most known catalytic-only

systems are not capable of sustained reforming operation in low-steam reforming conditions. There is an ongoing research effort to identify novel fuel reforming methods to either enhance or replace catalytic systems to reduce/eliminate unwanted by-products (coke, olefins) from steam-free operation and provide a pure fuel stream to allow fuel cells to run for longer durations with higher efficiency. Two ongoing projects will be described here: enhanced catalysis via RF electromagnetic fields; and low-temperature plasma-assisted reforming. Both of these research concepts relate to the SECA program goals of developing new, more efficient reforming methods to improve the performance of fuel cells.

RF-Enhanced Catalysis. The underlying concept of RF-enhanced catalysis is to provide targeted heating of the active metal sites of a catalyst, thereby enhancing their catalytic activity without increasing the gas temperature of the surrounding reactants. This concept allows one to control how energy is deposited into a reformer and avoids regimes of too high gas temperatures during partial oxidation, which can lead to the formation of unwanted byproducts, such as coke. An RF generation system was designed, built, and installed within a catalyst screening system to evaluate the effect of various RF frequencies (0-1,000 MHz) and power levels (0-100 W) on reforming using various catalysts. Figure 1 shows a schematic of the experimental setup along with a photo of the actual catalytic reactor with RF antenna.

Low-Temperature Plasma. Low-temperature plasmas have been investigated for their catalytic properties that can enhance fuel reforming by boosting

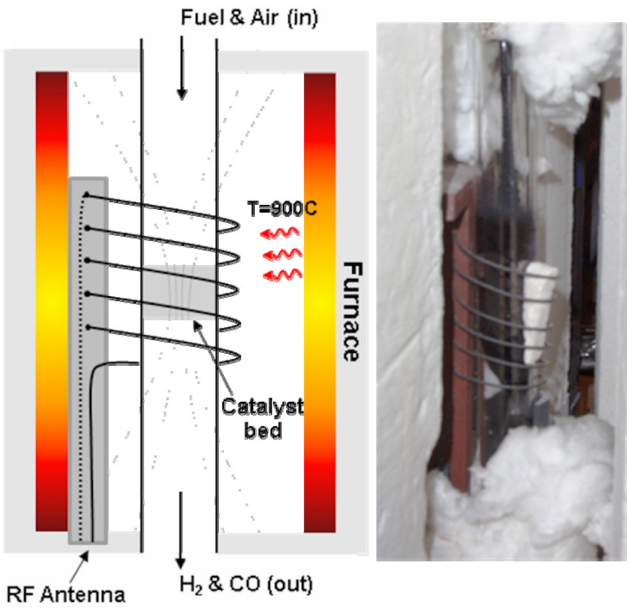

FIGURE 1. A Schematic and a Photo of the RF-Enhanced Catalytic Reactor

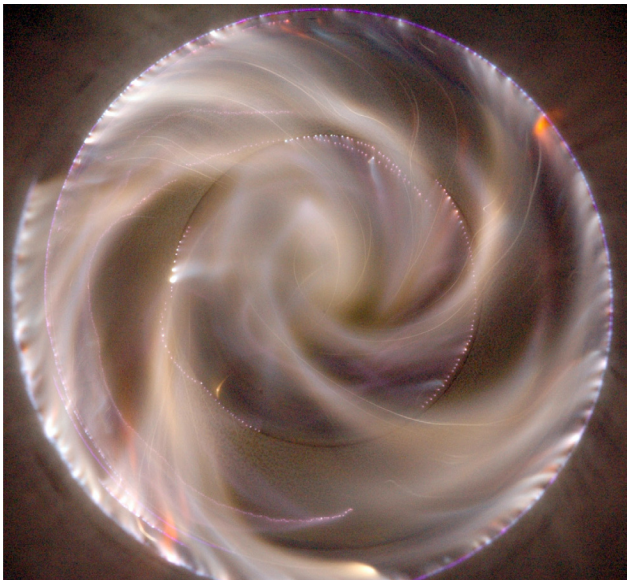

FIGURE 2. An Image of Gliding Arc Plasma as Taken from the Reactor Installed at NETL

syngas yields and avoiding by-product formation [1-3]. A particular type of plasma, named gliding arc, has shown some of the best reforming results in terms of syngas conversion and low electrical energy cost for syngas production, which is due in part to its moderate gas temperatures (~2,000 K) and high electron energy and density [1,4]. A gliding arc reformer was developed at Drexel University and installed in fuel processing unit to evaluate the effect of various plasma parameters (frequency, power) on energy conversion efficiency and product composition. Figure 2 shows an image of the gliding arc plasma stabilized in reverse vortex flow.

Approach

RF-Enhanced Catalysis: The main technical approach involves investigating various RF frequencies (range 0.1-1,000 MHz) and power levels (0-100 W) to find a regime of enhanced catalytic reforming. Enhanced reforming is determined by comparing results from RF-assisted catalytic experiments with control experiments using the same catalyst under identical conditions without the applied RF field. Previous work in this area was performed by Chevron (in conjunction with DOE) [5] and showed promising results at a frequency of 13.6 MHz. Initial experiments focused on this frequency, but other higher frequencies will be investigated. Dielectric permittivity measurements are also being performed to characterize how each of the various types of heterogeneous catalyst materials are absorbing RF radiation. Such information should provide clues to what frequencies will have the greatest positive influence on reforming. The targeted parameters for improvement include increasing syngas

yield, reduction of coking and/or olefin by-product formation, and minimizing the parasitic energy cost for the observed effect provided by the applied RF field. Gas chromatography and mass spectrometer measurements were used to determine product composition and temperature programmed oxidation runs were performed after each trial to measure the amount of carbon/coke formed. Additional types of catalysts are also being investigated. During installation of the RF system within the CSU, several technical problems were encountered which included disruption of lab equipment from electromagnetic interference and problems with several RF antennas. The vendor who provided the RF equipment (Radial Technology, LLC) worked to solve many of these problems and experiments were conducted starting in the third quarter.

Low-Temperature Plasma: Plasma is used in these trials as a potential catalyst to enhance the partial oxidation of commercial logistic fuels into syngas for use in fuel cells. The targets to be met therefore include: high conversion efficiency to syngas (and CH_4 up to 25%), minimization of solid coke/carbon or heavy hydrocarbon by-products, and low parasitic energy cost to drive the plasma. The approach used here includes demonstrating proof-of-concept results first using simple paraffin-like fuels (such as n-tetradecane) and then with complex fuels, such as diesel, containing difficult to reform aromatic compounds. Several parameters of plasma are to be investigated including the effect of varying plasma power (0-400 W) and the addition of steam as an oxidant and fuel contaminants (such as 1-methylnaphthalene) on reforming efficiency.

Results

RF-Enhanced Catalysis: Several technical problems were encountered during installation and configuration of the RF system which delayed the start of the experimental investigation by several months. These problems included electromagnetic interference created by the RF system which caused several system components (pumps, mass flow controllers, etc.) within the CSU to malfunction. These problems were eventually resolved and experiments were conducted with variable RF power at a fixed frequency (using a low-frequency antenna - range of 0.1-62 MHz) with a monolith coated with NETL's proprietary pyrochlore catalyst. The bulk of the experimental investigation took place at a frequency of 13.6 MHz as this frequency previously showed evidence of enhanced reforming [5]. Some preliminary evidence of enhanced syngas yields in the presence of the RF field was observed and is shown in Figure 3. The results show up to a 20% increase in H_2 and CO yields were obtained during n-tetradecane partial oxidation (O/C ratio 1.2) with RF assistance at various power levels (0-100 W). Baseline trials were performed without assistance from the RF field. The dotted line in

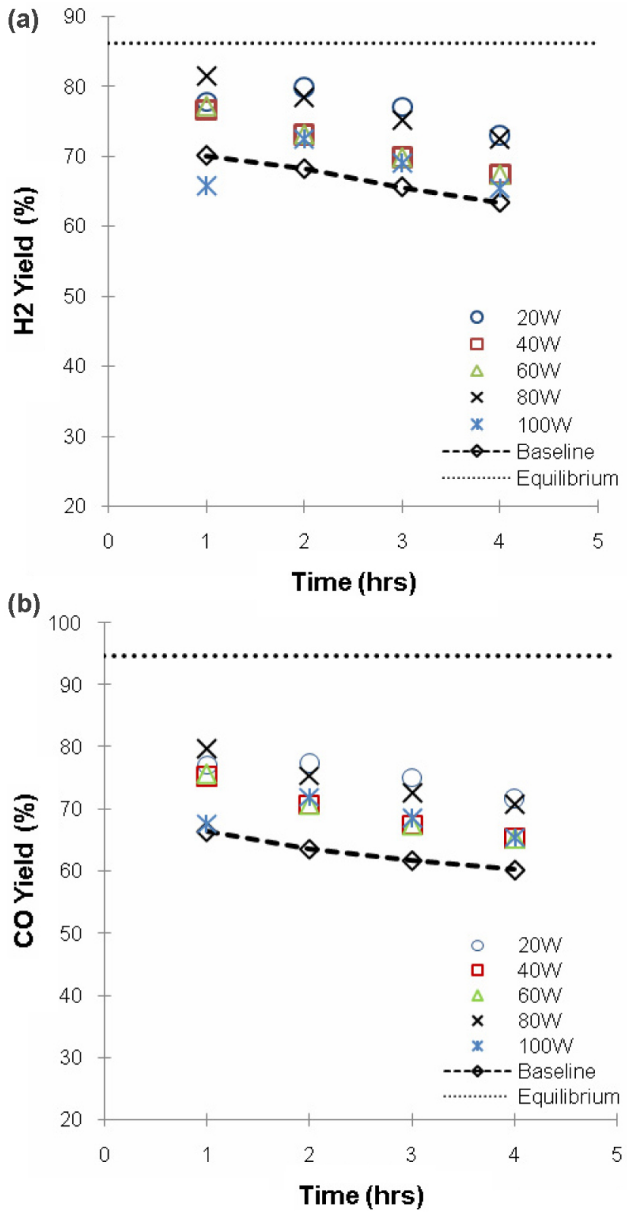

FIGURE 3. H_2 (a) and CO (b) Yields Versus Time for Various Cases of Applied RF Power at a Fixed Frequency of 13.6 MHz

Figures 3a and 3b show the thermodynamic equilibrium values of the maximum possible syngas yields that could be obtained under idealized conditions. Some evidence of a reduction in coke/carbon was observed, but further testing is needed to quantify these results. In addition, further testing is needed to quantify the levels of olefins and other light hydrocarbons products produced during trails with RF assistance.

Low-Temperature Plasma: Figure 4a shows the energy conversion efficiency as a function of the O/C ratio at a fixed plasma power of 200 W using n-tetradecane fuel. The solid and dashed lines in Figure 4a show the predicted thermodynamic

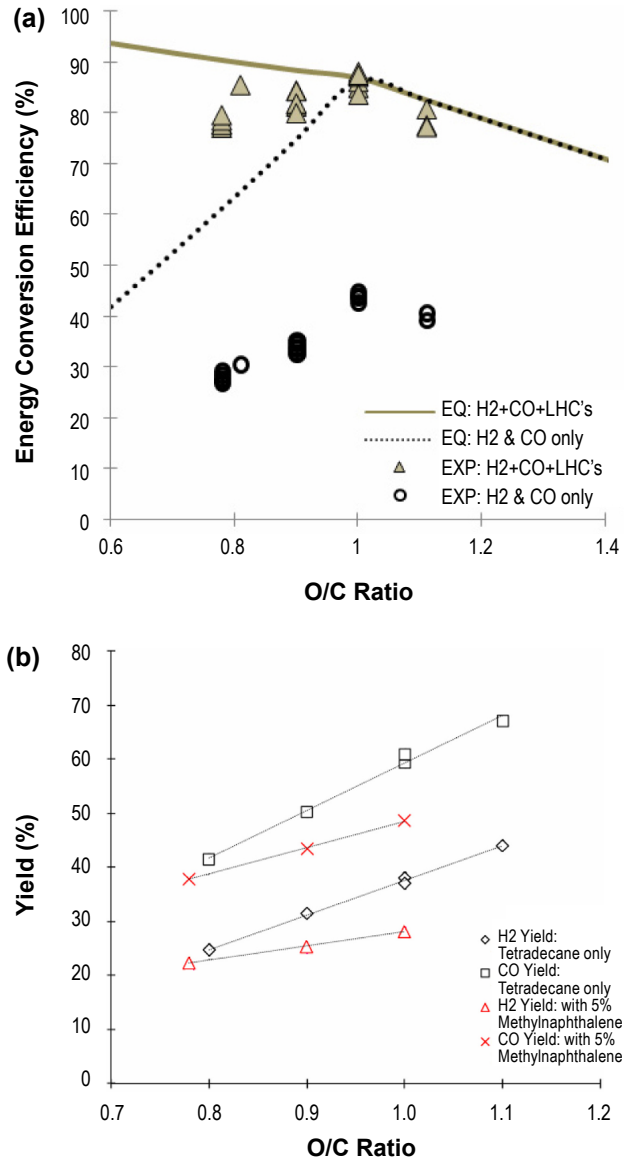

FIGURES 4. Energy conversion efficiency as a function of the O/C ratio for plasma-assisted reforming of n-tetradecane. Yields of H_2 and CO as a function of the O/C ratio for plasma-assisted reforming of 100% n-tetradecane and 95% n-tetradecane plus 5% 1-methylnaphthalene.

equilibrium energy conversion efficiency for H_2, CO, and light hydrocarbons (LHCs), and H_2 and CO only, respectively. The experimental points for energy conversion efficiency including LHCs match reasonably well to the equilibrium curves. This demonstrates that good conversion was achieved from fuel to products where most of the energy originally contained in the fuel was converted to a combination of syngas and light hydrocarbon fragments (3-5% CH_4, 2-4% C_2H_4, ≤1% C_2H_2). Conversion of fuel directly to syngas (H_2 and CO only) had an efficiency of approximately 50% with the remainder of energy (nearly 40%) bound in the form of LHCs. Little or no solid coke/carbon was observed during these trials and results from the atomic carbon balance (within ± 3-5%) corroborate this fact. A parametric study was initiated to understand which of the following factors influence plasma-assisted reforming the most: O/C ratio, plasma power (0-400 W), and the addition of steam and fuel contaminants. Increasing both the O/C ratio and plasma power increase conversion and syngas yields; however, there is an energy penalty associated with each: higher O/C ratio means lower maximum efficiency and higher plasma power increases the parasitic energy loss within the system. Figure 4b shows results of H_2 and CO yields of trials with pure n-tetradecane and n-tetradecane plus 5 wt% 1-methylnaphthalene. Yields with the fuel contaminant were slightly worse as would be expected due to the more complex structure of 1-methylnaphthalene. However, little or no coke was observed during reforming.

The plasma reformer was designed with the capability to recuperate heat from its own exhaust and this recovered heat is added to the premixed fuel and air just before it enters the reaction chamber and interacts with the plasma discharge. This heat recuperation scheme increased the overall energy efficiency of the reformer; however, it also created several problems in certain operating regimes. The main problem included overheating of the air and fuel reactants, which, in rich fuel/air mixtures, caused coking to occur outside of the reaction chamber. The coke material then provided a conductive path outside the reaction chamber where the plasma would preferentially discharge and cause damage. A new reactor was designed which avoids this problem by eliminating heat recuperation and providing precise control of the temperature of the fuel and air by means of a specially designed atomization nozzle. A schematic of the new plasma reactor is shown in Figure 5. This new reactor has been fabricated and the parametric studies are expected to resume during the fourth quarter.

Conclusions and Future Directions

RF-Enhanced Catalysis: Preliminary studies showed evidence of enhanced catalytic activity - up to a 20% increase in syngas yields was observed when RF fields were applied. The future work should involve continuation of the current investigation including the highest frequency range (300-1,000 MHz). In addition, there are several interesting research areas that should be explored including the influence of RF fields on aerogel catalysts and other coal-based reforming applications.

Low-Temperature Plasma: Plasma-assisted reforming has shown promising results in converting heavy hydrocarbon fuels into syngas with little or no coke/carbon residue and low levels of residual

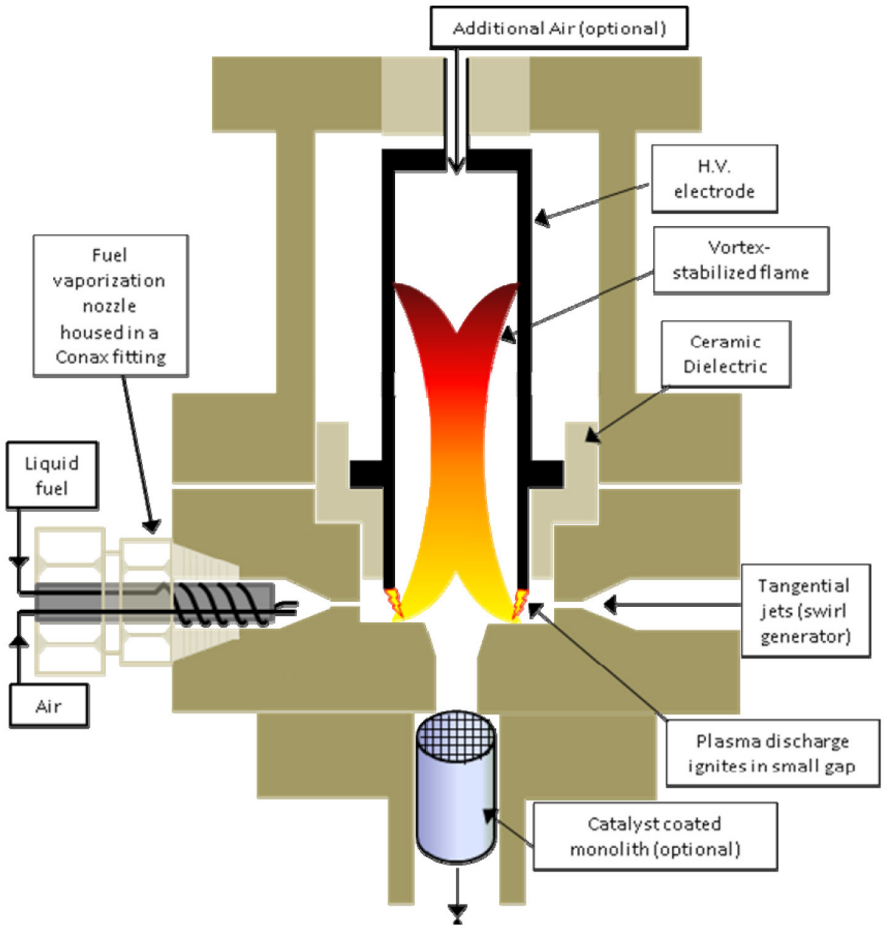

FIGURE 5. A Schematic of a New Type of Plasma Reformer Containing Specially Designed Atomization Nozzles for Precise Control of Reactant Temperatures

hydrocarbons. Future work will involve analyzing the types of light hydrocarbon species produced upon exposure to plasma and understanding the mechanisms for their formation. Large amounts of CH_4 were reported as one of the components of the LHCs, but 2% C_2H_4 and up to 1% C_2H_2 has also been reported. It is vital for SOFC performance targets that the formation of these olefin compounds be minimized. Understanding the plasma-chemical mechanisms occurring here may allow researchers to find optimal parameters to control the LHC species produced (i.e. use lower plasma current, and/or increase residence time in plasma zone).

FY 2010 Publications/Presentations

1. M.J. Gallagher, R. Geiger, A. Polevich, A. Rabinovich, A. Gutsol, A.A. Fridman, "On-Board Plasma-Assisted Conversion of Heavy Hydrocarbons into Synthesis Gas," Fuel, vol. 89:6, pp. 1187-1192, 2010.

2. M.J. Gallagher and A.A. Fridman, "Plasma Reforming for H_2-Rich Synthesis Gas," Fuel Processing for Fuel Cell Applications. Eds. D. Shekhawat, D. Berry, J.J. Spivey. Elsevier, in press.

References

1. A. Fridman, Plasma Chemistry. 2008, New York: Cambridge University Press. 978.

2. C.S. Kalra, A.F. Gutsol, and A. Fridman, "Gliding Arc Discharges as a Source of Intermediate Plasma for Methane Partial Oxidation," IEEE Transactions on Plasma Science, 2005. 33(1): p. 32.

3. H.L. Chen, H.M. Lee, S.H. Chen, Y. Chao, and M.B. Chang, "Review of Plasma Catalysis on Hydrogen Reforming for Hydrogen Production - Interaction, Integration, and Prospects," Applied Catalysis B: Environmental, 2008. 85: p. 1-9.

4. G. Petitpas, J.D. Rollier, A. Darmon, J. Gonzalez-Aguilar, R. Metkemeijer, and L. Fulcheri, "A Comparative Study of Non-Thermal Plasma Assisted Reforming Technologies," International Journal of Hydrogen Energy, 2007. 32(14): p. 2848-2867.

5. G.H. Dieckmann, "Nickel-Based Sulfur Resistant Reforming Catalyst with Radio-Frequency Coke Suppression," Presented at the SECA Diesel Fuel Processing Workshop, Pittsburgh, Pennsylvania, December 2005.

III.F.4 High-Methane Molten Carbonate Gasifier

Nicholas Siefert (Primary Contact),
Dushyant Shekhawat
U.S. Department of Energy
National Energy Technology Laboratory (NETL)
626 Cochrans Mill Road
Pittsburgh, PA 15236-0940
Phone: (412) 386-4404; Fax: (412) 386-6004
E-mail: Nicholas.Siefert@netl.doe.gov

Contract Number: 07-220611

Start Date: October 1, 2009
End Date: September 30, 2010

FY 2010 Objectives

- Construct a molten catalytic reactor for using molten alkali salts as steam-coal catalysts.
- Determine the kinetics of molten catalytic gasification of coal for a range of different alkali salt compositions, reactor temperatures and pressures.
- Determine the methane composition of the syngas for a range of different alkali salt compositions, reactor temperatures and reactor pressures.
- Conduct a literature review to determine the kinetics and compositions of previous molten salt reactors designed for gasifying coal and steam.

Accomplishments

- Completed design and fabrication of a molten catalytic reactor and associated experimental equipment.
- Began baseline testing of the reactor system.
- Completed literature review of molten catalytic gasification, surveying research from the Kellogg, the Rockwell International and the Esso Research and Engineering (Exxon) molten salt coal gasification processes.
- Published and presented results from literature review of "Integrating catalytic coal gasification with SOFCs" at the ASME Fuel Cell Science, Engineering & Technology Conference, Brooklyn, New York, June 2010.

Introduction

The United States (U.S.) currently uses coal to meet approximately 50% of its demand for electricity [1]. Almost all coal power plants currently in operation combust coal with air to provide the heat required to generate electricity in a Rankine vapor power cycle. The combustion process creates acid gases, greenhouse gases, and entrained particulates. Emissions of acid gases and particulates are currently regulated in the U.S. and the emission of greenhouses gases may soon be regulated. Current methods for capturing CO_2, NO_x, SO_x, and particulates from pulverized coal combustion (PCC) power plants cause decreased overall net energy efficiency and increased capital costs. The combination of these two effects causes the cost of electricity to increase compared with an unregulated coal power plant. The goal of future research on coal use should focus on generating electricity from coal with minimal air emissions and minimal water consumption in concert with decreasing the cost of electricity. As such, the DOE Office of Fossil Energy (FE) has set a 2015 energy goal of 60% electricity generation with greater than 90% capture and sequestration of greenhouse gases [2]. DOE/FE has also set a 2015 energy goal of multi-product capability, which includes co-generation of fuel/chemicals from a power plant during times of low electricity demand [2].

It appears that one of the only ways to achieve both of these goals is to integrate a catalytic coal gasifier with a solid oxide fuel cell (SOFC) [3-6]. Figure 1 shows a summary of different power plant designs that capture and compress >90% of the greenhouse gases generated produce electricity from coal. Integrated gasification fuel cell (IGFC) represents entrained-flow gasification followed by a 1 atm SOFC stack. Four cases of catalytic gasification are compared in Figure 1: 1 atm stack and no anode recycle to gasifier; 18 atm

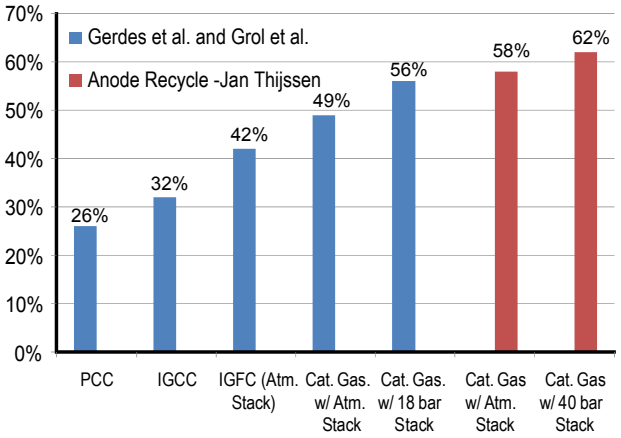

FIGURE 1. System efficiency for various configurations with carbon capture and compression to 150 atm. Of the four cases including catalytic gasification, two cases include anode recycle back to the gasifier and two cases include oxy-combustion of the anode tail gas.

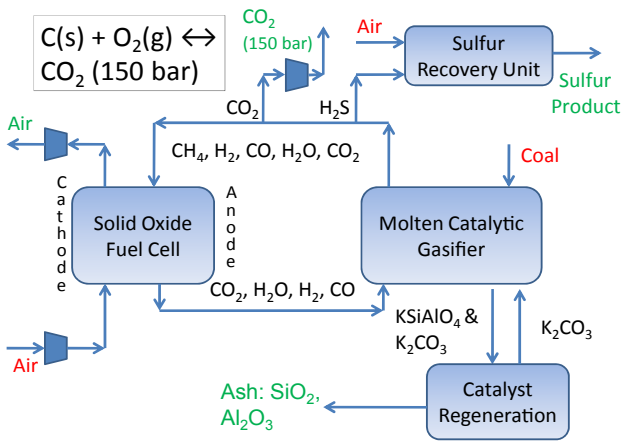

FIGURE 2. Molten catalytic gasification of coal integrated with a SOFC for an overall system efficiency near 60% and >90% capture of carbon dioxide.

stack with no anode recycle; 1 atm stack with anode recycle back to the gasifier; and 40 atm stack with anode recycle. Of the systems shown Figure 1, only the case that includes both anode recycle to the catalytic gasifier and pressurized operation of the fuel cell stack can reach DOE/FE 2015 Energy Goal of at least 60% overall system efficiencies. This overall system efficiency of 60% can be achieved if: a) the coal gasifier produces a syngas with a methane composition of roughly 25% on a dry volume basis; b) the methane-rich syngas is sent to a SOFC; and c) the off-gases from the SOFC are recycled back to coal gasifier (Figure 2). The overall generation of work (electricity) in the process described here (~60%) is larger than conventional IGFC processes (~42%) where available work is lost in entrained-flow, high-temperature coal gasification and in cooling a SOFC when the fuel is rich in hydrogen and low in methane. Some of the problems remaining before the "60% efficient/multi-product capable" process described above could be commercialized include scaling up each individual sub-system and reducing the cost of fresh catalyst or catalyst recovery.

Approach

The goal of NETL's research is to expand the operating range of molten salt gasifiers, compared with previous research by Esso Research and Engineering, Kellogg and Rockwell International in the 1970s [7-11] and compared with more recent work from Tokyo Institute and Nagoya University [12-13]. This will be done by lowering the temperature of the reactor by using eutectic (mixed) alkali salts and by lowering the pressure so as to improve integration with SOFCs that operate at or just above atmospheric pressures. Our goal is to operate a molten catalytic gasifier at pressures near 20 atm. This pressure was chosen as a balance between increased methane production at higher pressures and increased costs of associated turbines (to let down the pressure) and compressors (to compress the anode off-gas back to the pressure of the catalytic gasifier).

From a thermodynamic point of view, in order to operate at lower pressure and achieve at least 20% composition of methane in the syngas, the temperature of the reactor must be lowered. However, in order to maintain comparable kinetics, the use of pure potassium salts catalysts must be replaced with the use of eutectic alkali salt mixtures (sodium, potassium and lithium carbonates). The eutectic alkali salt mixture has a lower melting temperature, allowing the catalyst to be active at lower temperatures than pure potassium carbonate [14].

Potassium carbonate/hydroxide was found to catalyze both the steam-carbon reaction ($C+H_2O \leftrightarrow CO+H_2$) and the methanation reaction ($CO+H_2 \leftrightarrow \frac{1}{2}CH_4+\frac{1}{2}CO_2$) [14-15], whereas sodium carbonate/hydroxide was found to only catalyze the steam-carbon reaction. Figure 3 is a qualitative energy diagram showing the two-step process for generating methane from carbon. It is expected that mixtures of sodium, potassium and lithium carbonates should have the capability to catalyze the methanation reaction when there is a sizable portion of potassium in the mixture (>20%), and this will be one of main areas of experimental research because, to the best of our knowledge, there is no previous published literature on using molten carbonate eutectic mixtures for generating high methane content syngas.

In order to determine how to increase the reaction kinetics and increase methane composition without increasing the cost of catalyst use, a range of different experiments will be conducted using various alkali salt compositions, reactor temperatures and reactor pressures. In all cases, the kinetics of molten catalytic gasification of coal will be measured as well as the methane composition in the syngas. This research is required in order to determine whether the costs associated with catalytic steam-coal gasification can be decreased through the use of molten alkali salt mixtures.

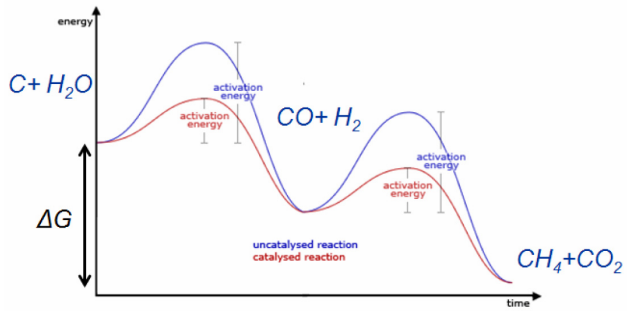

FIGURE 3. Gibbs free energy diagram vs. the reaction coordinate for the reaction of carbon and steam to methane and carbon dioxide (qualitative).

Results

NETL Office of Research and Development (ORD) has constructed a new molten catalytic reactor along with associated equipment required for operation of the reactor. This includes connecting together and testing all equipment, such as furnace heaters, controllers, flow meters, pressure regulators, pumps, steam generators, and diagnostic tools for syngas composition measurements. The reactor was designed for proof-of-concept scale in order to demonstrate the production of high methane-content syngas for SOFC applications. The reactor has successfully passed the required pressure checks and baseline testing of the system has been initiated. The reactor system and associated equipment are shown in Figure 4.

During thermodynamic modeling of the catalytic gasifiers, we determined that anode gas recycle to the gasifier has two significant benefits: a) increases overall efficiency of the process; and b) allows for autothermal operation of the catalytic gasifier. While the reaction of steam and carbon to make methane and carbon dioxide ($C+H_2O \leftrightarrow \frac{1}{2}CH_4+\frac{1}{2}CO_2$) is slightly exothermic, the steam gasification of coal to hydrogen and carbon monoxide reaction is quite endothermic. We found that if coal is reacted with steam, carbon dioxide, or a mixture of the two, then the operation of the catalytic gasifier is endothermic unless the temperature of the gasifier is below 523°C (Figure 5 for operation at 30 atm). This means that the gasifier would have to be heated externally in order to operate continuously at the temperatures required kinetically (700°C). However, the operation of a catalytic gasifier becomes slightly exothermic (for 700°C, 30 atm operation) if the coal is reacted with anode syngas that is incompletely combusted (Figure 6). If roughly 30% of the recycle gas

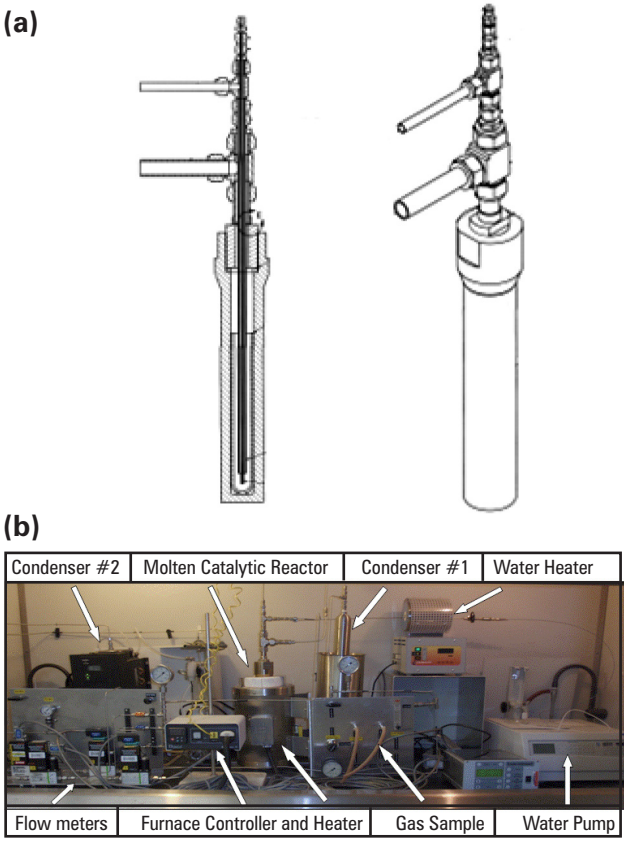

FIGURE 4. Molten catalytic reactor. a) design and b) laboratory experiment. Steam and coal react in a bed of molten alkali salts. The reactor is designed for a maximum pressure of 25 atm and temperature of 900°C.

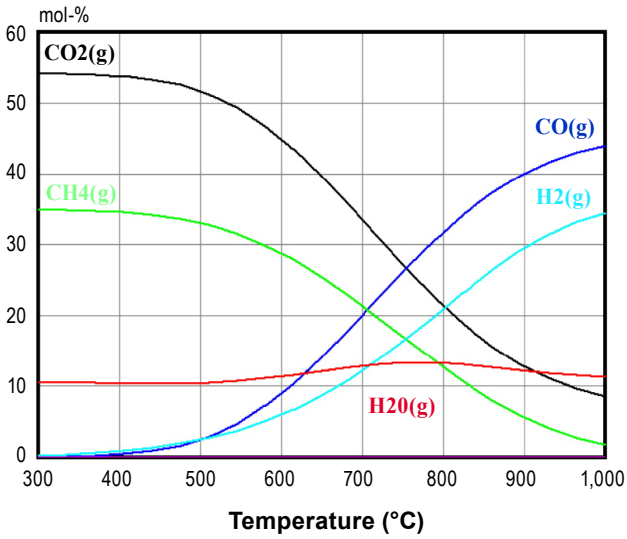

FIGURE 5. Thermodynamic equilibrium at 30 atm pressure for $C_{14}H_{10}(s) + 14\ H_2O(g) + 7\ CO_2(g)$. Autothermal operation corresponds to a temperature of 523°C.

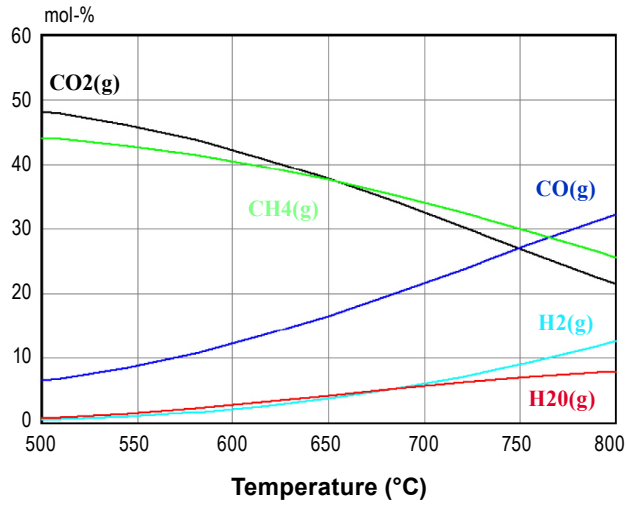

FIGURE 6. Thermodynamic equilibrium at 30 atm pressure for $C_{14}H_{10}(s) + 10\ H_2O(g) + 4\ H_2(g) + 5\ CO_2(g) + 2\ CO(g)$. Autothermal operation corresponds to a temperature of 700°C.

is incompletely combusted, such as 30% H_2/70% H_2O instead of 100% H_2O, then the exothermic reaction of hydrogen and carbon to form methane is sufficient to offset the endothermic steam gasification reactions. While initial experiments with molten alkali catalysts will be conducted using just steam and coal, future experiments will be conducted using coal with simulated anode recycle gases in order to simulate conditions that generate the highest overall system efficiency [3-4] and to simulate autothermal operation of the catalytic gasifier.

Conclusions and Future Directions

NETL/ORD has successfully built an experimental lab to measure the kinetics of catalytic coal gasification using molten alkali carbonate salts and to measure the composition of methane in the syngas. The goal for the next year is to conduct experiments with eutectic mixtures of sodium, potassium and lithium salts in order to lower the operating temperature compared with previous experimental studies. If the experiments produce the desired methane-composition and kinetic rates, then the results will be integrated into a full systems study using Aspen Plus® in order to determine overall efficiency, water consumption and air emissions. If the results from the systems studies are promising, then experiments will be conducted to test methods of minimizing the cost associated with the recovery of the alkali catalysts.

FY 2010 Publications/Presentations

1. Peer-Reviewed Publication: N. Siefert, D. Shekhawat, T. Kalapos, and D. Berry, "Integrating Catalytic Coal Gasifiers with Solid Oxide Fuel Cells," ASME Fuel Cell Science, Engineering & Technology Conference, Brooklyn, New York, June 2010.

2. Presentation: N. Siefert, D. Shekhawat, T. Kalapos, and D. Berry, "Integrating Catalytic Coal Gasifiers with Solid Oxide Fuel Cells," ASME Fuel Cell Science, Engineering & Technology Conference, Brooklyn, New York, June 2010.

References

1. U.S. Department of Energy, Energy Information Administration, International Energy Outlook 2006, DOE/EIA-0484 (2006).

2. W.A. Surdoval, 2008, "Clean Economic Energy in a Carbon Challenged World," Presentation at 2008 International Pittsburgh Coal Conference, September 30, 2008.

3. M. Li, A.D. Rao, J. Brouwer, and G.S. Samuelsen, 2010, "Design of Highly Efficient Coal-Based Integrated Gasification Fuel Cell Power Plants," J Power Sources, 195(17), pp. 5707-5718.

4. J. Thijssen, 2008, "Coal System Studies: Effects of Methane Content and High-Efficiency Catalytic Gasification," 2008 SECA Conference Proceedings.

5. K. Gerdes, E. Grol, D. Keairns, and R. Newby, 2009, "Integrated Gasification Fuel Cell Performance and Cost Assessment: DOE/NETL-2009/1361."

6. E. Grol and J. Wimer, 2009, "Systems Analysis of an Integrated Gasification Fuel Cell Combined Cycle: DOE/NETL - 40/080609."

7. R.L. Hirsch, J.E. Gallagher, R.R. Lessard, and R.D. Wesselhoft, 1982, "Catalytic Coal-Gasification - an Emerging Technology," Science, 215(4529), pp. 121-127.

8. C.A. Trilling, 1977, "Mass and Heat Balance for Coal-Gasification by Atomics Internationals Molten-Salt Gasification Process," Abstr Pap Am Chem S, 173(Mar20), pp. 17-17.

9. A.E. Cover, W.C. Schreine, and G.T. Skaperda, 1973, "Coal Gasification - Kelloggs Coal Gasification Process," Chem Eng Prog, 69(3), pp. 31-36.

10. C.A. Kumar, L.D. Fraley, and S.E. Handman, 1975, "Combined Power Cycle Using Low Btu Gas Produced from Kellogg Molten-Salt Coal Gasification Process," Abstr Pap Am Chem S, 170(Aug24), pp. 39-39.

11. C.L. Aldridge and D. Buben, "Production of Methane Rich Gases," U.S. Patent # 3,689,240, assigned to Esso Research and Engineering Co., September 5, 1972.

12. J. Matsunami, S. Yoshida, Y. Oku, O. Yokota, Y. Tamaura, and M. Kitamura, 2000, "Coal Gasification with CO_2 in Molten Salt for Solar Thermal/Chemical Energy Conversion," Energy, 25(1), pp. 71-79.

13. G. Jin, H. Iwaki, N. Arai, and K. Kitagawa, 2005, "Study on the Gasification of Wastepaper/Carbon Dioxide Catalyzed by Molten Carbonate Salts," Energy, 30(7), pp. 1192-1203.

14. A. Sheth, Y.D. Yeboah, A. Godavarty, Y. Xu, and P.K. Agrawal, 2003, "Catalytic Gasification of Coal Using Eutectic Salts: Reaction Kinetics with Binary and Ternary Eutectic Catalysts," Fuel, 82(3), pp. 305-317.

15. N.C. Nahas, 1983, "Exxon Catalytic Coal-Gasification Process - Fundamentals to Flowsheets," Fuel, 62(2), pp. 239-241.

III.F.5 Novel Water-Neutral Diesel Fuel Processor and Sulfur Trap

Subir Roychoudhury (Primary Contact), Christian Junaedi, Jeff Weissman and Dennis Walsh
Precision Combustion, Inc. (PCI)
410 Sackett Point Rd.
North Haven, CT 06473
Phone: (203) 287-3700 ext. 267; Fax: (203) 287-3710
E-mail: sroychoudhury@precision-combustion.com

DOE Project Manager: Joseph Stoffa
Phone: (304) 285-0285
E-mail: Joseph.Stoffa@netl.doe.gov

Contract Number: 84674

Start Date: August 15, 2008
End Date: August 14, 2010

FY 2010 Objectives

- Evaluate operational conditions, reactor performance, and catalyst durability of the autothermal reformer (ATR) operation under a water-neutral condition with water recovery via condensation or direct anode recycle approach.
- Further develop and optimize the low pressure drop fuel injector/nozzle to permit stable steady-state operation, cold start-up, and 5:1 turndown ratio. Map ATR performance with the low pressure drop nozzle and show coking avoidance with complete fuel conversion to C1 products and ~85% reforming efficiency while operating the reformer with low water usage.
- Compare different catalyst options and evaluate their performance to determine the optimal catalyst for reforming application to meet commercially viable auxiliary power unit (APU) system targets.

Accomplishments

In the second budget period of this two-year Phase II project, the operating conditions of the proposed water recovery approaches have been optimized and the reactor performance has been extensively characterized and evaluated. A durability test was performed to demonstrate stable catalyst performance under a water-neutral condition using simulated anode gas recycle (AGR) mixture. The feasibility of water-neutral operation via condensation of anode tail gas was also demonstrated. Operation of the fuel processor system integrated with stacks was demonstrated.

- **Evaluated and optimized direct anode recycle approach for water neutrality**: Performance mapping of a Microlith®-based fuel reformer has been completed with Tier II diesel to evaluate and optimize operating conditions using anode recycle approach for water recovery and water neutrality. Stable reformer operation was demonstrated. The reformate gas composition obtained experimentally was in good agreement with that obtained via ASPEN thermodynamic analysis.
- **Demonstrated feasibility of water-neutral operation via condensation approach**: An alternative approach to water-neutral operation using a condenser system was also demonstrated. Tests were performed to validate the maximum achievable water recovery from anode exhaust at different ambient/cooling air conditions and to compare experimental results with the predicted values. Test results indicated that sufficient amount of water can be recovered to allow for Microlith®-based fuel reformer operation under a water-neutral condition even in extremely hot weather conditions.
- **Further developed, optimized, and tested low pressure drop nozzle**: Tests were performed to study the spray pattern of the nozzle to ensure uniform reactant mixing and good atomization. Additional tests with a fuel reformer are ongoing to evaluate the reactor performance and durability during operation with Tier II diesel under a water-neutral condition. Preliminary results showed stable catalyst temperature profile and capability of cold-start with 5-to-1 turndown.
- **Developed coating technique for an alternative National Energy Technology Laboratory (NETL) catalyst and performed diesel ATR reforming**: A formulation was specifically developed to coat an alternative NETL catalyst on the Microlith® substrate for fuel reforming. Results from catalyst testing demonstrated potential for a low-cost, highly efficient reformer system that can accomplish complete fuel conversion and high reforming efficiency for reformation of diesel fuel.

Introduction

Fuel cell technology for auxiliary power or hybrid vehicle range extension offers the potential for major contributions towards long term DOE missions objectives of clean energy, efficiency, and independence. Yet fuel cell technology faces daunting entry barriers, notably including high unit costs amidst low sales volume as well as the absence of a hydrogen fueling

infrastructure. Thus, reforming of liquid fuels to produce hydrogen for fuel cell stacks is a practical approach for operating fuel cells due to the high energy density and the infrastructure availability. However, key barriers for the Solid State Energy Conversion Alliance industrial teams are the lack of a compact and economical diesel fuel processor capable of operating with long-term stability under a water-neutral condition (i.e., very low steam to carbon ratios) while being resistant to coke formation and sulfur poisoning. Fuel preparation for these reformers also remains problematic primarily due to the lack of good mixing at low air-pressure drop and resultant reactor non-uniformities leading to coke formation, among other things.

PCI is developing ultra-compact and sulfur-tolerant Microlith® fuel processor technology to reform conventional fuels such as diesel, gasoline, and liquid biofuels to the sulfur-free, hydrogen-rich fuels required by high temperature proton exchange membrane and SOFCs. By avoiding the need for a hydrogen fueling infrastructure, PCI's technology offers a major step advance towards a vital, self-sustaining American fuel cell industry. In this DOE Small Business Innovation Research Phase II, PCI has demonstrated this technology, along with improved catalyst effectiveness, demonstrated water-neutral operation, and substantially improved fuel injection pressure drop without performance loss, reducing parasitic losses of the overall system. The resulting fuel processor enables fuel cell use of selected conventional fuels including medium sulfur Jet Propellant 8 (JP-8) and ultra-low sulfur diesel (ULSD)/medium sulfur diesel. This system and balance-of-plant simplification will allow for cost optimization to meet commercially viable targets for the entire APU fuel cell system.

Approach

Reformer operation under water-neutral or waterless condition by avoiding the need for external water addition is a significant requirement for practical portable systems. Moreover, lower water usage can lead to faster start-up times, as less water needs to be vaporized at start-up. The reduction/elimination of water usage, however, can result in higher peak temperatures within the reactor/catalyst bed and can increase the production of higher hydrocarbons, particularly olefins, in the reformate stream. The former can compromise catalyst durability while the latter increases the likelihood of coking in the fuel cell stacks. It is important, therefore, to demonstrate long-term reformer operation at water-neutral condition using feasible water recovery approaches without catalyst degradation and coke formation.

The proposed concept being developed in this project builds upon PCI's Microlith® reforming technology which employs a mesh-based, short contact time catalyst as an integrated component of a novel reformer system involving fuel injector, reactor, steam generator, and sulfur trap. PCI's existing 5 kW_{th} system size is approximately 5 liters and weighs about 5 kg. This reactor starts up in partial oxidation mode and then transitions to ATR mode upon introduction of steam, operating at low steam-to-carbon ratios. It uses a limited amount of water that can be recovered from the system exhaust, either via a direct recycle approach or a condenser approach, while performing efficient fuel reformation without performance degradation and coke formation. Since the reformer is operated at very low steam-to-carbon ratios, sulfur compounds are readily adsorbed in a downstream desulfurizer bed. Appropriate thermal integration of the reformer, fuel cells, water recovery unit, and other balance-of-plant components in the APU system is also necessary to maximize the overall system efficiency and has been explored using ASPEN process simulation software.

Results

Key results from the second budget period of this Phase II project include: 1) the successful demonstration of fuel processor operation under water-neutral condition using direct anode recycle approach; 2) the validation of feasibility of water recovery via condensation approach for water-neutral operation of PCI's reformer; and 3) the development of low pressure drop nozzle that gave stable reformer performance for 5 kW_{th} operation.

Reformer Operation with Anode Recycle Gas for Water Neutrality

During Fiscal Year 2009, the feasibility of using PCI's Microlith® reactor to perform ATR operation using water from a simulated AGR mixture was demonstrated. During those tests, however, the steam-to-carbon (S/C) ratio was kept at >1.0, resulting in a more kinetically-limited reaction. The presence of steam as well as inerts (i.e., N_2 and CO_2) in the simulated AGR stream also quenched the catalyst bed, resulting in the presence of C2s (i.e., ethane and ethylene) and C3s (i.e., propane and propylene) in the reformate stream. This reduced the H_2 yield.

In order to optimize the operating conditions and to avoid C2s and C3s formation while operating the ATR reformer using a simulated AGR mixture, a more representative test setup simulating actual anode recycle was designed and built for performing a more extensive ATR test using the AGR approach. The test rig was equipped with the necessary mass flow controllers for simulating AGR mixture composition that consists of H_2, CO, CO_2, N_2, and steam. Additionally, an external steam generator and an electric heater were installed to

control the inlet mixture temperature prior to entering the reformer.

In these tests, the reactor was started under dry catalytic partial oxidation condition (i.e., waterless operation) by flowing ULSD (i.e., Tier II diesel containing 10 ppm_w sulfur) and air, and then transitioned to an ATR mode by introducing the AGR mixture consisting of H_2O along with H_2, CO, and inerts (based upon stack fuel utilization). As the AGR mixture, consisting of steam as well as CO_2 and N_2 inerts, was introduced to the reformer, the catalyst bed temperature decreased substantially and thus the air flow rate had to be increased accordingly. The performance map was developed by operating the reformer at different S/C ratios and AGR mixture temperatures. A slip stream was taken from the outlet of the reformer for gas chromatography analysis to measure the reformate gas composition. The experimental data showed that the reformate gas compositions obtained experimentally were in good agreement with those obtained via thermodynamic analysis.

Finally, a 50-hour ATR durability test using the AGR approach with Tier II diesel as fuel was performed at a S/C ratio of 0.7 and AGR mixture temperature of 400°C. The oxygen-to-carbon ratio was kept constant at ~1.24 to maintain the optimum reactor peak temperature throughout the test. The temperature profile of the catalyst bed was stable during the 50-hour test without any temperature excursions or catalyst deactivation due to sintering and coking. Here, the S/C ratio was defined as the molar ratio between the steam in the AGR mixture and the carbon in the inlet fuel and the O/C ratio was defined as the molar ratio of the oxygen atom in the feed air to the carbon in the inlet fuel.

Table 1 lists the operating condition and the average reformate composition (mole %, dry basis) obtained from the 50-hour ATR durability testing with AGR approach at S/C of 0.7 and AGR mixture temperature of 400°C. An equilibrium product composition obtained from the ASPEN modeling at the same operating condition is also listed for comparison. Table 1 indicated that the test results were in good agreement with equilibrium at those conditions as predicted by ASPEN.

TABLE 1. Operating condition and average reformate composition (mole %, dry basis) obtained from the 50-hour durability testing at S/C of 0.7 and inlet mixture temperature of 400°C. The conditions and result obtained from the ASPEN modeling are also listed for comparison.

	50-hour average	ASPEN model
O/C ratio	1.24	1.25
Component	**Conc. (mole %, dry basis)**	
H_2	12.4	12.4
CO	14.8	15.3
CO_2	12.6	10.9
N_2	60.2	61.4
CH_4	0.02	0

Water Recovery via Condensation Approach for Water Neutrality

An alternative approach to water recovery using a condenser unit was also demonstrated. Tests were performed to evaluate the maximum achievable water recovery from anode exhaust at different ambient/cooling air conditions and to compare experimental results with the predicted values. The goal of the tests was to assess the feasibility of collecting sufficient amount of water using a condensation approach to allow fuel reformer operation under a water-neutral condition.

The anode exhaust composition and flow rate were calculated using ASPEN modeling by implementing several assumptions based on the available SOFC stack data provided by a stack manufacturer. In these tests, steam was generated using an external steam generator and was mixed with H_2, CO, CO_2, and N_2 to simulate anode exhaust gas mixture. The temperature of the simulated anode exhaust was adjusted using an electrical heater to obtain the desired value. Flows of various gaseous components and the liquid water were controlled using mass flow controllers. Cooling air through the condensing heat exchanger fins was provided by an integrated fan with a constant flow. The ambient temperature around the condenser unit and the integrated cooling fan was adjusted using heat guns.

Several 3-hour tests were carried out to develop performance maps by varying the anode gas mixture temperature (100-800°C) and the ambient/cooling air temperature (20-50°C). At the end of each test, the water recovery (i.e., the ratio of water collected to the amount of water input) was calculated and the water mass balance was validated. Figure 1 shows the water recovery obtained from testing the condenser unit at different ambient/cooling air temperature. The maximum theoretical water recovery obtained from thermodynamic calculation is also included. In these tests, the temperature of the anode gas mixture entering the condenser unit was maintained at ~800°C and the water content was fixed at 32%. Test results indicated that as the ambient/cooling air was increased from 20°C to 50°C, the water recovery decreased from 93% to 65%. The experimental values were slightly below the maximum theoretical recovery. ASPEN modeling study of the integrated ATR-SOFC system operating at 75% fuel utilization indicated that 60% water recovery would be sufficient to provide the required amount of water for PCI's ATR operation at 5 kW_{th} with Tier II diesel. Indeed, test results validate the feasibility of water recovery via condensation approach for water-neutral operation of PCI's reformer.

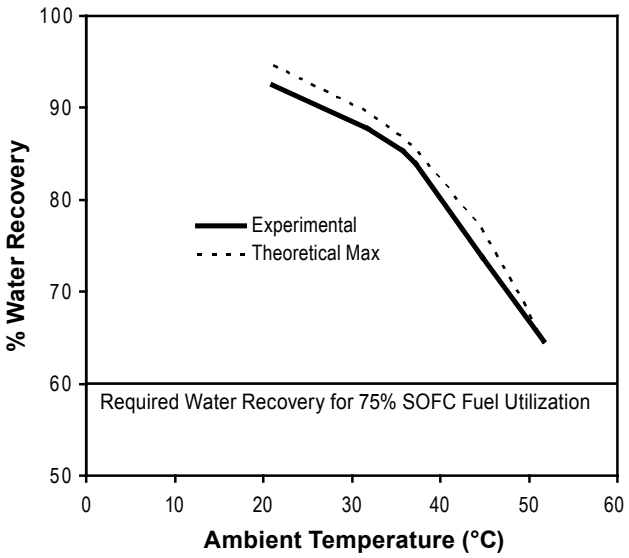

FIGURE 1. Percent water recovery as a function of ambient temperature obtained experimentally with anode gas mixture entering the condenser unit at ~800°C. The maximum theoretical water recovery is also included for comparison.

Development of a Low Pressure Drop Fuel Injector

A critical challenge for on-board fuel reforming is the use of low air pressure drop nozzles which allow uniform mixing of fuel, air and steam prior to entering the reactor. While lower pressure drop reduces parasitic losses, it generally compromises mixture quality, resulting in higher peak temperatures due to local unmixedness and higher propensity for catalyst deactivation due to sintering and coke formation. In this Phase II effort, PCI has successfully developed a novel low pressure nozzle and is also capable of cold-start with 5-to-1 turndown. This result is significant because it reduces parasitic power requirements significantly while providing more uniform flow over wide operating range.

Currently, additional tests with a fuel reformer are ongoing in order to evaluate the reactor performance and durability during operation with Tier II diesel under a water-neutral condition. Preliminary results showed stable catalyst temperature profile. More tests will be performed to fully characterize and optimize reactor operating conditions, and to evaluate durability of the nozzle and the catalyst.

Development of an Alternative NETL Catalyst for Water-Neutral Diesel Reformation

With fuel processor technology drawing substantial commercial interest, fuel processor costs in manufacture need to be substantially reduced to help fuel cells achieve economic viability compared to alternatives such as internal combustion gensets. The use of expensive precious metal catalysts in the reformer and fuel cell system mainly determines the high cost of this technology. Thus, it is key to develop a highly selective, sulfur tolerant multifunctional reforming catalyst for reformation of logistics fuels at low cost.

In Phase II, PCI synthesized, tested, and evaluated two different catalyst formulations for water-neutral diesel reformation: PCI's catalyst formulation and an alternative NETL catalyst coated on Microlith® substrate. A formulation was specifically developed to coat the alternative NETL catalyst on the Microlith® substrate. NETL has been developing this alternative reforming catalyst for some time for its potential in diesel processing. Results from testing the NETL catalyst demonstrated potential for a low cost, highly efficient reformer system that can accomplish complete fuel conversion and >80% reforming efficiency for reformation of diesel fuel. Based in part on that assessment, the NETL catalyst has been submitted as a potential research and developlment 100 innovation candidate.

Conclusions and Future Directions

PCI has demonstrated diesel ATR operation under a water-neutral condition using both direct anode recycle approach and condensation approach for recovering exhaust water. The operating conditions of the proposed water recovery approaches have been optimized and the reactor performance has been extensively characterized and evaluated. A durability test was performed to demonstrate stable catalyst performance under a water-neutral condition using simulated AGR mixture. Test results from this direct AGR approach indicated stable reformer performance without the presence of coke precursors or higher hydrocarbons in the reformate stream. The product gas composition obtained experimentally was in good agreement with that obtained via ASPEN thermodynamic analysis. For the condensation approach, test results showed that sufficient amount of water could be recovered to allow for Microlith®-based fuel reformer operation under a water-neutral condition.

PCI has also successfully developed and tested a novel low pressure nozzle prototype that operates with Tier II diesel (at 5 kW_{th} operation), and is also capable of cold-start with 5-to-1 turndown. This result is significant because it reduces parasitic power requirements of the APU system while providing more uniform flow over wide operating range. Finally, alternative NETL catalysts were evaluated in order to develop a highly selective, sulfur tolerant multifunctional reforming catalyst for reformation of logistics fuels at low cost. Results from preliminary catalyst testing demonstrated potential for a reduced cost, highly efficient reformer system that can accomplish complete fuel conversion and >80% reforming efficiency for reformation of diesel fuel. Further catalyst development and tests are ongoing

to characterize and optimize reformer performance and durability.

In summary, PCI has demonstrated a novel fuel reformer technology, along with improved catalyst effectiveness, demonstrated water-neutral operation, and substantially improved fuel injection pressure drop without performance loss, reducing parasitic losses of the overall system. The resulting fuel processor enables fuel cell use of widely available conventional fuels including medium sulfur JP-8 and ULSD/medium sulfur diesel.

FY 2010 Publications/Presentations

1. 2010 Power Sources Conference in Las Vegas, Nevada.

2. 2010 DOE SECA Meeting in Pittsburgh, Pennsylvania.

3. Abstract accepted for 2010 American Chemical Society meeting in Boston, Massachusetts.

4. Abstract accepted for 2010 Fuel Cell Seminar in San Antonio, Texas.

III. SECA CORE RESEARCH & DEVELOPMENT

G. Modeling and Simulation

III.G.1 Advanced Power Conditioning System Technologies for High-Megawatt Fuel Cell Power Plants

Allen R. Hefner, Jr.
National Institute of Standards and Technology (NIST)
100 Bureau Dr.
Gaithersburg, MD 20899
Phone: (301) 975-2071
E-mail: hefner@nist.gov

DOE Project Manager: Maria Reidpath
Phone: (304) 285-4140
E-mail: Maria.Reidpath@netl.doe.gov

Contract Number: 43042

Start Date: October 1, 2006
Project End Date: September 30, 2010

FY 2010 Objectives

- Identify advanced technologies that may significantly reduce the cost of the power conditioning systems (PCS) required for future high-megawatt fuel cell power plants.
- Determine fuel cell power plant PCS performance requirements, including requirements for fuel cell module interface and for Smart Grid interconnection.
- Develop simulation models for advanced PCS architectures, circuit topologies, and component technologies and perform simulations required to determine overall cost and performance benefits of advanced technologies.
- Coordinate related industry and federal government programs to enable the development of advanced high-megawatt PCS technologies necessary to meet the Solid State Energy Conversion Alliance (SECA) high-megawatt fuel cell power plant PCS goals.

Accomplishments

- Several High-Megawatt Power Converter Technology R&D Workshops have been convened at NIST since 2007 resulting in considerable consensus being reached on technology development needs for high-megawatt PCSs across a broad range of applications.
- The Interagency Advanced Power Group (IAPG) Electric Systems Working Group (ESWG) was reestablished to serve, in part, as an umbrella organization for coordination of federal programs in high-megawatt PCS technology. Several IAPG ESWG meetings have been held each year since 2007 and coordination is occurring on development of core high-megawatt PCS technologies.
- Considerable progress has been made in developing and demonstrating advanced high-voltage and medium-voltage SiC power devices that have the potential to enable significant cost reduction for high-megawatt PCSs.
- Simulation models for advanced PCS architectures, circuit topologies, and component technologies have been developed to verify the interactions between components to perform technology impact evaluations.

Introduction

High-megawatt PCSs are required to convert the low voltage power produced by fuel cell modules in central station-scale plants to the very much higher voltage levels required for delivery to the grid. The SECA power plant PCS cost goal of $40-$100/kW is generally recognized as a difficult stretch goal that cannot be met with today's technology. To address this challenge, DOE and NIST have entered into an interagency agreement to have NIST lead an effort to evaluate various advanced technology options for the PCSs and to identify technologies requiring development to meet the cost and efficiency goals of SECA central station fuel cell power plants.

Approach

This project aims to identify and enable development of advanced PCS architectures, circuit topologies, and component technologies that may significantly reduce the life cycle cost of the SECA central station fuel cell power plant. Various PCS approaches that focus on the use of advanced technologies for low-, medium-, and high-voltage architectures are considered. The advanced component technologies being considered include advanced power semiconductor devices made with the SiC material, advanced nano-crystalline magnetic materials for filters and transformers, advanced capacitor technologies, advanced power electronic component cooling systems, and modular power electronic package and interconnect approaches.

Each PCS approach is being evaluated for its ability to meet the performance requirements of the fuel cell power plant including requirements for interfacing to

fuel cell modules and for Smart Grid interconnection, as well as the cost of constructing and maintaining the PCS. The cost and performance estimates are made using tabular spreadsheet calculations where detailed circuit simulations are used to verify and refine the component interaction and system performance impacts used in the spreadsheet calculations. The project thus requires the development and validation of simulation models for advanced PCS architectures, circuit topologies, and component technologies.

Development and evaluation of the impact of advanced PCS technologies requires input from, and coordination with, the broad power electronics community. To initiate this interaction and to review the approach being used for the NIST/DOE Advanced High-Megawatt PCS Technology Impact Analysis, the first High-Megawatt Converter Workshop was held at NIST headquarters (in Gaithersburg, MD) on January 24, 2007 [1]. During the workshop, a consensus was reached on the parameters of the technology impact analysis. The participants of the workshop also agreed that a federal interagency task group for high-megawatt power converter technologies could play an important role in this area and that an industry roadmap process should be initiated to offer guidance for further development of more cost-effective and efficient PCSs.

Results

In response to the recommendations of the first High-Megawatt Converter Workshop held on January 24, 2007, an ongoing industry roadmapping process has been established involving periodic High-Megawatt Power Converter Technology R&D Roadmap Workshops convened at NIST, and an ongoing coordination and roadmapping process between federal government agencies has been established involving periodic meetings of the IAPG ESWG organized and led by NIST. As a result, considerable consensus has been achieved on the approach and goals of the NIST/DOE Advanced High-Megawatt PCS Technology Impact Analysis effort and considerable coordination has occurred between the organizations developing technologies necessary to meet the goals. Significant progress has been made in developing new advanced high-megawatt PCS technologies and in developing models for evaluating the impact of the new technologies in various PCS application.

Industry Roadmap on High-Megawatt PCS: The participants of the first High-Megawatt Converter Workshop that was held on January 24, 2007 agreed that an industry roadmapping process should be initiated to offer guidance for further development of PCSs that could meet the requirements for more cost-effective and efficient power conversion. A number of workshops have been convened at NIST since 2007 to coordinate the various activities in this area including the following (see Reference [1]):

- High-Megawatt Converter Workshop (January 24, 2007): goals included identifying technologies requiring development to meet DOE SECA PCS goals and to discuss approaches for achieving necessary technology development.
- High-Megawatt PCS Industry Roadmap Workshop (April 8, 2008): goals included initiating a roadmap process to offer guidance for further development of high-megawatt converter technology.
- National Science Foundation (NSF) Workshop on Advanced Power Conditioning for Alternate Energy Systems (May 15-16, 2008): goals included establishing power electronics curriculums and fundamental research programs for alternate energy power converters.
- Future Large CO_2 Compressors Workshop (March 30-31, 2009): goals included prioritizing research and development (R&D) gaps for future CO_2 compression systems at large central coal and natural gas plants.
- High Penetration Electronic Generators (December 11, 2009): goals included identifying the high-megawatt PCS technologies and manufacturing infrastructure required to achieve the goals of high penetration of renewable/clean energy systems.

Interagency Task Group on High-Megawatt PCS: The participants of the first High-Megawatt Converter Workshop that was held on January 24, 2007, agreed that a federal interagency task group for high-megawatt power converter technologies could play an important role in this area. It was also suggested that the IAPG would be a good organization to host such a task group. Subsequently during the IAPG Strategic Planning Meeting on April 3, 2007, the IAPG agreed that a reinitiated IAPG ESWG could serve, in part, as an umbrella organization for the High-Megawatt PCS Interagency Task Group. A number of meetings of the IAPG ESWG have been organized and chaired by NIST each year since 2007 resulting in significant progress on an interagency power electronics roadmap as well as the initiation of several new technology development programs that are coordinated with the NIST/DOE Advanced High-Megawatt PCS Technology Impact Analysis effort.

Advanced PCS Technology Impact Analysis: During the first High-Megawatt Converter Workshop in 2007, various aspects of the NIST/DOE Advanced PCS Technology Impact Analysis effort were reviewed including: the overall approach of the study, the current and voltage boundary conditions, the Smart Grid interconnection requirements, the fuel cell current regulation and ripple requirements, as well as, the topology and component technologies being considered

by the study. An 18 kV alternating current (AC) plant collection/distribution bus was chosen for the initial study because it is similar to that being considered for integrated gasification combined cycle gas turbine plants where central station fuel cell power islands may be tested.

Various approaches were evaluated that focus on the use of advanced technologies for low-, medium-, and high-voltage architectures to convert the unregulated direct current (DC) power produced by the fuel cell modules to that required for the 18 kV AC plant distribution. Figure 1 shows an example of a low- and high-voltage architecture for discussion, and Figure 2 shows the initial cost estimates for selected medium- and high-voltage inverter architectures and component technologies. The cost estimates in Figure 2 are based upon component selection and circuit performance being validated and refined using simulations. The following cost stretch goals are also used for the future component technologies including SiC devices and advance magnetic materials to determine the cost breakpoints for the new technologies:

- 1.2 kV Schottky diodes: $0.2/A
- 12 kV Schottky diodes: $1/A
- 12 kV half-bridge SiC metal-oxide-semiconductor field-effect transistor (MOSFET)/SiC-Schottky: $10/A
- 15 kV SiC-PiN: $0.4/A
- 15 kV SiC-insulated gate bipolar transistor (IGBT)/ SiC-PiN module: $3.3/A

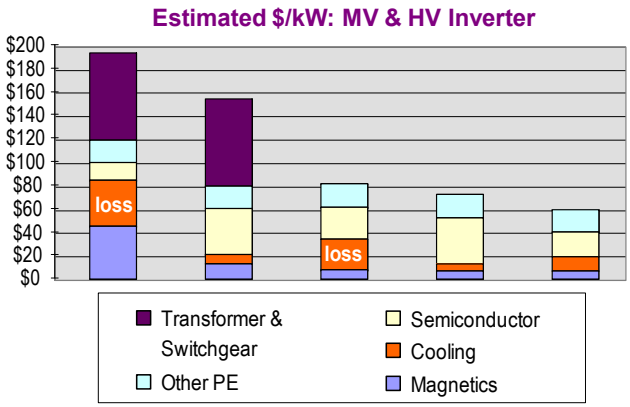

Inverter Voltage	Medium	Medium	High	High	High
HV-SiC Diode		Schottky	Schottky	Schottky	PiN
HV-SiC Switch		MOSFET	MOSFET		IGBT
HF Transformer	Nano	Nano	Nano	Nano	Nano
60 Hz Transformer	yes	yes			

Risk Level: Low | Moderate | Considerable | High

FIGURE 2. Initial cost estimates for selected medium- and high-voltage PCS architectures with different component technologies indicating that the high-voltage inverter options have the lowest cost.

- Nano-crystalline transformer: $2/kW
- Power electronics DC-DC, DC-AC: 150% overhead
- 60 Hz transformer and switchgear: 50% overhead

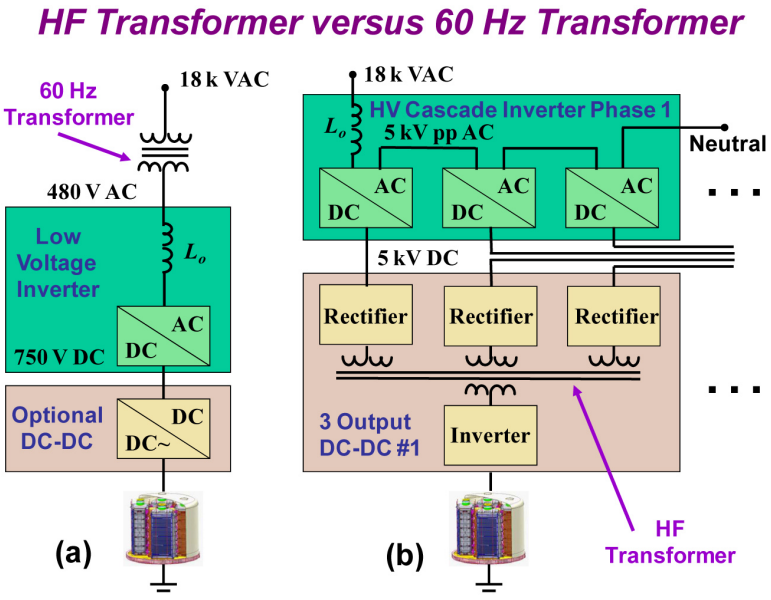

FIGURE 1. Example high-megawatt PCS architectures: (a) a 480 V AC inverter and a 60 Hz transformer to raise the output voltage to 18 kV AC for plant distribution and (b) an architecture that combines the output of multiple fuel cells each having a three-output DC-DC converter that steps the voltage up to 5 kV, followed by a high-voltage three-phase cascade inverter connected directly to the 18 kV AC power plant distribution.

The initial baseline power converter architecture for the study is a center-tapped fuel cell (approximately 700 V DC, 0.6 MW) with a DC-DC converter for fuel cell current regulation, a 480 V AC inverter, and a 60 Hz transformer to raise the output voltage to 18 kV AC for plant distribution (Figure 1a). This option was chosen as the baseline because it includes the individual functions necessary to expand to architectures having a DC common bus, and/or a medium-voltage or high-voltage inverter. The "present lowest-cost" option combines the DC-DC regulator and 480 V AC inverter functions into a single converter stage that uses the "present lowest-cost" switching power device, a 1.2 kV IGBT module. The low voltage inverter options were discussed in more detail in the previous fuel cell annual reports for this project.

The high-voltage inverter options being considered by this project use DC-DC voltage step-up converters to feed high voltage inverters connected directly to the 18 kV AC power plant distribution. For example, Figure 1b shows an

architecture that combines the output of multiple fuel cells each having a three output DC-DC converter that steps the voltage up to 5 kV, followed by a high voltage three-phase cascade inverter connected directly to the 18 kV AC power plant distribution bus. The three-output DC-DC converter is required because each fuel cell must power all three phases to reduce ripple current in the fuel cell.

In the case of the high-voltage inverter (e.g., architecture of Figure 1b), the voltage step-up and galvanic isolation are provided by the high-frequency transformer within the DC-DC converters rather than the 60 Hz transformers of the baseline low voltage inverter options (e.g., architecture of Figure 1a). The high-frequency transformer requires orders of magnitude less magnetic material and copper than the expensive conventional 60 Hz copper-iron transformer. The cost of the advanced magnetic materials (e.g., nano-crystalline magnetic materials) for the high frequency transformers can be reduced in the near future whereas the cost of the copper required by the 60 Hz transformers is expected to increase. The cost estimates shown in Figure 2 for several medium- and high-voltage PCS options indicating that the high-voltage inverter options have the lowest cost even with the relatively high cost SiC power semiconductor devices.

Advanced Component Technology Development: The high-voltage inverter PCS architectures are enabled by the rapidly advancing medium- and high-voltage semiconductor devices made with the SiC material [2]. The availability and cost of these advanced components are critically important and considerable R&D will be required to meet the cost goals. It is envisioned that early investment will permit the early adaptors to utilize and advance the technology so that it will be available for future high-megawatt PCS applications.

The development of the 10 kV, 100 A SiC MOSFET switch and 10 kV junction barrier Schottky (JBS) diode technology (represented by the second case from the right on Figure 2) was described in detail in the previous fuel cell annual reports for this project. Since then, prototype modules have been designed, produced, and demonstrated in a 1 MW level power converter [2-8]. Although the 10 kV SiC devices represent a transformational technology, it is expected to take some time before such products appear on the market, largely due to the relative lack of maturity of the SiC MOSFETs. The high voltage SiC IGBTs (represented by the last case on the right of Figure 2) will require even more development than the 10 kV MOSFET but it potentially provides advantages of higher voltage and higher current density than the 10 kV MOSFETS. Advanced Research Projects Agency-Energy recently announced a program to develop and advance high-voltage SiC IGBT technology [9].

On the other hand, medium-voltage SiC JBS diodes could be employed sooner than the high-voltage SiC technology since the medium-voltage SiC JBS diodes can be used as the anti-parallel diode for medium-voltage silicon IGBTs that have already been established in the marketplace [10] (this represents the third case from the right in Figure 2). For this case, a five-level cascade inverter would be required with bus voltages of approximately 2.5 kV rather than the three level 5 kV levels indicated in Figure 1 for the high-voltage device cases (last two cases on the right of Figure 2). It is expected that medium-voltage SiC JBS diodes may provide an early product offering that would enable more rapid development and acceptance of medium- and high-voltage SiC power device products. Reference 10 describes the development, characterization and modeling of a new 4.5 kV JBS Schottky diode and its application as the anti-parallel diode for 4.5 kV Silicon IGBTs.

Figure 3 demonstrates the performance of the 4.5 kV SiC JBS diodes and their interaction with

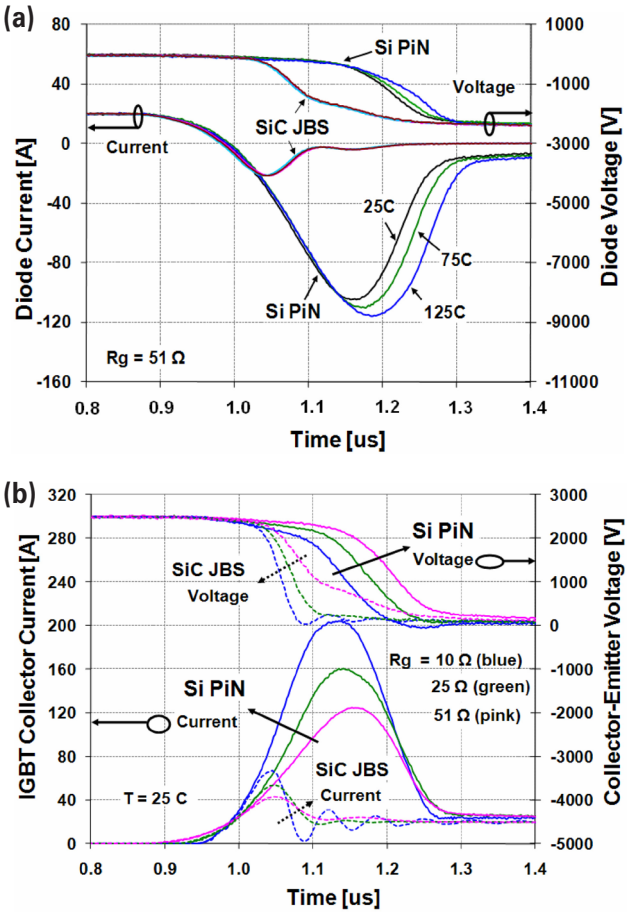

FIGURE 3. Performance evaluation of 4.5 kV SiC JBS and silicon PiN diodes and interaction with 4.5 kV silicon IGBTs: a) Comparison of reverse recovery versus temperature for silicon PiN and SiC JBS diodes, and b) Gate resistor dependence of Si IGBT turn-on for Si PiN and SiC JBS anti-parallel diodes.

4.5 kV Silicon IGBTs. Figure 3a shows the measured temperature dependence of the 4.5 kV, 60 A SiC JBS diode reverse recovery characteristics compared with those of the 4.5 kV, 60 A Si PiN diode that is used in commercial 4.5 kV IGBT modules. The peak reverse recovery current and the total reverse recovery charge (area under the reverse recovery peak) for the SiC JBS diodes remain unchanged with temperature. By contrast, the peak reverse recovery current for the Si PiN diode increases with temperature. Compared to the Si PiN, the SiC JBS diode reduces the peak reverse recovery current by more than a factor of five and reduces the total reverse recovery charge by more than a factor of ten.

The SiC JBS diode enables much higher switching frequency and lower loss with reduced current spike stress on the semiconductor die, package, and system. This is demonstrated in Figure 3b where the IGBT is switched with different gate resistances for both the SiC JBS and Silicon PiN diode types. The SiC JBS diode results in a lower IGBT current spike and does not result in a delayed voltage fall on the IGBT that occurs while the diode recovers in the SiC PiN case. The IGBT can also be switched with a lower gate resistance using the SiC JBS diode resulting in less switching loss and less switching delay.

Modeling Advanced PCS Technologies: Simulation models for advanced PCS architectures, circuit topologies, and component technologies are required to verify the interactions between components and for the technology impact evaluations. For this purpose, NIST has developed and validated models for 1.2 kV and 10 kV SiC MOSFETs and 1.2 kV, 3.2 kV, 4.5 kV and 10 kV SiC JBS diodes as well as models for various types and voltage ratings of Silicon IGBTs and other advanced low voltage device technologies such as super-junction MOSFETs. For example, Figure 4 show predicted and simulated current and voltage inductive load switching waveforms for 10 kV SiC MOSFET/JBS half-bridge modules for two different currents.

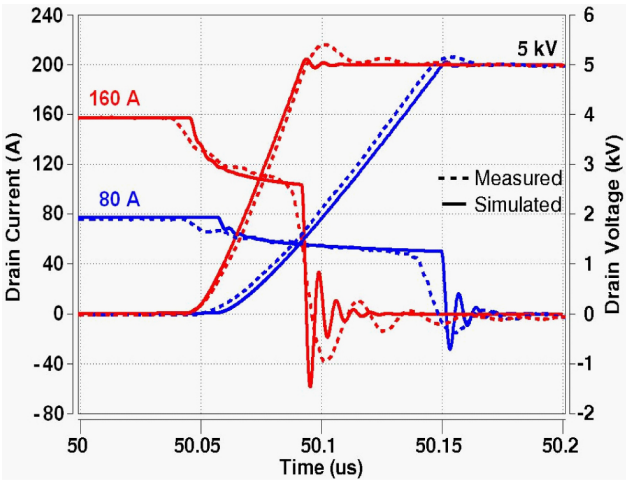

FIGURE 4. Predicted and simulated current and voltage inductive load switching waveforms for 10 kV SiC MOSFET/JBS half-bridge modules at two different switching currents.

Conclusions and Future Directions

It is generally recognized that the SECA cost goal of $40-$100/kW for the power plant PCS cannot be met with today's technology. To address this challenge, DOE and NIST have entered into an interagency agreement to have NIST lead an effort to evaluate various advanced technology options for high-megawatt PCSs. Several workshops have been held to review the approach being used for the NIST/DOE Advanced PCS Technology Impact Analysis and to coordinate the federal, industry, and academic high-megawatt PCS research and development activities.

Various PCS architectures and advanced technologies have been identified that may lead to the cost reductions required for central station fuel cell power plants. Initial cost estimates for low-, medium-, and high-voltage options indicate that HV-HF SiC power semiconductor devices are a transformational technology that can enable lower cost and improved performance of future PCS systems. It is envisioned that early investment in HV-HF SiC devices and medium-voltage SiC diodes will permit the early adaptors to utilize and advance the technology enabling cost reduction in future high-megawatt PCS applications. Predictive simulations including advanced technologies aid in validating the interaction between components and in demonstrating the overall system benefits of new high-megawatt PCS technologies.

Special Recognitions & Awards

1. In 2009, Dr. Hefner received a NIST Bronze Medal Award for technical leadership in development and application of the first high-voltage, high-frequency silicon-carbide switch mode power conversion devices.

References

1. Proceedings of the High Megawatt Converters and Machines Workshops: http://www.nist.gov/eeel/high_megawatt/.

2. A.R. Hefner, R. Sei-Hyung, B.A. Hull, D.W. Berning, C.E. Hood, J.M. Ortiz-Rodriguez, A. Rivera-Lopez, T. Duong, A. Akuffo, and M. Hernandez , "Recent Advances in High-Voltage, High-Frequency Silicon-Carbide Power Devices," Proceedings of the 2006 IEEE Industry Applications Society (IAS) Annual Meeting, October 8–12, 2006, pp. 330-337.

3. Allen R. Hefner and Sharon Beermann-Curtin, "Status of the DARPA WBST High Power Electronics Program

in SiC Device Development and Technology Transition," Proceedings of the Government Microcircuit Applications and Critical Technology Conference (GOMACTech) 2007, Lake Buena Vista, Florida, March 19-22, 2007, pp. 185-188.

4. J.M. Ortiz-Rodriguez, T. Duong, A. Rivera-Lopez, and A.R. Hefner, "High-Voltage, High-Frequency SiC Power MOSFETs Model Validation," in the Proceedings of the 2007 IEEE Power Electronics Specialists Conference (PESC), June 17–21, 2007, pp. 1018-1022.

5. J.M. Ortiz-Rodríguez, M. Hernández-Mora, T. Duong, S.G. Leslie, and A.R. Hefner, "Thermal Network Component Models for 10 kV SiC Power Module Packages," in the Proceedings of the 2008 IEEE Power Electronics Specialists Conference (PESC), June 15–19, 2008, pp. 4770-4775.

6. T.H. Duong, J.M. Ortiz-Rodriguez, R.N. Raju, and A.R. Hefner, "Circuit Simulation Model for a 100 A, 10 kV Half-Bridge SiC MOSFET/JBS Power Module," in the Proceedings of the 2008 IEEE Applied Power Electronics Conference (APEC), February 24–28, 2008, pp. 913-917.

7. T.H. Duong, J.M. Ortiz-Rodriguez, R.N. Raju, and A.R. Hefner, "Electro-thermal Simulation of a 100 A, 10 kV Half-Bridge SiC MOSFET/JBS Power Module," in the Proceedings of the 2008 IEEE Power Electronics Specialists Conference (PESC), June 15–19, 2008, pp. 1592-1597.

8. Allen R. Hefner, "Performance Analysis of 10 kV, 100 A SiC Half-Bridge Power Modules," in the Proceedings of the Government Microcircuit Applications and Critical Technology Conference (GOMACTech) 2008, March 17–20, 2008, pp. 361-364.

9. DOE Advanced Research Project Agency – Energy (ARPA-E) new project announcement entitled "Cree, Inc.: 15 kV SiC IGBT Power Modules for Grid Scale Power Conversion," http://arpa-e.energy.gov/ProgramsProjects/ADEPT/15kVSiCIGBTPowerModulesforGridScalePower.aspx.

10. Tam Duong, Allen Hefner, Karl Hobart, Sei-Hyung Ryu, David Grider, David Berning, Jose Ortiz, Eugene Imhoff, and Jerry Sherbondy, "Comparison of 4.5 kV SiC JBS and Si PiN Diodes for 4.5 kV Si IGBT Anti-parallel Diode Applications," to be published.

III.G.2 SOFC Modeling and Simulation Tools

Mohammad A. Khaleel (Primary Contact), Xin Sun, Wenning Liu, Elizabeth Stephens, Kurt Recknagle, Emily Ryan, Brian Koeppel, and Kevin Lai
Pacific Northwest National Laboratory (PNNL)
902 Battelle Blvd.
Richland, WA 99352
Phone: (509) 375-2438; Fax: (509) 375-4392
E-mail: moe.khaleel@pnl.gov

DOE Project Manager: Briggs White
Phone: (304) 375-2438
E-mail: Briggs.White@netl.doe.gov

Contract Number: FWP40552

Start Date: October 1, 2009
End Date: September 30, 2010

FY 2010 Objectives

- Develop and validate multi-physics (MP) modeling tools to simulate solid oxide fuel cell (SOFC) stack performance.
- Utilize computational techniques for the optimization of modular SOFC stack and system designs with mitigation of performance degradation.
- Disseminate/transfer modeling tools to Solid State Energy Conversion Alliance (SECA) industry teams and Core Technology Program (CTP) members.

Accomplishments

- Enhanced the PNNL-developed modeling tool SOFC-MP 2-dimensional (2D) with significantly improved algorithm and software. Many new features have been added such as allowing cell-to-cell variation parameters to enhance the 2D model capacity. The newly improved 2D model can simulate both co-flow and counter-flow large stacks with more complicated boundary conditions and some off-normal conditions.
- Enhanced the PNNL-developed modeling tool SOFC-MP 3-dimensional (3D) model by improving the numerical algorithm and resolving major memory management issues. With the new improvements, the model can simulate up to a 50-cell tall stack on a Linux server with reasonable computational effort.
- Continued to promote and support the use of SOFC-MP and Mentat-FC software packages with industry teams and CTP university researchers for modeling and development of SOFC stacks.
- Developed a detailed electrochemistry model that resolves the electric potential, charge density, and gas species distributions within the cell electrodes for the examination of secondary reactions that can also occur leading to degraded electrical and mechanical cell performance.
- Developed a model to examine the effect of operating pressure on the electrochemical and reforming performance of the SOFC, and used the model to perform a numerical study on the electrical and thermal performance of a pressurized 20 cm counter-flow stack.
- Used the developed constitutive model for sintering of porous materials to numerically characterize the densification sensitivities of candidate cathode contact materials currently under development.
- Performed simulations of SOFC anode with discrete microstructure in examining the effect of nickel–phosphorus interactions on anode structural integrity.
- Developed a continuum level model with mechanical analog to capture the temperature dependent mechanical properties of a self-healing glass seals.
- Developed an integrated modeling/experimental framework to predict the life of SOFC interconnect (IC) materials with and without spinel coatings.
- Demonstrated the effects of mechanical surface modification on life improvement of coated, 441 stainless steel interconnect materials.

Introduction

In order to efficiently develop and optimize planar SOFC stacks to meet technical performance targets, it is desirable to perform numerical experiments on the effects of geometry, material properties, operational parameters, and thermal-mechanical loading. The computations with representative baseline designs, validated by experimental data, have been used to develop better understanding of the stack behavior while avoiding costly and time-consuming experiments. In order to model the coupled physics associated with an SOFC stack, the simulation tool SOFC-MP was developed. This modeling tool combines the versatility of a commercial multi-physics code and a validated electrochemistry calculation routine to predict the gas flow distributions, current distribution, temperature field, and power output for stack-level simulations.

The fundamental building blocks of the modeling and simulation tools are electrochemical models, heat and mass transfer simulations, computational mechanics, and experimental data.

The modeling tools were then used to evaluate challenging issues anticipated for cell scale up. A systematic methodology was developed for quantifying the thermal and electrical performance improvements available with pressurized operation. For SOFC cathode contact materials and stack development, a sintering model was developed to explore/optimize the load distribution within the stack as a function of cathode contact densification and strength. The modeling tools developed were also used in studying current material development and degradation challenges. The mechanical durability of the surface scale present on metallic interconnects was evaluated for its ability to resist scale growth-induced spallation. The developed design methodology and stack analytical procedures have been documented as an American Society of Mechanical Engineers design basis for distribution within the SECA program.

Approach

The following technical approach has been taken in the modeling task to meet program goals:

- Maintain, enhance, and provide guidance for the integrated modeling tools developed under the SECA CTP for evaluating fuel cell stack design concepts by the industry teams.
- Explore scale up related topics such as enhanced cooling and performance boosting strategies.
- Investigate the effects of materials degradation on cell performance and life.
- Investigate the effects of cell geometric design, material property distributions, and operating conditions on SOFC reliability.
- Perform material experiments for property data essential to constitutive and numerical model development.

Results

Enhancement and Performance Improvement of Modeling Tools

The PNNL-developed SOFC-MP modeling tool was greatly enhanced during the past year. This modeling tool and the utilization of the tool played a greater role in continued support of SOFC technology development for the SECA industry team members:

- The SOFC-MP 2D model has been improved in many areas such as:
  - Its mesh size convergence has been improved, especially for the counter-flow simulation.
  - The electrochemistry and thermal numerical calculation has been made more accurate, robust, and computationally efficient.
  - Many new features have been added to the model and the model can now simulate mixed fuels with user-defined electrochemistry and reforming models.
  - The ability to include cell-to-cell variations for parameters allows simulation of off-normal operating conditions.
- The SOFC-MP 2D model has been validated by benchmarking with published results.
- The enhanced capabilities of SOFC-MP 2D model have been demonstrated to simulate many off-normal operating conditions.
- Major improvements have also been made on the 3D model such as improving the numerical algorithm and resolving major memory management issues. With the improvements, the model can now simulate up to a 50-cell tall stack on a Linux server with reasonable computational effort.

Detailed Electrochemistry Modeling Framework for Analysis of Secondary Reactions

During operation of the SOFC at normal to high electrical load, undesirable secondary reactions can occur within the electrodes in the bulk and near the electrolyte interface. Secondary reactions are any reactions that occur within the cell which are not directly related to the electrochemistry of the SOFC. Phases formed by these reactions may have adverse effects on the structural and electrochemical stability, and longevity of the cell and stack. Structural stability can be damaged by the formation of these phases that may affect the solid matrix, degrade the material properties, or create damaging levels of stress. The secondary reactions can also decrease the effective electrochemical activity and/or damage the electrical or ionic pathways to the triple-phase-boundaries needed for the charge transfer reactions.

- Developed a 2D detailed electrochemistry model to simulate the local volume of charge transfer, electric potential, current density, and gas species distributions through the thickness of the fuel cell using an effective properties approach. Figure 1 shows the model predicted charge density distributions for a typical “baseline” SOFC operating on wet hydrogen at 800°C, and cases of increased yttria-stabilized zirconia (YSZ) volume fraction, increased material network tortuousity, and a case with a 14-micron thick void in the electrical conductivity path. The differences in charge density

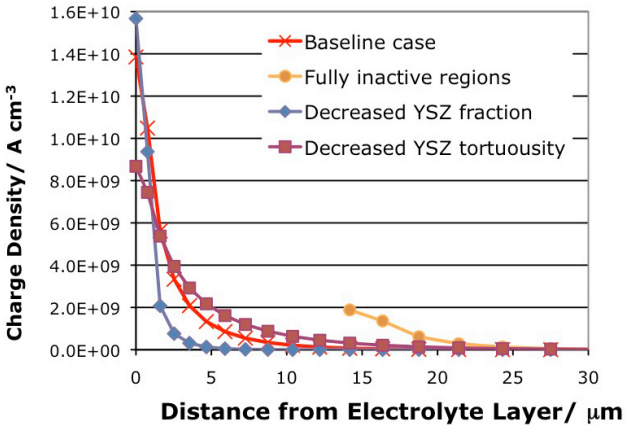

FIGURE 1. Charge density distributions for a typical "baseline" SOFC operating on wet hydrogen at 800°C, and cases of increased YSZ volume fraction, increased material network tortuousity, and a case with a 14-micron thick void in the electrical conductivity path as predicted by the electrochemical model.

calculated for these property variations serve to demonstrate the model capability to predict cell performance based on changes that may occur within the electrodes.

Modeling for Issues Related to Scale Up

As SOFCs continue to grow in size and power for use in stacks at the megawatt plant scale, so grows the need to manage the excess heat produced to make the power. The need for thermal management of these large stacks provided motivation to study scale up of cell dimensions. Stack builders must optimize the heat removal by conduction, convection, and radiation. Then to improve the thermal condition further involves removing additional heat from the stack, and/or decreasing the heat load by improving the electrical efficiency of the fuel cell. Additional heat removal can be achieved by operating the stack on methane enriched coal gas, and improved electrical efficiency can be achieved by operating the stack at elevated pressures. The following activities were performed to evaluate the effect of both on-cell reforming of methane and pressurized operation:

- The SOFC simulation capability, expanded with a model to characterize the enhanced electrochemical performance and the effect of pressurization on methane reforming, was exercised in a pressurization study. The numerical study examined the effect on thermal and electrical performance of a generic 20 x 20 cm counter-flow stack with methane reforming for operating pressures ranging from 1 to 10 atmospheres. The constant fuel utilization simulations showed that electrical and thermal performance increased monotonically with

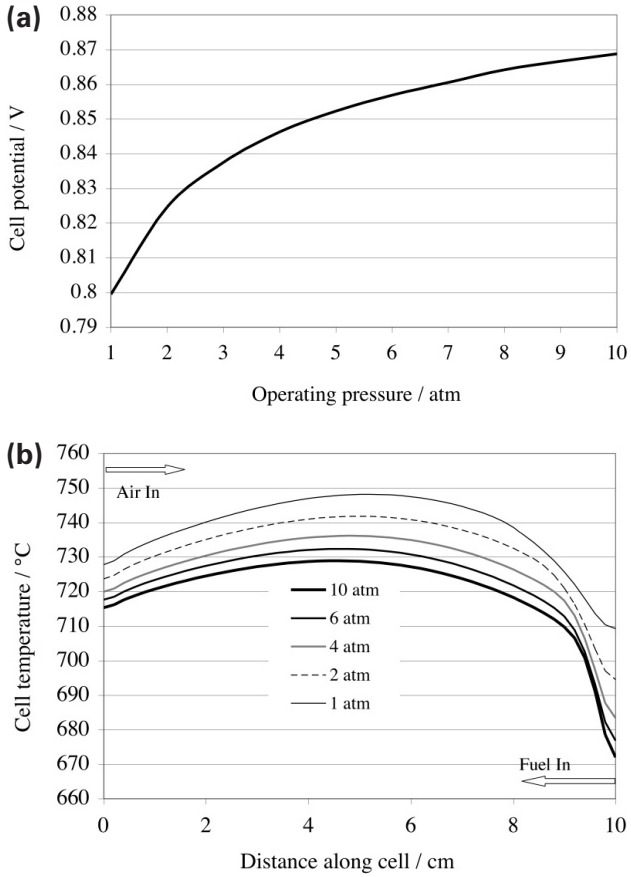

FIGURE 2. The a) electrochemical and b) thermal performance results of the constant fuel utilization simulations with increasing operating pressures.

increasing operating pressure as the cell voltage increased and the cell temperature decreased as shown in Figures 2a and 2b, respectively.

Modeling of Material Mechanical Behavior and Experiments

Candidate materials such as lanthanum strontium manganite, lanthanum strontium cobalt ferrite, and lanthanum nickel ferrite with sintering aids for lower temperature densification are being pursued for cathode contact layers. Dilatometric screening experiments were used to extract parameters for input to the previously developed densification constitutive model, and the sensitivity of contact materials to initial grain size, processing temperature, processing time, applied stress, and mechanical constraints was characterized. Sufficient densification in stack structures was predicted based on the available screening data, but once the preferred contact material is selected, additional mechanical testing and further stack modeling will be

done to evaluate the cell/seal/contact assembly stresses and reliability.

Modeling of Anode Structural Integrity

The anode is a porous material consisting of nickel (Ni) and YSZ, and works in a primarily reducing environment. Nickel, however, is highly susceptible to poisoning by multiple impurities, minor and trace elements, e.g., S, P, Se, As, Sb, that are naturally present in coals. If enough Ni present in the anode reacts with these impurities, the stress induced by volume expansion may be enough to lead to failure of the anode as well as the anode/electrolyte interface.

- An integrated experimental/modeling approach was utilized to assess the structural integrity of anode supports during the SOFC operation on coal gas containing trace amounts of phosphorus impurities. Finite element stress analyses were conducted using the actual anode support microstructures to assist in degradation mechanism explanation. Volume expansion induced by the Ni phase alteration was found to produce high stress levels such that local failure of the Ni–YSZ anode became possible under the operating conditions.

Computational Investigation of Performance of SCN-1 Glass used in SOFC Stacks

A self-healing glass seal has the potential of restoring its mechanical properties upon reheating to SOFC stack operating temperature, even when it has experienced some cooling induced damage/cracking at room temperature. Such a self-healing feature is desirable for achieving high-seal reliability during thermal cycling. On the other hand, self-healing glass is also characterized by its low mechanical stiffness and high creep rate at the typical operating temperature of SOFCs. Therefore, geometry stability and structural integrity of the glass seal system becomes critical to its successful application in SOFCs. It is crucial to be able to predict the effects of sealing system design and their structural stability under long term stack operating conditions, and to guide the design and optimization of a sealing system with a self-healing glass and appropriate containment mechanisms to achieve the ultimate goal of SOFC seal development.

- In Fiscal Year 2010, the geometry stability of the self-healing glass and the influence of various interfacial conditions of ceramic stoppers with the positive electrode – electrolyte – negative electrode (PEN), IC, and glass seal on the structural integrity of the glass seal during the operating and cooling down processes are studied using finite element analyses. For this purpose, the test cell used in the leakage tests for compliant glass seals conducted at PNNL is taken as the initial modeling geometry. The effect of the ceramic stopper on the geometry stability of the self-healing glass sealants is studied first. Two interfacial conditions of the ceramic stopper and glass seals, i.e., bonded (strong) or un-bonded (weak), are considered. Then the influences of interfacial strengths at various interfaces, i.e., stopper/glass, stopper/PEN, as well as stopper/IC plate, on the geometry stability and reliability of glass during the operating and cooling processes are examined.

Modeling for Interconnect Life Prediction

The interfacial strength between the oxide scale and the substrate is crucial to the reliability and durability of the metallic IC in SOFC operating environments. An integrated experimental/analytical methodology for quantifying the interfacial strength between the oxide scale and the different metallic interconnect candidates has been developed; therefore being able to predict the life of IC candidate materials under typical SOFC operating conditions. This integrated approach can also be used to quantify the effects of different surface finishes, coating layer thicknesses as well as different coating materials such that an optimized coating thickness as well as surface condition for the IC candidates can be developed to satisfy SECA life requirements.

Conclusions and Future Directions

During FY 2010, the modeling tools were improved and expanded with additional capabilities developed to address scale up, strength, and durability issues. Future modeling activities will continue to focus on these issues together with work on reliability, degradation, time-dependent response:

- Continue to enhance and maintain the modeling tools to meet the needs of the SECA program. Continue to promote the usage of the tools by the industry and academic teams.
- Continue to add improved material models and numerical procedures to the modeling tools for simulation of time-dependent mechanical response and reliability.
- Continue to develop modeling tools to examine secondary reactions that can take place within the cell electrodes and have detrimental effects on structural and electrochemical performance.
- Evaluate thermal management needs and reliability of seal/cell structures during cell scale up.
- Continue to support development of a robust test cell design.
- Investigate the geometric stability and structural integrity of self-healing glass in a sealing system with

ceramic stoppers (or other containment materials or design features) in a single-cell stack.

- Continue modeling work on ferritic stainless steel interconnects to meet SECA target on stack life.

FY 2010 Selected Publications/Presentations

1. K.P. Recknagle, E.M. Ryan, B.J. Koeppel, and M.A. Khaleel, "Modeling of Electrochemistry and Steam-Methane Reforming Performance for Simulating Pressurized Solid Oxide Fuel Cell Stacks," *Journal of Power Sources* 195 (19): 6637-6644, 2010.

2. W.N. Liu, X. Sun, B.J. Koeppel, and M.A. Khaleel, "Experimental Study of the Aging and Self-Healing of Glass/Ceramic Sealant Used in SOFCs," *International Journal of Applied Ceramic Technology* 7(1):22-29, 2010.

III.G.3 Optimization of Stack Load Path and Contact Materials

Brian J. Koeppel (Primary Contact), Wenning N. Liu, Elizabeth V. Stephens, and Moe A. Khaleel
Pacific Northwest National Laboratory (PNNL)
902 Battelle Blvd.
Richland, WA 99352
Phone: (509) 372-6816; Fax: (509) 375-6736
E-mail: brian.koeppel@pnl.gov

DOE Project Manager: Briggs White
Phone: (304) 285-5437
E-mail: Briggs.White@netl.doe.gov

Contract Number: FWP40552

Start Date: October 1, 2009
End Date: September 30, 2010

FY 2010 Objectives

- Use available property data from contact material screening tests to estimate input parameters for the densification constitutive model.
- Evaluate the sensitivity of contact material densification to material type, initial parameters, processing history, and geometry.
- Utilize finite element analysis (FEA) stack models to evaluate the effect of contact layers on mechanical load path development through planar stacks to reduce stresses in seal and cell layers.
- Evaluate the effect of stack assembly and densification behaviors on the stack load path and stresses at operating and shutdown conditions.

Accomplishments

- Used dilatometric test data from the materials development effort to estimate constitutive model parameters for lanthanum strontium manganite (LSM), lanthanum nickel ferrite (LNF), and lanthanum strontium cobalt ferrite (LSCF)-based materials with additions of various sintering aids.
- Evaluated the effects of initial grain size, processing temperature, processing time, applied load, and mechanical constraint on final predicted density for these candidate materials.
- Simulated densification of realistic materials within stacks and stack interconnect structures.
- Densification to high relative density predicted to be possible for low temperature processing based on available material data.
- Estimated peak contact layer stresses after densification to be ~10-15 MPa.

Introduction

Planar solid oxide fuel cell (SOFC) stack performance requires reliable uniform contact to carry the electrical current between the series-connected cells. On the cathode side, the contact layer must survive the oxidizing environment to maintain a durable bond between the ceramic electrode and the metallic interconnect. Stable but expensive noble metals have been used for contact materials, but less expensive alternatives are being investigated including ceramics with additions to aid sintering. Here the contact layer is often completed during stack assembly, so processing temperatures are limited for this interface when a metallic interconnect is used. Ceramic contact materials are desirable due to compatibility with the cathode and good oxidation resistance, but densification of the contact layer during assembly will result in volumetric changes that create residual stresses in the stack. Densification and other similar material behaviors during stack fabrication have not been typically included in thermal-stress analyses of SOFCs but do create an initial stress state. An understanding of these densification effects on the load distribution and stresses in the stack during assembly is necessary to quantify the mechanical reliability of the contact layer. Furthermore, if the structural ability of the contact layer can be improved sufficiently to carry and distribute the thermal mismatch loads between the cell and interconnect, mechanical reliability of the entire cell and seal layers can also be improved. Specifically, transmitting load to the ductile metallic interconnect was demonstrated to beneficially reduced the transmitted load through the cell's rigid perimeter seal. Numerical modeling can be used to evaluate these contact layer residual stresses in addition to the typical thermal-mechanical stresses at the operating temperature. The results of these modeling analyses will help stack designers reduce high stresses in the stack so that structural failures are prevented and high stack mechanical reliability is achieved to meet program technical targets.

Approach

The technical approach taken for this study was to develop the necessary model enhancements for densification analyses and transfer them to PNNL's existing SOFC modeling tool set. Potential constitutive

models were researched in the literature and evaluated for implementation to capture the mechanical effects of contact material densification. Based on a literature review, the continuum viscous sintering model [1] was selected as state-of-the-art and suitable for simulating volumetric material changes due to densification in the 3-dimensional (3D) stack modeling framework. This phenomenological constitutive model is a general nonlinear-viscous continuum model based on plastic deformation of porous materials. The model computes the inelastic strain rates as a function of grain size, relative density, mechanical properties, stress, and temperature. The model can capture the enhanced sintering behavior that occurs under applied stress and the influence of the mechanical constraint by the material layers being joined. The model was implemented into the MSC MARC general purpose FEA code through user defined subroutines. An existing single-cell FEA model for the first generation Solid State Energy Conversion Alliance test cell was used as the baseline stack geometry for evaluations. This FEA model was exercised in parametric studies to evaluate the loads and local stresses on seal and cell components as a function of the cathode contact material and interconnect properties. It was found that contact layer bonding and densification can beneficially reduce the structural load on the perimeter seal. Next, the densification behaviors of actual contact materials currently under development were evaluated to determine the influence of material, initial grain size, processing temperature, processing time, applied load, and constraint on the densification rate. The contact materials which exhibit good low temperature sintering and are selected for further development will be used in subsequent parametric evaluations of realistic stack geometries to optimize the load path and minimize stresses in the critical components.

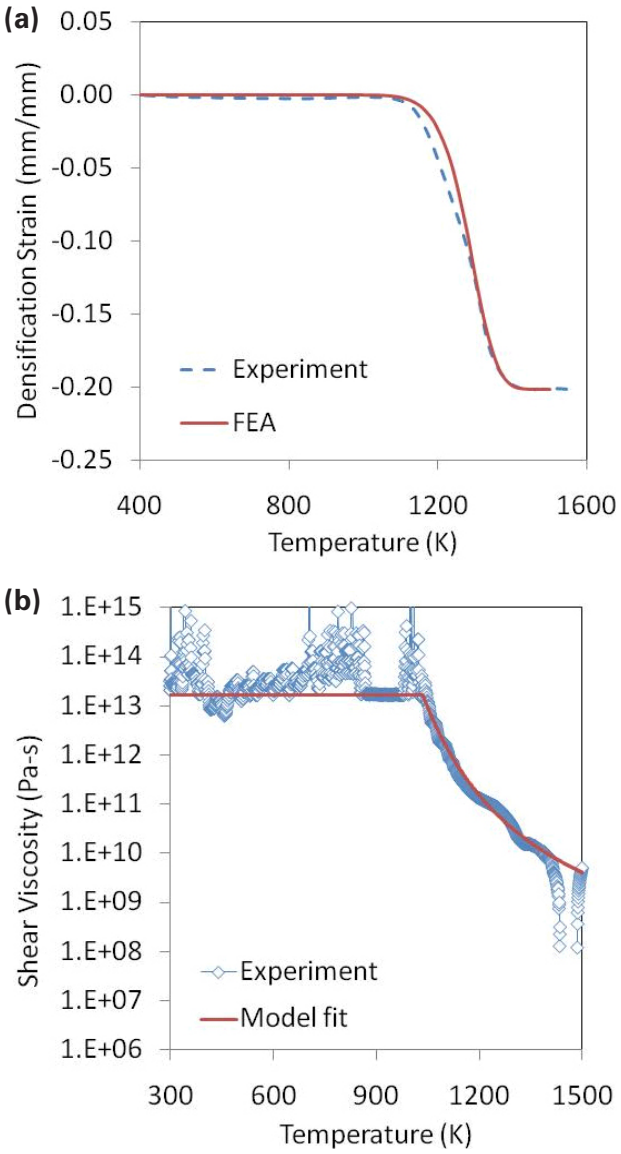

FIGURE 1. a) Densification strain during constant rate ramped temperature test and b) corresponding shear viscosity parameter (LSM + 3 mol% CuO+$BaCuO_2$).

Results

Estimation of Constitutive Model Parameters

The contact material developers used dilatometric testing under a constant heating rate to screen candidate materials. This simple test, with some assumptions, was used to estimate key parameters for the densification model. For example, the strain as a function of temperature for a candidate material (LSM with 3 mol% CuO+$BaCuO_2$ as a sintering aid) is shown in Figure 1a. Assuming that the strain is attributed entirely to densification under no load (i.e., free sintering), the densification strain rate as function of temperature is computed. Based on the constitutive model, this rate is related to the inherent driving force to minimize surface energy (i.e., the sintering stress), the particle size, and surface energy through a parameter equivalent to a shear viscosity. Particle growth was not measured, but the initial grain size was estimated from microscopy and growth rate data from the literature [2] was used. The surface energy for such ceramics does not vary considerably, so a constant value of 1.2 J/m was assumed. The shear viscosity parameter was then calculated as a function of temperature (Figure 1b). At low temperatures, no densification occurs so the viscosity term is simply capped for numerical stability. This procedure was also done for other materials such as LNF and LSCF with various sintering aids. The material parameters were then implemented in the FEA constitutive model and the original response curve from testing was verified (Figure 1a). This single test does not determine all of the required properties to

fully characterize the material for simulation, but this available data is presently adequate until the candidate materials are down selected and tested more thoroughly.

Effect of Material

Using the material data obtained from the dilatometry tests, the sintering of the LSM-based and LNF-based materials were compared under free sintering (Figure 2a and 2b). It is assumed that the processing temperature will be limited to 1,000°C maximum with metallic interconnects for durations up to 4 hours. The LSM-based material was observed to densify better than the LNF-based material in the expected processing window. The LSM-based material could achieve up to near full density even with a 2-hour treatment, while the best LNF-based material was still less than 80%. Higher densities are desirable since the bulk strength of porous materials increases with relative density. The LSM-based material showed a strong temperature sensitivity indicating that the sintering aid had reduced the temperature range to achieve good sintering rates around 950°C. It was also observed that the grain growth of the LSM was small from an initial 0.35 μm average size to 0.45 μm, which is consistent with general experimental observations.

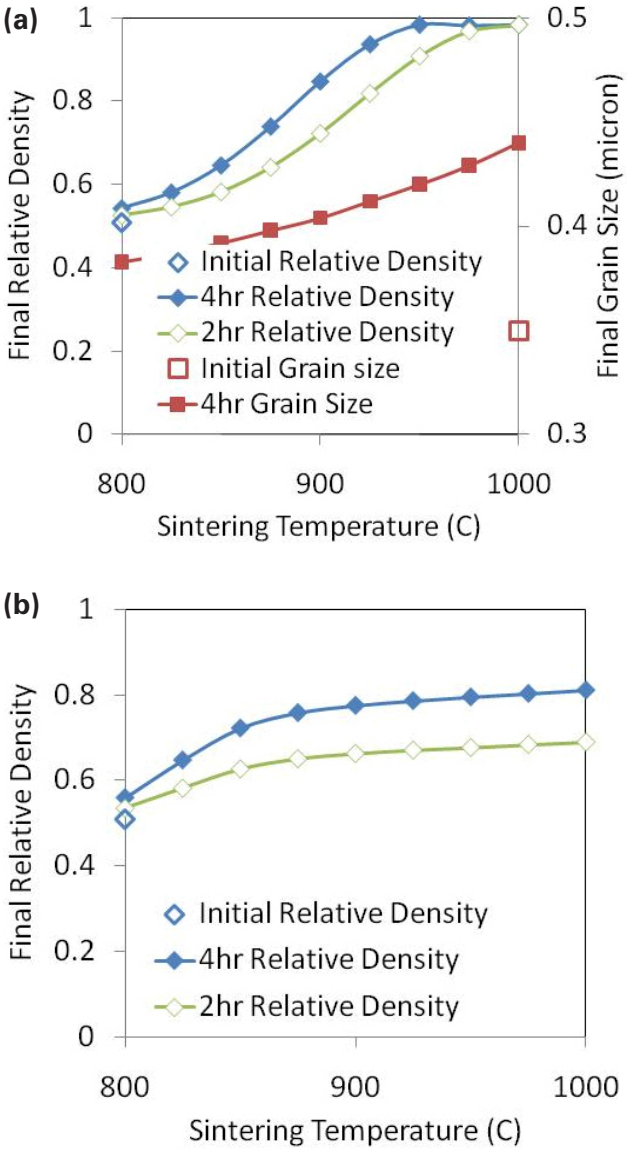

FIGURE 2. Predicted final relative density and grain size as a function of sintering temperature for a) LSM + 3 mol% $CuO+BaCuO_2$ and b) LNF +3 mol% Bi_2O_3 materials under 2 and 4-hour processing durations.

Effect of Initial Grain Size

The effect of initial grain size on the final density was also evaluated for the LSM-based material at a 950°C processing temperature (Figure 3). Smaller grain sizes have higher curvatures which increase the driving force to reduce surface energy. Strong sensitivity to achieve nearly full density was observed for grain sizes less than 0.5 μm. These small grained materials exhibited rapid sintering without excessive grain growth to achieve high density. If the starting materials can be economically milled to these small sizes and actual grain growth rates are low as assumed, then this approach may be advantageous for the low temperature regime.

Effect of Pressure

Remote compressive stresses provide additional driving force to aid the inherent sintering stress and increase the densification rate. The effect of remote

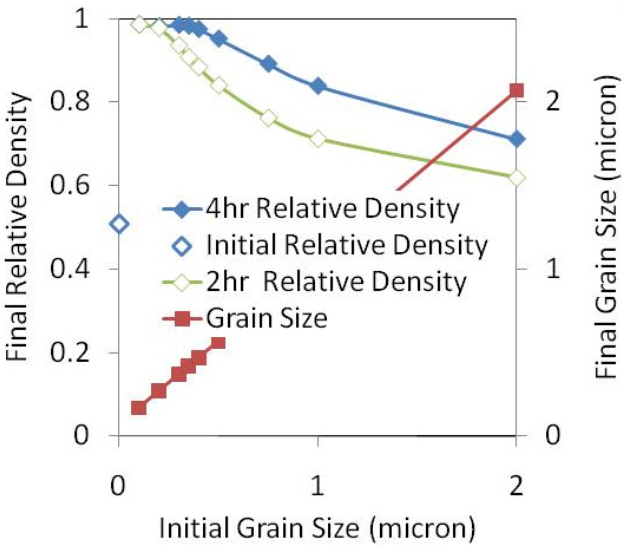

FIGURE 3. Predicted final relative density and grain size as a function of initial grain size for LSM + 3 mol% $CuO+BaCuO_2$ material under 2 and 4-hour processing durations.

uniaxial preload was evaluated for the LSM-based material. For a 2-hour treatment at 950°C without preload, the final relative density was about 91%. Preloads of 2 MPa and 5 MPa resulted in final densities of 93% and 98%, respectively. Applied stresses less than the sintering stress of ~5 MPa showed only small improvements while stresses near or greater than the sintering stress were much more beneficial. While the strains in all directions are the same for free sintering, the strains in pressurized sintering varied along different directions such that high preloads caused expansion lateral to the applied load even though the density still increased overall.

Effect of Constraints

The effect of kinematic constraints is important for sintering of SOFC layers. For materials sintered to other substrates, the bond with the other surface restricts the in-plane sintering strain while amplifying the out-of-plane sintering strain. This results in variation of not only the sintering strain rates but also the local stresses that they depend upon and ultimately the final local density. Therefore, constrained sintering layers are expected to exhibit variation in density and residual stresses depending on the relative properties of the contact and substrate materials. The contour of Figure 4a shows the final density of a bulk contact material specimen sandwiched between two thin substrates (not shown). The effect of the elastic constraints created a tensile region in the center that slowed densification and a compressive region at the corners that enhanced densification resulting in the contour profile. The effect of reducing the contact layer thickness is shown in Figure 4b. As the thickness was decreased to that characteristic of SOFC structures, it was observed that the maximum and minimum local densities converged to a more uniform value. For this material combination, the thin layer had lower out-of-plane stresses but in-plane residual stresses remained. Therefore, it is expected that for the more complex geometry of the SOFC interconnect structure, variation of contact stresses and density will likely depend on the stiffness of the design and how stack preload is distributed.

Densification in Stack Structures

Within the stack, it is expected that thin contact layers will bond the relatively stiff electrode and interconnect geometry. Simulations of stack structures like the rib geometry were performed. A 100 x 5 x 1 mm rib was bonded to a 2 mm ceramic substrate with a 0.2 mm LSM-based contact layer, and a 4-hour treatment at 950°C was simulated. It was found that for this combination of materials, the densification occurred faster at the edge but a uniform final density of 99% was predicted. Due to the constraint, the out-of-plane

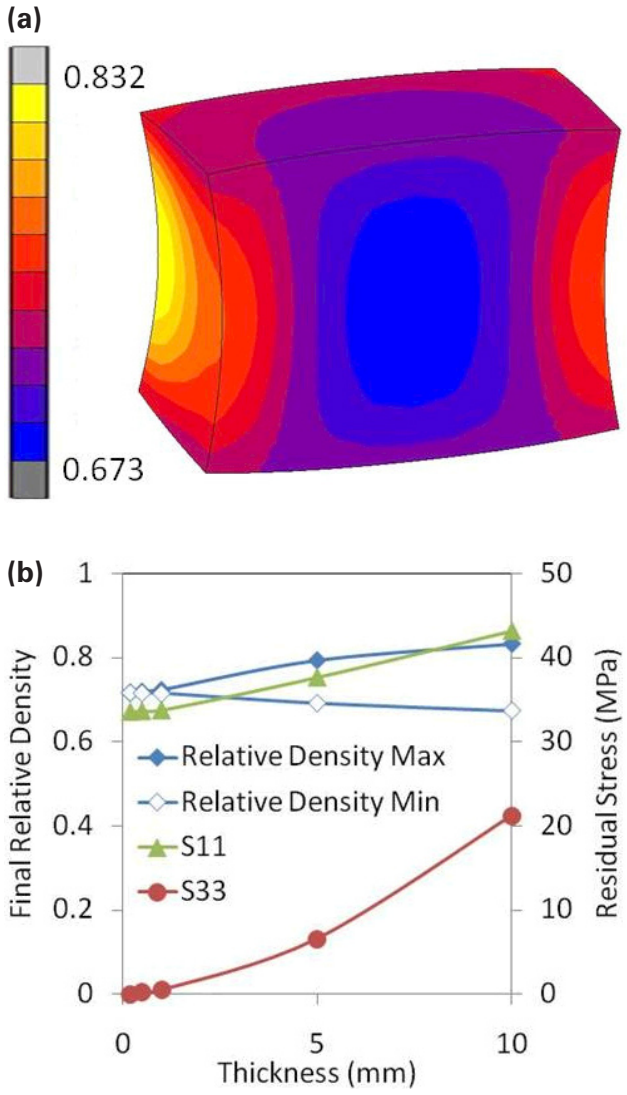

FIGURE 4. a) Contour of the final relative density for cross-section of a bulk contact layer sandwiched between upper and lower substrates and b) predicted final relative density, in-plane stress S11, and out-of-plane stress S33 for sandwiched contact layers as a function of thickness.

normal densification strains were 400X greater than the in-plane strains. The stresses in the contact layer varied considerably during processing and after densification (Figure 5). High tensile in-plane stresses up to 35 MPa were predicted in the layer during processing but were reduced to less than 6 MPa at the end. The high transient tensile stresses would be a concern though as actual decohesion of the material would stop sintering. The out-of-plane stresses were generally lower than 8 MPa both during and after processing, but there was a clear spatial variation of stresses between the specimen center and edges as well as between the cathode and interconnect interfaces. Maximum tensile normal stresses tended to occur at the center of the layer while maximum shear stresses occurred at the edges. These

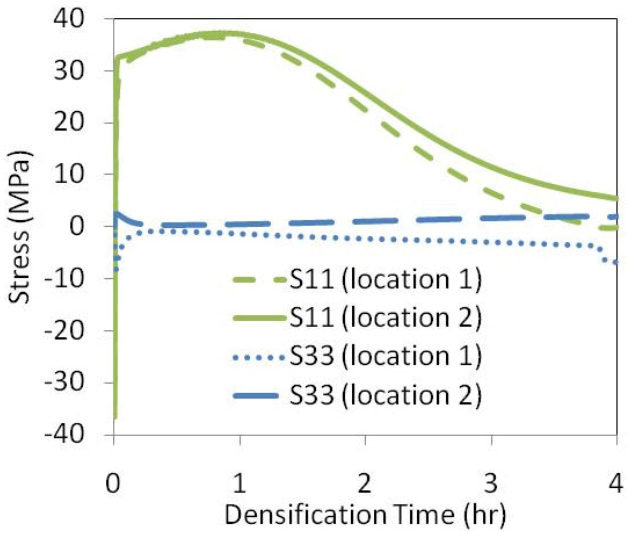

FIGURE 5. Predicted in-plane and out-of-plane stress histories at different locations within the rib contact layer during processing.

analyses along with the other stack analyses to date have suggested that the expected maximum stress levels (and therefore the required strength) in the contact layer will be up to 10-15 MPa.

Conclusions and Future Directions

During this year, the 3D continuum densification model was utilized to study contact layer behavior for realistic contact materials under development. The models showed that:

- Good densification of candidate material systems were predicted to be possible based on the dilatometric test results.
- The predicted benefits of small initial grain sizes less than 0.5 mm for higher final relative density were demonstrated.
- Constrained contact layers less than 1 mm have uniform density, although normal and shear stresses vary through the section.
- Expected maximum stress levels in stack structures predicted to be 10-15 MPa.

The densification rates predicted in these studies may be overestimated based on some experimental observations. This could be attributed to the presence of creep or plastic strains in the specimen in addition to the sintering strains. Therefore, testing which can discriminate between the deformation modes will be pursued to characterize the parameters for the constitutive model once the candidate contact materials are selected. Future activities will use the developed model with the chosen contact materials for parametric studies to improve stack reliability:

- Perform additional experiments to better characterize constitutive model parameters.
- Perform parametric studies to identify sensitivities of the stack load path and stresses to processing temperature, densification properties, and component design.
- Evaluate operation and shutdown conditions.
- Evaluate the mechanical reliability of stack assembly and interconnection through simultaneous refractory glass seal devitrification and cathode contact densification.

FY 2010 Publications/Presentations

1. W.N. Liu, B.J. Koeppel, X. Sun, and M.A. Khaleel, "Effect of Geometrical and Mechanical Properties of Various Components on Stresses of the Seals in SOFCs," 34th International Conference on Advanced Ceramics and Composites, Daytona Beach, Florida, January 2010.

References

1. E.U. Olevsky, "Theory of Sintering: From Discrete to Continuum," *Materials Science and Engineering* **R23**, 41-100 (1998).

2. A. Poirson, P. Decors, G. Caboche, and L.C. Dufour, "A Dilatometric Study of the $La_{0.8}Sr_{0.2}MnO_3$ Sintering Behavior," *Solid State Ionics* **99**, 287-295 (1997).

III.G.4 SOFC Multi-Physics Modeling and Simulation Tools

Kevin Lai (Primary Contact), Brian J. Koeppel, and Mohammad A. Khaleel
Pacific Northwest National Laboratory (PNNL)
902 Battelle Blvd.
Richland, WA 99352
Phone: (509) 372-6461; Fax: (509) 375-4392
E-mail: canhai.lai@pnl.gov

DOE Project Manager: Briggs White
Phone: (304) 285-5437
E-mail: Briggs.White@netl.doe.gov

Contract Number: FWP40552

Start Date: October 1, 2009
End Date: September 30, 2010

FY 2010 Objectives

- Develop and validate the tightly coupled multi-physics modeling tool SOFC-MP to simulate solid oxide fuel cell (SOFC) stack performance.
- Adapt the original 3-dimensional (3D) SOFC-MP modeling approach to a 2-dimensional (2D) approach for efficient evaluation of tall symmetric stacks and potential use with system-level models.
- Enhance the 3D model capabilities to handle larger stack models.
- Support industry teams use of the SOFC-MP tool for SOFC development.

Accomplishments

- Improved the 2D model in its mesh size convergence, making the electrochemistry and thermal calculation more accurate, robust, and computationally efficient.
- Developed a customized spreadsheet for automatic post-processing of 2D model results.
- Made many capability enhancements to the 2D model: 1) simulation of coal-based fuels; 2) user-specified CH_4 reforming rate; 3) user customized electrochemistry routines; 4) simulation on targeted average current density or fuel utilization; 5) simulation to obtain stack-wise current-voltage (I-V) curve; and 6) cell-to-cell variations on geometry, fuel and oxidant gas temperature, and flow rate.
- Validated the 2D model by benchmarking the results with the established Achenbach [1] one-cell model result. The work is included in a journal paper currently under revision.
- Demonstrated the capabilities of the 2D model in solving practical SOFC problems such as influence of measurement plates in the middle of stack and different flow rates caused by partial blockage, cell leaks, or by-pass in cells.
- Continued to promote and support the use of SOFC-MP and Mentat-FC software packages with industry teams and Core Technology Program (CTP) members for modeling and development of SOFC stacks.
- Made major improvements on the 3D model. Numerical algorithm has improved and major memory management issues resolved such that the model can simulate up to 50-cell tall stack on a Linux server with reasonable computational effort.

Introduction

In order to efficiently develop and optimize planar SOFC stacks to meet technical performance targets, it is desirable to perform numerical experiments on the effects of geometry, material properties, operational parameters, and thermal-mechanical loading. The computations with representative baseline designs, validated by experimental data, have been used to develop better understanding of the stack behavior while avoiding costly and time-consuming experiments. In order to model the coupled physics associated with an SOFC stack, the simulation tool SOFC-MP was developed. This modeling tool combines the versatility of a commercial multi-physics code and a validated electrochemistry calculation routine to predict the gas flow distributions, current distribution, temperature field, and power output for stack-level simulations. The fundamental building blocks of the modeling and simulation tools are electrochemical models, heat and mass transfer simulations, computational mechanics, and experimental data. The tool can be used standalone for stack engineering analysis to study operating conditions and the effects on power output, utilizations, temperatures, and temperature gradients. The tool can also be coupled with commercial finite element codes such as MSC MARC to evaluate structural integrity based on the predicted temperature field.

Approach

The following technical approach has been taken in the SOFC-MP modeling task to meet program goals:

- Develop the multi-physics solver SOFC-MP for computing the coupled 3D flow-thermal-

electrochemical response of multi-cell SOFC stacks. Utilize reduced order models where possible to increase numerical efficiency.
- Develop a graphical user interface for simplified user construction of planar stack models.
- Integrate the 3D multi-physics solver with a commercial finite element code to perform thermal-structural analysis based on the temperature results.
- Adapt the 3D SOFC-MP tool for 2D stack model computations of high numerical efficiency suitable for use with system analyses.
- Validate the models with published work and available data from industry teams.
- Maintain, enhance, and provide guidance for the integrated modeling tools developed under the Solid State Energy Conversion Alliance (SECA) CTP for evaluating fuel cell stack design concepts by the industry teams.

Results

Enhancements and Performance Improvement of SOFC-MP Modeling Tool

The PNNL-developed SOFC-MP modeling tool was greatly enhanced during the past year. This modeling tool and the utilization of the tool played a greater role in continued support of SOFC technology development for the SECA industry team members:

- The SOFC-MP 2D model has been improved in many areas:
  - Its mesh size convergence has been improved, especially for the counter flow simulation.
  - The electrochemistry and thermal numerical calculation has been made more accurate, robust, and computationally efficient.
  - Many new features have been added to the model and the model can now simulate mixed fuels with user-defined electrochemistry and reforming models.
  - The ability to include cell-to-cell variations for parameters allows simulation of off-normal operating conditions.
- Major improvements have also been made on the 3D model. The numerical algorithm has been improved and major memory management issues have been resolved such that the model can simulate up to 50-cell tall stack on a Linux server with reasonable computational effort.

Validation of 2D Model by Benchmarking with Established Data

The 2D model has been validated by benchmarking the simulations results with established data:

- Simulation results were comparable with those by Achenbach [1] for a one cell model.
- Simulation results are expected to be comparable with published data for a 5-cell stack.

A standard set of benchmark cases for SOFC operation and modeling have not been formally adopted by the fuel cell community, but two benchmark cases were previously established through collaborative activities of the International Energy Agency (IEA). Modeling predictions from a nine-member round-robin test were compared by Achenbach [1] for co-flow, counter-flow, and cross-flow geometries with non-reforming and reforming fuels. The SOFC-MP 2D model has been used to simulate the following four different cases:

- Co-flow with non-reforming fuel
- Counter-flow with non-reforming fuel
- Co-flow with reforming fuel
- Counter-flow with reforming fuel

As illustrated in Figure 1, the predicted results for voltage, power, efficiency, current density distribution, temperature distribution, and air/fuel outlet temperatures are all within the comparable ranges published by Achenbach [1].

Validation of the 2D model against published data of 5-cell stack is underway and it is expected that the model results are comparable to that of the published data also.

The validation of the two-dimensional model proved that SOFC-MP can be used reliably to predict the electrochemistry behavior of multi-cell SOFC systems at a relatively inexpensive computational cost. The comparison results have been summarized in a journal paper currently under revision.

Demonstration of SOFC-MP 2D Model Capabilities

Actual experiments with large multi-cell SOFC stacks may have variations of performance along the stack heights. Variations due to measurement plates, flow blockage, flow by-pass, degraded cell I-V performance, contact loss, etc. may affect stack performance. The enhanced features for cell-to-cell variation in the 2D model allow the user to evaluate the impact of such off-nominal behaviors which can help to maximize the understanding of experimental results from expensive stack testing. The baseline model for

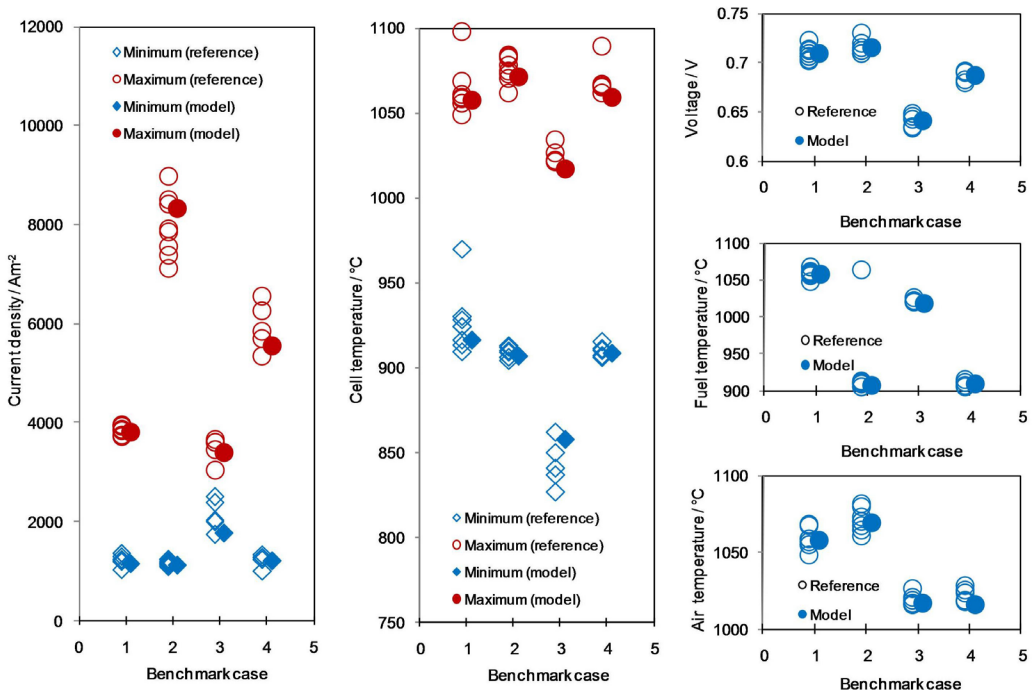

FIGURE 1. Simulation results for minimum/maximum current density, minimum/maximum cell temperature, voltage, fuel outlet temperature, and air outlet temperature for benchmark Cases 1-4 with comparisons to literature results.

the following examples is simulated under the following operating conditions: 96-cell stack, 625 cm^2 active area, wet H_2 fuel, 65% fuel utilization, 15% air utilization, and 750°C furnace environment. The baseline predicted performance is 25.5 kW for 0.5 A/cm^2 average current density and 0.85 V average cell voltage.

The first example involves the use of a measurement plate instrumented with thermocouples. Such structures may be introduced to a tall stack to determine the temperature profile across the cells during operation. However, the measurement itself can introduce an "observer effect" because the different thermal conductivity of the plate affects the lateral heat spreading ability and the measured temperature difference. For example, two 0.5" steel measurement plates were introduced at cells #32 and #64 in the 96-cell stack. Figure 2a shows the maximum, average, and minimum temperature for all 96 cells with the measurement plates, while Figure 2b shows the temperatures for the nominal stack without measurement plates. The enhanced thermal conductivity of the plate better spreads the temperatures so that locally the minimum temperature is increased and the maximum temperature is decreased. Therefore, the measured temperature difference (which is often an indicator of mechanical stress levels) is underestimated by 21% from the nominal stack. The model can help the user to understand effects due to measurement or load frame plates on the stack temperature distribution.

The second example evaluates the effects of flow maldistribution which may occur due to improper sealing or stack compression. It is assumed that the fuel flow is reduced 25% on cell #32 and air flow is reduced 50% on cell #64. The results indicated that the fuel flow reduction on cell #32 had the greatest impact on the stack. The cell had a reduced voltage of 0.81 V, current density consolidated near the fuel inlet, peak current density increased from 0.61 to 0.74 A/cm^2 (Figure 3a), cell average temperature increased from 790°C to 799°C (Figure 3b), and the cell fuel utilization increased from 65% to 85%. The air utilization is low so the effect on temperature and electrochemical performance for cell #64 was very small. Increased current density may be problematic for degradation and high fuel utilization areas are more susceptible to local reoxidation risk, so knowledge on the impact of such behaviors may be important to the fuel cell designer.

Conclusions and Future Directions

During FY 2010, the SOFC-MP modeling tool was greatly improved for both its 2D model and its 3D model. Future modeling activities will continue to focus on computational improvements, capability enhancements, and model validations. The specific tasks are listed as follows:

- Continue to improve the SOFC-MP modeling tool to meet the needs of the SECA program and

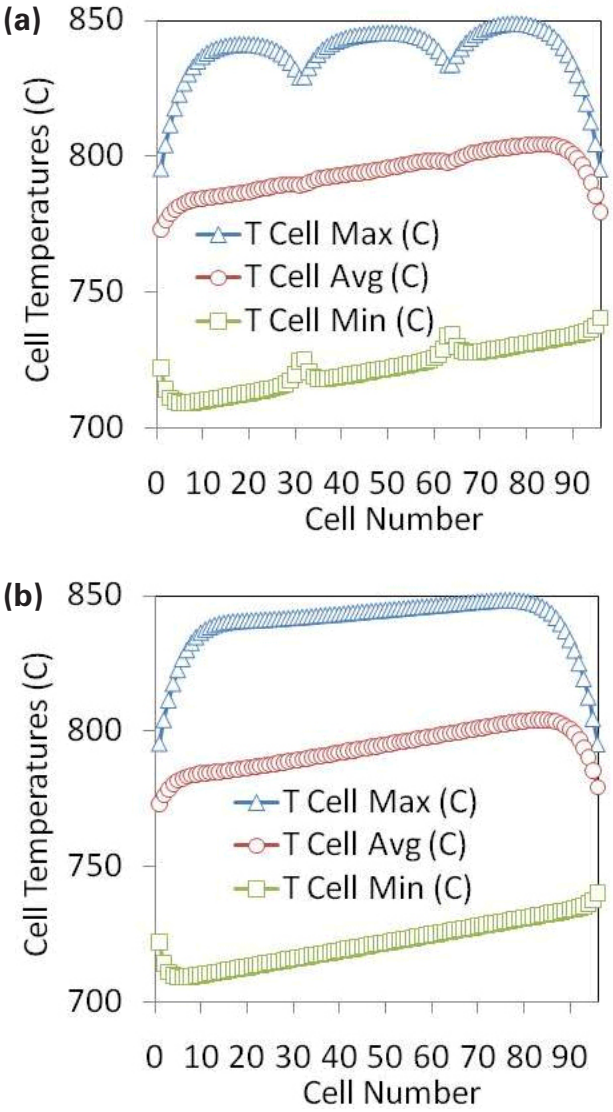

FIGURE 2. Minimum, average, and maximum cell temperatures for a 96-cell stack a) with and b) without measurement plates added at cells #32 and #64.

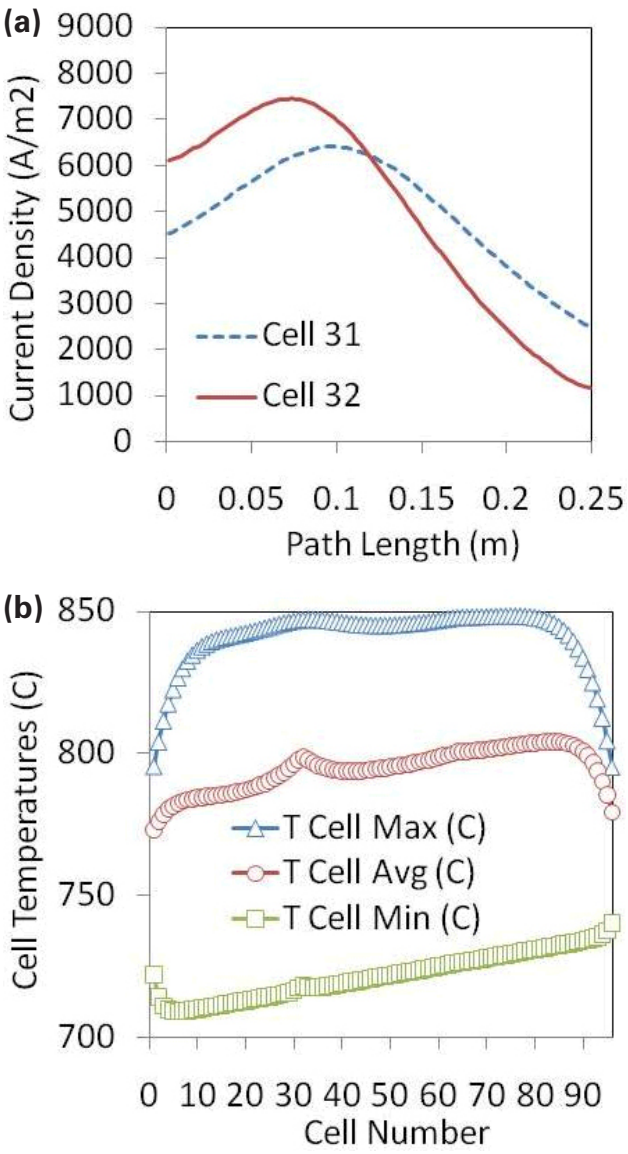

FIGURE 3. Results for a) current density as a function of cell length and b) temperature as a function of cell number for a 96-cell stack with 25% reduced fuel flow on cell #32 and 50% reduced air flow on cell #64.

continue to promote the usage of the tool by the industry and academic teams.

- Used the enhanced 2D model to complete a thorough parametric and sensitivity study. The enhanced capabilities, especially the cell-to-cell variation feature, will be utilized to analyze many practical problems in SOFC testing such as: a) influence of measurement plates in the middle of stack; b) different flow rates into cells along the stack height; c) different flow rates caused by partial blockage, cell leaks, or by-pass in cells; and d) different I-V performance of cells, etc. The SOFC-MP team will continue to work closely with existing projects to obtain experiment data for model validation and benchmarking. The results of the parametric study will be reported in a journal paper.
- Validate the enhanced 3D model by benchmarking the results with those from the existing 2D model, and document the 3D model and parametric study in a journal paper.

FY 2010 Selected Publications/Presentations

1. K. Lai, B. Koeppel, K. Choi, K. Recknagle, X. Sun, and M. Khaleel, "A Two-Dimensional Electrochemistry Modeling Tool for Planar Solid Oxide Fuel Cell Stacks," Currently under revision for Journal of Power Sources.

2. K. Lai, B. Koeppel, K. Choi, K. Recknagle, X. Sun, and M. Khaleel, "Overview of 2D SOFC-MP Modeling Tool for SOFC Stack Analysis," NETL Program Review, Pittsburgh, Pennsylvania, April 2010.

References

1. E. Achenbach, IEA Programme on R, D &D on Advanced Fuel Cells – Annex II: Modeling and Evaluation of Advanced Solid Oxide Fuel Cells, 31 March 1996, Forschungszentrum Jülich.

III. SECA CORE RESEARCH & DEVELOPMENT

H. Balance of Plant

III.H.1 Hybrid Ceramic/Metallic Recuperator for SOFC Generator

Mr. Anthony F. Litka (Primary Contact),
Dr. Norman Bessette
Acumentrics Corporation
20 Southwest Park
Westwood, MA 02090
Phone: (800) 332-0277; Fax: (781) 461-1261
E-mail: tlitka@acumentrics.com

DOE Project Manager: Robin Ames
Phone: (304) 285-0978
E-mail: Robin.Ames@netl.doe.gov

Contract Number: 84590

Start Date: June 28, 2006
End Date: August 7, 2009

FY 2010 Objectives

- Enable the use of inexpensive metallic alloys in a solid oxide fuel cell (SOFC) exhaust recuperator through the use of a ceramic heat exchange section in the high temperature region.
- Design and develop methods to mechanically integrate the ceramic and metallic sections into a recuperator assembly.
- Evaluate and characterize the performance of a hybrid ceramic/metallic recuperator under typical SOFC operating conditions.
- Demonstrate the performance and durability of the hybrid recuperator through both long-term steady-state and thermal cycle testing.

Accomplishments

- Evaluated foil recuperator designs and conducted prototype testing.
- Conducted brazing trials to reduce the cost of heat exchanger cores, plenum and stack integration components.
- Conducted thermal cycle testing of the ceramic monolith.
- Evaluated recuperator designs which are compatible with a "replaceable" cell bundle design.
- Developed concepts for stack cooling using integrated cathode air recuperation.

Introduction

Acumentrics Corporation is focused on the development of efficient, reliable, and low-cost SOFC generators for the residential and commercial markets. A key component of the SOFC generator is the heat exchanger, or recuperator, which preheats the incoming cathode air using available heat in the exhaust stream. Typical exhaust temperatures of an SOFC generator are in the range of 750 to 1,000°C and a recuperator effectiveness of >80% is required for high overall generator electrical efficiency.

While the use of full metallic recuperators requires expensive high-alloy metals for oxidation resistance, these operating temperatures are well within the capabilities of lower cost ceramic and refractory materials. The goal of this project is the development of a "hybrid" recuperator which utilizes ceramic and metallic materials to achieve the recuperator design goals of high effectiveness, low pressure drop, low cost and compact size. The hybrid configuration takes advantage of the high temperature, low fouling capability of the ceramic section, while enabling the use of lower grade metallic alloys in the medium-to-low temperature regions.

Approach

The design and construction of a high temperature, high effectiveness recuperator using a cast ceramic monolith technology in conjunction with a counter flow metallic recuperator was demonstrated in Fiscal Year 2009. The design goal of having the high temperature ceramic section reduce the exhaust side temperature sufficiently so that lower grade, lower cost, metals can be utilized in the metallic section was demonstrated. Figure 1 illustrates the design concept: a cross flow ceramic core is added to the air side outlet of a metallic recuperator. This core is encased in a metallic housing which directs the exhaust flow from the stack to the core exhaust passages and then directs the exhaust leaving the core to the inlet of the metallic recuperator. Expandable insulation is used to seal the core to the metallic casing preventing leakage from air to exhaust chambers. This configuration eliminates the need for complex plenums and allows for differential expansion of the heat exchange components through the use of flexible high-temperature ceramic gaskets similar to that used on catalytic converters and the linear arrangement of the metallic and ceramic cores. In FY 2010, work focused on the optimization of the overall recuperator and the reduction in size and cost of the metallic section. In addition, methods of including air recuperation within

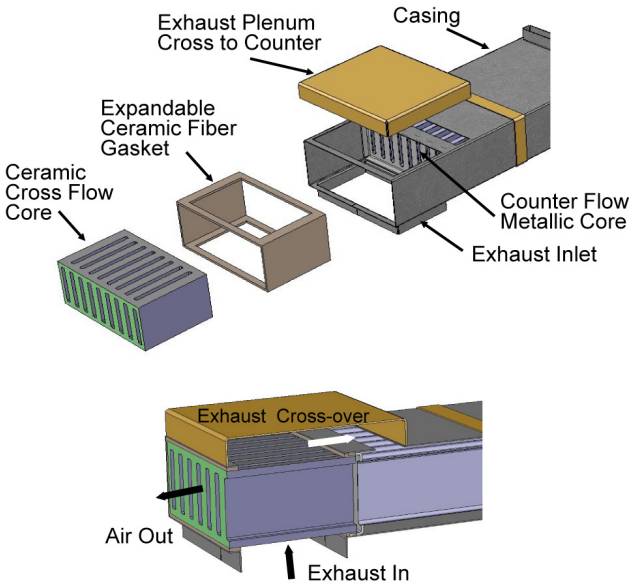

FIGURE 1. Hybrid Recuperator Assembly

the stack bundle were evaluated. Acumentrics' cell power density has increased substantially over the last several years as a result of improved manufacturing processes and material advancements, this in turn has pushed the need for internal stack heat recovery especially on small scale, partial oxidation fuel reformed generators.

Results

Testing was conducted on a foil recuperator manufactured by Catacel Incorporated. This recuperator

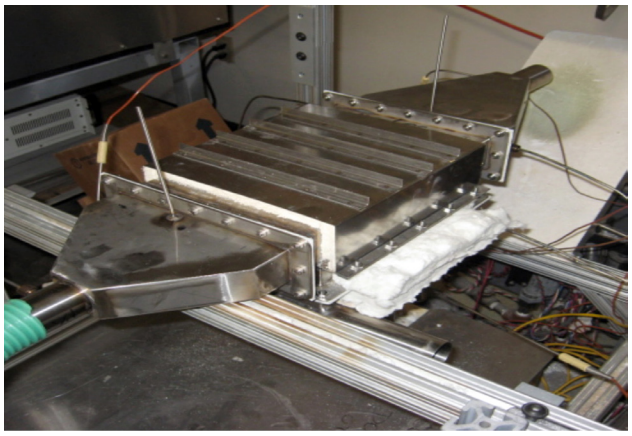

FIGURE 2. Catacel Foil Recuperator on Test

was designed as a single stage, counter flow unit capable of providing the heat recovery requirements of a 1 kW stack. This recuperator features a light weight foil construction with fin inserts; it has one-third the weight and one-half the volume of previously utilized rectangular tube, fin core recuperators. Since the flow geometry is identical with that used in the hybrid design, the technology also has the ability to serve as the metallic portion of a hybrid unit with proper adjustments to length and material selection. This recuperator was tested under various flow conditions as a stand alone unit as well as part of an integrated generator system. Figure 2 shows the recuperator on an Acumentrics recuperator test stand prior to final thermal insulation installation. Table 1 gives the performance of the unit over a range of operating conditions. Thermal cycling

TABLE 1. Foil Recuperator Effectiveness

Test Point	Exh Flow	Air Flow	Exhaust Diff Press	Air Diff Press	Exhaust Inlet Temp	Exhaust Outlet Temp	Air Outlet Temp	Air Inet Temp	Effec-tiveness
	slpm	slpm	Pa	Pa	C	C	C	C	
1	229	221	475	350	787	210	591	22	0.901
2	229	213	488	345	803	206	567	22	0.901
3	237	328	363	363	781	92	544	21	0.811
4	330	318	713	450	785	200	506	21	0.871
5	316	312	738	450	784	206	500	21	0.869
6	229	221	500	345	813	196	510	21	0.867
7	145	140	194	200	787	126	544	22	0.874
8	229	221	393	283	642	157	499	21	0.902
9	222	221	500	363	864	206	614	21	0.874
10	284	268	563	388	741	166	499	21	0.884
11	284	274	563	425	833	239	491	22	0.862
12	284	342	588	468	828	155	482	20	0.832
13	284	291	638	450	828	192	503	21	0.869
14	284	288	638	455	831	192	489	21	0.857
15	281	274	538	388	730	170	529	20	0.876
16	233	228	200	200	322	62	250	19	0.881

of the unit was also conducted. For the initial prototype unit, the leakage rate increased slightly after 20 thermal cycles but a modification was made on subsequent units to reduce the thermal stress at the high temperature end of the unit.

Additional testing was conducted to further characterize the heat transfer performance of the ceramic monolith manufactured by Blasch Precision Products. The graph in Figure 3 summarizes the performance of the two ceramic core types. Core 1 has air and exhaust side passage widths of 7 mm and a total heat transfer area of 810 cm^2 and Core 2 has passage widths of 3.3 mm and a heat transfer area of 1,425 cm^2. Thermal cycle testing was conducted on Core 2 and there was no change in performance or visual deterioration of the monolith or seals after 20 cycles. Figure 4 summarizes the performance during the thermal cycle testing.

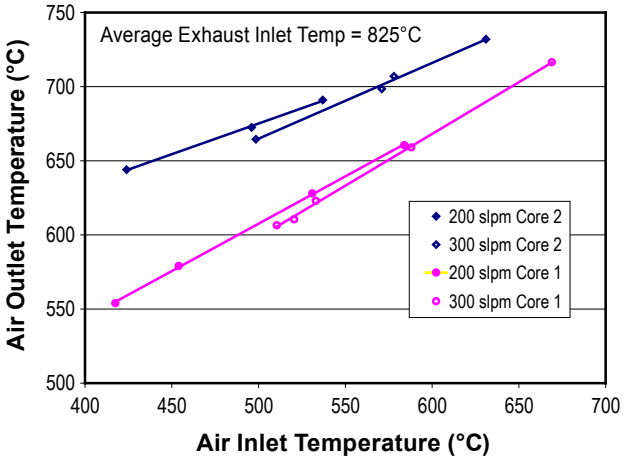

FIGURE 3. Ceramic Core Performance

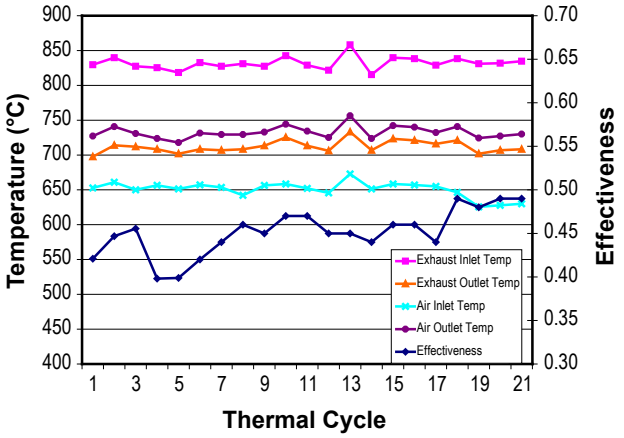

FIGURE 4. Ceramic Core Thermal Cycle Performance

An atmospheric braze furnace was acquired from CM Furnaces and brazing of recuperator parts undertaken. Corrugated panel recuperator sections have been fabricated which can be integrated into the fuel cell module to assist with the thermal management of the stack. For small-scale systems these panels can provide heat extraction from the cell bundle while minimizing thermal insulation requirements.

Conclusions and Future Directions

Acumentrics Corporation, in conjunction with Blasch Precision Ceramics, has successfully integrated a cross-flow ceramic monolith with a counter flow metallic recuperator and obtained greater than 80% effectiveness. A design has been developed which provides for a straightforward attachment of the ceramic monolith into the metallic section housing without the need for complex and expensive seals and plenums. Various configurations have been evaluated for the metallic core and the most promising from a cost perspective is a foil recuperator manufactured by Catacel Incorporated.

Future work under this project will involve

- The detailed design of a low cost recuperator incorporating features consistent with high volume manufacturing.
- Development of cost projections for the final recuperator design.
- Evaluate integral stack recuperation techniques utilizing aspects of the hybrid recuperator technology.
- Prepare a final report documenting the overall work conducted as part of the Small Business Innovation Research project.

III.H.2 Foil-Bearing Supported High-Speed Centrifugal Cathode Air Blower

Giri Agrawal (Primary Contact), Bill Buckley, Dennis Burr, Sam Rajendran
R&D Dynamics Corporation
49 West Dudley Town Road
Bloomfield, CT 06002
Phone: (860) 726-1204; Fax: (860) 726-1206
E-mail: agragiri@rddynamics.com
Web site: www.rddynamics.com

DOE Project Manager: Robin Ames
Phone: (304) 285-0978
E-mail: Robin.Ames@netl.doe.gov

Contract Number: 84616

Start Date: June 28, 2006
End Date: August 14, 2010

FY 2010 Objective

Develop a low cost cathode air blower meeting all the technical requirements of Solid State Energy Conversion Alliance (SECA) members for 3 to 10 kW solid oxide fuel cell (SOFC) systems. The manufacturing cost target for the blower is $100 per unit based upon a production volume of 50,000 units/year.

Accomplishments

- A Low Cost Cathode Blower (LCCB) with only 17 parts was designed. The following are unique features of the blower design :
  - Low cost
  - Maintenance free
  - Oil-free
  - High reliability
  - High efficiency
  - Scalability to different sizes
- Prototype units were manufactured and assembled for performance testing.
- A performance test rig was fabricated and blower testing was completed.
- Test data analysis was done.
- Acoustic testing of the blower was done.
- Preliminary quotes were received for pre-production quantities and vendor base were developed for volume production.
- SECA members were informed of advancements made in developing the low cost blower and support from SECA members were received for system testing the blower after completion of development.

Introduction

The goal of SECA is to develop commercially-viable ($400/kW) 3 to 10 kW SOFC systems by year 2010. SOFC power generation systems are attractive alternatives to current technologies in diverse stationary, mobile, and military applications. SOFC systems are very efficient, from 40 to 60 percent in small systems and up to 85 percent in larger co-generation applications. The electrochemical conversion in an SOFC takes place at a lower temperature (650 to 850°C) than combustion-based technologies, resulting in decreased emissions – particularly nitrogen oxides, sulfur oxides, and particulate matter. These systems all offer fuel flexibility, as they are compatible with conventional fuels such as hydrogen, coal, natural gas, gasoline, or diesel. Despite these advantages, advances in balance-of-plant component design must be developed before the SECA program goal can be realized.

SOFC systems require blowers to provide motive force to incoming atmospheric air, in order to overcome the pressure drop in the various valves and heat exchangers, and in the fuel cell stack. The energy required to drive this component is typically one of the largest parasitic loads for the SOFC system; consequently, high blower efficiency is paramount to high system efficiency. Furthermore, blower reliability is critical to ensure safe long-term system operation. A cathode air blower meeting following key requirements and specification has not been available in the market.

Key requirements of the cathode air blower are:

- Low cost
- High efficiency
- High reliability
- No oil contamination
- Low noise

Approach

In Phase I an LCCB was concepted and designed. A process using DFMA® (Design for Manufacturing and Assembly) techniques was developed for reducing manufactured cost of the LCCB to $100 per unit, based upon a production volume of 50,000 units per year. In Phase II a detailed design of the blower was completed and prototype blowers were manufactured and tested. Phase III will start the commercialization phase of the project.

Results

Less parts and hence low cost is the fundamental concept of the LCCB (Figure 1). The blower was cost reduced using DFMA® techniques. The estimated blower cost was $105.11 at a production rate of 50,000 units/year during Phase I research. A LCCB with only 17 parts was designed (Figure 1). To meet design point flow and pressure rise, the impeller was designed to be a centrifugal type. The rotating assembly was designed to be supported on foil gas bearings. Foil journal bearings handle the radial load and a pair of foil thrust bearings handles the thrust load of the blower. The LCCB was designed with a brushless permanent magnet synchronous motor controlled by a sensorless motor drive. The controller is mounted at the inlet of the blower being compact and cools itself without any external cooling features such as muffin fans.

A low cost controller was developed. The controller dominates 50% of the cost of entire blower assembly. A low cost reliable sensorless controller does not exist in the market. An innovative controller using commercial parts was developed. An innovative controller algorithm was developed to control the inverter over a range of operation envelope.

The prototype units were manufactured by machining and rapid prototyping. In production quantity all the metal components will be die cast, plastic components will be injection molded and sheet metal components will be stamped. Assembled prototype units are shown in Figure 2.

The test setup is shown in Figure 3. In this arrangement the unit was connected with an automated data acquisition system. The outlet of the blower is connected with an orifice flow meter setup where the pressure drop across the orifice plate was used to calculate flow. The exhaust was connected with a flow regulating valve which varies the flow rate of the blower at various speeds. The data acquisition system collects the data and the data were analyzed and performance maps were generated.

Figure 4 shows the performance of the blower. In Figure 4 the blue lines show the predicted performance and the red lines show the test data. The blower performed as predicted and the figure shows operation of the blower past the surge line without failure. The back pressure of the outlet flow line restricted the flow range over a narrow range. With higher outlet flow area the compressor can operate over a wide flow range at each speed. The blower performance data showed a turn down ratio of more than 5:1.

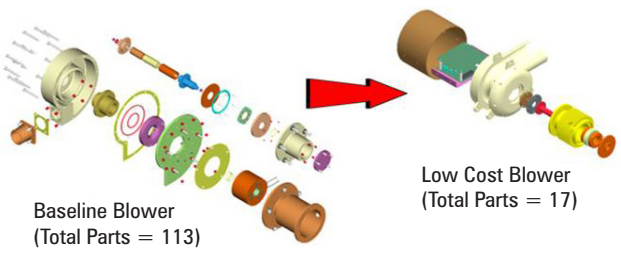

FIGURE 1. Low Cost Blower Concept

FIGURE 2. Manufactured Prototype Units

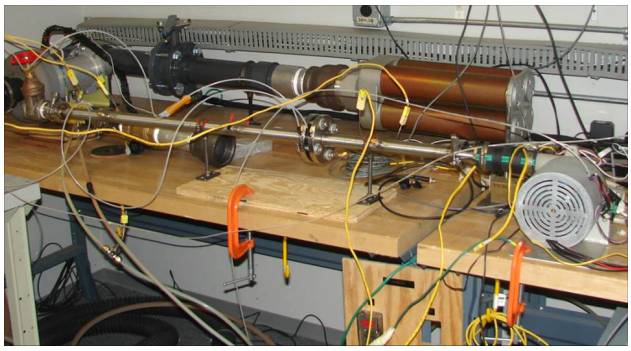

FIGURE 3. Test Rig for Performance Testing

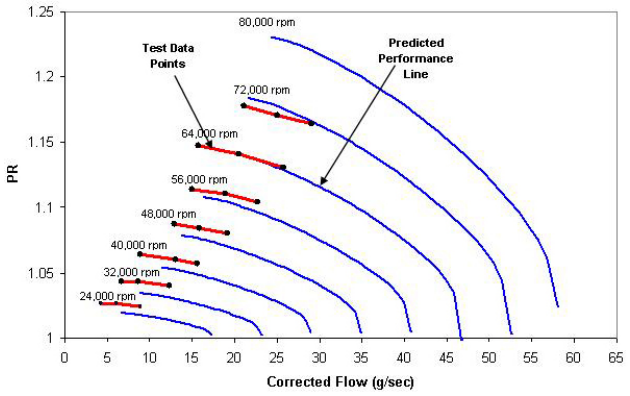

FIGURE 4. Performance Data

Acoustic Testing

Acoustic testing of the blower was completed. The compressor was tested over a wide variety of system configurations and flow conditions and acoustic signature was mapped. Lower noise is a key requirement of the blower. The blower noise level was 95 dBa, considerably lower than contact type roller element bearing blowers. However, in order to achieve 70 dBa noise level the air flow path is further being optimized.

Preliminary Quotes

Preliminary quotes for pre-production quantities of the blower were received from vendors. From preliminary quotes and estimations the blower cost was $146.97 at a production quantity of 50,000 units/year. Further optimization is being done to reduce the cost to target $100. Several vendors were identified for volume production of the blower.

System Testing

Periodic meeting and discussions with SECA members were conducted on advancements made in developing the low cost blower. SECA members have recently expressed their support to system test the blower and completion of development.

Schedule Status

The project is on schedule and all the key milestones have been achieved as planned. Key milestones that were achieved during the funding period are shown in Table 1.

TABLE 1. Schedule Status

Task	Date Completed
6 Month Progress Report	December 2008
DOE Review Meeting	March 2009
1 Year Progress Report	May 2009
DOE Review Meeting	November 2009
2nd Year Progress Report	December 2009
Blower Manufactured and Assembled	March 2010
Blower Tested	April 2010

The following milestones are planned for remaining project period:

- Improved Blower Testing - August 2010
- Final Report - August 2010

Technical Summary

The technical summary of the blower design is shown in Table 2.

TABLE 2. Blower Design

Blower Type	Centrifugal
Mechanical Speed	80,500 rpm
Weight	5.3 lbm
Bearings	Foil Gas Bearings
Motor Type	Permanent Magnet Motor
Controller Type	Sensorless Controller
Input Electric Power	769 watt
Overall Efficiency	61.6 %
Total Blower Cost	$105.11 @ 50,000 units/year
Life	>40,000 hrs

Conclusions and Future Directions

A LCCB was successfully designed, manufactured and tested per schedule. A viable energy efficient, reliable, contamination-free and maintenance-free low cost blower design was demonstrated. Support from SECA members was received for system testing the blower being developed. To make further improvements and meet design point specification the blower needs to run to a higher speed and so several components need to be further optimized. Planned tasks for the next year are:

- Optimization of motor that will provide higher power and run the blower efficiently at higher speed and meet cost target.
- Optimization of controller that will control the motor at higher power and speed efficiently and meet cost target.
- Noise abatement to further reduce blower noise.

With the improved blower design, performance and cost targets will be met. The future work planned is within the original work scope and is to be conducted during the supplemental extension period.

FY 2010 Publications/Presentations

1. WEBEX "Project Review Presentation," November 24, 2009, DOE NETL - Morgantown, West Virginia.

III.H.3 Foil Gas Bearing Supported High Temperature Cathode Recycle Blower

Giri Agrawal (Primary Contact), Bill Buckley, Dennis Burr, Sam Rajendran
R&D Dynamics Corporation
49 West Dudley Town Road
Bloomfield, CT 06002
Phone: (860) 726-1204; Fax: (860) 726-1206
E-mail: agragiri@rddynamics.com
Web site: www.rddynamics.com

DOE Project Manager: Robin Ames
Phone: (304) 285-0978
E-mail: Robin.Ames@netl.doe.gov

Contract Number: 85020

Start Date: June 30, 2008
End Date: August 14, 2011

FY 2010 Objective

Develop a high temperature capable (up to 850°C), energy efficient, reliable, maintenance-free, oil-free and low cost cathode and anode recycle blowers for large-scale solid oxide fuel cell (SOFC) power plants.

Accomplishments

- A suitable specification was chosen for design of the blower in discussion with SECA (Solid State Energy Conversion Alliance) members.
- A hermetically sealed blower concept that can be used dually as a cathode and anode recycle blower was developed.
- Detailed design and analysis of the blower was done.
- Detailed drawings of the blower were prepared.
- Long lead items such as motor lamination and magnets were manufactured.

Introduction

Fossil fuels are projected to remain the mainstay of energy consumption well into the 21st century. As the nation strives to reduce its reliance on imported energy sources, the DOE's Office of Fossil Energy (FE) supports research and development to help ensure that new technologies and methodologies will be in place to promote the efficient and environmentally sound use of the United State's abundant fossil fuels.

The SECA cost reduction goal is to develop and design a solid oxide fuel cell (SOFC) capable of manufacture at $400/kW. Concurrently, SECA coal-based systems will scale and integrate SECA SOFC technology for delivery to 5 MWe plant. Development of large (greater than 100 MWe) SOFC power blocks will enable affordable, efficient and environmentally friendly electrical power from coal.

SOFC-based power block configurations for coal-fueled central generation applications could benefit from recycling a portion of the high temperature (e.g., 800-850°C) cathode air effluent back to the incoming cathode air stream in order to improve the overall plant efficiency. System studies have indicated that a recycle ratio of (40-50%) would be desirable to assist in preheating incoming cathode air to the required stack inlet temperature (e.g., 600-650°C). The cathode recycle blower is utilized in the fuel cell power block as a means of improving thermal management of the fuel cell by controlling stack inlet temperature and through cathode recycle ratio. Thermal management benefits are balanced against auxiliary power requirement, oxygen utilization, cell operating parameters and power plant efficiency.

Key requirements of the cathode recycle blower are:

- Reliability at high temperature (up to 850°C), which is critical to ensure safe long-term operation
- Contamination-free operation (no oil or grease)
- Energy efficiency
- Scalability of design
- Minimum maintenance
- Low cost
- Low noise

In discussion with SECA members it was identified that a need for anode recycle blowers also exists for large size SOFC power plants. Following are additional requirements requested by SECA members in meeting the need for anode recycle blowers:

- Hermeticity
- Corrosion-free operation
- No metal outgassing
- No sulphur leak into fuel stream
- No free silica leak into fuel stream
- No heavy metal leak into fuel stream
- Purge gas undesirable

Currently, there is no blower available to meet these challenges; hence an innovative blower technology is needed.

Approach

- During Phase I the feasibility of the project was successfully proven by performing design and analysis of the blower.
- In Phase II detailed design of the blower was completed and detailed drawings were prepared for manufacturing. The blower will be manufactured, assembled and tested as an anode recycle blower. The same blower can also be dually used as a cathode recycle blower. The blower design will be optimized and cost reduced using the DFMA® (Design for Manufacturing and Assembly) model.
- In Phase III the blower will be tested in an actual SOFC system and will be commercialized and produced in quantities.

Results

The high temperature cathode/anode recycle blower is an innovative high temperature design where the hot fan side is separated from the motor. The blower was designed meeting all the stringent technical requirements as an anode recycle blower and can be easily used as a cathode recycle blower with minor modifications. Hence it would have dual use.

The hot fan side takes in the recycle gas and raises the pressure using an axial fan. The rotating assembly of the blower is supported on high reliability foil gas bearings. The blower is driven by a motor and controlled by sensorless controller. Figure 1 shows the three dimensional (3D) view of the blower assembly.

The blower design has following features:

- High temperature capable (up to 850°C)
- Highly reliable
- Highly energy efficient
- Low life cycle cost
- Oil-free
- Maintenance-free
- High design life (>40,000 hrs)
- Low noise (<70 dBa)
- Scalable
- Turn down ratio up to 5:1

The following detailed design and analysis work was performed in developing the blower.

Material Selection

The blower designed operates up to 850°C; hence, proper material selection is important for successful operation. To handle the corrosive environment, all the stationary components were designed as 316 stainless steel, rotating shafts are Inconel and to handle creep at high temperature, the rotor was designed to be made of

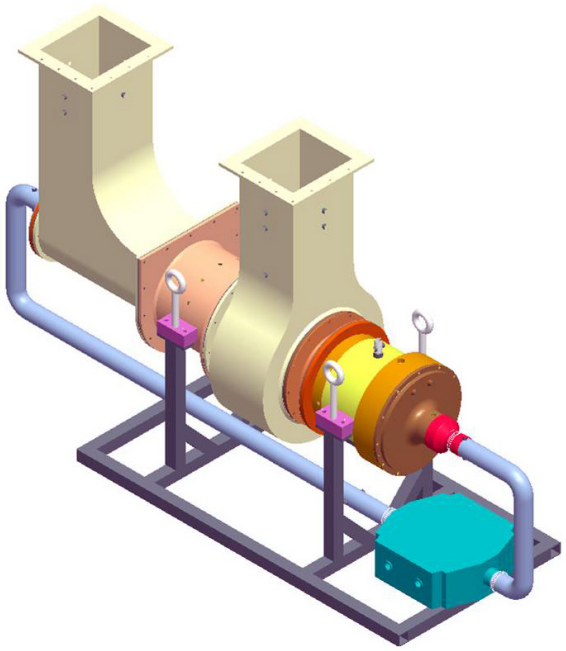

FIGURE 1. 3D View of the Blower

MAR M 247. High temperature ceramic materials are used as insulation wherever necessary.

Cooling Scheme

The blower was designed to be hermetically sealed. Heat generated due to bearings and heat leak from process gas are removed by recirculation of small amounts of process gas entrapped in the machine. The hot recirculation gas is cooled again by heat exchangers. The motor stator is cooled by water cooling jackets.

Heat Transfer Analysis

A heat transfer analysis was done using computational fluid dynamics tools. The hot end bearings were kept below 1,000°F by optimizing cooling flow and the circulation path. The motor end of the machine is kept below 400°F for safe operation.

Heat Exchanger Design

The heat exchanger controls the temperature of cooling flow recirculation inside the machine. The heat exchanger was designed as double pass water cooled. The hot cooling gas is baffled through water-cooled plates and drawn back into the machine through return channels. The heat exchanger was designed to have 6 to 10 gpm flow.

Seal Design

The hot process gas was designed to flow over the shaft through ducting. At the intersection of the shaft and housing labyrinth seals were designed to stop the

inflow of hot gas into the cooling flow circuit. Ceramic-metal gaskets were identified to seal all the joints.

Bearing Design

The blower was designed with high temperature foil gas bearings. The bearings were designed with high temperature coatings. A pair of journal thrust bearing handles the loads on the hot end and a separate set of bearings handle the loads on the cool end. By separating the bearings for rotating assemblies, they are allowed to act independently at large thermal gradients.

Coupling Design

The mechanical coupling connecting the hot end shaft and cool motor end was designed. The coupling was designed to be high strength tool steel which can transmit torque at high temperature without failure. The coupling was designed to be splined type to handle misalignments.

Stress Analysis

Stress analysis was done to ensure the material strength of the fan rotor, thrust discs, motor rotor containment, and shafts at high rotational speed.

Figure 2 shows the stress analysis results of the fan side thrust disc, where the max stress is 27,523 psi @ 30,000 rpm; the thrust disc material has 100,000 psi tensile strength @ 1,400°F which ensures a safety factor of 3.6.

Rotordynamic Analysis

Critical speed analysis of the hot end and motor end rotating assembly was performed. The fan side rotating assembly has 100% margin from the first bending mode.

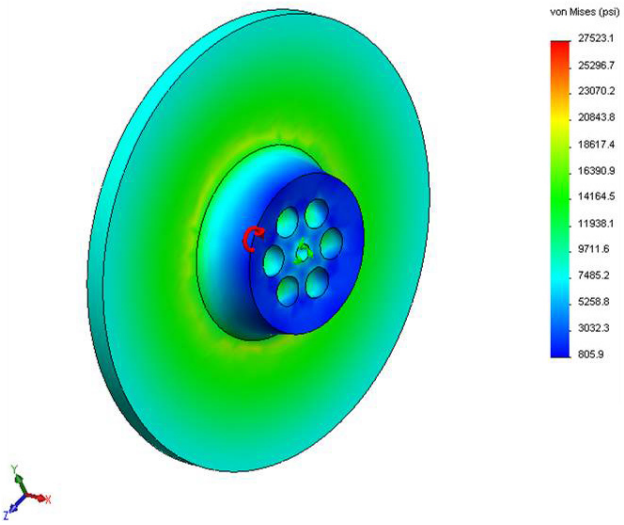

FIGURE 2. Stress Analysis of Thrust Disc

The rotating assembly design is safe. An undamped critical speed plot of the fan side rotating assembly is shown in Figure 3.

Thrust Load Analysis

Thrust load analysis of the blower was done. Thrust load of the machine is handled by a pair of thrust bearings. The maximum thrust load on the shaft was estimated as 5 psi. A typical foil gas bearing supported rotating assembly has a load capacity higher than 30 psi. Hence, the thrust bearing load are within safe limits.

Motor Design and Analysis

The axial fan of the blower was designed to be driven by a permanent magnet motor. Permanent magnet motors are the most efficient and operate over a wide range of off-design conditions with less performance degradation. The motor cooling scheme was designed innovatively to handle the heat removal with hermetic operation. Field analysis of the motor design was performed and motor design was optimized for high efficiency.

Controller Design and Analysis

The blower was designed to be controlled by a sensorless inverter. A sensorless inverter is highly efficient and effectively achieves wide operating power and speed ranges with less performance degradation. Controller simulation was done to optimize the performance of the electrical system. A simulation model was developed in MATLAB Simulink® and current waveforms were generated. The wave form showed a smooth sine curve with ripple less than 5%, hence high energy efficiency.

Detailed Drawings

Several optimizing iterations of the design were performed, and solid models were created using ProE.

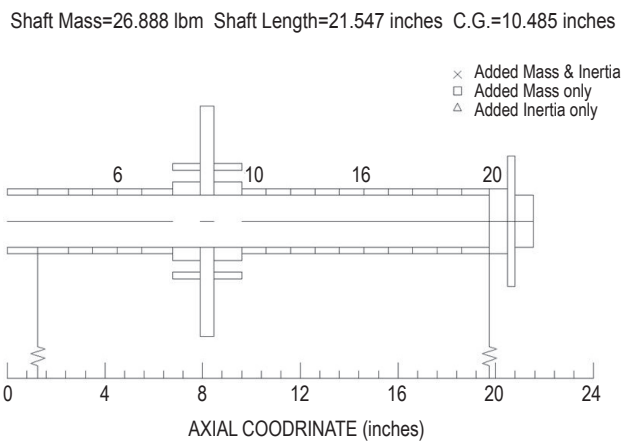

FIGURE 3. Undamped Critical Speed Plot

From thermal and stress analysis tolerance of various components were determined. Detailed drawings of the machine were completed considering all detailed analysis results, assembly aspects and manufacturing methods.

Part Manufacturing

The motor assembly is the longest lead item of the machine. By manufacturing motor stator lamination and motor rotor magnets in advance, the project is ahead of schedule. Key blower components such as bearings and rotating assembly will be manufactured in-house and vendors are being identified for manufacturing ducts, housings and support frames (Figure 4).

Schedule Status

The project is on schedule, and all the key milestones have been achieved as planned. The following key milestones were achieved during the first year of Phase II funding:

- DOE Review Meeting - November 2009
- 6 Month Progress Report - December 2009
- Design Review - February 2010
- 1 Year Progress Report - May 2010
- Detailed Drawings Completion - June 2010

The following milestones are planned for the second year of funding:

- Blower Assembly - November 2010
- Blower Testing - December 2010
- Second Year Progress Report - December 2010
- Blower Optimization & Cost Reduction - May 2011
- Field Testing & SECA Member Feedback - July 2011
- Final Report - August 2011

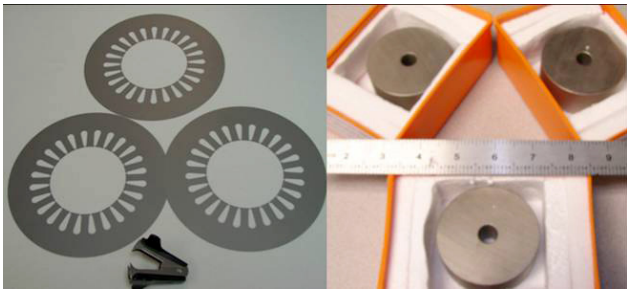

FIGURE 4. Parts Manufactured for Motor Assembly

The technical summary of the design is shown in Table 1.

TABLE 1. Technical Summary

Blower Type	Axial
Fan Diameter	9 inches
Mechanical Speed	26,520 rpm
Bearing Type	Foil Gas Bearings
Motor Type	Permanent Magnet Motor
Controller Type	Sensorless Controller
Overall Dimension	6.5 ft x 3.5ft x 3ft
Weight	700 lbs
Life	>40,000 hrs

Conclusions and Future Directions

Phase I research work was highly successful in meeting all the requirements of SECA members and proved the feasibility of the project. Phase II work has been progressing well and the milestones are being achieved as planned. A prototype unit will be manufactured and assembled by the end of 2010 and the unit will be tested for performance in early 2011.

FY 2010 Publications/Presentations

1. WEBEX "Project Review Presentation," November 24, 2009, DOE NETL - Morgantown, West Virginia.

IV. INNOVATIVE CONCEPTS

IV.1 Liquid Tin Anode Direct Coal Fuel Cell

Dr. Thomas Tao
CellTech Power, LLC
131 Flanders Road
Westborough, MA 01581
Phone: (508) 898-2223 x34; Fax: (508) 898-2690
E-mail: Tao@celltechpower.com

DOE Project Manager: Joseph Stoffa
Phone: (304) 285-0285
E-mail: Joseph.Stoffa@netl.doe.gov

Contract Number: NT0004111

Start Date: April 1, 2010
End Date: September 30, 2011

FY 2010 Objectives

- Design a "direct coal" single-cell fuel cell assembly capable of producing power from coal in a laboratory setting.
- Fabricate single-cell test articles for direct coal testing.
- Evaluate the operation of the liquid tin anode solid oxide fuel cell (LTA-SOFC) under coal-tin conditions to determine the fate of coal ash and contaminants in a continuous operating cell.
- Analyze the cell and test data to determine failure modes, contaminate levels and ash distribution associated with direct coal operation.

Accomplishments

- Design and analysis of direct coal experimental apparatus was completed.
- Coal feeder constructed and tested to conduct experiment in continuous operation.

Introduction

Electrochemical looping (ECL) [1] using the LTA fuel cell produces direct current electrical power in an electrochemical reaction powered by coal or other common fuels. For utility-scale applications the fuel oxidation step is carried out in a separate tin-coal reactor (TCR) as shown in Figure 1. The liquid tin "loops" between the fuel cell and the tin reactor, shuttling all of the oxygen used to convert the coal. The net effect is that power is produced directly and efficiently from coal or biomass without burning and with inherent separation/rejection of nitrogen. To verify, flowsheets were analyzed under another project to evaluate efficiency and cost. NOx is not formed because nitrogen does not participate in the reactions and sulfur emissions can be cleaned up using conventional technology. CO_2 can be captured in a pure stream from the ECL system in the tin reactor. CO_2 emissions and ash production are lower than other alternatives because less coal is used per kWh produced. Coal can incorporate a number of elements which are potentially harmful to the fuel cell. In Phase 1 of this project, initial testing of coal and tin was conducted. The results of this testing demonstrated that the tin can act as a purifier, rejecting some harmful contaminants (Nb, V, Mo, Cr, etc.) before they reach the fuel cell under certain conditions. To demonstrate harmful impact of potential coal contaminants a preliminary spiking testing was conducted in an actual cell containing five elements (Nb, V, Mo, Cr and As for a total of 1,600 ppm) during Phase I. The spiked cell had a measurable decay rate of 3% per 100 hours. This initial result demonstrates the technical feasibility of an LTA direct coal power plant. The result from the spiking test will provide a target for comparison of the future tin/coal experiments.

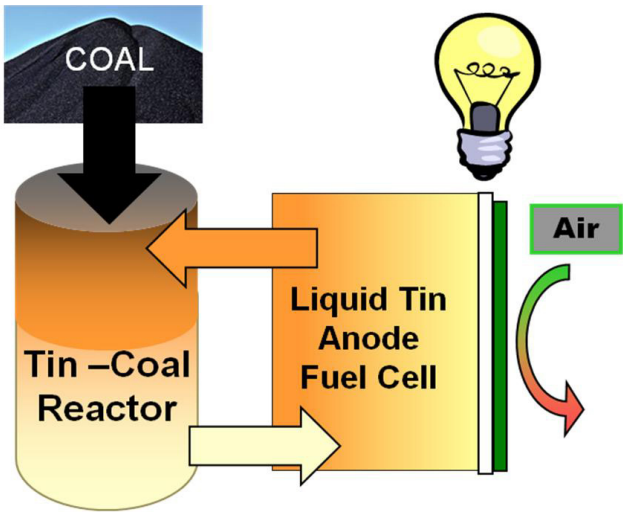

FIGURE 1. The Two Major Elements of the ECL Flowsheet Are the Tin-Coal Reactor, Which Processes the Coal, and the Liquid Tin Anode Fuel Cell, Which Produces Power

Approach

Coal impurities and ash and their impact on fuel cells can be a show-stopper for any direct coal conversion fuel cell. A mitigation strategy to

understand and deal with coal contaminants and ash is of paramount importance. As a result, the objective of this project is to develop an LTA cell technology which addresses the key issue of cell durability in a coal environment. The method of identifying durability issues is through long-term testing of single-cell test articles. In order to complete the testing, three areas of importance will be addressed. The first is the design and construction of a test apparatus and test articles that will contain a tin bath of reasonable size, up to 1 kg, the fuel cell and current collection in order to conduct the direct coal experiments. The second is to test the performance of the direct coal fuel cell under various conditions to determine the behavior of ash and impurities likely to be present in coal and their interaction with the tin bath and fuel cell materials. The third area consists of post mortem analysis of the fuel cell article and tin bath to measure the quantity and form of the ash and unused carbon, contamination levels in the tin and contamination levels at the electrolyte surface.

Molten tin has been demonstrated as being a potential media for separating, reducing or eliminating coal impurities under certain conditions similar to the tin/coal reactor. These previous tin chemistry studies have been narrowly focused, short in duration and have not systematically evaluated the equilibrium of tin-contaminants at conditions which are expected in the TCR. In another project, we have identified and modeled 10 metallic elements (V, Nb, W, Cr, Mo, Mn, As, Ta, U and Se) in coal that have the potential to be the most harmful to the ytrria-stabilized zirconia electrolyte. Additional non-metallic elements of F, Cl, Br, I, S, Si and P will be evaluated in conjunction with this project. Individual elements will be spiked into a Gen 3.1 fuel cell and tested to determine degradation under 100 hours of constant load. In this project the primary focus is the coal ash that is not largely dissolved in tin – and its physical separation with molten tin in an operating fuel cell. The testing will consist uniquely of Illinois #6 coal.

Results

- Coal properties have been compiled for Wyoming, Ohio, Illinois and West Virginia coal sources. The coal source selected for the direct coal experiments is Illinois #6 seam (Harris Seam) coal obtained from the Penn State Coal Sample Bank and Database as sample DECS-24. The properties of this coal are shown in Table 1. Advantages of testing with this source include lower moisture content, higher ash content and higher levels of potassium, sulfur and chlorine. Ash management will be realized in shorter test times and the higher levels of potassium, sulfur and chlorine will test the robust design of the fuel cell.

TABLE 1. Illinois #6 Seam (Harris Seam) Coal Analysis for Sample DECS-24

Illinois #6

Ultimate Analysis	As rec'd	Dry	Daf	dmmf (Parr)
% Ash	11.62	13.39		(17.5%MM)
% Carbon	57.33	66.05	76.26	80.06
% Hydrogen	3.98*	4.59	5.3	5.56
% Nitrogen	0.99	1.14	1.32	1.38
% Total Sulfur	4.8	5.53	6.38	
% Oxygen (diff.)	8.07*	9.3	10.74	12.99

* excluding H and O in moisture
Dry % Chlorine = 0.14
Dry % Carbon dioxide = 0.65

- Figure 2 shows the direct coal test apparatus concept. A bath of liquid tin is contained in an aluminum oxide vessel. The Gen 3.1 cell is submerged into the tin and covered with another aluminum oxide tube above the tin to separate any air from the tin bath environment. Coal is dropped onto the tin surface near the center of the tube and opposite the exhaust tube. Other tubes include a vibrating stir rod and an input for a cover gas.
- Figure 3 shows the continuous coal feeder that will be used to deliver coal at the start of the experiments. The feeder consists of a stepper motor, feed screw and hopper assembly.

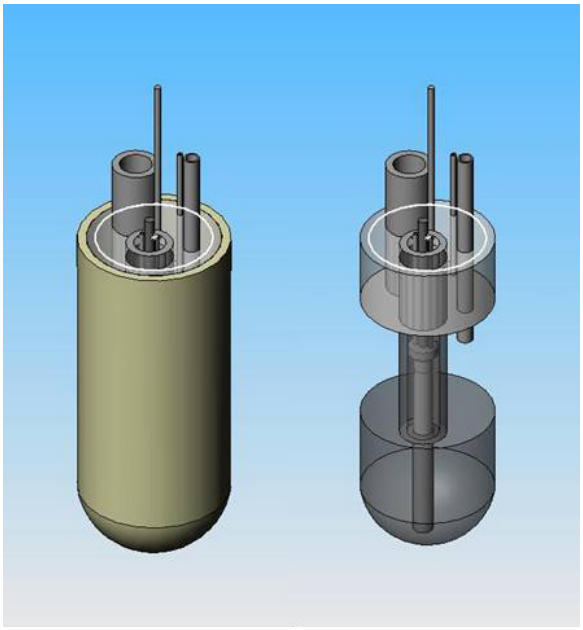

FIGURE 2. Direct Coal Tin Bath Test Apparatus

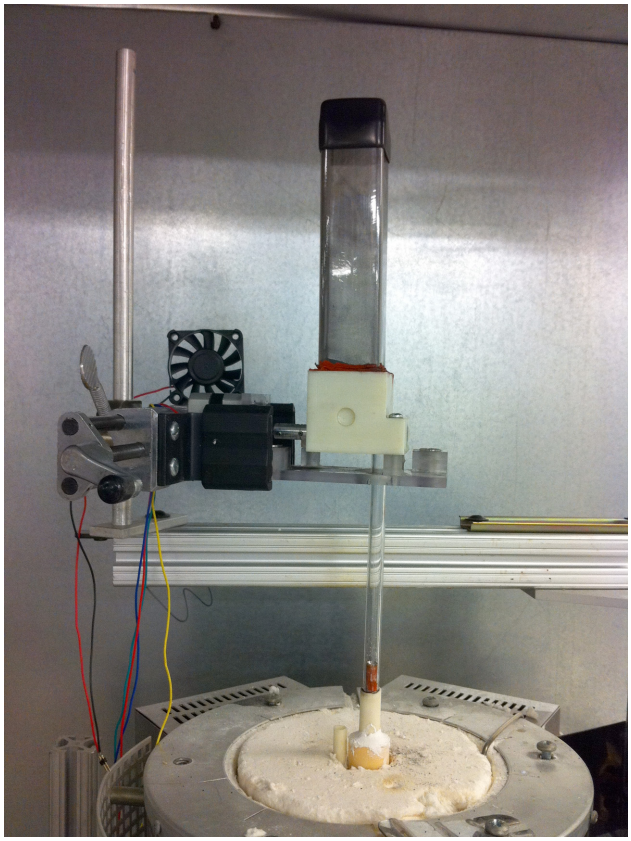

FIGURE 3. Direct Coal Continuous Delivery System

Conclusions and Future Directions

- Liquid tin has been found to be capable of separating, reducing or removing some key harmful elements under simulated TCR conditions of 1% H_2O in H_2. Oxides formed under these conditions were separated from bulk tin. This result/data seems to support a technical pathway to enable the isolation of coal contaminants and perhaps coal ash and slag in the TCR.
- The laboratory demonstration experimental setup is near completion.

FY 2010 Publications/Presentations

1. SECA – 2010.
2. Fuel Cell Seminar – 2010.

References

1. CellTech Power presentation at Fuel Cell Seminar 2009.

IV.2 Liquid Tin Anode Direct Coal Fuel Cell

Dr. Thomas Tao
CellTech Power, LLC
131 Flanders Road
Westborough, MA 01581
Phone: (508) 898-2223 x34; Fax: (508) 898-2690
E-mail: Tao@celltechpower.com

DOE Project Manager: Joseph Stoffa
Phone: (304) 285-0285
E-mail: Joseph.Stoffa@netl.doe.gov

Contract Number: 85006

Start Date: August 14, 2009
End Date: August 14, 2011

FY 2010 Objectives

- Install and commission a coal test stand with the capability of simulating tin-coal reactor (TCR) environments and uninterrupted operation for 1,000 hours.
- Determine the elemental solubility of coal contaminants in liquid tin at TCR conditions.
- Determine long-term cell performance and material stability impact for tin spiked with each coal contaminate element within their solubility limits.
- Analyze and evaluate experimental data/results, and continue to carry out remaining project.

Accomplishments

- Completed the coal simulation test stand which is capable of reliable operation for 1,000 hours.
- Established contaminant matrix found in coal including V, Nb, W, Cr, Mo, Mn, As, Ta, U, Se, F, Cl, Br, I, Na, S and P, and their subsequent evaluation procedures.
- Conducted coal contaminant solubility in tin by spiking individual elements into tin at environment equivalent to the electrochemical looping (ECL) conditions of tin after interaction with coal, i.e., 1% H_2O in H_2 or equivalent open circuit voltage of 1.1 V.
- Established baseline performance of liquid tin cells for long-term operations. Liquid tin cells spiked with individual elements are being made and under test.

Introduction

ECL using the liquid tin anode fuel cell [1] produces direct current electrical power in an electrochemical reaction powered by coal or other common fuels. For utility-scale applications the fuel oxidation step is carried out in a separate tin coal reactor as shown in Figure 1. The liquid tin "loops" between the fuel cell and the tin reactor, shuttling all of the oxygen used to convert the coal. The net effect is that power is produced directly and efficiently from coal or biomass without burning and with inherent separation/rejection of nitrogen. In Phase 1 of this Small Business Innovation Research, flowsheets for this concept were created and analyzed to evaluate efficiency and cost. NOx is not formed because nitrogen does not participate in the reactions and sulfur emissions can be cleaned up using conventional technology. CO_2 can be captured in a pure stream from the ECL system in the tin reactor. CO_2 emissions and ash production are lower than other alternatives because less coal is used per kWh produced. Coal can incorporate a number of elements which are potentially harmful to the fuel cell. Laboratory testing of tin/coal reactions has demonstrated that the tin coal reactor can act as a purifier, rejecting some harmful contaminants before they reach the fuel cell under certain conditions. This is a key positive finding demonstrating technical feasibility of liquid tin anode (LTA) direct coal power plant.

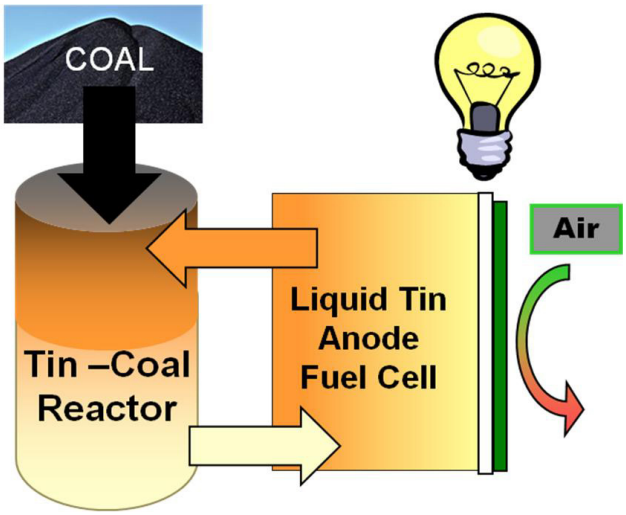

FIGURE 1. The two major elements of the ECL flowsheet are the tin-coal reactor which processes the coal and the liquid tin anode fuel cell which produces power.

Approach

Coal impurities and their impact on fuel cells can be a show-stopper for any direct coal conversion fuel cell. A mitigation strategy to understand and deal with coal contaminants is of paramount importance. As a result, the objective of this project is to develop an LTA cell technology which addresses the key issue of cell durability in a coal environment. The method of identifying durability issues is through long-term testing of single cell test articles. In order to complete the testing, three areas of importance will be addressed. The first is the implementation of a dedicated test stand which can reliably maintain test conditions over the duration of testing from 100 to 1,000 hours. The stand will simulate tin-coal reactor conditions for at least 1,000 hours. The second is to understand the behavior of impurities likely to be present in coal and their interaction with tin, in order to establish the spiking levels of contaminants of interest. This impurity solubility data will be obtained by specific tin/contaminant testing and analysis. The third area consists of long-term single fuel cell testing with each single element spiked into the tin. The long-term cell testing will identify specific contaminants which cause accelerated performance degradation and such finding shall allow evaluation of degradation mechanisms. Finally, the experimental data/results of solubility, cell performance and subsequent analysis of degradation mechanism will be used to propose future mitigation strategy including selection/optimization of materials, components and process to ensure long-term stable direct coal conversion in liquid tin.

Molten tin has been demonstrated as being a potential media for separating, reducing or eliminating coal impurities under certain conditions similar to the tin/coal reactor. These previous tin chemistry studies have been narrowly focused, short in duration and have not systematically evaluated the equilibrium of tin-contaminants at conditions which are expected in the TCR. In prior projects, we have identified and modeled 10 metallic elements (V, Nb, W, Cr, Mo, Mn, As, Ta, U and Se) in coal that have the potential to be the most harmful to the yttria-stabilized zirconia electrolyte. Additional non-metallic elements of F, Cl, Br, I, S, Si and P will be evaluated in this project also. Individual elements will be spiked into tin under an environment simulating the TCR exit. Analysis of the bulk tin will be completed to determine the solubility of the contaminate element. The results from this experiment with each element will be used to set the contamination levels for the long-term cell test. Preliminary contaminate testing in actual cells containing a number of contaminants (five elements, Nb, V, Mo, Cr and As to 1,600 ppm) in a single test had been conducted in Phase I at a measurable decay rate of 3% per 100 hours. In this project each element or contaminant will be tested individually to determine cell performance and degradation if any.

Results

- Tin oxide reduction by coal was performed to establish the coal contaminate solubility in tin and the disposition of coal ash. Samples of coal and tin oxide were premixed and heated to 1,000°C in order to oxidize the coal under operating conditions. The samples were sent for elemental analysis by glow discharge mass spectrometry (GDMS). Table 1 shows the results of one sample, #5, compared to the initial coal contamination. The analysis results indicated that the most harmful elements were not found in the tin. The data also implies that elements from coal found in the processed tin obey a simple rule of likes-dissolve-likes, predictable by their Gibb's free energy or Nernst potential of oxidation. The comparison of the Gibb's free energy to detectable contaminate solubility shows a threshold of 0.9 V. Above 0.9 V, the element in oxide form will be excluded from the liquid tin. Below 0.9 V, the element will have limited solubility in the liquid tin. The elements highlighted in Table 1 are of most interest for the long-term cell degradation studies.
- Figure 2 shows the completed DOE coal test stand for long-term testing. The capabilities include robust uninterrupted test capability for 1,000 hours, gas mixing to simulate TCR conditions and flexibility for direct coal testing.
- The solubility of coal contaminants was investigated by spiking individual metallic and non-metallic elements in tin and subjecting the material to a simulated TCR environment that is 1% H_2O in hydrogen for 5 hours. Figure 3 shows the surface and the cross-section of the tin samples from left to right spiked with Mn, W, Ta and Se. The surface of the Mn and Ta spiked samples show a large amount of powder which corresponds to oxide formation as indicated by their Gibb's free energy in Table 1. Table 2 shows the results from inductively coupled plasma optical emission spectroscopy (ICP-OES) elemental measurement on the interior/bulk of the spiked samples; substantial reduction of concentration was observed for V, Mo, Nb, W, Ta and Se at spiking levels of 4,000 ppm. The higher than expected concentration for Cr likely resulted from substantial entrainment of oxides in bulk tin.
- Cell performance testing with spiked elements has begun with the establishment of a pure tin cell baseline. Figure 4 shows a baseline of pure tin cell under hydrogen under a load of 4.8 amps for 100 hours approaching stable state with initial cell potential drop of less than 2%. The data from a previous test of five spiked elements and a single element Ta test are also shown. The reduction in the cell voltage for the other data is 7.9% and 6.9% over the 100-hour period. Testing of all contaminate elements of interest will continue.

TABLE 1. Coal Contaminate Element Solubility Results Ranked by Nernst Potential

Element	Oxide, stable valance state	Nernst Potential @1,000C	Coal Impurity Test Levels (ppm wt)	#5 GDMS Results (ppm wt)
Ca	2	2.6	2,165	<0.01
Sr	2	2.4	32	<0.005
Mg	2	2.39	374	<0.01
Zr	4	2.22	3.15	<0.005
Al	3	2.2	1,181	<0.05
Ti	4	1.85	98	<0.005
Si	4	1.77	1,968	<0.01
Ta	5	1.55		<5
U	6	1.55		<0.005
Nb	5	1.4		<0.005
Na	1	1.27	177	<0.01
Ga	3	1.16		<0.005
Zn	2	1.1	1.18	<0.01
Mn	3	1.09	1.97	<0.005
V	5	1.07	2.16	<0.001
Cr	4	1.07	0.59	<0.005
K	1	1.01	39	<0.01
P	5	0.93	51	<0.01
Mo	4	0.93		<0.01
W	6	0.9		<0.01
Ti	3	**0.9**		**0.04**
In	3	**0.89**		**58**
Ge	4	**0.87**		**<0.01**
Fe	3	**0.85**	453	**51**
Sn	4	**0.82**		**Matrix**
S	4	**0.75**		**23**
Co	2	**0.75**		**0.28**
Cd	2	**0.67**	ND <0.2	**<0.05**
Sb	3	**0.66**		**400**
Ni	2	**0.65**	0.394	**2.9**
Te	2	**0.56**		**<0.1**
Pb	2	**0.49**	0.984	**150**
Bi	3	**0.4**		**13**
Cu	1	**0.39**	1.771	**29**
As	5	**0.34**	0.197	**8.8**
Rh	3	**0.06**		**<0.005**
Se	6	**-0.2**	0.394	**<0.01**
Ag	1	**-0.24**	ND <0.2	**1.1**

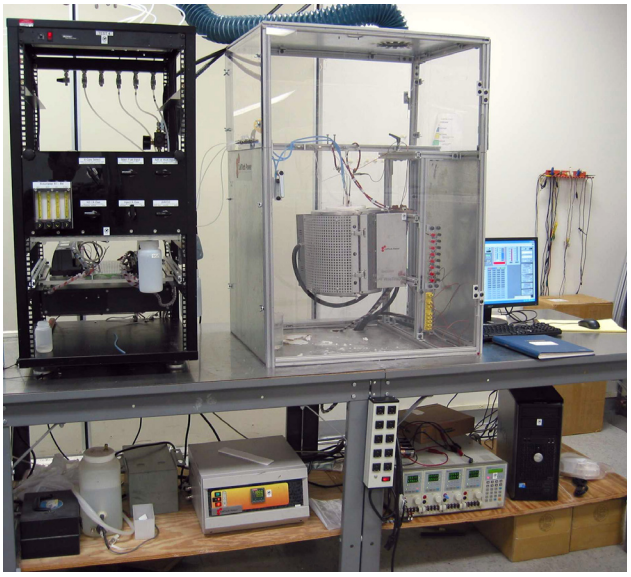

FIGURE 2. CellTech DOE Coal Test Stand

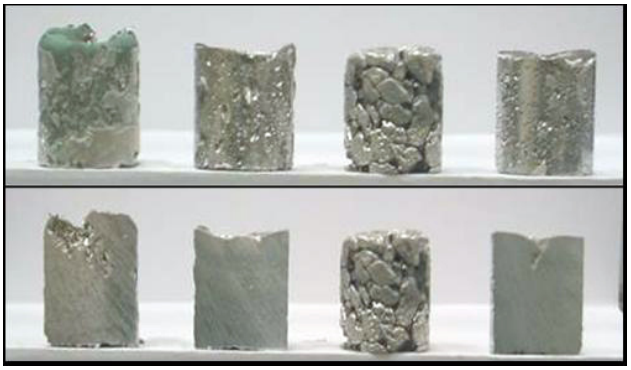

FIGURE 3. Coal Contaminate Element Solubility in Tin Samples Showing the Contaminate Expelled from the Tin

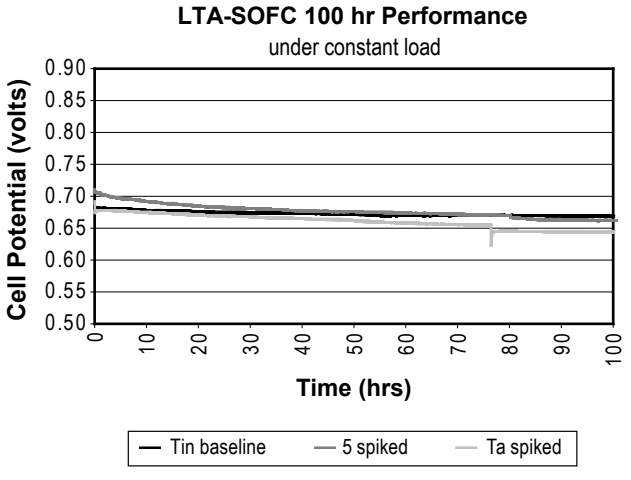

FIGURE 4. Cell Performance Comparison of LTA-Solid Oxide Fuel Cell (SOFC) Baseline and Contaminate Spiked LTA-SOFC Cells

TABLE 2. Elemental Analysis of Spiked Tin Samples under Simulated TCR Conditions

Spiked Element	Initial amount (ppm wt)	ICP-OES Results (ppm wt)	Pure Sn GDMS results (ppm wt)
Cr	4,000	1,098	2.7
V	4,000	10	<0.001
Mo	4,000	9	<0.01
Nb	4,000	115	<0.005
As	4,000	2,535	1
Mn	4,000	2,405	0.2
W	4,000	60	<0.01
Ta	4,000	8	<5
Se	4,000	44.7	<0.01
Cl	4,000		<0.01
S	4,000		0.07
P	4,000		0.08
Si	4,000		<0.01
Br	4,000		<0.05
I	4,000		<0.05

Conclusions and Future Directions

- Liquid tin has been found to be capable of separating/reducing/removing some key harmful elements under simulated TCR conditions of 1% H_2O in H_2–forming oxides thus separated from bulk tin. This result/data seems to support a technical pathway to enable the isolation of coal contaminants and perhaps coal ash and slag in the TCR.
- The electrochemical testing of cells with spiked elements has started and initial results show that for those most harmful elements projected there seems to be some cell degradation. Cell testing for 100 and 1,000 hours will continue in the next year.

FY 2010 Publications/Presentations

1. SECA - 2010
2. Fuel Cell Seminar - 2010

References

1. CellTech Power presentation at Fuel Cell Seminar 2009.

IV.3 Performance Degradation of LSCF Cathodes

Matthew Alinger
GE Global Research
1 Research Circle, MB277
Niskayuna, NY 12309
Phone: (518) 387-5124; Fax: (518) 387-5576
E-mail: alinger@ge.com

DOE Project Manager: Joseph Stoffa
Phone: (304) 285-0285
E-mail: Joseph.Stoffa@netl.doe.gov

Subcontractors:
- Rensselaer Polytechnic Institute, Troy, NY
- NexTech Materials, Lewis Center, OH

Contract Number: NT0004109

Start Date: October 1, 2008
End Date: September 30, 2010

FY 2010 Objectives

- Validate degradation mitigation strategies on representative area cells (25 cm^2).
- Develop kinetic oxidation model for ferritic stainless steel alloys GE-13L and AL441 at relevant operating temperatures.
- Measure the effect of interconnect contact geometry on contact resistance.
- Develop processing method to increase cathode interconnect coating density to minimize chromium volatilization.
- Identify potential anode degradation mechanisms.
- Evaluate alternative cell manufacturing approaches to address barrier layer adhesion.

Accomplishments

- Demonstrated that interconnect geometry does not influence contact resistance degradation.
- Validated that the power density degradation behavior using AL441 ferritic stainless steel current collectors decreases with time from ~3%/1,000 h for the initial 1,000 h and ~0.5%/1,000 h for subsequent 600 h.
- Identified the anode contact paste as a degradation mechanism responsible for area specific resistance (ASR) increases of 5-15 mΩ-cm^2/1,000 h and developed mitigation strategy.
- Optimized processing to create a dense current collector chromium barrier coating to prevent chromium volatilization in support of 40,000 h fuel cell interconnect life.

Introduction

Through research and development efforts conducted within the DOE Solid State Energy Conversion Alliance (SECA) fuel cell program, considerable progress has been made towards the realization of current solid oxide fuel cell (SOFC) stack cost goals. However, performance degradation of high-performance SOFC cathodes, in particular $La_{1-x}Sr_xCo_{1-y}Fe_yO_{3-\delta}$ (LSCF), remains a technical barrier to the commercial viability of SOFC technology. The objective of this project is to identify the dominant degradation mechanisms, and to develop and implement cost-effective mitigation strategies to retain high electrochemical performance in LSCF-based cathodes over the operational lifetime of an SOFC stack (>40,000 h). The project goal is to reduce power density degradation rates to less than 1% per 1,000 h while maintaining high initial power densities (>0.75 W/cm^2).

Approach

The LSCF-based cathode degradation mechanisms will be identified and evaluated using the state-of-the-art SOFC characterization laboratory at the GE Global Research Center, Niskayuna, New York. The approach relies on the electrochemical testing of SOFCs under realistic operating conditions. However, given the complexity of SOFCs, off-line laboratory testing including sintering studies, contact resistance, and diffusion couples will be leveraged to isolate and understand specific mechanisms under representative conditions. The structural and chemical degradation components will be identified using advanced characterization techniques such as high-resolution transmission electron microscopy, scanning electron microscopy microprobe, and high-angular resolution synchrotron X-ray diffraction.

As the contact integrity of critical interfaces has been recently identified as a major degradation mechanism, alternative cell manufacturing approaches will also be evaluated. In particular, approaches will be evaluated for improved barrier layers to provide enhanced cathode interfacial strength. In addition, interconnect chromium barrier coatings will be evaluated and optimized, with a focus on $(Mn,Co)_3O_4$,

for thin and dense coatings to mitigate the well-known chromium poisoning degradation mechanism. Combined, these results will enable the development of structure-property-performance correlations. These will be used to guide the identification and development of cost-effective solutions to reduce the degradation of high-performance LSCF-based SOFCs.

Results

Cathode-side degradation mechanisms comprise contributions of various ohmic (e.g., oxide scale growth and interaction/reaction layers between the metal interconnect and cathode) and non-ohmic (destruction of catalytically active sites and diffusion pathways for oxygen reduction within the cathode) mechanisms. A summary of potential mechanisms is presented in Figure 1. A combination of electrochemical cell testing and electrical contact resistance experiments has been employed to simulate the configuration and conditions of operating SOFCs. A quantitative comparison of the results from the experiments, in conjunction with existing models, will furnish an understanding of the degradation processes that contribute to the performance degradation of LSCF-based SOFCs.

In order to isolate and study specific degradation mechanisms, idealized but representative testing configurations are useful. For example, a gold mesh embedded in the cathode contact layer measures the voltage drop, and corresponding resistance, between the stainless steel current collector and cathode. Figure 2 shows the evolution of the ohmic contribution of ASR of the interface as a function of time for three different current collector geometries, normalized to the active cathode area. These tests were conducted at 800°C and operated at 0.25 A/cm^2 for ~4,500 h and the voltages were continuously measured. For all three geometries, solid disk, 7-hole perforated disk and 19-hole perforated disk, the change in ASR is very similar. Figure 3 shows the average change in ASR for all geometries as a function of time (red circles). It can be seen that the average ASR increase is about 7 mΩ-cm^2 after 4,144 hours. Empirical curve fitting of this long-term contact resistance data indicates that the ASR evolution follows a power law with a time exponent of 0.49. A time exponent of ~0.5 is indicative of diffusion limited processes such as the thermally grown chromium oxide on the interconnect, supporting the hypothesis that current collector oxide scale growth is responsible for the increase in ASR increase. This data is the critical degradation component of the operating fuel cell and can be used to develop long-term performance models to support the low degradation targets of the SECA program.

Another approach to isolating a specific region or interface of an SOFC is to modify a layer of interest and measure the resulting performance and degradation responses. The anode contact layer has generally been beyond the scope of this work, but recently has been identified as a potentially significant degradation mechanism. Three different anode contact pastes were applied on two cells each, and the performance was monitored using gold mesh cathode current collectors. Figure 4 shows the power density as a function of

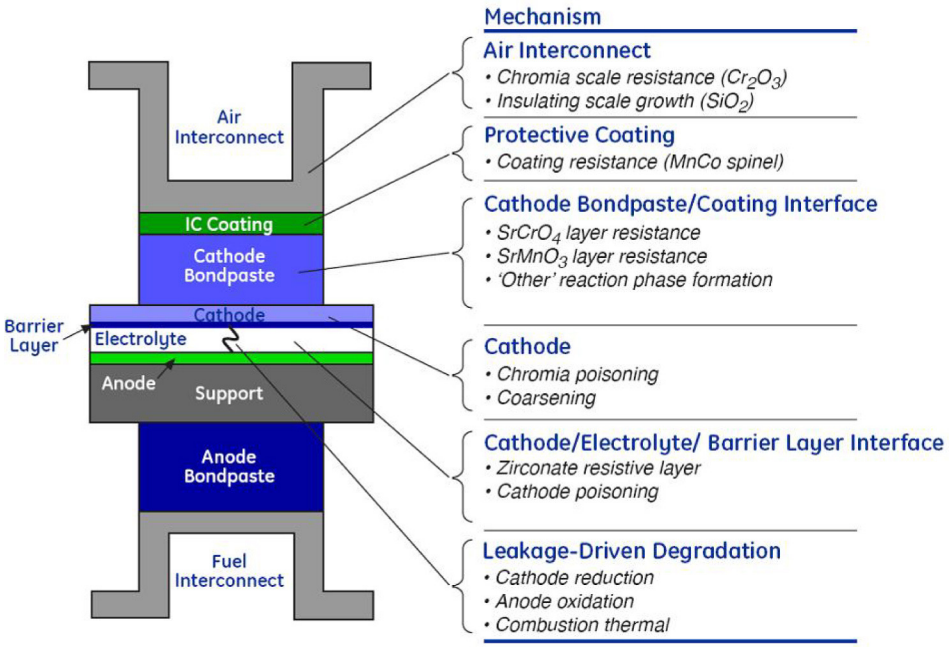

FIGURE 1. Schematic of an SOFC Highlighting Potential Degradation Mechanisms

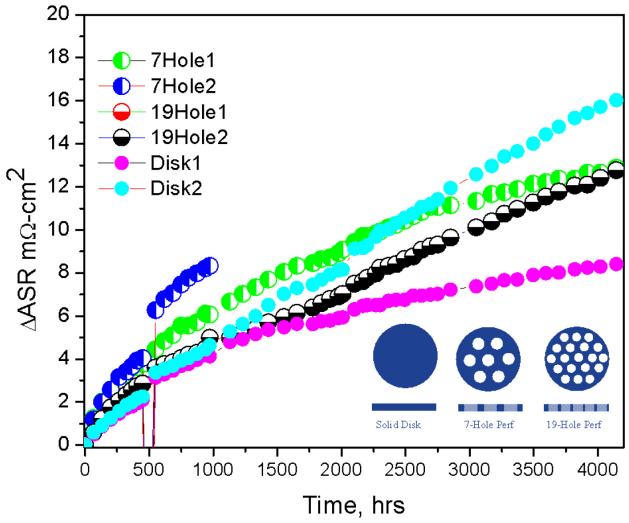

FIGURE 2. Evolution of the Ohmic Interfacial Current Collector-Cathode Contact ASR (Normalized to the Active Cathode Area) for Three Current Collector Geometries as a Function of Time

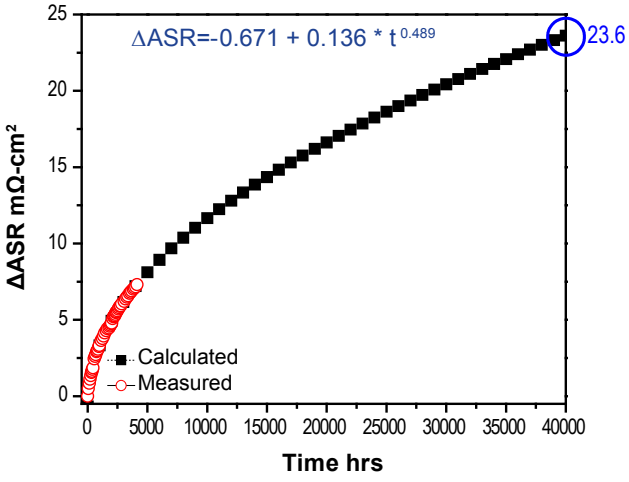

FIGURE 3. Averaged Contact Resistance Data (red circles) and Calculated Fit (black diamonds) Extrapolated to 40,000 Hours

time for these cells. The cells with anode contact paste C show greater initial power densities and lower degradation rates than the cells with anode contact pastes A or B. The average power density and ASR over the lifetime of the test for the three contact pastes is shown on the plot. The power density degradation rate, determined after a 24 h conditioning period, is 2.3±0.3, 2.7±0.6 and 1.0±0.7 %/1,000 h for contact paste A, B and C, respectively. The corresponding ASR degradation rate is 5±1, 14±3 and 0±3 mΩ-cm^2/1,000 h for contact paste A, B and C, respectively. With this understanding, anode contact pastes can be optimized so that they ensure electrical pathways without interfering with the electrochemical performance of the cells.

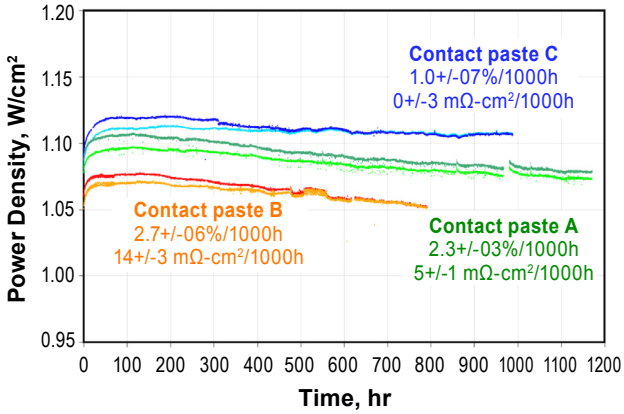

FIGURE 4. Power Density as a Function of Testing Time for the Three Anode Contact Pastes Run on Button Cells under Constant Current Condition (1.25 A/cm^2) with Gold Mesh Current Collectors

This approach of careful analysis of selected regions of SOFCs has enabled significant progress in the identification of degradation mechanisms. With this fundamental knowledge, cost-effective mitigation strategies have been devised and successfully implemented.

Conclusions and Future Directions

The inherent stability and high electrochemical performance entitlement of LSCF cathode-based SOFCs has been demonstrated. The high performance of this material system plays a major role in decreasing the cost per kilowatt of SOFCs. However, a reliable solution to the degradation behavior requires a more detailed understanding of the kinetics of the dominant mechanisms and requires additional investigation. Ultimately, a degradation mitigation solution for high performance (>0.75 W/cm^2) SOFCs with ferritic steel interconnects, having a repeatable performance degradation of <1%/1,000 h, will be demonstrated.

FY 2010 Publications/Presentations

1. Quarterly Report for 4th calendar quarter 2009, January 30, 2009.

2. Quarterly Report for 1st calendar quarter 2010, April 30, 2010.

3. V.S Dheeradhada, H. Cao, E.H. Hearn, D.A. Wark, and M.J. Alinger, "Oxidation of Ferritic Stainless Steel Interconnects: Thermodynamic Assessment and Experimental Validation," Poster Presentation, 10th Annual SECA Workshop, Pittsburgh, Pennsylvania, July 2009.

IV.4 Validation of Novel Planar Cell Design for MW-Scale SOFC Power Systems

Michael J. Day, Ph.D. (Primary Contact), Robin Kimbrell, Lora Thrun, and Scott Swartz
NexTech Materials, Ltd.
404 Enterprise Drive
Lewis Center, OH 43035
Phone: (614) 842-6606; Fax: (614) 842-6607
E-mail: m.day@nextechmaterials.com

DOE Project Manager: Briggs White
Phone: (304) 285-5437
E-mail: Briggs.White@netl.doe.gov

Subcontractor:
Professor Mark Walter, The Ohio State University
Columbus, OH

Contract Number: NT0004113

Start Date: October 1, 2008
End Date: September 30, 2011

FY 2010 Objectives

The overall goal of this project is to validate the performance, robustness, cost and scalability of a novel electrolyte-supported planar cell design, termed the *FlexCell*, for use in coal-based solid oxide fuel cell (SOFC) power systems. Specific objectives of the project include:

- Demonstrate that high performance can be achieved in *FlexCells* made with yttrium-stabilized zirconia (YSZ), instead of scandium-stabilized zirconia (ScSZ) as the electrolyte material. This objective was met by achieving a power density exceeding 300 mW/cm^2 at 800°C (>0.7 volts and 70 percent fuel utilization) with diluted hydrogen as fuel.
- Demonstrate that *FlexCells* have sufficient mechanical robustness for SOFC applications. This objective was met through finite element analyses of the *FlexCell* architecture at The Ohio State University.
- Demonstrate potential of achieving stack manufacturing cost of less than $100/kW using *FlexCells*. This objective was met by performing a comprehensive manufacturing and cost analysis and confirming that cell costs will be less than $50/kW at full-scale production (250 MW/year).
- Demonstrate scalability of the *FlexCell* design by fabricating *FlexCells* having a total cell area of at least 500 cm^2 and an active cell area of at least 350 cm^2. *This objective will be met by fabricating a minimum of 20 large-area cells and achieving a production yield of greater than 80 percent.*
- Demonstrate that high performance can be achieved in large-area *FlexCells*. *This objective will be met by performing single-cell SOFC tests on large-area FlexCells and achieving a power density of 300 mW/cm^2 at 800ºC (>0.7 volts and 70 percent fuel utilization).*
- Demonstrate stable performance of YSZ-based *FlexCells* operating with syngas that is typical of gasified coal after syngas cleanup operations. *This objective will be met by achieving a steady-state degradation rate of <1% per 1,000 hours over 500 hours of single-cell testing.*

Accomplishments

- Evaluated the effects of membrane geometry on SOFC performance, and achieved an area-specific power density of up to 475 mW/cm^2 at 800°C (0.7 volts and 70 percent fuel utilization).
- Successfully fabricated YSZ-based *FlexCells* with varying geometries. The largest YSZ-based *FlexCell* fabricated to date has a total cell area of 470 cm^2 and active area of 330 cm^2.
- Completed a manufacturing cost analysis and confirmed that full-scale production costs (250 MW) of *FlexCells* will be less than $50/kW, and identified paths to reduce costs to less than $40 per kilowatt.
- Established a finite element analysis model of mechanical robustness, which has been applied to the design of large-area (500-cm^2 area) *FlexCells* for subsequent fabrication and testing (Ohio State).

Introduction

This Solid State Energy Conversion Alliance (SECA) Core Technology project is aimed at advancing planar SOFC technology for coal-based, megawatt-scale power generation systems. It is anticipated that such systems will be comprised of a multitude of SOFC stack modules to achieve targeted power outputs. In order to increase the power output per stack module (and reduce the number of modules in the system), planar SOFC cells with large areas will be required. NexTech Materials has established a novel electrolyte-supported planar cell design, termed the *FlexCell*, which offers intrinsic scalability to large areas, as well as other

important performance attributes. The *FlexCell* is based on a patent-pending, electrolyte-supported planar membrane. As shown in Figure 1, the *FlexCell* is a two-layer structure comprising a thin electrolyte membrane layer that is mechanically supported by a "honeycomb" mesh layer of electrolyte material. With the *FlexCell*, 60 to 80 percent of the electrolyte membrane within the active area is thin (less than 40 microns), and the periphery of the cell is dense.

NexTech established its *FlexCell* membrane design using ScSZ as the electrolyte material. Although ScSZ offers an excellent combination of high oxygen ion conductivity and high mechanical strength, its cost is expected to be prohibitive for large-scale power generation systems. Thus, the focus of work on this project is on fabrication and testing of *FlexCell* membranes made with lower-cost YSZ as the electrolyte material. Phase I of this project, competed in March of 2010, focused on validating manufacturability and performance capabilities of YSZ-based *FlexCells* under conditions expected for coal-based SOFC systems. Specific tasks include fabrication of 100-cm^2 area *FlexCells*, testing of these *FlexCells* under application-specific conditions, finite element analysis of mechanical robustness of *FlexCell* membranes, and manufacturing cost analysis. Ongoing work in Phase II is aimed at fabrication and testing of large-area *FlexCells* (nominally 500 cm^2), and validation of the cost model established in Phase I.

Approach

Partially stabilized YSZ electrolyte compositions are being used to fabricate *FlexCells* in this project. Although ionic conductivity of partially stabilized compositions (3 to 6 mol% Y_2O_3) is lower than that of fully stabilized compositions (8 to 10 mol% YSZ), partially stabilized compositions have significantly higher mechanical strength. The optimal YSZ composition is a trade-off between these two endpoints. Commercially sourced YSZ powder was used to prepare green tape, from which *FlexCell* membranes were prepared using NexTech's standard procedures. NexTech's proprietary anode and cathode layers then are applied in separate deposition/sintering steps, with the anode applied to the support (corrugated) face of the *FlexCell* membrane and the cathode applied to the non-corrugated face. Successfully fabricated *FlexCells* are subjected to SOFC performance testing following NexTech's existing single-cell testing methods. Manifolds for these tests are made a high-chrome alloy (Crofer). The active cell area for these tests is 28 cm^2, as defined by the area of the current collector meshes. Finite element analysis work on this project is being performed at The Ohio State University. Manufacturing cost analyses were performed using costing principles established by SECA.

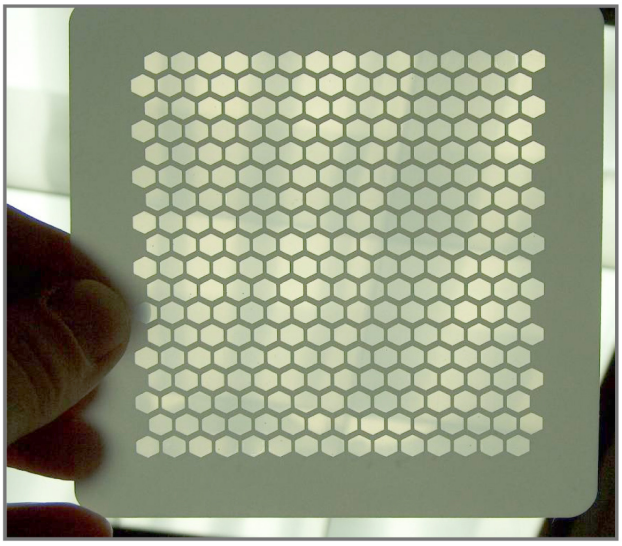

FIGURE 1. Example of a *FlexCell* Membrane

Results

YSZ-based *FlexCells* have been successfully fabricated. The primary geometric variables that can be modified in the *FlexCell* are thickness of the support layer, thickness of the membrane layer, and the percentage of unsupported (thin) membrane within the active cell area. The focus of *FlexCell* fabrication work to date in the project has been on changing thicknesses of the support and membrane layers and evaluating the impact of geometry on performance. A considerable amount of compositional and process development work was conducted with the aims of improving sintered density of YSZ-based *FlexCell* membranes, reducing defect density, and improving electrochemical performance. This work was highly successful, and led to the successful fabrication of *FlexCells* with 476 cm^2 total area (see Figure 2). NexTech also has fabricated *FlexCells* with 320 cm^2 area for use in stacks being fabricated and tested at NexTech (also shown in Figure 2). An important focus of work in Phase II will be on testing of these large-area YSZ-based *FlexCells*.

Two types of SOFC performance tests were performed on *FlexCells* with 28-cm^2 active areas. In the first set of tests, current-voltage (I-V) data were collected with constant fuel and air flow rates of 450 sccm H_2 and 1,500 sccm air. Under these conditions, cells are tested at low fuel utilization, which allows intrinsic performance characteristics to be assessed and area-specific resistance (ASR) values to be calculated. In the second set of tests, I-V data (pole curves) were recorded under conditions of constant fuel utilization (50 to 80 percent) at different temperatures (700 to 850°C), with diluted hydrogen (50% H_2, 50% N_2) as fuel. Results are summarized below:

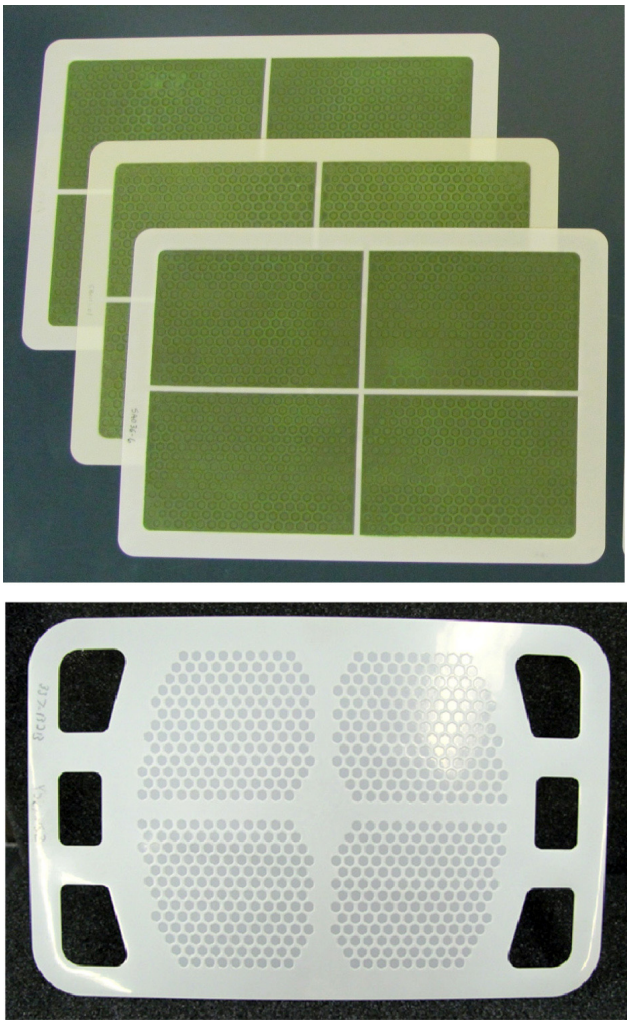

FIGURE 2. Examples of *FlexCells* Made with 476 cm^2 Area (top) and 330 cm^2 Area (bottom)

- The compositional and process improvements led to significant improvements in SOFC performance, with an ASR value (calculated from 0.8 to 0.6 volts, with H_2 fuel at low utilization) of 0.30 Ω-cm^2 obtained at 800°C, and area-specific power density exceeding 800 mW/cm^2 at 0.7 volts at 800°C (see Figure 3). At temperatures of 800 and 850°C, the performance of YSZ-based *FlexCells* is essentially the same as ScSZ-based *FlexCells* of identical geometry. At 750°C, the lower ionic conductivity of YSZ-based *FlexCells* leads to slightly reduced comparative performance (see Figure 4).
- Data obtained from constant utilization pole curve tests confirmed the intrinsic attributes of the *FlexCell* architecture. At 800°C, a power density value of 475 mW/cm^2 was obtained at 70 percent fuel utilization and 0.7 volts. Very tight spreads of pole curves were obtained over the range of 50 and 80 percent fuel utilization (see Figure 5). These data illustrate the fact that thin anode layers that are intrinsic to the *FlexCell* lead to reduced gas diffusion limitations (i.e., fuel in and steam out). When tested at 800°C with 70% fuel utilization, the highest performing YSZ-based *FlexCell* achieved

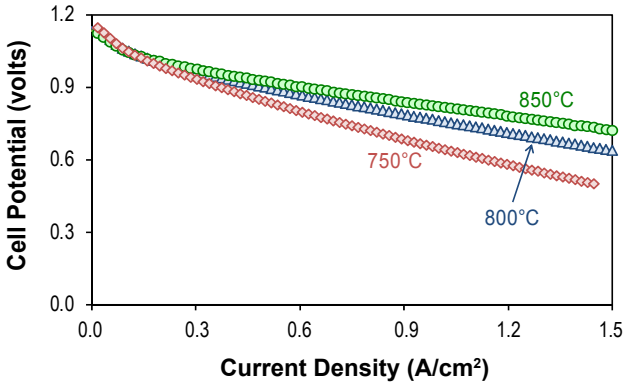

FIGURE 3. SOFC Performance of YSZ-Based *FlexCell* under Conditions of Low Fuel Utilization

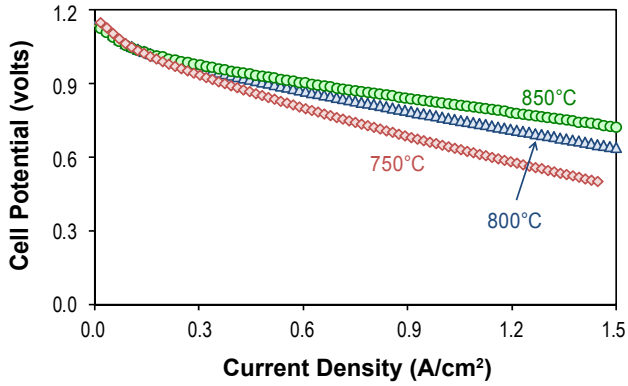

FIGURE 4. Comparison of SOFC Performance at 850 and 750°C for Identical *FlexCell* Made with YSZ and ScSZ Membranes

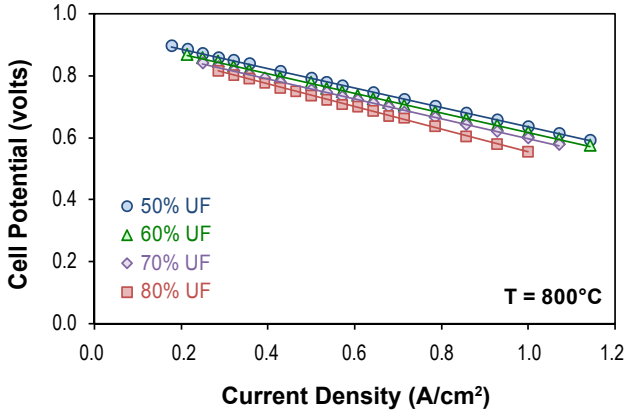

FIGURE 5. Pole Curves Obtained at 800°C with Different Fuel Utilizations for the YSZ-Based *FlexCell*

power densities of 287 and 475 mW/cm^2 at 0.8 and 0.7 volts, respectively (see Figure 6), which far exceeds the original performance milestone targets for this project.

A manufacturing cost analysis was completed for the manufacturing of large-area *FlexCells* at the 250 MW/year volume level. A seven-day, three-shift operation was assumed to maximize capacity of the highly automated manufacturing equipment. Gas-fired tunnel kilns were assumed for sintering electrolyte substrates, while electrically-heated tunnel kilns were assumed for annealing of electrodes. The capital equipment cost needed for the full-scale (250 MW) *FlexCell* production facility was determined through vendor quotes for each manufacturing operation. Raw material costs for the full-scale production plant were based on large-scale production estimates and raw material costs provided by SECA. Based on these assumptions and a complete accounting for costs associated with building and operating the production facility, a manufactured cost estimate of $45 per kW was estimated (see Table 1). Several approaches were identified to provide a path toward reduction of manufacturing cost to the $35/kW level.

TABLE 1. Breakdown of *FlexCell* production costs at 250 MW/year scale.

Cost Category	Yearly Cost	Cost Per Cell	Cost Per kW
Raw Materials	$3,389,653	$1.69	$13.56
Depreciation	$3,032,925	$1.52	$12.13
Operating Labor	$1,833,930	$0.92	$7.34
Utilities	$1,146,435	$0.57	$4.59
Operating Supplies	$677,931	$0.34	$2.71
Local Taxes	$808,780	$0.40	$3.24
Maintenance & Repairs	$67,793	$0.03	$0.27
Insurance	$323,512	$0.16	$1.29
Total	**$11,280,958**	**$5.64**	**$45.12**

In Phase I of the project, NexTech collaborated with The Ohio State University to measure material properties and generate predictive models of the mechanical robustness of *FlexCells*. Simulations were conducted both on the small, repeating unit scale as well as the large scale. Figure 7 is a schematic of the *FlexCell* active area with honeycomb (hexagonal) mesh layer. Each rectangle shown in the center of Figure 7 is a unit cell that can be repeated vertically and horizontally. With appropriate boundary conditions, the stresses, strains, and displacements in the unit cell are representative of the entire area. Figure 8 depicts equivalent stress contours for a unit cell. The frame

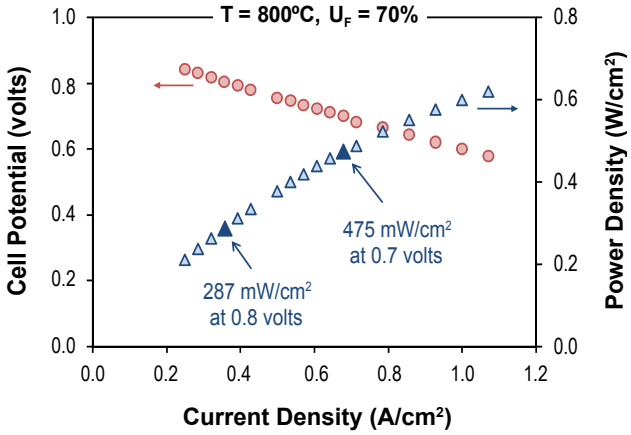

FIGURE 6. Constant Stoichiometry Pole Curve Data Obtained at 800°C with 70% Fuel Utilization for the YSZ-Based *FlexCell*

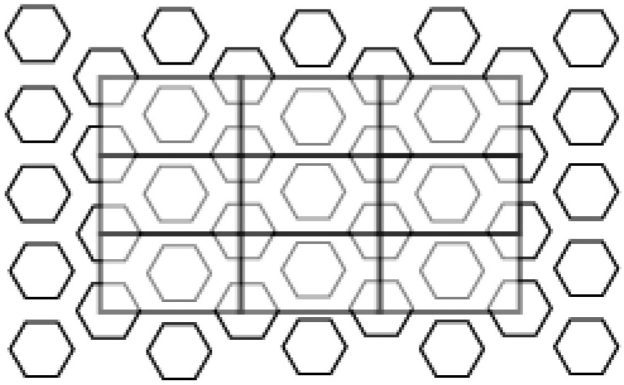

FIGURE 7. Illustration of the Repeating Unit Cell Used in Conjunction with Periodic Boundary Conditions to Approximate Large Area Membranes

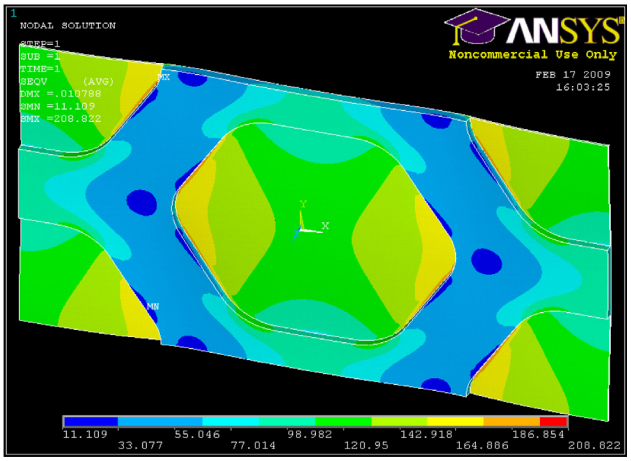

FIGURE 8. Contour Map Showing Equivalent Stresses Associated with Uniform Stretching of the Unit Cell

(mesh) around the hexagonal center portion provides the necessary mechanical strength. The geometry of the repeating unit has been varied to simulate different active areas, including those with circular support mesh cutouts and different size supports.

The large area finite element simulations with shell elements have been developed during the current reporting period. To qualify the approach, simple cantilever beams were simulated with solid brick elements and with shell elements and results from both simulations were compared to theory. Simple beams simulated with shell elements with spatially varying properties and thicknesses were also found to behave well. The active areas within the frame and outside the ribs are composed of the different hexagonally and circularly-thinned geometries simulated with the unit cells described earlier. Thus effective materials properties for active areas are obtained from the unit cell simulations. Current simulations of large area membranes are being undertaken with the intent to determine how much internal support is necessary for actual applications. Figure 9 shows one membrane with both vertical and horizontal support ribs. Other geometries under investigation have no ribs or different rib thicknesses.

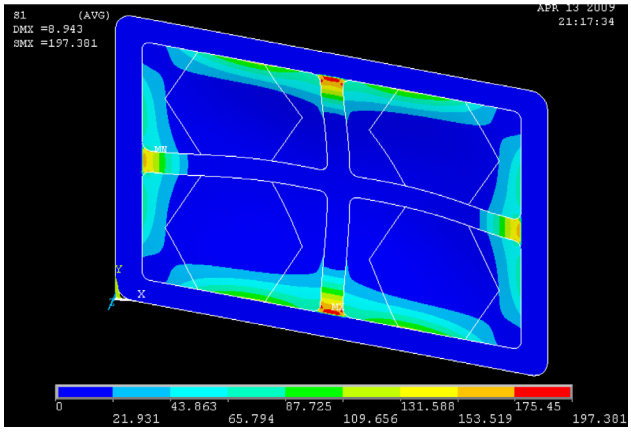

FIGURE 9. Principle stress contours for a large-area electrolyte membrane with vertical and horizontal support ribs. The loading profile is uniform pressure on the entire membrane with the outer frame area being fully constrained.

Conclusions and Future Directions

To date in this project, NexTech has successfully demonstrated the fabrication of *FlexCell* membranes made with YSZ as the electrolyte material. Electrochemical testing has confirmed that SOFC performance of YSZ-based *FlexCells* is essentially the same as that achieved with *FlexCells* made with ScSZ electrolyte material at 800ºC. The fabrication of YSZ-based was successfully scaled-up to 476 cm^2 areas. Finite element analysis modeling of the *FlexCell* architecture performed at The Ohio State University has identified geometric modifications providing improved mechanical robustness. Additional work on the project includes the following:

- Fabrication and testing of large-area *FlexCells* (>300 cm^2 active area), with the goal of replicating the performance achieved on smaller *FlexCells* (28 cm^2 active area).
- Long-term testing on simulated coal gas with the goal of demonstrating stable performance over a minimum of 1,000 hours of testing.
- Refinements to the manufacturing cost analysis, based on results of large-area *FlexCell* testing, with the goal of confirming that targeted *FlexCell* manufacturing costs can be achieved.

FY 2010 Publications/Presentations

1. Quarterly Status Report #3 (July 31, 2009).
2. Quarterly Status Report #4 (October 30, 2009).
3. Quarterly Status Report #5 (January 31, 2010).
4. Quarterly Status Report #6 (April 30, 2010).
5. Topical Report on Manufacturing Cost Analysis for YSZ-Based *FlexCells* (July 31, 2009).
6. Presentation at SECA Core Technology Workshop (July 16, 2009).
7. Interim Review Meeting Presentation (August 26, 2009).
8. Interim Review Meeting Presentation (January 8, 2010).
9. Interim Review Meeting Presentation (March 9, 2010).

V. ADVANCED RESEARCH

V.1 Proton Conducting Solid Oxide Fuel Cell

S. (Elango) Elangovan (Primary Contact), J. Hartvigsen, F. Zhao
Ceramatec, Inc.
2425 South 900 West
Salt Lake City, UT 84119-1517
Phone: (801) 978-2162; Fax: (801) 972-1925
E-mail: Elango@ceramatec.com

DOE Project Manager: Joseph Stoffa
Phone: (304) 285-0285
E-mail: Joseph.Stoffa@netl.doe.gov

Contract Number: 84595

Start Date: August 8, 2007
End Date: August 7, 2009

FY 2010 Objectives

- Identification of dopant type and concentration in a perovskite host to achieve high proton conductivity and high protonic transference number under solid oxide fuel cell (SOFC) operating conditions.
- Evaluation of a ceramic composite approach to provide chemical stability to CO_2- and H_2O-containing gases.
- Evaluation of electrode materials using symmetric cells and full cells in button cell configuration.
- Test button cells using selected perovskite compositions.
- Test short stacks.

Accomplishments

- Dopant type was identified to achieve a high protonic conductivity of $1x10^{-2}$ to 3×10^{-2} S/cm at 800°C to 900°C.
- Addition of doped ceria was found to improve stability of $BaCeO_3$ in the presence of syngas ($H_2O + CO_2$).
- High ionic transference number was demonstrated as indicated by open circuit voltage in button cells.
- A proton transference number of 0.7 was estimated at 800°C.
- Potential for high efficiency operation using a proton conductor-based SOFC relative to oxygen conductor-based SOFC was demonstrated.
- Electrode evaluation was completed using thick electrolyte discs.
- Tape cast process was developed to enable fabrication of thin electrolytes.
- Anode supported cells were shown to exhibit high performance characteristics.
- Stable cell performance demonstrated with high CO_2-containing fuel compositions.
- Stack performance evaluated using anode supported cells.

Introduction

One of the prime attractions of fuel cells is the possibility of realizing energy conversion efficiencies much higher than possible with the thermal cycle systems. The basis of this difference is that thermal cycle system efficiencies are bounded by Carnot cycle thermodynamics, whereas fuel cell efficiencies are determined by chemical equilibrium thermodynamics and non-equilibrium force-flux relationships that govern charge, mass, momentum and energy transport. Materials have been developed which function as high temperature solid electrolytes in fuel cell applications. Two of the most widely considered materials are yttria doped ZrO_2 (YSZ) which transports oxygen ions and gadolinium-doped $BaCeO_3$ which transports protons [1].

The thermodynamic difference between proton and oxygen ion cells is manifest in reversible potential variation with reactant utilization as a function of product water location. Excess air flow, used to remove the heat generated by cell operation, results in a lower water concentration in the cathode stream of a proton cell than in the anode stream of an O^{2-} cell.

Reversible potential variation with fuel utilization is shown for both proton and oxygen ion cells in Figure 1. The proton cell has a substantially higher reversible potential across the full range of fuel utilization. An interesting observation is that steam ratios greater than stoichiometric (S/C=2) increase the high utilization potential of a proton cell while oxygen ion cell potentials are uniformly higher with sub-stoichiometric steam ratios. This is due to the use of carbon monoxide via the shift reaction. The oxygen ion cell generates water in the anode stream so inlet compositions can be water deficit (high potential) and still have sufficient water to drive the shift reaction as utilization increases. The proton cell, on the other hand, must have sufficient or even excess water at the inlet to drive the shift reaction at high utilizations. However, water in the anode stream does not directly enter in the calculation of proton cell potentials and thus has little effect on the potential until higher utilizations where shift-produced hydrogen is important. Thus, high temperature proton conductors

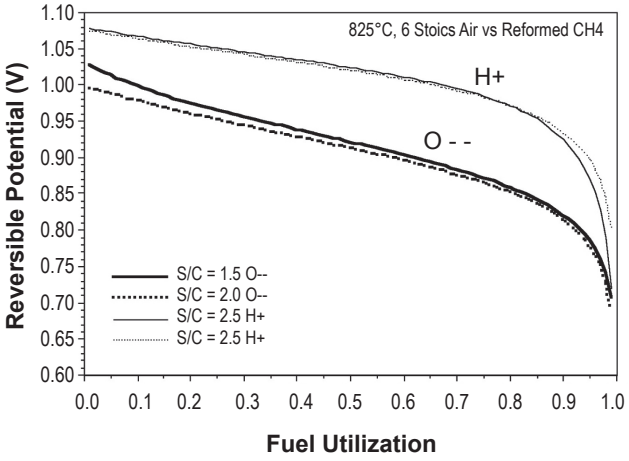

FIGURE 1. Comparison of Reversible Cell Potential

have a thermodynamic advantage over oxygen ion conductors.

Comparable electrolyte ionic conductivities are required to take practical advantage of the thermodynamic benefit. Applications driven by maximizing efficiency at the expense of power density would favor proton cells. Thus, the opportunity for very high efficiency operation is one of the primary motivating factors for investigating proton-conducting SOFCs (P-SOFCs). The challenges that have been encountered in P-SOFC systems are discussed below.

Proton Conductivity

As mentioned earlier, the differences in electrolyte ionic conductivity may be greater than differences in driving force and must be included in any comparison of an operating cell at a fixed current density. In general the protonic conductivity of commonly known perovskite materials such as doped $SrCeO_3$ and $BaCeO_3$ are considerably lower than the oxygen ion conductivity of YSZ. The proton conductivity ranges from 5×10^{-3} to 2×10^{-2} S/cm at 800°C [2-6]. While the high end of this range is comparable to the oxygen conductivity of 8-YSZ, the perovskite materials also possess some level of oxygen ion conductivity and electronic conductivity at various temperatures. Thus, the protonic transference number varies as a function of temperature. While the doped $BaCeO_3$ composition functions as an effective electrolyte, an increase in hydrogen conductivity is preferable to fully exploit the benefit of high efficiency with high power density.

Stability

One of the biggest technical challenges lies in maintaining the chemical stability of the perovskite in the presence of CO_2 and moisture, both are present in a typical hydrocarbon fuel. Numerous studies have confirmed the instability of the perovskite compositions.

It has been shown [7] that partial replacement of the B-site dopant with Zr completely eliminates this reaction. A similar improvement in stability in moist conditions was also reported with Zr substitution [8]. However, the stability improvement is at the expense of protonic conductivity. The proton conductivity was found to decrease monotonically with increasing Zr content [9-11].

Thus, what is required for successful development of a P-SOFC is an electrolyte material that has high proton conductivity to achieve a low area specific resistance, high protonic transference number relative to oxygen transference number to realize high efficiency, and stability in CO_2 and H_2O without compromising protonic conductivity for cell operation using practical hydrocarbon fuels.

Approach

Perovskite compositions that are known to exhibit protonic conductivity were evaluated for dopant study. The B-site dopants, typcially rare earth metals, have been shown to increase the proton conductivity of perovskites such as $BaCeO_3$. Several dopants and dopant levels were screened to identify compositions that have high conducivity and stability. Selected compositions were evaluated in button cell tests.

As the reaction product of the pervoskite material when exposed to CO_2 and H_2O is ceria, a composite of perovskite-ceria was evaluated for stability in syngas.

Results

A variety of B-site dopants were evaluated for their effect in total ionic conductivity and proton transference number. Protonic conductivity as high as 0.015 S/cm at 700°C and 0.02 to 0.03 S/cm at 800°C was measured. In addtion, the estimated protonic transference number ranged from 0.6 to 0.7 at 800°C, while the total ionic transference number was around 0.9.

Selected compositions, baseline and composite perovskites, were also exposed to syngas at 900°C. Comparison of powder X-ray diffraction patterns showed a significant reduction in the $BaCeO_3$ for for the composite relative to the baseline material as shown in Figure 2. As the target cell operating temperature is 700°C, various ratios of ceria-perovskite composites were exposed to syngas at 700°C. It was shown (Figure 3) that even 10 vol% addition of ceria provides a significant improvement to the stability.

Button cell tests with 500 µm thick doped $BaCeO_3$ pellets were conducted. The cell performance was somewhat low. Post-test examination showed poor

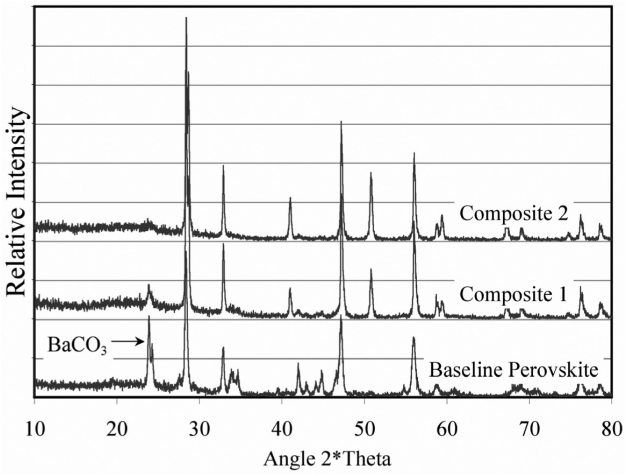

FIGURE 2. Comparsion of Sintered Density with and without the Addition of a Sintering Aid

anode bonding to the electrolyte. However, comparison of proton and oxygen conducting electrolyte fuel gas potential as a function of cell current density, as measured by independent reference electrodes, showed the high efficiency potential for the proton SOFCs. This is shown in Figure 4.

Comparison of the reference voltage trace provides several interesting points.

- First, at open circuit the proton open circuit voltage (OCV) is lower than that of oxygen OCV. This again is a confirmation of pure ionic conduction of zirconia electrolyte providing near theoretical Nernst potential. The lower OCV of the proton cell is indication of the ionic transference number, t_{ion} being less than one, in this case about 0.96.
- As a function of utilization however, the driving potential of the oxygen cell drops more steeply than the proton cell again confirming the benefit of proton cell in maintaining higher driving force.
- Because of t_{ion} being less than 1, the true benefit of proton cell does not manifest itself until the cell reaches much higher utilization. The driving potential in this case will cross over at about 10 to 15% fuel utilization. It is theoretically possible to achieve very high utilization at higher operating voltage with a proton cell.

In order to improve performance through better anode adhesion and thinner electrolyte, an anode supported cell was tested. The cell test results are shown in Figure 5. The cell was also tested using very dilute hyrogen and high CO_2 fuel (90% CO_2 – 10% humidified hydrogen) to evaluate performance at simulated high utilization condition. Very stable cell performance was observed as shown in Figure 6.

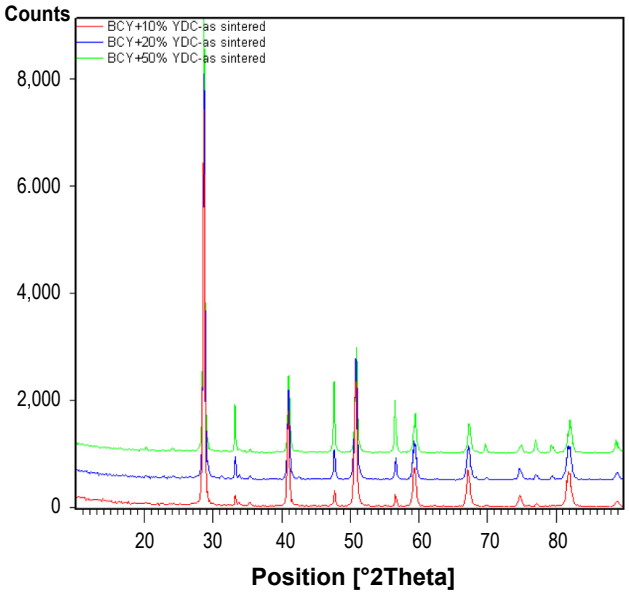

As-Sintered Composite (scan bottom to top: 10, 20, 50 vol% ceria)

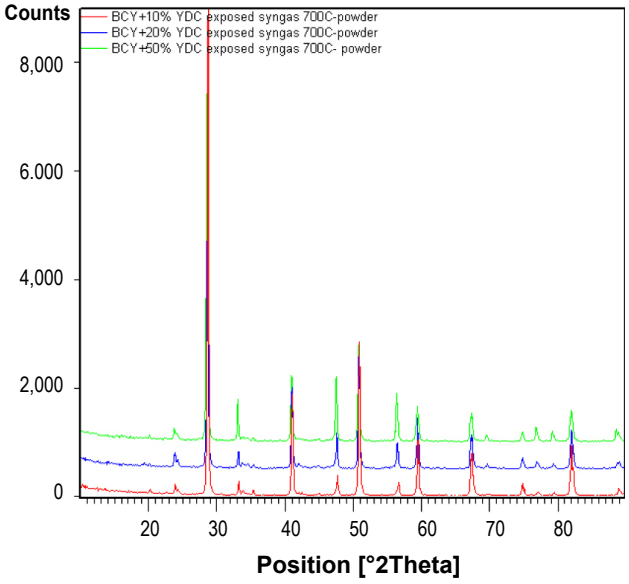

Exposed Crushed Composite Pellets (scan bottom to top: 10, 20, 50 vol% ceria)

FIGURE 3. Powder X-ray Diffraction Patterns of 900°C Syngas Exposed Baseline and 50 vol% Ceria-Perovskite Composite

A short stack using anode supported 10 x 10 cm cells were tested. The performance stability plot is shown in Figure 7. Reasonable stability were observed in simulated syngas fuel condition. However, the overall performance was compromised by defects in the electrolyte casued by unoptimized fabrication conditions. Further processing improvements are needed to overcome the fabrication defects.

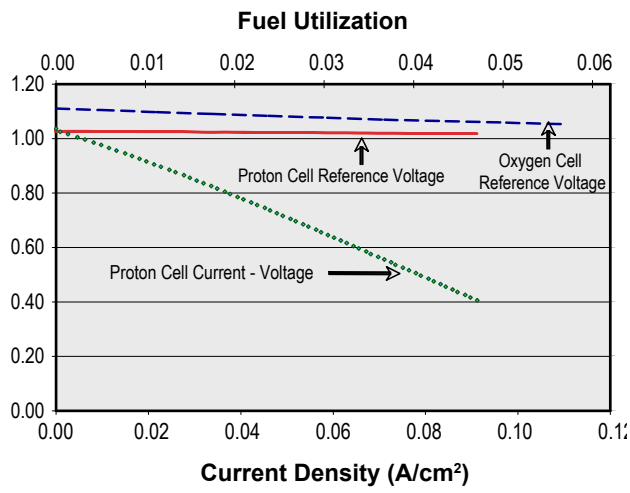

FIGURE 4. Comparison Between Proton SOFC and Oxygen SOFC: Fuel Potential as a Function of Fuel Utilization

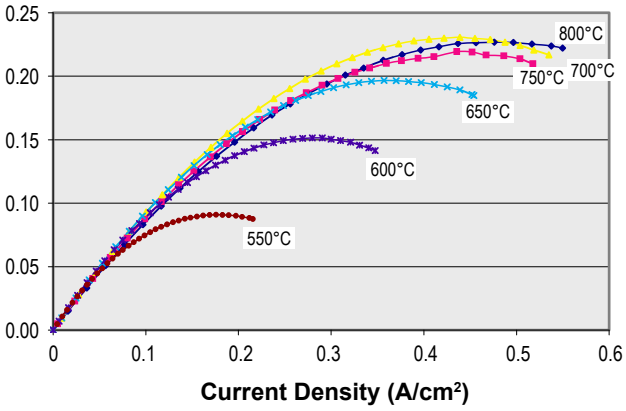

FIGURE 5. Anode Supported Cell Performance in Humidified Hydrogen Fuel

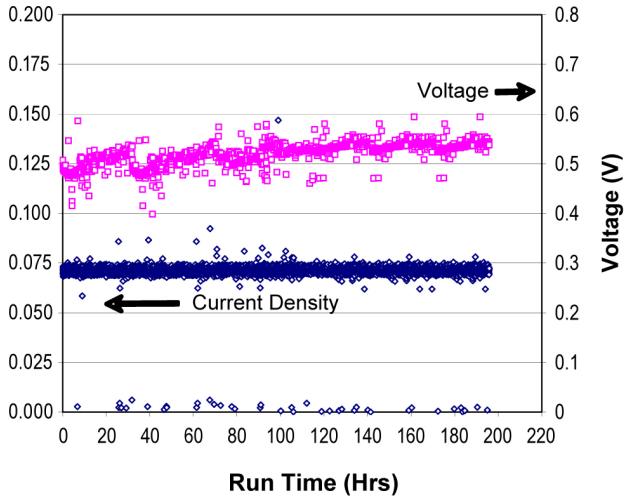

FIGURE 6. Stability of P-SOFC Cell at 700°C in High Concentration of CO_2 Containing Fuel (90% CO_2 – 10% humidifed H_2)

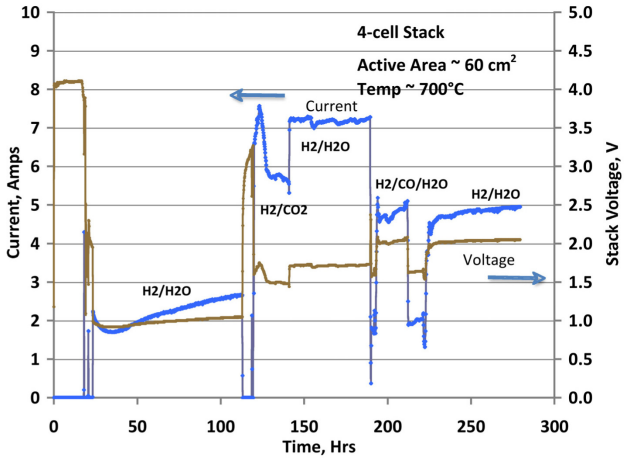

FIGURE 7. Performance Stability of Anode Supported Cell Stack

Conclusions and Future Directions

The project results reconfirms the high efficieny potential for P-SOFCs. By proper B-site doping very high proton conductivity, comparable to that of the oxygen ion conductivity of yttria-doped zirconia can be achieved to enable high performance cell operation. Stability in syngas can be achieved by using a composite electrolyte. The inherent mixed ionic conductivity in the $BaCeO_3$ type of material limit the efficiency benefit to some extent depending on the operating conditions. When the cell is operated at high utlization, significantly higher electrochemical efficieny can be realized compared to an oxygen ion conductor-based SOFC.

References

1. H. Iwahara, T. Hibino, and M. Yamada, Proc. 3rd International Symposium on Solid Oxide Fuel Cells, p. 137, Singhal and Iwahara eds., Honolulu, Hawaii, 1993.

2. H. Iwahara, T. Esaka, H. Uchida, and N. Maeda, Solid State Ionics 3/4, 359 (1981).

3. H. Iwahara, H. Uchida, and N. Maeda, J. Power Sources 7, 193 (1982).

4. H. Iwahara, H. Uchida, and I. Yamasaki, Int. J. Hydrogen Energy 12, 73 (1987).

5. H. Iwahara, Solid State Ionics 28–30, 573 (1988).

6. N. Bonanos, K.S. Knight, and B. Ellis, Solid State Ionics 79 (1995) 61.

7. T.R. Armstrong et al., "Stability of Perovskite Hydrogen Separation Membranes," AR Materials Conference, Baltimore, Maryland, April 2003.

8. N. Taniguchi et al., "Endurance against Moisture for Protonic Conductors of Perovskite-Type Ceramics and Preparation of Practical Conductors," Solid State Ionics 145, 349–355 (2001).

9. K.H. Ryu and S.M. Haile, "Chemical Stability and Proton Conductivity of Doped Perovskite Oxides in the $BaCeO_3$-$BaZrO_5$ System," Solid State Ionics 125 (1999) 355-367.

10. K. Katahira, Y. Kohchi, T. Shimura, H. Iwahara, "Protonic Conduction in Zr-Substituted $BaCeO_3$", Solid State Ionics 138, 91-98 (2000).

11. S. Wienströer and H.-D. Wiemhöfer, "Investigation of the Influence of Zirconium Substitution on the Properties of Neodymium-Doped Barium Cerates," Solid State Ionics 101-103, 1113-1117 (1997).

V.2 Oxide Contaminant Removal in Liquid Tin Anode Fuel Cells by Direct Reduction with Coal

William O'Connor (Primary Contact) and Ben Nielsen
National Energy Technology Laboratory
Process Development Division
1450 Queen Ave. SW
Albany, OR 97321
Phone: (541) 967-5834; (541) 918-8073
Fax: (541) 967-5958
E-mail: William.Oconnor@netl.doe.gov
Benjamin.Nielsen@ur.netl.doe.gov

Contract Number: 08-220696

Start Date: October 1, 2008
End Date: September 30, 2010

FY 2010 Objectives

- Evaluate reduction efficiency of tin/tin oxide mixture using both solid and gas reductants and evaluate products for contaminants.
- Evaluate reduction efficiency using CO gas as a function of temperature for the pure tin oxide system.
- Relocate Harrop furnace from Building 3 to Building 34 due to demolition of Building 3.
- Complete new Safety Analysis and Review System (SARS) package, 0927 Building 34 Melt Lab, to receive permit for operation of Harrop furnace at new location.

Accomplishments

- Reduction efficiency of pure tin oxide with three solid reductant materials was determined as a function of temperature and stoichiometric carbon addition. Reduction efficiencies decreased with increasing coal addition, from 100% to 130% stoichiometric, for both the eastern (Pittsburgh Seam) and western (Wyodak Seam) coals, while those for the coke reductant showed a reverse trend. The western coal required a greater mass addition relative to the eastern coal due to its lower fixed carbon content.
- Contaminant concentrations in the tin product were indiscernible between the three solid reductant materials, while the contaminants reported predominantly to the slag product. For the 10 critical contaminants identified by prior studies (As, Cr, Mo, Nb, Se, Ta, Te, U, V, W), all partitioned to the slag product at 90% or higher, with the exception of Te, which reported favorably (~60-70%) to the tin metal.
- The evaluation of the reduction efficiencies of gas reductants, and the evaluation of the reduction efficiency using CO gas as a function of temperature, were canceled based on program review comments from 5 January 2010. The emphasis was placed on direct reduction of tin oxide with coal within the fuel cell, or simulations of that environment, thus gas reduction was not considered pertinent to the goals of the liquid tin anode (LTA) project.
- Revision of the objectives resulted from the project review comments, to include conduct of direct reduction tests of dilute tin oxide within a molten tin bath. Yttria-stabilized zirconia crucibles were purchased to simulate the fuel cell media, and high-purity tin shot was obtained to produce a 10:1 tin/tin oxide ratio in the molten bath.
- The Harrop furnace was moved to its new location in Building 34, refitted with a new electrical supply/disconnect, control/process thermocouples, and hood tied into the existing blower/baghouse infrastructure.
- The hazard analysis for the new 0927 Building 34 Melt Lab SARS package has been conducted and hazard charts have been prepared and submitted to the Engineering Research Division for approval.

Introduction

The National Energy Technology Laboratory (NETL) Fuel Cell Program has identified tin (Sn) as a possible material to support concurrent electrochemistry and fossil fuel utilization. In this concept, liquid tin provides a 'fuel' for the electrochemical step, but is oxidized to some degree within the cell during the process. Coal is introduced into the liquid tin to convert the tin oxide back to tin at the same rate that the 'fuel' is consumed. This project investigates the in situ or direct reduction of tin oxide with coal within the fuel cell. The ultimate goal is to develop a process to recycle tin oxide into tin without contamination of the fuel cell, by sequestering the contaminants introduced by the coal in a separate, recoverable slag component. To this end, NETL has performed a number of tin oxide reduction tests in an effort to determine reductant-specific reduction efficiencies at the fuel cell operating conditions, and the fate of contaminants supplied by the coal ash component. Results have demonstrated that reduction efficiencies

of 90% or greater can be achieved for both eastern and western coals at the fuel cell operating temperature of 1,000°C, while virtually all critical contaminants report at >90% to the slag component.

Approach

Although the reduction tests were conducted in Fiscal Year 2009, complete analytical results were not received until mid-FY 2010, thus a brief description of the tests is provided here for reference. A test matrix was designed to investigate three reductant materials at three stoichiometric carbon levels and three temperatures (800, 1,000, and 1,200°C). Reductants included two coals acquired from the Penn State Coal Bank, DECS-26 Wyodak Seam Coal (Wyoming), DECS-34 Pittsburgh Seam Coal (Pennsylvania), and metallurgical coke, which was included as a baseline. A high purity tin oxide sample was acquired from Universal Photonics, with a typical chemical analysis of 99.7% SnO_2 (78.65% as Sn) and 0.02% Fe. Chemical analyses for the major constituents and trace elements were acquired for all three reductants and the tin oxide sample from CONSOL Energy Inc., R&D. The carbon addition to the tin oxide was based on the chemistry of the tin oxide, fixed carbon content of the reductant, and the following stoichiometric reduction equations.

$$SnO_2 + 2C \Rightarrow Sn + 2CO$$
$$SnO_2 + 2CO \Rightarrow Sn + 2CO_2$$

Table 1 lists the charge weights for each of the 27 reduction tests, grouped by reductant. Three theoretical

TABLE 1. Charge Weights for the Tin Oxide Reduction Tests

Temp., deg. C	Reductant	Stoich., C %	Number	Reductant wt, pct	Tin oxide wt, pct	Total feed wt, pct
800	Pittsburgh Seam	100	1	12.76	87.24	100.00
		115	2	14.40	85.60	100.00
		130	3	15.98	84.02	100.00
	Wyodak Seam	100	4	14.30	85.70	100.00
		115	5	16.10	83.90	100.00
		130	6	17.83	82.17	100.00
	Coke	100	7	8.35	91.65	100.00
		115	8	9.49	90.51	100.00
		130	9	10.59	89.41	100.00
1000	Pittsburgh Seam	100	10	12.76	87.24	100.00
		115	11	14.40	85.60	100.00
		130	12	15.98	84.02	100.00
	Wyodak Seam	100	13	14.30	85.70	100.00
		115	14	16.10	83.90	100.00
		130	15	17.83	82.17	100.00
	Coke	100	16	8.35	91.65	100.00
		115	17	9.49	90.51	100.00
		130	18	10.59	89.41	100.00
1200	Pittsburgh Seam	100	19	12.76	87.24	100.00
		115	20	14.40	85.60	100.00
		130	21	15.98	84.02	100.00
	Wyodak Seam	100	22	14.30	85.70	100.00
		115	23	16.10	83.90	100.00
		130	24	17.83	82.17	100.00
	Coke	100	25	8.35	91.65	100.00
		115	26	9.49	90.51	100.00
		130	27	10.59	89.41	100.00

carbon additions were investigated: 100% (1 mole carbon/mole SnO_2); 115%; and 130% stoichiometric. The materials were blended for approximately 10 minutes in a multi-speed bench-top Hobart blender, weighed out into 100 g allotments, and sealed in plastic bags prior to their addition to the crucible. The vessels used for the reduction tests were 100 cm^3 high-alumina crucibles, fitted with high-alumina lids which were drilled to provide inlet and outlet holes. The empty crucibles were purged with 99.9% argon gas for ~1 min at a flow rate of 1,000 cm^3/min. Following the Ar purge, the lids were removed and the crucibles were loaded with the 100 g feed mixture. The lids were then replaced, and the loaded crucible was re-purged for ~30 sec at the same Ar flow rate. The Ar purge was intended to provide an inert atmosphere above the bed of material and prevent oxidation of the carbon reductant with air. The crucibles were laid out in a 3x3 grid, with each row representing one reductant at the three carbon levels. This procedure was repeated for each of the three temperatures investigated, with duplicate tests conducted at 800°C and 1,000°C, for a total of 54 reduction tests.

A Harrop SiC element furnace with a nominal 1 ft^3 hearth was used for the reduction tests. The furnace was ramped up to temperature and allowed to stabilize prior to loading the nine crucibles onto the hearth. A thermocouple was placed within one of the crucibles, into the bed of feed material, to monitor bed temperature. Once the targeted bed temperature was reached, a 1 hour soak was conducted, followed by removal of all the crucibles at temperature. This methodology was used to rapidly cool the molten tin in an effort to prevent re-oxidation.

Results

Analytical data for most of the 61 metal, slag, and sinter products from 27 reduction tests were received by the end of Quarter 1, with the remainder received by the end of Quarter 2. These data, along with feed analyses acquired previously, were compiled to permit the calculation of the mean feed and product analyses, trace element concentrations of the feed and products, and distribution of trace elements among the furnace products. Tin recovery to metal (reduction efficiency) was determined based on the material balance for each test and the chemical analyses of the feed and products, and is reported graphically in Figure 1, grouped by reductant.

Tin recovery to the metal product was ~90% at 1,000ºC for each reductant, although at differing carbon additions. The coke required a 130% stoichiometric carbon addition to achieve roughly the same reduction efficiency achieved by both coals at the 100% level. This appears to be an illustration of the greater reactivity

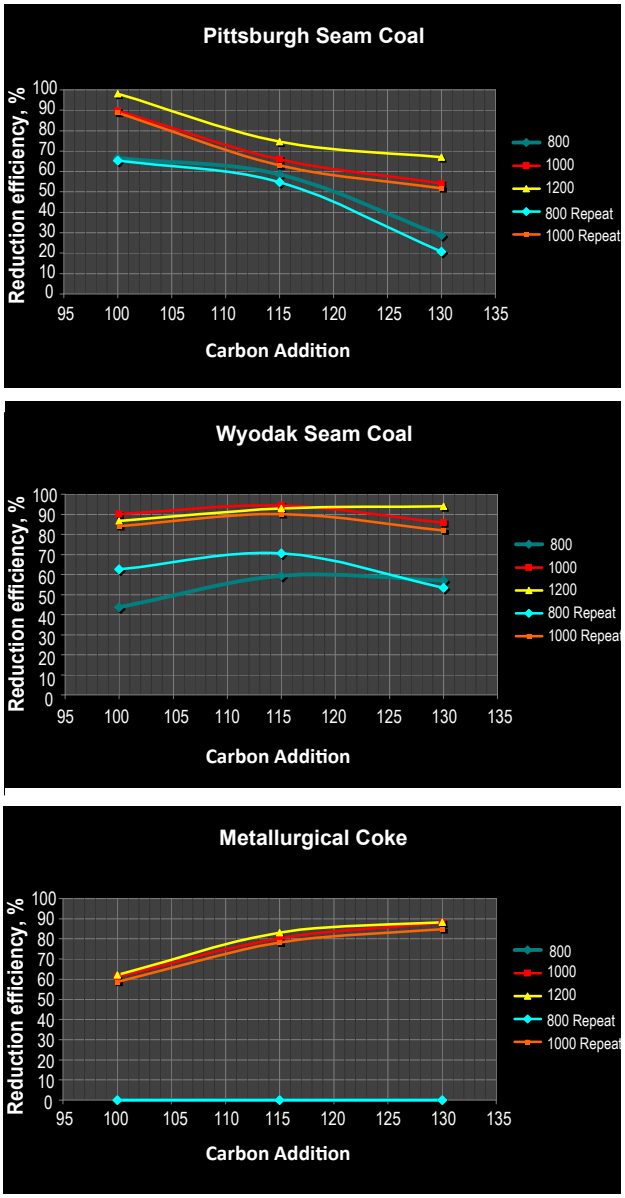

FIGURE 1. Reduction Efficiencies for Each of the Reduction Tests

of the coals, and their crystalline carbon, relative to the coke, which is comprised primarily of amorphous carbon. The higher moisture and lower fixed carbon content of the western coal required a greater mass addition to reach the 100% stoichiometric level, compared to the eastern coal, resulting in higher ash content in the feed and slightly greater slag generation for the western coal.

CONSOL Energy R&D, the contract lab conducting the analyses, has explained that the tin oxide matrix represents an extremely difficult sample matrix for the inductively coupled plasma (ICP) mass spectrometry and/or ICP-atomic emission spectoscopy analytical method used. Part of this difficulty is due to the

tendency for the tin oxide to coat instrumentation, requiring significant effort to flush the device and all infrastructure for each sample. However, the more significant limitation is caused by the concentration of tin oxide in each slag or sinter sample, which tends to mask other elemental signatures, leading to higher detection limits. For example, detection limits for several of the critical elemental contaminants (As, Cr, Mo, Nb, Se, Ta, Te, U, V, W) are 50 ppm or higher in the slag products, due to the matrix effect of the tin oxide in the slag. Conversely, detection limits for these same critical elements are very good for the metallic tin product, often as low as 0.1 ppm. To best represent the tin produced from each reductant, the weighted mean concentrations were calculated for all of the metallic tin products from each group of tests. Using this methodology, the trace element concentrations in the metallic tin products are very consistent, and appear to be generally independent of the reductant used, as depicted graphically in Figure 2.

Elemental mass distributions among the furnace products were calculated for each of the reductant materials, using the equation below. Concentrations below the detection limit were assumed to be at the detection limit for the calculation. Mass balance (MB) and elemental mass distributions between the metal and slag products are included in Figure 3.

$$D_{ij} = c_{ij} m_j / \sum_j (c_{ij} m_j) \text{ x } 100$$

Where
D = Distribution (mass fraction) in %
I = Element I
J = Product (metal, slag)
c = Mass concentration
m = Mass of each product

Clearly, the trace elements depicted in Figure 3 report predominantly to the slag product, even though the overwhelming mass distribution among the solid products is to the metal. The one exception is Te, which reports favorably to the metal (~60-70%). This trend

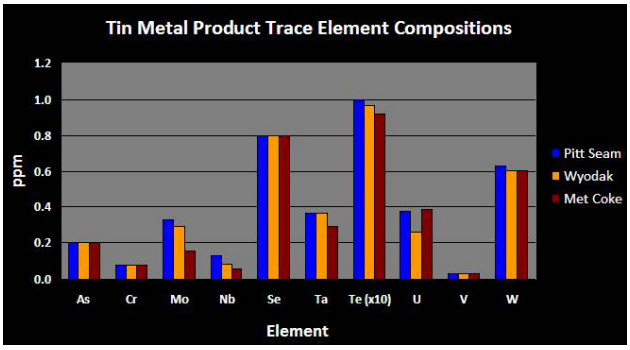

FIGURE 2. Trace Element Concentrations in the Tin Metal Products

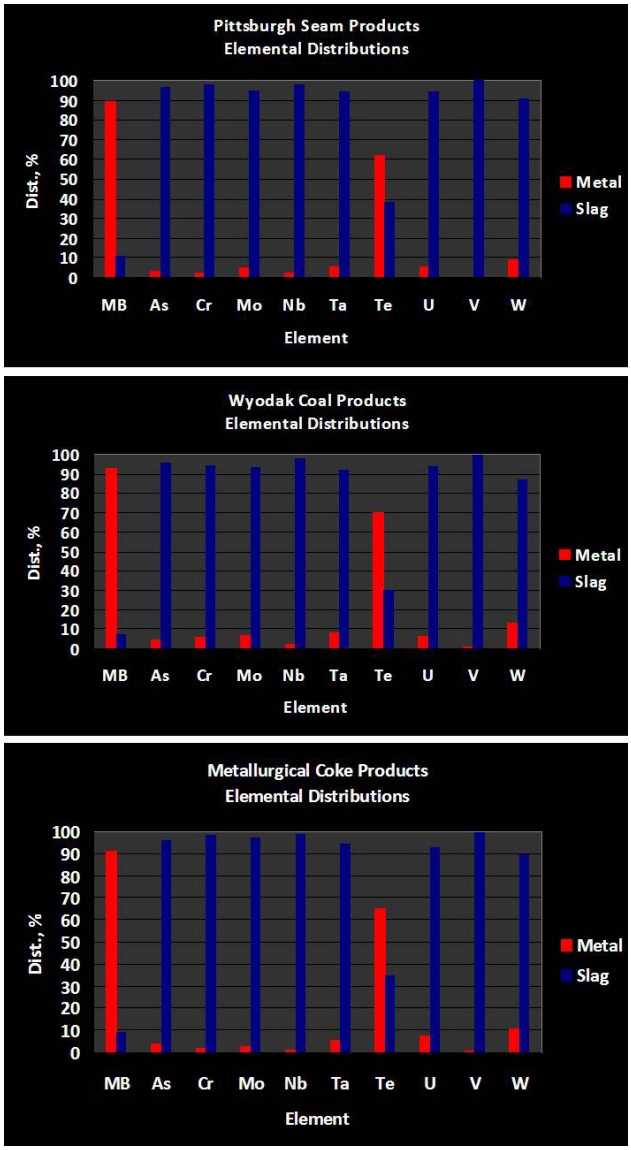

FIGURE 3. MB and Elemental Distributions among the Metal and Slag Products

is independent of the reductant used, and suggests that effective slag cleaning of these contaminants is possible.

Conclusions and Future Directions

Reduction efficiency of pure tin oxide with three solid reductant materials was determined as a function of temperature and stoichiometric carbon addition. Reduction efficiencies decreased with increasing coal addition, from 100% to 130% stoichiometric, for both the eastern (Pittsburgh Seam) and western (Wyodak Seam) coals, while those for the coke showed a reverse trend. The western coal required a greater mass addition relative to the eastern coal due to its lower fixed carbon content.

Contaminant concentrations in the tin product were indiscernible between the three solid reductant materials, while the contaminants reported predominantly to the slag product. The 10 critical contaminants identified by prior studies (As, Cr, Mo, Nb, Se, Ta, Te, U, V, W), reported predominantly to the slag product, even though the overwhelming mass distribution among the solid products is to the metal. The one exception is Te, which reports favorably to the metal (~60-70%). This trend is independent of the reductant used, and suggests that effective slag cleaning of these contaminants is possible.

During the 5 January 2010 Project Review meeting, concerns were expressed that the reduction tests conducted and reported on here did not reflect or effectively simulate the fuel cell environment. These were in fact "worse case" scenarios because a 100% solid tin oxide sample was reduced, rather than a relatively small percentage of molten tin oxide within a bath of molten tin. This latter scenario could best be reproduced by conducting the reduction tests in a LTA fuel cell. Because the Albany site has no such fuel cell, an alternative scenario was proposed.

A second series of reduction tests will be conducted in which the powder mixture of solid tin oxide and coal/coke reductant will be reacted within a larger crucible filled with metallic tin shot. These tests will be conducted in 250 cm^3 crucibles, which will provide sufficient volume for 33 g of powder mixture and roughly 330 g of tin shot. This will provide for a dilution factor of over 10:1, molten tin to tin oxide, which is intended to better simulate the actual fuel cell environment. The tests will also be conducted in yttria-stablized zirconia crucibles, the same ceramic used in the LTA fuel cell, to better simulate the wetting characteristics and/or molten bath/ceramic interaction of the actual fuel cell.

This second group of tests will include three series, three tests per series, based on the results from the initial reduction tests and the modifications described above. All tests will be conducted at 1,000°C, and each reductant will be added at the optimum stoichiometric level determined in the prior tests. A baseline series will repeat the initial tests, but in the molten tin bath scenario. A second series will be conducted with slag former additions intended to fluidize the product slag, based on the ash composition of each reductant. A third series will repeat the slag former tests, but the tin oxide/reductant powder mixture will be spiked with several of the critical trace elements. This is intended to increase their concentrations in the furnace products to ensure that their levels will be above the instrumental detection limits.

Due to the demolition of Building 3 at the Albany site, the Harrop furnace used for the reduction tests was moved to a new location, and a new SARS permit is required prior to conduct of the next series of tests. The 0927 Building 34 Melt Lab SARS package is in process.

V.3 DOE/NETL In-House LTA SOFC R&D

Kirk Gerdes
U.S. Department of Energy
National Energy Technology Laboratory
3610 Collins Ferry Rd.
Morgantown, WV 26507
Phone: (304) 285-4342; Fax: (304) 285-4469
E-mail: Kirk.Gerdes@netl.doe.gov

Contract Number: 10-220621 6923
(In-house LTA SOFC R&D)

Start Date: October 1, 2009
End Date: September 30, 2010

FY 2010 Objectives

- Measure oxygen/hydrogen solubility and oxygen diffusivity in liquid tin and liquid tin alloys at two or more temperatures between 800 and 1,000°C.
- Create of a model for the operation of a liquid tin anode (LTA) solid oxide fuel cell (SOFC) using experimentally-determined parameters.
- Report results directly to industrial collaborators (CellTech, Inc.) and to general public in the form of conference presentation or journal publication. Reports detail methodologies, results, and conclusions from experimental and modeling work.

Accomplishments

- Test stand data quality improved and electrochemical operations have been completed at 750-1,000°C for current densities of 1-20 mA/cm^2. System is extremely well sealed (no oxygen leaks) and consequently data noise is limited to a few microamps.
- Collected data were matched to oxygen transport model with high accuracy.
- Collected data indicate oxygen diffusion at 800°C. Diffusion coefficient of ~10^{-4} cm^2/sec agrees with reported literature values.
- Test fixture modifications completed that permit spatial resolution of key parameters (temperature, potential).
- Performed microscopic/spectroscopic analysis of tin samples doped with trace materials, evaluated partitioning of contaminant material between material phases.

Introduction

In 2009, electricity consumers in the United States were supplied with 68% of their electricity from fossil fuels, with 44% of the total electric power generated from coal fuel alone. Sustained, economically feasible production of electric power will require continued consumption of substantial amounts of coal. Improving the electricity generation efficiency using coal fuel extends the lifetime of coal reserves and reduces the amount of carbon dioxide and other pollutants produced per kilowatt of electricity (relative to lower efficiency processes). High efficiency production from coal is possible in power plant designs that include fuel cell technology.

Most fuel cell systems leveraging coal as a fuel source require gasification of the coal to produce synthesis gas, which significantly increases system cost and complexity. By replacing the traditional ceramic fuel electrode of a typical high temperature SOFC with a liquid metal anode (LMA) such as tin, pulverized coal and other solid carbon-containing fuels (plastics, biomass) can be fed directly into the fuel cell and their chemical energy converted to electricity. Direct utilization of the coal facilitates decreased cost and complexity of the total system, features which serve to offset the lower power density of this novel unit relative to traditional SOFC. This project investigates the basic performance features of an LMA-SOFC to produce fundamental data that will be useful for designing commercially significant systems.

Approach

Utilization of coal directly in an LMA-SOFC requires fundamental knowledge of the processes of oxygen transport in such a system. Oxygen from the air is captured and reduced at the cathode and ionically transported across the electrolyte layer. The oxygen then reacts to oxidize the metal (tin in the present case), forming a tin-oxygen specie that travels through the tin layer to the fuel. The oxidized tin then releases its oxygen as the fuel source is oxidized and the tin oxide reduces to tin metal. This oxygen exchange process produces electricity and an exhaust gas containing steam and carbon dioxide.

The transport and exchange processes pertinent to the operation of an LMA system are depicted in Figure 1 and include: 1) the rate at which oxygen diffuses through the liquid metal anode; and 2) the total solubility of oxygen and other fuel components (carbon, hydrogen)

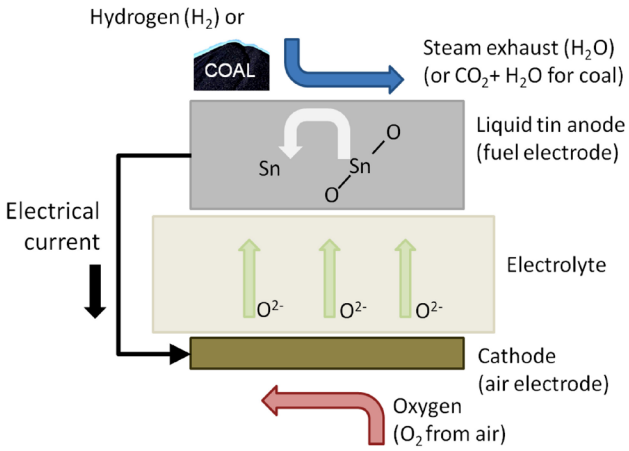

FIGURE 1. Illustration of the Oxygen Transport Path Through the Liquid Metal Anode SOFC

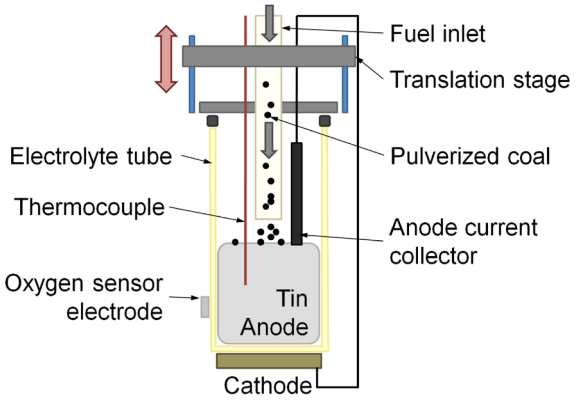

FIGURE 2. Schematic of the LTA-SOFC Test System Operated by NETL

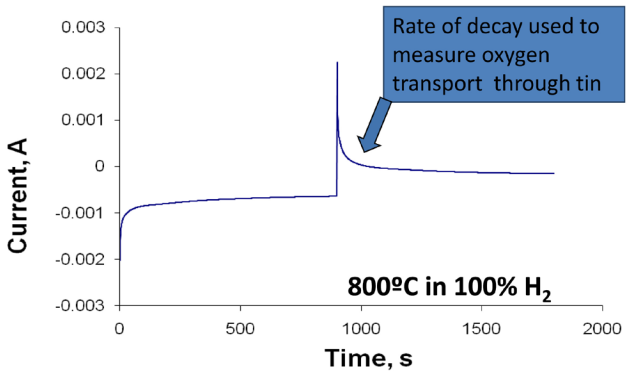

FIGURE 3. Current response to 50 mV step in potential in LTA-SOFC operated at 800°C in hydrogen. The quality of the current trace (low noise) is of particular note and indicates a well-sealed system.

in the liquid metal. The Fiscal Year 2010 research effort has evaluated these system properties in order to generate fundamental data that are necessary to design larger systems capable of producing commercially significant electricity. The data collected in this effort are compared to basic models and literature reported data.

Results

The LMA-SOFC system was operated using tin as the anode, and the cell is therefore referred to as the LTA-SOFC system. Figure 2 shows the configuration of the liquid tin fuel cell test apparatus operated at NETL. The tin is contained in a crucible made of the fuel cell electrolyte material, which has a cathode painted on the bottom. The fuel is fed through an interior tube oriented co-axially with the outer tube. One current collecting electrode is attached to the painted cathode and one electrode is submerged inside the tin. The electrodes are connected externally to instrumentation that can probe the current/voltage/power characteristics and perform electrochemical impedance spectroscopy experiments on the cell. A thermocouple is also immersed in the tin to measure the temperature at different depths. Figure 2 depicts an oxygen sensor attached to the wall of the tube to measure the amount of oxygen inside the tin bath. In the most recent tests, the thermocouple and the oxygen sensor have each been attached to a translation stage to facilitate movement of the probes. Probe translation allows spatial resolution of liquid tin bath temperature and potential to ensure that key assumptions in the transport models are satisfied during the experiments.

A series of typical cell results is shown in Figure 3 for a cell operated at 800°C with hydrogen fuel. In a single experiment, small step changes in voltage are applied to the cell and the current response is measured as a function of time. Measurement of the electrical response is repeated for temperatures between 800-1,000°C and for different fuel sources (hydrogen, carbon, coal). By monitoring changes in operating current, the mechanisms of oxygen transport are isolated and quantified for each step along the path into, through, and out of the tin layer.

The quality of the trace reported in Figure 3 is excellent, as indicated by noise band of less than 10 microamps observed as the system relaxes to the equilibrium potential. The data quality was the result of diligent testing and repeated refining of the experimental apparatus. In particular, a special assembly method was adopted which keeps the cell seal in a location that both prevents oxygen leakage into the test cell, and directs any trace leakage to the fuel exhaust line. The noise-free relaxation data demonstrate a shape that closely approaches the theoretically predicted result and the data have been used to calculate an oxygen diffusion coefficient that is similar to those predicted in the literature at 10^{-4} cm^2/sec.

The test system at NETL has been primarily operated on hydrogen, but results have also been obtained using carbon and coal as fuels. Data comparing the operation of the system on hydrogen and carbon are shown in Figure 4. Results show that operation using carbon as fuel results in greater impedances (reduced efficiency) than in the hydrogen fueled condition. The result certainly indicates that the hydrogen reaction proceeds faster than the carbon reaction, but the source of the greater hydrogen reaction rate is not precisely known. Hypotheses for the superior hydrogen reaction rate include improved hydrogen/electrode contact relative to carbon, greater surface diffusion rates of hydrogen, or modest solubility of hydrogen in the liquid tin.

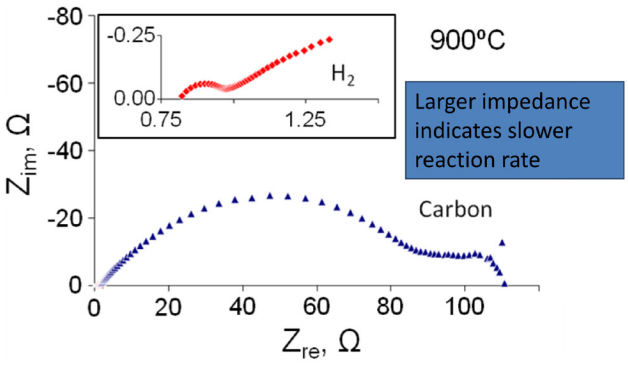

FIGURE 4. Comparison of Cell Impedance When the NETL Test System Is Operated on Hydrogen or on Carbon

Conclusions and Future Directions

Publicly reported performance information for the state-of-the-art LMA-SOFC indicates that the system can generate roughly 0.2 W/cm^2 of power, compared to over 1 W/cm^2 for a high tech SOFC system. While the LTA-SOFC is more fuel flexible, is more tolerant to fuel contaminants, and does not need a gasifier to run on coal, the system cost could be further lowered by pushing its performance closer to that of a traditional SOFC. The power can be increased by decreasing the tin layer thickness, by improving the contact between the anode and the fuel (and electrolyte), or by boosting the amount of oxygen that can be carried in the tin (by adding other chemicals to the tin bath).

Future efforts will primarily focus on the adoption of novel metal alloys of tin and characterization of the oxygen transport and solubility. Promising alloys will be identified through thermodynamic analysis and tested using the types of tests described here. After an alloy is identified that produces an electrode having good transport features, the stability of the metal will be evaluated to ensure that the anode will remain stable over the course of operations. In particular, the alloy constituents must not react with the electrolyte or produce undesirable phases with any trace metals that the coal may contain.

FY 2010 Publications/Presentations

1. Poster presentation, "Oxygen Diffusion and Solubility in a LTA-SOFC," SECA 2010, Pittsburgh, Pennsylvania.

2. Liquid Tin Anode review meeting, January 2010, hosted by SECA/NETL.

3. H. Abernathy, R. Gemmen, K. Gerdes, and R. Pineault, "Experimental Characterization of a Direct Carbon Solid Oxide Fuel Cell with a Liquid Tin Anode," Materials Science & Technology 2009, Pittsburgh, Pennsylvania, October 2009.

4. H. Abernathy, R. Gemmen, K. Gerdes, M. Koslowske, W.A. McPhee, and T. Tao, "Fundamentals of Liquid Tin Anode Solid Oxide Fuel Cell (LTA-SOFC) Operation" (in submission).

V.4 Testing and Evaluation of Solid Oxide Fuel Cells in Extreme Conditions

A. Alan Burke (Primary Contact),
Louis G. Carreiro
Naval Undersea Warfare Center, Division Newport (NUWCDIVNPT)
1176 Howell Street, Bldg. 1302/1
Newport, RI 02841
Phone: (401) 832-6675; Fax: (401) 832-6202
E-mail: Adrian.Burke@navy.mil

DOE Project Manager: Maria Reidpath
Phone: (304) 285-4140
E-mail: Maria.Reidpath@netl.doe.gov

Subcontractors:
- Versa Power Systems, Littleton, CO
- Delphi Corporation, Troy, MI

Contract Number: 43247

Start Date: July 23, 2009
End Date: December 31, 2010

FY 2010 Objectives

- Examine solid oxide fuel cell (SOFC) performance under extreme conditions (pure oxygen and reformate) to benefit future coal gasification plants, as well as NUWCDIVNPT's unmanned, undersea vehicles (UUVs).
- Provide independent testing and evaluation of SOFC stacks being developed under the DOE's Solid State Energy Conversion Alliance (SECA) program.
- Identify key performance targets to ensure reliable, steady-state operation by preventing coking and having acceptable recycle flow rate.
- Demonstrate Versa Power Systems (VPS) SOFC stack in notional UUV system test.
- Demonstrate Delphi Corporation SOFC stack and fuel processor using JP-10, RP-1, and other diesel-type fuels.

Accomplishments

- VPS stacks were evaluated in simulated UUV conditions.
- Hardware has been delivered from Delphi Corporation for SOFC stack and reformer testing in Fiscal Year 2010.
- Clear guidelines have been established regarding system reliability and efficiency as dependent upon CO_2 (scrubber) removal, water feed into steam reformer, and anode recycle ratio.

Introduction

The objective of this work is to conduct independent testing and evaluation of SOFC stacks being developed within the DOE's SECA program under "extreme" conditions – pure oxygen on the cathode side. The Naval Undersea Warfare Center is developing SOFC-based power sources for UUVs that must operate in an air-free scenario. Oxygen-blown coal gasifiers could be designed to provide pure oxygen feed to the SOFC power plant block. Understanding SOFC performance under these extreme conditions will be useful for future coal gasification plants as well as NUWCDIVNPT's UUVs. SOFCs operating on pure oxygen instead of air are unique to the SOFC research community but are of common interest to both NUWCDIVNPT and DOE.

NUWCDIVNPT has been testing a variety of SOFCs being developed under the SECA program as well as related components such as fuel processors. This year's effort focused on system demonstrations with a VPS stack, as well as analysis of Delphi Corporation's SOFC stack and endothermic fuel processor.

Approach

The system demonstrations are being accomplished in two phases. In the first phase, a VPS stack was integrated with a R&D Dynamics anode recycle blower, an InnovaTek steam reformer, and CO_2 sorbent from TDA Research. The aim was to continue extended lifetime studies of these four prototype technologies. In the second phase, a Delphi Corporation stack will be tested with a steam reformer, also manufactured by Delphi. However, the reformer will predominately be run in steam reforming mode instead of catalytic partial oxidation/autothermal reforming mode, as Delphi typically uses in their auxiliary power unit system.

In addition to the experimental validation, continual refinement of the system model for a UUV application is being conducted in order to better comprehend the effects of water feed/recycle into the reformer, rate of CO_2 removal, and recycle ratio in the anode exhaust stream. A better understanding is needed regarding how these parameters affect system reliability; namely, steam-to-carbon ratio (S/C) at the reformer exhaust and maximum flow rate in the anode recycle loop. With minimal system-level data available, an iterative

approach is used to refine the system model after experimental validation, which offers insight as to what system performance metrics are practical.

Results

A 28-cell, SOFC stack was manufactured by VPS for testing at NUWCDIVNPT. The stack was externally compressed and was tested in a proof-of-concept system demonstration as shown in Figure 1. Several hours of operation were conducted and steady transition from hydrogen cylinder gas to liquid fuel was achieved at 22 amp draw from the stack, see Figure 2. However, when higher power levels were attempted, the flows were not sustainable, as shown in Figure 3. Air leakage into the anode gas stream, gas leakage from the anode loop, and limitations with blower flow rate capacity forced this test to be terminated prematurely. It can be seen here that careful coordination between fuel feed rate, current, and blower rpm is required when changing power level. Additionally, this finely tuned control system is compromised if there is considerable gas leakage or air intake. Figure 4 shows performance data for the VPS stack under cylinder gas. In these tests, utilizations of fuel and oxygen up to 80% were achieved without recycle.

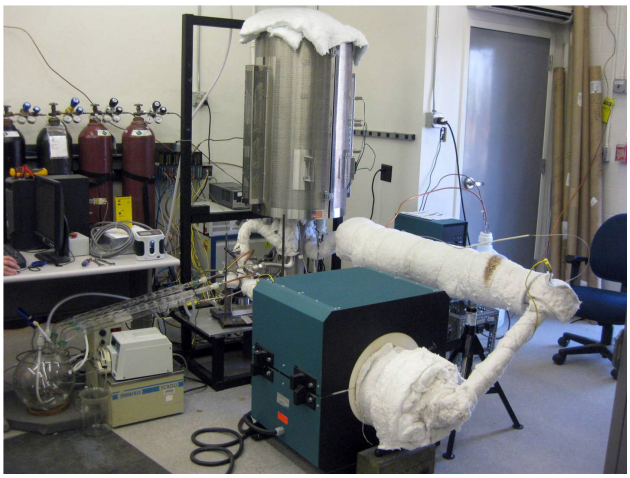

FIGURE 1. SOFC system set-up for VPS stack testing with R&D Dynamics anode recycle blower, TDA CO_2 sorbent, and InnovaTek steam reformer.

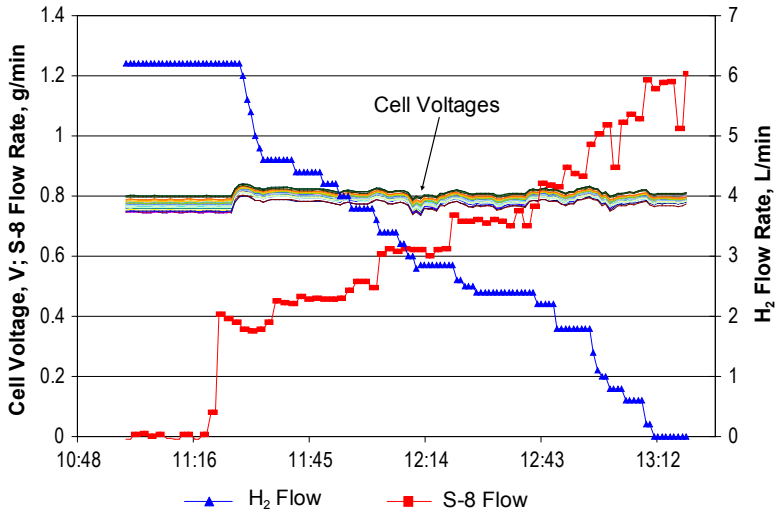

FIGURE 2. Steady transition from H_2 cylinder gas to S-8 liquid fuel feed. Cell voltages were stable at 22 amps, ~500 W, and 75% U_{fuel}. The anode was operated in closed-loop recycle.

Hardware for the Delphi SOFC stack and endothermic reformer test is currently being installed and will be tested in the calendar year.

Concerning the system modeling, a minimum CO_2 removal percentage from each scrubber bed appears to be near 70% in order to keep the overall steam-to-carbon ratio acceptable at the reformer exhaust (>2.0). Higher removal percentages would be preferred, but it is not clear at this time what will actually be attainable in the final system. Continuing studies by TDA Research on their sorbent material are investigating the effects of space velocity and pressure. At this point, 70% seems the minimum acceptable removal level in order to avoid excessive purging and water recycle (either of which may cool the system too much or lower efficiency). By splitting scrubber beds into equal portions, each can operate in its optimum temperature range at the exhaust of the SOFC and reformer. If the maximum sustainable scrubber performance were 70% CO_2 removal from each bed, then a reliable steady-state point would use 85% anode recycle with a water feed of 8 mol/hr (see Figure 5). This is deemed "reliable" because all variables can change slightly without approaching coking conditions (S/C <2.0) or unacceptably high flow rates (>150 L/min). Anode recycle over 88% generally results in exceedingly high flow rate unless CO_2 scrubber performance can be further increased.

Conclusions and Future Directions

With the non-hermetic sealing of the VPS stack, concern remains over gas leakage for the intended UUV application, as any leakage across the cells or mixing with the reactant atmospheres cannot be tolerated in the system design. Leakage both consumes and dilutes intended reactant streams, thus decreasing efficiency while elevating stack temperature. Additionally, the steam exhaust from the fuel cell needs to

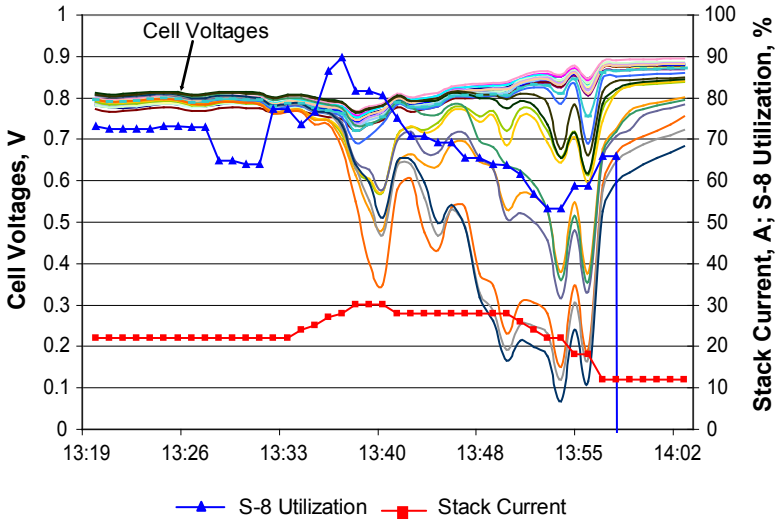

FIGURE 3. Instability at higher fuel utilization. Fuel starvation was seen in the SOFC after current was ramped at a faster rate in proportion to fuel delivery. Gas leakage and air intake amplified the problem of fuel dilution in the anode recycle loop, making higher power levels unattainable in this system demonstration.

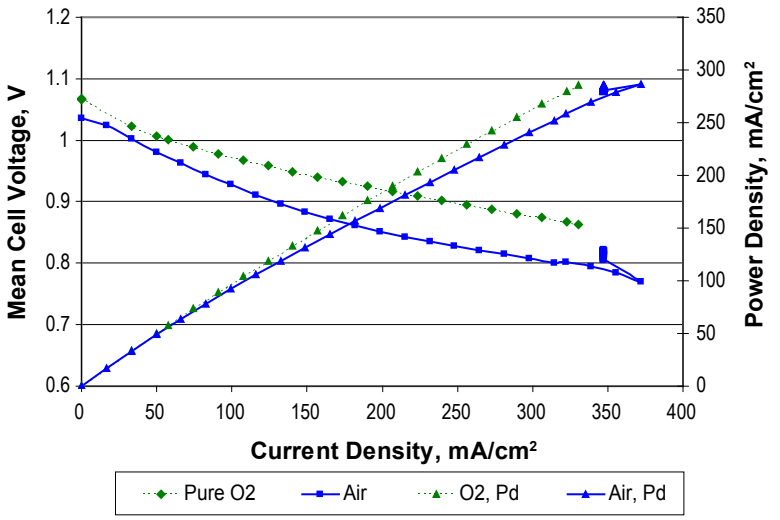

FIGURE 4. Isolated tests on VPS SOFC stack. Performance using 10 L/min pure O_2 versus 30 L/min air at the cathode. Anode feed was 20 L/min H_2, 10 L/min N_2, and 3% water vapor. Roughly 3% gain from pure oxygen versus air. Up to 80% fuel or oxygen utilization achieved.

be recycled to drive the steam reformer. If a significant amount of steam is leaking out of the fuel cell or into the cathode chamber, the anode recycle system design will be unsteady and unsustainable.

Delphi's SOFC stack, which uses brazed cassettes and glass-based sealing for stack assembly will be tested again with focus placed on reformer operation and characterization. The reformer will run off the hot anode exhaust stream from the SOFC stack. Liquid fuel will be blended into the stream and the reforming reaction will be driven primarily by the latent heat in the anode recycle stream.

FY 2010 Publications/Presentations

1. A. Alan Burke, Louis G. Carreiro, and R. Craig Urian, "Results Using Processed Acetylene Fuel Stream in SOFC Stack," Journal of Fuel Cell Science and Technology, vol. 7, iss. 3, 034502 (2010).

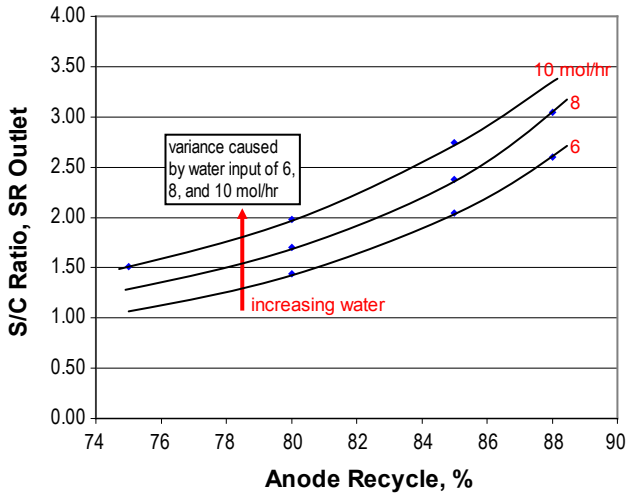

FIGURE 5. Scrubbers operating at 70% removal for all cases. Operating map for S/C ratio as a function of water input and anode recycle percentage.

2. A. Alan Burke, Louis G. Carreiro, and R. Craig Urian, "Self-Contained SOFC Power System Using Calcium Carbide and Hydrogen Peroxide as Reactants," Fuel Cell Seminar and Exhibition 2009, Palm Springs, California, 16–19 November 2009. Poster and Extended Abstract.

VI. Acronyms & Abbreviations

°	Degree
°C	Degree(s) Celsius
Δ	Change, delta
~	Approximately
≈	Equals approximately
>	Greater than
≥	Greater than or equal to
≤	Less than or equal to
<	Less than
@	At
#	Number
%	Percent
®	Registered trademark
μm	Micrometer(s), micron(s)
η	Viscosity
Ω	Ohm(s)
Ω/cm^2	Ohm(s) per square centimeter
$	United States dollars
2D	Two dimensional
3D	Three dimensional
441	A ferritic stainless steel
8YSZ	Eight mol% yttria-stabilized zirconia
A	Ampere(s), amp(s)
Å	Angstrom(s)
ABO_3	Perovskite type materials
Abstr.	Abstract
A/cm^2	Amp(s) per square centimeter
Adv.	Advanced
Ag	Silver
AGR	Anode gas recycle
AIChE	American Institute of Chemical Engineers
AISI	American Iron and Steel Institute
AISI 441	A ferritic stainless steel
Al	Aluminum
AL	Alabama
AL441	A ferritic stainless steel alloy
Al_2O_3	Alumina, aluminum oxide, sapphire
Am.	American
Amer.	American
Amp	Ampere
ANL	Argonne National Laboratory
ANL-APS	Argonne National Laboratory Advanced Photon Source
ANN	Artificial neural network
ANOVA	Analysis of variance
APEC	Applied Power Electronics Conference
Appl.	Applied
APS	Advanced Photon Source
APU	Auxiliary power unit
arb.	Arbitrary
As	Arsenic
ASD	Aerosol spray deposition
AsH_3	Arsine
ASM	American Society for Microbiology
ASME	American Society of Mechanical Engineers
ASPEN	Modeling software, computer code for process analysis
ASR	Area specific resistance
ASTM	ASTM International, originally known as the American Society for Testing and Materials
ATI	Allegheny Technologies Incorporated
atm	Atmosphere(s)
ATR	Autothermal reformer
a.u.	Arbitrary unit
Ave.	Average
B	Boron
Ba	Barium
$BaCeO_3$	Barium cerate
BaO	Barium oxide
bar_a	Bar absolute
BATAN	Indonesian National Nuclear Energy Agency
BCAS	Barium-calcium-aluminum-boron silicate
BCC	Body centered cubic
BET	Brunauer-Emmett-Teller
Bi	Bismuth
Bldg.	Building
BNHA	Ni-substituted barium hexaaluminate
B_2O_3	Boron (III) oxide
BOP	Balance of plant
Br	Bromine
C	Carbon
C	Celsius
Ca	Calcium
CA	California
Catal.	Catalysis

CBS	Coal-based systems
CCM	Cathode contact material
Cd	Cadmium
Ce	Cerium
CeO_2	Ceric oxide
Ceram.	Ceramics
Ch.	Chapter
CH_4	Methane
C_2H_2	Acetylene
C_2H_4	Ethylene
chem.	Chemistry
Cl	Chlorine
cm	Centimeter(s)
cm^2	Square centimeter(s)
CMU	Carnegie Mellon University
CO	Carbon monoxide
CO	Colorado
Co	Cobalt
Co.	Company
CO_2	Carbon dioxide
COE	Cost of electricity
Comm.	Communications
CPD	Contact potential difference
CPOX	Catalytic partial oxidation
Cr	Chromium
Cr_2O_3	Chromic oxide
CRPLAW	A user-defined subroutine in the MARC model
CT	Connecticut
CTE	Coefficient of thermal expansion
CTP	Core Technology Program
Cu	Copper
CuO	Copper oxide
d	Distance
DARPA	Defense Advanced Research Projects Agency
dBA	Decibel(s)
DBT	Dibenzothiophene
DC	Direct current
DC-DC	Direct current to direct current
DECS-24	A sample of coal from the Penn State Coal Sample Bank
DFMA	Design for Manufacturing and Assembly
DFT	Density functional theory
DICTRA	Diffusion controlled transformations
dmmf	Dry mineral matter free
DOE	U.S. Department of Energy
DOI	U.S. Department of Interior
Dr.	Doctor
DREAM SOFC	A multi-dimensional modeling tool
DSC	Differential scanning calorimetry
Dy	Dysprosium
$DyScO_3$	Dysprosium scandium oxide
ECL	Electrochemical looping
ECR	Electrical conductivity relaxation
ECS	The Electrochemical Society
ed.	Edition
eds, Eds.	Editors
EDS	Energy dispersive spectroscopy
EDX	Energy dispersive X-ray spectroscopy
e.g.	exempli gratia, for example
EG&G	EG&G Technical Services, a division of URS Corporation
EIA	Energy Information Administration
EIS	Electrochemical impedance spectroscopy
Electrochem.	Electrochemical
E-MRS	European Materials Research Society
EPD	Electrophoretic deposition
EPSCOR	Experimental Program to Stimulate Competitive Research
ESL	Electroscience Laboratories
ESWG	Electrical Systems Working Group
et al.	et alii, and others
etc.	et cetera, and so on
Eur.	European
eV	Electron volt(s)
exch.	Exchange
EXP	Experimental
ext.	Extension
F	Fluorine
FC	Fuel cell
FCC	Face centered cubic
FCC/BCC	Face centered cubic/body centered cubic
FCE	FuelCell Energy, Inc.
Fe	Iron
FE	U.S. Department of Energy Office of Fossil Energy
FEA	Finite element analysis
FF	Form factor
FPS	Fuel processing system
FY	Fiscal year
g	Gram(s)
Ga	Gallium

GA	Georgia
GC-ICP/MS	Gas chromatograph-inductively coupled plasma/mass spectrometer
GCO	Gadolinium doped ceric oxide
GCO/YSZ	Gadolinium doped ceric oxide/yttria-stabilized zirconia
Gd	Gadolinium
GDC	Gadolinia-doped ceria
GDMS	Glow discharge mass spectrometry
GE	General Electric
Ge	Germanium
Gen	Generation
GHSV	Gas hourly space velocity
GNP	Glycine-nitrate process
GOMACTech	Government Microcircuit Applications and Critical Technology
gpm	Gallon(s) per minute
GRNN	Generalized regression neural network
GT	Gas turbine
GT/ST	Gas turbine/steam turbine
h	Hour(s)
H	Hydrogen
H_2	Diatomic hydrogen
H/C	Hydrogen to carbon ratio
HCl	Hydrogen chloride
HF	High frequency
Hg	Mercury
HHV	Higher heating value
H_2O	Water
HP	High pressure
hr	Hour(s)
hrs.	Hours
HRTEM	High resolution transmission electron microscopy
H_2S	Hydrogen sulfide
HT	High temperature
HTXRD	High temperature X-ray diffractometer
HV	High voltage
Hz	Hertz
I	Current
I	Iodine
IAPG	Interagency Advanced Power Group
IAS	Industry Applications Society
IASR	Internal air-steam reforming
IC	Interconnect
ICACC	International Conference and Exhibition on Advanced Ceramics and Composites
ICP	Inductively-coupled plasma
ICP/MS	Inductively coupled plasma/mass spectrometer
ICP-OES	Inductively-coupled plasmañoptical emission spectroscopy
IDR	Internal dry reforming
i.e.	id est, that is
IEEE	Institute of Electrical and Electronics Engineering
IGBT	Insulated gate bipolar transistor
IGFC	Integrated gasification fuel cell
IL	Illinois
Im	Impedance
In	Indium
in.	Inch(es)
Inc.	Incorporated
Int.	International
Intíl	International
I/O	Input/output
IP	Integrated-planar
IP	Ionization potential
IP-SOFC	Integrated-planar solid oxide fuel cell
Ir	Iridium
ISBN	International Standard Book Number
ISR	Internal steam reforming
iss.	Issue
IT	Intermediate temperature
IT-SOFC	Intermediate temperature solid oxide fuel cell
I-V	Current-voltage
J	Joule(s)
J.	Journal
JBS	Junction barrier Schottky
JP-10	Jet Propellant 10, a jet fuel
Jpn.	Japan
K	Kelvin
K	Potassium
kg	Kilogram(s)
kgf	Kilogram(s) force
kHz	Kilohertz
kJ	Kilojoule(s)
kJ/mol	Kilojoule(s) per mole
KPS	Kelvin probe spectroscopy
kV	Kilovolt(s)
kW	Kilowatt(s)
kWac	Kilowatt(s) alternating current
kWe	Kilowatt(s) electric

kWh	Kilowatt-hour(s)
L	Liter(s)
La	Lanthanum
$LaAlO_3$	Lanthanum aluminum oxide
$LaCrO_3$	Lanthanum chromite
$LaMnO_3$	Lanthanum manganite
LAO	Lanthanum aluminum oxide
LaSr	Lanthanum strontium
lb.	Pound(s)
LBC	Lanthanum barium cobalt oxide
LBCO	Lanthanum barium cobalt oxide
lbm	Pound(s)-mass
LBNL	Lawrence Berkeley National Laboratory
LCC	Lanthanum calcium chromite
LCCB	Low-cost cathode blower
LCRh1ZY	Rhodium-substituted pyrochlore
LDC	Lanthanum-doped ceria
Lett.	Letter
LF	Low frequency
LHV	Lower heating value
Li	Lithium
LLC	Limited Liability Company
LMA	Liquid metal anode
L/min	Liter(s) per minute
LMO	Lanthanum manganite ($LaMnO_3$)
LNF	Lanthanum nickel ferrite
Log	Logarithm
LSC	Lanthanum strontium cobaltite, lanthanum strontium cobalt oxide
LSCF	Lanthanum strontium cobalt ferrite, lanthanum strontium cobalt iron oxide
LSCMF	Lanthanum strontium cobalt manganese ferrite
LSCuF	Lanthanum strontium copper ferrite, lanthanum strontium copper iron oxide
LSF	Lanthanum strontium ferrite
LSM	Lanthanum strontium manganite, strontium-doped lanthanum manganite, lanthanum strontium manganese oxide
LSMO	Lanthanum strontium manganite oxide
LSM/YSZ	Lanthanum strontium manganite/yttria-stabilized zirconia
LSN	Lanthanum strontium nickel oxide
LSTMO	Lanthanum strontium transition metal oxide
LSZ	Lanthanum strontium zirconium oxide
LTA	Liquid tin anode
LTA-SOFC	Liquid tin anode solid oxide fuel cell
m	Meter(s)
M	Million
MA	Massachusetts
mA	Milliampere(s)
mA/cm^2	Milliampere(s) per square centimeter
MARC	A fuel cell stack computer model
MARC-SECA	A solid oxide fuel cell stack computer model
Mat.	Material
Mater.	Material
mbar	Millibar
MC	Manganese cobalt oxide, $(Mn,Co)_3O_4$
MCO	Manganese-cobalt spinel, $(MnCo)_3O_4$
MDU	Module Demonstration Unit
Meet.	Meeting
meV	Milli electron volt(s)
MFC	Multi-function controller
Mg	Magnesium
MgO	Magnesium oxide
MI	Michigan
MIEC	Mixed ionic-electronic conductor
min	Minute(s)
MIT	Massachusetts Institute of Technology
mm	Millimeter(s)
Mn	Manganese
MN	1-Methylnapthalene
MnCo	Manganese cobalt
$MnCo_2O_4$	Manganese cobalt oxide
MnO_3	Manganate
Mo	Molybdenum
MO	Missouri
mΩ	Milli-ohm(s)
$m\Omega{\cdot}cm^2$	Milli-ohm square centimeter(s)
MOB2	A diffusity database
MOD	Modification
mol	Mole(s)
mol%	Mole percent
MOSFET	Metal-oxide semiconductor field-effect transistor
MP	Multi-physics
MPa	Megapascal(s)
MRS	Materials Research Society
MS	Mail stop
MS&T	Materials Science and Technology
MSC MARC	A fuel cell stack model
MSRI	Materials and Systems Research, Inc.
Mtg.	Meeting

mTorr	Millitorr
mV	Millivolt(s)
MW	Megawatt(s)
mW	Milliwatt(s)
mW/cm^2	Milliwatt(s) per square centimeter
MWe	Megawatt(s) electric
N	Newton(s)
N	Nitrogen
N_2	Diatomic nitrogen
Na	Sodium
NaCl	Sodium chloride
Nb	Niobium
NCC	Neodymium cerium copper oxide
NCCC	National Carbon Capture Center
Nd	Neodymium
NETL	National Energy Technology Laboratory
NG	Natural gas
NGO	Neodymium gadolinium oxide, $NdGaO_3$
Ni	Nickel
$NiMn_2O_4$	Nickel manganese oxide
NIMTE	Ningbo Institute of Material Technology and Engineering
NiO	Nickel oxide
Ni_5P_2	Nickel phosphide
$Ni_{12}P_5$	Nickel phosphide
Ni_xP_y	Nickel phosphides
NIST	National Institute of Standards and Technology
NJ	New Jersey
nm	Nanometer(s)
NOC	Normal operating conditions
NOx	Oxides of nitrogen
NSF	National Science Foundation
NUWC	Naval Undersea Warfare Center
NUWC/DIVNPT	Naval Undersea Warfare Center Division Newport
NV	Nevada
NW	Northwest
NY	New York
O	Oxygen
O_2	Diatomic oxygen
O_3	Ozone
O/C	Oxygen to carbon ratio
OCV	Open circuit voltage
OH	Ohio
OR	Oregon
ORAU	Oak Ridge Associated Universities
ORNL	Oak Ridge National Laboratory
ORR	Oxygen reduction rate
Os	Osmium
p.	Page
P	Performance
P	Phosphorus
P	Pressure
PA	Pennsylvania
Pa	Pascal(s)
Pap.	Paper
Pa-s, Pa.s	Pascal-second(s)
Pb	Lead
PBCO	Praseodymium barium cobalt oxide, $PrBaCo_2O_{5+x}$
PCC	Pulverized coal combustion
PCI	Precision Combustion Inc.
PCS	Power conditioning system
Pd	Palladium
PEN	Positive electrode-electrolyte-negative electrode
PESC	Power Electronics Specialists Conference
PH_3	Phosphine
Phys.	Physics
PiN	P-intrinsic-N
PLD	Pulsed laser deposition
PNAS	Proceedings of the National Academy of Sciences
PNNL	Pacific Northwest National Laboratory
PO, P.O.	Post office
pO_2, P_{O2}	Partial pressure of oxygen
pp.	Pages
PP	Polarizing power
ppb	Part(s) per billion
ppbv	Part(s) per billion by volume
ppm	Part(s) per million
ppmw	Part(s) per million by weight
Pr	Praseodymium
Proc.	Proceedings
PSDF	Power Systems Development Facility
psi	Pound(s) per square inch
psid	Pound(s) per square inch differential
P-SOFC	Proton conducting solid oxide fuel cell
Pt	Platinum
PVL	Process verification line
r, R	Rate
R	Resistance

R&D	Research and development
Rd.	Road
RD&D	Research, development, and demonstration
Re	Resistance
RE	Rare earth
RE	Reactive elements
Res.	Research
Rev.	Review
RF	Radio frequency
Rh	Rhodium
Rm	Room
RO	Alkaline earth oxides
RP-1	A diesel type fuel
RRFCS	Rolls Royce Fuel Cell Systems
RT	Room temperature
Ru	Ruthenium
s	Second(s)
S	Siemen(s)
S	Sulfur
SARS	Safety Analysis and Review System
Sb	Antimony
SBIR	Small Business Innovation Research
SBSC	Samarium barium strontium cobalt oxide
Sc	Scandium
S/C	Steam to carbon ratio
sccm	Standard cubic centimeter(s) per minute
Sci.	Science
S/cm	Siemen(s) per centimeter
SCM	A barium alkali silicate glass
SCN, SCN-1	Glasses belonging to the system SiO_2-CaO-Na_2O
ScSZ	Scandium-stabilized zirconia
SDC	Scandia-doped ceria
SDC	Samarium-doped ceria
Se	Selenium
sec	Second(s)
SECA	Solid State Energy Conversion Alliance
SEM	Scanning electron microscopy
SEM/EDS	Scanning electron microscopy/energy dispersive spectroscopy
SEM/EDX	Scanning electron microscopy/energy dispersive X-ray spectroscopy
Si	Silicon
Si	Stream interface
SiC	Silicon carbide
slpm	Standard liter(s) per minute
Sm	Samarium
SMO	Strontium manganate, $SrMnO_3$
Sn	Tin
Soc.	Society
SOFC	Solid oxide fuel cell
SOFC-MP	Solid oxide fuel cell multi-physics
Sol.	Solid
Sr	Strontium
$SrMnO_3$	Strontium manganate
$SrTiO_3$	Strontium titanate
$SrZrO_3$	Strontium zirconiate
SS, ss	Stainless steel
SSC	Strontium samarium cobalt oxide
SSM	Sign sheeting materials
St.	Saint
St.	Street
ST	Steam turbine
STM	Scanning tunneling microscopy
STO	Strontium titanate, $SrTiO_3$
STTM	South Texas Technology Management
STTR	Small Business Technology Transfer
Surf.	Surface
SW	Southwest
Symp.	Symposium
t	Time
T	Temperature
Ta	Tantalum
TC	Thermocouple channel
TCFe6	A thermodynamic database
TCR	Tin-coal reactor
TD	n-Tetradecane
TDA	TDA Research
Te	Tellurium
TEC	Thermal expansion coefficient
Tech.	Technology
TEM	Transmission electron microscopy
Tg, T_g	Glass transition temperature
Ti	Titanium
T_L	Liquidus temperature
TMA	Thermomechanical analysis
TMS	The Metallurgical Society
TN	Tennessee
TPD	Temperature-programmed desorption
TPO	Temperature-programmed oxidation
TPR	Temperature-programmed reduction
Trans.	Transactions

T_s	Softening point temperature
TSC	Tape casting–Screen printing–Co-firing
TX	Texas
U	Uranium
UHV	Ultra-high vacuum
UNLV	University of Nevada, Las Vegas
UNS	Unified Numbering System
US, U.S.	United States
USA	United States of America
USD	United States dollar
UT	Utah
UTC	United Technologies Company
UTRC	United Technologies Research Center
UTSA	University of Texas at San Antonio
UUV	Unmanned undersea vehicle
V	Vanadium
V	Version
V	Volt(s)
VA	Virginia
VCH	Verlag Chemie
V-I	Volt-current
vol, Vol.	Volume
VPS	Versa Power Systems
W	Tungsten
W	Watt(s)
WA	Washington
WBST	Wide-bandgap semiconductor technology
W/cm^2	Watt(s) per square centimeter
WE	Working electrode
WEBEX	Web exchange internet conferencing
WF	Work function
WGS	Water-gas shift
wt	Weight
wt%	Weight percent
WV	West Virginia
WVU	West Virginia University
x	Times
XAS	X-ray adsorption spectroscopy
XES	X-ray emission spectroscopy
XPS	X-ray photon spectroscopy, X-ray photoelectron spectroscopy
XRD	X-ray diffraction
XRS	X-ray resonant scattering
Y	Yttrium
YBC	Yttrium barium cobalt oxide
YDC	Yttria-doped ceria
Y_2O_3	Yttrium oxide (yttria)
YSZ	Yttria-stabilized zirconia
Z	Impedance
Zn	Zinc
ZnO	Zinc oxide
Zr	Zirconium
ZrO_2	Zirconium dioxide (zirconia)

VII. Primary Contact Index

VIII. Organization Index

IX. Contract Number Index

X. Index of Previous Projects

Projects Discontinued Since the FY 2009 Annual Report

Contract Number	Performer	Project Topic
41567	Virginia Polytechnic Institute and State University	A Low-Cost Soft-Switched DC-DC Converter for Solid Oxide Fuel Cells
41817	American Society of Mechanical Engineers (ASME)	SOFC Design Basis Development Project
41817	Carnegie Mellon University	TEM Investigations of SOFCs: Stability of LSCF-based Cathodes
41817	University of California	High Efficiency Coal Gasification-Based SOFC Power Plants
42219	Georgia Institute of Technology	Novel Sulfur-Tolerant Anodes for Solid Oxide Fuel Cells
42533	Tennessee Technological University	Novel Composite Materials for SOFC Cathode-Interconnect Contact
42613	Siemens Energy, Inc.	Coal Gas-Fueled SOFC Hybrid Power Systems with CO_2 Separation
42735	Georgia Institute of Technology	Characterization of Atomic and Electronic Structure of Electrochemically Active SOFC Cathode Surfaces
43063	University of Texas at San Antonio	Novel Low Temperature Solid State Fuel Cells
44036	Montana State University	SECA Coal-Based Systems Core Research – Montana State University
84209	Phoenix Analysis & Design Technologies	Anode and Cathode Blower Systems for SOFC
84210	R&D Dynamics Corporation	Foil Gas Bearing Supported High-Speed Centrifugal Anode Gas Recycle Blower

Note: Previous contract number FWP44036 (Pacific Northwest National Laboratory) is now reported under FWP40552. Contract number NT0003893 [Rolls-Royce Fuel Cell Systems (U.S.) Inc.] has been changed to FE0000303.

Projects Discontinued Since the FY 2008 Annual Report

Contract Number	Performer	Project Topic
05690	American Society of Mechanical Engineers	SOFC Design Basis Development Project (project transferred to RDS41817.3130105-036)
08-220692	National Energy Technology Laboratory	Materials Development for the Solid Oxide Fuel Cell Environment
41572	Georgia Institute of Technology	Functionally Graded Cathodes for Solid Oxide Fuel Cells
42221	Missouri University of Science & Technology	Thermochemically Stable Sealing Materials for Solid Oxide Fuel Cells
42223	Tennessee Technological University	Development of Low-Cr Fe-Ni-Based Alloys for Intermediate Temperature SOFC Interconnect Application
42225	Arcomac Surface Engineering, LLC	Oxidation Resistant, Cr Retaining, Electrically Conductive Coatings on Metallic Alloys for SOFC Interconnects
42227	University of Cincinnati	Innovative Seals for Solid Oxide Fuel Cells (SOFCs)
42229	Delavan d.b.a. Goodrich Turbine Fuel Technologies	An Innovative Injection and Mixing System for Diesel Fuel Reforming
42471	Ceramatec, Inc.	Intermediate Temperature Solid Oxide Fuel Cell Development
42516	University of Michigan	Carbon Tolerant Steam Reforming and SOFC Anode Catalysts
42527	Ohio University	Combined Theoretical and Experimental Investigation and Design of H_2S Tolerant Anode for Solid Oxide Fuel Cells
42614	GE Global Research	Solid Oxide Fuel Cell Coal-Based Power Systems
42623	University of Utah	A High Temperature Electrochemical Energy Storage System Based on Sodium Beta Alumina Solid Electrolyte (BASE)
42627	SRI International	Effect of Coal Contaminants on Solid Oxide Fuel Cell System Performance and Service Life
44036	University of Florida	SECA Coal-Based Systems Core Research - University of Florida
49071	Massachusetts Institute of Technology	Local Electronic Structure and Surface Chemistry of SOFC Cathodes
68250	Sandia National Laboratories	Reliable Seals for Solid Oxide Fuel Cells
84662	Aspen Products Group, Inc.	Waterless 5 kWe Diesel Reformer
84663	Ceramatec, Inc.	SOFC Integrated Multi-Mode Diesel Reformer
84673	Lynntech, Inc.	Low Cost, Compact Plasma Fuel Reformer for APUs
84881	NexTech Materials Ltd.	Intermediate Temperature Solid Oxide Fuel Cell Cathode Enhancement through Infiltration Fabrication Techniques

Projects Discontinued Since the FY 2007 Annual Report

Contract Number	Performer	Project Topic
41838	Acumentrics Corporation	Development of a Low Cost 10 kW Tubular SOFC Power System
41245	GE Global Research	Solid State Energy Conversion Alliance (SECA) Solid Oxide Fuel Cell Program
42175	University of Missouri-Rolla	Resilient Sealing Materials for Solid Oxide Fuel Cells
41247	Siemens Power Generation	Small-Scale Low Cost Solid Oxide Fuel Cell Power Systems
42220	University of Utah	Electrically Conductive, Corrosion-Resistant Coatings through Defect Chemistry for Metallic Interconnects
42741	Virginia Polytechnic Institute and State University	Digital Manufacturing of Gradient Meshed SOFC Sealing Composites with Self-Healing Capabilities
84611	Mesta Electronics Inc.	DC-AC Inverter with Reactive-Power-Management Functionality
84616	R&D Dynamics Corporation	Foil-Bearing Supported High-Speed Centrifugal Cathode Air Blower
84624	TIAX LLC	Low-Cost, High-Temperature Recuperators for SOFC Fabricated from Titanium Aluminum Carbide (Ti_2AlC)
83795	TDA Research, Inc.	Sorbents for Desulfurization of Natural Gas and LPG
84608	Materials and Systems Research, Inc.	A Thin Film, Anode-Supported Solid Oxide Fuel Cell Based on High Temperature Proton Conducting Membrane for Operation at 400 to 700°C
86280	Materials and Systems Research, Inc.	A High Temperature (400 to 650°C) Secondary Storage Battery Based on Liquid Sodium and Potassium Anodes
86140	FuelCell Energy, Inc.	Advanced Control Modules for Hybrid Fuel Cell/Gas Turbine Power Plants
86283	NexTech Materials, Ltd.	Component Manufacturing and Optimization of Protonic SOFCs
41244	Cummins Power Generation	10 kW Solid Oxide Fuel Cell Power System Commercialization
42184	University at Albany – SUNY	Feasibility of a SOFC Stack Integrated Optical Chemical Sensor
42624	Massachusetts Institute of Technology	Photo-Activated Low Temperature, Micro Fuel Cell Power Source
42625	Northwest University	High Temperature Fuel Cells for Co-Generation of Chemicals and Electricity
42626	United Technologies Research Center	Techno-Economic Feasibility of Highly Efficient Cost Effective Thermoelectric-SOFC Hybrid Power Generation Systems

Projects Discontinued Since the FY 2006 Annual Report

Contract Number	Performer	Project Topic
FEAA067	Oak Ridge National Laboratory	Power Electronics for Solid Oxide Fuel Cells
FWP49100	Argonne National Laboratory	Technology Development in Support of SECA
34139	Siemens Power Generation	High Temperature Solid Oxide Fuel Cell Development
40798	FuelCell Energy, Inc.	Direct Fuel Cell/Turbine Power Plant
41562	University of Florida	Determination of Electrochemical Performance and Thermo-Mechanical-Chemical Stability of SOFCs from Defect Modeling
41566	University of Washington	Advanced Measurement and Modeling Techniques for Improved SOFC Cathodes
41569	Ceramatec, Inc.	Metal Interconnect for Solid Oxide Fuel Cell Power Systems
41571	Georgia Institute of Technology	An Integrated Approach to Modeling and Mitigating SOFC Failure
41574	[1]University of Illinois at Chicago [2]Ceramatec Inc. [3]Virginia Polytechnic Institute and State University [4]Oak Ridge National Laboratory [5]Pacific Northwest National Laboratory	An Investigation of Resolve the Interaction between Fuel Cell, Power Conditioning System and Application Load
41575	NexTech Materials, Ltd.	Continuous Process for Low-Cost, High-Quality YSZ Powder
41578	University of Pittsburgh	Fundamental Studies of the Durability of Materials for Interconnects in Solid Oxide Fuel Cells
41915	Southern University and A&M College	Dense Membranes for Anode Supported All-Perovskite IT-SOFCs
41959	University of Florida	Electrocatalytically Active High Surface Area Cathodes for Low Temperature SOFCs
41960	University of Houston	New Cathode Materials for Intermediate Temperature Solid Oxide Fuel Cells
42222	Chevron Energy Research and Technology Company	Development of Ni-Based Sulfur-Resistant Catalyst for Diesel Reforming
42228	Connecticut Global Fuel Cell Center University of Connecticut	Low-Cost Integrated Composite Seal for SOFC: Materials and Design Methodologies
42514	Franklin Fuel Cells, Inc.	Novel Cathodes Prepared by Impregnation Procedures
42515	Georgia Institute of Technology Center for Innovative Fuel Cell and Battery Technologies	Quantitative Characterization of Chromium Poisoning of Cathode Activity
42517	University of Michigan	Desulfurization of High-Sulfur Jet Fuels by Adsorption and Ultrasound-Assisted Sorbent Regeneration
73138	Ceramatec, Inc.	Advanced Net-Shape Insulation for Solid Oxide Fuel Cells
83528	NexTech Materials, Ltd.	Highly Textured Glass Composite Seals for Intermediate-Temperature SOFCs
84387	FuelCell Energy, Inc.	Diesel Plasma Reformer
84212	Spinworks, LLC	Low-Cost/High-Temperature Heat Exchanger for SOFCs Using Near-Net-Shape Ceramic Powder Forming Process

Projects Discontinued Since the FY 2005 Annual Report

Contract Number	Performer	Project Topic
FE09	Los Alamos National Laboratory	Diesel Reforming for Solid Oxide Fuel Cell Auxiliary Power Units
40779	General Electric	SOFC Hybrid System for Distributed Power Generation
41539	Boston University	Materials System for Intermediate-Temperature SOFC
41602	University of Utah	Active Cathodes for Super-High Power Density SOFC Through Space Change Effects
41631	California Institute of Technology	Enhanced Power Stability for Proton-Conducting Solid Oxide Fuel Cells
41801	Virginia Polytechnic Institute and State University	Modeling and Design for a Direct Carbon Fuel Cell with Entrained Fuel and Oxidizer
41803	University of Akron	Carbon-based Fuel Cell
41804	Duke University	Carbon Ionic Conductors for Use in Novel Carbon-Ion Fuel Cells
83212	Ceramatec, Inc.	Lanthanum Gallate Electrolyte Based Intermediate-Temperature Solid Oxide Fuel Cell Development

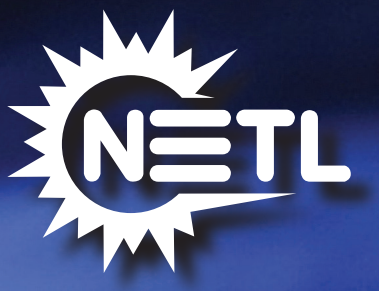

National Energy Technology Laboratory

1450 Queen Avenue SW
Albany, OR 97321-2198
541-967-5892

3610 Collins Ferry Road
P.O. Box 880
Morgantown, WV 26507-0880
304-285-4764

626 Cochrans Mill Road
P.O. Box 10940
Pittsburgh, PA 15236-0940
412-386-4687

Dr. Shailesh D. Vora
Technology Manager, Fuel Cells
412-386-7515
shailesh.vora@netl.doe.gov

Visit the NETL website at:
www.netl.doe.gov

Customer Service:
1-800-553-7681

DOE/NETL-2010-1439 October 2010